

NASA/CR-2006-214281



STAGS Example Problems Manual

Norman F. Knight, Jr.

General Dynamics – Advanced Information Systems, Inc., Chantilly, Virginia

Charles C. Rankin

Rhombus Consultants Group, Inc., Palo Alto, California

March 2006

The NASA STI Program Office . . . in Profile

Since its founding, NASA has been dedicated to the advancement of aeronautics and space science. The NASA Scientific and Technical Information (STI) Program Office plays a key part in helping NASA maintain this important role.

The NASA STI Program Office is operated by Langley Research Center, the lead center for NASA's scientific and technical information. The NASA STI Program Office provides access to the NASA STI Database, the largest collection of aeronautical and space science STI in the world. The Program Office is also NASA's institutional mechanism for disseminating the results of its research and development activities. These results are published by NASA in the NASA STI Report Series, which includes the following report types:

- **TECHNICAL PUBLICATION.** Reports of completed research or a major significant phase of research that present the results of NASA programs and include extensive data or theoretical analysis. Includes compilations of significant scientific and technical data and information deemed to be of continuing reference value. NASA counterpart of peer-reviewed formal professional papers, but having less stringent limitations on manuscript length and extent of graphic presentations.
- **TECHNICAL MEMORANDUM.** Scientific and technical findings that are preliminary or of specialized interest, e.g., quick release reports, working papers, and bibliographies that contain minimal annotation. Does not contain extensive analysis.
- **CONTRACTOR REPORT.** Scientific and technical findings by NASA-sponsored contractors and grantees.

- **CONFERENCE PUBLICATION.** Collected papers from scientific and technical conferences, symposia, seminars, or other meetings sponsored or co-sponsored by NASA.
- **SPECIAL PUBLICATION.** Scientific, technical, or historical information from NASA programs, projects, and missions, often concerned with subjects having substantial public interest.
- **TECHNICAL TRANSLATION.** English-language translations of foreign scientific and technical material pertinent to NASA's mission.

Specialized services that complement the STI Program Office's diverse offerings include creating custom thesauri, building customized databases, organizing and publishing research results ... even providing videos.

For more information about the NASA STI Program Office, see the following:

- Access the NASA STI Program Home Page at <http://www.sti.nasa.gov>
- E-mail your question via the Internet to help@sti.nasa.gov
- Fax your question to the NASA STI Help Desk at (301) 621-0134
- Phone the NASA STI Help Desk at (301) 621-0390
- Write to:
NASA STI Help Desk
NASA Center for AeroSpace Information
7121 Standard Drive
Hanover, MD 21076-1320

NASA/CR-2006-214281



STAGS Example Problems Manual

Norman F. Knight, Jr.

General Dynamics – Advanced Information Systems, Inc., Chantilly, Virginia

Charles C. Rankin

Rhombus Consultants Group, Inc., Palo Alto, California

National Aeronautics and
Space Administration

Langley Research Center
Hampton, Virginia 23681-2199

Prepared for Langley Research Center
under NASA Task Order NNL05AC09T

March 2006

Available from:

NASA Center for AeroSpace Information (CASI)
7121 Standard Drive
Hanover, MD 21076-1320
(301) 621-0390

National Technical Information Service (NTIS)
5285 Port Royal Road
Springfield, VA 22161-2171
(703) 605-6000

Introduction	4
Historical Setting.....	4
Pre-STAGS Days.....	4
Early STAGS Years	5
Initial NASA Langley Efforts.....	5
Finite Element Years.....	6
Nonlinear Solution Procedures.....	6
Global Function Effort	7
STAGS Restructuring Effort	7
STAGSC-1 Era.....	8
QSTAGS to the Present	8
STAGS Version 5.0	9
STAGS Functional Modules	9
Usage.....	9
Demonstration Example Problems	10
Cook Membrane Problem.....	11
Background.....	11
Modeling and Analysis Process.....	11
Numerical Results and Discussion	13
STAGS Input Files	16
Problem References.....	18
Euler-Column Buckling Problem.....	19
Background	19
Modeling and Analysis Process.....	20
Numerical Results and Discussion.....	22
STAGS Input Files	23
Problem References.....	28
Free Vibration of Straight Beam	29
Background.....	29
Modeling and Analysis Process.....	30
Numerical Results and Discussion	31
STAGS Input Files	34
Problem References.....	39
Free Vibration of Circular Ring	40
Background.....	40
Modeling and Analysis Process.....	41
Numerical Results and Discussion	42
STAGS Input Files	44
Problem References.....	51
Buckling of Blade-Stiffened Flat Panels	52
Background.....	52
Modeling and Analysis Process.....	53
Numerical Results and Discussion.....	57
STAGS Input Files	66
Problem References.....	79
Raasch Curved Hook Problem	80
Background.....	80
Modeling and Analysis Process.....	80
Numerical Results and Discussion.....	83

STAGS Input Files	83
Problem References.....	87
Buckling and Collapse of Circular Cylinder with Square Cutouts	88
Background.....	88
Modeling and Analysis Process.....	88
Numerical Results and Discussion.....	92
STAGS Input Files	100
Problem References.....	108
Scordelis-Lo Barrel Roof Problem	109
Background.....	109
Modeling and Analysis Process.....	109
Numerical Results and Discussion.....	112
STAGS Input Files	114
Problem References.....	118
Transient Response of Truncated Conical Shell	119
Background.....	119
Modeling and Analysis Process.....	119
Numerical Results and Discussion.....	122
STAGS Input Files	126
Problem References.....	129
Snap-Through of Hinged Shallow Cylindrical Shell	130
Background.....	130
Modeling and Analysis Process.....	130
Numerical Results and Discussion.....	132
STAGS Input Files	141
Problem References.....	147
Advanced-Features Example Problems.....	148
Buckling of Sandwich Panels.....	149
Background.....	149
Modeling and Analysis Process.....	150
Numerical Results and Discussion.....	154
STAGS Input Files	157
Problem References.....	173
Crack Growth Simulation for Middle-Crack Tension Panel.....	174
Background.....	174
Modeling and Analysis Process.....	175
Numerical Results and Discussion.....	179
STAGS Input Files	191
Problem References.....	210
Hybrid Quasi-Static/Transient Solution Procedures Application	211
Background.....	211
Modeling and Analysis Process.....	213
Numerical Results and Discussion.....	214
STAGS Input Files	218
Problem References.....	224
Progressive Failure Analysis of Postbuckled Shear Panel	226
Background.....	226
Modeling and Analysis Process.....	227
Numerical Results and Discussion.....	228
STAGS Input Files	233
Problem References.....	242

Membrane Wrinkling Problems	243
Background	243
Modeling and Analysis Process.....	246
Numerical Results and Discussion	249
STAGS Input Files	257
Problem References.....	269
Actuator Problems.....	273
Background	273
Modeling and Analysis Process.....	273
Numerical Results and Discussion.....	273
STAGS Input Files	277
Problem References.....	279
Summary.....	280
References	280

Introduction

NASA Langley has been involved with shell analysis research and development for many decades. Much of the early shell analysis research enabled space flight through the thorough understanding of shell theory and development of computerized shell design tools. This development occurred during an epoch when several technological advancements were taking place; in particular, the development of electronic computations and associated numerical methods such as finite difference and finite element methods. STAGS had its beginnings as an Lockheed Missiles & Space Company research code and evolved into a powerful shell analysis code offering unique capabilities such as advanced nonlinear solution procedures, load relaxation for re-establishing equilibrium, sandwich elements, fastener elements, generalized imperfection modeling, constraint definitions, and constitutive modeling utilities.

STAGS is an acronym for Structural Analysis of General Shells. Development of STAGS' technology and analysis tools began in 1963, nearly forty years ago, at the Lockheed Palo Alto Research Laboratory (Applied Mechanics Group) of the Lockheed Missiles & Space Company (LMSC) in Palo Alto, CA.* Initially casted as a finite difference code (finite elements were just appearing and computer systems were quite limited in capability), STAGS evolved to a finite element code in the late 1970's. It is based on a small-strain, large-deformation, large-rotation energy formulation including nonlinear material behavior. Historically STAGS has been a shell analysis tool; however, three-dimensional nonlinear analysis capabilities have been incorporated in recent years. STAGS continues to serve as both a structural mechanics research tool for shell analysis and nonlinear mechanics as well as an advanced structural analysis tool for aerospace structures.

Historical Setting

A brief historical summary of the development of the STAGS shell analysis code is given here. This summary is not intended to review all shell analysis work but rather those aspect contributing to computerized shell analysis and the STAGS code. The summary covers the early LMSC effort through the current effort resulting in STAGS Version 5.0. Reference citations to STAGS documents are given when they can be identified.

Pre-STAGS Days

Computer analysis of shell structure was well under way in the early 1960's at LMSC. NASA Marshall Space Flight Center sponsored some of the early shell analysis formulations and implementations from 1963 to 1968 [1-3]. Much of the work focused on developing equilibrium equations for cylinders, cones and spheres and then applying finite difference approximations to arrive at a set of algebraic equations to solve using matrix algebra. However, the system of equations was unsymmetric. Another aspect of the work investigated the use of an energy formulation to pose the buckling problem wherein finite difference approximations are used for derivative terms. Stationary conditions on the energy functional then gave rise to a symmetric set of nonlinear algebraic equations. This approach, led by Bo O. Almroth, was a significant advancement and provided the basis for future shell analysis tools developed at LMSC and elsewhere.

* This organization is now the Lockheed Martin Advanced Technology Center of Lockheed Martin Missiles & Space (LMMS).

Following the NASA Marshall Space Flight Center contract, LMSC continued their shell analysis research and development work under internal research and development funding. During this time, methods research computer codes were developed, extended and sometimes abandoned. Most likely, an internal LMSC research code called STAGS came into being while not formally released - like many of our own special-purpose research codes. However, this work was not done in a vacuum either. Government agencies, in particular the military, were also involved in shell analysis research.

It should be noted that other shell analysis research was also underway during this time including others at LMSC, NASA, AFFDL, NSRDC, and many universities. However, much of this work was directed towards shells of revolution and not general shell structures. Shell analysis codes such as BOSOR, FASOR, SRA, GIRLS, SALORS and others were developed during this period.

Early STAGS Years

STAGS initial development was an outgrowth of LMSC work sponsored by NASA Marshall Space Flight Center in 1963. NSRDC sponsored work at LMSC that resulted in an analysis capability for stiffened shells with cutouts [4, 5]. Then the Air Force (SAMSO and AFFDL) sponsored additional work including bifurcation buckling, thermal effects, plasticity, and general coordinate systems [6]. The work on arbitrary non-orthogonal coordinates led by Marlowe was based on his PhD work with Flugge at Stanford University [7]. The geometrically nonlinear equations were discretized using a half-station finite difference approach where u and v were defined at the nodes and u and v were defined at half-station points. The resulting code called STAGSA (some use STAGS-A) was released in 1972 to the structural analysis community. Formal users documentation was released through AFFDL in 1973 [8, 9].

During this period, competition between research groups was very keen. Selected shell analysis problems were defined and tossed down as challenges and provide, even today, a gauntlet of difficult nonlinear shell analysis problems. References 11-13 are cited as key references from this period.

Initial NASA Langley Efforts

NASA Langley funding of STAGS-related efforts appears to have begun in the early 1970's - although this date is somewhat uncertain because of NASA Langley's involvement with the BOSOR development at LMSC. Dr. Paul Cooper was the first NASA LaRC contract monitor for shell analysis work at LMSC, followed by Dr. James Starnes, Dr. Wendell Stephens, Dr. Jerrold Housner, Dr. Gaylen Thurston, Dr. James Starnes, and finally Dr. Richard Young.

To resolve some issues present in STAGSA, a new version, STAGSB, was developed based on a modified finite difference approach with all displacement unknowns at grid points (whole-station finite difference approach). STAGSB was released in 1974 [14]. STAGSB also permitted the use of segmented or branched shells.

Then because finite element technology was maturing, a comparative study between the finite difference and finite element approaches for nonlinear shell collapse problems was needed. This study was enabled, in part, by STAGSC [15, 16], an analysis code with the whole-station finite difference approach having different areas of integration for bending and membrane energy contributions and also the first implementation of shell finite elements. Other LMSC shell finite element analysis work (*e.g.*, REXBAT) began to be implemented with the STAGS code. The 4-node QUAF (quadrilateral flat) element originated by Almroth and Brogan from a combination of

the Melosh QB12 bending element [17] with the Willam membrane element [18]. Tuning this element (410 element) has occurred over the years, and it remains the workhorse shell element of STAGS [19]. The Ahmad thick shell elements [20] were added for isotropic shells. Basic plotting capabilities such as finite element geometry, deformed shapes, and contour plots were developed and called STAPL by leveraging on NASA LaRC work [21].

Finite Element Years

STAGSC-1 represented the first complete finite-element-only version of STAGS [22]. In 1981, Almroth and Brogan evaluated the STAGS finite element capabilities and computational efficiencies [23]. Early in the STAGSC-1 development, an evaluation of STAGSC-1 was performed by Thomas and Sobel in 1981 [24]. Their report discussed many test cases and documented some of the internal programming aspects of STAGS, which had never been documented before. Woytowicz [25] also released a sample problems manual providing some illustrative examples of STAGS usage.

Unfortunately, Bo Almroth's death in February 1983 left a major void in the STAGS development team. After some time, Dr. Charles Rankin emerged as the LMSC contact for STAGS and structural mechanics research and development continued. This time period also saw a shift towards more focused program support and less basic research. Ref. 26 is a collection of papers honoring Bo Almroth.

Several releases of STAGSC-1 occurred during the 1980's without any name change or version number except the release date printed in the output. For the most part, NASA Langley was the primary sponsor of the mechanics technology implemented in STAGS including arc-length control [27-30], corotation formulation [31-34], nonlinear springs [33], contact [34], and the Thurston bifurcation processor based on the equivalence transformation [35-37].

During this same time period, NSRDC funded the development of STAGS-2000 which was to be a modern version of STAGS based on a database manager developed by Peter Stehlin. It was to be completely modular and consistent with software standards for extendibility and maintainability. This version was never installed at NASA Langley.

Nonlinear Solution Procedures

Nonlinear solution procedures are cornerstone concepts of the STAGS shell analysis code. From STAGS' initial beginnings, nonlinear solution procedures have been played a significant role in advancing shell analysis technology. Shell collapse using nonlinear methods was considered first followed by bifurcation buckling methods as an alternative approach to collapse analyses.

The nonlinear analysis procedures implemented within STAGS are based on an incremental iterative procedure using the Newton-Raphson approach. STAGS takes great care to formulate and evaluate consistent first and second variations of the energy functional. Both full and modified Newton-Raphson implementations are available. Because of the speed of the sparse matrix equation solver, the use of a full Newton-Raphson approach for even very large problems (>100,000 degrees of freedom) has become routine. Each solution step requires an initial "guess" or starting solution. STAGS uses the previous step's converged solution as the initial guess until three converged solutions are obtained. Then quadratic extrapolation can be used to form the initial guess for the next step. Solution control sensors include error norms based on the iterative change in the solution and on the residual or imbalance forces. During the iterative process for each step, these error indicators, total elastic energy, determinant of the stiffness matrix, maximum component in the residual vector are printed. These values can be monitored and provide some added insight into the overall behavior of the structure.

STAGS offers three different solution control procedures: load control, displacement control, and arc-length control. STAGS has offered the arc-length-control procedure developed by Riks since the early 1980's. The direct involvement of Dr. Riks with LMMS staff over the years has led to very robust, accurate, and stable nonlinear solution procedures. The arc-length constraint equation implemented within STAGS is based on the normal-plane constraint equation which has been very reliable for a wide range of nonlinear problems. The implementation does not solve the constraint equation (which is quadratic) directly as Crisfield does because of the questions surrounding which root of the quadratic equation to use. STAGS solves the constraint equation in a manner analogous to the approach used to solve the nonlinear equilibrium equations - expand in a Taylor series. This approach provides a very robust method for selecting the appropriate path rather than heuristics for root selection. STAGS is capable of solving nonlinear problems including those exhibiting snap-through and snap-back behavior.

Global Function Effort

In attempt to reduce the computational cost associated with nonlinear shell analysis, Almroth et al. [38, 39] proposed the use of global functions as a Rayleigh-Ritz procedure on the discretized global system of equations. In this approach, the vector of nodal degrees of freedom is transformed to a "reduced system" through the use of transformation matrix. The columns of the transformation matrix are essentially previous nonlinear solutions for the "full system" or global functions. RRSYS implemented the global function approach as a predictor using the reduced system and STAGSC-1 as the corrector for a reduced system formulation using the full system for nonlinear static problems.

This formulation provides an effective solution procedure for problems that do not exhibit any path dependence due to material nonlinearities or mode jumping. If the solution throughout the range of loading exhibits a self-similar behavior, then reduction methods are attractive. However as a solution procedure for general structural analysis problems, the limitations restricted its further development to academic issues.

STAGS Restructuring Effort

Early STAGS development (pre-STAGS through STAGSC; early 1960's through mid 1970's) evolved from an LMSC internal research computer code to a computer code distributed outside LMSC. STAGS had a demonstrated capability for solving practical aerospace shell structures problems. Mechanics research was driven by space applications and military funding. Research directions were generally set by the sponsor in concert with Lockheed; however, LMSC had considerable flexibility in their STAGS methods research thrusts.

The early STAGS development team was a small core group (4-6 people) from Lockheed with technical interaction from their government sponsors. Few researchers outside of Lockheed waded into the actual STAGS source code. Sponsoring agencies tended to be more focused on extending features, adding new capabilities, and developing advanced methods rather than on the more mundane, albeit necessary, tasks associated with software maintenance, documentation, and migration to newer computer systems. This tendency resulted in limited theoretical and system documentation. In addition and perhaps more critical is the fact that during this period, most methods developers (not just STAGS developers) were more focused on the methods work rather than software maintainability and longevity of their computer code. As a result, computer codes evolved into very difficult programming environments to maintain (*i.e.*, the era of "spaghetti" codes).

The early period of STAGS development was also the early period of computing systems development. As a result, programming techniques and standards were just developing and attention focused on computer memory management and computational efficiency. STAGS development work proceeded from a UNIVAC computer system to a DEC VAX VMS computer system. During this same period, commercial finite element codes were also under development focusing on general-purpose structural analysis needs.

STAGSC-1 Era

Later STAGS development (STAGSC-1 era extends from the mid 1970's through the early 1990's) continued along the same path with the primary sponsor being the NASA Langley Research Center. Structural mechanics research was driven by aerospace applications. Research directions were still generally set by the sponsor in concert with LMSC; however, LMSC still had considerable flexibility in their methods research thrusts.

The STAGS development environment did not change significantly. Lockheed had 3-4 people working on STAGS with about that many more working on related projects (*e.g.*, modeling and analysis tasks, coupling STAGS to the underwater shock analysis code USA to form USA-STAGS). Sponsoring agencies continued to be more focused on extending features, adding new capabilities, and developing advanced methods rather than on software infrastructure tasks although an awareness of its importance had emerged.

Computing systems had evolved some during this period. Lockheed was using a VAX VMS computer system as their main development environment while NASA LaRC had access only to CDC Cyber-class computers. Computer-word-length issues (*i.e.*, 32-bit versus 60-bit words; single versus double precision) related to data and memory management needed to be addressed relative to the impact on accuracy, computational speed, and overall solution efficiency. Software changes to STAGS were delivered to NASA LaRC periodically in UPDATE-format with either bug fixes or new features or both. The NASA LaRC contact person then installed the updates on NASA computers (or arranged for installation) and notified STAGS users of the new version.

QSTAGS to the Present

In 1984, NASA Langley initiated a new activity called the Computational Structural Mechanics or CSM. Its aim was to define the next generation of structural analysis tools and provide a framework for structural mechanics research. LMSC served as the prime contractor for this activity for a 5-year period from 1987 to 1992. The STAGS work at LMSC continued under independent funding from NASA Langley. As a result, a new restructured STAGS emerged called QSTAGS or quick STAGS that in essence was STAGS Version 1.0 in the current naming convention. QSTAGS then served as the main research version of STAGS at LMSC for a few years as new capabilities and old restrictions (*e.g.*, limit on the number of shell units) were removed.

In the mid 1980's, LMSC worked to transform the STAGS internal architecture from a file-based system (*i.e.*, TAPE21 and TAPE22 or the MOD and SOD files, respectively) to a database system. This conversion enabled the technology transfer from STAGS to the CSM Testbed. In 1988, NSRDC sponsored the development of a STAGS-to-Testbed interface in order to provide them a mechanism to transfer their STAGS finite element models to the CSM Testbed.

In 1994, STAGS Version 2.0 was released. This version represented a major software enhancement with significant portions of the code being re-written. In addition, the STAGS users

documentation was overhauled. Additional versions were released nearly every year until Version 2.4 was released in 1997.

Some of the major new features in this version included the Generic Constitutive Processor or GCP for constitutive research, the 9-node ANS element, mesh refinement transition elements (E510 and E710) for the E410 shell element, new STAGS database access routines, crack growth analysis tools, load relaxation and hybrid static/transient analysis option and various post-processing features for results displays, xy-plotting, and access to PATRAN or I-DEAS. MSC.Software, Inc. was also contracted to provide a STAGS-preference with PATRAN for developing STAGS finite element models and results post-processing.

The current STAGS development strategy (QSTAGS through current version; mid 1990's to present) has not changed significantly over the past decade. Historically, the STAGS development team has always been a small core group from Lockheed with technical interaction from their government sponsors. However, many of the STAGS key developers are now retired and work as consultants.

STAGS Version 5.0

STAGS Version 5.0 is the current release of STAGS. This version has been available for approximately two years and represents a complete integration of various developments by the STAGS key developers as well as others. New capabilities include user-defined materials, user-defined elements, user-defined fabrications, progressive failure methodologies, actuator elements, Stein-Hedgpeth membrane wrinkling model, and Hahn nonlinear elastic material model. New documentation has been generated as well. STAGS is available on several UNIX systems (SUN, SGI, and HP), on the Apple OS X, and on both 32-bit and 64-bit Linux systems. Documentation supporting STAGS Version 5.0 is given in References 65-74.

STAGS Functional Modules

STAGS is actually a small set of executable computer programs (S1, S2, and STAPL). Users typically execute the S1 processor to read basic finite element modeling data and build essential geometry and material tables. The S2 processor performs the element stiffness evaluations, global assembly of vectors and matrices, application of boundary conditions, matrix decompositions, solution procedures (linear or nonlinear, static, transient, or eigenvalue), and recovery of secondary fields. The STAPL processor is a stand-alone, static graphical tool for undeformed and deformed geometry plots as well as contour plots. The XYTRANS processor creates xy-plotting data from the STAGS databases directly. The PITRANS processor creates ASCII files from the STAGS databases for post-processing by PATRANS or I-DEAS. User documentation includes four manuals - two are preliminary forms. Much of the formulation and development for the newer features are documented directly in the users manual. Some basic training materials were developed about 10 years ago.

Usage

STAGS usage is essentially the same as any other finite element analysis code. The user prepares the input, submits the input file to STAGS processors for execution, and once execution is completed, post-processes the numerical results. Three input files are typically defined. The STAGS S1 processor reads an input file with an extension *.inp (e.g., my_problem.inp). The S1 processor evaluates the geometry data, boundary conditions, loading definitions, constraints, and other finite element data. Successful execution of the S1 processor results in the generation of a PDF file of the problem finite element model in the file my_problem_m.pdf.

Next, the STAGS S2 processor reads an input file with an extension `*.bin` (e.g., `my_problem.bin`). The S2 processor is the computational processor and performs the finite element solution based on the parameters contained in the `*.bin` file. Postprocessing can be accomplished using the STAGS STAPL processor for batch graphical files generation. The STAPL processor can be executed as an interactive command and the user provides answers to STAPL queries, which generates an input file with the extension `*.pin` (e.g., `my_problem.pin`). This is a simple way to generate a new STAPL input file that may be used to generate many plots by copying the input generated by the interactive approach and editing the lines for additional plots. Batch execution usually follows and a PDF file results that can be viewed.

Demonstration Example Problems

A series of commonly used demonstration problems are described, modeled, analyzed, and results presented. STAGS capabilities to solve these demonstration problems are illustrated through results comparison with available reference solutions and/or finite element mesh refinement studies. Each demonstration problem is first described and background information provided. The modeling and analysis process using STAGS is then described. Numerical results are presented and compared to reference solutions. Listings of selected STAGS input files are given for completeness and easy reference for the reader. References specific to each demonstration problem are provided to close each section.

Cook Membrane Problem

Background

The membrane problem posed by Cook (1987) involves a trapezoidal-shaped membrane fixed along one edge and loaded by in-plane shear loading along the opposite edge. The geometry of the membrane has the appearance of a swept-wing plan-form as shown in Figure 1. The dimensions, material properties and loading are defined in Figure 1 using U. S. customary units.

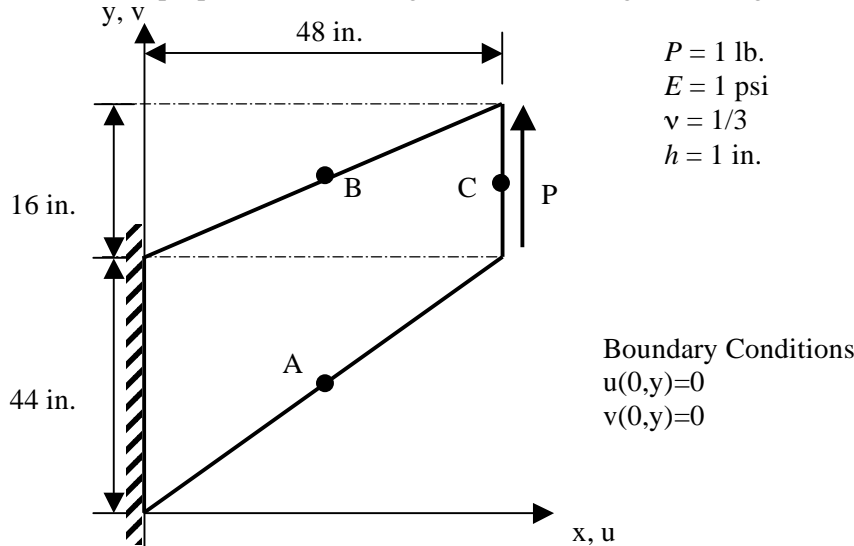
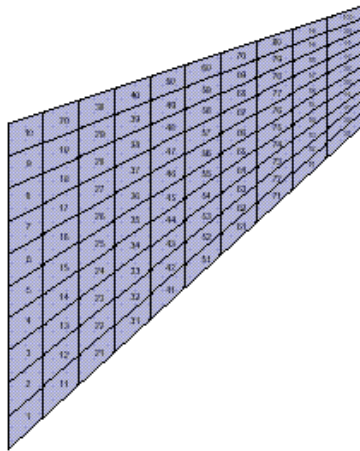


Figure 1. Cook membrane problem: geometry, material properties, and loading.

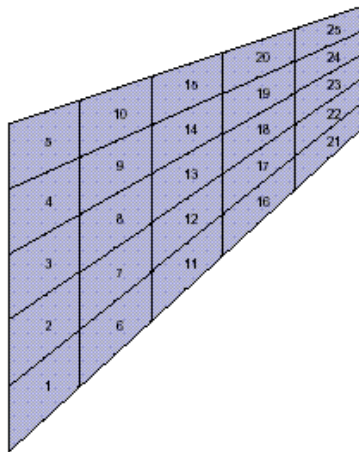
The membrane has a unit thickness and a unit in-plane shear load along the vertical edge at $x=48$ inches. The four corners of the membrane (starting at the origin and moving in a clockwise manner) have (x,y) coordinate values in inches of $(0, 0)$, $(0, 44)$, $(48, 60)$, and $(48, 44)$ – all coordinates are given in inches. This problem provides a good measure of the robustness of the elements since the fixed-end of the panel and its shape cause a stress gradient throughout the membrane, and it is frequently used to assess membrane elements (*e.g.*, see Davis, 1995). The reference solutions obtained by Ibrahimbegovic, Taylor and Wilson (1990) for stresses and Cook (1993) for deflections are used for comparison.

Modeling and Analysis Process

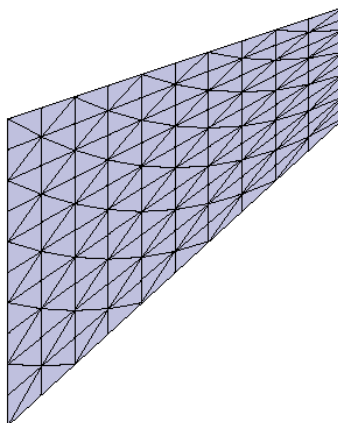
The STAGS model is generated using a single shell unit with the quadrilateral plate surface geometry (ISHELL=3). Material properties and membrane construction are defined using both the *historical* STAGS approach and the current GCP approach. Mesh discretization studies include different levels of mesh refinement and different element types. Mesh refinement is readily performed by changing the number of nodes N in each direction on the F-1 record (*i.e.*, the mesh is defined as $N \times N$ mesh of nodes). Element type is selected using the N-1 record (KELT). Representative finite element meshes using 3-node, 4-node and 9-node shell elements are shown in Figure 2.



4-node E410 quadrilateral shell element.



9-node E480 (9ANS) quadrilateral shell element.



3-node E330 (MIN3) triangular shell element.

Figure 2. Representative finite element discretizations for $N=11$

Material modeling for an elastic isotropic material using the historical STAGS approach requires data on the I-1 and I-2 records to define the material properties and the K-1 and K-2 records to define the construction or fabrication data. Material modeling using the current GCP approach requires data on the I-5a and I-6a records to define the material properties and the I-5a, I-21a, I-21b, I-21c, I-21d, and I-21e records to define the fabrication.

Loading is specified as a uniformly distributed shear load across the right end of the membrane. It is specified as a line load ($N_{xy} = 1/16$ lb/in.) using the Q-1, Q-2, and Q-3 records. As a check on the loading, the summation of the equilibrium forces across the loaded edge in the direction of applied loading should equal unity (*i.e.*, total force equal to edge length times line load).

Boundary condition on the displacements are specified using the P-1 and P-2 records. All out-of-plane degrees of freedom are suppressed since only a membrane response is needed. The drilling degrees of freedom are suppressed for the E330 and E480 elements but they are retained for the E410 element. These freedoms are constrained using the Q-3 records with the exterior looping feature (see sample S1 input file).

Numerical Results and Discussion

Results are presented for the tip deflection at point C (48, 52) in the y -direction denoted by v_c and the reference solution of Cook (1993) is 23.91 inches. Results are presented for the maximum principal stress at point A (24, 22) denoted by σ_A and the reference solution by Ibrahimbegovic *et al.* (1990) is 0.237 psi. Results are also presented for the minimum principal stress at point B (24, 52) denoted by σ_B , and the reference solution by Ibrahimbegovic *et al.* (1990) is -0.202 psi. The principal stresses at a point for a plane stress problem are computed using:

$$\sigma_{1,2} = \frac{\sigma_x + \sigma_y}{2} \pm \tau_{\max} \quad \text{and} \quad \tau_{\max} = \sqrt{\left(\frac{\sigma_x - \sigma_y}{2}\right)^2 + (\tau_{xy})^2}$$

These computations have been incorporated into the stress output subroutines for the E410 element in the STAGS S2 processor.

Tip displacement results shown in Table 1 indicate that models using the E480 9ANS shell element converge quickly to the reference solution, while models using the E330 and E410 shell elements converge at a slower rate. For the E480 element, the membrane response is approximated in a biquadratic manner. For the E410 element, the membrane response is nearly bilinear except for the contribution of the drilling degrees of freedom. Since every element in the finite element mesh is a trapezoid, element sensitive to mesh distortion is clearly evident. Effort should be expended by the analyst to minimize element distortion when using the E410 element in a membrane dominant problem. Contour plot of the v -displacement component is shown in Figure 3.

Table 1. Mesh refinement study for three shell elements in STAGS – reference solution is 23.91 inches (Cook, 1993).

Number of Nodes per Edge, N	Tip Deflection at Point C, v_c (inches)		
	E330 Element	E410 Element	E480 Element
3	9.897	11.101	22.735
5	16.297	17.697	23.618
7	19.493	20.562	23.813
9	21.105	21.836	23.886
11	22.001	22.512	23.911
13	22.537	22.910	23.925
15	22.885	23.163	23.932
17	23.118	23.334	23.937
19	23.285	23.454	23.940
21	23.405	23.542	23.942

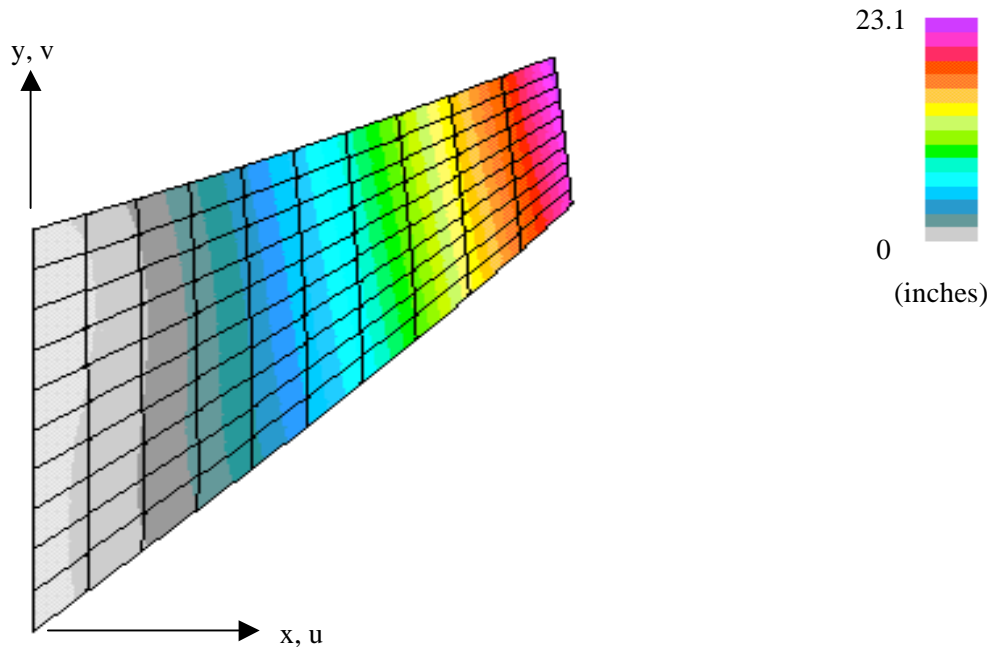


Figure 3. Contour plot of the v -displacement component from the linear solution for $N=11$ and the E410 element.

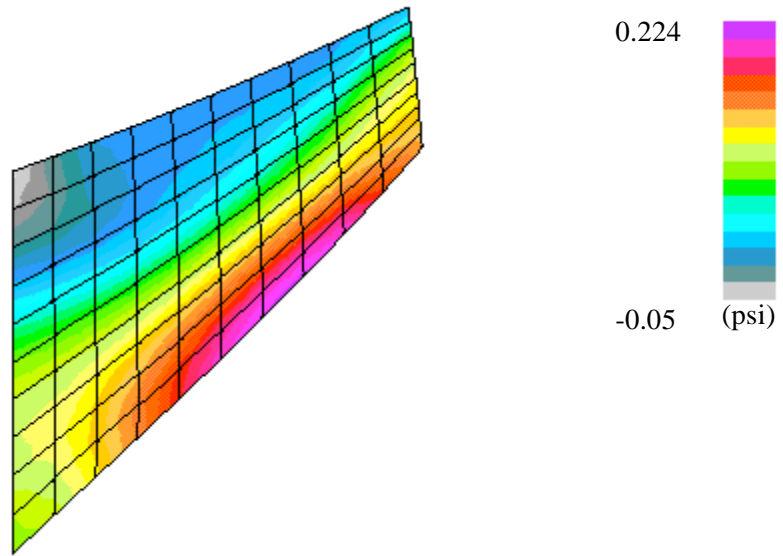


Figure 4. Contour plot of the maximum principal stress component from the linear solution for $N=11$ and the E410 element.

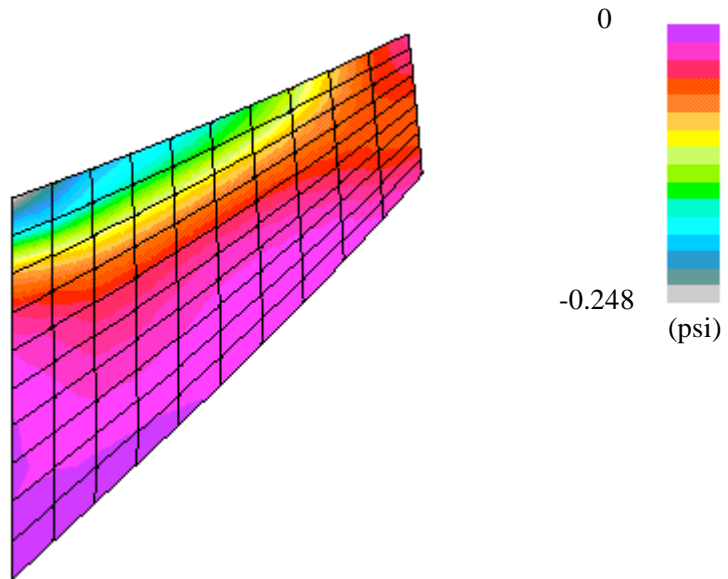


Figure 5. Contour plot of the minimum principal stress component from the linear solution for $N=11$ and the E410 element.

Principal stress values near Points A and B for the $N=11$ mesh using the E410 element are consistent with the reference values. The principal stress distributions are shown in Figures 4 and 5 for the $N=11$ mesh of E410 elements. Values taken at element integration points from either size of these reference locations (see Figure 2a) are:

Near Point A: Element 41 = 0.222; Element 51 = 0.223 (Point A Ref. Value = 0.237)

Near Point B: Element 50 = -0.184; Element 60 = -0.186 (Point B Ref. Value = -0.202)

STAGS Input Files

These STAGS input files are located under the following subdirectory:

\$STAGSHOME/Sample-Testcases/Cook

Typical 2D Shell Model Input Files

The following text files give the input for the plane stress membrane model using the E410 4-node shell element in STAGS with eleven nodes per edge ($N=11$).

cook2D.inp (for S1 processor)

```

COOK TRAPEZOIDAL MEMBRANE PROBLEM           $A-1
C
C TRAPEZOIDAL MEMBRANE WITH INPLANE SHEAR TIP LOAD
C
C REF.: COOK, "AN ELEMENT ERROR INDICATOR AND A RELATED
C        STRESS-IMPROVEMENT PROCEDURE," COMM. IN NUMERICAL
C        METHODS IN ENGINEERING, VOL. 9, 1993, PP. 207-217.
C
C MODEL INPUT CONTROLS
0      0      1      0      0      0      0      $B-1
1      10*0
1      0      1      0      0      1      $B-2 INCLUDE GCP INPUT
11     11     $F-1 DISCRETIZATION:  NROWS, NCOLS OF NODES
C
C HISTORICAL STAGS MATERIAL DEFINITION
C
1      $I-1 MATERIAL NO. 1 (HISTORICAL STAGS APPROACH)
1.0  0.33  0.0  0.10  $I-2 ISOTROPIC ELASTIC MATERIAL
C =====
C BEGIN GCP INPUT FOR MATERIAL AND FABRICATION
C
ISOELASTIC_MATERIAL 1 1 1 0 0 $I-5A MATERIAL NO. 1 (GCP APPROACH)
1.0,      $I-6A YOUNG'S MODULUS, PSI
0.33,     $I-6A POISSON'S RATIO
2.588E-4, $I-6A MASS DENSITY
4*0.0     $I-6A UNUSED MATERIAL PARAMETERS
SHELL_FABRICATION 1 1 0 0 0 $I-5A GCP SHELL FABRICATION RECORD
1      $I-21A GCP LAYER MATERIAL ID
1.0    $I-21C GCP LAYER THICKNESS, INCHES
0.0    $I-21D GCP LAYER ORIENTATION, DEGREES
END    $I-5A END GCP INPUT
C END GCP INPUT FOR MATERIAL AND FABRICATION
C =====
C
C HISTORICAL STAGS SHELL FABRICATION DEFINITION
C
1      1      1      0      $K-1 SHELL WALL RECORD
1      1.0    0.0    0      $K-2 LAYERED WALL
C
C SHELL UNIT 1 MODEL DEFINITION
C

```

```

3      0      4*0      $M-1  QUADRILATERAL PLATE GEOMETRY
  0.0    0.0,          $M-2  (X1, Y1)
  0.0   44.0,          $M-2  (X2, Y2)
48.0   60.0,          $M-2  (X3, Y3)
48.0   44.0           $M-2  (X4, Y4)
-1  0  0.0  0.0  0  0  0      $M-5 SHELL WALL RECORD, USE GCP FAB. # 1
410  0  0  $N-1 DISCRETIZATION RECORD, ELEMENT SELECTION
2  0  0  0  $P-1  EDGE 1 IS CLAMPED
110  000  $P-2  EDGE 2 IS FREE INPLANE, OTHERWISE FIXED
110  000  $P-2  EDGE 3 IS FREE INPLANE, OTHERWISE FIXED
110  000  $P-2  EDGE 4 IS FREE INPLANE, OTHERWISE FIXED
1  0  0  0  $Q-1  LOADING SUMMARY
1  2  0      $Q-2  LOAD SET SUMMARY
-0.0625  2  2  11  0  0      $Q-3  NXY=1/16 LB/IN ACROSS RIGHT END
  0.0  -1  3  0  0  0  3  1  0  0  $Q-3  EXTERIOR LOOPING TO SET
C
1      1      0      1      $R-1  OUTPUT CONTROL FOR SHELL UNIT 1

```

cook2D.bin (for S2 processor)

```

COOK TRAPEZOIDAL MEMBRANE PROBLEM  $A-1
  0      1      5*0      -1      $B-1 ANALYSIS CONTROL
  1.0      $C-1  LOAD MULTIPLIERS

```

cook2D.pin (for STAPL processor)

```

Cook Membrane problem          $A-1
  6  0  0  0  $PL-2  NPLOT,IPREP,IPRS,KDEV
C plot undeformed geometry with global node numbers
  0  0  6  0  0  0  0  0  $PL-3  KPLOT,VIEW,ITEM,STEP,MODE,IFRNG,COLOR,ICOMP
  0.0  3  0.0  0.0  0.0  $PL-5  DSCALE,NROTS,LWSALE,RNGMIN,RGMAX
  1  0.0 / 2  0.0 / 3  0.0  $PL-6  rotations
C plot undeformed geometry with global element numbers
  0  0  1  0  0  0  0  0  $PL-3  KPLOT,VIEW,ITEM,STEP,MODE,IFRNG,COLOR,ICOMP
  0.0  3  0.0  0.0  0.0  $PL-5  DSCALE,NROTS,LWSALE,RNGMIN,RGMAX
  1  0.0 / 2  0.0 / 3  0.0  $PL-6  rotations
C plot deformed and undeformed geometry
  1  0  1  0  0  0  0  0  $PL-3  KPLOT,VIEW,ITEM,STEP,MODE,IFRNG,COLOR,ICOMP
  0.0  3  0.0  0.0  0.0  $PL-5  DSCALE,NROTS,LWSALE,RNGMIN,RGMAX
  1  0.0 / 2  0.0 / 3  0.0  $PL-6  rotations
C plot v-displ contours on deformed geometry
  2  0  1  0  0  0  0  2  $PL-3  KPLOT,VIEW,ITEM,STEP,MODE,IFRNG,COLOR,ICOMP
  0.0  3  0.0  0.0  0.0  $PL-5  DSCALE,NROTS,LWSALE,RNGMIN,RGMAX
  1  0.0 / 2  0.0 / 3  0.0  $PL-6  rotations
C plot S1P principal stress on the deformed geometry
  2  0  7  0  0  0  0  7  $PL-3  KPLOT,VIEW,ITEM,STEP,MODE,IFRNG,COLOR,ICOMP
  0.0  3  0.0  0.0  0.0  $PL-5  DSCALE,NROTS,LWSALE,RNGMIN,RGMAX
  1  0.0 / 2  0.0 / 3  0.0  $PL-6  rotations
C plot S2P principal stress on the deformed geometry
  2  0  7  0  0  0  0  8  $PL-3  KPLOT,VIEW,ITEM,STEP,MODE,IFRNG,COLOR,ICOMP
  0.0  3  0.0  0.0  0.0  $PL-5  DSCALE,NROTS,LWSALE,RNGMIN,RGMAX
  1  0.0 / 2  0.0 / 3  0.0  $PL-6  rotations

```

Problem References

Cook, R. D., "A Plane Hybrid Element with Rotational D. O. F. and Adjustable Stiffness," *International Journal for Numerical Methods in Engineering*, Vol. 24, 1987, pp. 1499-1508.

Cook, R. D., "An Element Error Indicator and a Related Stress-Improvement Procedure," *Communications in Numerical Methods in Engineering*, Vol. 9, 1993, pp. 207-217.

Ibrahimbegovic, A., Taylor, R. L., and Wilson, E. L., "A Robust Quadrilateral Membrane Finite Element with Drilling Degrees of Freedom," *International Journal for Numerical Methods in Engineering*, Vol. 30, 1990, pp. 445-457.

Davis, Timothy S., *Assessment of High-Order Serendipity and Lagrangian Quadrilateral Membrane Elements*, Master's Thesis, Department of Aerospace Engineering, Old Dominion University, Norfolk, VA, December 1995.

Euler-Column Buckling Problem

Background

Stiffened panels are a common configuration in the aerospace industry. Modeling the stiffeners affects the buckling predictions. For stiffened panels exhibiting overall buckling behavior, the stiffeners participate with the panel skin in the buckling mode. As a result, the stiffener models need to be capable of modeling an in-plane buckling behavior (*i.e.*, in the x - y plane). For beam models, this represents an Euler column-buckling problem about a specific axis of the beam cross-section. For plate models, the finite elements need to be capable of exhibiting in-plane buckling behavior. The geometry, material properties, and loading of the column are defined in Figure 6 using U. S. customary units.

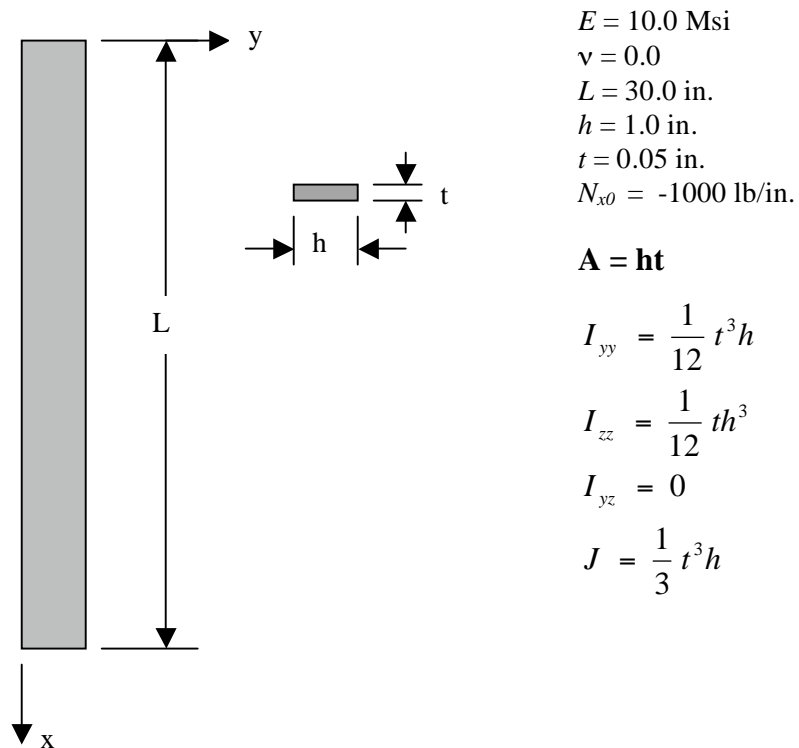


Figure 6. Euler column buckling problem: geometry, material properties, and loading.

The analytical solution for linear bifurcation buckling of a long slender column simply supported at its ends is given by Brush and Almroth (1975):

$$N_x^{cr} = \frac{P_{Euler}}{h} = \frac{\pi^2 EI}{hL^2} = \lambda_{Euler} N_{x0}$$

where E is Young's elastic modulus (10 Msi), I_{zz} is the moment of inertia equal to $th^3 / 12$ (.0041666 in.⁴), L is the column length (30 in.), t is the column thickness (0.05 in.), h is the column width (1.0 in.), and N_{x0} is the uniform compressive longitudinal pre-stress value (-1000 lb/in.). Using these values, the critical buckling factor λ_{Euler} evaluates to:

$$\lambda_{Euler} = \frac{5\pi^2}{108} = 0.456926$$

The buckling mode shape corresponds to a single half wave along the column length ($n=1$). The higher eigenvalues and corresponding mode shapes are in proportion to the factor n^2 ; that is,

$$P_n = n^2 \frac{\pi^2 EI}{L^2}$$

Hence the first four eigenvalues will be a multiple of λ_{Euler} by factors of 1, 4, 9, and 16, respectively.

Modeling and Analysis Process

Three separate STAGS finite element models are considered in this test case problem: 1D beam model, 2D plate model, and 3D solid model. Each model has 31 equally spaced nodes along the column length. These finite element models are shown in Figure 7. A summary of each model includes:

1. Beam model – Model the column using discrete beam elements in an element unit. This model will predict general buckling mode shapes – no cross-sectional deformation of the column.
2. Plate model – Model the column with plate elements in a single shell unit.
3. Solid model – Model the column with solid elements in a single shell unit

Material properties and laminate construction are defined using both the *historical* STAGS approach (*i.e.*, STAGS versions prior to GCP) and the current GCP approach. Material modeling for an elastic isotropic material using the historical STAGS approach requires data on the I-1 and I-2 records to define the material properties and the K-1 and K-2 records to define shell fabrication data. Material modeling using the current GCP approach requires data on the I-5a and I-6a records to define the material properties and the I-5a, I-21a, I-21b, I-21c, I-21d, and I-21e records to define the fabrication. Note that a zero Poisson ratio is used in the 2D and 3D analyses in order to correlate with the 1D beam-column solution – no biaxial stress. Also the current GCP implementation does not support beam elements. Hence beam cross-sectional properties (A , I_{yy} , I_{zz} , J) are defined using the J-1 and J-2 records.



(a) Beam model.



(b) Plate model.



(c) Solid model.

Figure 7. Finite element models studied for the Euler column buckling problem.

Loading is specified as an applied end shortening at the $x=0$ end of the column using the Q-1, Q-2, and Q-3 records. Boundary condition on the displacements are specified using the P-1 and P-2 records for the plate model. For the beam model, the boundary conditions are specified on the user point record (S-1 record). The boundary conditions are such that buckling about the “strong” axis occurs as the lowest buckling mode. For the plate and solid models, two sets of boundary conditions are needed: one to generate the pre-stress state and another to simulate in-plane simple-support boundary conditions. All degrees of freedom associated with out-of-plane displacements and bending rotations are suppressed.

Numerical Results and Discussion

The pre-buckling stress distributions is specified rather than computed. For a pre-stress in-plane longitudinal stress resultant loading of $N_{x0}=1000$ lb/in. In order to apply the loading in the same manner for the three idealizations considered (1D, 2D, and 3D), an applied end shortening δ at one end of the column is specified. For the uniform pre-stress state, the corresponding end shortening is:

$$\delta = \frac{N_{x0}L}{Et} = 0.06 \text{ in.}$$

The eigenvalue analysis has a convergence tolerance of 10^{-4} and the number of eigenpairs requested is four. No shift is used in the eigen solution.

Results of the STAGS analyses are summarized in Table 2 where the eigenvalues are normalized by the first analytical eigenvalue λ_{Euler} . The first eigenvalue agrees very well with the analytical solution. Contour plots of the eigenvectors or mode shapes for the 2D plate model are shown in Figure 8. The displacement component v in the y direction are shown in the figure.

Table 2. Normalized Eigenvalue Solutions for Euler Column Buckling Problem.

n	Normalized Eigenvalues, λ/λ_{Euler}			
	Analytical Solution	1D Beam Model – E210	2D Plate Model – E410	3D Solid Model – E885
1	1	1.0000	0.9953	0.9970
2	4	4.0000	3.9555	3.9520
3	9	9.0001	8.8057	8.7633
4	16	16.0011	15.4280	15.2780

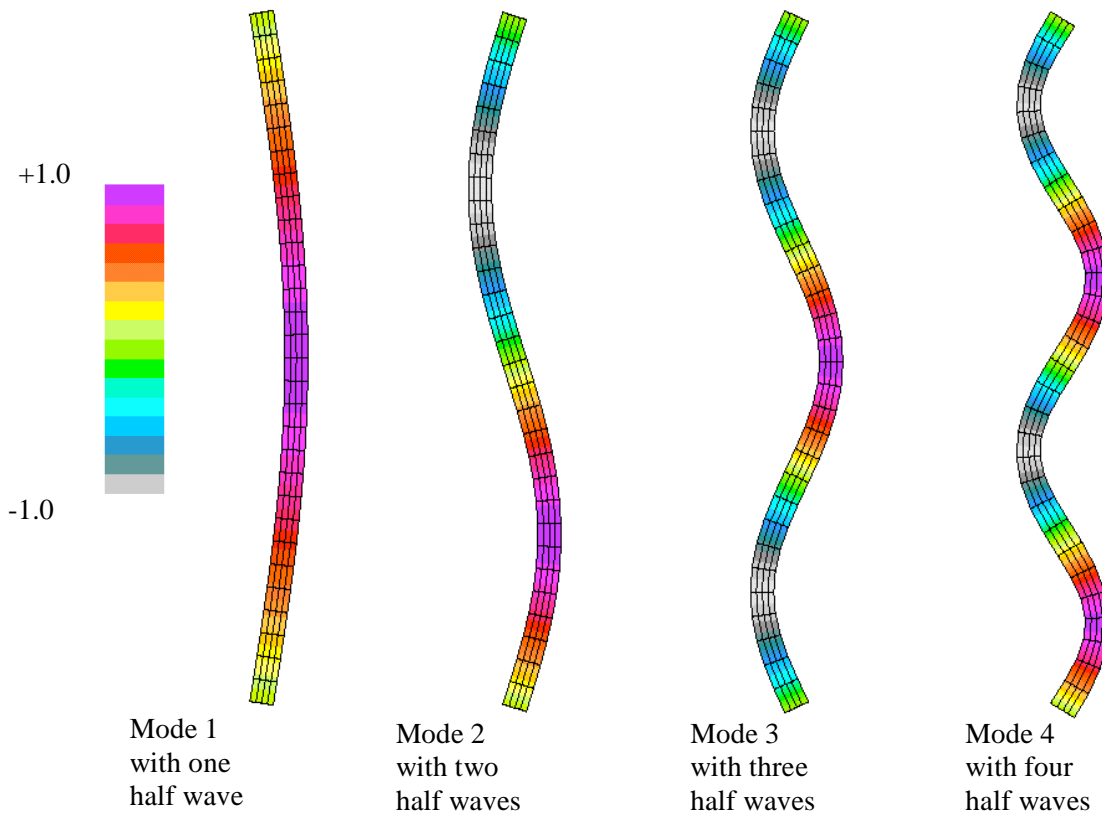


Figure 8. Contour plots of the in-plane displacement component v of the mode shapes from the 2D plate model.

STAGS Input Files

These STAGS input files are located under the following subdirectory:
 \$STAGSHOME/Sample-Testcases/Euler-column

1D Beam Model Input Files

euler1d.inp (for S1 processor)

```
Euler column-buckling problem - 1-D model           $A-1
C
C Thin strip, Euler column buckling from uniform axial compression
C
C REF.: Brush and Almroth, "Buckling of Bars, Plates
C       and Shells," 1975.
C
C MODEL INPUT CONTROLS
0      0      1      0      0      3      0  $B-1
1 0.0 / 2 0.0 / 3 -90.0  $B-1b model rotations
0      1      0      $B-2
1      1      1      0      0      1  $B-3 USE GCP INPUT
C
C Define Element Unit data
C
32 0 30 0 0 0 $h-1 No. of points and No. of beam elements
C
```

```

C HISTORICAL STAGS MATERIAL DEFINITION
C
1          $I-1 MATERIAL NO. 1(HISTORICAL STAGS APPROACH)
10.0e+6  0.0    0.0    0.10  $I-2 ISOTROPIC ELASTIC MATERIAL
C =====
C BEGIN GCP INPUT FOR MATERIAL AND FABRICATION
C
ISOELASTIC_MATERIAL 1 1 1 0 0 $I-5A MATERIAL NO. 1 (GCP APPROACH)
10.0E+6,          $I-6A YOUNG'S MODULUS, PSI
0.0 ,            $I-6A POISSON'S RATIO
2.588E-4,        $I-6A MASS DENSITY
4*0.0           $I-6A UNUSED MATERIAL PARAMETERS
SHELL_FABRICATION 1 1 0 0 0 $I-5A GCP SHELL FABRICATION RECORD
1          $I-21A GCP LAYER MATERIAL ID
0.05      $I-21C GCP LAYER THICKNESS, INCHES
0.0       $I-21D GCP LAYER ORIENTATION, DEGREES
END       $I-5A END GCP INPUT
C END GCP INPUT FOR MATERIAL AND FABRICATION
C =====
C
C Beam cross-sectional properties
C
1 1 1 0 4.1666E-5 0.0 0.0 0 0 0 $j-1
0.05 1.041666E-5 4.1666E-3 0.0 $j-2
C
C HISTORICAL STAGS SHELL FABRICATION DEFINITION
C
1 1 1 0 $K-1 SHELL WALL RECORD
1 0.05 0.0 0 $K-2 LAYERED WALL
C
C ELEMENT UNIT 1 MODEL DEFINITION
C
1 0 0 0 0.0 0.0 0.0 100 001 $s-1 end point at x=0
2 0 0 0 1.0 0.0 0.0 110 001 0 29 0 $s-1
1 0 0 0 1.0 0.0 0.0 $s-1a incrementation
31 0 0 0 30.0 0.0 0.0 000 001 0 $s-1 end point at x=L
32 0 0 0 15.0 1.0 0.0 111 111 $s-1 reference node
C
C Generate beam elements
C
1 2 32 210 1 0.0 0.0 0.0 0 0 30 $T-2
1 1 0 $T-2a generate 30 elements
C
C generate loads - applied end shortening
C
1 0 $u-1 Loads summary
1 1 0 $u-2 Load set summary
6.0e-2 -1 1 1 $u-3 end shortening at x=0 end
1 0 0 $v-1 output control

```

euler1d.bin (for S2 processor)

```

Euler column-buckling PROBLEM          $A-1
C
C Thin strip, Euler column buckling from uniform axial compression
C
C REF.: Brush and Almroth, "Buckling of Bars, Plates
C       and Shells," 1975.
C
1 1 0 0 0 0 0 -1 $b-1 buckling analysis
1.0 1.0 1.0 $c-1 load factors
100 1.0e-4 0 $d-2 eigenvalue control

```

2D Plate Model Input Files**euler2d.inp** (for S1 processor)

```

Euler column-buckling problem - 2D model          $A-1
C
C Thin strip, Euler column buckling from uniform axial compression
C
C REF.: Brush and Almroth, "Buckling of Bars, Plates
C       and Shells," 1975.
C
C MODEL INPUT CONTROLS
0      0      1      0      0      3      0      $B-1
1  0.0 / 2  0.0 / 3  -90.0          $B-1b model rotations
1      10*0          $B-2
1      0      1      0      0      1          $B-3 INCLUDE GCP INPUT
31     5          $F-1 DISCRETIZATION:  NROWS, NCOLS OF NODES
C
C HISTORICAL STAGS MATERIAL DEFINITION
C
1          $I-1 MATERIAL NO. 1 (HISTORICAL STAGS APPROACH)
10.0e+6  0.0    0.0    0.10  $I-2 ISOTROPIC ELASTIC MATERIAL
C =====
C BEGIN GCP INPUT FOR MATERIAL AND FABRICATION
C
ISOELASTIC_MATERIAL  1  1  1  0  0  $I-5A MATERIAL NO. 1 (GCP APPROACH)
10.0E+6,             $I-6A YOUNG'S MODULUS, PSI
0.0 ,               $I-6A POISSON'S RATIO
2.588E-4,           $I-6A MASS DENSITY
4*0.0              $I-6A UNUSED MATERIAL PARAMETERS
SHELL_FABRICATION  1  1  0  0  0  $I-5A GCP SHELL FABRICATION RECORD
1          $I-21A GCP LAYER MATERIAL ID
0.05      $I-21C GCP LAYER THICKNESS, INCHES
0.0       $I-21D GCP LAYER ORIENTATION, DEGREES
END       $I-5A END GCP INPUT
C END GCP INPUT FOR MATERIAL AND FABRICATION
C =====
C
C HISTORICAL STAGS SHELL FABRICATION DEFINITION
C
1          1          1          0          $K-1 SHELL WALL RECORD
1          0.05      0.0          0          $K-2 LAYERED WALL
C
C SHELL UNIT 1 MODEL DEFINITION
C
2          0          4*0          $M-1 Rectangular PLATE GEOMETRY
0.0  30.0  0.0  1.0          $M-2 L=30 in.; h=1.0 in.
-1  0  0.0  0.0  0  0  0  $M-5 SHELL WALL RECORD, USE GCP FAB. # 1
410  0  0          $N-1 DISCRETIZATION RECORD, ELEMENT SELECTION
0  0  0  0  1          $P-1 EDGES 1 & 3 simple support; Edges 2 & 4 free
100 001
110 001
000 001
110 001
0  0  0  0          $P-1 EDGES 1 & 3 simple support; Edges 2 & 4 free
100 001
110 001
100 001
110 001
1  0  0  0          $Q-1 LOADING SUMMARY - force inplane buckling
1  4          $q-2

```

```

6.0e-2 -1 1 1 0 0 $q-3 u=constant at x=0
0.0 -1 3 0 0 0 $q-3 w=0 everywhere
0.0 -1 4 0 0 0 $q-3 ru=0 everywhere
0.0 -1 5 0 0 0 $q-3 rv=0 everywhere
1 1 0 0 $R-1 OUTPUT CONTROL FOR SHELL UNIT 1

```

euler2d.bin (for S2 processor)

```

Euler column-buckling PROBLEM $A-1
C
C Thin strip, Euler column buckling from uniform axial compression
C
C REF.: Brush and Almroth, "Buckling of Bars, Plates
C and Shells," 1975.
C
1 1 0 0 0 0 -1 $b-1 buckling analysis
1.0 1.0 1.0 $c-1 load factors
100 1.0e-4 0 $d-2 eigenvalue control
4 $d-3 cluster definition

```

euler2d.pin (for STAPL processor)

```

Euler column-buckling problem - uniform compression
4 0 0 0 $PPL-2 NPLOT,IPREP,IPRS,KDEV
2 0 4 0 1 0 0 2 $PPL-3 KPLOT,VIEW,ITEM,STEP,MODE,IFRNG,COLOR,ICOMP
0.0 3 0.0 -1.0 1.0 $PPL-5 DSCALE,NROTS,LWSALE,RNGMIN,RGMAX
1 0.0 / 2 0.0 / 3 -90.0
2 0 4 0 2 0 0 2 $PPL-3 KPLOT,VIEW,ITEM,STEP,MODE,IFRNG,COLOR,ICOMP
0.0 3 0.0 -1.0 1.0 $PPL-5 DSCALE,NROTS,LWSALE,RNGMIN,RGMAX
1 0.0 / 2 0.0 / 3 -90.0
2 0 4 0 3 0 0 2 $PPL-3 KPLOT,VIEW,ITEM,STEP,MODE,IFRNG,COLOR,ICOMP
0.0 3 0.0 -1.0 1.0 $PPL-5 DSCALE,NROTS,LWSALE,RNGMIN,RGMAX
1 0.0 / 2 0.0 / 3 -90.0
2 0 4 0 4 0 0 2 $PPL-3 KPLOT,VIEW,ITEM,STEP,MODE,IFRNG,COLOR,ICOMP
0.0 3 0.0 -1.0 1.0 $PPL-5 DSCALE,NROTS,LWSALE,RNGMIN,RGMAX
1 0.0 / 2 0.0 / 3 -90.0

```

3D Solid Model Input Files

euler3d.inp (for S1 processor)

```

Euler column-buckling problem - 3D solid model $A-1
C
C Thin strip, Euler column buckling from uniform axial compression
C
C REF.: Brush and Almroth, "Buckling of Bars, Plates
C and Shells," 1975.
C
C MODEL INPUT CONTROLS
0 0 1 1 0 3 0 $B-1
1 0.0 / 2 0.0 / 3 -90.0 $B-1b model rotations
1 10*0 $B-2
1 0 1 0 0 1 $B-3 INCLUDE GCP INPUT
31 5 $F-1 DISCRETIZATION: NROWS, NCOLS OF NODES
C
C HISTORICAL STAGS MATERIAL DEFINITION
C
1 $I-1 MATERIAL NO. 1 (HISTORICAL STAGS APPROACH)
10.0e+6 0.0 0.0 0.10 $I-2 ISOTROPIC ELASTIC MATERIAL
C =====
C BEGIN GCP INPUT FOR MATERIAL AND FABRICATION

```

```

C
ISOELASTIC_MATERIAL 1 1 1 0 0 $I-5A MATERIAL NO. 1 (GCP APPROACH)
10.0E+6,          $I-6A YOUNG'S MODULUS, PSI
0.0 ,            $I-6A POISSON'S RATIO
2.588E-4,        $I-6A MASS DENSITY
4*0.0           $I-6A UNUSED MATERIAL PARAMETERS
SOLID_FABRICATION 1 1 0          $I-5A GCP Solid Fabrication Record
0.05 $I-22a element thickness
SHELL_FABRICATION 1 1 0 0 0 $I-5A GCP SHELL FABRICATION RECORD
1 $I-21A GCP LAYER MATERIAL ID
0.05 $I-21C GCP LAYER THICKNESS, INCHES
0.0 $I-21D GCP LAYER ORIENTATION, DEGREES
END $I-5A END GCP INPUT
C END GCP INPUT FOR MATERIAL AND FABRICATION
C =====
C
C HISTORICAL STAGS SHELL FABRICATION DEFINITION
C
1 1 1 0 $K-1 SHELL WALL RECORD
1 0.05 0.0 0 $K-2 LAYERED WALL
C
C UNIT 1 MODEL DEFINITION (one solid element thickness)
C
2 0 0 0 1 1 $M-1 Rectangular PLATE GEOMETRY
0.0 30.0 0.0 1.0 $M-2 L=30 in.; h=1.0 in.
-1 0 0.0 0.0 0 0 0 $M-5 SHELL WALL RECORD, USE GCP FAB. # 1
885 0 0 $N-1 DISCRETIZATION RECORD, ELEMENT SELECTION
3 3 3 3 $p-1 free - BC given on q-records
2 $q-1 basic and incremental BCs (homogeneous constraints)
1 12 0 $q-2 load set summary
6.0e-2 -1 1 1 0 0 0 0 0 0 1 $q-3 u=u0 at x=0; layer 1
6.0e-2 -1 1 1 0 0 0 0 0 0 2 $q-3 u=u0 at x=0; layer 2
6.0e-2 -1 1 1 0 0 0 0 0 0 3 $q-3 u=u0 at x=0; layer 3
0.0 -1 2 1 0 0 0 0 0 0 1 $q-3 v=0 at x=0; layer 1
0.0 -1 2 1 0 0 0 0 0 0 2 $q-3 v=0 at x=0; layer 2
0.0 -1 2 1 0 0 0 0 0 0 3 $q-3 v=0 at x=0; layer 3
0.0 -1 1 31 0 0 2 1 0 0 1 $q-3 u=v=0 at x=L layer 1
0.0 -1 1 31 0 0 2 1 0 0 2 $q-3 u=v=0 at x=L layer 2
0.0 -1 1 31 0 0 2 1 0 0 3 $q-3 u=v=0 at x=L layer 3
0.0 -1 3 0 0 0 0 0 0 0 1 $q-3 w=0 everywhere; layer 1
0.0 -1 3 0 0 0 0 0 0 0 2 $q-3 w=0 everywhere; layer 2
0.0 -1 3 0 0 0 0 0 0 0 3 $q-3 w=0 everywhere; layer 3
C Incremental BC's for buckling (be sure to set INCBC=1 on B-1 record)
2 9 0
0.0 -1 2 1 0 0 0 0 0 0 1 $q-3 v=0 at x=0; layer 1
0.0 -1 2 1 0 0 0 0 0 0 2 $q-3 v=0 at x=0; layer 2
0.0 -1 2 1 0 0 0 0 0 0 3 $q-3 v=0 at x=0; layer 3
0.0 -1 2 31 0 0 0 0 0 0 1 $q-3 v=0 at x=L; layer 1
0.0 -1 2 31 0 0 0 0 0 0 2 $q-3 v=0 at x=L; layer 2
0.0 -1 2 31 0 0 0 0 0 0 3 $q-3 v=0 at x=L; layer 3
0.0 -1 3 0 0 0 0 0 0 0 1 $q-3 w=0 everywhere; layer 1
0.0 -1 3 0 0 0 0 0 0 0 2 $q-3 w=0 everywhere; layer 2
0.0 -1 3 0 0 0 0 0 0 0 3 $q-3 w=0 everywhere; layer 3
1 1 0 0 $R-1 OUTPUT CONTROL FOR SHELL UNIT 1

```

euler3d.bin (for S2 processor)

```

Euler column-buckling PROBLEM          $A-1
C
C Thin strip, Euler column buckling from uniform axial compression
C
C REF.: Brush and Almroth, "Buckling of Bars, Plates

```

C and Shells," 1975.
C
1 1 0 0 0 0 0 -1 \$b-1 buckling analysis
1.0 1.0 1.0 \$c-1 load factors
100 1.0e-4 0 \$d-2 eigenvalue control
4 \$d-3 cluster definition

Problem References

Brush D. O. and Almroth, B. O., *Buckling of Bars, Plates and Shells*, McGraw-Hill Book Company, New York, 1975.

Free Vibration of Straight Beam

Background

Free vibration of a straight cantilevered beam modeled using both one- and two-dimensional elements is studied. Two vibration cases are considered: in-plane vibration and lateral vibration. The geometry and material properties of the beam are defined in Figure 9 using U. S. customary units.

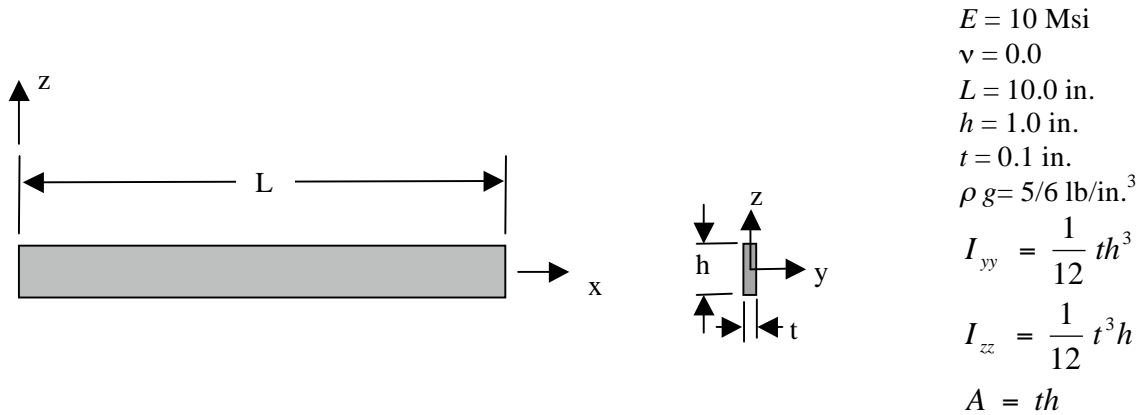


Figure 9. Straight cantilevered beam problem: geometry and material properties.

The analytical solutions for linear free vibration of a straight cantilevered beam are given by Timoshenko, Young and Weaver (1974). The frequencies for longitudinal axial vibration are given by Timoshenko *et al.* (1974, p. 369) as:

$$\omega_m = \frac{(2m-1)\pi}{2L} \sqrt{\frac{E}{\rho}}$$

where E is Young's elastic modulus (10 Msi), ρ is the mass density, L is the column length (10 in.), and m is the number of halfwaves along the beam, and ω_m is the circular frequency (radians per second) for the m -th vibration mode. The value used for the acceleration due to gravity is 386.4 in./s^2 and is specified on the B-4 record of the S1 input file. In terms of cycles per second or hertz, the frequency for the m -th mode is given by:

$$f_m = \frac{\omega_m}{2\pi}$$

The frequencies for in-plane (x - z plane) flexural vibration are given by Timoshenko *et al.* (1974, p. 426) as:

$$\omega_m = k_m^2 \sqrt{\frac{EI_{yy}}{\rho A}}$$

where I_{yy} is the moment of inertia about the y -axis, A is the cross-sectional area, t is the beam thickness (0.1 in.), h is the beam width (1.0 in.), and k_m is a constant obtained from the roots of the following equation:

$$\cos(k_m L) \cosh(k_m L) + 1 = 0$$

The consecutive roots of this equation are given by Timoshenko *et al.* (1974, p. 426) as:

m	$k_m L$
1	1.875
2	4.694
3	7.855
4	10.996
5	14.137
6	17.279

For higher values of m, the roots are approximated by the expression:

$$k_m L = \frac{(2m-1)\pi}{2}$$

The frequencies for lateral (x-y plane) flexural vibration are given by Timoshenko *et al.* (1974, p. 426) as:

$$\omega_m = k_m^2 \sqrt{\frac{EI_{zz}}{\rho A}}$$

where I_{zz} is the moment of inertia about the z-axis. Using this formula, the frequencies for the different vibration modes are computed and given in Table 3.

Table 3. Analytical vibration frequencies for cantilevered straight beam.

m	Type of Mode	ω_m^2	f_m
1	Flexural-xy	4.776×10^3	10.999
2	Flexural-xy	187.590×10^3	68.933
1	Flexural-xz	4.776×10^5	109.990
3	Flexural-xy	1471.031×10^3	193.033
4	Flexural-xy	5649.057×10^3	378.275
2	Flexural-xz	187.590×10^5	689.326
1	Extensional	1144.085×10^5	1702.351
3	Flexural-xz	1471.031×10^5	1930.328
4	Flexural-xz	5649.057×10^5	3782.754
2	Extensional	10296.761×10^5	5107.054

Modeling and Analysis Process

Three separate STAGS finite element models are considered in this sample test case problem: beam model, shell model, and solid model. In each case, the number of nodes along the beam length is either 21 or 41; however, for the 3-D 20-node solid element model, the number of

elements along the beam length is half that of the beam and shell models. A summary of each model includes:

1. 1-D beam model – Model the beam using 2-node beam elements in an element unit.
2. 2-D shell model – Model the beam with 4-node shell elements (x - z plane) in a single shell unit.
3. 3-D solid model – Model beam with 20-node solid elements in a single shell unit.

Material properties and laminate construction are defined using both the *historical* STAGS approach (*i.e.*, STAGS versions prior to GCP) and the current GCP approach. Material modeling for an elastic orthotropic material using the historical STAGS approach requires data on the I-1 and I-2 records to define the material properties and the K-1 and K-2 records to define the laminate fabrication data. Section properties for the beam elements can only be accomplished using the *historical* STAGS approach using the J series of records. Material modeling using the current GCP approach requires data on the I-5a and I-6a records to define the material properties and records I-5a, I-21a, I-21b, I-21c, I-21d, and I-21e to define the fabrication.

Boundary condition on the displacements are specified using the P-1 and P-2 records. The boundary condition on the left end is clamped with all degrees of freedom restrained at that edge ($x=0$). All other nodes are free. For the 1-D beam model the nodal degrees of freedom are specified on the node point definition records (S-1 records). For the 2-D shell model, the degrees of freedom on the boundary edges are specified on the P-1 record. For the 3-D solid model, the nodal degrees of freedom for each nodal layer through the thickness are specified using applied displacement loading conditions on the Q-records. The E885 20-node solid element is used so that even though the number of nodes along the beam length is the same in the different models, only half the number of elements is required.

Numerical Results and Discussion

Free vibration of the beam is analyzed for three types of vibration modes: axial, in-plane (xz) flexural, and lateral (xy) flexural. There is no external load on the beam – vibration about an unstressed state. The eigenvalue analysis has a convergence tolerance of 10^{-4} and the number of eigenpairs (eigenvalue and corresponding eigenmode) requested is sixteen. No shift is used in the eigenvalue solution.

The results for 21 and 41 nodes along the beam length are given in Tables 4, 5 and 6 for the beam, shell, and solid element models, respectively. Representative vibration mode shapes for flexural modes in the xy -plane are shown in Figure 10 for the 1-D beam model.

Table 4. Vibration analysis results for 1-D beam model.

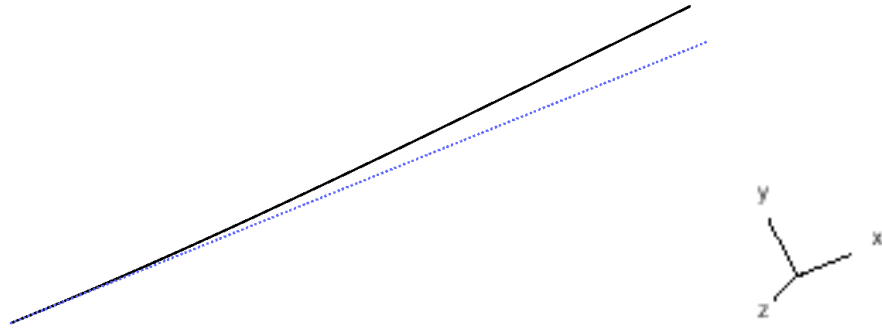
Mode	Mode Type	Frequency, Hertz		
		Analytical	E210 Beam Model	
			20 elements	40 elements
1	Flexural-xy	10.999	10.987	10.997
2	Flexural-xy	68.933	68.662	68.867
3	Flexural-xz	109.990	109.873	109.968
4	Flexural-xy	193.033	191.766	192.706
5	Flexural-xy	378.275	374.796	377.378
6	Flexural-xy	625.249	617.911	623.423
7	Flexural-xz	689.326	686.619	688.667
8	Flexural-xy	934.062	920.507	930.667
9	Flexural-xy	1304.563	1281.933	1298.983
10	Extensional	1702.351	1701.337	1702.245

Table 5. Vibration analysis results for 2-D shell model.

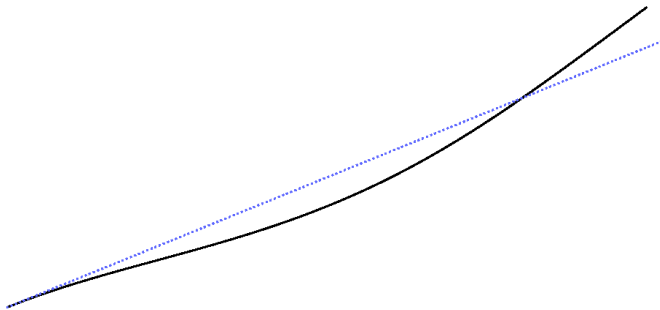
Mode	Mode Type	Frequency, Hertz		
		Analytical	E410 Shell Model	
			20 elements	40 elements
1	Flexural-xy	10.999	10.939	10.802
2	Flexural-xy	68.933	68.517	67.660
3	Flexural-xz	109.990	109.831	109.925
4	Flexural-xy	193.033	192.085	189.376
5	Flexural-xy	378.275	377.546	370.992
6	Flexural-xy	625.249	627.193	613.166
7	Flexural-xz	689.326	686.353	688.400
8	Flexural-xy	934.062	943.564	915.905
9	Flexural-xy	1304.563	1330.481	1279.306
10	Extensional	1702.351	1701.242	1701.564

Table 6. Vibration analysis results for 3-D solid model.

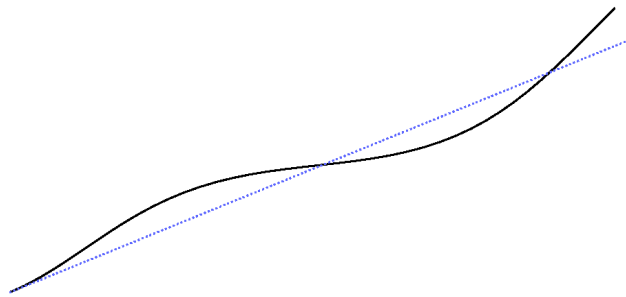
Mode	Mode Type	Frequency, Hertz		
		Analytical	E885 Solid Model	
			10 elements	20 elements
1	Flexural-xy	10.999	10.970	10.992
2	Flexural-xy	68.933	68.312	68.734
3	Flexural-xz	109.990	108.824	109.044
4	Twisting	---	163.963	153.970
5	Flexural-xy	193.033	190.197	191.966
6	Flexural-xy	378.275	370.477	374.784
7	Twisting	---	493.116	493.611
8	Flexural-xy	625.249	608.260	616.127
9	Flexural-xz	689.326	647.861	652.075
10	Flexural-xy	934.062	---	---



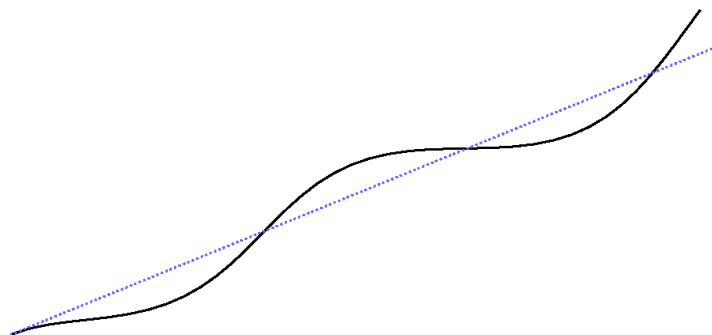
(a) Mode 1, flexural mode in xy -plane, 10.997 hertz.



Mode 2, flexural mode in xy -plane, 68.867 hertz.



Mode 4, flexural mode in xy -plane, 192.706 hertz.



Mode 5, flexural mode in xy -plane, 377.378 hertz.

Figure 10. Representative flexural vibration mode shapes from the 1-D beam model.

STAGS Input Files

These STAGS input files are located under the following directory:
\$STAGSHOME/Sample-Testcases/Beam-Vibration

Model using 1-D Beam Elements

The following text file provides the input for a beam finite element model using forty 2-node E210 beam elements along the beam length.

beam1d.inp (for S1 processor)

```
Straight beam free vibration problem - 1-D model          $A-1
C
C Thin straight strip, free vibration problem
C
C REF.: Timoshenko, Young, and Weaver, "Vibration Problems
C       in Engineering," 1974.
C
C MODEL INPUT CONTROLS
1      0      1      0      0      3      0  $B-1
1 0.0 / 2 0.0 / 3 -90.0          $B-1b model rotations
0      1      0          $B-2
1      1      1      0      0      1          $B-3 INCLUDE GCP INPUT
386.4          $B-4 acceleration due to gravity, g (in/s/s)
C
C Define Element Unit data
C
42 0 40 0 0 0 $h-1 No. of points and No. of beam elements
C
C HISTORICAL STAGS MATERIAL DEFINITION
C
1          $I-1 MATERIAL NO. 1 (HISTORICAL STAGS APPROACH)
10.0e+6 0.0 0.0 0.83333 $I-2 ISOTROPIC ELASTIC MATERIAL
C =====
C BEGIN GCP INPUT FOR MATERIAL AND FABRICATION
C
ISOELASTIC_MATERIAL 1 1 1 0 0 $I-5A MATERIAL NO. 1 (GCP APPROACH)
10.0E+6,          $I-6A YOUNG'S MODULUS, PSI
0.0 ,          $I-6A POISSON'S RATIO
2.1583354E-3,    $I-6A MASS DENSITY
4*0.0          $I-6A UNUSED MATERIAL PARAMETERS
SHELL_FABRICATION 1 1 0 0 0 $I-5A GCP SHELL FABRICATION RECORD
1          $I-21A GCP LAYER MATERIAL ID
0.10      $I-21C GCP LAYER THICKNESS, INCHES
0.0       $I-21D GCP LAYER ORIENTATION, DEGREES
END      $I-5A END GCP INPUT
C END GCP INPUT FOR MATERIAL AND FABRICATION
C =====
C
C Beam cross-sectional properties
C
1 1 1 0 8.3333E-5 0.0 0.0 0 0 0 $j-1
0.1 8.3333E-3 8.3333E-5 0.0          $j-2
C
C HISTORICAL STAGS SHELL FABRICATION DEFINITION
C
1      1      1      0          $K-1 SHELL WALL RECORD
1      0.10    0.0      0          $K-2 LAYERED WALL
C
C ELEMENT UNIT 1 MODEL DEFINITION
C
1 0 0 0 0.0 0.0 0.0 000 000          $s-1 end point at x=0
```

```

2 0 0 0 0.25 0.0 0.0 111 111 0 40 0 $s-1 BC's for x-z inplane
vibration
1 0 0 0 0.25 0.0 0.0 $s-1a user point
incrementation
42 0 0 0 5.0 1.0 0.0 111 111 $s-1 reference node
C
C Generate beam elements
C
1 2 42 210 1 0.0 0.0 0.0 0 0 40 $T-2
1 1 0 $T-2a generate 20 elements
C
C generate loads - applied end shortening
C
0 0 $u-1 Loads summary
1 0 0 $v-1 output control

```

beam1d.bin (for S2 processor)

```

Straight beam free vibration problem - 1-D model $A-1
C
C Thin straight strip, free vibration problem
C
C REF.: Timoshenko, Young, and Weaver, "Vibration Problems
C in Engineering," 1974.
C
2 1 0 0 0 0 0 -1 $b-1 free vibration analysis
1.0 1.0 1.0 $c-1 load factors
100 1.0e-4 0 $d-2 eigenvalue control
20 $d-3 cluster definition

```

beam1d.pin (for STAPL processor)

```

Straight cantilevered beam - free vibration problem
16 0 0 0 $P1-2 NPLOT,IPREP,IPRS,KDEV
1 0 4 0 1 0 0 2 $P1-3 KPLOT,VIEW,ITEM,STEP,MODE,IFRNG,COLOR,ICOMP
0.0 0 0.0 0.0 0.0 $P1-5 DSCALE,NROTS,LWSCALE,RNGMIN,RGMAX
1 0 4 0 2 0 0 2 $P1-3 KPLOT,VIEW,ITEM,STEP,MODE,IFRNG,COLOR,ICOMP
0.0 0 0.0 0.0 0.0 $P1-5 DSCALE,NROTS,LWSCALE,RNGMIN,RGMAX
1 0 4 0 3 0 0 2 $P1-3 KPLOT,VIEW,ITEM,STEP,MODE,IFRNG,COLOR,ICOMP
0.0 0 0.0 0.0 0.0 $P1-5 DSCALE,NROTS,LWSCALE,RNGMIN,RGMAX
1 0 4 0 4 0 0 2 $P1-3 KPLOT,VIEW,ITEM,STEP,MODE,IFRNG,COLOR,ICOMP
0.0 0 0.0 0.0 0.0 $P1-5 DSCALE,NROTS,LWSCALE,RNGMIN,RGMAX
1 0 4 0 5 0 0 2 $P1-3 KPLOT,VIEW,ITEM,STEP,MODE,IFRNG,COLOR,ICOMP
0.0 0 0.0 0.0 0.0 $P1-5 DSCALE,NROTS,LWSCALE,RNGMIN,RGMAX
1 0 4 0 6 0 0 2 $P1-3 KPLOT,VIEW,ITEM,STEP,MODE,IFRNG,COLOR,ICOMP
0.0 0 0.0 0.0 0.0 $P1-5 DSCALE,NROTS,LWSCALE,RNGMIN,RGMAX
1 0 4 0 7 0 0 2 $P1-3 KPLOT,VIEW,ITEM,STEP,MODE,IFRNG,COLOR,ICOMP
0.0 0 0.0 0.0 0.0 $P1-5 DSCALE,NROTS,LWSCALE,RNGMIN,RGMAX
1 0 4 0 8 0 0 2 $P1-3 KPLOT,VIEW,ITEM,STEP,MODE,IFRNG,COLOR,ICOMP
0.0 0 0.0 0.0 0.0 $P1-5 DSCALE,NROTS,LWSCALE,RNGMIN,RGMAX
1 0 4 0 9 0 0 2 $P1-3 KPLOT,VIEW,ITEM,STEP,MODE,IFRNG,COLOR,ICOMP
0.0 0 0.0 0.0 0.0 $P1-5 DSCALE,NROTS,LWSCALE,RNGMIN,RGMAX
1 0 4 0 10 0 0 2 $P1-3 KPLOT,VIEW,ITEM,STEP,MODE,IFRNG,COLOR,ICOMP
0.0 0 0.0 0.0 0.0 $P1-5 DSCALE,NROTS,LWSCALE,RNGMIN,RGMAX
1 0 4 0 11 0 0 2 $P1-3 KPLOT,VIEW,ITEM,STEP,MODE,IFRNG,COLOR,ICOMP
0.0 0 0.0 0.0 0.0 $P1-5 DSCALE,NROTS,LWSCALE,RNGMIN,RGMAX
1 0 4 0 12 0 0 2 $P1-3 KPLOT,VIEW,ITEM,STEP,MODE,IFRNG,COLOR,ICOMP
0.0 0 0.0 0.0 0.0 $P1-5 DSCALE,NROTS,LWSCALE,RNGMIN,RGMAX
1 0 4 0 13 0 0 2 $P1-3 KPLOT,VIEW,ITEM,STEP,MODE,IFRNG,COLOR,ICOMP
0.0 0 0.0 0.0 0.0 $P1-5 DSCALE,NROTS,LWSCALE,RNGMIN,RGMAX
1 0 4 0 14 0 0 2 $P1-3 KPLOT,VIEW,ITEM,STEP,MODE,IFRNG,COLOR,ICOMP

```

```

0.0  0  0.0  0.0  0.0  $PL-5  DSCALE,NROTS,LWSCALE,RNGMIN,RGMAX
1   0  4   0  15  0  0   2   $PL-3  KPLOT,VIEW,ITEM,STEP,MODE,IFRNG,COLOR,ICOMP
0.0  0  0.0  0.0  0.0  $PL-5  DSCALE,NROTS,LWSCALE,RNGMIN,RGMAX
1   0  4   0  16  0  0   2   $PL-3  KPLOT,VIEW,ITEM,STEP,MODE,IFRNG,COLOR,ICOMP
0.0  0  0.0  0.0  0.0  $PL-5  DSCALE,NROTS,LWSCALE,RNGMIN,RGMAX

```

Model using 2-D Shell Elements

The following text file provides the input for a beam finite element model using forty 4-node E410 shell elements along the beam length and one element across the beam width.

beam2d.inp (for S1 processor)

```

Straight beam free vibration problem - 2-D model          $A-1
C
C Thin straight strip, free vibration problem
C
C REF.: Timoshenko, Young, and Weaver, "Vibration Problems
C       in Engineering," 1974.
C
C MODEL INPUT CONTROLS
1   0          1          0          0          3          0  $B-1
1  0.0 / 2  0.0 / 3  -90.0          $B-1b model rotations
1          10*0          $B-2
1   0          1          0          0          1          $B-3 INCLUDE GCP INPUT
386.4          $b-4 acceleration due to gravity g (in/s/s)
41   2          $F-1 DISCRETIZATION: NROWS, NCOLS OF NODES
C
C HISTORICAL STAGS MATERIAL DEFINITION
C
1          $I-1 MATERIAL NO. 1 (HISTORICAL STAGS APPROACH)
10.0e+6  0.0    0.0    0.83333 $I-2 ISOTROPIC ELASTIC MATERIAL
C =====
C BEGIN GCP INPUT FOR MATERIAL AND FABRICATION
C
ISOELASTIC_MATERIAL 1 1 1 0 0 $I-5A MATERIAL NO. 1 (GCP APPROACH)
10.0E+6,          $I-6A YOUNG'S MODULUS, PSI
0.0 ,            $I-6A POISSON'S RATIO
2.1583354E-3,    $I-6A MASS DENSITY
4*0.0            $I-6A UNUSED MATERIAL PARAMETERS
SHELL_FABRICATION 1 1 0 0 0 $I-5A GCP SHELL FABRICATION RECORD
1          $I-21A GCP LAYER MATERIAL ID
1.0       $I-21C GCP LAYER THICKNESS, INCHES
0.0       $I-21D GCP LAYER ORIENTATION, DEGREES
END       $I-5A END GCP INPUT
C END GCP INPUT FOR MATERIAL AND FABRICATION
C =====
C HISTORICAL STAGS SHELL FABRICATION DEFINITION
C
1   1          1          0          $K-1 SHELL WALL RECORD
1   1.0        0.0        0          $K-2 LAYERED WALL
C
C SHELL UNIT 1 MODEL DEFINITION
C
2   0          4*0          $M-1 Rectangular PLATE GEOMETRY
0.0  10.0  0.0  0.1          $M-2 L=10 in.; t=0.1 in.
-1  0  0.0  0.0  0  0  0  $M-5 SHELL WALL RECORD, USE GCP FAB. # 1
410 0  0          $N-1 DISCRETIZATION RECORD, ELEMENT SELECTION
2  3  3  3          $P-1 Cantilevered beam simulation
0  0  0  0          $Q-1 No applied load - free vibration
1  0  0  0          $R-1 OUTPUT CONTROL FOR SHELL UNIT 1

```


beam2d.bin (for S2 processor)

```
Straight beam free vibration problem - 1-D model          $A-1
C
C Thin straight strip, free vibration problem
C
C REF.: Timoshenko, Young, and Weaver, "Vibration Problems
C         in Engineering," 1974.
C
2 1 0 0 0 0 0 -1 $b-1 free vibration analysis
1.0 1.0 1.0 $c-1 load factors
100 1.0e-4 0 $d-2 eigenvalue control
16          $d-3 cluster definition
```

beam2d.pin (for STAPL processor)

```
Straight cantilevered beam - free vibration problem
16 0 0 0 $P1-2 NPL0T,IPREP,IPRS,KDEV
 2 0 4 0 1 0 0 2 $P1-3 KPL0T,VIEW,ITEM,STEP,MODE,IFRNG,COLOR,ICOMP
0.0 0 0.0 0.0 0.0 0.0 $P1-5 DSCALE,NROTS,LWSCALE,RNGMIN,RGMAX
 2 0 4 0 2 0 0 2 $P1-3 KPL0T,VIEW,ITEM,STEP,MODE,IFRNG,COLOR,ICOMP
0.0 0 0.0 0.0 0.0 0.0 $P1-5 DSCALE,NROTS,LWSCALE,RNGMIN,RGMAX
 2 0 4 0 3 0 0 2 $P1-3 KPL0T,VIEW,ITEM,STEP,MODE,IFRNG,COLOR,ICOMP
0.0 0 0.0 0.0 0.0 0.0 $P1-5 DSCALE,NROTS,LWSCALE,RNGMIN,RGMAX
 2 0 4 0 4 0 0 2 $P1-3 KPL0T,VIEW,ITEM,STEP,MODE,IFRNG,COLOR,ICOMP
0.0 0 0.0 0.0 0.0 0.0 $P1-5 DSCALE,NROTS,LWSCALE,RNGMIN,RGMAX
 2 0 4 0 5 0 0 2 $P1-3 KPL0T,VIEW,ITEM,STEP,MODE,IFRNG,COLOR,ICOMP
0.0 0 0.0 0.0 0.0 0.0 $P1-5 DSCALE,NROTS,LWSCALE,RNGMIN,RGMAX
 2 0 4 0 6 0 0 2 $P1-3 KPL0T,VIEW,ITEM,STEP,MODE,IFRNG,COLOR,ICOMP
0.0 0 0.0 0.0 0.0 0.0 $P1-5 DSCALE,NROTS,LWSCALE,RNGMIN,RGMAX
 2 0 4 0 7 0 0 2 $P1-3 KPL0T,VIEW,ITEM,STEP,MODE,IFRNG,COLOR,ICOMP
0.0 0 0.0 0.0 0.0 0.0 $P1-5 DSCALE,NROTS,LWSCALE,RNGMIN,RGMAX
 2 0 4 0 8 0 0 2 $P1-3 KPL0T,VIEW,ITEM,STEP,MODE,IFRNG,COLOR,ICOMP
0.0 0 0.0 0.0 0.0 0.0 $P1-5 DSCALE,NROTS,LWSCALE,RNGMIN,RGMAX
 2 0 4 0 9 0 0 2 $P1-3 KPL0T,VIEW,ITEM,STEP,MODE,IFRNG,COLOR,ICOMP
0.0 0 0.0 0.0 0.0 0.0 $P1-5 DSCALE,NROTS,LWSCALE,RNGMIN,RGMAX
 2 0 4 0 10 0 0 2 $P1-3 KPL0T,VIEW,ITEM,STEP,MODE,IFRNG,COLOR,ICOMP
0.0 0 0.0 0.0 0.0 0.0 $P1-5 DSCALE,NROTS,LWSCALE,RNGMIN,RGMAX
 2 0 4 0 11 0 0 2 $P1-3 KPL0T,VIEW,ITEM,STEP,MODE,IFRNG,COLOR,ICOMP
0.0 0 0.0 0.0 0.0 0.0 $P1-5 DSCALE,NROTS,LWSCALE,RNGMIN,RGMAX
 2 0 4 0 12 0 0 2 $P1-3 KPL0T,VIEW,ITEM,STEP,MODE,IFRNG,COLOR,ICOMP
0.0 0 0.0 0.0 0.0 0.0 $P1-5 DSCALE,NROTS,LWSCALE,RNGMIN,RGMAX
 2 0 4 0 13 0 0 2 $P1-3 KPL0T,VIEW,ITEM,STEP,MODE,IFRNG,COLOR,ICOMP
0.0 0 0.0 0.0 0.0 0.0 $P1-5 DSCALE,NROTS,LWSCALE,RNGMIN,RGMAX
 2 0 4 0 14 0 0 2 $P1-3 KPL0T,VIEW,ITEM,STEP,MODE,IFRNG,COLOR,ICOMP
0.0 0 0.0 0.0 0.0 0.0 $P1-5 DSCALE,NROTS,LWSCALE,RNGMIN,RGMAX
 2 0 4 0 15 0 0 2 $P1-3 KPL0T,VIEW,ITEM,STEP,MODE,IFRNG,COLOR,ICOMP
0.0 0 0.0 0.0 0.0 0.0 $P1-5 DSCALE,NROTS,LWSCALE,RNGMIN,RGMAX
 2 0 4 0 16 0 0 2 $P1-3 KPL0T,VIEW,ITEM,STEP,MODE,IFRNG,COLOR,ICOMP
0.0 0 0.0 0.0 0.0 0.0 $P1-5 DSCALE,NROTS,LWSCALE,RNGMIN,RGMAX
```

Model using 3-D Solid Elements

The following text file provides the input for a beam finite element model using twenty 20-node E885 solid elements along the beam length and one element across the beam width and across the beam depth.

beam3d.inp (for S1 processor)

```
Straight beam free vibration problem - 3-D model          $A-1
C
```

```

C Thin straight strip, free vibration problem
C
C REF.: Timoshenko, Young, and Weaver, "Vibration Problems
C       in Engineering," 1974.
C
C MODEL INPUT CONTROLS
1      0      1      1      0      3      0  $B-1
1 0.0 / 2 0.0 / 3 -90.0      $B-1b rotations for model plot
1      10*0
1      0      1      0      0      1      $B-2
386.4  $b-4 acceleration due to gravity, g (in./s/s)
41     3      $F-1 DISCRETIZATION: NROWS, NCOLS OF NODES
C
C HISTORICAL STAGS MATERIAL DEFINITION
C
1      $I-1 MATERIAL NO. 1 (HISTORICAL STAGS APPROACH)
10.0e+6 0.0 0.0 0.83333 $I-2 ISOTROPIC ELASTIC MATERIAL
C =====
C BEGIN GCP INPUT FOR MATERIAL AND FABRICATION
C
ISOELASTIC_MATERIAL 1 1 1 0 0 $I-5A MATERIAL NO. 1 (GCP APPROACH)
10.0E+6,          $I-6A YOUNG'S MODULUS, PSI
0.0 ,            $I-6A POISSON'S RATIO
CC2.1583354E-3,   $I-6A MASS DENSITY
2.1566598E-3,    $I-6A MASS DENSITY
4*0.0           $I-6A UNUSED MATERIAL PARAMETERS
SOLID_FABRICATION 1 1 0      $I-5A GCP Solid Fabrication Record
1.0      $I-22a element thickness
SHELL_FABRICATION 1 1 0 0 0 $I-5A GCP SHELL FABRICATION RECORD
1      $I-21A GCP LAYER MATERIAL ID
1.0    $I-21C GCP LAYER THICKNESS, INCHES
0.0    $I-21D GCP LAYER ORIENTATION, DEGREES
END    $I-5A END GCP INPUT
C END GCP INPUT FOR MATERIAL AND FABRICATION
C =====
C
C HISTORICAL STAGS SHELL FABRICATION DEFINITION
C
1      1      1      0      $K-1 SHELL WALL RECORD
1      1.0    0.0    0      $K-2 LAYERED WALL
C
C UNIT 1 MODEL DEFINITION (one solid element thickness)
C
2 0 0 0 1 1      $M-1 Rectangular PLATE GEOMETRY
0.0 10.0 0.0 0.1 $M-2 L=30 in.; t=1.0 in.
-1 0 0.0 0.0 0 0 0 $M-5 SHELL WALL RECORD, USE GCP FAB. # 1
885 0 0      $N-1 DISCRETIZATION RECORD, ELEMENT SELECTION
3 3 3 3      $P-1 BC imposed on q-records
1 $q-1 homogeneous BC's imposed on q-records for 3D elements
1 3 0 $q-2 (E881 has 2 nodal layers; E883, E885 has three)
0.0 -1 1 1 0 0 3 1 0 0 1 $q-3 u=v=w=0 at clamped end for layer 1
0.0 -1 1 1 0 0 3 1 0 0 2 $q-3 u=v=w=0 at clamped end for layer 2
0.0 -1 1 1 0 0 3 1 0 0 3 $q-3 u=v=w=0 at clamped end for layer 3
1 0 0 0      $R-1 OUTPUT CONTROL FOR SHELL UNIT 1

```

beam3d.bin (for S2 processor)

```

Straight beam free vibration problem - 1-D model      $A-1
C
C Thin straight strip, free vibration problem
C
C REF.: Timoshenko, Young, and Weaver, "Vibration Problems

```

```

C      in Engineering," 1974.
C
2 1 0 0 0 0 0 -1 $b-1 free vibration analysis
1.0 1.0 1.0 $c-1 load factors
100 1.0e-4 0 $d-2 eigenvalue control
16      $d-3 cluster definition

```

beam3d.pin (for STAPL processor)

Straight cantilevered beam - free vibration problem

```

16 0 0 0 $PL-2 NPLOT,IPREP,IPRS,KDEV
 2 0 4 0 1 0 0 2 $PL-3 KPLOT,VIEW,ITEM,STEP,MODE,IFRNG,COLOR,ICOMP
0.0 0 0.0 0.0 0.0 $PL-5 DSCALE,NROTS,LWSCALE,RNGMIN,RGMAX
 2 0 4 0 2 0 0 2 $PL-3 KPLOT,VIEW,ITEM,STEP,MODE,IFRNG,COLOR,ICOMP
0.0 0 0.0 0.0 0.0 $PL-5 DSCALE,NROTS,LWSCALE,RNGMIN,RGMAX
 2 0 4 0 3 0 0 2 $PL-3 KPLOT,VIEW,ITEM,STEP,MODE,IFRNG,COLOR,ICOMP
0.0 0 0.0 0.0 0.0 $PL-5 DSCALE,NROTS,LWSCALE,RNGMIN,RGMAX
 2 0 4 0 4 0 0 2 $PL-3 KPLOT,VIEW,ITEM,STEP,MODE,IFRNG,COLOR,ICOMP
0.0 0 0.0 0.0 0.0 $PL-5 DSCALE,NROTS,LWSCALE,RNGMIN,RGMAX
 2 0 4 0 5 0 0 2 $PL-3 KPLOT,VIEW,ITEM,STEP,MODE,IFRNG,COLOR,ICOMP
0.0 0 0.0 0.0 0.0 $PL-5 DSCALE,NROTS,LWSCALE,RNGMIN,RGMAX
 2 0 4 0 6 0 0 2 $PL-3 KPLOT,VIEW,ITEM,STEP,MODE,IFRNG,COLOR,ICOMP
0.0 0 0.0 0.0 0.0 $PL-5 DSCALE,NROTS,LWSCALE,RNGMIN,RGMAX
 2 0 4 0 7 0 0 2 $PL-3 KPLOT,VIEW,ITEM,STEP,MODE,IFRNG,COLOR,ICOMP
0.0 0 0.0 0.0 0.0 $PL-5 DSCALE,NROTS,LWSCALE,RNGMIN,RGMAX
 2 0 4 0 8 0 0 2 $PL-3 KPLOT,VIEW,ITEM,STEP,MODE,IFRNG,COLOR,ICOMP
0.0 0 0.0 0.0 0.0 $PL-5 DSCALE,NROTS,LWSCALE,RNGMIN,RGMAX
 2 0 4 0 9 0 0 2 $PL-3 KPLOT,VIEW,ITEM,STEP,MODE,IFRNG,COLOR,ICOMP
0.0 0 0.0 0.0 0.0 $PL-5 DSCALE,NROTS,LWSCALE,RNGMIN,RGMAX
 2 0 4 0 10 0 0 2 $PL-3 KPLOT,VIEW,ITEM,STEP,MODE,IFRNG,COLOR,ICOMP
0.0 0 0.0 0.0 0.0 $PL-5 DSCALE,NROTS,LWSCALE,RNGMIN,RGMAX
 2 0 4 0 11 0 0 2 $PL-3 KPLOT,VIEW,ITEM,STEP,MODE,IFRNG,COLOR,ICOMP
0.0 0 0.0 0.0 0.0 $PL-5 DSCALE,NROTS,LWSCALE,RNGMIN,RGMAX
 2 0 4 0 12 0 0 2 $PL-3 KPLOT,VIEW,ITEM,STEP,MODE,IFRNG,COLOR,ICOMP
0.0 0 0.0 0.0 0.0 $PL-5 DSCALE,NROTS,LWSCALE,RNGMIN,RGMAX
 2 0 4 0 13 0 0 2 $PL-3 KPLOT,VIEW,ITEM,STEP,MODE,IFRNG,COLOR,ICOMP
0.0 0 0.0 0.0 0.0 $PL-5 DSCALE,NROTS,LWSCALE,RNGMIN,RGMAX
 2 0 4 0 14 0 0 2 $PL-3 KPLOT,VIEW,ITEM,STEP,MODE,IFRNG,COLOR,ICOMP
0.0 0 0.0 0.0 0.0 $PL-5 DSCALE,NROTS,LWSCALE,RNGMIN,RGMAX
 2 0 4 0 15 0 0 2 $PL-3 KPLOT,VIEW,ITEM,STEP,MODE,IFRNG,COLOR,ICOMP
0.0 0 0.0 0.0 0.0 $PL-5 DSCALE,NROTS,LWSCALE,RNGMIN,RGMAX
 2 0 4 0 16 0 0 2 $PL-3 KPLOT,VIEW,ITEM,STEP,MODE,IFRNG,COLOR,ICOMP
0.0 0 0.0 0.0 0.0 $PL-5 DSCALE,NROTS,LWSCALE,RNGMIN,RGMAX

```

Problem References

Timoshenko, S., Young, D. H., and Weaver, W., Jr., *Vibration Problems in Engineering*, Fourth Edition, John Wiley & Sons, Inc., New York, 1974.

Free Vibration of Circular Ring

Background

Free vibration of a circular ring modeled using both one- and two-dimensional elements is studied. Two vibration cases are considered: extensional vibration and in-plane flexural vibration. The geometry and material properties of the circular ring with a square cross sectional area are defined in Figure 11 using U. S. customary units.

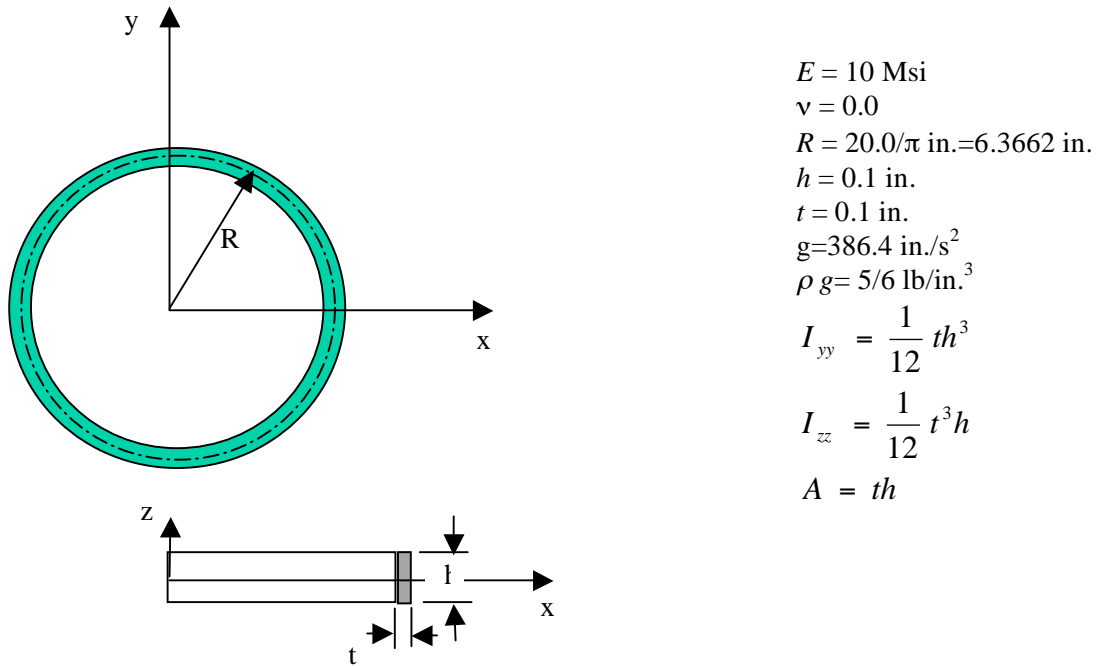


Figure 11. Circular ring problem: geometry and material properties.

The analytical solutions for linear free vibration of a circular ring are given by Timoshenko, Young and Weaver (1974). The frequencies for extensional vibration are given by Timoshenko *et al.* (1974, pp. 476-477) as:

$$\omega_m = \sqrt{\frac{E(1 + m^2)}{\rho R^2}}$$

where E is Young's elastic modulus (10 Msi), ρ is the mass density, R is the radius of the centerline of the ring ($20/\pi$ in.), and m is the number of full waves ($m=0$ is the pure radial vibration case), and ω_m is the circular frequency (radians per second) for the m -th vibration mode. In terms of cycles per second or hertz, the frequency for the m -th mode is given by:

$$f_m = \frac{\omega_m}{2\pi}$$

Using these formula, the frequencies for the in-plane (x - z plane) extensional vibration modes are computed as follows:

m	Type of Mode	ω_m^2	f_m
0	Pure radial	1.1441×10^8	1702.351
1	Extension	2.2882×10^8	2407.488
2	Extension	5.7204×10^8	3806.573
3	Extension	11.4408×10^8	5383.308

The frequencies for in-plane (x - y plane) flexural vibration of the circular ring are given by Timoshenko *et al.* (1974, pp. 479-481) as:

$$\omega_m = \sqrt{\frac{EI_{zz} m^2 (1 - m^2)^2}{\rho A R^4 (1 + m^2)}}$$

where I_{zz} is the moment of inertia about the z -axis, A is the cross-sectional area, t is the ring thickness (0.1 in.), h is the ring width (1.0 in.), and ω_m is the circular frequency (radians per second) for the m -th vibration mode. For $m=1$, the frequency is zero indicating that the ring moves as a rigid body.

Using this formula, the frequencies for the in-plane flexural vibration modes are computed as follows:

m	Type of Mode	ω_m^2	f_m
1	Rigid Body	0	0
2	Flexural	16937.49	20.713
3	Flexural	135499.94	58.585
4	Flexural	498161.55	112.332
5	Flexural	1302884.10	181.666
6	Flexural	2803841.71	266.500
7	Flexural	5311597.88	366.803
8	Flexural	9193150.18	482.561

Modeling and Analysis Process

Three separate STAGS finite element models are considered in this test case problem: beam elements, shell elements, and solid elements. A summary of each model includes:

1. 1-D beam model – Model the beam using discrete beam elements using an element unit where node records (S records) are generated using an external FORTRAN code to compute nodal coordinates and output each record.
2. 2-D plate model – Model the beam with plate elements (x - y plane) in a single shell unit using the annular plate shell geometry.

For each model, a full 360-degree model of the ring is used (*i.e.*, a 360° segment) with boundary conditions applied to constrain the motion to the xy plane. The annular plate shell geometry does not include extensions for 3-D elements – presumably because of the possible pole at the center. Therefore a 3-D solid model is not consider; however, a 3-D model could be developed as an element unit using MSC.Patran or other external finite element modeling approach.

Material properties and fabrication construction are defined using both the *historical* STAGS approach (*i.e.*, STAGS versions prior to GCP) and the current GCP approach. Material modeling for an elastic material using the historical STAGS approach requires data on the I-1 and I-2 records to define the material properties and the K-1 and K-2 records to define the fabrication data. Section properties for the beam elements can only be accomplished using the *historical* STAGS approach using the J records. Material modeling using the current GCP approach requires data on the I-5a and I-6a records to define the material properties and records I-5a, I-21a, I-21b, I-21c, I-21d, and I-21e to define the fabrication.

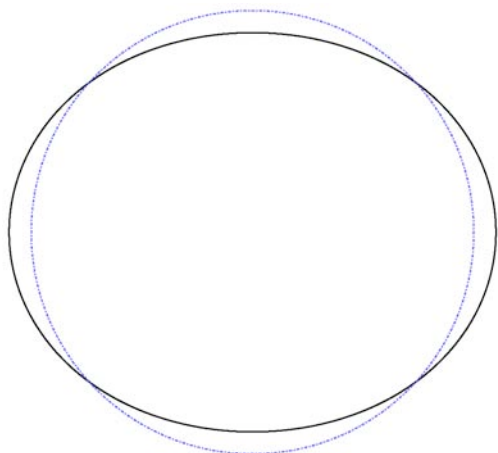
Boundary condition on the displacements are specified using the P-1 and P-2 records. The in-plane edges of the 2-D shell model are free. The out-of-plane degrees of freedom are constrained using the Q records to specify homogeneous conditions. The drilling freedom is retained as an active degree of freedom for the E410 shell element since it contributes to the membrane response of the element.

Numerical Results and Discussion

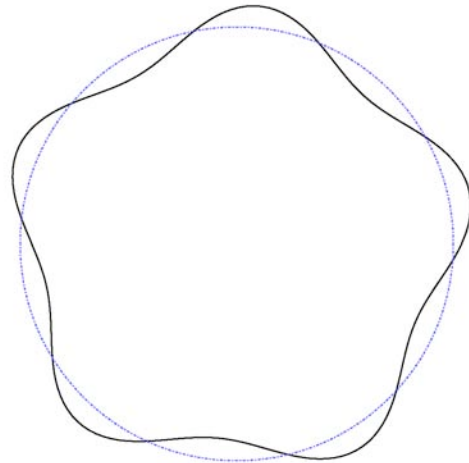
Free vibration of the circular ring is analyzed for two types of vibration modes: in-plane extensional and in-plane flexural. There is no external load on the ring – vibration about an unstressed state. The eigenvalue analysis has a convergence tolerance of 10^{-4} and the number of eigenpairs (eigenvalue and corresponding eigenmode) requested is six. No shift is used in the eigenvalue solution. In both the 1-D and 2-D models, three rigid body modes are extracted first (zero frequencies) and then the various modes (in pairs) are computed. The flexural modes occur in pairs because of the periodicity of the solutions with one mode rotated relative to the other by an angle corresponding to a half cycle. These mode shapes are shown in Figure 12 for the 1-D beam model. Comparison of vibration frequencies for the models analyzed is given in Table 7. The ring cross-sectional area is square. In the 1-D model no deformations occur in the cross-sectional plane; however, in the 2-D model, in-plane deformations of the cross section may occur. This added flexibility results in slightly lower vibration frequencies for the 2-D model.

Table 7. Vibration analysis results for circular ring.

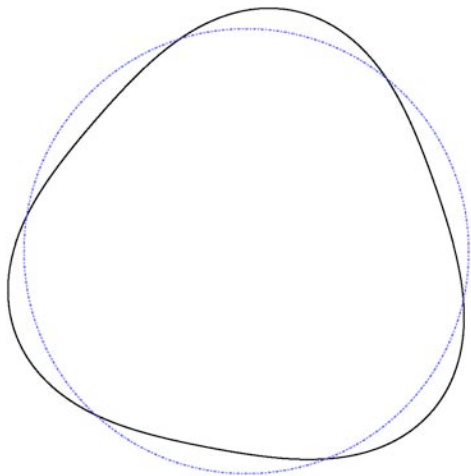
Number of Full Waves, m	Mode Type	Frequency, Hertz		
		Analytical	Finite Element Model	
			1-D Model	2-D Model
2	Flexural	20.713	20.717	19.095
3	Flexural	58.585	58.597	53.957
4	Flexural	112.332	112.36	103.40
5	Flexural	181.666	181.70	167.15
6	Flexural	266.500	266.56	245.09
7	Flexural	366.803	366.88	337.17
8	Flexural	482.561	482.66	443.33



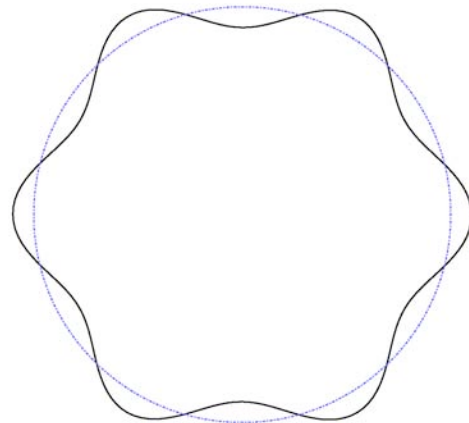
(a) Mode 4, $m=2$



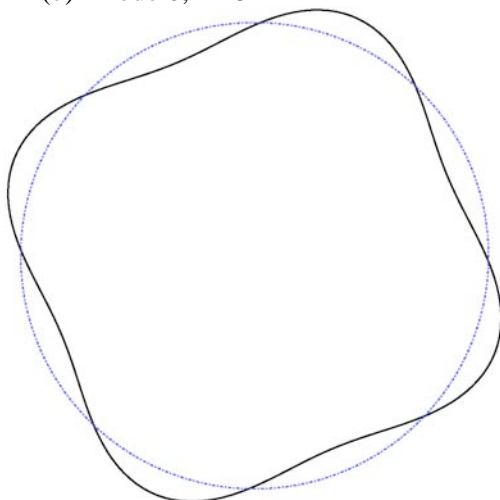
(d) Mode 10, $m=5$



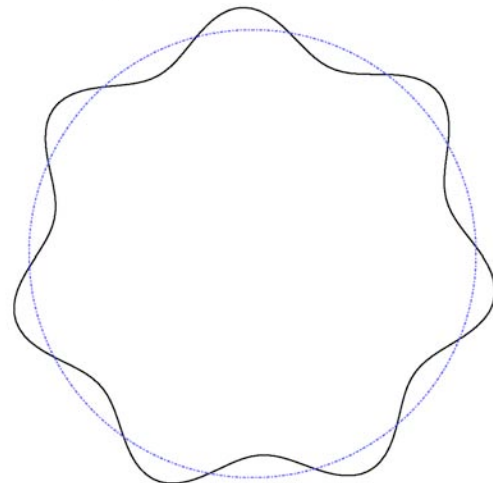
(b) Mode 6, $m=3$



(e) Mode 12, $m=6$



(c) Mode 8, $m=4$



(f) Mode 14, $m=7$

Figure 12. Representative in-plane free vibration mode shapes.

STAGS Input Files

These STAGS input files are located under the following directory:
\$STAGSHOME/Sample-Testcases/Ring-Vibration

Model using 1-D Beam Elements

The following text file provides the input for a beam finite element model using forty 2-node E210 beam elements along the ring circumference.

ring1d.inp (for S1 processor)

```
Circular ring free vibration problem - 1-D model          $A-1
C
C Thin straight strip, free vibration problem
C
C REF.: Timoshenko, Young, and Weaver, "Vibration Problems
C       in Engineering," 1974.
C
C MODEL INPUT CONTROLS
1      0      1      0      0      3      0  $B-1
1 0.0 / 2 0.0 / 3 -90.0          $B-1b model rotations
0      1      0          $B-2
1      1      1      0      0      1          $B-3 INCLUDE GCP INPUT
386.4          $B-4 acceleration due to gravity, g (in/s/s)
C
C Define Element Unit data
C
181 0 180 0 0 0 $h-1 No. of points and No. of beam elements
C
C HISTORICAL STAGS MATERIAL DEFINITION
C
1                                $I-1 MATERIAL NO. 1 (HISTORICAL STAGS APPROACH)
10.0e+6 0.0      0.0  0.83333 $I-2 ISOTROPIC ELASTIC MATERIAL
C =====
C BEGIN GCP INPUT FOR MATERIAL AND FABRICATION
C
ISOELASTIC_MATERIAL 1 1 1 0 0 $I-5A MATERIAL NO. 1 (GCP APPROACH)
10.0E+6,          $I-6A YOUNG'S MODULUS, PSI
0.0 ,            $I-6A POISSON'S RATIO
2.15666E-3,      $I-6A MASS DENSITY
4*0.0           $I-6A UNUSED MATERIAL PARAMETERS
SHELL_FABRICATION 1 1 0 0 0 $I-5A GCP SHELL FABRICATION RECORD
1      $I-21A GCP LAYER MATERIAL ID
0.10   $I-21C GCP LAYER THICKNESS, INCHES
0.0    $I-21D GCP LAYER ORIENTATION, DEGREES
END    $I-5A END GCP INPUT
C END GCP INPUT FOR MATERIAL AND FABRICATION
C =====
C
C Beam cross-sectional properties
C
1 1 1 0 0.3333E-4 0.0 0.0 0 0 0 $j-1
0.01 0.083333E-4 0.083333E-4 0.0          $j-2
C
C HISTORICAL STAGS SHELL FABRICATION DEFINITION
C
1      1      1      0          $K-1 SHELL WALL RECORD
1      0.10   0.0      0          $K-2 LAYERED WALL
C
C ELEMENT UNIT 1 MODEL DEFINITION
```


C

1	0	0	0	6.366198	0.000000	0.0	110	001	0	\$s-1
2	0	0	0	6.362320	0.222177	0.0	110	001	0	\$s-1
3	0	0	0	6.350690	0.444084	0.0	110	001	0	\$s-1
4	0	0	0	6.331323	0.665449	0.0	110	001	0	\$s-1
5	0	0	0	6.304242	0.886003	0.0	110	001	0	\$s-1
6	0	0	0	6.269481	1.105479	0.0	110	001	0	\$s-1
7	0	0	0	6.227081	1.323607	0.0	110	001	0	\$s-1
8	0	0	0	6.177094	1.540123	0.0	110	001	0	\$s-1
9	0	0	0	6.119582	1.754762	0.0	110	001	0	\$s-1
10	0	0	0	6.054614	1.967263	0.0	110	001	0	\$s-1
11	0	0	0	5.982269	2.177368	0.0	110	001	0	\$s-1
12	0	0	0	5.902636	2.384820	0.0	110	001	0	\$s-1
13	0	0	0	5.815811	2.589366	0.0	110	001	0	\$s-1
14	0	0	0	5.721901	2.790757	0.0	110	001	0	\$s-1
15	0	0	0	5.621019	2.988749	0.0	110	001	0	\$s-1
16	0	0	0	5.513289	3.183099	0.0	110	001	0	\$s-1
17	0	0	0	5.398842	3.373571	0.0	110	001	0	\$s-1
18	0	0	0	5.277817	3.559933	0.0	110	001	0	\$s-1
19	0	0	0	5.150362	3.741957	0.0	110	001	0	\$s-1
20	0	0	0	5.016632	3.919423	0.0	110	001	0	\$s-1
21	0	0	0	4.876790	4.092113	0.0	110	001	0	\$s-1
22	0	0	0	4.731007	4.259818	0.0	110	001	0	\$s-1
23	0	0	0	4.579459	4.422333	0.0	110	001	0	\$s-1
24	0	0	0	4.422333	4.579459	0.0	110	001	0	\$s-1
25	0	0	0	4.259818	4.731007	0.0	110	001	0	\$s-1
26	0	0	0	4.092113	4.876790	0.0	110	001	0	\$s-1
27	0	0	0	3.919423	5.016632	0.0	110	001	0	\$s-1
28	0	0	0	3.741957	5.150362	0.0	110	001	0	\$s-1
29	0	0	0	3.559933	5.277817	0.0	110	001	0	\$s-1
30	0	0	0	3.373571	5.398842	0.0	110	001	0	\$s-1
31	0	0	0	3.183099	5.513289	0.0	110	001	0	\$s-1
32	0	0	0	2.988749	5.621019	0.0	110	001	0	\$s-1
33	0	0	0	2.790757	5.721901	0.0	110	001	0	\$s-1
34	0	0	0	2.589366	5.815811	0.0	110	001	0	\$s-1
35	0	0	0	2.384820	5.902636	0.0	110	001	0	\$s-1
36	0	0	0	2.177368	5.982269	0.0	110	001	0	\$s-1
37	0	0	0	1.967263	6.054614	0.0	110	001	0	\$s-1
38	0	0	0	1.754762	6.119582	0.0	110	001	0	\$s-1
39	0	0	0	1.540123	6.177094	0.0	110	001	0	\$s-1
40	0	0	0	1.323607	6.227081	0.0	110	001	0	\$s-1
41	0	0	0	1.105479	6.269481	0.0	110	001	0	\$s-1
42	0	0	0	0.886003	6.304242	0.0	110	001	0	\$s-1
43	0	0	0	0.665449	6.331323	0.0	110	001	0	\$s-1
44	0	0	0	0.444084	6.350690	0.0	110	001	0	\$s-1
45	0	0	0	0.222177	6.362320	0.0	110	001	0	\$s-1
46	0	0	0	0.000000	6.366198	0.0	110	001	0	\$s-1
47	0	0	0	-0.222177	6.362320	0.0	110	001	0	\$s-1
48	0	0	0	-0.444084	6.350690	0.0	110	001	0	\$s-1
49	0	0	0	-0.665449	6.331323	0.0	110	001	0	\$s-1
50	0	0	0	-0.886003	6.304242	0.0	110	001	0	\$s-1
51	0	0	0	-1.105479	6.269481	0.0	110	001	0	\$s-1
52	0	0	0	-1.323607	6.227081	0.0	110	001	0	\$s-1
53	0	0	0	-1.540123	6.177094	0.0	110	001	0	\$s-1
54	0	0	0	-1.754762	6.119582	0.0	110	001	0	\$s-1
55	0	0	0	-1.967263	6.054614	0.0	110	001	0	\$s-1
56	0	0	0	-2.177368	5.982269	0.0	110	001	0	\$s-1
57	0	0	0	-2.384820	5.902636	0.0	110	001	0	\$s-1
58	0	0	0	-2.589366	5.815811	0.0	110	001	0	\$s-1
59	0	0	0	-2.790757	5.721901	0.0	110	001	0	\$s-1
60	0	0	0	-2.988749	5.621019	0.0	110	001	0	\$s-1
61	0	0	0	-3.183099	5.513289	0.0	110	001	0	\$s-1
62	0	0	0	-3.373571	5.398842	0.0	110	001	0	\$s-1

63	0	0	0	-3.559933	5.277817	0.0	110	001	0	\$s-1
64	0	0	0	-3.741957	5.150362	0.0	110	001	0	\$s-1
65	0	0	0	-3.919423	5.016632	0.0	110	001	0	\$s-1
66	0	0	0	-4.092113	4.876790	0.0	110	001	0	\$s-1
67	0	0	0	-4.259818	4.731007	0.0	110	001	0	\$s-1
68	0	0	0	-4.422333	4.579459	0.0	110	001	0	\$s-1
69	0	0	0	-4.579459	4.422333	0.0	110	001	0	\$s-1
70	0	0	0	-4.731007	4.259818	0.0	110	001	0	\$s-1
71	0	0	0	-4.876790	4.092113	0.0	110	001	0	\$s-1
72	0	0	0	-5.016632	3.919423	0.0	110	001	0	\$s-1
73	0	0	0	-5.150362	3.741957	0.0	110	001	0	\$s-1
74	0	0	0	-5.277817	3.559933	0.0	110	001	0	\$s-1
75	0	0	0	-5.398842	3.373571	0.0	110	001	0	\$s-1
76	0	0	0	-5.513289	3.183099	0.0	110	001	0	\$s-1
77	0	0	0	-5.621019	2.988749	0.0	110	001	0	\$s-1
78	0	0	0	-5.721901	2.790757	0.0	110	001	0	\$s-1
79	0	0	0	-5.815811	2.589366	0.0	110	001	0	\$s-1
80	0	0	0	-5.902636	2.384820	0.0	110	001	0	\$s-1
81	0	0	0	-5.982269	2.177368	0.0	110	001	0	\$s-1
82	0	0	0	-6.054614	1.967263	0.0	110	001	0	\$s-1
83	0	0	0	-6.119582	1.754762	0.0	110	001	0	\$s-1
84	0	0	0	-6.177094	1.540123	0.0	110	001	0	\$s-1
85	0	0	0	-6.227081	1.323607	0.0	110	001	0	\$s-1
86	0	0	0	-6.269481	1.105479	0.0	110	001	0	\$s-1
87	0	0	0	-6.304242	0.886003	0.0	110	001	0	\$s-1
88	0	0	0	-6.331323	0.665449	0.0	110	001	0	\$s-1
89	0	0	0	-6.350690	0.444084	0.0	110	001	0	\$s-1
90	0	0	0	-6.362320	0.222177	0.0	110	001	0	\$s-1
91	0	0	0	-6.366198	0.000000	0.0	110	001	0	\$s-1
92	0	0	0	-6.362320	-0.222177	0.0	110	001	0	\$s-1
93	0	0	0	-6.350690	-0.444084	0.0	110	001	0	\$s-1
94	0	0	0	-6.331323	-0.665449	0.0	110	001	0	\$s-1
95	0	0	0	-6.304242	-0.886003	0.0	110	001	0	\$s-1
96	0	0	0	-6.269481	-1.105479	0.0	110	001	0	\$s-1
97	0	0	0	-6.227081	-1.323607	0.0	110	001	0	\$s-1
98	0	0	0	-6.177094	-1.540123	0.0	110	001	0	\$s-1
99	0	0	0	-6.119582	-1.754762	0.0	110	001	0	\$s-1
100	0	0	0	-6.054614	-1.967263	0.0	110	001	0	\$s-1
101	0	0	0	-5.982269	-2.177368	0.0	110	001	0	\$s-1
102	0	0	0	-5.902636	-2.384820	0.0	110	001	0	\$s-1
103	0	0	0	-5.815811	-2.589366	0.0	110	001	0	\$s-1
104	0	0	0	-5.721901	-2.790757	0.0	110	001	0	\$s-1
105	0	0	0	-5.621019	-2.988749	0.0	110	001	0	\$s-1
106	0	0	0	-5.513289	-3.183099	0.0	110	001	0	\$s-1
107	0	0	0	-5.398842	-3.373571	0.0	110	001	0	\$s-1
108	0	0	0	-5.277817	-3.559933	0.0	110	001	0	\$s-1
109	0	0	0	-5.150362	-3.741957	0.0	110	001	0	\$s-1
110	0	0	0	-5.016632	-3.919423	0.0	110	001	0	\$s-1
111	0	0	0	-4.876790	-4.092113	0.0	110	001	0	\$s-1
112	0	0	0	-4.731007	-4.259818	0.0	110	001	0	\$s-1
113	0	0	0	-4.579459	-4.422333	0.0	110	001	0	\$s-1
114	0	0	0	-4.422333	-4.579459	0.0	110	001	0	\$s-1
115	0	0	0	-4.259818	-4.731007	0.0	110	001	0	\$s-1
116	0	0	0	-4.092113	-4.876790	0.0	110	001	0	\$s-1
117	0	0	0	-3.919423	-5.016632	0.0	110	001	0	\$s-1
118	0	0	0	-3.741957	-5.150362	0.0	110	001	0	\$s-1
119	0	0	0	-3.559933	-5.277817	0.0	110	001	0	\$s-1
120	0	0	0	-3.373571	-5.398842	0.0	110	001	0	\$s-1
121	0	0	0	-3.183099	-5.513289	0.0	110	001	0	\$s-1
122	0	0	0	-2.988749	-5.621019	0.0	110	001	0	\$s-1
123	0	0	0	-2.790757	-5.721901	0.0	110	001	0	\$s-1
124	0	0	0	-2.589366	-5.815811	0.0	110	001	0	\$s-1
125	0	0	0	-2.384820	-5.902636	0.0	110	001	0	\$s-1

```

126 0 0 0 -2.177368 -5.982269 0.0 110 001 0 $s-1
127 0 0 0 -1.967263 -6.054614 0.0 110 001 0 $s-1
128 0 0 0 -1.754762 -6.119582 0.0 110 001 0 $s-1
129 0 0 0 -1.540123 -6.177094 0.0 110 001 0 $s-1
130 0 0 0 -1.323607 -6.227081 0.0 110 001 0 $s-1
131 0 0 0 -1.105479 -6.269481 0.0 110 001 0 $s-1
132 0 0 0 -0.886003 -6.304242 0.0 110 001 0 $s-1
133 0 0 0 -0.665449 -6.331323 0.0 110 001 0 $s-1
134 0 0 0 -0.444084 -6.350690 0.0 110 001 0 $s-1
135 0 0 0 -0.222177 -6.362320 0.0 110 001 0 $s-1
136 0 0 0 0.000000 -6.366198 0.0 110 001 0 $s-1
137 0 0 0 0.222177 -6.362320 0.0 110 001 0 $s-1
138 0 0 0 0.444084 -6.350690 0.0 110 001 0 $s-1
139 0 0 0 0.665449 -6.331323 0.0 110 001 0 $s-1
140 0 0 0 0.886003 -6.304242 0.0 110 001 0 $s-1
141 0 0 0 1.105479 -6.269481 0.0 110 001 0 $s-1
142 0 0 0 1.323607 -6.227081 0.0 110 001 0 $s-1
143 0 0 0 1.540123 -6.177094 0.0 110 001 0 $s-1
144 0 0 0 1.754762 -6.119582 0.0 110 001 0 $s-1
145 0 0 0 1.967263 -6.054614 0.0 110 001 0 $s-1
146 0 0 0 2.177368 -5.982269 0.0 110 001 0 $s-1
147 0 0 0 2.384820 -5.902636 0.0 110 001 0 $s-1
148 0 0 0 2.589366 -5.815811 0.0 110 001 0 $s-1
149 0 0 0 2.790757 -5.721901 0.0 110 001 0 $s-1
150 0 0 0 2.988749 -5.621019 0.0 110 001 0 $s-1
151 0 0 0 3.183099 -5.513289 0.0 110 001 0 $s-1
152 0 0 0 3.373571 -5.398842 0.0 110 001 0 $s-1
153 0 0 0 3.559933 -5.277817 0.0 110 001 0 $s-1
154 0 0 0 3.741957 -5.150362 0.0 110 001 0 $s-1
155 0 0 0 3.919423 -5.016632 0.0 110 001 0 $s-1
156 0 0 0 4.092113 -4.876790 0.0 110 001 0 $s-1
157 0 0 0 4.259818 -4.731007 0.0 110 001 0 $s-1
158 0 0 0 4.422333 -4.579459 0.0 110 001 0 $s-1
159 0 0 0 4.579459 -4.422333 0.0 110 001 0 $s-1
160 0 0 0 4.731007 -4.259818 0.0 110 001 0 $s-1
161 0 0 0 4.876790 -4.092113 0.0 110 001 0 $s-1
162 0 0 0 5.016632 -3.919423 0.0 110 001 0 $s-1
163 0 0 0 5.150362 -3.741957 0.0 110 001 0 $s-1
164 0 0 0 5.277817 -3.559933 0.0 110 001 0 $s-1
165 0 0 0 5.398842 -3.373571 0.0 110 001 0 $s-1
166 0 0 0 5.513289 -3.183099 0.0 110 001 0 $s-1
167 0 0 0 5.621019 -2.988749 0.0 110 001 0 $s-1
168 0 0 0 5.721901 -2.790757 0.0 110 001 0 $s-1
169 0 0 0 5.815811 -2.589366 0.0 110 001 0 $s-1
170 0 0 0 5.902636 -2.384820 0.0 110 001 0 $s-1
171 0 0 0 5.982269 -2.177368 0.0 110 001 0 $s-1
172 0 0 0 6.054614 -1.967263 0.0 110 001 0 $s-1
173 0 0 0 6.119582 -1.754762 0.0 110 001 0 $s-1
174 0 0 0 6.177094 -1.540123 0.0 110 001 0 $s-1
175 0 0 0 6.227081 -1.323607 0.0 110 001 0 $s-1
176 0 0 0 6.269481 -1.105479 0.0 110 001 0 $s-1
177 0 0 0 6.304242 -0.886003 0.0 110 001 0 $s-1
178 0 0 0 6.331323 -0.665449 0.0 110 001 0 $s-1
179 0 0 0 6.350690 -0.444084 0.0 110 001 0 $s-1
180 0 0 0 6.362320 -0.222177 0.0 110 001 0 $s-1
181 0 0 0 0.000000 0.000000 0.0 110 000 0 $s-1

```

C

C Generate beam elements

C

```

1 2 181 210 1 0.0 0.0 0.0 0 0 179 $T-2
1 1 0 $T-2a generate 20 elements
180 1 181 210 1 0.0 0.0 0.0 0 0 0 $T-2

```

C

```

C generate loads - applied end shortening
C
0 0          $u-1 Loads summary
1 0 0       $v-1 output control

```

ringld.bin (for S2 processor)

```

Straight beam free vibration problem - 1-D model          $A-1
C
C Thin straight strip, free vibration problem
C
C REF.: Timoshenko, Young, and Weaver, "Vibration Problems
C         in Engineering," 1974.
C
2 1 0 0 0 0 0 -1 $b-1 free vibration analysis
1.0 1.0 1.0 $c-1 load factors
100 1.0e-4 0 $d-2 eigenvalue control
20 -1.0     $d-3 cluster definition

```

ringld.pin (for STAPL processor)

```

Straight cantilevered beam - free vibration problem
16 0 0 0 $PL-2 NPLOT,IPREP,IPRS,KDEV
 1 0 4 0 1 0 0 2 $PL-3 KPLOT,VIEW,ITEM,STEP,MODE,IFRNG,COLOR,ICOMP
0.0 3 0.0 0.0 0.0 $PL-5 DSCALE,NROTS,LWSCALE,RNGMIN,RGMAX
1 0.0 / 2 0.0 / 3 0.0
 1 0 4 0 2 0 0 2 $PL-3 KPLOT,VIEW,ITEM,STEP,MODE,IFRNG,COLOR,ICOMP
0.0 3 0.0 0.0 0.0 $PL-5 DSCALE,NROTS,LWSCALE,RNGMIN,RGMAX
1 0.0 / 2 0.0 / 3 0.0
 1 0 4 0 3 0 0 2 $PL-3 KPLOT,VIEW,ITEM,STEP,MODE,IFRNG,COLOR,ICOMP
0.0 3 0.0 0.0 0.0 $PL-5 DSCALE,NROTS,LWSCALE,RNGMIN,RGMAX
1 0.0 / 2 0.0 / 3 0.0
 1 0 4 0 4 0 0 2 $PL-3 KPLOT,VIEW,ITEM,STEP,MODE,IFRNG,COLOR,ICOMP
0.0 3 0.0 0.0 0.0 $PL-5 DSCALE,NROTS,LWSCALE,RNGMIN,RGMAX
1 0.0 / 2 0.0 / 3 0.0
 1 0 4 0 5 0 0 2 $PL-3 KPLOT,VIEW,ITEM,STEP,MODE,IFRNG,COLOR,ICOMP
0.0 3 0.0 0.0 0.0 $PL-5 DSCALE,NROTS,LWSCALE,RNGMIN,RGMAX
1 0.0 / 2 0.0 / 3 0.0
 1 0 4 0 6 0 0 2 $PL-3 KPLOT,VIEW,ITEM,STEP,MODE,IFRNG,COLOR,ICOMP
0.0 3 0.0 0.0 0.0 $PL-5 DSCALE,NROTS,LWSCALE,RNGMIN,RGMAX
1 0.0 / 2 0.0 / 3 0.0
 1 0 4 0 7 0 0 2 $PL-3 KPLOT,VIEW,ITEM,STEP,MODE,IFRNG,COLOR,ICOMP
0.0 3 0.0 0.0 0.0 $PL-5 DSCALE,NROTS,LWSCALE,RNGMIN,RGMAX
1 0.0 / 2 0.0 / 3 0.0
 1 0 4 0 8 0 0 2 $PL-3 KPLOT,VIEW,ITEM,STEP,MODE,IFRNG,COLOR,ICOMP
0.0 3 0.0 0.0 0.0 $PL-5 DSCALE,NROTS,LWSCALE,RNGMIN,RGMAX
1 0.0 / 2 0.0 / 3 0.0
 1 0 4 0 9 0 0 2 $PL-3 KPLOT,VIEW,ITEM,STEP,MODE,IFRNG,COLOR,ICOMP
0.0 3 0.0 0.0 0.0 $PL-5 DSCALE,NROTS,LWSCALE,RNGMIN,RGMAX
1 0.0 / 2 0.0 / 3 0.0
 1 0 4 0 10 0 0 2 $PL-3 KPLOT,VIEW,ITEM,STEP,MODE,IFRNG,COLOR,ICOMP
0.0 3 0.0 0.0 0.0 $PL-5 DSCALE,NROTS,LWSCALE,RNGMIN,RGMAX
1 0.0 / 2 0.0 / 3 0.0
 1 0 4 0 11 0 0 2 $PL-3 KPLOT,VIEW,ITEM,STEP,MODE,IFRNG,COLOR,ICOMP
0.0 3 0.0 0.0 0.0 $PL-5 DSCALE,NROTS,LWSCALE,RNGMIN,RGMAX
1 0.0 / 2 0.0 / 3 0.0
 1 0 4 0 12 0 0 2 $PL-3 KPLOT,VIEW,ITEM,STEP,MODE,IFRNG,COLOR,ICOMP
0.0 3 0.0 0.0 0.0 $PL-5 DSCALE,NROTS,LWSCALE,RNGMIN,RGMAX
1 0.0 / 2 0.0 / 3 0.0
 1 0 4 0 13 0 0 2 $PL-3 KPLOT,VIEW,ITEM,STEP,MODE,IFRNG,COLOR,ICOMP
0.0 3 0.0 0.0 0.0 $PL-5 DSCALE,NROTS,LWSCALE,RNGMIN,RGMAX

```

```

1 0.0 / 2 0.0 / 3 0.0
1 0 4 0 14 0 0 2 $P1-3 KPLOT,VIEW,ITEM,STEP,MODE,IFRNG,COLOR,ICOMP
0.0 3 0.0 0.0 0.0 $P1-5 DSCALE,NROTS,LWSCALE,RNGMIN,RGMAX
1 0.0 / 2 0.0 / 3 0.0
1 0 4 0 15 0 0 2 $P1-3 KPLOT,VIEW,ITEM,STEP,MODE,IFRNG,COLOR,ICOMP
0.0 3 0.0 0.0 0.0 $P1-5 DSCALE,NROTS,LWSCALE,RNGMIN,RGMAX
1 0.0 / 2 0.0 / 3 0.0
1 0 4 0 16 0 0 2 $P1-3 KPLOT,VIEW,ITEM,STEP,MODE,IFRNG,COLOR,ICOMP
0.0 3 0.0 0.0 0.0 $P1-5 DSCALE,NROTS,LWSCALE,RNGMIN,RGMAX
1 0.0 / 2 0.0 / 3 0.0

```

Model using 2-D Shell Elements

The following text file provides the input for a finite element model using 360 4-node E410 shell elements along the ring circumference.

ring2d.inp (fpr S1 processor)

```

Circular ring free vibration problem - 2-D model $A-1
C
C Thin 90-degree segment of circular ring, free vibration problem
C
C REF.: Timoshenko, Young, and Weaver, "Vibration Problems
C in Engineering," 1974.
C
C MODEL INPUT CONTROLS
1 0 1 0 0 0 $B-1
CCX1 0.0/ 2 90.0 / 3 0.0
1 0 0 1 $B-2
1 0 1 0 0 1 $B-3 INCLUDE GCP INPUT
386.4 $b-4 acceleration due to gravity g (in/s/s)
2 361 $F-1 DISCRETIZATION: NROWS, NCOLS OF NODES
1 2 1 4 $g-1 complete ring, full 360-degrees
C
C HISTORICAL STAGS MATERIAL DEFINITION
C
1 $I-1 MATERIAL NO. 1 (HISTORICAL STAGS APPROACH)
10.0e+6 0.0 0.0 0.83333 $I-2 ISOTROPIC ELASTIC MATERIAL
C =====
C BEGIN GCP INPUT FOR MATERIAL AND FABRICATION
C
ISOELASTIC_MATERIAL 1 1 1 0 0 $I-5A MATERIAL NO. 1 (GCP APPROACH)
10.0E+6, $I-6A YOUNG'S MODULUS, PSI
0.0 , $I-6A POISSON'S RATIO
2.15666E-3, $I-6A MASS DENSITY
4*0.0 $I-6A UNUSED MATERIAL PARAMETERS
SHELL_FABRICATION 1 1 0 0 0 $I-5A GCP SHELL FABRICATION RECORD
1 $I-21A GCP LAYER MATERIAL ID
0.1 $I-21C GCP LAYER THICKNESS, INCHES
0.0 $I-21D GCP LAYER ORIENTATION, DEGREES
END $I-5A END GCP INPUT
C END GCP INPUT FOR MATERIAL AND FABRICATION
C =====
C
C HISTORICAL STAGS SHELL FABRICATION DEFINITION
C
1 1 1 0 $K-1 SHELL WALL RECORD
1 0.1 0.0 0 $K-2 LAYERED WALL
C
C SHELL UNIT 1 MODEL DEFINITION
C
4 0 4*0 $M-1 Annular PLATE GEOMETRY
CC5.8662 6.8662 0.0 360.0 $M-2 Ra, Rb, theta-a, theta-b
6.3162 6.4162 0.0 360.0 $M-2 Ra, Rb, theta-a, theta-b

```

```

-1 0 0.0 0.0 0 0 0 $M-5 SHELL WALL RECORD, USE GCP FAB. # 1
410 0 0 $N-1 DISCRETIZATION RECORD, ELEMENT SELECTION
3 6 3 6 $P-1 symmetric quarter of a ring simulation
1 0 0 0 $Q-1 No applied load - free vibration
1 3
0.0 -1 3 0 0
0.0 -1 4 0 0
0.0 -1 5 0 0
CC0.0 -1 6 0 0
1 0 0 0 $R-1 OUTPUT CONTROL FOR SHELL UNIT 1

```

ring2d.bin (for S2 processor)

```

Circular ring free vibration problem - 1-D model $A-1
C
C Thin 90-deg segment of circular ring, free vibration problem
C
C REF.: Timoshenko, Young, and Weaver, "Vibration Problems
C in Engineering," 1974.
C
2 1 0 0 0 0 0 -1 $b-1 free vibration analysis
1.0 1.0 1.0 $c-1 load factors
100 1.0e-4 0 $d-2 eigenvalue control
16 -1.0 $d-3 cluster definition

```

ring2d.pin (for STAPL processor)

```

Straight cantilevered beam - free vibration problem
16 0 0 0 $P1-2 NPLOT,IPREP,IPRS,KDEV
1 0 4 0 1 0 0 0 $P1-3 KPLOT,VIEW,ITEM,STEP,MODE,IFRNG,COLOR,ICOMP
0.0 3 0.0 0.0 0.0 $P1-5 DSCALE,NROTS,LWSCALE,RNGMIN,RGMAX
1 0.0 / 2 90.0 / 3 0.0
1 0 4 0 2 0 0 0 $P1-3 KPLOT,VIEW,ITEM,STEP,MODE,IFRNG,COLOR,ICOMP
0.0 3 0.0 0.0 0.0 $P1-5 DSCALE,NROTS,LWSCALE,RNGMIN,RGMAX
1 0.0 / 2 90.0 / 3 0.0
1 0 4 0 3 0 0 0 $P1-3 KPLOT,VIEW,ITEM,STEP,MODE,IFRNG,COLOR,ICOMP
0.0 3 0.0 0.0 0.0 $P1-5 DSCALE,NROTS,LWSCALE,RNGMIN,RGMAX
1 0.0 / 2 90.0 / 3 0.0
1 0 4 0 4 0 0 0 $P1-3 KPLOT,VIEW,ITEM,STEP,MODE,IFRNG,COLOR,ICOMP
0.0 3 0.0 0.0 0.0 $P1-5 DSCALE,NROTS,LWSCALE,RNGMIN,RGMAX
1 0.0 / 2 90.0 / 3 0.0
1 0 4 0 5 0 0 0 $P1-3 KPLOT,VIEW,ITEM,STEP,MODE,IFRNG,COLOR,ICOMP
0.0 3 0.0 0.0 0.0 $P1-5 DSCALE,NROTS,LWSCALE,RNGMIN,RGMAX
1 0.0 / 2 90.0 / 3 0.0
1 0 4 0 6 0 0 0 $P1-3 KPLOT,VIEW,ITEM,STEP,MODE,IFRNG,COLOR,ICOMP
0.0 3 0.0 0.0 0.0 $P1-5 DSCALE,NROTS,LWSCALE,RNGMIN,RGMAX
1 0.0 / 2 90.0 / 3 0.0
1 0 4 0 7 0 0 0 $P1-3 KPLOT,VIEW,ITEM,STEP,MODE,IFRNG,COLOR,ICOMP
0.0 3 0.0 0.0 0.0 $P1-5 DSCALE,NROTS,LWSCALE,RNGMIN,RGMAX
1 0.0 / 2 90.0 / 3 0.0
1 0 4 0 8 0 0 0 $P1-3 KPLOT,VIEW,ITEM,STEP,MODE,IFRNG,COLOR,ICOMP
0.0 3 0.0 0.0 0.0 $P1-5 DSCALE,NROTS,LWSCALE,RNGMIN,RGMAX
1 0.0 / 2 90.0 / 3 0.0
1 0 4 0 9 0 0 0 $P1-3 KPLOT,VIEW,ITEM,STEP,MODE,IFRNG,COLOR,ICOMP
0.0 3 0.0 0.0 0.0 $P1-5 DSCALE,NROTS,LWSCALE,RNGMIN,RGMAX
1 0.0 / 2 90.0 / 3 0.0
1 0 4 0 10 0 0 0 $P1-3 KPLOT,VIEW,ITEM,STEP,MODE,IFRNG,COLOR,ICOMP
0.0 3 0.0 0.0 0.0 $P1-5 DSCALE,NROTS,LWSCALE,RNGMIN,RGMAX
1 0.0 / 2 90.0 / 3 0.0
1 0 4 0 11 0 0 0 $P1-3 KPLOT,VIEW,ITEM,STEP,MODE,IFRNG,COLOR,ICOMP
0.0 3 0.0 0.0 0.0 $P1-5 DSCALE,NROTS,LWSCALE,RNGMIN,RGMAX

```

```

1 0.0 / 2 90.0 / 3 0.0
1 0 4 0 12 0 0 0 $PL-3 KPLOT,VIEW,ITEM,STEP,MODE,IFRNG,COLOR,ICOMP
0.0 3 0.0 0.0 0.0 $PL-5 DSCALE,NROTS,LWSCALE,RNGMIN,RGMAX
1 0.0 / 2 90.0 / 3 0.0
1 0 4 0 13 0 0 0 $PL-3 KPLOT,VIEW,ITEM,STEP,MODE,IFRNG,COLOR,ICOMP
0.0 3 0.0 0.0 0.0 $PL-5 DSCALE,NROTS,LWSCALE,RNGMIN,RGMAX
1 0.0 / 2 90.0 / 3 0.0
1 0 4 0 14 0 0 0 $PL-3 KPLOT,VIEW,ITEM,STEP,MODE,IFRNG,COLOR,ICOMP
0.0 3 0.0 0.0 0.0 $PL-5 DSCALE,NROTS,LWSCALE,RNGMIN,RGMAX
1 0.0 / 2 90.0 / 3 0.0
1 0 4 0 15 0 0 0 $PL-3 KPLOT,VIEW,ITEM,STEP,MODE,IFRNG,COLOR,ICOMP
0.0 3 0.0 0.0 0.0 $PL-5 DSCALE,NROTS,LWSCALE,RNGMIN,RGMAX
1 0.0 / 2 90.0 / 3 0.0
1 0 4 0 16 0 0 0 $PL-3 KPLOT,VIEW,ITEM,STEP,MODE,IFRNG,COLOR,ICOMP
0.0 3 0.0 0.0 0.0 $PL-5 DSCALE,NROTS,LWSCALE,RNGMIN,RGMAX
1 0.0 / 2 90.0 / 3 0.0

```

Problem References

Timoshenko, S., Young, D. H., and Weaver, W., Jr., *Vibration Problems in Engineering*, Fourth Edition, John Wiley & Sons, Inc., New York, 1974.

Buckling of Blade-Stiffened Flat Panels

Background

Stiffened panels are a common configuration in the aerospace industry. Stiffened panels may be modeled in at least three ways. One way is to *smear* the stiffener stiffness over the panel skin – smeared-stiffener model. Another way is to model the stiffeners as discrete beams located along discrete lines in the model and without cross-sectional deformations – discrete-stiffener model. The third way is to model the stiffeners using shell elements – branched-plate model. Stroud, Greene, and Anderson (1984) studied several stiffened-panel configurations subjected to in-plane compression and shear loads. Their results are often cited as reference solutions for comparative purposes. The basic geometry of the panel and the repeating blade-stiffener segment considered in this study are defined in Figure 13 using U. S. customary units.

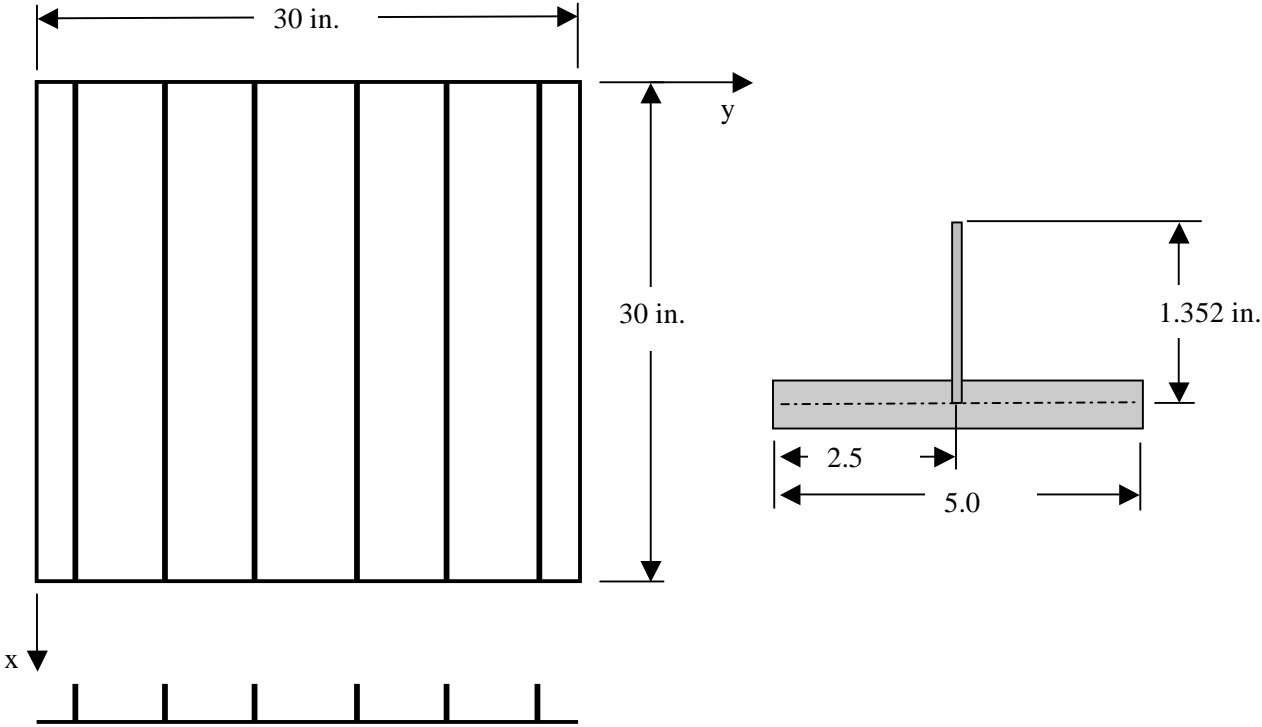


Figure 13. Blade-stiffened panel problem: geometry and repeating element – all dimensions are given in inches.

These demonstration test cases involve a flat, square panel with six blade stiffeners (six repeating elements). The panel has a length L equal to 30 inches and an overall panel width W of 30 inches (six repeating elements of width 5.0 inches). No offsets are assumed for attaching the blade stiffeners to the panel skin in the branched-plate model approach (*i.e.*, there is a small amount of overlapping of material at their connection point). The reference surface of the panel skin is defined as the middle surface of the skin. Three panel configurations are considered.

Panel 1 corresponds to Example 1 in NASA TP-2215 – a composite blade-stiffened panel. The panel skin and blade stiffeners are laminated composite structures. The material definitions for the panel skin and stiffener have the same linear elastic mechanical properties for an orthotropic material: $E_1=19.0$ Msi, $E_2=1.89$ Msi, $G_{12}=0.93$ Msi, $\nu_{12}=0.38$, and $\nu_{21}=0.0378$. The fabrication of the panel skin is a laminated composite with a stacking sequence defined as $[\pm 45 / \mp 45 / 0 / 90_9]_s$ – a 28-ply laminate, and the stacking sequence of the blade stiffeners is defined as $[\pm 45 / \mp 45 / 0_2]_s$ – a 12-ply laminate. The average ply thickness is 0.0055 inches. Two loading cases are considered here. The pure compression case ($N_x=1000$ lb/in.) results in a load distribution of 811.35 lb/in. in each skin segment and 697.67 lb/in. in each blade stiffener according to NASA TP-2215. The buckling load factor is 1.0030 with an overall Euler buckling mode shape obtained from the EAL finite element code. The pure shear case ($N_{xy}=1000$ lb/in.) results in all the load going into the skin segments and nothing in the blade stiffeners. The buckling load factor is 1.5525 with a skewed mode shape having one halfwave in the stiffener direction and two halfwaves across the panel.

Panel 2 corresponds to Example 2 in NASA TP-2215 – a metal blade-stiffened panel with a thick skin. The panel skin is 0.084-inches thick, and the blade stiffeners are 0.058-inches thick. The material definitions for the panel skin, and blade stiffeners are the same linear elastic mechanical properties for an isotropic material: $E=10.5$ Msi and $\nu=0.32$. The pure compression case ($N_x=1000$ lb/in.) results in a load distribution of 842.67 lb/in. in each skin segment and 581.84 lb/in. in each blade stiffener according to NASA TP-2215. The buckling load factor is 0.9759 with an overall Euler buckling mode shape obtained from the EAL finite element code. The pure shear case ($N_{xy}=1000$ lb/in.) results in all the load going into the skin segments and nothing in the blade stiffeners. The buckling load factor is 0.8138 with a skewed mode shape having one halfwave in the stiffener direction and three halfwaves across the panel.

Panel 3 corresponds to Example 4 in NASA TP-2215 – a metal blade-stiffened panel with a thin skin. The panel skin is 0.050-inches thick, and the blade stiffeners are 0.058-inches thick. The material definitions from Panel 2 are used here as well. The pure compression case ($N_x=1000$ lb/in.) results in a load distribution of 761.23 lb/in. in each skin segment and 883.03 lb/in. in each blade stiffener according to NASA TP-2215. The buckling load factor is 0.2965 with an stiffened panel buckling mode shape having six halfwaves between each stiffener obtained from the EAL finite element code (Whetstone, 1986). The pure shear case ($N_{xy}=1000$ lb/in.) results in all the load going into the panel skin segments and nothing in the blade stiffeners. The buckling load factor is 0.2767 with a skewed mode shape having one halfwave in the stiffener direction and four halfwaves across the panel.

The reference solutions obtained by Stroud, Greene, and Anderson (1984) for linear bifurcation buckling loads and buckling mode shapes are used for comparison.

Modeling and Analysis Process

Three separate STAGS finite element models are considered in these demonstration test case problems: smeared-stiffener model, discrete-stiffener model, and branched-plate model. The basic finite element discretization for the panel skin is the same in each modeling approach – 36 elements across the panel length and width. A summary of each model includes:

Smearred-stiffener model – Model the stiffened panel with a single shell unit for the panel skin and STAGS automatically “smears” the stiffness of the blade stiffeners across the panel skin. Each stiffener is defined in STAGS in the same manner as would be required for the discrete-stiffener model. A rectangular subelement is defined using the J-1 and J-3b records for the metal stiffeners and STAGS internally computes and outputs the beam stiffnesses. For the composite panel, the general stiffness option for defining beam stiffnesses ($EA, EI_{yy}, EI_{zz}, EI_{yz}, GJ$) using the J-1 and J-2b records. These properties are defined relative to the stiffener cross-sectional centroid. The stiffener spacing and eccentricity relative to the shell reference surface are defined using the K-6 record as part of the panel skin fabrication data. This model will predict general buckling behavior but no skin-stiffener buckling modes – essentially orthotropic panel buckling mode shapes. This model is shown in Figure 14.

Discrete-stiffener model – Model the stiffened panel with a single shell unit for the panel skin and model the blade stiffeners as discrete beams located along discrete lines on the panel skin (lines of constant values of y). The blade stiffeners are defined using the J records as in the smearred-stiffener model. These discrete-beam stiffeners are located on the shell reference surface using the O-2a and O-2b records. This discrete-stiffener model will predict general and skin-stiffener buckling mode shapes – essentially stiffened-panel buckling mode shapes but no cross-sectional deformation of the stiffeners is permitted and skin-stiffener interaction is limited to the nodal line attaching each stiffener. This model is shown in Figure 15 with the discrete-beam stiffeners shown as darker lines.

Branched-plate model – Model the stiffened panel with multiple shell units – for both panel skin and stiffeners. Two approaches could be used. First, each segment could be individually modeled (*e.g.*, skin, blade, skin, blade, etc.). This would result in seven shell units for the various panel skin segments and six shell units for the stiffeners (one for each blade stiffener) – total of 13 shell units. The other approach would be model the skin as a single shell unit with the six stiffener shell units attached within the skin shell unit. The model using 13 shell units (each shell unit is indicated by a different color or shade) used in these studies is shown in Figure 16. There are two 4-node shell elements (three columns of nodes) across the blade-stiffener height in the branched-plate model. The same finite element model is used for the composite and metal panels with changes in the shell fabrication number and the membrane loads for the panel skin and blade stiffeners.

In the analysis of this structure using either the discrete-stiffener or smearred-stiffener modeling approach, the stiffness terms of the blade stiffener need to be provided to STAGS. For the metal panel case, the rectangular geometry of the blade stiffener can be defined to STAGS and STAGS will compute the necessary terms. The x -direction is along the stiffener axis, the z -direction is perpendicular to the panel skin, and the y -direction is perpendicular to the x - z plane of the stiffener. The quantities needed include:

$$A = bt \quad I_{yy} = \frac{b^3t}{12} \quad I_{zz} = \frac{bt^3}{12} \quad I_{yz} = 0 \quad J = \frac{bt^3}{3}$$

where b is the blade width or height (1.352 in.) and t is the blade thickness (0.058 in.). The centroid of the blade cross-sectional area is $b/2$ (0.676 inches) above the panel skin reference surface.

For the composite panel case, the blade stiffeners are also laminated structures. Currently there is no automatic feature in STAGS to treat laminated beams. The approach used herein is define the laminate of the blade and perform a laminate analysis using STAGS in order to obtain the coefficients of the so-called ABD matrices. A *dummy* material is defined with all moduli defined as a million and the Poisson’s ratio set to zero (see the I-records). Then the stiffness terms for the composite blades are computed as followed:

$$EA = b \left[A_{11} - \frac{(A_{12})^2}{A_{22}} \right]$$

$$EI_{yy} = \frac{1}{12} EAb^2 \quad EI_{zz} = D_{11}b \quad EI_{yz} = 0$$

$$GJ = 4b \left[\frac{D_{12}}{2} + D_{66} \right]$$

Taking the computed values from these evaluations and dividing by a million gives the values used on the J-records since the dummy material terms are defined as a million. The centroid of the blade cross-sectional area is $b/2$ (0.676 inches) above the panel skin reference surface.

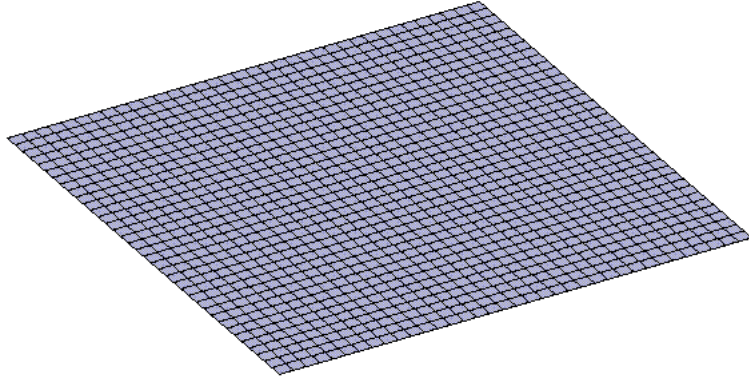


Figure 14. Model of blade-stiffened panel using smeared-stiffener-modeling approach.

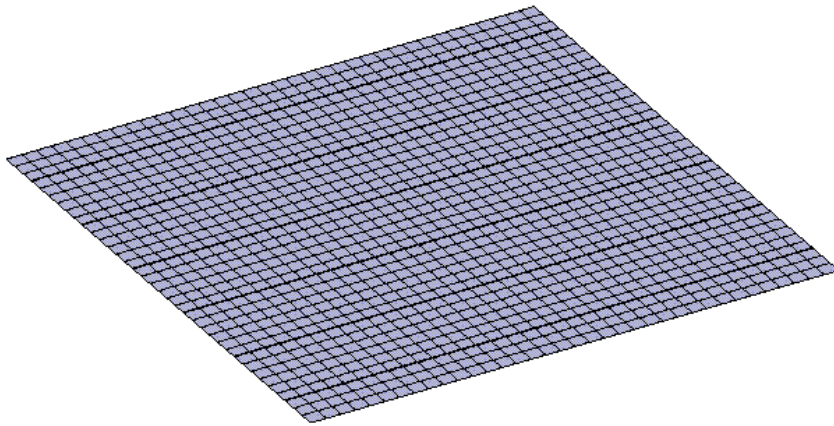


Figure 15. Model of blade-stiffened panel using discrete-stiffener-modeling approach.

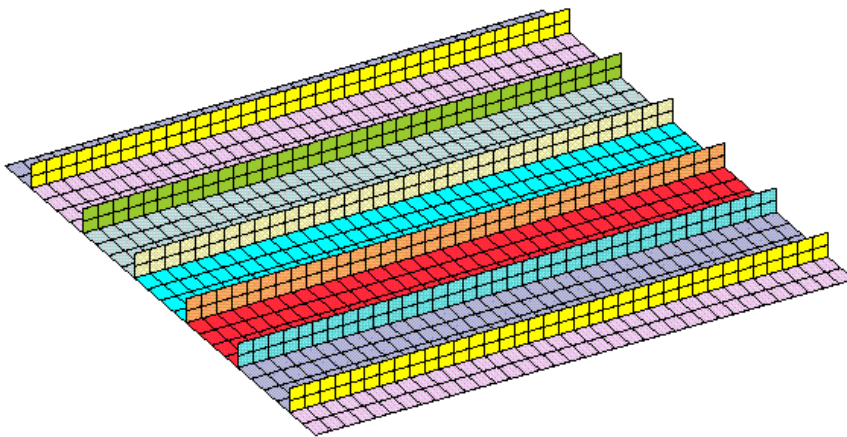


Figure 16. Model of blade-stiffened panel using branched-plate-modeling approach.

Material properties and laminate construction are defined using both the *historical* STAGS approach (*i.e.*, STAGS versions prior to GCP) and the current GCP approach. Material modeling for an elastic orthotropic material using the historical STAGS approach requires data on the I-1 and I-2 records to define the material properties and the K-1 and K-2 records to define the laminate fabrication data. Material modeling using the current GCP approach requires data on the I-5a and I-6a records to define the material properties and the I-5a, I-21a, I-21b, I-21c, I-21d, and I-21e records to define the fabrication.

The blade stiffeners have a rectangular cross-sectional area. For the metal panels, the stiffeners have a thickness of 0.58 inches and a height of 1.352 inches. Using the J-1 and J-3b records, the corners of the rectangular subelement are defined with the origin of the stiffener cross-sectional coordinate systems located at the subelement's center. Input on the K-6 record identifies the offset of the stiffener center from the shell reference surface.

Loading is specified as a uniform membrane pre-buckling load in the panel skin and blade stiffeners. It is specified using the Q-1 and Q-5 records. Boundary condition on the displacements are specified using the P-1 and P-2 records. The buckling boundary conditions along the four edges of the panel skin are simply supported and defined by:

$$\text{At } x=0, L; v=w=\theta_x=0$$

$$\text{At } y=0, W; u=w=\theta_y=0$$

Numerical Results and Discussion

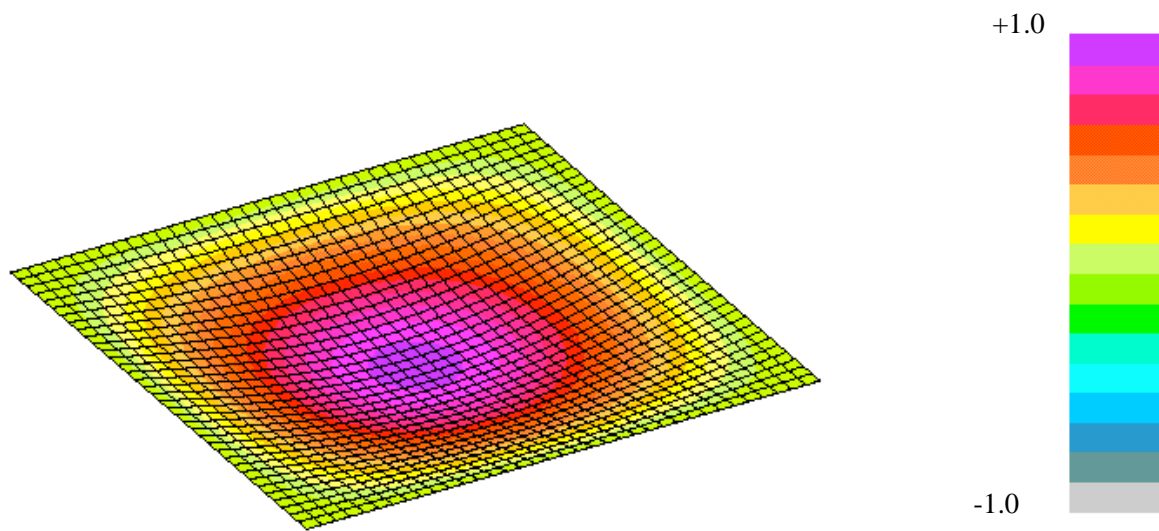
The uniform pre-buckling membrane stress distributions in the panel skin and blade stiffeners are taken from Stroud, Greene, and Anderson (1984). For a pre-stress in-plane longitudinal stress resultant loading of $N_x=1000$ lb/in., the load distribution between the panel skin and the blade stiffeners has been given earlier and depends on the fabrication of the skin and stiffeners. For a pre-stress in-plane shear stress resultant loading of $N_{xy}=1000$ lb/in., the entire in-plane shear load is carried by the panel skin and no shear load is carried by the blade stiffeners. The eigenvalue analysis has a convergence tolerance of 10^{-4} and the number of eigenpairs requested is four. No shift is used in the eigen solution.

A summary of the buckling analysis results is given in Table 8. These results are consistent with the finite element reported by Stroud, Greene and Anderson (1984) using the EAL finite element code. Buckling mode shapes for compression and shear loadings are shown in Figures 17 and 18 for the smeared-stiffener model, in Figures 19 and 20 for the discrete-stiffener model, and in Figures 21 and 22 for the branched-plate model. The smeared-stiffener model essentially gives an orthotropic plate solution that in some cases is sufficient. The discrete-stiffener model does permit stiffened-panel-buckling modes to be predicted (modes with local skin buckling between stiffeners). The branched-plate model permits stiffened-panel-buckling modes to be predicted as well as cross-sectional deformations within the plane-stress formulation used to model the cross-sectional elements of the stiffeners.

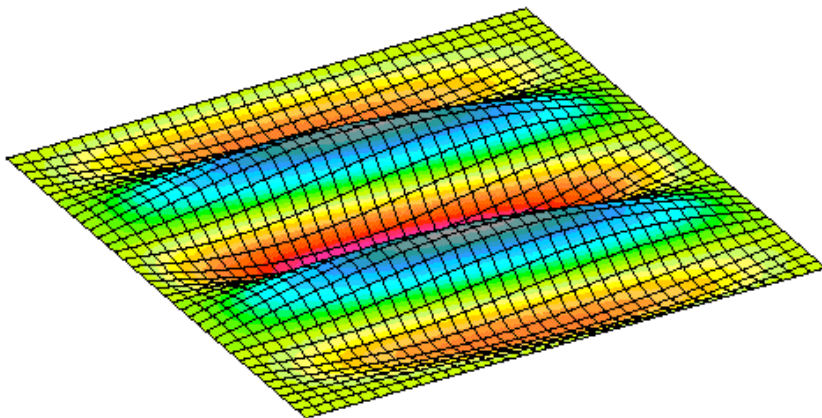
Table 8. Summary of buckling factors for compression and shear loads for three different panel configurations using different finite element modeling approaches.

Panel No.	Applied Load, lb/in.		Buckling Factor				
			NASA TP-2215		STAGS		
	N_x	N_{xy}	Smeared	EAL	Smeared	Discrete	Branched
1	1000	0	0.9970	1.0030	1.0268	0.8499	1.0189
1	0	1000	1.4683	1.5525	1.6924	1.6279	1.5805
2	1000	0	0.9969	0.9759	1.0094	0.8269	0.9807
2	0	1000	0.9823	0.8138	1.0690	0.8651	0.8309
3	1000	0	0.9097	0.2965	0.9270	0.3008	0.3121
3	0	1000	0.6062	0.2767	0.6825	0.3208	0.2906

Buckling analyses were performed for different panels under different loading conditions and using different finite element modeling approaches. The results are summarized in Table 8 and are shown to be consistent with results from NASA TP-2215. Contour plots of the out-of-plane component of the buckling mode shapes corresponding to both compression and shear load cases are shown in Figures 17 through 23. Under compression load, the smeared-stiffener models predict a overall buckling mode shape with one half wave in each direction (see Figures 17a and 18a). Under shear loading, the smeared-stiffener models predict one longitudinal half wave and several half waves across the panel perpendicular to the stiffener direction (see Figures 17b and 18b). As the fidelity of the finite element model is increased to a discrete-stiffener model, Panels 3 and 2 still exhibit long wavelength shear buckles as shown in Figures 19b and 20b, respectively. However, Panel 3 (metal panel with a thin skin) exhibits a stiffened panel buckling model with eight half waves along the panel length and one half wave between stiffeners (see Figure 19a). The thick skin panel (Panel 2) exhibits an overall buckling mode (see Figure 20a). Increasing the modeling fidelity further to a branched-plate model allows cross-sectional deformations of the blade stiffeners to be simulated. The buckling modes are shown in Figures 21 through 23 for Panels 3, 2, and 1, respectively. The compression-loaded Panels 2 and 1 exhibit Euler buckling mode shapes and demonstrate the need to plate elements to be capable of buckling in their own plane.

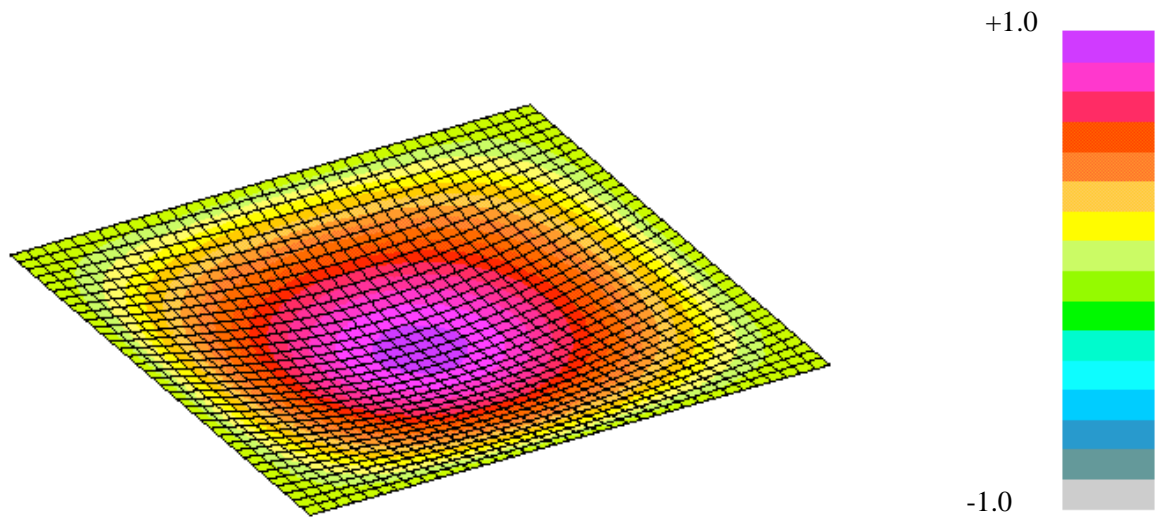


(a) Pure membrane compression prebuckling stress state, $N_x=1000$ lb/in.

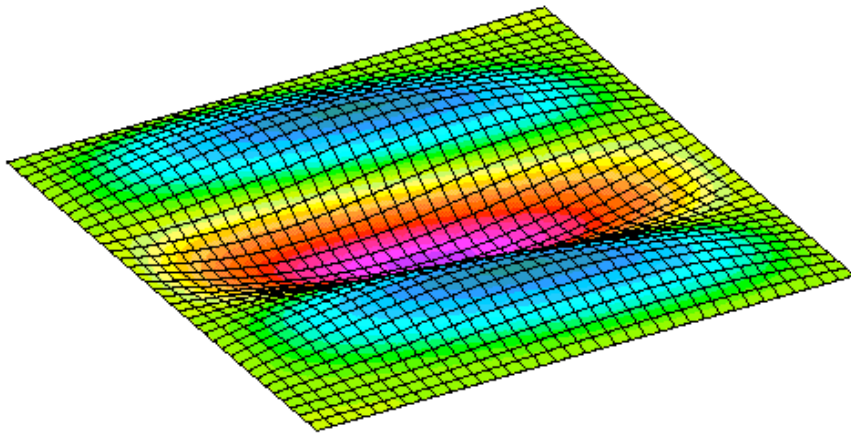


(b) Pure membrane shear prebuckling stress state, $N_{xy}=1000$ lb/in.

Figure 17. Buckling mode shapes for the metal blade-stiffened panel with a thin skin (Panel 3) obtained using the smeared-stiffener modeling approach.

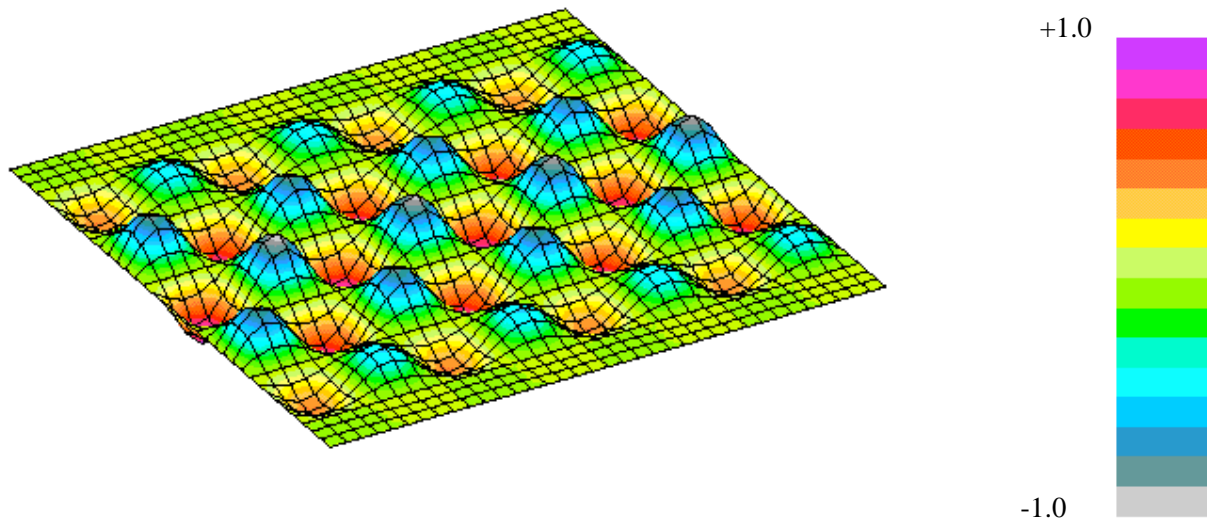


(a) Pure membrane compression prebuckling stress state, $N_x=1000$ lb/in.

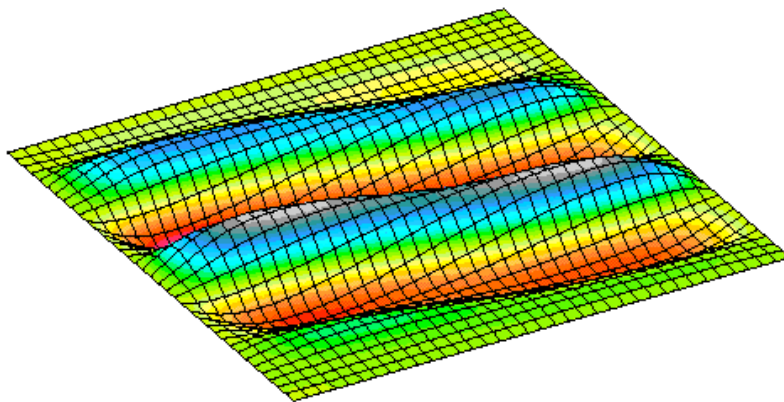


(b) Pure membrane shear prebuckling stress state, $N_{xy}=1000$ lb/in.

Figure 18. Buckling mode shapes for the metal blade-stiffened panel with a thick skin (Panel 2) obtained using the smeared-stiffener modeling approach.

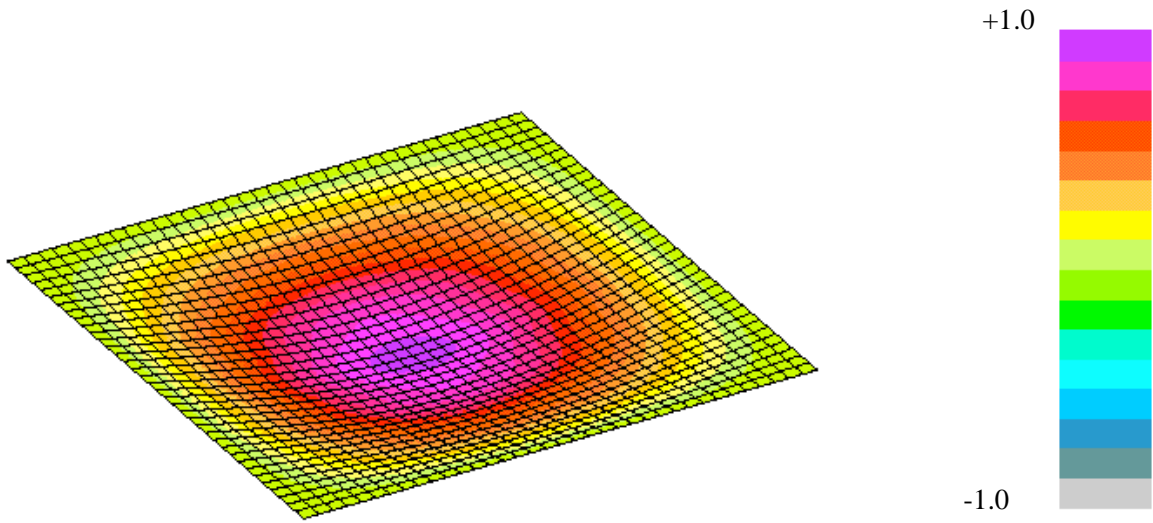


(a) Pure membrane compression prebuckling stress state, $N_x=1000$ lb/in.

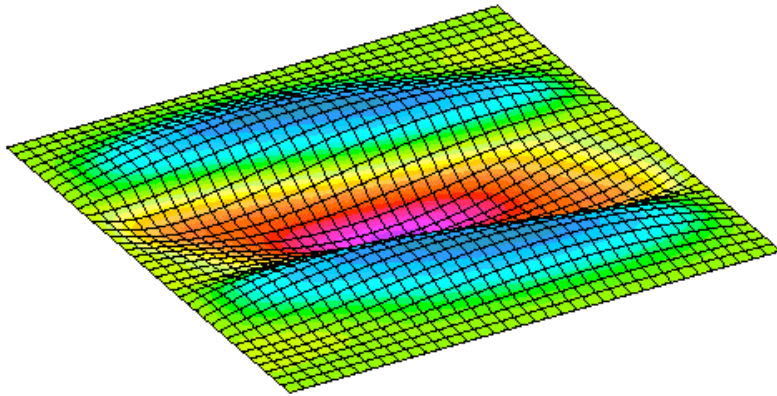


(b) Pure membrane shear prebuckling stress state, $N_{xy}=1000$ lb/in.

Figure 19. Buckling mode shapes for the metal blade-stiffened panel with a thin skin (Panel 3) obtained using the discrete-stiffener modeling approach.

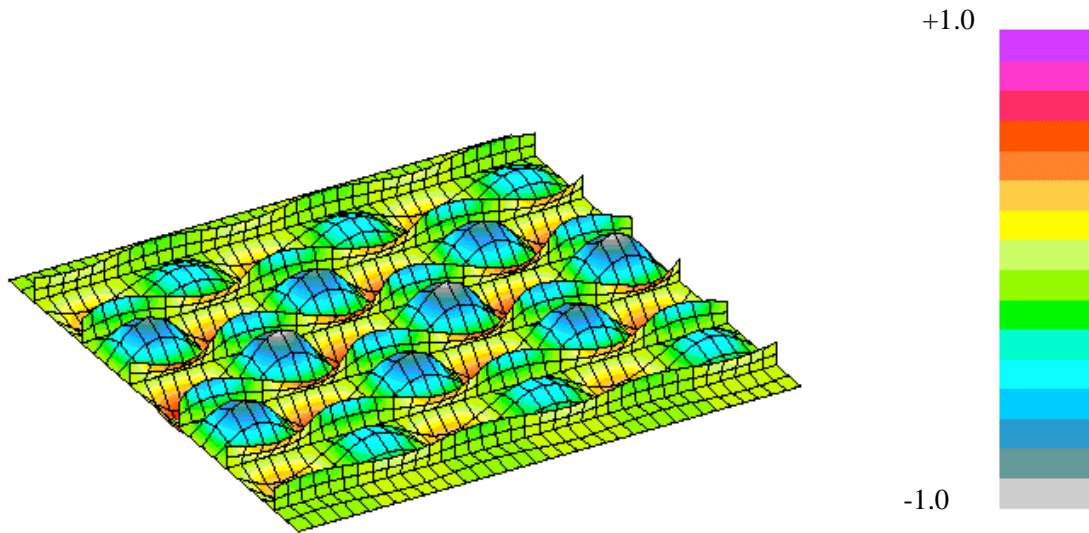


(a) Pure membrane compression prebuckling stress state, $N_x=1000$ lb/in.

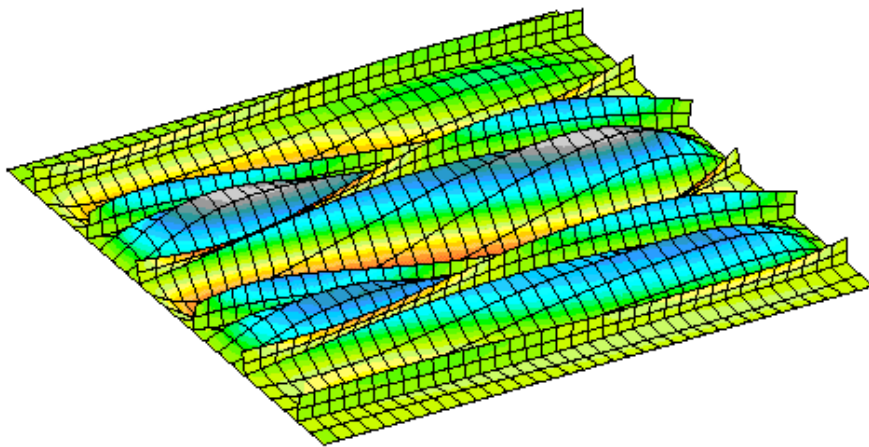


(b) Pure membrane shear prebuckling stress state, $N_{xy}=1000$ lb/in.

Figure 20. Buckling mode shapes for the metal blade-stiffened panel with a thick skin (Panel 2) obtained using the discrete-stiffener modeling approach.

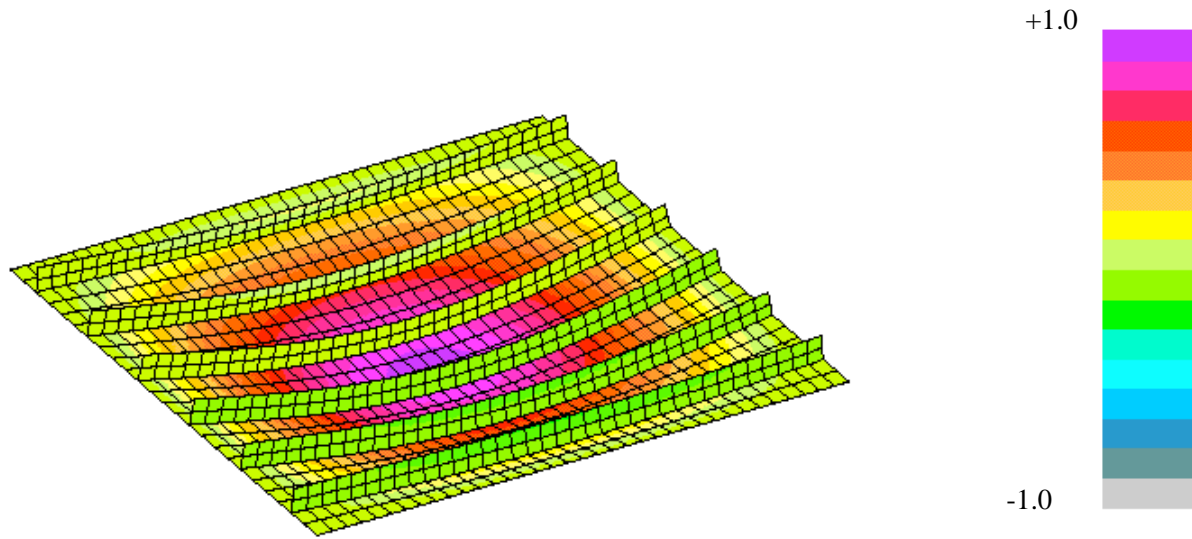


(a) Pure membrane compression prebuckling stress state, $N_x=1000$ lb/in.

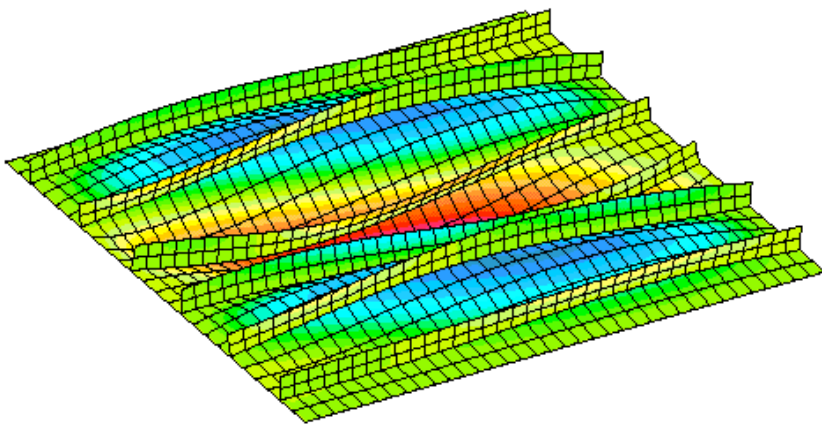


(b) Pure membrane shear prebuckling stress state, $N_{xy}=1000$ lb/in.

Figure 21. Buckling mode shapes for the metal blade-stiffened panel with a thin skin (Panel 3) obtained using the branched-plate modeling approach.

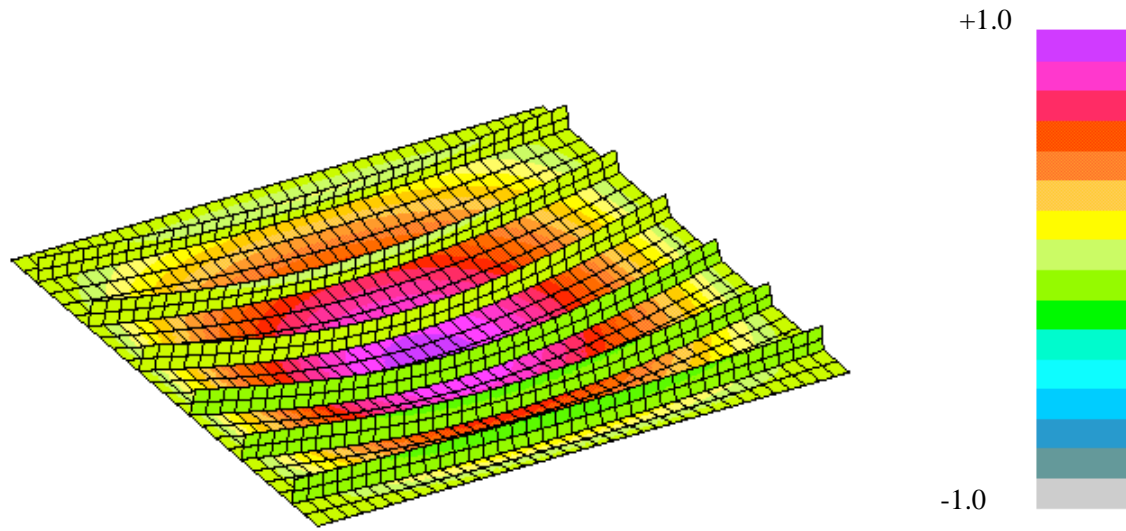


(a) Pure membrane compression prebuckling stress state, $N_x=1000$ lb/in.

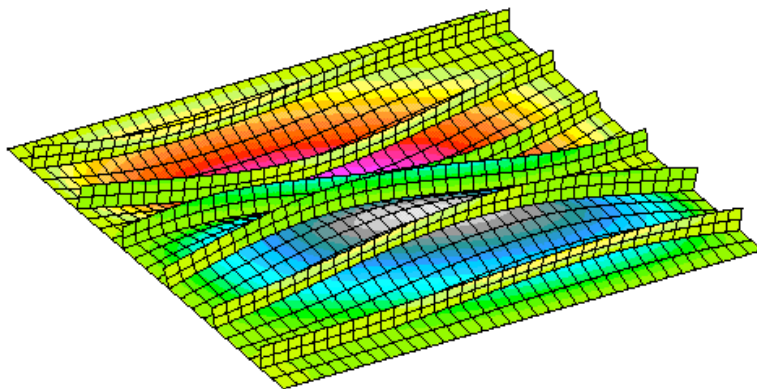


(b) Pure membrane shear prebuckling stress state, $N_{xy}=1000$ lb/in.

Figure 22. Buckling mode shapes for the metal blade-stiffened panel with a thick skin (Panel 2) obtained using the branched-plate modeling approach.



(a) Pure membrane compression prebuckling stress state, $N_x=1000$ lb/in.



(b) Pure membrane shear prebuckling stress state, $N_{xy}=1000$ lb/in.

Figure 23. Buckling mode shapes for the composite blade-stiffened panel (Panel 1) obtained using the branched-plate modeling approach.

STAGS Input Files

The STAGS input files are provided in several subdirectories based on the panel configuration (Panel 1, Panel 2, or Panel 3), pre-buckling membrane stress state (compression or shear), and modeling approach (branched plate approach, discrete-stiffener approach, or smeared-stiffener approach). These subdirectories are located under the following subdirectory:

\$STAGSHOME/Sample-Testcases/Stiffened-panel

Subdirectories for this test case are organized by specific panel number (Panel-1, Panel-2, or Panel-3). Under each panel number subdirectory the two load cases (Compression and Shear) are defined as subdirectories. Then under each load case, an additional subdirectory structure is defined for the different structural modeling approaches (Branched-plate, Discrete-stiffener, and Smeared-stiffener). Representative input file listings are provided to illustrate the various modeling approaches and required STAGS input records.

Branched Model of Panel 1 (composite)

Panel 1 is a composite blade-stiffened panel with a laminated panel skin and laminated blade stiffeners. This configuration corresponds to Example 1 in NASA TP-2215. The input file included here is for the uniform compression case with an overall N_x membrane loading of -1000 lb/in. This compression load is carried partly by the skin and partly by the stiffeners as indicated by the load magnitudes specified on the Q-5 records. The load distributions were taken from NASA TP-2215. These input files are given in:

../Stiffened-panel/Panel-1/Compression/Branched-plate

cbranched.inp (for S1 processor)

```
Blade stiffened panel with laminated skin - TP 2215 Example 1 $a-1
0 0 0 0 0 3 $b-1
1 -240.0 / 2 0.0 / 3 -30.0 $b-1b model rotations
13 0 0 12 0 $b-2
3 2 5 0 0 1 $b-3
37 3 37 3 37 5 37 3 37 5 37 3 37 5 ,
37 3 37 5 37 3 37 5 37 3 37 3 $f-1
1 2 2 4 $g-1 connections
1 2 3 4
3 2 4 4
3 2 5 4
5 2 6 4
5 2 7 4
7 2 8 4
7 2 9 4
9 2 10 4
9 2 11 4
11 2 12 4
11 2 13 4 $ g-1 connections
C
C Material definition for Example 2 and 4
C
1 $i-1 material data
10.5e6 .32 $i-2 aluminium
C
C Material definition for Example 1
C
2 $i-1 G/E material data
```

```

19.0E+6  0.0378  0.93E+6  0.1  0.0  1.89E+6  $i-2
C
C Dummy material data tas multipliers for composite stringer
C stiffness terms (EA, EIyy, EIZZ, GJ)
C
3 $i-1 dummy material multipliers
1.0E6  0.0  1.0E6  0.1  0.0  1.0E6  $i-2
C
C ---- GCP Input -----
C
C Material for Examples 2 and 4
C
ISOELASTIC  1  1  1  $I-5
10.5E+6  0.32  2.0E-5  4*0.0  $i-6a  E, Nu, rho
C
C Material for Example 1
C
ORTHOELAST  2  1  1  $I-5
19.0E6  1.89E6  1.89E6,  $I-7a  E11, E22, E33
0.93E6  0.93E6  0.93E6,  $I-7a  G12, G13, G23
0.38  0.38  0.38,  $I-7a  nu12, nu13, nu23
2.0E-5,  $i-7a  rho
3*0.0,  $i-7a  CTE's
3*0.0,  $i-7a  CME's
0.0  0.0  $i-7a  ref. temp. and moisture
C
C Fabrication data
C
SHELL_FABRICATION  1  1  0  0  0  $I-21a  Panel skin for Example 2
1  $I-21a  isotropic material
0.084  $I-21c  thick skin
0.0  $i-21d
SHELL_FABRICATION  2  1  0  0  0  $I-21a  Panel skin for Example 2
1  $I-21a  isotropic material
0.050  $I-21c  thin skin
0.0  $i-21d
SHELL_FABRICATION  3  1  0  0  0  $I-21a  Blade stiffeners for Examples 2 and 4
1  $I-21a  isotropic material
0.058  $I-21c  blade stiffeners
0.0  $i-21d
SHELL_FABRICATION  4  28  0  0  0  $I-21a  Panel skin for Example 1
28*2  $I-21a  orthotropic material
28*0.0055  $I-21c  laminated skin [ +/-45 / -/+45 /0/90_9]_s
+45. -45. -45. 45. 0.0 ,  $i-21d
90. 90. 90. 90. 90. 90. 90. 90. ,  $i-21d
90. 90. 90. 90. 90. 90. 90. 90. ,  $i-21d
0.0 +45. -45. -45. 45.  $i-21d
SHELL_FABRICATION  5  12  0  0  0  $I-21a  Blade stiffeners for Example 1
12*2  $I-21a  orthotropic material
12*0.0055  $I-21c  laminated stiffener [ +/-45 / -/+45 /0_2]_s
+45. -45. -45. 45. 0.0 0.0 ,  $i-21d
0.0 0.0 +45. -45. -45. 45.  $i-21d
END
C
C --- End GCP input ---
C
C metal stringers
C
1 3 1 1 8.5481e-5 0.0 0.0 $j-1 stringer stiffener
-.029 +.029 -0.676 +0.676 $j-3b
C
C composite stringers
C

```

```

2 1 3 0 0.00092 0.0 0.0 $j-1 general stiffener
0.7609 0.1159 0.00023 0.0 $j-2a A, Iyy, Izz, Iyz
C
C Fabrication definitions
C (thick skin; thin skin; stringer)
C
1 1 1 $k-1 panel skin thickness - Example 2
1 0.084 $k-2 thick skin
2 1 1 $k-1 panel skin thickness - Example 4
1 0.050 $k-2 thin skin
3 1 1 $k-1 blade stringer thickness - Examples 2 & 4
1 0.058 $k-2
4 1 28 $k-1 laminated panel skin - Example 1
2 0.0055 +45.0 $k-2
2 0.0055 -45.0 $k-2
2 0.0055 -45.0 $k-2
2 0.0055 +45.0 $k-2
2 0.0055 0.0 $k-2
2 0.0055 90.0 $k-2
2 0.0055 90.0 $k-2
2 0.0055 90.0 $k-2
2 0.0055 90.0 $k-2
2 0.0055 90.0 $k-2
2 0.0055 90.0 $k-2
2 0.0055 90.0 $k-2
2 0.0055 90.0 $k-2
2 0.0055 90.0 $k-2
2 0.0055 90.0 $k-2
2 0.0055 90.0 $k-2
2 0.0055 90.0 $k-2
2 0.0055 90.0 $k-2
2 0.0055 90.0 $k-2
2 0.0055 90.0 $k-2
2 0.0055 90.0 $k-2
2 0.0055 90.0 $k-2
2 0.0055 0.0 $k-2
2 0.0055 +45.0 $k-2
2 0.0055 -45.0 $k-2
2 0.0055 -45.0 $k-2
2 0.0055 +45.0 $k-2
5 1 12 $k-1 laminated stringer - Example 1
2 0.0055 +45.0 $k-2
2 0.0055 -45.0 $k-2
2 0.0055 -45.0 $k-2
2 0.0055 +45.0 $k-2
2 0.0055 0.0 $k-2
2 0.0055 0.0 $k-2
2 0.0055 0.0 $k-2
2 0.0055 0.0 $k-2
2 0.0055 +45.0 $k-2
2 0.0055 -45.0 $k-2
2 0.0055 -45.0 $k-2
2 0.0055 +45.0 $k-2
C
C ----- Define shell units: skin segment then stringer, etc
C
C
C Panel Skin Segment
C
2 $m-1
0.0 30.0 0.0 2.5 $m-2
4 $m-5 laminated panel skin

```



```

410 $n-1
1 6 1 1 $p-1
0 0 0 1 $q-1
-811.35 0.0 0.0 $q-5 Nx in skin for overall Nx=1000
1 $r-1
C
C Stringer Segment
C
2 4$m-1
0.0 30.0 0.0 1.352 $m-2
0.0 2.5 0.0 $m-4d iglobe=4
-90.0 0.0 0.0 $m-4e
5 $m-5 laminated stringer
410 $n-1
1 3 1 6 $p-1
0 0 0 1 $q-1
-697.67 0.0 0.0 $q-5 Nx in stringer for overall Nx=1000
1 $r-1
C
C Panel Skin Segment
C
2 4$m-1
0.0 30.0 0.0 5.0 $m-2
0.0 2.5 0.0 $m-4d iglobe=4
0.0 0.0 0.0 $m-4e
4 $m-5 laminated panel skin
410 $n-1
1 6 1 6 $p-1
0 0 0 1 $q-1
-811.35 0.0 0.0 $q-5 Nx in skin for overall Nx=1000
1 $r-1
C
C Stringer Segment
C
2 4$m-1
0.0 30.0 0.0 1.352 $m-2
0.0 7.5 0.0 $m-4d iglobe=4
-90.0 0.0 0.0 $m-4e
5 $m-5 laminated stringer
410 $n-1
1 3 1 6 $p-1
0 0 0 1 $q-1
-697.67 0.0 0.0 $q-5 Nx in stringer for overall Nx=1000
1 $r-1
C
C Panel Skin Segment
C
2 4$m-1
0.0 30.0 0.0 5.0 $m-2
0.0 7.5 0.0 $m-4d iglobe=4
0.0 0.0 0.0 $m-4e
4 $m-5 laminated panel skin
410 $n-1
1 6 1 6 $p-1
0 0 0 1 $q-1
-811.35 0.0 0.0 $q-5 Nx in skin for overall Nx=1000
1 $r-1
C
C Stringer Segment
C
2 4$m-1
0.0 30.0 0.0 1.352 $m-2
0.0 12.5 0.0 $m-4d iglobe=4

```

```

-90.0 0.0 0.0 $m-4e
5 $m-5 laminated stringer
410 $n-1
1 3 1 6 $p-1
0 0 0 1 $q-1
-697.67 0.0 0.0 $q-5 Nx in stringer for overall Nx=1000
1 $r-1
C
C Panel Skin Segment
C
2 4$m-1
0.0 30.0 0.0 5.0 $m-2
0.0 12.5 0.0 $m-4d iglobe=4
0.0 0.0 0.0 $m-4e
4 $m-5 laminated panel skin
410 $n-1
1 6 1 6 $p-1
0 0 0 1 $q-1
-811.35 0.0 0.0 $q-5 Nx in skin for overall Nx=1000
1 $r-1
C
C Stringer Segment
C
2 4$m-1
0.0 30.0 0.0 1.352 $m-2
0.0 17.5 0.0 $m-4d iglobe=4
-90.0 0.0 0.0 $m-4e
5 $m-5 laminated stringer
410 $n-1
1 3 1 6 $p-1
0 0 0 1 $q-1
-697.67 0.0 0.0 $q-5 Nx in stringer for overall Nx=1000
1 $r-1
C
C Panel Skin Segment
C
2 4$m-1
0.0 30.0 0.0 5.0 $m-2
0.0 17.5 0.0 $m-4d iglobe=4
0.0 0.0 0.0 $m-4e
4 $m-5 laminated panel skin
410 $n-1
1 6 1 6 $p-1
0 0 0 1 $q-1
-811.35 0.0 0.0 $q-5 Nx in skin for overall Nx=1000
1 $r-1
C
C Stringer Segment
C
2 4$m-1
0.0 30.0 0.0 1.352 $m-2
0.0 22.5 0.0 $m-4d iglobe=4
-90.0 0.0 0.0 $m-4e
5 $m-5 laminated stringer
410 $n-1
1 3 1 6 $p-1
0 0 0 1 $q-1
-697.67 0.0 0.0 $q-5 Nx in stringer for overall Nx=1000
1 $r-1
C
C Panel Skin Segment
C
2 4$m-1

```

```

0.0 30.0 0.0 5.0 $m-2
0.0 22.5 0.0 $m-4d iglobe=4
0.0 0.0 0.0 $m-4e
4 $m-5 laminated panel skin
410 $n-1
1 6 1 6 $p-1
0 0 0 1 $q-1
-811.35 0.0 0.0 $q-5 Nx in skin for overall Nx=1000
1 $r-1
C
C Stringer Segment
C
2 4$m-1
0.0 30.0 0.0 1.352 $m-2
0.0 27.5 0.0 $m-4d iglobe=4
-90.0 0.0 0.0 $m-4e
5 $m-5 laminated stringer
410 $n-1
1 3 1 6 $p-1
0 0 0 1 $q-1
-697.67 0.0 0.0 $q-5 Nx in stringer for overall Nx=1000
1 $r-1
C
C Panel Skin Segment
C
2 4$m-1
0.0 30.0 0.0 2.5 $m-2
0.0 27.5 0.0 $m-4d iglobe=4
0.0 0.0 0.0 $m-4e
4 $m-5 laminated panel skin
410 $n-1
1 1 1 6 $p-1
0 0 0 1 $q-1
-811.35 0.0 0.0 $q-5 Nx in skin for overall Nx=1000
1 $r-1

```

cbranched.bin (for S2 processor)

```

Blade stiffened panel with laminated skin - TP-2215, Example 1 $a-1
1 1 0 $b-1
1.0 1.0 1.0 $c-1
1000 .0001 0 $d-2
4 $d-3

```

cbranched.pin (for STAPL processor)

```

Blade-stiffened Panel - TP-2215
4 0 0 0 $PL-2 NPLOT,IPREP,IPRS,KDEV
2 0 4 0 1 0 0 3 $PL-3 KPLOT,VIEW,ITEM,STEP,MODE,IFRNG,COLOR,ICOMP
0.0 3 0.0 -1.0 1.0 $PL-5 DSCALE,NROTS,LWSCALE,RNGMIN,RGMAX
1 -240.0 / 2 0.0 / 3 -30.0
2 0 4 0 2 0 0 3 $PL-3 KPLOT,VIEW,ITEM,STEP,MODE,IFRNG,COLOR,ICOMP
0.0 3 0.0 -1.0 1.0 $PL-5 DSCALE,NROTS,LWSCALE,RNGMIN,RGMAX
1 -240.0 / 2 0.0 / 3 -30.0
2 0 4 0 3 0 0 3 $PL-3 KPLOT,VIEW,ITEM,STEP,MODE,IFRNG,COLOR,ICOMP
0.0 3 0.0 -1.0 1.0 $PL-5 DSCALE,NROTS,LWSCALE,RNGMIN,RGMAX
1 -240.0 / 2 0.0 / 3 -30.0
2 0 4 0 4 0 0 3 $PL-3 KPLOT,VIEW,ITEM,STEP,MODE,IFRNG,COLOR,ICOMP
0.0 3 0.0 -1.0 1.0 $PL-5 DSCALE,NROTS,LWSCALE,RNGMIN,RGMAX
1 -240.0 / 2 0.0 / 3 -30.0

```

Branched Model of Panel 3 (metal)

Panel 3 is a metal blade-stiffened panel with a thin skin. This configuration corresponds to Example 4 in NASA TP-2215. The input file included here is for the uniform compression case with an overall N_x membrane loading of -1000 lb/in. This compression load is carried partly by the skin and partly by the stiffeners as indicated by the load magnitudes specified on the Q-5 records. The load distributions were taken from NASA TP-2215. These input files are given in:

../Stiffened-panel/Panel-3/Compression/Branched-plate

branched.inp (for S1 processor)

```
Blade stiffened panel with thin skin - TP 2215 Example 4 $a-1
0 0 0 0 0 3 $b-1
1 -240.0 / 2 0.0 / 3 -30. $b-1b model rotations
13 0 0 12 0 $b-2
2 0 5 $b-3
37 3 37 3 37 5 37 3 37 5 37 3 37 5 ,
37 3 37 5 37 3 37 5 37 3 37 3 $f-1
1 2 2 4 $g-1 connections
1 2 3 4
3 2 4 4
3 2 5 4
5 2 6 4
5 2 7 4
7 2 8 4
7 2 9 4
9 2 10 4
9 2 11 4
11 2 12 4
11 2 13 4 $ g-1 connections
C
C Material definition for Example 2 and 4
C
1 $i-1 material data
10.5e6 .32 $i-2 aluminium
C
C Material definition for Example 1
C
2 $i-1 G/E material data
19.0E+6 0.0378 0.93E+6 0.1 0.0 1.89E+6 $i-2
C
C Fabrication definitions
C (thick skin; thin skin; stringer)
C
1 1 1 $k-1 panel skin thickness - Example 2
1 0.084 $k-2 thick skin
2 1 1 $k-1 panel skin thickness - Example 4
1 0.050 $k-2 thin skin
3 1 1 $k-1 blade stringer thickness - Examples 2 & 4
1 0.058 $k-2
4 1 28 $k-1 laminated panel skin - Example 1
2 0.0055 +45.0 $k-2
2 0.0055 -45.0 $k-2
2 0.0055 -45.0 $k-2
2 0.0055 +45.0 $k-2
2 0.0055 0.0 $k-2
2 0.0055 90.0 $k-2
2 0.0055 90.0 $k-2
2 0.0055 90.0 $k-2
2 0.0055 90.0 $k-2
```

```

2 0.0055 90.0 $k-2
2 0.0055 90.0 $k-2
2 0.0055 90.0 $k-2
2 0.0055 90.0 $k-2
2 0.0055 90.0 $k-2
2 0.0055 90.0 $k-2
2 0.0055 90.0 $k-2
2 0.0055 90.0 $k-2
2 0.0055 90.0 $k-2
2 0.0055 90.0 $k-2
2 0.0055 90.0 $k-2
2 0.0055 90.0 $k-2
2 0.0055 90.0 $k-2
2 0.0055 0.0 $k-2
2 0.0055 +45.0 $k-2
2 0.0055 -45.0 $k-2
2 0.0055 -45.0 $k-2
2 0.0055 +45.0 $k-2
5 1 12 $k-1 laminated stringer - Example 1
2 0.0055 +45.0 $k-2
2 0.0055 -45.0 $k-2
2 0.0055 -45.0 $k-2
2 0.0055 +45.0 $k-2
2 0.0055 0.0 $k-2
2 0.0055 0.0 $k-2
2 0.0055 0.0 $k-2
2 0.0055 0.0 $k-2
2 0.0055 +45.0 $k-2
2 0.0055 -45.0 $k-2
2 0.0055 -45.0 $k-2
2 0.0055 +45.0 $k-2
C
C ----- Define shell units: skin segment then stringer, etc
C
C
C Panel Skin Segment
C
2 $m-1
0.0 30.0 0.0 2.5 $m-2
2 $m-5 shell wall-thin skin
410 $n-1
1 6 1 1 $p-1
0 0 0 1 $q-1
-761.23 0.0 0.0 $q-5 Nx in thin skin for overall Nx=1000
1 $r-1
C
C Stringer Segment
C
2 4$m-1
0.0 30.0 0.0 1.352 $m-2
0.0 2.5 0.0 $m-4d iglobe=4
-90.0 0.0 0.0 $m-4e
3 $m-5 shell wall
410 $n-1
1 3 1 6 $p-1
0 0 0 1 $q-1
-883.03 0.0 0.0 $q-5 Nx in stringer for thin skin for overall Nx=1000
1 $r-1
C
C Panel Skin Segment
C
2 4$m-1

```

```

0.0 30.0 0.0 5.0 $m-2
0.0 2.5 0.0 $m-4d iglobe=4
0.0 0.0 0.0 $m-4e
2 $m-5 shell wall-thin skin
410 $n-1
1 6 1 6 $p-1
0 0 0 1 $q-1
-761.23 0.0 0.0 $q-5 Nx in thin skin for overall Nx=1000
1 $r-1
C
C Stringer Segment
C
2 4$m-1
0.0 30.0 0.0 1.352 $m-2
0.0 7.5 0.0 $m-4d iglobe=4
-90.0 0.0 0.0 $m-4e
3 $m-5 shell wall
410 $n-1
1 3 1 6 $p-1
0 0 0 1 $q-1
-883.03 0.0 0.0 $q-5 Nx in stringer for thin skin for overall Nx=1000
1 $r-1
C
C Panel Skin Segment
C
2 4$m-1
0.0 30.0 0.0 5.0 $m-2
0.0 7.5 0.0 $m-4d iglobe=4
0.0 0.0 0.0 $m-4e
2 $m-5 shell wall-thin skin
410 $n-1
1 6 1 6 $p-1
0 0 0 1 $q-1
-761.23 0.0 0.0 $q-5 Nx in thin skin for overall Nx=1000
1 $r-1
C
C Stringer Segment
C
2 4$m-1
0.0 30.0 0.0 1.352 $m-2
0.0 12.5 0.0 $m-4d iglobe=4
-90.0 0.0 0.0 $m-4e
3 $m-5 shell wall
410 $n-1
1 3 1 6 $p-1
0 0 0 1 $q-1
-883.03 0.0 0.0 $q-5 Nx in stringer for thin skin for overall Nx=1000
1 $r-1
C
C Panel Skin Segment
C
2 4$m-1
0.0 30.0 0.0 5.0 $m-2
0.0 12.5 0.0 $m-4d iglobe=4
0.0 0.0 0.0 $m-4e
2 $m-5 shell wall-thin skin
410 $n-1
1 6 1 6 $p-1
0 0 0 1 $q-1
-761.23 0.0 0.0 $q-5 Nx in thin skin for overall Nx=1000
1 $r-1
C
C Stringer Segment

```

```

C
2 4$m-1
0.0 30.0 0.0 1.352 $m-2
0.0 17.5 0.0 $m-4d iglobe=4
-90.0 0.0 0.0 $m-4e
3 $m-5 shell wall
410 $n-1
1 3 1 6 $p-1
0 0 0 1 $q-1
-883.03 0.0 0.0 $q-5 Nx in stringer for thin skin for overall Nx=1000
1 $r-1
C
C Panel Skin Segment
C
2 4$m-1
0.0 30.0 0.0 5.0 $m-2
0.0 17.5 0.0 $m-4d iglobe=4
0.0 0.0 0.0 $m-4e
2 $m-5 shell wall-thin skin
410 $n-1
1 6 1 6 $p-1
0 0 0 1 $q-1
-761.23 0.0 0.0 $q-5 Nx in thin skin for overall Nx=1000
1 $r-1
C
C Stringer Segment
C
2 4$m-1
0.0 30.0 0.0 1.352 $m-2
0.0 22.5 0.0 $m-4d iglobe=4
-90.0 0.0 0.0 $m-4e
3 $m-5 shell wall
410 $n-1
1 3 1 6 $p-1
0 0 0 1 $q-1
-883.03 0.0 0.0 $q-5 Nx in stringer for thin skin for overall Nx=1000
1 $r-1
C
C Panel Skin Segment
C
2 4$m-1
0.0 30.0 0.0 5.0 $m-2
0.0 22.5 0.0 $m-4d iglobe=4
0.0 0.0 0.0 $m-4e
2 $m-5 shell wall-thin skin
410 $n-1
1 6 1 6 $p-1
0 0 0 1 $q-1
-761.23 0.0 0.0 $q-5 Nx in thin skin for overall Nx=1000
1 $r-1
C
C Stringer Segment
C
2 4$m-1
0.0 30.0 0.0 1.352 $m-2
0.0 27.5 0.0 $m-4d iglobe=4
-90.0 0.0 0.0 $m-4e
3 $m-5 shell wall
410 $n-1
1 3 1 6 $p-1
0 0 0 1 $q-1
-883.03 0.0 0.0 $q-5 Nx in stringer for thin skin for overall Nx=1000
1 $r-1

```

```

C
C Panel Skin Segment
C
2 4$m-1
0.0 30.0 0.0 2.5 $m-2
0.0 27.5 0.0 $m-4d iglobe=4
0.0 0.0 0.0 $m-4e
1 $m-5 shell wall-thin skin
410 $n-1
1 1 1 6 $p-1
0 0 0 1 $q-1
-761.23 0.0 0.0 $q-5 Nx in thin skin for overall Nx=1000
1 $r-1

```

branched.bin (for S2 processor)

```

Blade stiffened panel with thin skin - TP-2215, Example 4 $a-1
1 1 0 $b-1
1.0 1.0 1.0 $c-1
1000 .0001 0 $d-2
4 $d-3

```

branched.pin (for STAPL processor)

```

Blade-stiffened Panel - TP-2215
4 0 0 0 $PL-2 NPLOT,IPREP,IPRS,KDEV
2 0 4 0 1 0 0 3 $PL-3 KPLOT,VIEW,ITEM,STEP,MODE,IFRNG,COLOR,ICOMP
0.0 3 0.0 -1.0 1.0 $PL-5 DSCALE,NROTS,LWSCALE,RNGMIN,RGMAX
1 -240.0 / 2 0.0 / 3 -30.0
2 0 4 0 2 0 0 3 $PL-3 KPLOT,VIEW,ITEM,STEP,MODE,IFRNG,COLOR,ICOMP
0.0 3 0.0 -1.0 1.0 $PL-5 DSCALE,NROTS,LWSCALE,RNGMIN,RGMAX
1 -240.0 / 2 0.0 / 3 -30.0
2 0 4 0 3 0 0 3 $PL-3 KPLOT,VIEW,ITEM,STEP,MODE,IFRNG,COLOR,ICOMP
0.0 3 0.0 -1.0 1.0 $PL-5 DSCALE,NROTS,LWSCALE,RNGMIN,RGMAX
1 -240.0 / 2 0.0 / 3 -30.0
2 0 4 0 4 0 0 3 $PL-3 KPLOT,VIEW,ITEM,STEP,MODE,IFRNG,COLOR,ICOMP
0.0 3 0.0 -1.0 1.0 $PL-5 DSCALE,NROTS,LWSCALE,RNGMIN,RGMAX
1 -240.0 / 2 0.0 / 3 -30.0

```

Discrete-Stiffener Model of Panel 3 (metal)

Panel 3 is a metal blade-stiffened panel with a thin skin. This configuration corresponds to Example 4 in NASA TP-2215. The input file included here is for the uniform compression case with an overall N_x membrane loading of -1000 lb/in. These input files are given in:

../Stiffened-panel/Panel-3/Compression/Discrete-stiffener

discrete.inp (for S1 processor)

```

Discretely stiffened panel with thin skin - TP 2215 Example 4 $a-1
0 0 0 0 0 3 $b-1
1 -240.0 / 2 0.0 / 3 -30.0 $b-1b model rotations
1 0 1 $b-2
1 1 2 $b-3
37 37 $f-1
1 0 6 $ f-2 discrete stiffeners including along boundaries
1 $i-1 material records
10.5e6 .32 $i-2
1 3 1 1 8.5481e-5 0.0 0.0 $j-1 stringer stiffener

```



```

-.029 +.029  -0.676  +0.676  $j-3b
1  1  1  0  0  $k-1
1 .084  $k-2  thick skin
2  1  1  0  0  $k-1
1 .050  $k-2  thin skin
2  0  $m-1
0.0 30.0  0.0  30.0  $m-2a
2  $m-5 thin skin case - example 4 in TP 2215
410 $n-1
1  0.0  0.0  0.676  $o-2a  discrete stringers (constant y)
0  0  0  2.5  0.0  30.0  $o-2b
1  0.0  0.0  0.676  $o-2a  discrete stringers (constant y)
0  0  0  7.5  0.0  30.0  $o-2b
1  0.0  0.0  0.676  $o-2a  discrete stringers (constant y)
0  0  0  12.5  0.0  30.0  $o-2b
1  0.0  0.0  0.676  $o-2a  discrete stringers (constant y)
0  0  0  17.5  0.0  30.0  $o-2b
1  0.0  0.0  0.676  $o-2a  discrete stringers (constant y)
0  0  0  22.5  0.0  30.0  $o-2b
1  0.0  0.0  0.676  $o-2a  discrete stringers (constant y)
0  0  0  27.5  0.0  30.0  $o-2b
1  1  1  1  $p-1
0  0  0  1  $q-1
-1000.0 000.0  0.0  $q-5
1  0  0  $r-1

```

discrete.bin (for S2 processor)

Discretely stiffened panel with thin skin - TP 2215 Example 4 \$a-1

```

1  1  0  $b-1
1.0 1.0 1.0  $c-1
1000 .0001 0  $d-2
4  $d-3

```

discrete.pin (for STAPL processor)

Blade-stiffened Panel - TP-2215

```

4  0  0  0  $PL-2  NPLOT,IPREP,IPRS,KDEV
2  0  4  0  1  0  0  3  $PL-3  KPLOT,VIEW,ITEM,STEP,MODE,IFRNG,COLOR,ICOMP
0.0  3  0.0  -1.0  1.0  $PL-5  DSCALE,NROTS,LWSCALE,RNGMIN,RGMAX
1  -240.0 / 2  0.0 / 3  -30.0
2  0  4  0  2  0  0  3  $PL-3  KPLOT,VIEW,ITEM,STEP,MODE,IFRNG,COLOR,ICOMP
0.0  3  0.0  -1.0  1.0  $PL-5  DSCALE,NROTS,LWSCALE,RNGMIN,RGMAX
1  -240.0 / 2  0.0 / 3  -30.0
2  0  4  0  3  0  0  3  $PL-3  KPLOT,VIEW,ITEM,STEP,MODE,IFRNG,COLOR,ICOMP
0.0  3  0.0  -1.0  1.0  $PL-5  DSCALE,NROTS,LWSCALE,RNGMIN,RGMAX
1  -240.0 / 2  0.0 / 3  -30.0
2  0  4  0  4  0  0  3  $PL-3  KPLOT,VIEW,ITEM,STEP,MODE,IFRNG,COLOR,ICOMP
0.0  3  0.0  -1.0  1.0  $PL-5  DSCALE,NROTS,LWSCALE,RNGMIN,RGMAX
1  -240.0 / 2  0.0 / 3  -30.0
0  0  0  0  0  0  0  0  $PL-3  KPLOT,VIEW,ITEM,STEP,MODE,IFRNG,COLOR,ICOMP
-0.5  3  0.0  0.0  0.0  $PL-5  DSCALE,NROTS,LWSCALE,RNGMIN,RGMAX
1  -240.0 / 2  0.0 / 3  -30.0

```

Smearred-Stiffener Model of Panels 3 (metal)

Panel 3 is a metal blade-stiffened panel with a thin skin. This configuration corresponds to Example 4 in NASA TP-2215. The input file included here is for the uniform compression case with an overall N_x membrane loading of -1000 lb/in. These input files are given in:

../Stiffened-panel/Panel-3/Compression/Smearred-stiffener

smearred.inp (for S1 processor)

```
Smearred stiffened panel with thin skin - TP-2215, Example 4 $a-1
0 0 0 0 0 3 $b-1
1 -240.0 / 2 0.0 / 3 -30.0 $b-1b model rotations
1 0 0 0 0 $b-2
1 1 2 $b-3
37 37 $f-1
1 $i-1 material records
10.5e6 .32 $i-2
1 3 1 1 8.5481e-5 0.0 0.0 $j-1 stringer stiffener
-.029 +.029 -0.676 +0.676 $j-3b
1 1 1 0 1 $k-1 thick skin with smearred stringers
1 .084 $k-2 thick skin
1 5.0 0.0 0.0 .676 $k-6 smearred stringers
2 1 1 0 1 $k-1 thin skin with smearred stringers
1 .050 $k-2 thin skin
1 5.0 0.0 0.0 .676 $k-6 smearred stringers
2 0 $m-1
0.0 30.0 0.0 30.0 $m-2a
2 $m-5 thin skin case (example 4 in TP 2215)
410 $n-1
1 1 1 1 $p-1
0 0 0 1 $q-1
-1000.0 0.0 0.0 $q-5 Nx=-1000.0 uniform stress state
1 0 0 $r-1
```

smearred.bin (for S2 processor)

```
Smearred stiffened panel with thin skin - TP-2215, Example 4 $a-1
1 1 0 $b-1
1.0 1.0 1.0 $c-1
1000 .0001 0 $d-2
4 $d-3
```

smearred.pin (for STAPL processor)

```
Blade-stiffened Panel - TP-2215
4 0 0 0 $PL-2 NPLOT,IPREP,IPRS,KDEV
2 0 4 0 1 0 0 3 $PL-3 KPLOT,VIEW,ITEM,STEP,MODE,IFRNG,COLOR,ICOMP
0.0 3 0.0 -1.0 1.0 $PL-5 DSCALE,NROTS,LWSCALE,RNGMIN,RGMAX
1 -240.0 / 2 0.0 / 3 -30.0
2 0 4 0 2 0 0 3 $PL-3 KPLOT,VIEW,ITEM,STEP,MODE,IFRNG,COLOR,ICOMP
0.0 3 0.0 -1.0 1.0 $PL-5 DSCALE,NROTS,LWSCALE,RNGMIN,RGMAX
1 -240.0 / 2 0.0 / 3 -30.0
2 0 4 0 3 0 0 3 $PL-3 KPLOT,VIEW,ITEM,STEP,MODE,IFRNG,COLOR,ICOMP
0.0 3 0.0 -1.0 1.0 $PL-5 DSCALE,NROTS,LWSCALE,RNGMIN,RGMAX
1 -240.0 / 2 0.0 / 3 -30.0
2 0 4 0 4 0 0 3 $PL-3 KPLOT,VIEW,ITEM,STEP,MODE,IFRNG,COLOR,ICOMP
0.0 3 0.0 -1.0 1.0 $PL-5 DSCALE,NROTS,LWSCALE,RNGMIN,RGMAX
1 -240.0 / 2 0.0 / 3 -30.0
```

Problem References

Rankin, C. C., Brogan F. A., Loden, W., and Cabiness, H., *Structural Analysis of General Shells – STAGS User Manual, Version 4.0*, Lockheed Martin Advanced Technology Center, Palo Alto, CA, June 2000.

Stroud, W. Jefferson, Greene, William H., and Anderson, Melvin S., Buckling Loads of Stiffened Panels Subjected to Combined Longitudinal Compression and Shear: Results Obtained with PASCO, EAL, and STAGS Computer Programs, NASA TP-2215, January 1984.

Whetstone, W. D., “EISI-EAL: A General Engineering Analysis and Design Language,” *Finite Elements in Analysis and Design*, Vol. 2, Nos. 1-2, April 1986, pp. 219-235

Raasch Curved Hook Problem

Background

The Raasch curved hook problem was first publicly report by Harder at the Structures Technical Forum during the 1991 MSC World Users' Conference. The problem is essentially a curved 2-D structure with a reverse in shape near the boundary. The opposite end (or tip) is loaded by a unit in-plane shear loading. The issue with this test case is that shell elements without shear flexibility tend to converge to within 5% of the 3D solution, while models with shear flexibility tend not to converge unless shell normal (drilling) degrees of freedom are included. Hoff *et al.* (1995), Knight (1997), and MacNeal *et al.* (1998) have studied this problem using a variety of element formulations and mesh discretizations. The dimensions, material properties and loading are defined in Figure 24 using U. S. customary units.

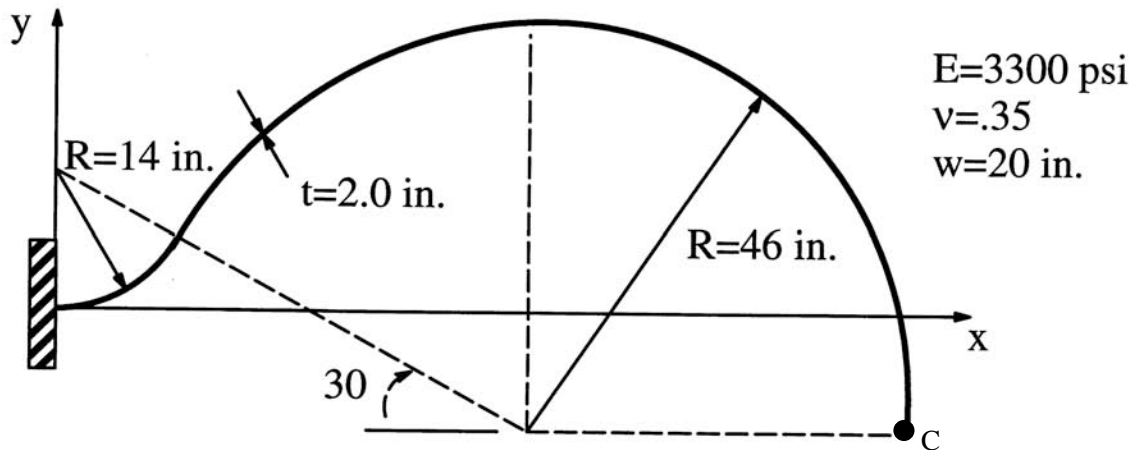


Figure 24. Raasch curved hook problem: geometry, material properties, and loading.

The hook has a uniform thickness t , and has width (in the z -direction) w , and an in-plane shear load P along the free edge at point C having a magnitude of unity. The response of the hook exhibits coupling between bending, extension, and twist. The mesh is defined as the number of elements in the width direction n_w by the number of elements along the hook length n_L (*i.e.*, $n_w \times n_L$). Meshes involving triangular elements are developed by subdividing each 4-node quadrilateral element into two triangular elements. The nodes are distributed equally in each direction. The reference solution for the tip deflection w_{ref} in the direction of the loading is taken as 4.9352 inches as done by Knight (1997).

Modeling and Analysis Process

The STAGS model is generated using two shell units with the cylindrical shell surface geometry (ISHELL=5). Material properties and membrane construction are defined using both the *historical* STAGS approach and the current GCP approach. Mesh discretization studies include different levels of mesh refinement and different element types. Mesh refinement is readily performed by changing the number of nodes in each direction on the F-1 record (*i.e.*, the mesh is defined a $n_w \times n_L$ as mesh of elements, one less than the number of nodes). Element type is selected using the N-1 record (KELT). Representative finite element meshes using 3-node, 4-node, and 9-node shell elements and 8-node solid element are shown in Figure 25 for the 10×68 mesh.

Material modeling for an elastic isotropic material using the historical STAGS approach requires data on the I-1 and I-2 records to define the material properties and the K-1 and K-2 records to define the construction or fabrication data. Material modeling using the current GCP approach requires data on the I-5a and I-6a records to define the material properties and the I-5a, I-21a, I-21b, I-21c, I-21d, and I-21e records to define the fabrication.

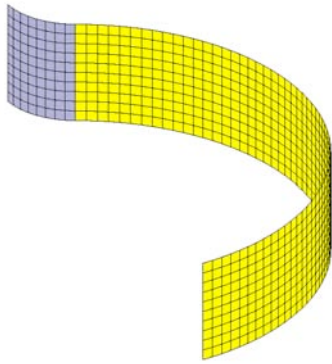
Loading is specified as a uniformly distributed shear load across the free end of the curved hook. For the 2D shell elements, it is specified as a line load ($N_{xy} = 1/20$ lb/in.) using the Q-1, Q-2, and Q-3 records. For the 3D 8-node solid element (E881), the nodal loads are specified manually by computing the work-equivalent nodal forces per element face and then defining the assembled nodal loads for that face of the hook. As a check on the loading, the summation of the equilibrium forces across the loaded edge in the direction of applied loading should equal unity (*i.e.*, total force equal to edge length times line load for 2D elements and equal to face traction times the face area for 3D elements).

For the 3D meshes, only two 8-node solid elements are used through the hook thickness. The loaded face involves the number of elements along the hook width or n_w . Thus the nodal force for each element on that face of the hook is given by:

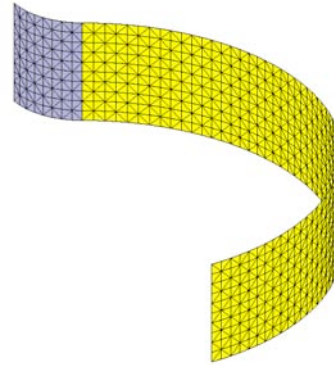
$$P_n = \frac{P}{4n_e}$$

where P is the total unit in-plane shear load and n_e is the total number of element faces across the loaded face – assuming equal area for the element faces. As a result corner nodes on the loaded face will have an applied force of P_n , other nodes on the bounding edges of the loaded face will have an applied force of $2 P_n$, and interior nodes of the face will have an applied force of $4 P_n$. The sum of all the nodal forces should equal the total applied shear load – which has a value of unity.

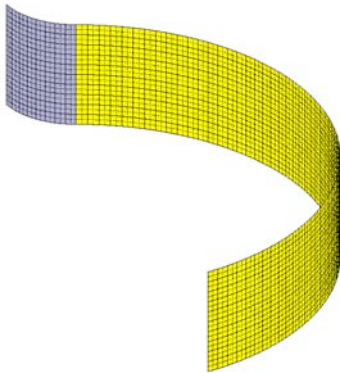
Boundary condition on the displacements are specified using the P-1 and P-2 records for the shell element models. Finite element models using the solid elements have the homogeneous boundary conditions imposed using the applied displacement loading records (Q-records) for each nodal layer through the hook thickness. The one end is fully clamped and all other edges are free. The drilling degrees of freedom are suppressed for the E480 element and they are retained for the E410 element. These drilling freedoms are constrained for the E480 element using the Q-3 records with the exterior looping feature. The E330 (MIN3) element does not introduce artificial drilling stiffness (a small number times the smallest diagonal term of the element stiffness matrix) automatically. Hence two cases are considered: one case restrains all drilling degrees of freedom and the other case leaves all the drilling degrees of freedom unrestrained and uses the penalty approach implemented within the element. Results are presented for both cases.



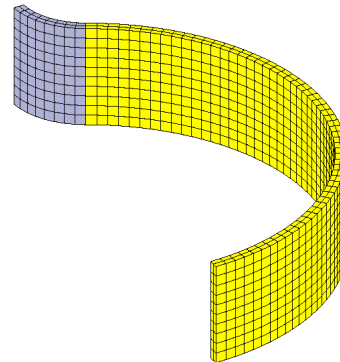
(a) 4-node E410 quadrilateral shell element.



(b) 3-node E330 (MIN3) triangular shell element.



(c) 9-node E480 (ANS) quadrilateral shell element.



(d) 8-node E881 (ANS) solid brick element.

Figure 25. Representative finite element discretization (10×68 mesh) of Raasch curved hook.

Table 9. Mesh refinement study for three shell finite element and one solid finite elements in STAGS – reference solution is 4.9352 inches (Knight, 1997).

Mesh of Elements $n_w \times n_L$	Normalized Tip Deflection w_c/w_{ref}			
	E330 Shell Element**	E410 Shell Element	E480 Shell Element**	E881 Solid Element*
1×9	0.4407 (1.0656) ⁺	0.9083	0.9776	0.7445
3×17	0.3749 (1.1336) ⁺	0.9398	0.9993	0.9484
5×34	0.5505 (1.2623) ⁺	0.9512	1.0085	0.9702
10×68	0.7963 (1.6547) ⁺	0.9541	1.0164	0.9856
20×136	1.1548 (2.8374) ⁺	0.9548	1.0182	0.9967
40×272	1.2243 (3.4904) ⁺	0.9550	1.0056	---

*For the solid element models, only two 8-node solid elements through the thickness are considered.

**The shear correction factors are set equal to 5/6.

+The number inside the parentheses was computed with the drilling degrees of freedom unrestrained and a penalty parameter is used with the drilling stiffness, while the outside number was computed by restraining all drilling degrees of freedom to zero.

Numerical Results and Discussion

Results are presented for the tip deflection at free end in the z -direction denoted by w_c normalized by the reference solution w_{ref} equal to 4.9352 inches (Knight, 1997).

Tip displacement results shown in Table 9 indicate that finite element models using the E410 and E480 shell elements and the E881 solid element converge quickly to the reference solution, while finite element models using the E330 shell element do not appear to be converging – with or without the drilling degrees of freedom. For the E410 element, the membrane response is nearly bilinear except for the contribution to edge's in-plane normal displacement from the drilling degrees of freedom. These results are consistent with available published solutions.

STAGS Input Files

These STAGS input files are located under the following subdirectory:

\$STAGSHOME/Sample-Testcases/Raasch

Typical 2D Shell Model Input Files

The following text files give the input for the hook model using the E480 9-node ANS shell element in STAGS with a 10×68 ($n_w \times n_L$) mesh of elements.

hook2D.inp (for S1 processor)

```
Raasch Curved Hook Problem - 2D      $a-1
C
C Curved hook problem with unit in-plane shear load at tip
C Reference solution for w/t=10 is 4.9352 in. for tip
C displacement in the direction of the loading
C
```

```

C Problem originally posed by Ingo Raasch, BMW in Germany
C at the 1995 MSC User's Forum
C
C Ref. Knight, "Raasch Challenge for Shell Elements"
C AIAA Journal, Vol. 35, No. 2, Feb. 1997,
C pp. 375-381.
C
0 0 0 0 0 3 $b-1
1 30.0 / 2 30.0 / 3 -90.0 $ b-1b Model rotations
2 0 0 1 0 $b-2
1 0 1 0 0 1 $b-3
C
C Mesh discretization
C
CC 2 2 2 9 $f-1 mesh in both units ( 1 x 9 mesh of 4-node elements)
CC 4 3 4 16 $f-1 mesh in both units ( 3 x 17 mesh of 4-node elements)
CC 6 5 6 31 $f-1 mesh in both units ( 5 x 34 mesh of 4-node elements)
CC11 9 11 61 $f-1 mesh in both units (10 x 68 mesh of 4-node elements)
CC21 16 21 121 $f-1 mesh in both units (20 x 136 mesh of 4-node elements)
CC 3 3 3 17 $f-1 mesh in both units ( 1 x 9 mesh of 9-node elements)
CC 7 5 7 31 $f-1 mesh in both units ( 3 x 17 mesh of 9-node elements)
CC11 9 11 61 $f-1 mesh in both units ( 5 x 34 mesh of 9-node elements)
21 17 21 121 $f-1 mesh in both units (10 x 68 mesh of 9-node elements)
CC41 31 41 241 $f-1 mesh in both units (20 x 136 mesh of 9-node elements)
C
C Connect the shell units
C
1 2 2 2 $g-1 shell unit connection
C
C Material definition (traditional approach)
C
1 0 $i-1 material data
3300.0 0.35 0.0 0.03861 $i-2 Modulus, Poisson's ratio, weight density
C
C =====
C Begin GCP Input for material and fabrication data
C
ISOELASTIC_MATERIAL 1 1 1 0 0 $i-2 isotropic elastic
3300.0, $i-6a Young's modulus, psi
0.35, $i-6a Poisson's ratio
1.0e-4, $i-6a Mass density, slugs/in^3
4*0.0 $i-6a unused values
SHELL_FABRICATION 1 1 0 1 0 $i-5a shell fabrication
1 $i-21a Layer material ID
2.0 $i-21c Layer thickness, in.
0.0 $i-21d Layer orientation angle, degrees
0.8333 0.8333 $i-21e shear correction factors
SOLID_FABRICATION 1 1 0 0 $i-5a solid fabrication
1.0 $i-22a element thickness
C
END $I-5a End GCP input
C =====
C
C Shell wall fabrication (traditional approach)
1 1 1 $k-1 wall card
1 2.0 0.0 $k-2 Mat ID, thickness, orientation
C
C define first segment
C
5 4 0 0 0 0 $m-1 Cylinder geometry
0.0 20.0 0.0 60.0 14.0 $m-2
0.0 14.0 0.0 $m-4d Orient shell unit
90.0 0.0 0.0 $m-4e

```



```

-1          $m-5 Fabrication
480        $n-1 Element selection
3 6 3 2    $p-1 boundary conditions
1          $q-1 no loading
1 1        $q-2 For E430, E480 elements only
0.0 -1 6 0 0 0 $q-3 zero-out drilling freedom
0          $r-1
C
C define second segment
C
5 4 0 0 0 0    $m-1 Cylinder geometry
0.0 20.0 0.0 150.0 46.0 $m-2
0.0 -16.0 51.96152422 $m-4d Orient shell unit
0.0 0.0 0.0    $m-4e
-1          $m-5 Fabrication
480        $n-1 Element selection
3 6 3 3    $p-1 boundary conditions
C
C Tip loading (across column of edge 1)
C
1 0          $q-1 Applied tip load
1 2 0        $q-2
0.05 3 1 0 1 0 $q-3 Uniform line load along tip
C          $ For E480 elements only
0.0 -1 6 0 0 0 $q-3 zero-out drilling freedom
0 0 0 0 0 0 1 $r-1 Selected displacements at tip
0 1          $r-2

```

hook2D.bin (for S2 processor)

```

Raasch hook problem execution parameters $a-1
C
C linear stress analysis
C
0 1 0 0 0 0 0 -1 $b-1
0.202626033 $c-1 reciprocal of reference solution

```

Typical 3D Solid Model Input Files

The following text files give the input for the hook 3D model using the E881 8-node solid element in STAGS with a 10×68 ($n_w \times n_L$) mesh of elements and just two 8-node solid elements through the hook thickness).

hook3D.inp (for S1 processor)

```

Raasch Curved Hook Problem - 3D          $a-1
C
C Curved hook problem with unit in-plane shear load at tip
C Reference solution for w/t=10 is 4.9352 in. for tip
C displacement in the direction of the loading
C
C Problem originally posed by Ingo Raasch, BMW in Germany
C at the 1991 MSC User's Forum
C
C Ref. Knight, "Raasch Challenge for Shell Elements"
C      AIAA Journal, Vol. 35, No. 2, Feb. 1997,
C      pp. 375-381.
C
0 0 0 0 0 3 $b-1
1 30.0 / 2 30.0 / 3 -90.0 $ b-1b Model rotations
2 0 0 1 0 $b-2

```

```

1 0 1 0 0 1 $b-3
C
C Mesh discretization
C
CC 2 2 2 9 $f-1 mesh in both units ( 1 x 9 mesh of 4-node elements)
CC 4 3 4 16 $f-1 mesh in both units ( 3 x 17 mesh of 4-node elements)
CC 6 5 6 31 $f-1 mesh in both units ( 5 x 34 mesh of 4-node elements)
  11 9 11 61 $f-1 mesh in both units (10 x 68 mesh of 4-node elements)
CC21 16 21 121 $f-1 mesh in both units (20 x 136 mesh of 4-node elements)
C
C Connect the shell units
C
1 2 2 2 $g-1 shell unit connection
C
C Material definition (traditional approach)
C
1 0 $i-1 material data
3300.0 0.35 0.0 0.03861 $i-2 Modulus, Poisson's ratio, weight density
C
C =====
C Begin GCP Input for material and fabrication data
C
ISOELASTIC_MATERIAL 1 1 1 0 0 $i-2 isotropic elastic
3300.0, $i-6a Young's modulus, psi
0.35, $i-6a Poisson's ratio
1.0e-4, $i-6a Mass density, slugs/in^3
4*0.0 $i-6a unused values
SHELL_FABRICATION 1 1 0 1 0 $i-5a shell fabrication
1 $i-21a Layer material ID
2.0 $i-21c Layer thickness, in.
0.0 $i-21d Layer orientation angle, degrees
0.8333 0.8333 $i-21e shear correction factors
SOLID_FABRICATION 1 1 0 0 $i-5a solid fabrication
1.0 $i-22a element thickness
C
END $I-5a End GCP input
C =====
C
C Shell wall fabrication (traditional approach)
C
1 1 1 $k-1 wall card
1 2.0 0.0 $k-2 Mat ID, thickness, orientation
C
C define first segment
C
5 4 0 0 2 1 $m-1 Cylinder geometry, 2 layers
0.0 20.0 0.0 60.0 14.0 $m-2
0.0 14.0 0.0 $m-4d Orient shell unit by translation
90.0 0.0 0.0 $m-4e and rotation
-1 $m-5 Fabrication
881 $n-1 Element selection
3 6 3 3 $p-1 boundary conditions
1 $q-1 Impose clamped BCs on end
1 3 $q-2
0.0 -1 1 0 1 0 3 1 0 0 1 $q-3 Set u=v=w=0 on Layer 1 along Column 1
0.0 -1 1 0 1 0 3 1 0 0 2 $q-3 Set u=v=w=0 on Layer 2 along Column 1
0.0 -1 1 0 1 0 3 1 0 0 3 $q-3 Set u=v=w=0 on Layer 3 along Column 1
1 $r-1
C
C define second segment
C
5 4 0 0 2 1 $m-1 Cylinder geometry, 2 layers
0.0 20.0 0.0 150.0 46.0 $m-2

```

```

0.0 -16.0 51.96152422 $m-4d Orient shell unit by translation
0.0 0.0 0.0 $m-4e and rotation
-1 $m-5 Fabrication
881 $n-1 Element selection
3 6 3 3 $p-1 boundary conditions
C
C Tip loading (across column of edge 1)
C where Pn = P/4/(number of elements on tip face)
C for 8-node solid elements with equal face areas
C Mesh Ne_tipface Pn
C 1x9 2 0.1250
C 3x17 4 0.0625
C 5x34 10 0.0250
C 10x68 20 0.0125
C 20x136 40 0.00625
C
1 0 $q-1 Applied tip load
1 9 0 $q-2
0.0125 1 1 1 1 0 0 0 0 0 1 $q-3 Corner (1,1) on Layer 1, Pn
0.0125 1 1 11 1 0 0 0 0 0 1 $q-3 Corner (nrow,1) on Layer 1, Pn
0.0125 1 1 1 1 0 0 0 0 0 3 $q-3 Corner (1,1) on Layer 3, Pn
0.0125 1 1 11 1 0 0 0 0 0 3 $q-3 Corner (nrow,1) on Layer 3, Pn
0.0250 1 1 1 1 0 0 0 0 0 2 $q-3 Midside at (1,1) on Layer 2, 2Pn
0.0250 1 1 11 1 0 0 0 0 0 2 $q-3 Midside at (nrow,1) on Layer 2, 2Pn
0.0250 1 1 2 1 0 9 0 1 0 1 $q-3 Edge 1 on Layer 1, 2Pn
0.0250 1 1 2 1 0 9 0 1 0 3 $q-3 Edge 1 on Layer 3, 2Pn
0.0500 1 1 2 1 0 9 0 1 0 2 $q-3 Interior centerline at Layer 2, 4Pn
C
C Output
C
0 0 0 0 0 0 1 $r-1 Selected displacements at tip
0 1 $r-2

```

hook3D.bin (for S2 processor)

```

Raasch hook problem execution parameters $a-1
C
C linear stress analysis
C
0 1 0 0 0 0 0 -1 $b-1
0.202626033 $c-1 reciprocal of reference solution

```

Problem References

Harder, R. L., "The Raasch Challenge," presentation charts (12 charts) from the Structures Technical Forum at the 1991 MSC World Users' Conference, Los Angeles, CA, 1991.

Hoff, C. C., Harder, R. L., Campbell, G., MacNeal, R. H., and Wilson, C. T., "Analysis of Shell Structures using MSC/NASTRAN's Shell Elements with Surface Normals," *Proceedings of the 1995 MSC World Users' Conference* (University City, CA), MacNeal-Schwendler Corp., Paper No. 26, Los Angeles, CA 1995, 18 pages.

Knight, Norman F., Jr., "Raasch Challenge for Shell Elements," *AIAA Journal*, Vol. 35, No. 2, February 1997, pp. 375-381.

MacNeal, R. H., Wilson, C. T., Harder, R. L., Hoff, C. C., "The Treatment of Shell Normals in Finite Element Analysis," *Finite Element in Analysis and Design*, Vol. 30, No. 3, August 1998, pp. 235-242.

Buckling and Collapse of Circular Cylinder with Square Cutouts

Background

To verify the nonlinear solution algorithm and nonlinear aspects of the shell element and corotational formulations, the elastic collapse of a circular cylinder ($R/t=433$ and $L/R=1.5$) with two opposing central rectangular cutouts (45° by $L/3$ in size) loaded by uniform end-shortening is studied. This problem involves local radial deflections along the straight edges of the cutout that develop at a low load level and become large prior to collapse. This shell problem was part of experimental and analytical studies by Almroth and Holmes (1972) and extended to dynamic buckling by Almroth, Meller and Brogan (1974). Hartung and Ball (1973) included this shell structure as one of the three challenge problems to assess shell structural analysis capabilities. Almroth and Brogan (1981) studied the computational efficiency and capability of the shell finite elements implemented in the STAGS finite element code. Knight *et al.* (1989, 1995) also used this problem to assess the CSM Testbed capabilities for the static collapse of elastic shell. The geometry and material properties of the problem are defined in Figure 26 using U.S. customary units.

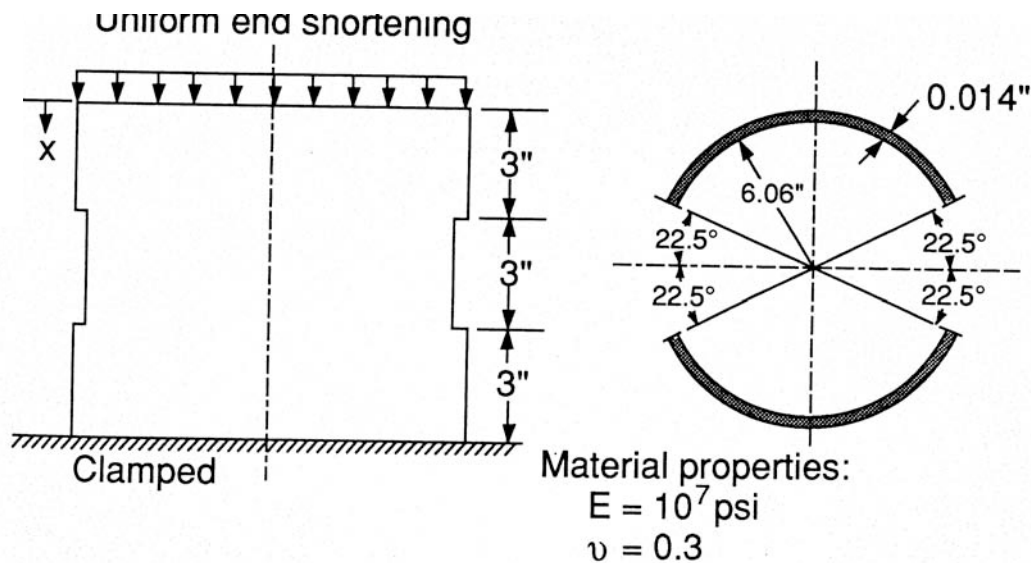


Figure 26. Cylinder with cutouts: geometry and material properties.

Modeling and Analysis Process

Three separate STAGS finite element models are considered in this test case problem – both involve shell elements. A summary of each model includes:

2-D shell model – Model the shell with shell finite elements in a single shell unit and using the irregular grid modeling option – cutout1.inp.

2-D shell model – Model shell with shell finite elements in three shell units to model around the cutout – `cutout3.inp`.

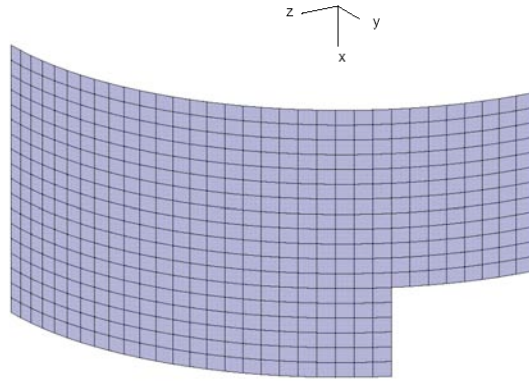
2-D shell model – Model the shell with shell finite elements in two shell units and use the connection across a portion of a shell unit option – `cutout2.inp`.

The STAGS model is generated using a single shell unit with the cylindrical shell surface geometry (ISHELL=5). Material properties and shell wall construction are defined using both the *historical* STAGS approach and the current GCP approach. Mesh discretization studies include different levels of mesh refinement and different element types. Mesh refinement is readily performed by changing the number of rows and columns of nodes in each direction on the F-1 record. Element type is selected using the N-1 record (KELT). Note that E430 uses two E330 triangular elements for each 4-node quadrilateral subdomain.

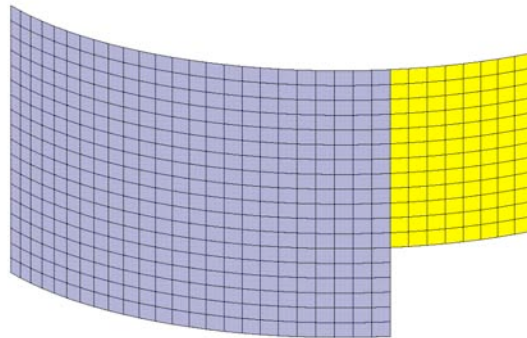
Representative finite element models using Mesh 3 (19×33 mesh of nodes on the shell surface) are shown in Figure 27 for different shell unit modeling approaches. The single shell unit model shown in Figure 27a illustrates the use of the irregular mesh option (see the N-8 records) for easy inclusion of rectangular cutouts. However, the irregular mesh option is not available for use with the triangular elements or solid elements. Alternatively, two or three shell units may be used as shown in Figures 27b and 27c, respectively. The two shell unit model requires special consideration for the shell unit junction along only a portion of a shell unit boundary (see the G-2 records of the `cutout2.inp` input file). The three shell unit model is straightforward to create in that three rectangular domains are defined and discretized (see the `cutout3.inp` input file). Finite element models labeled as Mesh 3 using the 3-node, 4-node, and 9-node shell elements are shown in Figure 28.

The S1 input file for the single shell unit model (`cutout1.inp`) contains input records (F-1 and N-8 records) for different finite element discretizations. The different meshes can be exercised by editing the input file and changing the records that are “commented.”

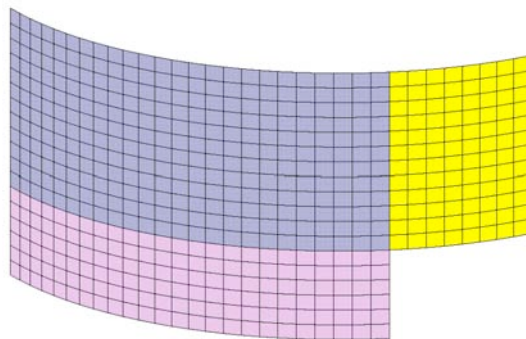
The nonlinear solutions were obtained using the perfect shell geometry – no initial geometric surface imperfections. The cutouts served as a sufficient “trigger” for the geometric nonlinearities to develop. The material behavior is treated as linear elastic – no elastic-plastic behavior was considered. The value of the collapse load reported by Almroth and Holmes (1972) is 2250 pounds or 0.3045 P_0 . Almroth and Brogan (1981) reported a nearly converged elastic collapse load of 2750 pounds or 0.3722 P_0 obtained using the STAGS E411 shell element. Difference may be attributed to thickness variations in the test cylinder while uniform thickness in the analysis; initial surface imperfections that are not included in the analysis; elastic material properties that differ from nominal values used in the analysis; and possible local material yielding that is not accounted for in the analysis.



(a) Mesh 3 using a single shell unit with the E410 4-node shell elements.

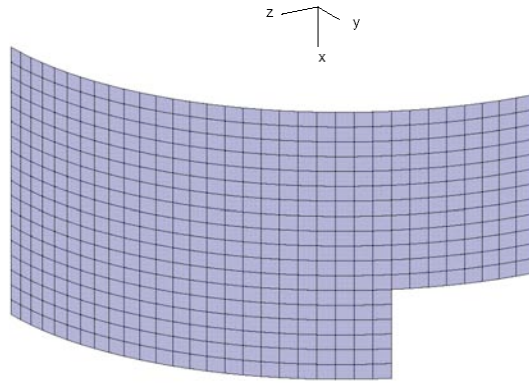


(b) Mesh 3 using two shell units with the E410 4-node shell elements.

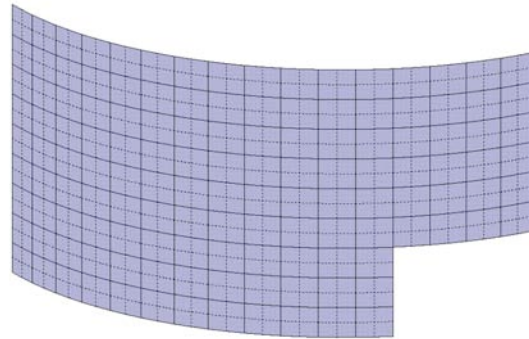


(c) Mesh 3 using three shell units with the E410 4-node shell elements.

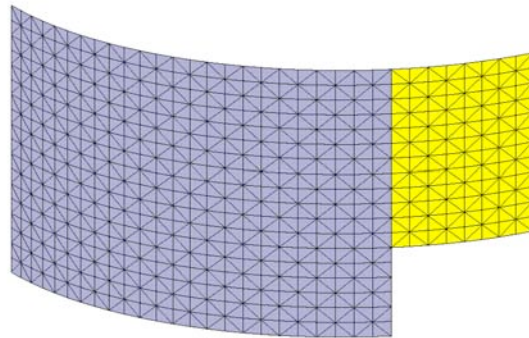
Figure 27. Representative finite element models of the cylinder with cutouts using different numbers of shell units – Mesh 3.



(a) Mesh 3 using a single shell unit with the E410 4-node shell elements.



(b) Mesh 3 using a single shell unit with the E480 9-node shell elements.



(c) Mesh 3 using two shell units with the E430 3-node shell elements.

Figure 28. Representative finite element models of the cylinder with cutouts using different shell elements – Mesh 3 with 4-node, 9-node and 3-node 2-D shell elements.

Material properties and shell-wall construction are defined using both the *historical* STAGS approach (*i.e.*, STAGS versions prior to GCP) and the current GCP approach. Material modeling for an elastic isotropic material using the historical STAGS approach requires data on the I-1 and I-2 records to define the material properties and the K-1 and K-2 records to define the shell fabrication data. Material modeling using the current GCP approach requires data on the I-5a and I-6a records to define the material properties and records I-5a, I-21a, I-21b, I-21c, I-21d, and I-21e to define the shell fabrication data.

Boundary condition on the displacements are specified using the P-1 and P-2 records. The boundary conditions along the curved boundary are clamped, while the boundary edges around the cutout are free. Symmetry boundary conditions are imposed on the straight and curved edges interior to the shell.

A point load is applied at one point on the shell edge equal to one quarter of the total base load P_0 because of the symmetry conditions. The base load given on the Q-3 record is $0.25 P_0$ where $P_0 = 1.2\pi Et^2$. Then the load factor on the C-1 record of the S2 input file gives the total load amplitude (*i.e.*, the load factor PA is related to the total load on the shell). Since the load condition is defined as uniform end-shortening loading, partial compatibility constraints on the G-2 records are employed to equate the end shortening everywhere on the loaded edge to the end shortening at the loading point. The internal force at that node and in the direction of the loading can be computed and used for plotting as well via the XYTRANS utility.

Numerical Results and Discussion

Results for this problem involve the elastic nonlinear collapse response of the shell structure with localized deformations near the cutouts. The response exhibits buckling at a low value of the applied load followed by a substantial postbuckling response before elastic collapse is detected. Elastic collapse is defined here as the first occurrence of a negative root in the tangent stiffness matrix upon convergence for a given solution step. The nonlinear solutions were obtained using the arc-length control procedure that automatically adjusts the solution step size and using the full Newton-Raphson approach (*i.e.*, -20 for NEWT on the D-1 record of the S2 input file).

First a series of linear bifurcation buckling analyses were performed using the single-shell-unit modeling approach and the various finite element meshes. The finite element mesh is defined by the number of equally spaced rows and columns of nodes on the shell surface. The irregular mesh option is used to eliminate those nodes and elements in the cutout region. The results are presented in Table 10 for the E410 and E480 shell elements. Models for a given mesh (say Mesh 1) have the same number of nodes but the model using the E410 element will have four times as many elements as the model using the E480 element – same number of degrees of freedom.

Table 10. Effect of Mesh Refinement on the Buckling and Collapse Loads

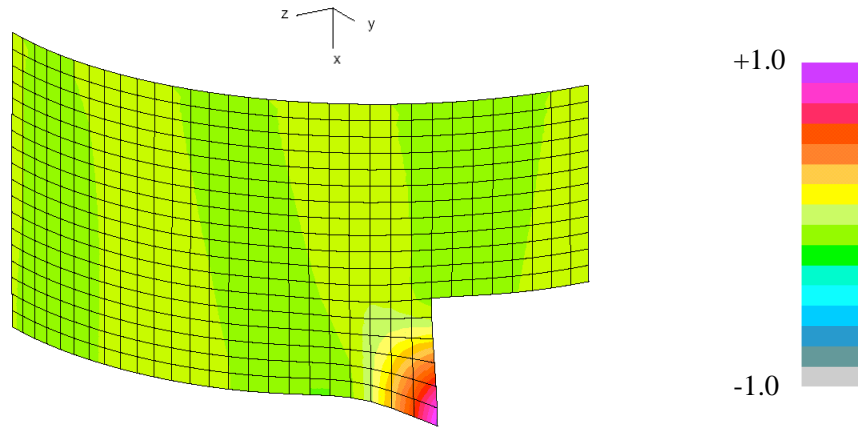
Mesh	NROWS × NCOLS	Buckling Load, P/P ₀		Collapse Load, P/P ₀	
		E410	E480	E410	E480
1	7×13	0.0948	0.1739	---	0.3604
2	13×25	0.1364	0.1489	0.4072	0.4144
3	19×33	0.1372	0.1411	0.3911	0.3748
4	25×49	0.1366	0.1366	0.3845	0.3801

Convergence studies were performed for buckling solutions using the E410 and E480 shell elements. Results for Mesh 1 are significantly away from the converged value. The E410 models appear to converge to a value faster than the E480 models for the same number of nodes. It needs to be noted that the Mesh 4 has four times the number of E410 shell elements as it has E480 shell elements. The lowest five buckling modes correspond to localized patterns near the cutout straight edges. The sixth mode is roughly an axisymmetric-like pattern, and the ninth mode is roughly a diamond- or checkerboard-like pattern. These modes are illustrated on Figure 29.

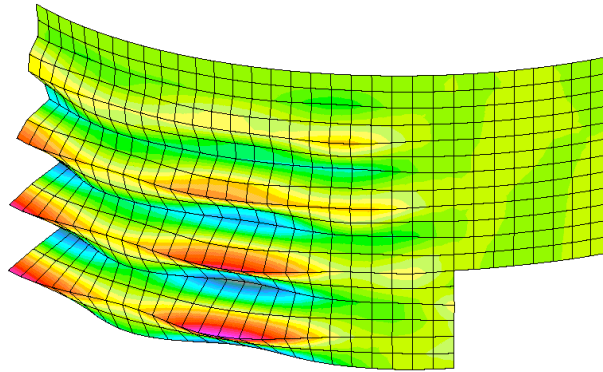
Convergence studies were also performed for the elastic nonlinear collapse solutions using the E410 and E480 shell elements. Results obtained using Mesh 1 and the E410 shell element did not clearly indicate “collapse” as defined here (negative root in the tangent stiffness matrix upon convergence). Convergence to a value of 0.38 P₀ occurs at approximately the same rate for both element types.

Results shown in Figures 30 and 31 are for different levels of discretization using the E410 4-node and E480 9-node shell elements, respectively. Clearly Mesh 1 results the more different results for the E410 models – perhaps due to geometry modeling issues. Results shown in Figure 32 compare the response predicted using Mesh 3 for three shell elements (E410, E480, and E430). The results obtained using the E430 triangular shell elements are somewhat stiffer than the quadrilateral shell elements. The elastic collapse load predicted by the E430 model using Mesh 3 is 0.4052 P₀.

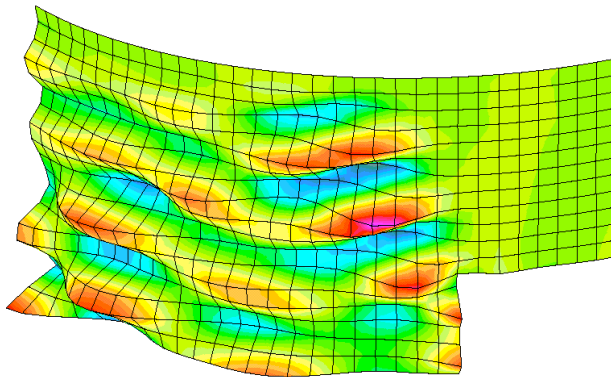
Contour plots of the axial stress distribution for selected solution steps including after buckling, just prior to collapse, and just after collapse are shown in Figure 33. These plots indicate the redistribution of stress away from just over the cutout, the tensile axial stress near the cutout corners and a compressive axial stress concentration along the middle of the straight edge of the cutout.



(a) Mode 1, $P/P_0=0.1372$ – localized near cutout.



(b) Mode 6, $P/P_0=0.7937$ – axisymmetric-like pattern except near cutouts.



(c) Mode 9, $P/P_0=0.8113$ – nearly diamond pattern except near cutouts.

Figure 29. Contour plots of the out-of-plane displacement component of the buckling mode shapes for the single-shell-unit model using Mesh 3 and the E410 shell element.

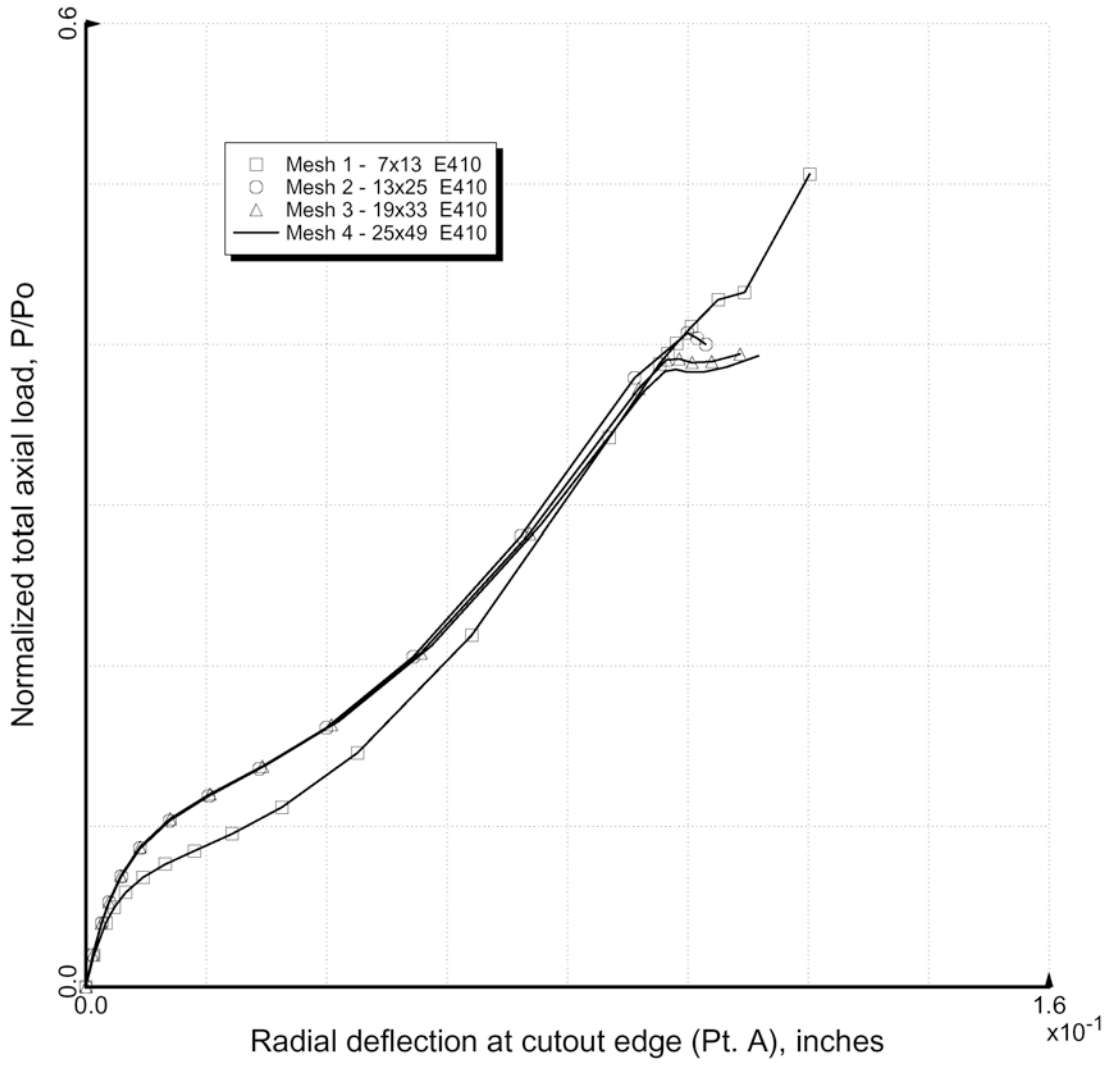


Figure 30. Effect of mesh refinement using the E410 shell element on the elastic nonlinear collapse response.

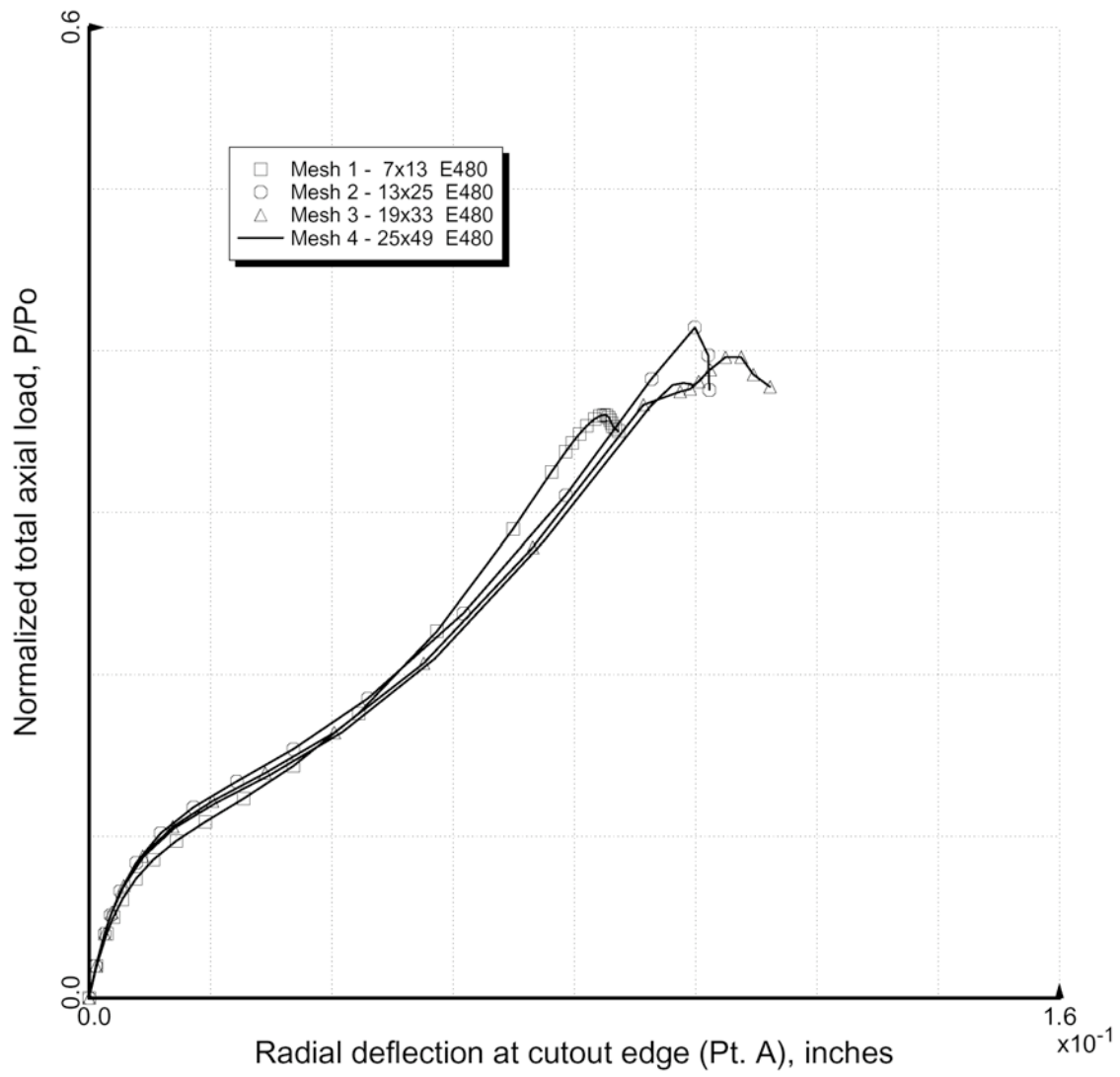


Figure 31. Effect of mesh refinement using the E410 shell element on the elastic nonlinear collapse response.

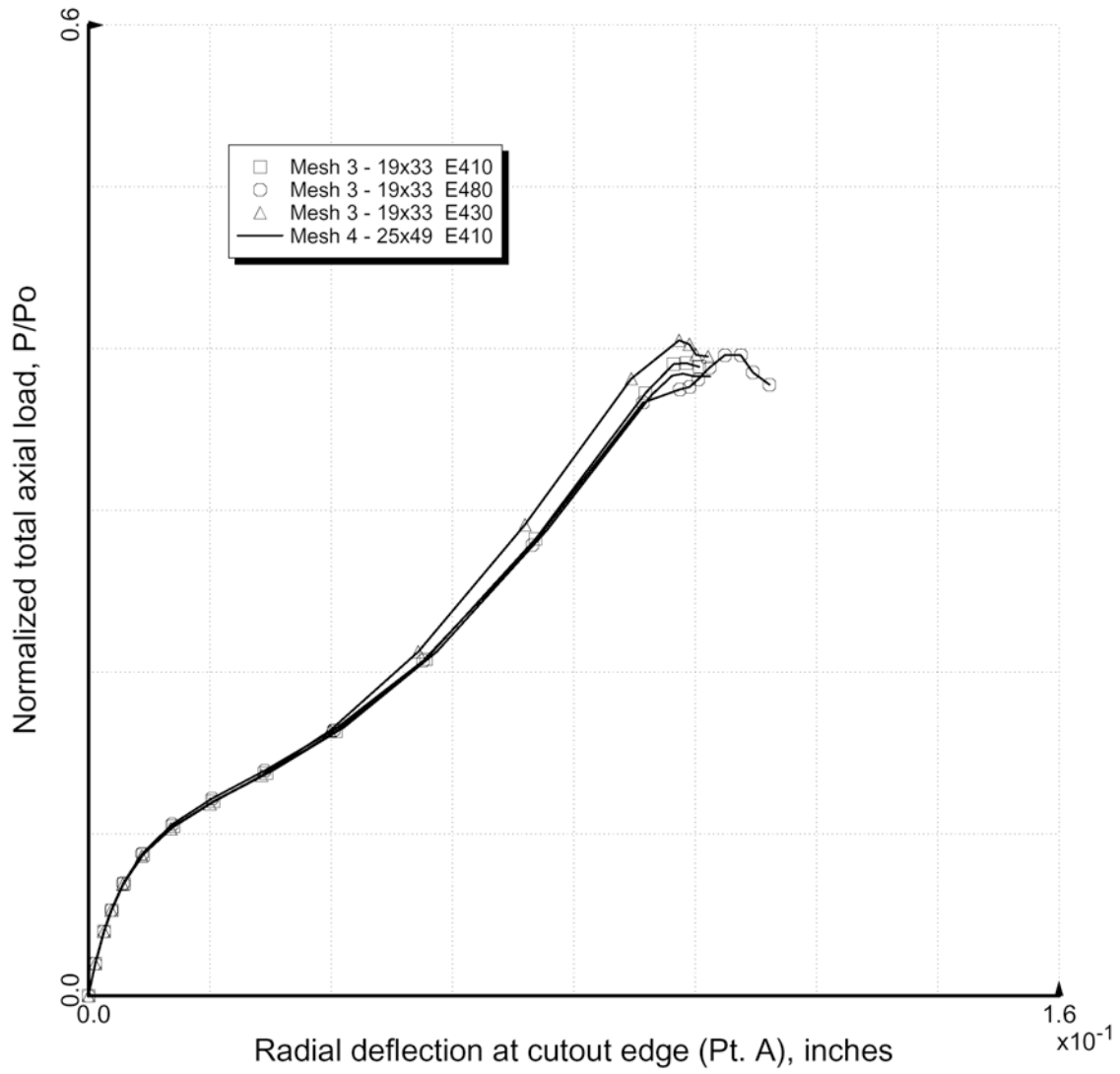
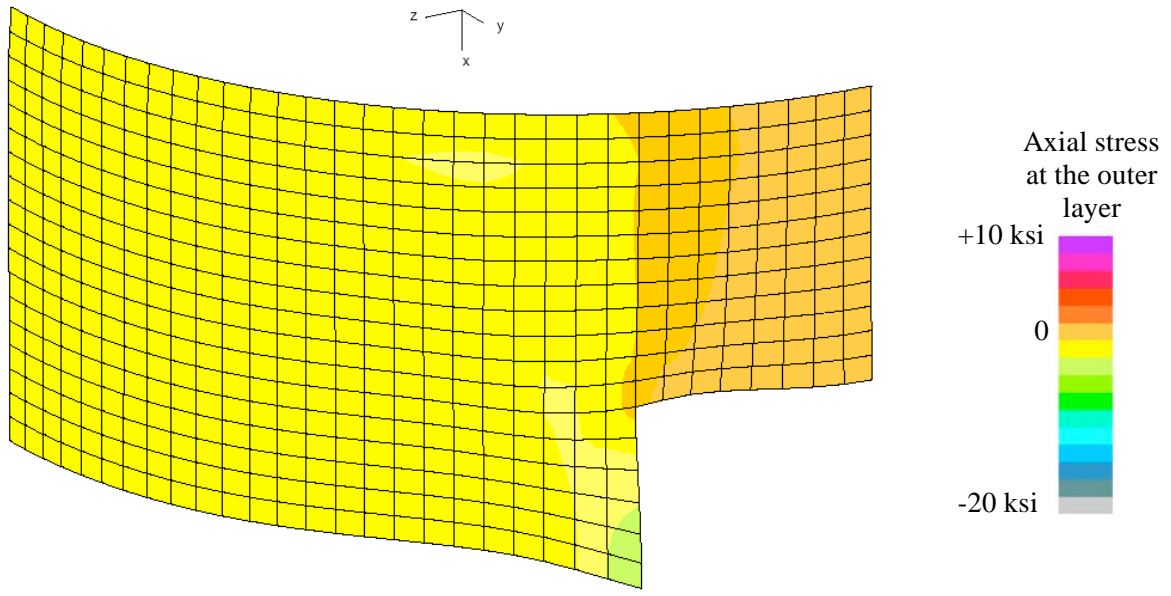
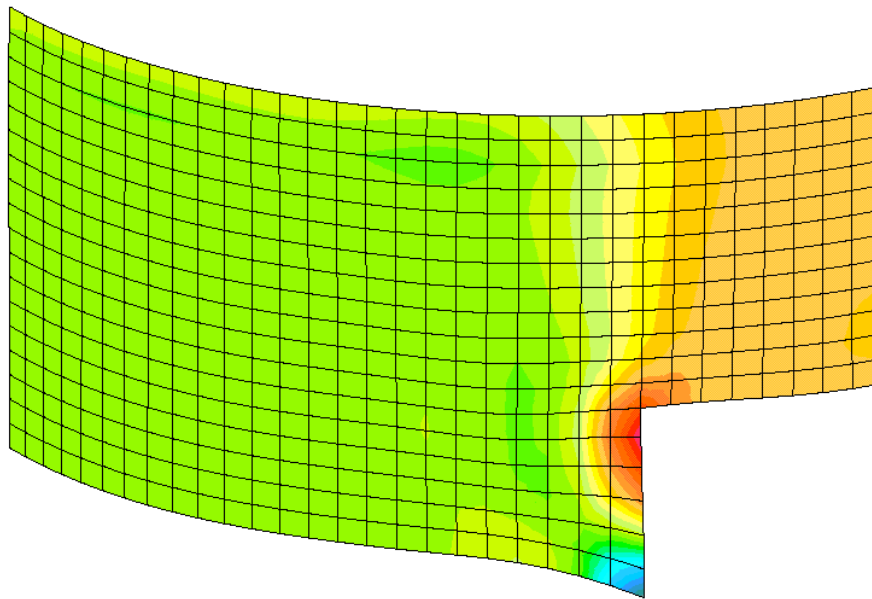


Figure 32. Effect of element type using Mesh 3 on the elastic nonlinear collapse response.

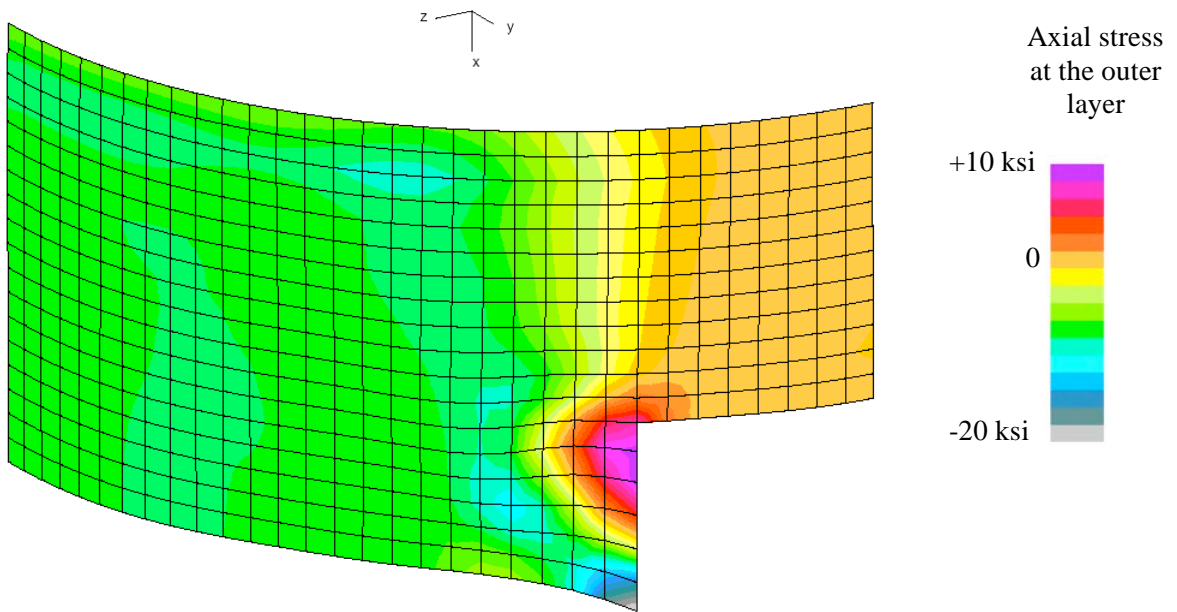


(a) Step 6, $P=0.1049 P_0$

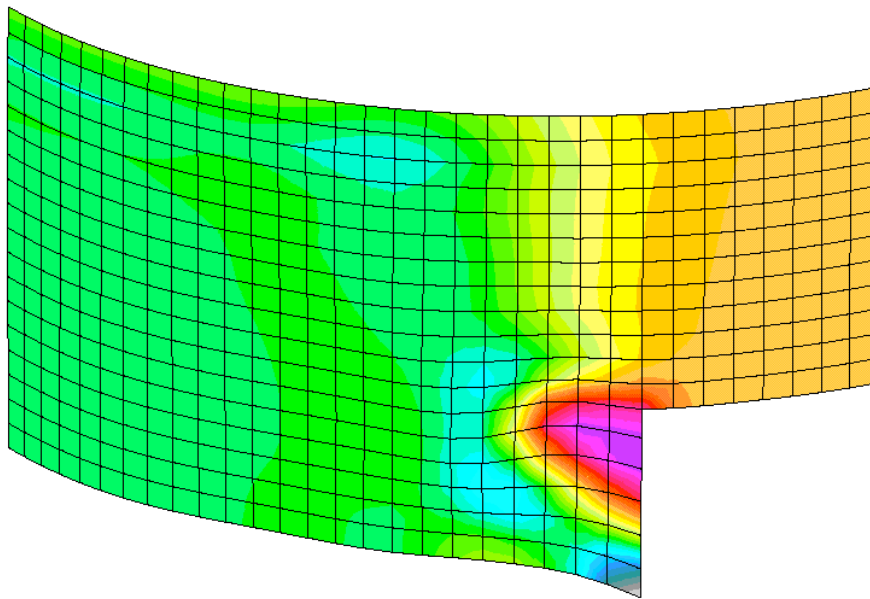


(b) Step 11, $P=0.2825 P_0$

Figure 33. Contour plots of the axial stress in the outer surface displayed on the deformed geometry at selected solution steps.



(c) Step 13, $P=0.3905 P_0$



(d) Step 15, $P=0.3888 P_0$

Figure 33. Concluded.

STAGS Input Files

These STAGS input files are located under the following subdirectory:

\$STAGSHOME/Sample-Testcases/Cyl-with-Cutouts

Under this directory are the files for the 2D shell finite element models and analyses described in this section.

Single Shell Unit Input Files

The following text files give the input for the cylinder with cutouts using the E410 4-node shell element with an 19x33 mesh of nodes on the shell surface. These files are in the 2D/ subdirectory. The S2 input file contains input sufficient to perform the buckling computations and the elastic nonlinear collapse analysis. While all records of the S2 input file are read, only those associated with the first analysis type are active. Similarly all the records of the STAPL input file are read even though only the number of plots specified on the PL-2 record will be drawn.

cutout1.inp (for S1 processor)

```
2D circular cylinder with two rectangular cutouts $A-1
C
C Cylinder with cutouts 180-degrees apart at cylinder
C mid-length; clamped at the ends and loaded by applied
C end-shortening. Elastic postbuckling response.
C R=6.06 in., L=9.0 in. (total), t=0.014 in.
C R/t=433, L/R=1.5
C
C Loading is a point axial load plus constraints for uniform u
C Px = 0.25*Po = 0.25 * (1.2*pi*E*t^2) = 1847.256 pounds
C Critical eigenvalue is 0.137
C Linear Buckling Load = 1012.3 lbs. = 0.137 * Po
C Collapse Load from STAGS (Mesh 4, E410) = 0.3845 Po
C Collapse Load from Test [1] = 2200 lbs = 0.2977 * Po
C
C Perfect geometry assumed for linear buckling analysis
C and for the elastic collapse analysis. Use of initial
C geometric imperfections would influence the collapse load
C prediction.
C
C References:
C 1. Almroth, B. O. and Holmes, A. M. C., "Buckling of Shells with
C Cutouts, Experiment and Analysis," International Journal
C of Solids and Structures, Vol. 8, No. 8, 1972, pp. 1057-1071.
C 2. Hartung, R. F. and Ball, R. E., "A Comparison of Several
C Computer Solutions to Three Structural Shell Analysis
C Problems," AFFDL TR-73-15, 1973
C 3. Almroth, B. O. and Brogan, F. A., "Computational Efficiency
C of Shell Elements," in Nonlinear Finite Element Analysis
C of Plates and Shells, Hughes, Pifko, & Jay (editors),
C ASME AMD Vol. 48, 1981, pp. 147-165.
C 4. Knight, et al., "Large-Scale Structural Analysis: The
C Structural Analyst, The CSM Testbed, and The NAS System,"
C NASA TM-100643, March 1989.
C
0 0 0 0 0 3 0 $b-1
1 20.0 / 2 -60.0 / 3 -90.0 $b-1b model rotations
1 0 0 0 1 0 0 $b-2
1 0 1 0 0 1 $b-3
C
C FE Mesh Study
C Nrcols x Ncols
```



```

C
C7 13 $F-1 Mesh 1
C13 25 $F-1 Mesh 2
19 33 $F-1 Mesh 3
C25 49 $F-1 Mesh 4
C37 65 $F-1 Mesh 5
C
1 1 1 1 1 1 0 1 $G-2 set end shortening to be uniform
C
C Material Record using Historical Approach
C
1 0 $I-1 material table
10.0E+6 0.3 0.0 .1 $i-2 E, nu, G=E/2/(1+nu), rho (for volume check)
C
C GCP Input
C
ISOELASTIC_MATERIAL 1 1 1 $i-5
10.0E+6, $i-6a Young's modulus, psi
0.3, $i-6a Poisson's ratio
2.59E-4, $i-6a Mass density
4*0.0 $i-6a unused properties
C
C Shell wall fabrications
C
SHELL_FABRICATION 1 1 0 0 0 $i-5a fabid, nlayer, ipt, ishr, isym
1 $I-21a matid
0.014 $i-21c thickness, inches
0.0 $i-21d angle
C
END $I-5a end GCP input
C
C Wall Record using Historical Approach
C
1 1 1 0 $k-1 thickness, inches
1 0.014 0.0 $k-2
C
C Shell Unit Definition - using 2D shell elements
C
5 0 0 0 0 0 0 $m-1 cylindrical shell geometry
0.0 4.50 0.0 90.0 6.06 $m-2 x1, x4, y1, y2, R
-1 0 0.0 0.0 0 0 $m-5 shell wall selection
410 0 0 1 $n-1 element options
C
C Irregular mesh option for cutout boundaries
C (only works for quadrilateral shell elements)
C
C5 7 9 13 $N-8 Mesh 1 values
C9 13 19 25 $N-8 Mesh 2 values
13 19 25 33 $N-8 Mesh 3 values
C17 25 37 49 $N-8 Mesh 4 values
C25 37 49 65 $N-8 Mesh 5 values
C
C Boundary conditions
C
0 4 4 4 $p-1 clamped-sym-sym-sym
100 000 $p-2 end shortening on clamped end
C
C Loading - point load at center
C P_base = 0.25 * Po = 0.25 * (1.2 pi E t^2)
C then the load factor is related to P/Po
C
1 0 $q-1 load summary
1 1 0 $q-2

```

```

1847.256 1 1 1 1 0 $Q-3 imposed axial load at one node and then G-1
C0.0 -1 6 0 0 0 $Q-3 imposed RW=0 everywhere for E480 and E330
0 0 0 0 0 1 0 0 $r-1 Output selection
1 0 $r-2 selected displacement output

```

cutout1.bin (for S2 processor)

```

Cylinder with two rectangular cutouts $A-1
C
C Linear buckling analysis
C
1 1 0 0 0 0 0 -1 $b-1
1.0 0.0 1.0 $c-1
1000 1.0e-4 0 $d-2
10 .137 $d-3 Number of modes
C
C Nonlinear static solution control
C
3 1 5*0 -1 $B-1 ANALYSIS CONTROL
0.02 0.02 1.0 $C-1 LOAD MULTIPLIERS
0 3000 5 -20 0 1.0e-4 1.0 $d-1 strategy parameters
0 0 0 $et-1

```

cutout1.pin (for STAPL processor)

```

Cylinder with two rectangular cutouts
4 0 0 0 $PL-2 NPLOT,IPREP,IPRS,KDEV
C plot axial stress contours
2 0 7 6 0 0 0 1 $PL-3 KPLOT,VIEW,ITEM,STEP,MODE,IFRNG,COLOR,ICOMP
0.0 3 0.0 -20000.0 10000.0 $PL-5 DSCALE,NROTS,LWSCALE,RNGMIN,RGMAX
1 20.0 / 2 -60.0 / 3 -90.0
2 0 7 11 0 0 0 1 $PL-3 KPLOT,VIEW,ITEM,STEP,MODE,IFRNG,COLOR,ICOMP
0.0 3 0.0 -20000.0 10000.0 $PL-5 DSCALE,NROTS,LWSCALE,RNGMIN,RGMAX
1 20.0 / 2 -60.0 / 3 -90.0
2 0 7 13 0 0 0 1 $PL-3 KPLOT,VIEW,ITEM,STEP,MODE,IFRNG,COLOR,ICOMP
0.0 3 0.0 -20000.0 10000.0 $PL-5 DSCALE,NROTS,LWSCALE,RNGMIN,RGMAX
1 20.0 / 2 -60.0 / 3 -90.0
2 0 7 15 0 0 0 1 $PL-3 KPLOT,VIEW,ITEM,STEP,MODE,IFRNG,COLOR,ICOMP
0.0 3 0.0 -20000.0 10000.0 $PL-5 DSCALE,NROTS,LWSCALE,RNGMIN,RGMAX
1 20.0 / 2 -60.0 / 3 -90.0
C plot stress resultant Nx at different steps
2 0 5 6 0 2 1 1 $PL-3 KPLOT,VIEW,ITEM,STEP,MODE,IFRNG,COLOR,ICOMP
0.0 3 0.0 -150.0 0.0 $PL-5 DSCALE,NROTS,LWSCALE,RNGMIN,RGMAX
1 20.0 / 2 -60.0 / 3 -90.0
2 0 5 11 0 2 1 1 $PL-3 KPLOT,VIEW,ITEM,STEP,MODE,IFRNG,COLOR,ICOMP
0.0 3 0.0 -150.0 0.0 $PL-5 DSCALE,NROTS,LWSCALE,RNGMIN,RGMAX
1 20.0 / 2 -60.0 / 3 -90.0
2 0 5 13 0 2 1 1 $PL-3 KPLOT,VIEW,ITEM,STEP,MODE,IFRNG,COLOR,ICOMP
0.0 3 0.0 -150.0 0.0 $PL-5 DSCALE,NROTS,LWSCALE,RNGMIN,RGMAX
1 20.0 / 2 -60.0 / 3 -90.0
2 0 5 15 0 2 1 1 $PL-3 KPLOT,VIEW,ITEM,STEP,MODE,IFRNG,COLOR,ICOMP
0.0 3 0.0 -150.0 0.0 $PL-5 DSCALE,NROTS,LWSCALE,RNGMIN,RGMAX
1 20.0 / 2 -60.0 / 3 -90.0
C plot buckling modes
2 0 4 0 1 0 0 3 $PL-3 KPLOT,VIEW,ITEM,STEP,MODE,IFRNG,COLOR,ICOMP
0.0 3 0.0 -1.0 1.0 $PL-5 DSCALE,NROTS,LWSCALE,RNGMIN,RGMAX
1 20.0 / 2 -60.0 / 3 -90.0
2 0 4 0 6 0 0 3 $PL-3 KPLOT,VIEW,ITEM,STEP,MODE,IFRNG,COLOR,ICOMP
0.0 3 0.0 -1.0 1.0 $PL-5 DSCALE,NROTS,LWSCALE,RNGMIN,RGMAX
1 20.0 / 2 -60.0 / 3 -90.0
2 0 4 0 9 0 0 3 $PL-3 KPLOT,VIEW,ITEM,STEP,MODE,IFRNG,COLOR,ICOMP

```

```

0.0 3 0.0 -1.0 1.0 $PL-5 DSCALE,NROTS,LWSCALE,RNGMIN,RGMAX
1 20.0 / 2 -60.0 / 3 -90.0
2 0 4 0 4 0 0 3 $PL-3 KPLOT,VIEW,ITEM,STEP,MODE,IFRNG,COLOR,ICOMP
0.0 3 0.0 -1.0 1.0 $PL-5 DSCALE,NROTS,LWSCALE,RNGMIN,RGMAX
1 20.0 / 2 -60.0 / 3 -90.0
2 0 4 0 5 0 0 3 $PL-3 KPLOT,VIEW,ITEM,STEP,MODE,IFRNG,COLOR,ICOMP
0.0 3 0.0 -1.0 1.0 $PL-5 DSCALE,NROTS,LWSCALE,RNGMIN,RGMAX
1 20.0 / 2 -60.0 / 3 -90.0
2 0 4 0 6 0 0 3 $PL-3 KPLOT,VIEW,ITEM,STEP,MODE,IFRNG,COLOR,ICOMP
0.0 3 0.0 -1.0 1.0 $PL-5 DSCALE,NROTS,LWSCALE,RNGMIN,RGMAX
1 20.0 / 2 -60.0 / 3 -90.0
2 0 4 0 7 0 0 3 $PL-3 KPLOT,VIEW,ITEM,STEP,MODE,IFRNG,COLOR,ICOMP
0.0 3 0.0 -1.0 1.0 $PL-5 DSCALE,NROTS,LWSCALE,RNGMIN,RGMAX
1 20.0 / 2 -60.0 / 3 -90.0
2 0 4 0 8 0 0 3 $PL-3 KPLOT,VIEW,ITEM,STEP,MODE,IFRNG,COLOR,ICOMP
0.0 3 0.0 -1.0 1.0 $PL-5 DSCALE,NROTS,LWSCALE,RNGMIN,RGMAX
1 20.0 / 2 -60.0 / 3 -90.0
2 0 4 0 9 0 0 3 $PL-3 KPLOT,VIEW,ITEM,STEP,MODE,IFRNG,COLOR,ICOMP
0.0 3 0.0 -1.0 1.0 $PL-5 DSCALE,NROTS,LWSCALE,RNGMIN,RGMAX
1 20.0 / 2 -60.0 / 3 -90.0
2 0 4 0 10 0 0 3 $PL-3 KPLOT,VIEW,ITEM,STEP,MODE,IFRNG,COLOR,ICOMP
0.0 3 0.0 -1.0 1.0 $PL-5 DSCALE,NROTS,LWSCALE,RNGMIN,RGMAX
1 20.0 / 2 -60.0 / 3 -90.0
2 0 1 10 0 0 0 3 $PL-3 KPLOT,VIEW,ITEM,STEP,MODE,IFRNG,COLOR,ICOMP
0.0 3 0.0 0.0 0.0 $PL-5 DSCALE,NROTS,LWSCALE,RNGMIN,RGMAX
1 20.0 / 2 -60.0 / 3 -90.0
2 0 1 20 0 0 0 3 $PL-3 KPLOT,VIEW,ITEM,STEP,MODE,IFRNG,COLOR,ICOMP
0.0 3 0.0 0.0 0.0 $PL-5 DSCALE,NROTS,LWSCALE,RNGMIN,RGMAX
1 20.0 / 2 -60.0 / 3 -90.0

```

cutout1.pxy (for XYTRANS processor)

This input is generated and saved during the first execution of XYTRANS (so called journal file). Once created it can be used over and over again to extract the same information from a STAGS run.

```

P          $ (P)lotps or (S)pread_Sheet output
cutout1   $ STAGS solution 'Case Name'
F          $ (F)ull or (C)ondensed Model
Y          $ (Y)es-(N)o: setup data for another plot
5         $ x-axis variable = choice (1 to 15)
0         $ node no. (0 = ask for Unit,Row,Col)
1 19 25   $ (U)nit, (R)ow, (C)ol - Node No. = 619
3         $ comp no., dis,vel,acc (1-6) = u,v,w,ru,rv,rw
S         $ (G)lobal or (S)hell ref surface
N         $ (Y)es-(N)o: specify x-variable scale factor
2         $ y-axis variable = choice (1 to 15)
N         $ (Y)es-(N)o: specify y-variable scale factor
N         $ (Y)es-(N)o: specify subrange of loadsteps
Y         $ (Y)es-(N)o: plotted points start at origin
N         $ (Y)es-(N)o: setup data for another plot

```

Two-Shell-Unit Model Input Files

The following text files give the input for the cylinder with cutouts using the E410 4-node shell element with a 19×33 mesh of nodes on the shell surface. The input files for S2 and STAPL are the same as those given for the single-shell-unit model.

cutout2.inp (for S1 processor)

```
2D circular cylinder with two rectangular cutouts - 2 shell units $A-1
C
C Mesh 3 (19 x 33) only
C
C Cylinder with cutouts 180-degrees apart at cylinder
C mid-length; clamped at the ends and loaded by applied
C end-shortening. Elastic postbuckling response.
C Only a 1/8 symmetric model is considered.
C
C R=6.06 in., L=9.0 in. (total), t=0.014 in.
C R/t=433, L/R=1.5
C
C Loading is a point axial load plus constraints for uniform u
C Px = 0.25*Po = 0.25 * (1.2*pi*E*t^2) = 1847.256 pounds
C Critical eigenvalue is 0.137
C Linear Buckling Load = 1012.3 lbs. = 0.137 * Po
C Collapse Load from STAGS (Mesh 4, E410) = 0.3845 * Po
C Collapse load from test [1] = 2200 lbs = 0.2977 * Po
C
C Perfect geometry assumed for linear buckling analysis
C and for the elastic collapse analysis. Use of initial
C geometric imperfections would influence the collapse load
C prediction.
C
C References:
C 1. Almroth, B. O. and Holmes, A. M. C., "Buckling of Shells with
C Cutouts, Experiment and Analysis," International Journal
C of Solids and Structures, Vol. 8, No. 8, 1972, pp. 1057-1071.
C 2. Hartung, R. F. and Ball, R. E., "A Comparison of Several
C Computer Solutions to Three Structural Shell Analysis
C Problems," AFFDL TR-73-15, 1973
C 3. Almroth, B. O. and Brogan, F. A., "Computational Efficiency
C of Shell Elements," in Nonlinear Finite Element Analysis
C of Plates and Shells, Hughes, Pifko, & Jay (editors),
C ASME AMD Vol. 48, 1981, pp. 147-165.
C 4. Knight, et al., "Large-Scale Structural Analysis: The
C Structural Analyst, The CSM Testbed, and The NAS System,"
C NASA TM-100643, March 1989.
C
0 0 0 0 0 3 0          $b-1
1 20.0 / 2 -60.0 / 3 -90.0 $b-1b model rotations
2 0 0 0 3 0 0          $b-2
1 0 1 0 0 1           $b-3
C FE mesh Nrcols x Ncols
19 25 13 9          $F-1 Resulting mesh is 19 x 33
1 1 1 1 1 1 0 1    $G-2 set end shortening to be uniform
1 1 1 1 2 1 0 1    $G-2 set end shortening to be uniform
1 0 25 0 2 0 1 0   1 13 1 1 13 1 $G-2
C
C Material Record using Historical Approach
C
1 0 $I-1 material table
10.0E+6 0.3 0.0 .1 $i-2 E, nu, G=E/2/(1+nu), rho (for volume check)
C
C GCP Input
C
```

```

ISOELASTIC_MATERIAL 1 1 1 $i-5
10.0E+6,          $i-6a Young's modulus, psi
0.3,             $i-6a Poisson's ratio
2.59E-4,         $i-6a Mass density
4*0.0           $i-6a unused properties
C
C Shell wall fabrications
C
SHELL_FABRICATION 1 1 0 0 0 $i-5a fabid, nlayer, ipt, ishr, isym
1      $I-21a matid
0.014 $i-21c thickness, inches
0.0   $i-21d angle
C
END    $I-5a end GCP input
C
C Wall Record using Historical Approach
C
1 1 1 0      $k-1 thickness, inches
1 0.014 0.0  $k-2
C
C Shell Unit Definition - using 2D shell elements
C
C      =====
C      Shell unit 1 (top left side)
C      =====
5 0 0 0 0 0 0      $m-1 cylindrical shell geometry
0.0 4.50 0.0 67.5 6.06 $m-2 x1, x4, y1, y2, R
-1 0 0.0 0.0 0 0   $m-5 shell wall selection
410 0 0 0          $n-1 element options
C
C Boundary conditions
C
0 3 4 4      $p-1 clamped-juncture-juncture-sym
100 000      $p-2 end shortening on clamped end
C
C Loading - point load at center
C
1 0          $q-1 load summary
1 1 0        $q-2
1847.256 1 1 1 1 0 $Q-3 imposed axial load at one node and then G-1
C0.0 -1 6 0 0 0 $Q-3 RW=0 everywhere for E480 & E430
0 0 0 0 0 1 0 0 $r-1 Output selection
1 0          $r-2 selected displacement output
C
C      =====
C      Shell unit 2 (top right side over cutout)
C      =====
5 0 0 0 0 0 0      $m-1 cylindrical shell geometry
0.0 3.00 67.5 90.0 6.06 $m-2 x1, x4, y1, y2, R
-1 0 0.0 0.0 0 0   $m-5 shell wall selection
410 0 0 0          $n-1 element options
C
C Boundary conditions
C
0 4 3 3      $p-1 clamped-sym-free-juncture
100 000      $p-2 end shortening on clamped end
C
0 0          $q-1 No loads
C1 0         $q-1 Zero out drilling freedoms for E480 & E430
C1 1 0       $q-2
C0.0 -1 6 0 0 0 $Q-3 RW=0 everywhere
0 0 0 0 0 1 0 0 $r-1 Output selection
1 0          $r-2 selected displacement output

```

Three-Shell-Unit Model Input Files

The following text files give the input for the cylinder with cutouts using the E430 3-node shell element with a 19x33 mesh of nodes on the shell surface. Notice in this case that the drilling freedoms are suppressed everywhere in the finite element model (*i.e.*, requires Q-3 records for each shell unit). The input files for S2 and STAPL are the same as those given for the single-shell-unit model.

cutout3.inp (for S1 processor)

```
2D circular cylinder with two rectangular cutouts - 3 shell units $A-1
C
C Mesh 3 (19 x 33) only
C
C Cylinder with cutouts 180-degrees apart at cylinder
C mid-length; clamped at the ends and loaded by applied
C end-shortening. Elastic postbuckling response.
C Only a 1/8 symmetric model is considered.
C
C R=6.06 in., L=9.0 in. (total), t=0.014 in.
C R/t=433, L/R=1.5
C
C Loading is a point axial load plus constraints for uniform u
C Px = 0.25*Po = 0.25 * (1.2*pi*E*t^2) = 1847.256 pounds
C Critical eigenvalue is 0.137
C Linear Buckling Load = 1012.3 lbs. = 0.137 * Po
C Collapse Load from STAGS (Mesh 4, E410) = 0.3845 * Po
C Collapse Load from Test [1] = 2200 lbs = 0.2977 * Po
C
C Perfect geometry assumed for linear buckling analysis
C and for the elastic collapse analysis. Use of initial
C geometric imperfections would influence the collapse load
C prediction.
C
C References:
C 1. Almroth, B. O. and Holmes, A. M. C., "Buckling of Shells with
C Cutouts, Experiment and Analysis," International Journal
C of Solids and Structures, Vol. 8, No. 8, 1972, pp. 1057-1071.
C 2. Hartung, R. F. and Ball, R. E., "A Comparison of Several
C Computer Solutions to Three Structural Shell Analysis
C Problems," AFFDL TR-73-15, 1973
C 3. Almroth, B. O. and Brogan, F. A., "Computational Efficiency
C of Shell Elements," in Nonlinear Finite Element Analysis
C of Plates and Shells, Hughes, Pifko, & Jay (editors),
C ASME AMD Vol. 48, 1981, pp. 147-165.
C 4. Knight, et al., "Large-Scale Structural Analysis: The
C Structural Analyst, The CSM Testbed, and The NAS System,"
C NASA TM-100643, March 1989.
C
0 0 0 0 0 3 0 $b-1
1 20.0 / 2 -60.0 / 3 -90.0 $b-1b model rotations
3 0 0 2 2 0 0 $b-2
1 0 1 0 0 1 $b-3
C FE mesh Nrcols x Ncols
13 25 13 9 7 25 $F-1 Resulting mesh is 19 x 33
1 2 2 4 $g-1 Shell unit connectivity
1 3 3 1 $g-1 Shell unit connectivity
1 1 1 1 1 0 1 $G-2 set end shortening to be uniform
1 1 1 1 2 1 0 1 $G-2 set end shortening to be uniform
C
C Material Record using Historical Approach
C
1 0 $I-1 material table
```

```

10.0E+6  0.3  0.0  .1  $i-2  E, nu, G=E/2/(1+nu), rho (for volume check)
C
C  GCP Input
C
ISOELASTIC_MATERIAL  1  1  1  $i-5
10.0E+6,             $i-6a  Young's modulus, psi
0.3,                 $i-6a  Poisson's ratio
2.59E-4,             $i-6a  Mass density
4*0.0                 $i-6a  unused properties
C
C  Shell wall fabrications
C
SHELL_FABRICATION  1  1  0  0  0  $i-5a  fabid, nlayer, ipts, ishr, isym
1      $I-21a  matid
0.014  $i-21c  thickness, inches
0.0    $i-21d  angle
C
END      $I-5a  end GCP input
C
C  Wall Record using Historical Approach
C
1  1  1  0      $k-1  thickness, inches
1  0.014  0.0  $k-2
C
C  Shell Unit Definition - using 2D shell elements
C
C      =====
C      Shell unit 1 (top left side)
C      =====
5  0  0  0  0  0  0      $m-1  cylindrical shell geometry
0.0  3.00  0.0  67.5  6.06  $m-2  x1, x4, y1, y2, R
-1  0  0.0  0.0  0  0      $m-5  shell wall selection
430  0  0  0      $n-1  element options
C
C  Boundary conditions
C
0  6  6  4      $p-1  clamped-juncture-juncture-sym
100  000  $p-2  end shortening on clamped end
C
C  Loading - point load at center
C
1  0      $q-1  load summary
1  2  0      $q-2
1847.256  1  1  1  1  0  $Q-3  imposed axial load at one node and then G-1
0.0  -1  6  0  0  0      $q-3  RW=0 everywhere
0  0  0  0  0  1  0  0  $r-1  Output selection
1  0  $r-2  selected displacement output
C
C      =====
C      Shell unit 2 (top right side over cutout)
C      =====
5  0  0  0  0  0  0      $m-1  cylindrical shell geometry
0.0  3.00  67.5  90.0  6.06  $m-2  x1, x4, y1, y2, R
-1  0  0.0  0.0  0  0      $m-5  shell wall selection
430  0  0  0      $n-1  element options
C
C  Boundary conditions
C
0  4  3  6      $p-1  clamped-sym-free-juncture
100  000  $p-2  end shortening on clamped end
C
1  0      $q-1  Suppress drilling freedoms
1  1      $q-2
0.0  -1  6  0  0  0      $q-3  RW=0 everywhere

```

```

0 0 0 0 0 0 1 0 0      $r-1  Output selection
1 0  $r-2  selected displacement output
C      =====
C      Shell unit 3 (bottom side left of cutout)
C      =====
5 0 0 0 0 0 0          $m-1  cylindrical shell geometry
3.0 4.50 0.0 67.5 6.06  $m-2  x1, x4, y1, y2, R
-1 0 0.0 0.0 0 0      $m-5  shell wall selection
430 0 0 0            $n-1  element options
C
C  Boundary conditions
C
6 3 4 4      $p-1  juncture-free-sym-sym
C
C
1 0          $q-1  Suppress drilling freedoms
1 1          $q-2
0.0 -1 6 0 0 0  $q-3  RW=0 everywhere
0 0 0 0 0 0 0 0  $r-1  Output selection

```

Problem References

Almroth, B. O. and Holmes, A. M. C., "Buckling of Shells with Cutouts, Experiment and Analysis," *International Journal of Solids and Structures*, Vol. 8, 1972, pp. 1057-1071.

Hartung, R. F. and Ball R. E., A Comparison of Several Computer Solutions to Three Structural Shell Analysis Problems, AFFDL Report No. AFFDL-TR-73-15, April 1973.

Almroth, B. O., Meller, E., and Brogan, F. A., "Computer Solutions for Static and Dynamic Buckling of Shells," in *Buckling of Structures*, B. Budiansky (editor), proceedings of the IUTAM Symposium, June 17-21, 1974, Springer-Verlag, Berlin, 1976, pp. 52-66.

Almroth, B. O. and Brogan, F. A., "Computational Efficiency of Shell Elements," in *Nonlinear Finite Element Analysis of Plates and Shells*, T. J. R. Hughes, A. Pifko, and A. Jay (editors), ASME AMD-Vol. 48, 1981, pp. 147-165.

Knight, N. F., Jr., McCleary, S. L., Macy, S. C., and Aminpour, M. A., *Large-Scale Structural Analysis: The Structural Analyst, The CSM Testbed, and The NAS System*, NASA TM-100643, March 1989.

Knight, N. F., Jr., Macy, S. C., and McCleary, S. L., "Assessment of Structural Analysis Technology for Static Collapse of Elastic Cylindrical Shells," *Finite Elements in Analysis and Design*, Vol. 18, No. 4, January 1995, pp. 403-431.

Hurlbut, B. J., Stanley, G. M., and Kang, D. S., *The Computational Structural Mechanics (CSM) Testbed Applications Manual*, Lockheed Contract Report No. LMSC-F333007, May 1989.

Rankin, C. C., Brogan, F. A., Loden, W., and Cabiness, H., *Structural Analysis of General Shells – STAGS User Manual, Version 4.0*, Lockheed Martin Advanced Technology Center, Palo Alto, CA, June 2000.

Scordelis-Lo Barrel Roof Problem

Background

The Scordelis-Lo barrel roof (or vault) is a singly curved shell structure shown in Figure 34 loaded by a gravity load or uniform dead load (UDL, loading by its own weight). This cylindrical shell is supported along the curved ends by rigid diaphragms ($v=w=0$) while the straight edges are free. This problem is a common linear static shell analysis (*e.g.*, Forsberg, 1971; Parisch, 1979; Thomas and Sobel, 1981; MacNeal and Harder, 1985; Belytschko and Liu, 1986; Zienkiewicz and Taylor, 1991; Phaal and Calladine, 1992; Rengarajan *et al.*, 1995). This problem tests an element's ability to represent membrane states. Most of the strain energy is stored in the stretching mode with little inextensional flexural response. It is one of the MacNeal-Harder standard test problems and one of the Belytschko-Liu shell obstacle course problems.

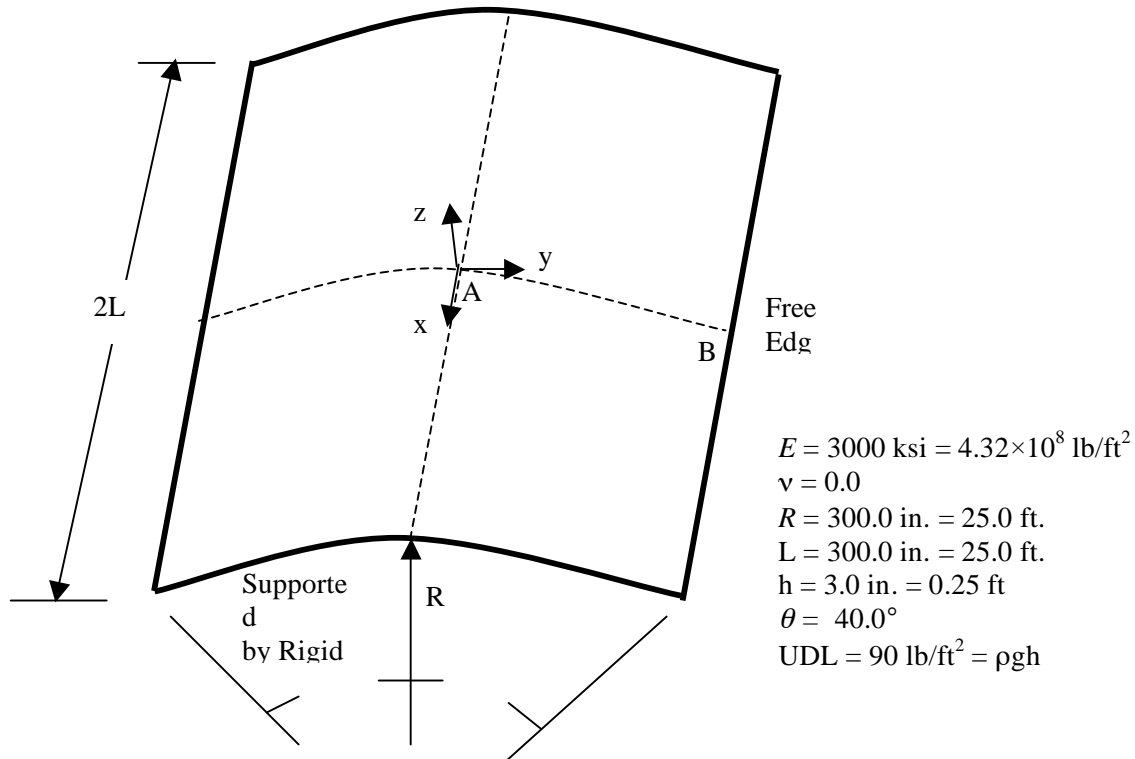


Figure 34. Scordelis-Lo barrel roof problem: geometry and material properties.

Modeling and Analysis Process

Two separate STAGS finite element models are considered in this test case problem: shell elements and solid elements. A summary of each model includes:

2-D shell models – Model the shell with plate elements (x - y plane) in a single shell unit as shown in Figure 35.

3-D solid models – Model shell with solid elements in a single shell unit using one and two solid elements through the thickness of the shell as shown in Figure 36.

The STAGS model is generated using a single shell unit with the cylindrical shell surface geometry (ISHELL=5) using the mid-surface as the shell reference surface. Material properties and membrane construction are defined using both the *historical* STAGS approach and the current GCP approach. Mesh discretization studies include different levels of mesh refinement and different element types. Mesh refinement is readily performed by changing the number of rows and columns of nodes in each direction on the F-1 record. Element type is selected using the N-1 record (KELT). Multiple solid elements through the thickness are specified using the NLAYS and NFABS parameters on the M-1 record in combination with a set of NFABS M-5 records.

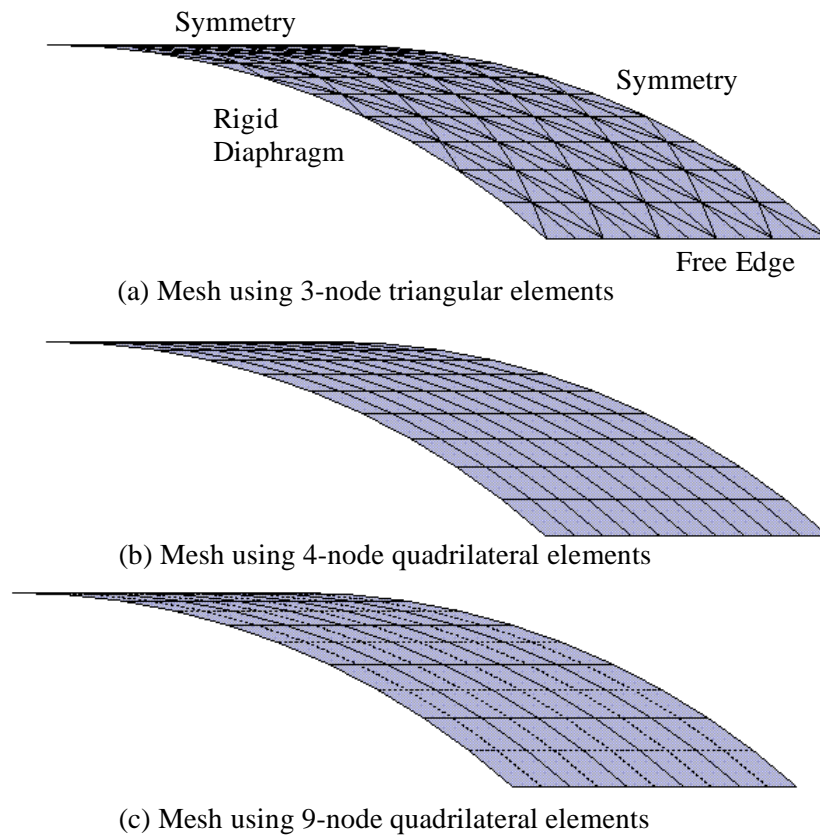
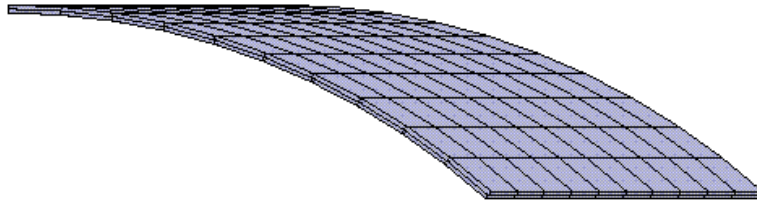
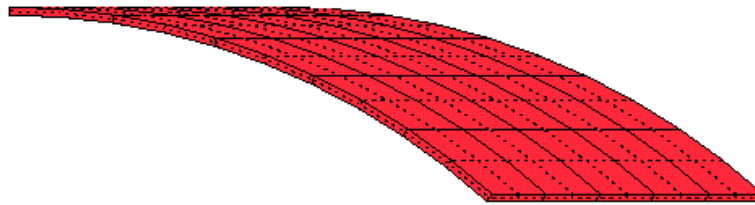


Figure 35. Shell finite element models having 11 nodes per edge.



(a) Mesh using 8-node hexahedral elements – NEZ=2



(b) Mesh using 27-node hexahedral elements – NEZ=1)

Figure 36. Solid element models having 11 nodes per edge.

Material properties and laminate construction are defined using both the *historical* STAGS approach (*i.e.*, STAGS versions prior to GCP) and the current GCP approach. Material modeling for an elastic orthotropic material using the historical STAGS approach requires data on the I-1 and I-2 records to define the material properties and the K-1 and K-2 records to define the laminate fabrication data. Material modeling using the current GCP approach requires data on the I-5a and I-6a records to define the material properties and records I-5a, I-21a, I-21b, I-21c, I-21d, and I-21e to define the shell fabrication. In addition, records I-5a, I-22a, and I-22b are used to define the solid fabrication. As a basic check on the finite element model, the total weight of the structure is computed and printed in the initial portion of the S2 output file. The total weight of one quarter of the shell is 12500π pounds.

Boundary condition on the displacements could be specified using the P-1 and P-2 records for the shell models as indicated in the input file. However, for compatibility with the solid element models, the boundary conditions are imposed using specified zero displacements through the Q-records for both shell and solid models. The boundary conditions along the curved boundary are those of a rigid diaphragm with no circumferential or transverse displacements ($v=w=0$), and the boundary conditions along the straight boundary are free. Symmetry boundary conditions are imposed on the remaining straight and curved interior edges. The uniform dead load (UDL) is applied as an inertial loading (B-6 records) acting parallel to the negative z -coordinate direction. Essentially the weight density of the shell material generates the distributed load. The weight density is computed as the UDL divided by the shell thickness or 360 lbs/in.³. The inertial loading is due to the shell mass density and the acceleration due to gravity. The default gravitational constant g in STAGS is 386.1 in./sec.² (32.175 ft/ sec.²) which may be changed using the B-4 record in the S1 input file. For this test case, a value of 386.4 in./sec.² (32.2 ft/ sec.²) is used.

Numerical Results and Discussion

Numerical results are presented to indicate the effect of uniform mesh refinement. The vertical deflection at point B (on the free edge at panel midlength) is commonly used as the metric to judge performance. Since STAGS prints the displacement solution in the coordinate system of the shell unit (cylindrical coordinates for this case), the displacements at the node points need to be transformed to the global rectangular coordinate system using the following relation:

$$w_B^{global} = v_B^{local} \sin \theta - w_B^{local} \cos \theta$$

where θ is measured from the crown of the cylindrical panel, w is the radial displacement and v is the tangential displacement at point B on the shell. Alternatively XYTRANS may be used to extract the displacement in global coordinates. Theoretical solutions are given by Cowper *et al.* (1970) for shallow shell theory (3.703 in. or 0.3086 ft) and by Forsberg (1970) and Thomas and Sobel (1981) for deep shell theory (3.592 in. or 0.2994 ft). Parisch (1979) quotes a value of 2.610 in. or 0.3008 ft. for a deep shell solution. MacNeal and Harder (1985) and Belytschko and Liu (1986) normalize their solutions using a value of 3.6288 in. or 0.3024 ft. This value has become the *de facto* standard value for comparison purposes. The computed values obtained from STAGS are normalized by this latter value in order to be compared with other published solutions.

Table 11 summarizes the 2D shell analysis results obtained using different STAGS shell elements and different levels of uniform mesh refinement. Element aspect ratio is unity for all meshes considered. Element E320 is a 3-node classical triangular shell element in STAGS; drilling degrees of freedom are not present and hence suppressed. Element E330 is the 3-node MIN3 shear-deformable shell element; drilling degrees of freedom are not present and hence suppressed. Element E410 is the 4-node classical shell element in STAGS – workhorse shell element; drilling degrees of freedom are present and free. Element E480 is the 9-node ANS shear-deformable shell element; drilling degrees of freedom are not present and hence suppressed. The mesh is defined by the number of nodes along each edge of the finite

element model so that each finite element model has essentially the same number nodes and degrees of freedom even though the number of elements is different.

Table 12 summarizes the 3D analysis results obtained using different STAGS solid elements and different levels of uniform mesh refinement. The same planar mesh discretizations as considered for the shell elements are used herein in combination with either one (NEZ=1) or two (NEZ=2) solid elements through the thickness of the structure. For the case of one solid element through the thickness, the through-the-thickness element aspect ratio varies from 50 for the coarsest mesh to 10 for the most refined. For the case of two solid elements through the thickness, the through-the-thickness element aspect ratio varies from 25 for the coarsest mesh to 5 for the most refined. Element E881 is an 8-node ANS-based solid element. Element E883 is a 27-node ANS-based solid element. Element E885 is a 20-node displacement based solid element. The value of the normalized deflection reported in Table 12 for the solid element cases represents the value from the inner surface at Point B – only a slight variation in this value occurs through the thickness.

Table 11. Convergence behavior of the STAGS shell elements for the Scordelis-Lo barrel roof problem.

Mesh	Normalized free edge vertical deflection at panel midlength (Point B)			
	E320	E330	E410	E480
3×3	0.9267	1.0235	1.3776	0.7705
5×5	0.7236	0.7322	1.0476	0.9544
7×7	0.8220	0.8273	1.0143	0.9852
9×9	0.8840	0.8893	1.0047	0.9914
11×11	0.9198	0.9255	1.0006	0.9933

Table 12. Convergence behavior of the STAGS solid elements for the Scordelis-Lo barrel roof problem.

Mesh	Normalized free edge vertical deflection at panel midlength (Point B)					
	E881		E883		E885	
	NEZ=1	NEZ=2	NEZ=1	NEZ=2	NEZ=1	NEZ=2
3×3×NEZ	1.3032	1.3046	1.0020	1.0021	0.8778	0.8784
5×5×NEZ	1.0271	1.0272	0.9435	0.9436	0.9628	0.9629
7×7×NEZ	1.0047	1.0047	0.9774	0.9775	1.0087	1.0088
9×9×NEZ	0.9965	0.9965	0.9837	0.9838	1.0014	1.0015
11×11×NEZ	0.9928	0.9928	0.9855	0.9856	0.9968	0.9969

STAGS Input Files

These STAGS input files are located under the following subdirectory:
\$STAGSHOME/Sample-Testcases/Roof

Typical 2D Shell Model Input Files

The following text files give the input for the 2D shell model using the E410 4-node shell element in STAGS with 11 nodes per edge.

roof2d.inp (for S1 processor)

```
2D Scordelis-Lo barrel roof under self weight $A-1
C
C 2D shell model: Reference solution for vertical deflection
C                   at free edge at mid-length = 3.6288" = 0.3024 ft.
C                   vertical deflection = v*sin(theta) - w*cos(theta)
C
1 0 0 0 0 3 0      $b-1
1 -90.0 $b-1b rotation about x
2 0.0 $b-1b rotation about y
3 -110.0 $b-1b rotation about z
1 0 0 0 0 0 0 1 $b-2
1 0 1 0 0 1      $b-3
386.4            $b-4 gravitational constant
1 1 0 0 0      $b-6 inertial load set
0.0 0.0 386.4  $b-6a gravity loading in z-direction
11 11          $f-1 grid (nrows by ncols)
C
C Material Record using Historical Approach
C
1 0            $I-1 material table
3000000. 0.0 0.0 .208333 $i-2 E, nu, G=E/2/(1+nu), rho (90 lb/ft^2)
C
C GCP Input
C
ISOELASTIC_MATERIAL 1 1 1 $i-5
3000000.0,      $i-6a Young's modulus, psi
0.0,           $i-6a Poisson's ratio
5.3916494E-4,  $i-6a Mass density
4*0.0          $i-6a unused properties
C
C Solid fabrications - element thicknesses NOT total wall thickness!
C
SOLID_FABRICATION 1 1 0 0 $i-5a for one element through thickness
3.0               $i-22a element thickness
SOLID_FABRICATION 2 1 0 0 $i-5a for two elements through thickness
1.50              $i-22a element thickness
SOLID_FABRICATION 3 1 0 0 $i-5a for four elements through thickness
0.75              $i-22a element thickness
C
C Shell wall fabrications
C
SHELL_FABRICATION 1 1 0 1 0 $i-5a fabid, nlayer, ipt, ishr, isym
1                $I-21a matid
3.0              $i-21c thickness - thick
0.0              $i-21d angle
1.0 1.0          $i-21e shear factors
C
END $I-5a end GCP input
C
C Wall Record using STAGS Historical Approach
C
```

```

1 1 1 0      $k-1  thick shell
1 3.0 0.0    $k-2
C
C Shell Unit Definition - using 2D shell elements
C
5 0 0 0 0 0      $m-1  cylindrical shell geometry
0.0 300.0 0.0 40.0 300.0  $m-2  x1, x4, y1, y2, R
-1 0 0.0 0.0 0 0    $m-5  shell wall selection
330 11*0          $n-1  element options
C
C Boundary conditions - specified using the Q-records
C
3 3 3 3      $p-1  completely free - see Q-records
C 4 3 0 4    $p-1  sym-free- rigid diaphragm-sym
C 100 000 $p-2  v=w=0  on curved boundary (rigid diaphragm)
C
C Loading - uniform dead load using inertial loading (B-6 records)
C
1 0          $q-1  load summary
1 8          $q-2  load set summary
C
C Impose symmetry on edge 1 (u=rv=rw=0); all layers
C
0.0 -1 1 1 1 0 11 0 0 1      1 $q-3  u=0 on edge 1, layer 1
0.0 -1 5 1 1 0 11 0 0 1      1 $q-3  rv=0 on edge 1, layer 1
0.0 -1 6 1 1 0 11 0 0 1      1 $q-3  rw=0 on edge 1, layer 1
C
C Impose symmetry on edge 4 (v=ru=rw=0); all layers
C
0.0 -1 2 1 1 0 11 0 1 0      1 $q-3  v=0 on edge 4, layer 1
0.0 -1 4 1 1 0 11 0 1 0      1 $q-3  ru=0 on edge 4, layer 1
0.0 -1 6 1 1 0 11 0 1 0      1 $q-3  rw=0 on edge 4, layer 1
C
C Impose condition v=w=0 on edge 3; all layers
C
0.0 -1 2 11 1 0 11 0 0 1      1 $q-3  v=0 on edge 1, layer 1
0.0 -1 3 11 1 0 11 0 0 1      1 $q-3  w=0 on edge 1, layer 1
C
C Zero out all drilling DOF for elements w/o them (E320, E330, E480)
C
C 0.0 -1 6 0 0 0 0 0 0 0      0 $q-3  rw=0 everywhere
C
1 0 0 0 0 0 1 0 1      $r-1  Output selection
1 0          $r-2  selected displacement output

```

roof2d.bin (for S2 processor)

```

Scordelis-Lo barrel roof problem  $A-1
0      1      5*0      -1      $B-1 ANALYSIS CONTROL
1.0 1.0 1.0          $C-1 LOAD MULTIPLIERS

```

roof2d.pin (for STAPL processor)

```

Scordelis-Lo 2D roof problem
1 0 0 0      $PL-2  NPLOT,IPREP,IPRS,KDEV
2 0 1 0 0 0 0 3  $PL-3  KPLOT,VIEW,ITEM,STEP,MODE,IFRNG,COLOR,ICOMP
0.0 3 0.0 0.0 0.0 $PL-5  DSCALE,NROTS,LWSCALE,RNGMIN,RGMAX
1 -90.0 / 2 0.0 / 3 -110.0  $PL-6 rotations

```

Typical 3D Solid Model Input Files

The following text files give the input for the 3D shell model using the E881 8-node solid element in STAGS with 11 nodes per edge and two elements through the thickness or three planes of nodes (NEZ=2).

roof3d.inp (for S1 processor)

```
3D Scordelis-Lo barrel roof under self weight $A-1
C
C 3D solid model: Reference solution for vertical deflection
C                   at free edge at mid-length = 3.6288" = 0.3024 ft.
C                   vertical deflection = v*sin(theta) - w*cos(theta)
C
1 0 0 0 0 3 0      $b-1
1 -90.0 $b-1b rotation about x
2 0.0 $b-1b rotation about y
3 -110.0 $b-1b rotation about z
1 0 0 0 0 0 0 1 $b-2
1 0 1 0 0 1      $b-3
386.4            $b-4 gravitational constant
1 1 0 0 0      $b-6 inertial load set
0.0 0.0 386.4  $b-6a gravity loading in z-direction
11 11          $f-1 grid (nrows by ncols)
C
C Material Record using Historical Approach
C
1 0            $I-1 material table
3000000. 0.0 0.0 .208333 $i-2 E, nu, G=E/2/(1+nu), rho (90 lb/ft^2)
C
C GCP Input
C
ISOELASTIC_MATERIAL 1 1 1 $i-5
3000000.0,      $i-6a Young's modulus, psi
0.0,           $i-6a Poisson's ratio
5.3916494E-4,  $i-6a Mass density
4*0.0         $i-6a unused properties
C
C Solid fabrications - element thicknesses NOT total wall thickness!
C
SOLID_FABRICATION 1 1 0 0 $i-5a for one element through thickness
3.0 $i-22a element thickness
SOLID_FABRICATION 2 1 0 0 $i-5a for two elements through thickness
1.50 $i-22a element thickness
SOLID_FABRICATION 3 1 0 0 $i-5a for four elements through thickness
0.75 $i-22a element thickness
C
C Shell wall fabrications
C
SHELL_FABRICATION 1 1 0 0 0 $i-5a fabid, nlayer, ipt, ishr, isym
1 $I-21a matid
3.0 $i-21c thickness
0.0 $i-21d angle
C
END $I-5a end GCP input
C
C Wall Record using STAGS Historical Approach
C
1 1 1 0 $k-1 thick shell
1 3.0 0.0 $k-2
C
C Shell Unit Definition - using 3D shell elements
C 2 881-solid elements of the same material through the thickness
C this results in three layers of nodes
```



```

C
5 0 0 0 2 1 $m-1 cylindrical shell geometry, 2 layers of elements
0.0 300.0 0.0 40.0 300.0 $m-2 x1, x4, y1, y2, R
-2 0 0.0 0.0 0 0 $m-5 shell wall selection
881 11*0 $n-1 element options
C
C Boundary conditions - specified using the Q-records
C
3 3 3 3 $p-1 completely free - see Q-records
C
C Loading - uniform dead load using inertial loading (B-6 records)
C
1 0 $q-1 load summary
1 12 $q-2 load set summary
C
C Impose symmetry on edge 1 (u=0); all layers
C
0.0 -1 1 1 1 0 11 0 0 1 1 $q-3 u=0 on edge 1, layer 1
0.0 -1 1 1 1 0 11 0 0 1 2 $q-3 u=0 on edge 1, layer 2
0.0 -1 1 1 1 0 11 0 0 1 3 $q-3 u=0 on edge 1, layer 3
C
C Impose symmetry on edge 4 (v=0); all layers
C
0.0 -1 2 1 1 0 11 0 1 0 1 $q-3 v=0 on edge 4, layer 1
0.0 -1 2 1 1 0 11 0 1 0 2 $q-3 v=0 on edge 4, layer 2
0.0 -1 2 1 1 0 11 0 1 0 3 $q-3 v=0 on edge 4, layer 3
C
C Impose condition v=w=0 on edge 3; all layers
C
0.0 -1 2 11 1 0 11 0 0 1 1 $q-3 v=0 on edge 3, layer 1
0.0 -1 2 11 1 0 11 0 0 1 2 $q-3 v=0 on edge 3, layer 2
0.0 -1 2 11 1 0 11 0 0 1 3 $q-3 v=0 on edge 3, layer 3
0.0 -1 3 11 1 0 11 0 0 1 1 $q-3 w=0 on edge 3, layer 1
0.0 -1 3 11 1 0 11 0 0 1 2 $q-3 w=0 on edge 3, layer 2
0.0 -1 3 11 1 0 11 0 0 1 3 $q-3 w=0 on edge 3, layer 3
C
1 0 0 0 0 1 0 1 $r-1 Output selection
1 0 $r-2 selected displacement output

```

roof3d.bin (for S2 processor)

```

Scordelis-Lo barrel roof problem $A-1
0 1 5*0 -1 $B-1 ANALYSIS CONTROL
1.0 1.0 1.0 $C-1 LOAD MULTIPLIERS

```

Problem References

- Scordelis, A. C. and Lo, K. S., "Computer Analysis of Cylindrical Shells," *Journal of the American Concrete Institute*, Vol. 61, No. 5, May 1964, pp. 539-561.
- Cowper, G. R., Lindberg, G. M., and Olson, M.D., "A Shallow Shell Finite Element of Triangular Shape," *International Journal of Solids and Structures*, Vol. 6, No. 8, August 1970, pp. 1133-1156.
- Forsberg, Kevin, "An Evaluation of Finite Difference and Finite Element Techniques for Analysis of General Shells," in *High Speed Computing of Elastic Structures*, B. Fraeijs de Veubeke (editor), IUTAM, University of Liège, 1971, pp.837-859.
- Parisch, H., "A Critical Survey of the 9-Node Degenerated Shell Element with Special Emphasis on Thin Shell Application and Reduced Integration," *Computer Methods in Applied Mechanics and Engineering*, Vol. 20, No. 3, December 1979, pp. 323-350.
- Thomas, Kevin and Sobel, L. H., *Evaluation of the STAGSC-1 Shell Analysis Computer Code*, Report No. WARD-10881, Westinghouse Electric Corporation, Madison, PA, August 1981.
- MacNeal, R. H. and Harder, R. L., "A Proposed Standard Set of Problems to Test Finite Element Accuracy," *Finite Element Analysis and Design*, Vol. 1, No. 1, April 1985, pp. 1-20.
- Belytschko, T. and Liu, W. K., "Test Problems and Anomalies in Shell Finite Elements," in *Reliability of Methods for Engineering Analysis*, K. J. Bathe and D. R. J. Owen (editors), Pineridge Press, 1986, pp. 393-406.
- Zienkiewicz, O. C. and Taylor, R. L., *The Finite Element Method – Volume 2: Solid and Fluid Mechanics, Dynamics and Non-linearity*, Fourth Edition, McGraw-Hill Book Company, 1991, pp. 123, 127, 176-179.
- Phaal, R. and Calladine, C. R., "A Simple Class of Finite Elements for Plate and Shell Problems. II: An Element for Thin Shells, with Only Translational Degrees of Freedom," *International Journal for Numerical Methods in Engineering*, Vol. 35, No. 5, September 1992, pp. 979-996.
- Muhanna, Rafi L., "New Assumed Natural Strain Formulation of the Shallow Shell Element," *Communications in Numerical Methods in Engineering*, Vol. 9, No. 12, December 1993, pp. 989-1004.
- Rengarajan, G., Aminpour, M. A., and Knight, N. F., Jr. "Improved Assumed-Stress Hybrid Shell Element with Drilling Degrees of Freedom for Linear Stress, Buckling and Free Vibration Analyses," *International Journal for Numerical Methods in Engineering*, Vol. 38, No. 11, June 1995, pp. 1917-1943.

Transient Response of Truncated Conical Shell

Background

To verify the transient solution algorithm, the linear elastic collapse of a truncated conical shell subjected to an impulse load (initial velocity). Hartung (1971) presented this problem as part of an assessment of shell analysis capabilities and Hartung and Ball (1973) included this shell structure as one of the three challenge problems to assess shell structural analysis capabilities of various computer codes. Knight *et al.* (1989) also used this problem to assess the CSM Testbed capabilities for the linear elastic transient dynamic analysis of shells. The geometry and material properties of the problem are defined in Figure 37 using U.S. customary units.

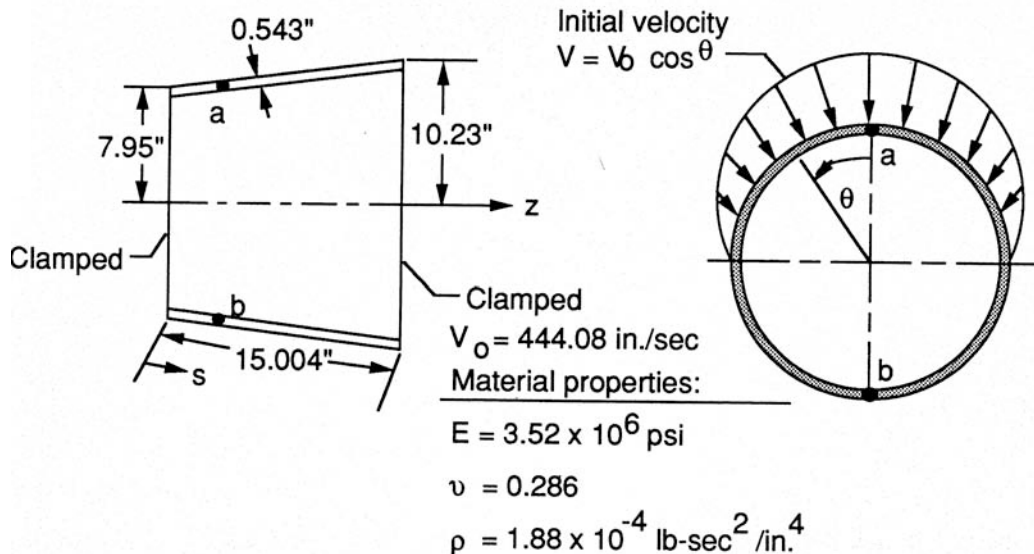


Figure 37. Truncated conical shell problem: geometry and material properties.

Modeling and Analysis Process

The STAGS finite element model considered in this test case problem involves a single shell unit and only 2-D shell elements. Symmetry conditions are exploited and only a 180-degree model of the conical shell is used. The loading is a cosine distribution of a normal initial velocity load distributed over the upper 90-degree segment (see Figure 37). The impulse is uniform along the axis of the shell.

The STAGS model is generated using a single shell unit with the conical shell surface geometry (ISHHELL=6). Material properties and shell wall construction are defined using both the *historical*

STAGS approach and the current GCP approach. Mesh discretization studies include different levels of mesh refinement and different element types. Mesh refinement is readily performed by changing the number of rows and columns of nodes in each direction on the F-1 record. Element type is selected using the N-1 record (KELT). Representative finite element model using 31×19 mesh of nodes is shown in Figure 38 for the 4-node shell elements.

Material properties and shell-wall construction are defined using both the *historical* STAGS approach (*i.e.*, STAGS versions prior to GCP) and the current GCP approach. Material modeling for an elastic isotropic material using the historical STAGS approach requires data on the I-1 and I-2 records to define the material properties and the K-1 and K-2 records to define the shell fabrication data. Material modeling using the current GCP approach requires data on the I-5a and I-6a records to define the material properties and records I-5a, I-21a, I-21b, I-21c, I-21d, and I-21e to define the shell fabrication data. While not used, records I-5a, I-22a, and I-22b are used to define the solid fabrication data.

Boundary condition on the displacements are specified using the P-1 and P-2 records. The symmetry boundary conditions along the straight boundary, while the curved boundaries are clamped. The STAGS definition of these conditions is used.

The impulse loading condition is defined as an initial velocity condition using the Q-records. The looping option on all rows is exploited to impose a uniform initial velocity condition along the shell at each circumferential location (see the Q-3 records in the `trcone.inp S1` input file). However, the magnitude of the initial velocity at each node must be computed externally for each finite element discretization change in the circumferential direction. A FORTRAN computer code is developed that creates the loading records for a given finite element mesh of uniformly distributed nodes. A listing of this code is given in Figure 39. The output is written to FORTRAN unit 6 (standard output) – typically the screen. The user may then “cut-and-paste” these lines directly into the input file.

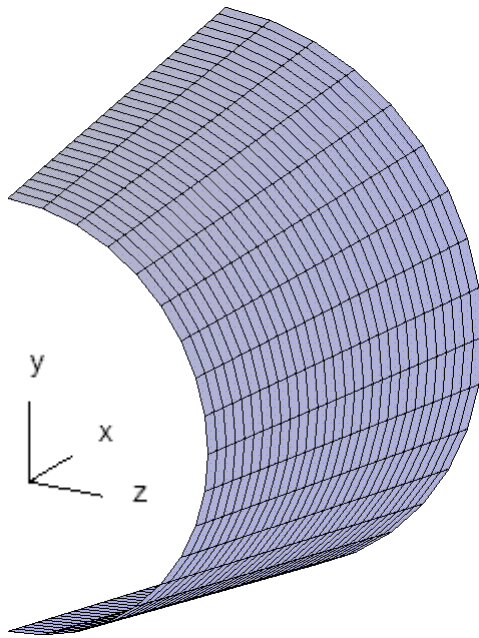


Figure 38. Representative finite element models of the truncated conical shell
 - 31×19 mesh of nodes on the shell surface.

```

      program velocity
      double precision dtheta, vel, V0
      integer ncols,nstart,nele, i
      double precision pi, dtr

c
      pi = acos(-1.0d0)
      dtr = pi/180.0d0

c
      ncols = 19
      nstart = (ncols-1)/2+1
      nele = ncols-nstart
      dtheta = 90.0d0/nele
      V0 = 444.08
      print *, nele, dtheta

c
      do i=1,nele
      vel=V0*sin(dtr*i*dtheta)
      irow = nstart+i
      write(6,100) vel,irow
100    format(F10.5,' -1 3 0 ',i2,
1      3x,'$Q-3 initial velocity loading')
      end do

      stop
      end
  
```

Figure 39. Listing of the FORTRAN computer code used to generate the initial velocity loading for the truncated conical shell.

Numerical Results and Discussion

The linear transient dynamic response is computed using the Park 3-step implicit direct time integration procedure with a fixed time step size Δt of two microseconds for a duration of 1500 microseconds (750 time steps). The predicted linear transient response for two points on the shell is given in Figure 40 for the transverse normal (radial) deflection component. Both points are located 6.5 inches from the clamped, small diameter edge: one at $\theta=90^\circ$ (point a) and one at $\theta=-90^\circ$ (point b). Point a is directly under the maximum initial velocity and immediately responds to the impulse. Point b is 180-degrees away and has no initial velocity, and hence some time passes before the point deflects.

The transient behavior of the hoop stress resultant for selected times during the linear transient dynamic analysis is given in Figure 41. The contour levels are held constant for all plots, and the contours are displayed on the deformed geometry shapes of the shell wherein the deflections are exaggerated for viewing. Note that from Figure 40 the amplitude of the transverse normal deflections at points a and b is less than ten percent of the shell thickness.

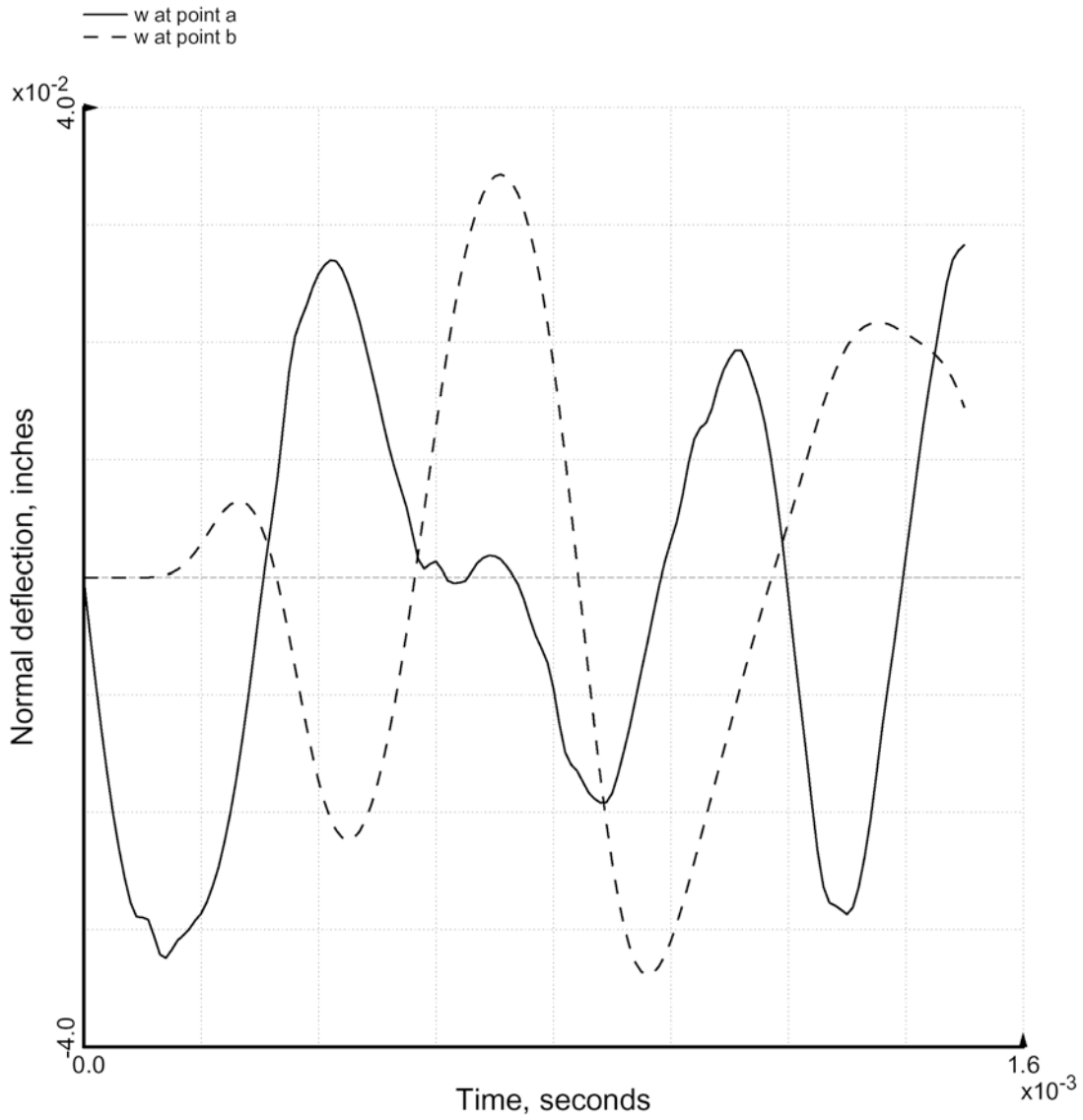


Figure 40. Linear transient response of truncated conical shell due to impulse load obtained using 31 \times 19 mesh of nodes and the E410 4-node quadrilateral shell element.

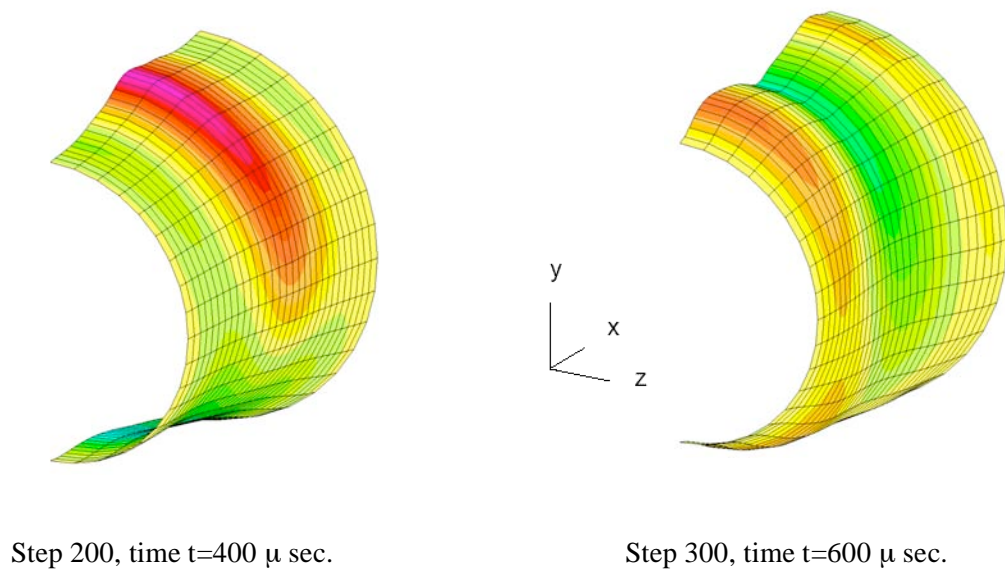
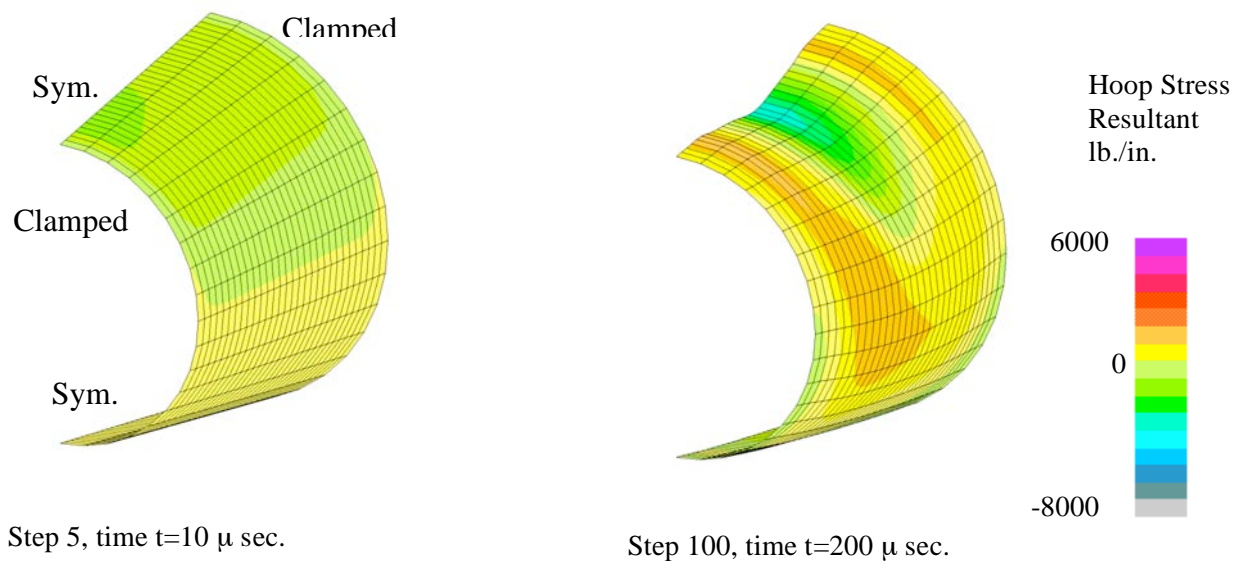
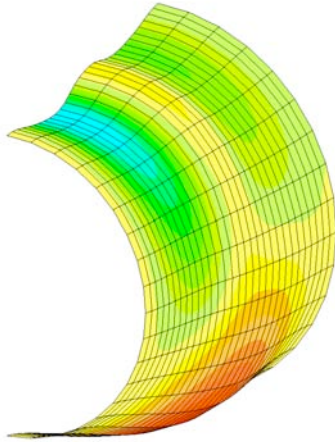
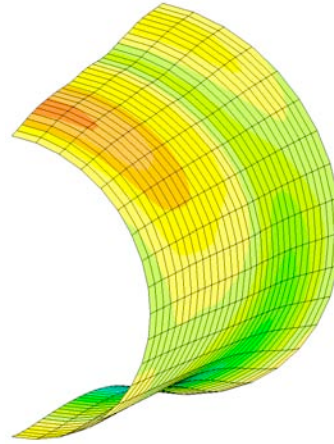


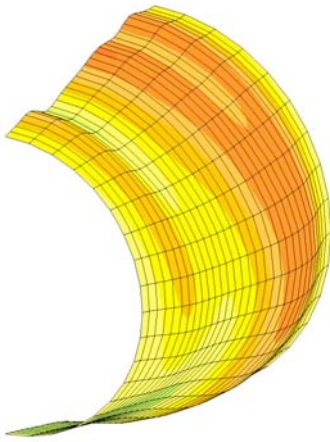
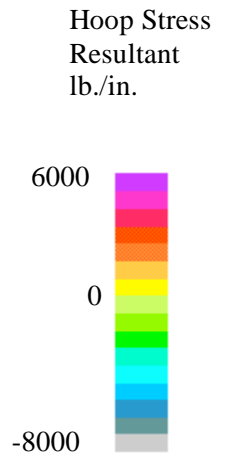
Figure 41. Contour plots of the hoop stress resultant on the deformed geometry shapes of the clamped truncated conical shell subjected to an impulse load: E410 shell element, 31×19 mesh of nodes.



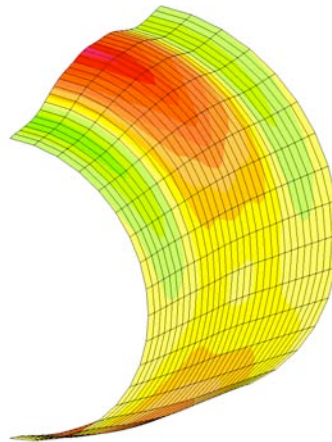
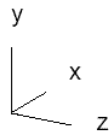
Step 400, time $t=800 \mu \text{ sec.}$



Step 500, time $t=1000 \mu \text{ sec.}$



Step 600, time $t=1200 \mu \text{ sec.}$



Step 750, time $t=1500 \mu \text{ sec.}$

Figure 41. Concluded

STAGS Input Files

These STAGS input files are located under the following subdirectory:

 \$STAGSHOME/Sample-Testcases/Truncated-cone

Under this directory are the files for the 2D shell finite element models and analysis.

2D Shell Model Input Files

The following text files give the input for the hinged cylindrical shell using the E410 4-node shell element with a 31×19 mesh of nodes on the shell surface. The S2 input file contains input sufficient to use the transient analysis procedure.

trcone.inp (for S1 processor)

```
2D truncated cone subjected to impulsive loading    $A-1
C
C Elastic linear transient response of a truncated conical
C shell with clamped ends and impulsively loaded by an
C initial velocity
C
C References:
C 1. Hartung, R. F., "An Assessment of Current Capability
C    for Computer Analysis of Shell Structures," Computers
C    and Structures, Vol. 1, 1971, pp. 3-32.
C 2. Hartung, R. F. and Ball, R. E., "A Comparison of Several
C    Computer Solutions to Three Structural Shell Analysis
C    Problems," Technical Report No. AFFDL-TR-73-15, April 1973.
C 3. Knight, et al., "Large-Scale Structural Analysis: The
C    Structural Analyst, The CSM Testbed, and The NAS System,"
C    NASA TM-100643, March 1989.
C
0 0 0 0 0 3 0      $b-1
1 20.0 / 2 60.0 / 3 0.0  $b-1b model rotations
1 0 0 0 0 0 0      $b-2
1 0 1 0 0 1        $b-3
31 19  $f-1 Nrows (length) x Ncols (circumference)
C
C Material Record using Historical Approach
C
1 0  $I-1 material table
3.52E+6 0.286 0.0 .0726  $i-2 E, nu, G=E/2/(1+nu), rho (for volume check)
C
C GCP Input
C
ISOELASTIC_MATERIAL 1 1 1 $i-5
3.52E+6,          $i-6a Young's modulus, psi
0.286,           $i-6a Poisson's ratio
1.88E-4,         $i-6a Mass density
4*0.0            $i-6a unused properties
C
C Solid fabrications - element thicknesses NOT total wall thickness!
C
SOLID_FABRICATION 1 1 0 0  $i-5a
0.543  $i-22a element thickness
SOLID_FABRICATION 2 1 0 0  $i-5a
0.2715 $i-22a element thickness
C
C Shell wall fabrications
C
SHELL_FABRICATION 1 1 0 0 0  $i-5a fabid, nlayer, ipts, ishr, isym
1      $I-21a matid
```

```

0.543 $i-21c thickness, inches
0.0 $i-21d angle
C
END $I-5a end GCP input
C
C Wall Record using Historical Approach
C
1 1 1 0 $k-1 thickness, inches
1 0.543 0.0 $k-2
C
C Shell Unit Definition - using 2D shell elements
C
6 0 0 0 0 0 0 $m-1 truncated cone geometry
0.0 15.004 -90.0 90.0 7.95 10.23 $m-2 x1, x4, y1, y2, Ra, Rb
-1 0 0.0 0.0 0 0 $m-5 shell wall selection
410 0 0 0 $n-1 element options
C
C Boundary conditions
C
2 4 2 4 $p-1 clamped-sym-clamped-sym
C
C Loading - point load at center
C
0 1 $q-1 load summary
-1 9 0 $q-2
-77.11368 -1 3 0 11 $Q-3 initial velocity loading
-151.88431 -1 3 0 12 $Q-3 initial velocity loading
-222.04000 -1 3 0 13 $Q-3 initial velocity loading
-285.44912 -1 3 0 14 $Q-3 initial velocity loading
-340.18502 -1 3 0 15 $Q-3 initial velocity loading
-384.58456 -1 3 0 16 $Q-3 initial velocity loading
-417.29870 -1 3 0 17 $Q-3 initial velocity loading
-437.33343 -1 3 0 18 $Q-3 initial velocity loading
-444.08000 -1 3 0 19 $Q-3 initial velocity loading
0 0 0 0 0 2 0 0 $r-1 Output selection
13 1 $r-2 selected displacement output (bottom)
13 19 $r-2 selected displacement output (top)

```

trcone.bin (for S2 processor)

```

Truncated conical shell with initial velocity impulsive loading $a-1
C
C Linear transient dynamic solution control
C
7 5 0 0 0 0 0 -1 $b-1
0.0 0.0 0.0 $c-1
0 400 10 -20 0 1.0e-4 $d-1
0.0 1500.E-6 2.0e-6 0.04 $e-1 Time integration parameters
0 4 0 0 0 0 0 $e-2

```

trcone.pin (for STAPL processor)

```

Truncated conical shell with impulsive loading $A-1
16 0 1 0 $PL-2 NPLLOT,IPREP,IPRS,KDEV
C
C stress resultant plots for linear solution
C
2 0 5 5 0 0 0 2 $PL-3 KPLOT,NUNIT,ITEM,STEP,MODE,IFRNG,COLOR,ICOMP
-1.0 2 0.0 -8000.0 6000.0 $PL-5 DSCALE,NROTS,LWSCALE
1 20.0 / 2 60.0
2 0 5 50 0 0 0 2 $PL-3 KPLOT,NUNIT,ITEM,STEP,MODE,IFRNG,COLOR,ICOMP

```

```

0.0  2  0.0 -8000.0 6000.0 $PL-5 DSCALE,NROTS,LWSCALE
1  20.0 / 2 60.0
2  0  5 100 0 0 0 2 $PL-3 KPLOT,NUNIT,ITEM,STEP,MODE,IFRNG,COLOR,ICOMP
0.0  2  0.0 -8000.0 6000.0 $PL-5 DSCALE,NROTS,LWSCALE
1  20.0 / 2 60.0
2  0  5 150 0 0 0 2 $PL-3 KPLOT,NUNIT,ITEM,STEP,MODE,IFRNG,COLOR,ICOMP
0.0  2  0.0 -8000.0 6000.0 $PL-5 DSCALE,NROTS,LWSCALE
1  20.0 / 2 60.0
2  0  5 200 0 0 0 2 $PL-3 KPLOT,NUNIT,ITEM,STEP,MODE,IFRNG,COLOR,ICOMP
0.0  2  0.0 -8000.0 6000.0 $PL-5 DSCALE,NROTS,LWSCALE
1  20.0 / 2 60.0
2  0  5 250 0 0 0 2 $PL-3 KPLOT,NUNIT,ITEM,STEP,MODE,IFRNG,COLOR,ICOMP
0.0  2  0.0 -8000.0 6000.0 $PL-5 DSCALE,NROTS,LWSCALE
1  20.0 / 2 60.0
2  0  5 300 0 0 0 2 $PL-3 KPLOT,NUNIT,ITEM,STEP,MODE,IFRNG,COLOR,ICOMP
0.0  2  0.0 -8000.0 6000.0 $PL-5 DSCALE,NROTS,LWSCALE
1  20.0 / 2 60.0
2  0  5 350 0 0 0 2 $PL-3 KPLOT,NUNIT,ITEM,STEP,MODE,IFRNG,COLOR,ICOMP
0.0  2  0.0 -8000.0 6000.0 $PL-5 DSCALE,NROTS,LWSCALE
1  20.0 / 2 60.0
2  0  5 400 0 0 0 2 $PL-3 KPLOT,NUNIT,ITEM,STEP,MODE,IFRNG,COLOR,ICOMP
0.0  2  0.0 -8000.0 6000.0 $PL-5 DSCALE,NROTS,LWSCALE
1  20.0 / 2 60.0
2  0  5 450 0 0 0 2 $PL-3 KPLOT,NUNIT,ITEM,STEP,MODE,IFRNG,COLOR,ICOMP
0.0  2  0.0 -8000.0 6000.0 $PL-5 DSCALE,NROTS,LWSCALE
1  20.0 / 2 60.0
2  0  5 500 0 0 0 2 $PL-3 KPLOT,NUNIT,ITEM,STEP,MODE,IFRNG,COLOR,ICOMP
0.0  2  0.0 -8000.0 6000.0 $PL-5 DSCALE,NROTS,LWSCALE
1  20.0 / 2 60.0
2  0  5 550 0 0 0 2 $PL-3 KPLOT,NUNIT,ITEM,STEP,MODE,IFRNG,COLOR,ICOMP
0.0  2  0.0 -8000.0 6000.0 $PL-5 DSCALE,NROTS,LWSCALE
1  20.0 / 2 60.0
2  0  5 600 0 0 0 2 $PL-3 KPLOT,NUNIT,ITEM,STEP,MODE,IFRNG,COLOR,ICOMP
0.0  2  0.0 -8000.0 6000.0 $PL-5 DSCALE,NROTS,LWSCALE
1  20.0 / 2 60.0
2  0  5 650 0 0 0 2 $PL-3 KPLOT,NUNIT,ITEM,STEP,MODE,IFRNG,COLOR,ICOMP
0.0  2  0.0 -8000.0 6000.0 $PL-5 DSCALE,NROTS,LWSCALE
1  20.0 / 2 60.0
2  0  5 700 0 0 0 2 $PL-3 KPLOT,NUNIT,ITEM,STEP,MODE,IFRNG,COLOR,ICOMP
0.0  2  0.0 -8000.0 6000.0 $PL-5 DSCALE,NROTS,LWSCALE
1  20.0 / 2 60.0
2  0  5 750 0 0 0 2 $PL-3 KPLOT,NUNIT,ITEM,STEP,MODE,IFRNG,COLOR,ICOMP
0.0  2  0.0 -8000.0 6000.0 $PL-5 DSCALE,NROTS,LWSCALE
1  20.0 / 2 60.0

```

trcone.pxy (for XYTRANS processor)

This input file is generated and saved during the first execution of XYTRANS (so called journal file). Once created it can be used over and over again to extract the same information from a STAGS run.

```
P          $ (P)lotps or (S)pread_Sheet output
trcone    $ STAGS solution 'Case Name'
F          $ (F)ull or (C)ondensed Model
Y          $ (Y)es-(N)o: setup data for another plot
 4         $ x-axis variable = choice (1 to 15)
N          $ (Y)es-(N)o: specify x-variable scale factor
 5         $ y-axis variable = choice (1 to 15)
 0         $ node no. (0 = ask for Unit,Row,Col)
 1 14 19   $ (U)nit, (R)ow, (C)ol - Node No. = 266
 3         $ comp no., dis,vel,acc (1-6) = u,v,w,ru,rv,rw
S         $ (G)lobal or (S)hell ref surface
N          $ (Y)es-(N)o: specify y-variable scale factor
N          $ (Y)es-(N)o: specify subrange of loadsteps
Y          $ (Y)es-(N)o: plotted points start at origin
Y          $ (Y)es-(N)o: setup data for another plot
 4         $ x-axis variable = choice (1 to 15)
N          $ (Y)es-(N)o: specify x-variable scale factor
 5         $ y-axis variable = choice (1 to 15)
 0         $ node no. (0 = ask for Unit,Row,Col)
 1 14 1    $ (U)nit, (R)ow, (C)ol - Node No. = 248
 3         $ comp no., dis,vel,acc (1-6) = u,v,w,ru,rv,rw
S         $ (G)lobal or (S)hell ref surface
N          $ (Y)es-(N)o: specify y-variable scale factor
N          $ (Y)es-(N)o: specify subrange of loadsteps
Y          $ (Y)es-(N)o: plotted points start at origin
N          $ (Y)es-(N)o: setup data for another plot
```

Problem References

Hartung, R. F., "An Assessment of Current Capability for Computer Analysis of Shell Structures," *Computers and Structures*, Vol. 1, 1971, pp. 3-32.

Hartung, R. F. and Ball R. E., A Comparison of Several Computer Solutions to Three Structural Shell Analysis Problems, AFFDL Report No. AFFDL-TR-73-15, April 1973.

Knight, N. F., Jr., McCleary, S. L., Macy, S. C., and Aminpour, M. A., *Large-Scale Structural Analysis: The Structural Analyst, The CSM Testbed, and The NAS System*, NASA TM-100643, March 1989.

Hurlbut, B. J., Stanley, G. M., and Kang, D. S., *The Computational Structural Mechanics (CSM) Testbed Applications Manual*, Lockheed Contract Report No. LMSC-F333007, May 1989.

Rankin, C. C., Brogan, F. A., Loden, W., and Cabiness, H., *Structural Analysis of General Shells – STAGS User Manual, Version 4.0*, Lockheed Martin Advanced Technology Center, Palo Alto, CA, June 2000.

Snap-Through of Hinged Shallow Cylindrical Shell

Background

To verify the nonlinear solution algorithm and nonlinear aspects of the shell element and corotational formulations, the snap-through response of a hinged cylindrical shallow shell under a central point force is studied. This problem involves only moderate geometric nonlinearities and exhibits a limit point in the nonlinear response. This problem posed by Sabir and Lock (1972) is a very popular test case for shell elements and nonlinear solution procedures for quasi-static behavior (*e.g.*, Gass and Tabarrok, 1976; Ramm, 1981; Hinton and Lo, 1982; Jeusette *et al.*, 1989; Eriksson, 1989; Hurlbut *et al.*, 1989; Moy and Lam, 1991). The geometry and material properties of the problem are defined in Figure 42 using U.S. customary units and SI units. Three values of shell thickness are considered: 1.00 in. (25.4 mm); 0.50 in. (12.7 mm); and 0.25 in. (6.35 mm). The rise of the shell H is 0.5 inches (12.7 mm).

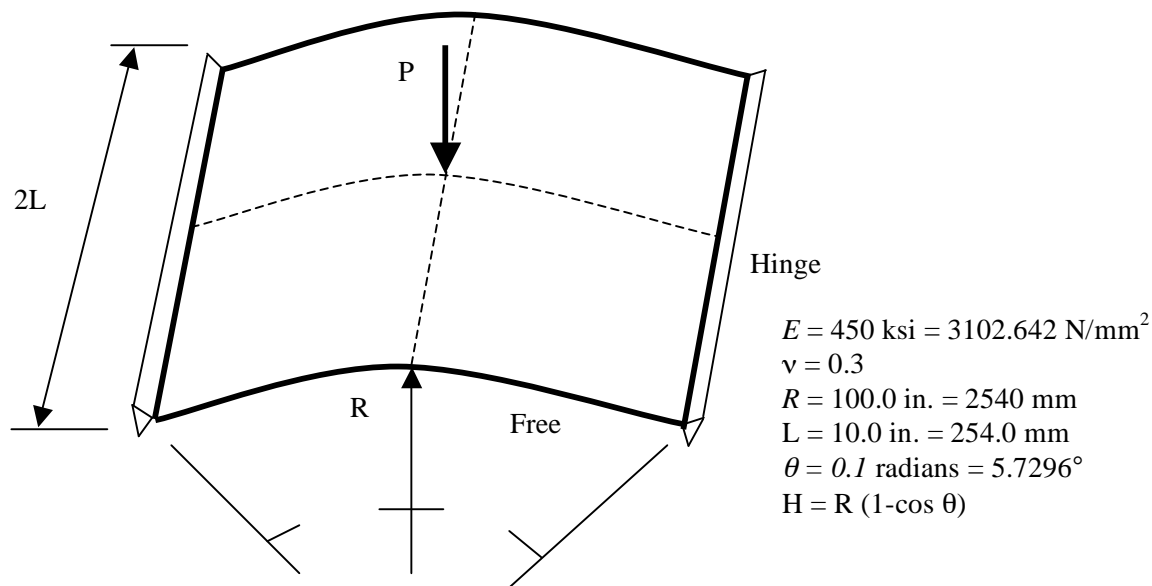


Figure 42. Hinged cylindrical shallow shell problem: geometry and material properties.

Modeling and Analysis Process

Two separate STAGS finite element models are considered in this test case problem: shell elements and solid elements. A summary of each model includes:

2-D shell model – Model the shell with plate elements (x - y plane) in a single shell unit.

3-D solid model – Model shell with solid elements in a single shell unit and having multiple elements through the shell thickness.

The STAGS model is generated using a single shell unit with the cylindrical shell surface geometry (ISHELL=5). Material properties and shell wall construction are defined using both the *historical* STAGS approach and the current GCP approach. Mesh discretization studies include different levels of mesh refinement and different element types. Mesh refinement is readily performed by changing the number of rows and columns of nodes in each direction on the F-1 record. Element type is selected using the N-1 record (KELT). Note that E430 uses two E330 triangular elements for each 4-node quadrilateral subdomain. Multiple solid elements through the thickness are specified using the NLAYS and NFABS parameters on the M-1 record in combination with NFABS sets of M-5 records. For this study, only two and four solid elements through the shell wall thickness are used. Representative finite element models using 11x11 mesh of nodes in the plane are shown in Figure 42 for the 3-node, 4-node, and 9-node shell elements as well as for the 8-node solid element with four elements in the thickness direction.

Material properties and shell-wall construction are defined using both the *historical* STAGS approach (*i.e.*, STAGS versions prior to GCP) and the current GCP approach. Material modeling for an elastic isotropic material using the historical STAGS approach requires data on the I-1 and I-2 records to define the material properties and the K-1 and K-2 records to define the shell fabrication data. Material modeling using the current GCP approach requires data on the I-5a and I-6a records to define the material properties and records I-5a, I-21a, I-21b, I-21c, I-21d, and I-21e to define the shell fabrication data. In addition, records I-5a, I-22a, and I-22b are used to define the solid fabrication data.

Boundary condition on the displacements are specified using the P-1 and P-2 records. The boundary conditions along the straight boundary are hinged ($v=w=0$ and $ry=rz=0$), while the curved boundary are free. Symmetry boundary conditions are imposed on the interior straight and curved edges. For the 3D finite element models, the displacement boundary conditions are imposed using the Q-3 records and on each nodal layer in the model.

A point load is applied at the center of the panel that is at the origin of the finite element model coordinate frame. Because of the symmetry conditions, only one fourth of the applied load is used on the quarter model. The base load given on the Q-3 record is 0.25 and then the load factor on the C-1 record of the S2 input file gives the total load amplitude (*i.e.*, the load factor PA is related to the total load on the shell). The internal force at that node and in the direction of the loading can be computed and used for plotting as well via the XYTRANS utility.

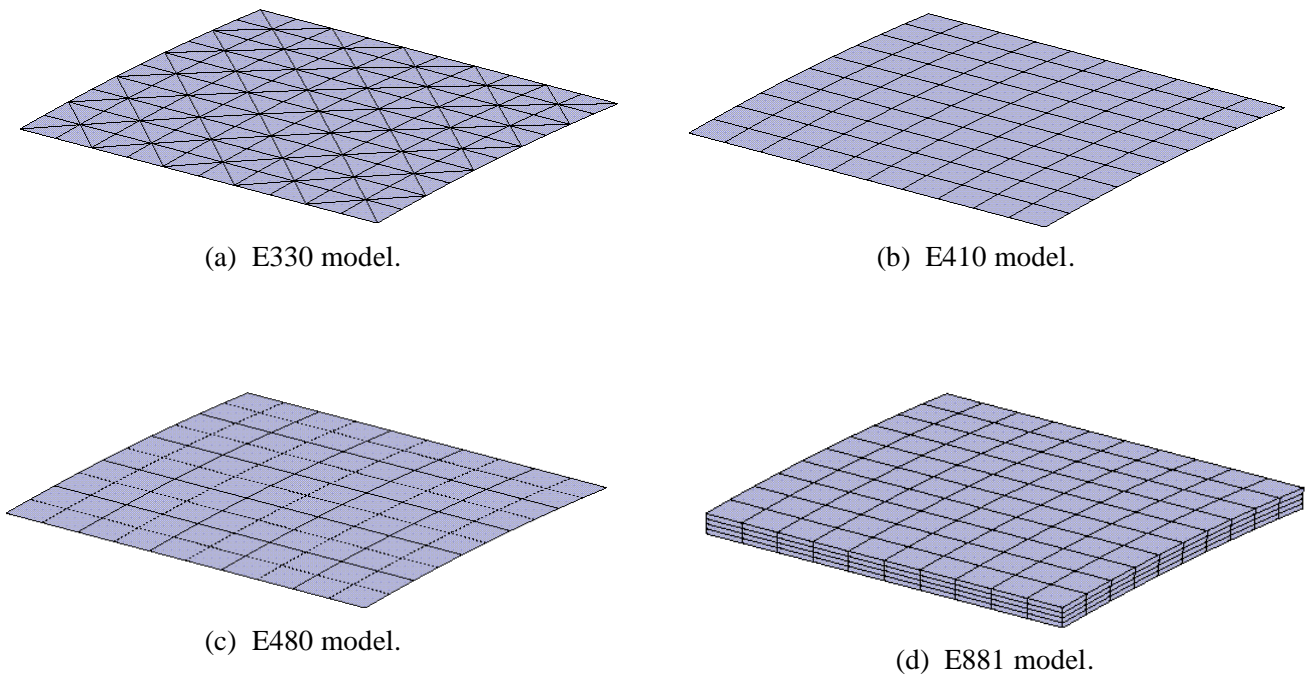


Figure 42. Representative finite element models of the hinged cylinder
 - 11×11 mesh of nodes on the shell surface.

Numerical Results and Discussion

Results for this problem are more complicated to present because of the nonlinear snap-through response of the shell structure. Three different values of the shell thickness are studied: 25.40-mm thick, 12.70-mm thick, and 6.35-mm thick. For the 25.40-mm-thick shell, the nonlinear response exhibits an inflection point but does not snap through. For the 12.70-mm-thick shell, the nonlinear response exhibits a limit point and using displacement-control or the arc-length-control procedure the unstable branch of the nonlinear response can be traced. For the 6.35-mm-thick shell, the nonlinear response exhibits a horizontal limit point and a vertical limit (snap-through and snap-back behavior, respectively). These characteristics are displayed in Figure 43 for an 11×11 mesh of nodes and the E410 4-node quadrilateral shell element. The solutions were obtained using the arc-length control procedure that automatically adjusts the solution step size.

Convergence studies were performed for the E410 and E480 shell elements. Results shown in Figures 44 through 46 are for different levels of discretization using the E410 4-node and E480 9-node shell elements for the three shell thickness values considered. These convergence studies included meshes where the number of nodes per edge equaled 3, 5, 7, 11, and 21. For the E410 element, these meshes correspond to 2, 4, 6, 10, and 20 4-node elements per edge, respectively. For the E480 element, these meshes correspond to 1, 2, 3, 5, and 10 9-node elements per edge, respectively.

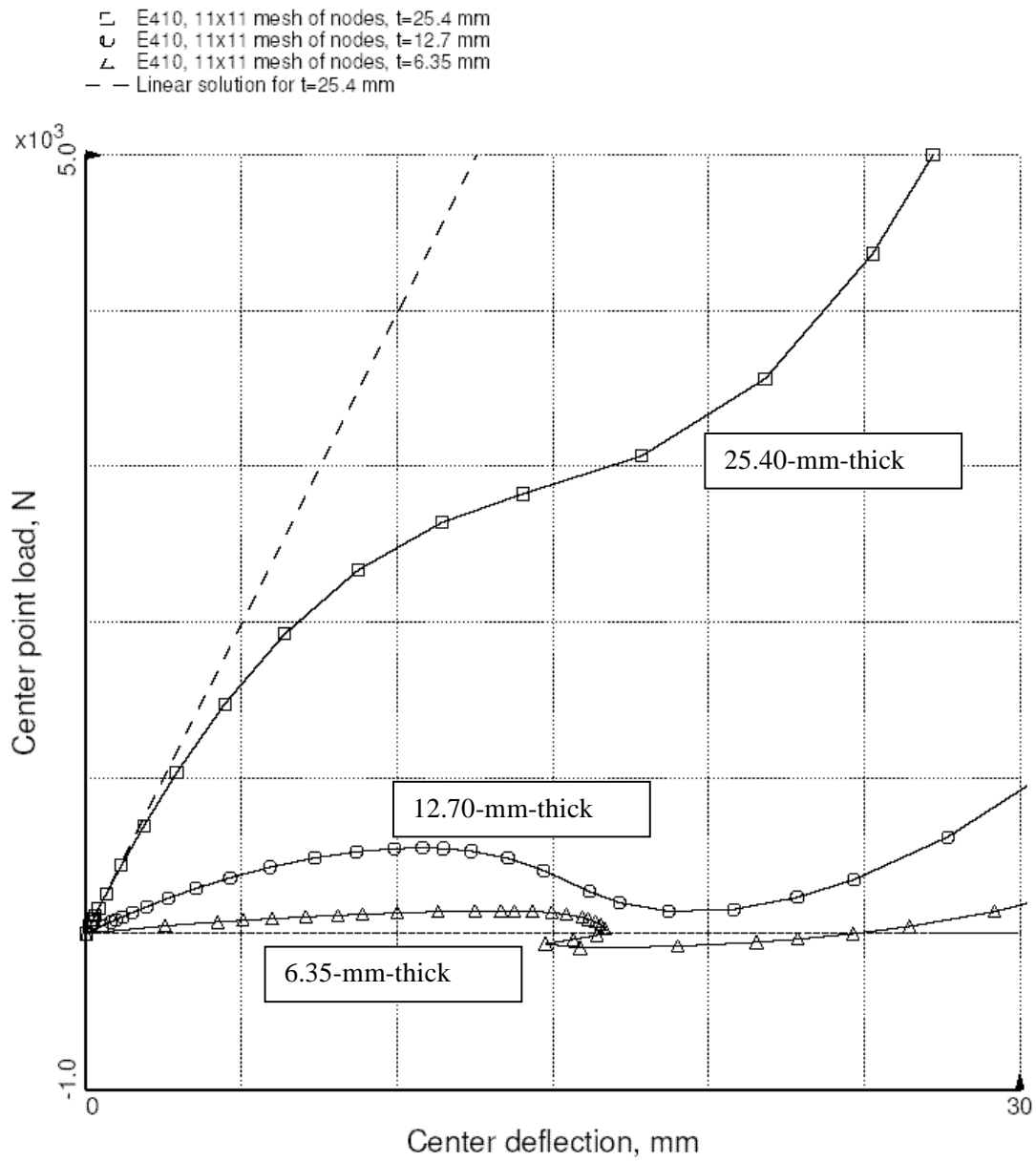
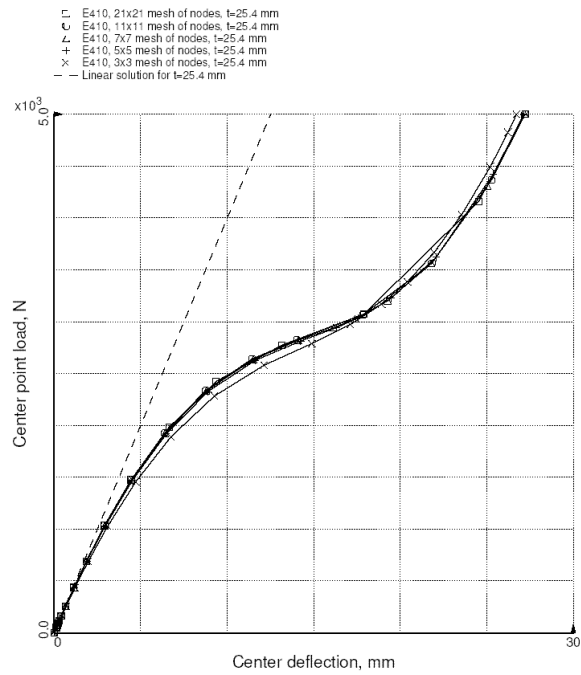
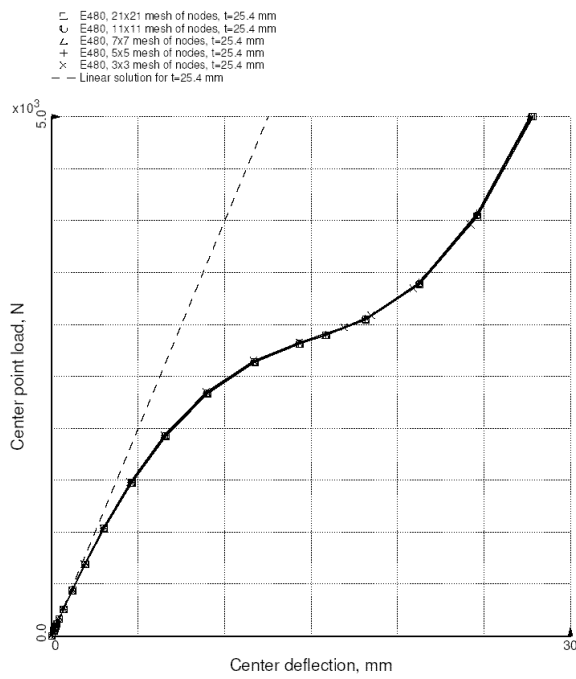


Figure 43. Basic hinged cylindrical shell response for three values of shell thickness obtained using 11×11 mesh of nodes and the E410 4-node quadrilateral element.

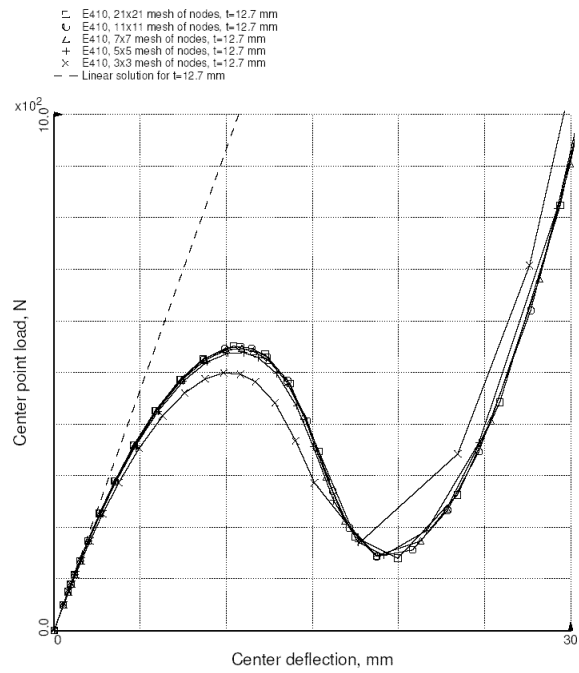


(a) 4-node E410 shell element.

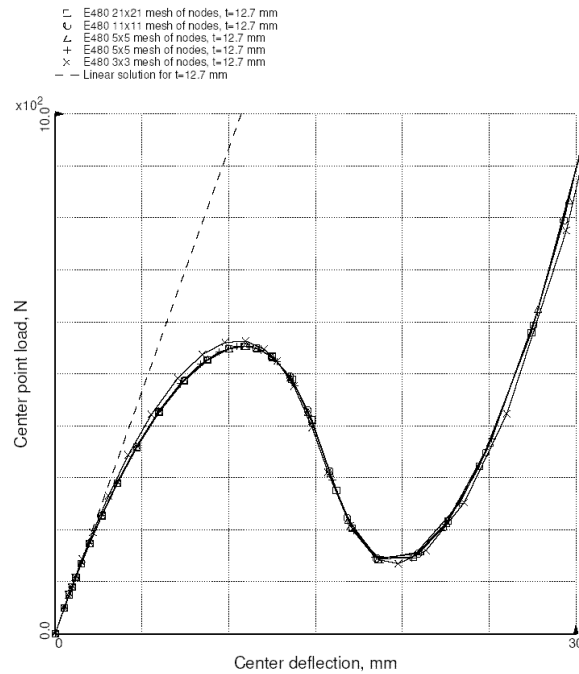


(b) 9-node E480 shell element.

Figure 44. Hinged cylindrical shell response to a central point load – 25.40-mm thick.

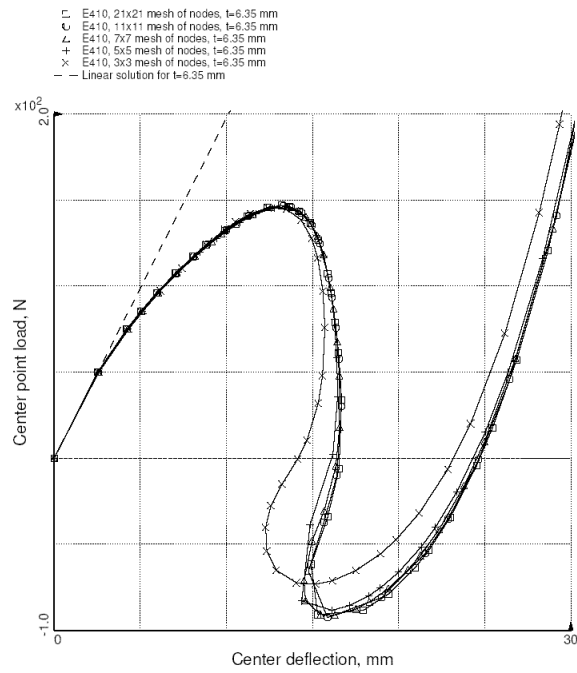


(a) 4-node E410 shell element.

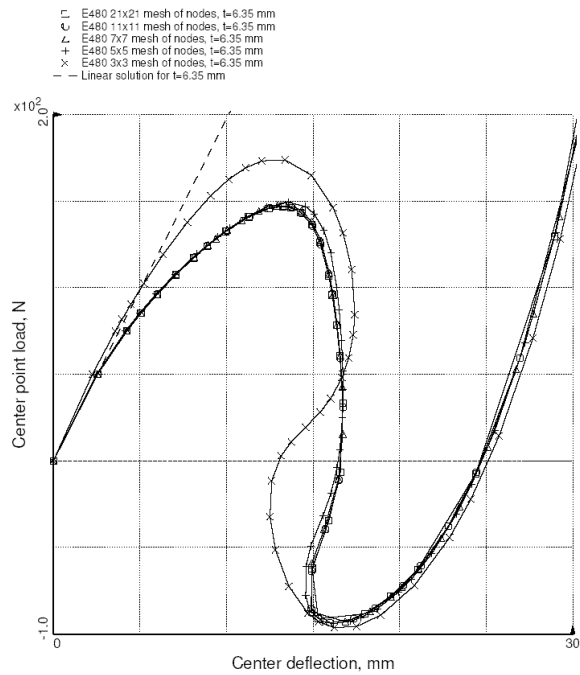


(b) 9-node E480 shell element.

Figure 45. Hinged cylindrical shell response to a central point load – 12.70-mm thick.



(a) 4-node E410 shell element.



(b) 9-node E480 shell element.

Figure 46. Hinged cylindrical shell response to a central point load – 6.35-mm thick.

These results indicate that good solutions can be obtained even with just one or two elements along an edge of the quarter model. As the shell thickness decreases, the number of elements required for a converged solution increases. It is interesting that with as few as two elements per edge, the E410 shell element captures the first limit point very well for even the thinnest shell but the response exhibits a greater degree of snap-back. With a single E480 shell element, the basic behavior is captured, but additional elements are required to capture the snap-through and snap-back behavior.

Contour plots of the transverse normal deflection for the 12.70-mm-thick shell are shown in Figure 47 for an 11×11 mesh of nodes and the E410 shell element. Initially the center point deflects and pulls the shell surface down. As the limit point is approached, the shell deflection patterns approach that of an arch response. Following complete snap through, the center point deflects further, causing stretching of the middle surface.

Prediction of the hinged cylindrical shell response using the E330 MIN3 triangular shell elements in STAGS was not as readily obtained. Note that STAGS will automatically subdivide a 4-node subregion into two 3-node regions. Users typically use the designation E430 on the N-1 record to cause this result. First, in all other simulations the response was obtained using no more than five step size cuts – the E330 model required more but fewer than ten. Second, the E330 element has artificial drilling stiffness based on a penalty approach. Leaving the drilling degrees of freedom free or unrestrained caused the solution to bog down and well below the first limit point as shown in Figure 48. Constraining all drilling degrees of freedom resulted in a solution comparable to that obtained using the E410. Note the E410 element does have drilling degrees of freedom; however, these freedoms contribute to the in-plane displacement field approximations and do not use artificial stiffness for those freedoms.

Results obtained using the E881 8-node ANS solid element are shown in Figure 49. For the solid models, the symmetry boundary conditions were imposed on all nodes on the symmetry plane. To simulate the hinged condition, the transverse normal deflection was restrained on all nodes on the hinged plane, while the in-plane circumferential displacement was only restrained at the midplane of shell. Three different discretizations of the shell surface are considered: 11 nodes per edge, 21 nodes per edge and 41 nodes per edge. The solid models had either two or four elements through the shell thickness. Results from the E410 simulation are included for comparison. These results indicate that increasing the number of elements through the thickness had only a minor effect on the center transverse normal deflection. Increasing the number of nodes per edge had a significant effect on the response; however, even with 41 nodes per edge, the second limit point was still not accurately predicted – the first limit point was predicted satisfactorily.

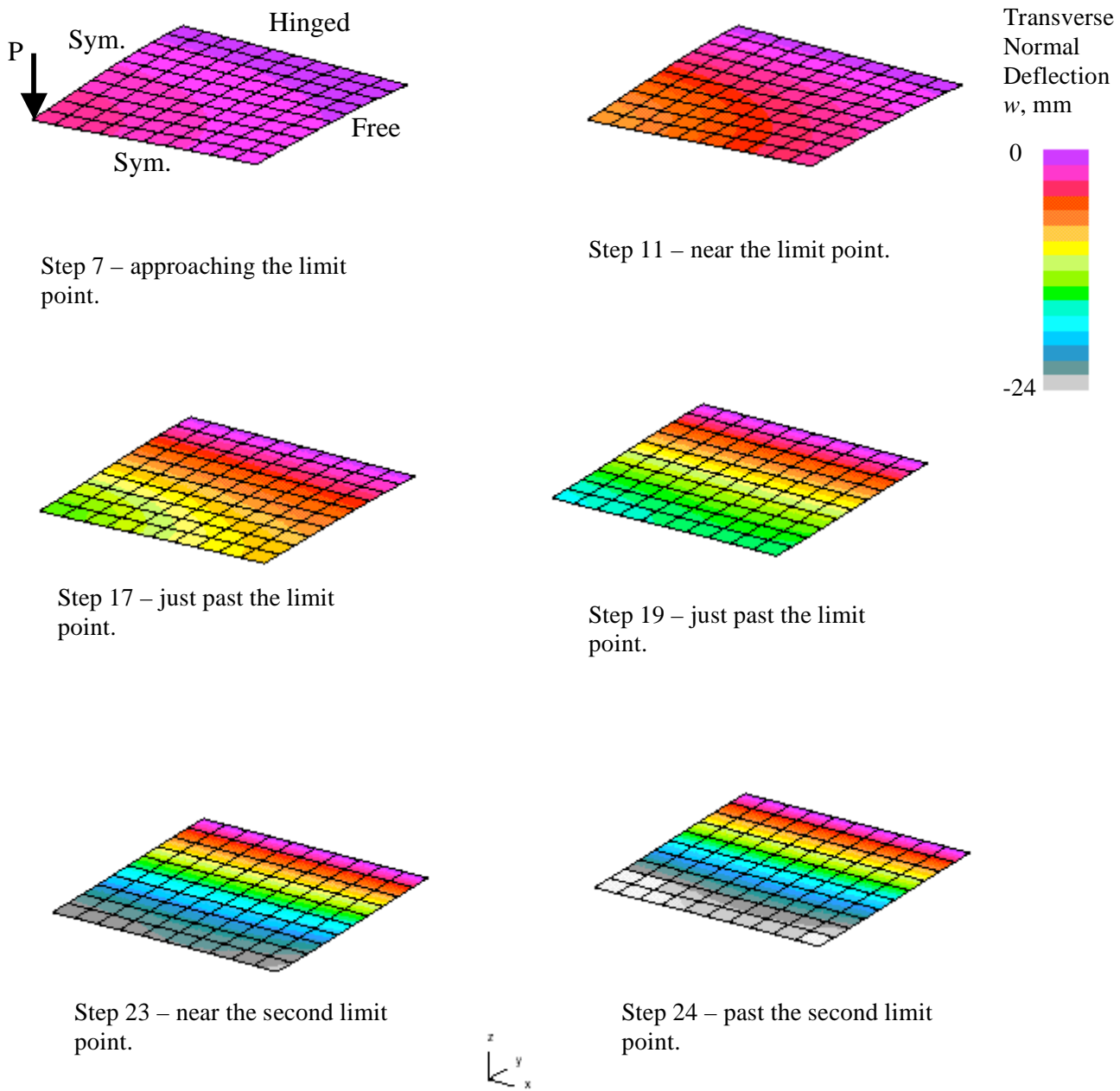


Figure 47. Contour plots of the transverse normal deflection on the deformed surface for selected values of the applied point load – 12.7-mm-thick shell, E410 element, 11×11 mesh of nodes.

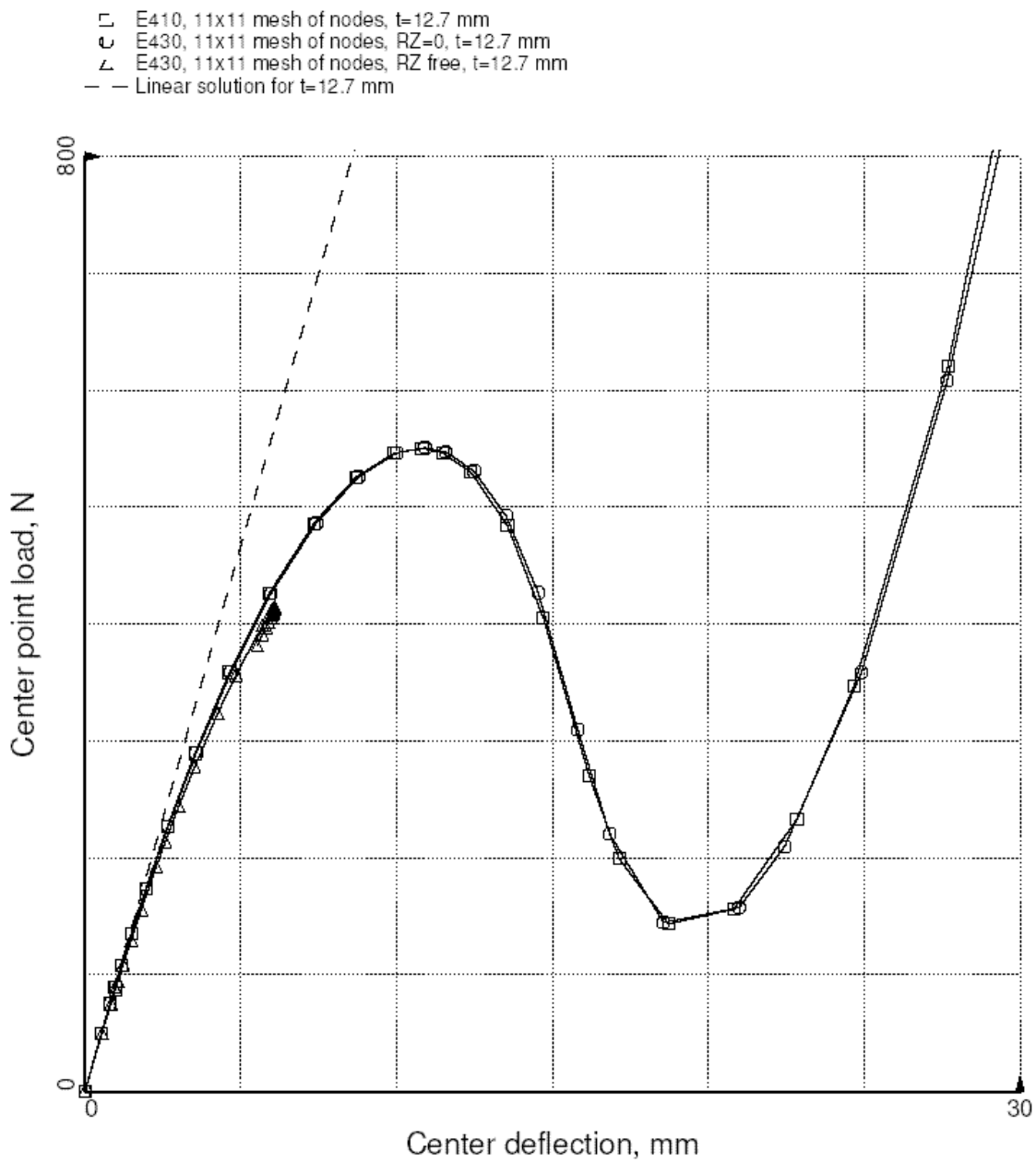


Figure 48. Hinged cylindrical shell response to a central point load – 12.70-mm thick.

- E410, 11x11 mesh of nodes, t=12.7 mm
- ◐ E881, 11x11 mesh of nodes, 4 elements through thickness, t=12.7 mm
- △ E881, 11x11 mesh of nodes, 2 elements through thickness, t=12.7 mm
- + E881, 21x21 mesh of nodes, 2 elements through thickness, t=12.7 mm
- × E881, 21x21 mesh of nodes, 4 elements through thickness, t=12.7 mm
- ◁ E881, 41x41 mesh of nodes, 4 elements through thickness, t=12.7 mm
- Linear solution for t=12.7 mm

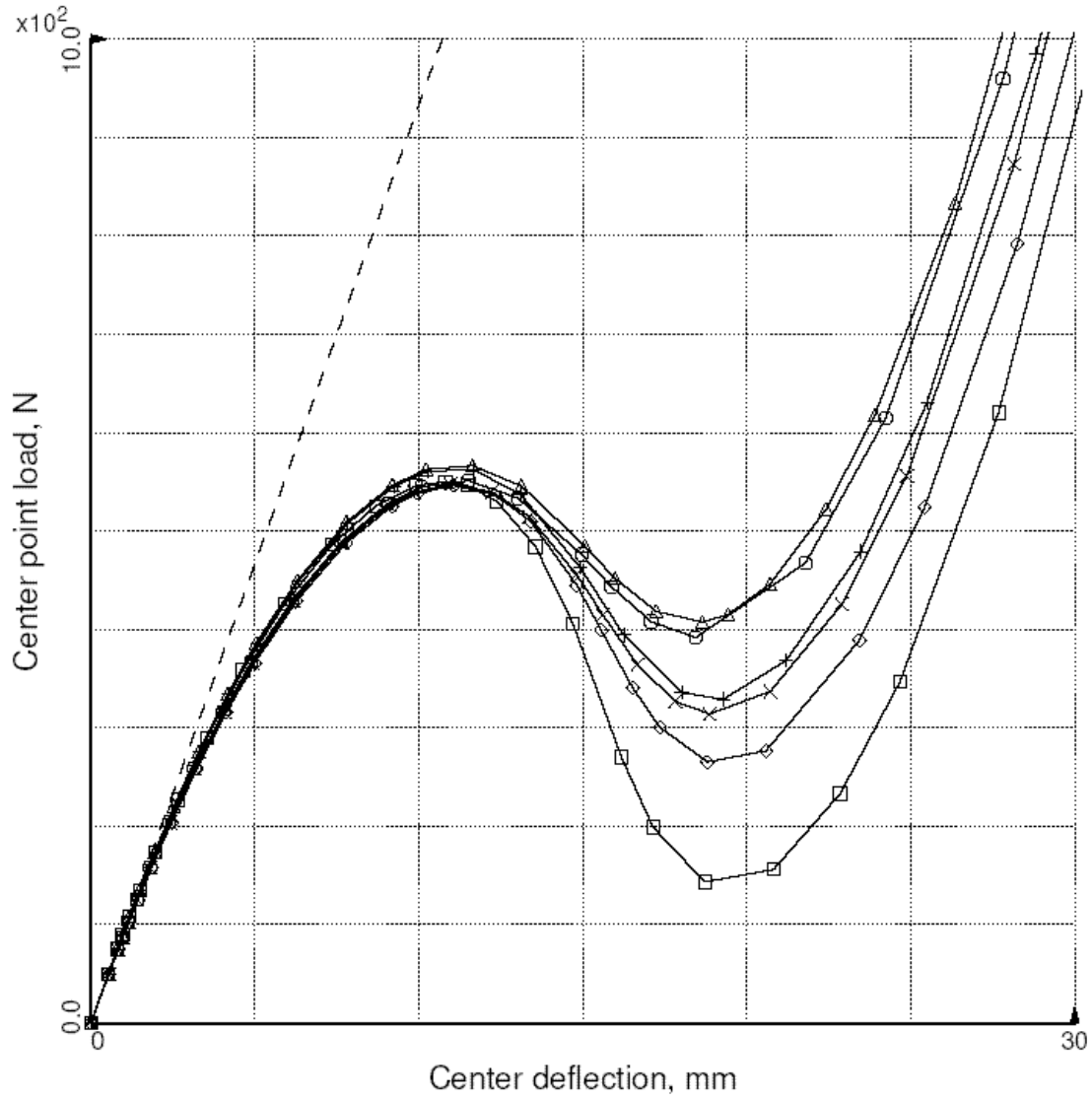


Figure 49. Hinged cylindrical shell response to a central point load – 12.7-mm thick.

STAGS Input Files

These STAGS input files are located under the following subdirectory:

\$STAGSHOME/Sample-Testcases/Snap-Through

Under this directory are two subdirectories: 2D/ contains the files for the 2D shell finite element models and analyses and 3D/ contains the files for the 3D solid finite element models and analyses.

2D Shell Model Input Files

The following text files give the input for the hinged cylindrical shell using the E410 4-node shell element with an 11×11 mesh of nodes on the shell surface. These files are in the 2D/ subdirectory. The S2 input file contains input sufficient to use the hybrid transient-static procedure in the event a load control solution algorithm is used for the nonlinear static analysis. If so, then the solution will stop at or near the limit point. Then using information from a linear vibration analysis, a nonlinear transient analysis can be started using a higher load to cause the shell to snap through – too small a value will just bring you closer to the limit point. After the transient is completed, the nonlinear static analysis can be resumed starting with a load relaxation step to guarantee equilibrium is re-established.

hinge2d.inp (for S1 processor)

```
2D Hinged Cylindrical Shallow Shell with Central Point Load    $A-1
0 0 0 0 0 3 0          $b-1
1 -67.0 / 2 0.0 / 3 -34.0 $b-1b model rotations
1 0 0 0 0 0 0          $b-2
2 0 3 0 0 1           $b-3
11 11 $f-1 grid (nrows by ncols of NODES)
C
C Material Record using Historical Approach
C
1 0 $I-1 material table
450000. 0.3 0.0 .1 $i-2 E, nu, G=E/2/(1+nu), rho (for volume check)
2 0 $I-1 material table
3.10275E3 0.3 0.0 0.1 $i-2 N/mm^2
C
C GCP Input
C
ISOELASTIC_MATERIAL 1 1 1 $i-5
450000.0,          $i-6a Young's modulus, psi
0.3,              $i-6a Poisson's ratio
2.58799E-4,       $i-6a Mass density
4*0.0             $i-6a unused properties
ISOELASTIC_MATERIAL 2 1 1 $i-5
3.10275E3,        $i-6a Young's modulus, N/mm^2
0.3,              $i-6a Poisson's ratio
2.58799E-4,       $i-6a Mass density
4*0.0             $i-6a unused properties
C
C Solid fabrications - element thicknesses NOT total wall thickness!
C
SOLID_FABRICATION 1 1 0 0 $i-5a
25.4 $i-22a element thickness
SOLID_FABRICATION 2 1 0 0 $i-5a
12.7 $i-22a element thickness
SOLID_FABRICATION 3 1 0 0 $i-5a
6.35 $i-22a element thickness
C
C Shell wall fabrications (total thicknesses)
C
SHELL_FABRICATION 1 1 0 1 0 $i-5a fabid, nlayer, ipts, ishr, isym
2 $I-21a matid
```

```

25.4          $i-21c  thickness - thick
0.0           $i-21d  angle
0.83333 0.83333 $i-21e shear correction factors
SHELL_FABRICATION 2 1 0 1 0 $i-5a  fabid, nlayer, ipt, ishr, isym
2           $I-21a  matid
12.7         $i-21c  thickness - thin
0.0          $i-21d  angle
0.83333 0.83333 $i-21e shear correction factors
SHELL_FABRICATION 3 1 0 1 0 $i-5a  fabid, nlayer, ipt, ishr, isym
2           $I-21a  matid
6.35         $i-21c  thickness - very thin
0.0          $i-21d  angle
0.83333 0.83333 $i-21e shear correction factors
C
END      $I-5a  end GCP input
C
C Wall Record using Historical Approach (total thicknesses)
C
1 1 1 0      $k-1  thick shell
2 25.40 0.0  $k-2
2 1 1 0      $k-1  thin shell
2 12.7 0.0   $k-2
3 1 1 0      $k-1  very thin shell
2 6.35 0.0   $k-2
C
C Shell Unit Definition - using 2D shell elements
C
5 0 0 0 0 0 0      $m-1  cylindrical shell geometry
0.0 254.0 0.0 5.7296 2540.0 $m-2  x1, x4, y1, y2, R
-2 0 0.0 0.0 0 0   $m-5  shell wall selection
410      $n-1  element options
C
C Boundary conditions
C
4 0 3 4 $p-1  sym-hinged-free-sym
100 100 $p-2  v=w=0 and ry=rz=0 on straight boundary (hinged; immovable)
C
C Loading - point load at center
C
1 0          $q-1  load summary
1 1 0        $q-2
C0.0      -1 6 0 0 0 $Q-3  Set RW=0 for E480 and E330 elements
-0.25E+3 1 3 1 1 0 $Q-3  0.25*P*1000 at panel center
0 0 0 0 0 1 0 1   $r-1  Output selection
1 0          $r-2  selected displacement output

```

hinge2d.bin (for S2 processor)

```

Hinged Cylindrical Shallow Shell Problem $A-1
C
C Nonlinear static solution control
C
3      1      5*0      -1      $B-1 ANALYSIS CONTROL
0.2 0.1 20.0      $C-1 LOAD MULTIPLIERS
0 1000 5 20 0 1.0e-4 1.0 $d-1 strategy parameters
0 0 0      $et-1
C
C Nonlinear static restart after transient
C with load relaxation as a first step
C
3      1      5*0      -1      $B-1 ANALYSIS CONTROL
2.3 0.1 20.0      $C-1 LOAD MULTIPLIERS

```

```

32 100 5 20 1 1.0e-4 1.0      $d-1 strategy parameters
5 0 1 $et-1 do load relaxation and use previous solution as estimate
C
C Nonlinear transient dynamic solution control from static solution
C
6 1 1 0 0 0 0 -1 $b-1
2.20430 0.0 2.20430 $c-1
10 200 10 -20 0 1.0e-4 $d-1
0.0 200.0 1.0e-3 100.0 0.1295 0.772 $e-1
0 4 1 0 0 1 0 $e-2
2.30 0.0 0.0 1000.0 1000.0 0.0 $e-3
C
C Linear free vibration analysis
C
2 1 1 0 0 0 0 -1 $b-1
1.0 0.0 1.0
0 0 0
2
C
C Nonlinear transient dynamic solution control from static solution
C
6 1 1 0 0 0 0 -1 $b-1
2.20430 0.0 2.20430 $c-1
10 200 10 -20 0 1.0e-4 $d-1
0.0 0.2 1.0e-8 100.0 0.1295 0.772 $e-1
0 4 1 0 0 1 0 $e-2
2.20430 0.0 0.0 100.0 100.0 0.0 $e-3

```

hinge2d.pin (for STAPL processor)

```

Hinged Cylindrical Shell with center point load $a-1 shell thickness = 12.7mm
6 0 0 0 $SPL-2 NPLOT,IPREP,IPRS,KDEV
C contour plots of w-deflection with fixed range of values (-24mm to 0)
2 0 1 7 0 0 0 3 $SPL-3 KPLOT,VIEW,ITEM,STEP,MODE,IFRNG,COLOR,ICOMP
0.0 3 0.0 -24.0 1.0e-8 $SPL-5 DSCALE,NROTS,LWSCALE,RNGMIN,RGMAX
1 -67.0 / 2 0.0 / 3 -34.0
2 0 1 11 0 0 0 3 $SPL-3 KPLOT,VIEW,ITEM,STEP,MODE,IFRNG,COLOR,ICOMP
0.0 3 0.0 -24.0 1.0e-8 $SPL-5 DSCALE,NROTS,LWSCALE,RNGMIN,RGMAX
1 -67.0 / 2 0.0 / 3 -34.0
2 0 1 17 0 0 0 3 $SPL-3 KPLOT,VIEW,ITEM,STEP,MODE,IFRNG,COLOR,ICOMP
0.0 3 0.0 -24.0 1.0e-8 $SPL-5 DSCALE,NROTS,LWSCALE,RNGMIN,RGMAX
1 -67.0 / 2 0.0 / 3 -34.0
2 0 1 19 0 0 0 3 $SPL-3 KPLOT,VIEW,ITEM,STEP,MODE,IFRNG,COLOR,ICOMP
0.0 3 0.0 -24.0 1.0e-8 $SPL-5 DSCALE,NROTS,LWSCALE,RNGMIN,RGMAX
1 -67.0 / 2 0.0 / 3 -34.0
2 0 1 23 0 0 0 3 $SPL-3 KPLOT,VIEW,ITEM,STEP,MODE,IFRNG,COLOR,ICOMP
0.0 3 0.0 -24.0 1.0e-8 $SPL-5 DSCALE,NROTS,LWSCALE,RNGMIN,RGMAX
1 -67.0 / 2 0.0 / 3 -34.0
2 0 1 24 0 0 0 3 $SPL-3 KPLOT,VIEW,ITEM,STEP,MODE,IFRNG,COLOR,ICOMP
0.0 3 0.0 -24.0 1.0e-8 $SPL-5 DSCALE,NROTS,LWSCALE,RNGMIN,RGMAX
1 -67.0 / 2 0.0 / 3 -34.0
2

```

hinge2d.pxy (for XYTRANS processor)

This input is generated and saved during the first execution of XYTRANS (so called journal file). Once created it can be used over and over again to extract the same information from a STAGS run.

```

P          $ (P)lotps or (S)pread_Sheet output
hinge2d   $ STAGS solution 'Case Name'
F          $ (F)ull or (C)ondensed Model
Y          $ (Y)es-(N)o: setup data for another plot

```

```

5          $ x-axis variable = choice (1 to 15)
          0          $ node no. (0 = ask for Unit,Row,Col)
1      1      1$ (U)nit, (R)ow, (C)ol - Node No. =      1
3          $ comp no., dis,vel,acc (1-6) = u,v,w,ru,rv,rw
G          $ (G)lobal or (S)hell ref surface
8          $ y-axis variable = choice (1 to 15)
          0          $ node no. (0 = ask for Unit,Row,Col)
1      1      1$ (U)nit, (R)ow, (C)ol - Node No. =      1
3          $ comp no., int-for (1-6) = Fu,Fv,Fw,Mu,Mv,Mw
G          $ (G)lobal or (S)hell ref surface
N          $ (Y)es-(N)o: specify subrange of loadsteps
Y          $ (Y)es-(N)o: plotted points start at origin
N          $ (Y)es-(N)o: setup data for another plot

```

3D Solid Model Input Files

The following text files give the input for the hinged cylindrical shell using the E881 8-node solid element with an 11×11 mesh of nodes on the shell surface and four elements through the shell thickness (five nodal layers). These files are under the 3D/ subdirectory.

hinge3d.inp (for S1 processor)

```

3D Hinged Cylindrical Shell with Central Point Load    $A-1
0 0 0 0 0 3 0          $b-1
1 -67.0 / 2 0.0 / 3 -34.0 $b-1b model rotations
1 0 0 0 0 0 0          $b-2
2 0 3 0 0 1          $b-3
21 21          $f-1 grid (nrows by ncols of NODES)
C
C Material Record using Historical Approach
C
1 0 $I-1 material table (US Customary UNITS)
450000. 0.3 0.0 .1 $i-2 E, nu, G=E/2/(1+nu), rho (for volume check)
2 0 $I-1 material table (Metric)
3.10275E3 0.3 0.0 0.1 $i-2 N/mm^2
C
C GCP Input
C
ISOELASTIC_MATERIAL 1 1 1 $i-5
450000.0,          $i-6a Young's modulus, psi
0.3,          $i-6a Poisson's ratio
2.58799E-4,          $i-6a Mass density
4*0.0          $i-6a unused properties
ISOELASTIC_MATERIAL 2 1 1 $i-5
3.10275E3,          $i-6a Young's modulus, N/mm^2
0.3,          $i-6a Poisson's ratio
2.58799E-4,          $i-6a Mass density
4*0.0          $i-6a unused properties
C
C Solid fabrications - element thicknesses NOT total wall thickness!
C Note: these models have 2 or more elements through the thickness
C
SOLID_FABRICATION 1 2 0 0 $i-5a
12.7 $i-22a element thickness
SOLID_FABRICATION 2 2 0 0 $i-5a
6.35 $i-22a element thickness
SOLID_FABRICATION 3 2 0 0 $i-5a
3.175 $i-22a element thickness
C
C Shell wall fabrications ( these are total thicknesses)
C
SHELL_FABRICATION 1 1 0 0 0 $i-5a fabid, nlayer, ipts, ishr, isym

```

```

2      $I-21a  matid
25.4   $i-21c  thickness - thick
0.0    $i-21d  angle
SHELL_FABRICATION 2 1 0 0 0  $i-5a  fabid, nlayer, ipt, ishr, isym
2      $I-21a  matid
12.7   $i-21c  thickness - thin
0.0    $i-21d  angle
SHELL_FABRICATION 3 1 0 0 0  $i-5a  fabid, nlayer, ipt, ishr, isym
2      $I-21a  matid
6.35   $i-21c  thickness - very thin
0.0    $i-21d  angle
C
END    $I-5a  end GCP input
C
C Wall Record using Historical Approach (total thicknesses)
C
1 1 1 0      $k-1  thick shell
2 25.4 0.0   $k-2
2 1 1 0      $k-1  thin shell
2 12.7 0.0   $k-2
3 1 1 0      $k-1  very thin shell
2 6.35 0.0   $k-2
C
C Shell Unit Definition - using 3D solid elements
C
5 0 0 0 4 4      $m-1  cylindrical shell geometry
0.0 254.0 0.0 5.7296 2540.0 $m-2  x1, x4, y1, y2, R
-3 0 0.0 0.0 0 0      $m-5  shell wall selection
-3 0 0.0 0.0 0 0      $m-5  shell wall selection
-3 0 0.0 0.0 0 0      $m-5  shell wall selection
-3 0 0.0 0.0 0 0      $m-5  shell wall selection
881      $n-1  element options
C
C Boundary conditions (see q-3 records)
C   BC: sym-hinged-free-sym
C
3 3 3 3      $p-1  all edges free
C
C Loading - point load at center
C
1 0      $q-1  load summary
1 16 0    $q-2
-0.25E+3 1 3 1 1 0 0 0 0 0 1  $Q-3  0.25*P*1000 at panel center
0.0 -1 1 1 0 0 0 0 0 0 1  $q-3  u=0 on Row 1 of Layer 1
0.0 -1 1 1 0 0 0 0 0 0 2  $q-3  u=0 on Row 1 of Layer 2
0.0 -1 1 1 0 0 0 0 0 0 3  $q-3  u=0 on Row 1 of Layer 3
0.0 -1 1 1 0 0 0 0 0 0 4  $q-3  u=0 on Row 1 of Layer 4
0.0 -1 1 1 0 0 0 0 0 0 5  $q-3  u=0 on Row 1 of Layer 5
0.0 -1 2 0 1 0 0 0 0 0 1  $q-3  v=0 on Col 1 of Layer 1
0.0 -1 2 0 1 0 0 0 0 0 2  $q-3  v=0 on Col 1 of Layer 2
0.0 -1 2 0 1 0 0 0 0 0 3  $q-3  v=0 on Col 1 of Layer 3
0.0 -1 2 0 1 0 0 0 0 0 4  $q-3  v=0 on Col 1 of Layer 4
0.0 -1 2 0 1 0 0 0 0 0 5  $q-3  v=0 on Col 1 of Layer 5
0.0 -1 3 0 21 0 0 0 0 0 1  $q-3  v=w=0 on Col NCOL of Layer 1
0.0 -1 3 0 21 0 0 0 0 0 2  $q-3  v=w=0 on Col NCOL of Layer 2
0.0 -1 2 0 21 0 2 1 0 0 3  $q-3  v=w=0 on Col NCOL of Layer 3
0.0 -1 3 0 21 0 0 0 0 0 4  $q-3  v=w=0 on Col NCOL of Layer 4
0.0 -1 3 0 21 0 0 0 0 0 5  $q-3  v=w=0 on Col NCOL of Layer 5
0 0 0 0 0 0 1 0 1  $r-1  Output selection
1 0  $r-2  selected displacement output

```

hinge3d.bin (for S2 processor)

Hinged Cylindrical Shallow Shell Problem \$A-1

```

C
C Nonlinear static solution control
C
3      1      5*0      -1      $B-1 ANALYSIS CONTROL
0.2  0.1  20.0      $C-1 LOAD MULTIPLIERS
0  6000  5  20  0  1.0e-4  1.0      $d-1 strategy parameters
0  0  0      $et-1

```

hinge3d.pin (for STAPL processor)

```

Hinged Cylindrical Shell with center point load $a-1
5 0 0 0 $PL-2 NPLLOT,IPREP,IPRS,KDEV
C contour plots of w-deflection on deformed shape
2 0 1 9 0 0 0 3 $PL-3 KPLOT,VIEW,ITEM,STEP,MODE,IFRNG,COLOR,ICOMP
0.0 3 0.0 0.0 0.0 0.0 $PL-5 DSCALE,NROTS,LWSCALE,RNGMIN,RGMAX
1 -67.0 / 2 0.0 / 3 -34.0
2 0 1 12 0 0 0 3 $PL-3 KPLOT,VIEW,ITEM,STEP,MODE,IFRNG,COLOR,ICOMP
0.0 3 0.0 0.0 0.0 0.0 $PL-5 DSCALE,NROTS,LWSCALE,RNGMIN,RGMAX
1 -67.0 / 2 0.0 / 3 -34.0
2 0 1 18 0 0 0 3 $PL-3 KPLOT,VIEW,ITEM,STEP,MODE,IFRNG,COLOR,ICOMP
0.0 3 0.0 0.0 0.0 0.0 $PL-5 DSCALE,NROTS,LWSCALE,RNGMIN,RGMAX
1 -67.0 / 2 0.0 / 3 -34.0
2 0 1 22 0 0 0 3 $PL-3 KPLOT,VIEW,ITEM,STEP,MODE,IFRNG,COLOR,ICOMP
0.0 3 0.0 0.0 0.0 0.0 $PL-5 DSCALE,NROTS,LWSCALE,RNGMIN,RGMAX
1 -67.0 / 2 0.0 / 3 -34.0
2 0 1 25 0 0 0 3 $PL-3 KPLOT,VIEW,ITEM,STEP,MODE,IFRNG,COLOR,ICOMP
0.0 3 0.0 0.0 0.0 0.0 $PL-5 DSCALE,NROTS,LWSCALE,RNGMIN,RGMAX
1 -67.0 / 2 0.0 / 3 -34.0

```

Problem References

Sabir, A. B. and Lock, A. C., "The Application of Finite Elements to the Large Deflection Geometrically Nonlinear Behaviour of Cylindrical Shells," in *Variational Methods in Engineering – Volume II*, C. A. Brebbia and H. Tottenham (editors), Southampton University Press, 1972, pp. 7/66-7/75.

Gass, N. and Tabarrok, B., "Large Deformation Analysis of Plates and Cylindrical Shells by a Mixed Finite Element Method," *International Journal for Numerical Methods in Engineering*, Vol. 10, No. 4, 1976, pp. 731-746.

Ramm, E., "Strategies for Tracing the Nonlinear Response Near Limit Points," in *Nonlinear Finite Element Analysis in Structural Mechanics*, W. Wunderlich, E. Stein, and K.-J. Bathe (editors), Springer-Verlag, Berlin, 1981, pp. 63-89

Hinton, E. and Lo, C. S., "Large Deflection Analysis of Imperfect Mindlin Plates using the Modified Riks Method," in *The Mathematics of Finite Elements and Applications IV*, MAFELAP 1981, J. R. Whiteman (editor), Academic Press, London, 1982, pp. 111-118.

Jeusette, Jean-Pierre, Laschet, Gottfried, and Idelsohn, Sergio, "An Effective Automatic Incremental/Iterative Method for Static Nonlinear Structural Analysis," *Computers and Structures*, Vol. 32, No. 1, 1989, pp. 125-135.

Eriksson, Anders, "On Linear Constraints for Newton-Raphson Corrections and Critical Point Searches in Structural F. E. Problems," *International Journal for Numerical Methods in Engineering*, Vol. 28, No. 6, June 1989, pp. 1317-1334.

Hurlbut, B. J., Stanley, G. M., and Kang, D. S., *The Computational Structural Mechanics (CSM) Testbed Applications Manual*, Lockheed Contract Report No. LMSC-F333007, May 1989.

Moy, S. S. J. and Lam, S. S. E., "Geometrically Non-Linear Analysis of Shell Structures," *Communications in Applied Numerical Methods*, Vol. 7, No. 5, July 1991, pp. 377-391.

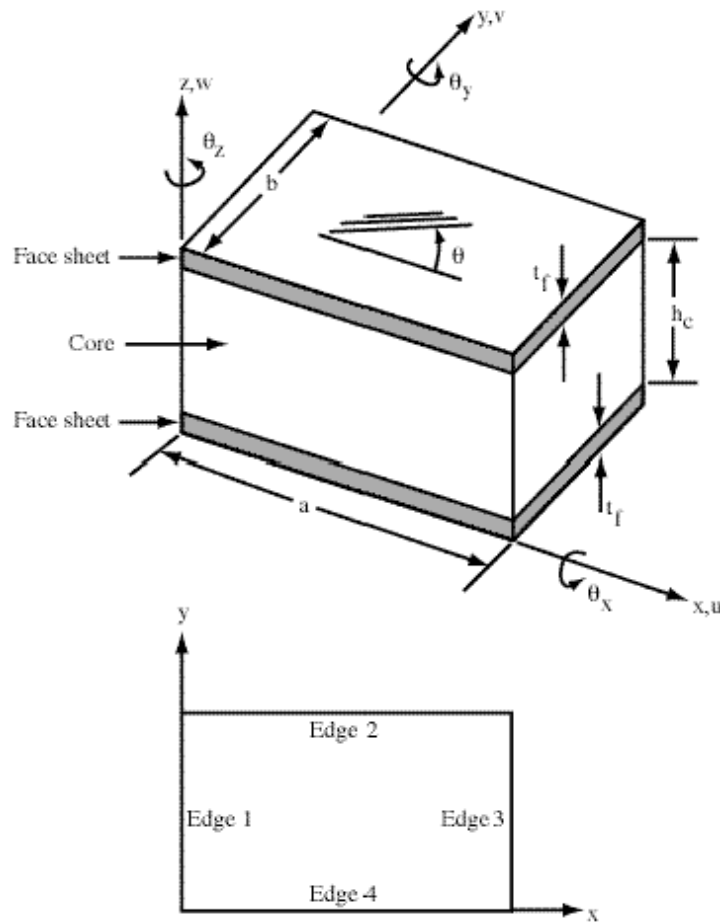
Advanced-Features Example Problems

The advanced-features example problems focus on the application of recent STAGS enhancements and unique capabilities. These problems illustrate how to use and interpret results for these applications. The problems include the analysis of a sandwich panel, the crack propagation of a middle-crack-tension panel and a panel with multiple site damage, the application of the hybrid solution procedure using a composite curved panel with a central circular hole, the progressive failure analysis of a composite square panel loaded in in-plane shear, two membrane wrinkling problems, and an actuator problem.

Buckling of Sandwich Panels

Background

Sandwich panels are generally described by two face sheets held apart by material referred to as the core. The face sheets can be isotropic, orthotropic, or laminated, and each face sheet can be distinctly different. The core material is often a foam or honeycomb material *modeled* as an orthotropic continuum. The core material usually has low in-plane stiffness compared to its transverse normal stiffness. The geometry and material properties of the problem are defined in Figure 50 using U.S. customary units and SI units.



Geometry:

$$a = 20.0 \text{ in.} = 508.0 \text{ mm}$$

$$b = 10.0 \text{ in.} = 254.0 \text{ mm}$$

Face Sheet Material:

$$E = 10.0 \text{ Msi} = 68.95 \text{ GPa}$$

$$\nu = 0.3$$

$$t_f = \begin{cases} 0.02 \text{ in.} = 0.508 \text{ mm} \\ 0.11 \text{ in.} = 2.794 \text{ mm} \end{cases}$$

Core Material:

$$E_{cx} = 0.1 \text{ ksi} = 0.6895 \text{ MPa}$$

$$E_{cy} = 0.1 \text{ ksi} = 0.6895 \text{ MPa}$$

$$E_{cz} = 10.0 \text{ ksi} = 68.95 \text{ MPa}$$

$$G_{cxy} = 0.0384 \text{ ksi} = 0.265 \text{ MPa}$$

$$G_{cxz} = 12.000 \text{ ksi} = 82.74 \text{ MPa}$$

$$G_{cyz} = 7.200 \text{ ksi} = 49.64 \text{ MPa}$$

$$\nu_{cxy} = 0.30$$

$$\nu_{cxz} = 0.01$$

$$\nu_{cyz} = 0.01$$

$$h_c = \begin{cases} 0.20 \text{ in.} = 5.08 \text{ mm} \\ 5.50 \text{ in.} = 139.70 \text{ mm} \end{cases}$$

Figure 50. Sandwich panel problem: geometry and material properties.

Modeling and Analysis Process

Sandwich panel finite element modeling has generally taken one of three approaches depending on panel geometry and constituent materials. The buckling behavior of a sandwich panel is dependent on the sandwich panel geometry and properties and may involve a general instability mode, a local instability mode, or an interaction between the two. Accurate prediction of general or overall instability modes requires adequate representation of the sandwich stiffnesses whereas prediction of local instabilities requires detailed through-the-thickness modeling. The first modeling approach exploits standard shell finite elements. These models are referred to herein as layered shell models (using either E410, E330, or E480 shell elements), and for thin sandwich panels may provide a first approximation of the global behavior. The second approach uses standard shell finite elements for the face sheets and solid three-dimensional finite elements for the core. These models are referred to as layered shell/solid models (uses E480 shell element for each face sheet and E883 solid element for the core) and provide a modeling approach for both general and local response predictions. The accuracy of this approach, as well as its computational cost, is related to the through-the-thickness modeling of the core material and the displacement field compatibility between the shell and solid elements (both quadratic). The third approach is a full three-dimensional finite element model, in which solid three-dimensional elements are used to model both the face sheets and the core. These models are referred to as three-dimensional solid models (using either E881, 883, or 885 solid elements) and they are typically reserved for detailed local modeling because of their computational cost. Recently, an additional modeling approach has been implemented in the STAGS nonlinear finite element code. This modeling approach, referred to herein as sandwich element models (see Riks and Rankin, 2001, 2002), uses a specialty element developed specifically for the analysis of sandwich structures (E840 sandwich element). Sandwich element models embody the kinematics and stiffness of the sandwich structure for less computational cost than the layered shell/solid models. Sandwich element models provide a cost-effective analysis approach for capturing sandwich behavior for large-scale sandwich structure simulations and avoid the through-the-thickness element aspect ratio issue associated with the use of solid elements. Sandwich elements provide accurate solutions for detailed local analyses as well. Several STAGS finite element models are considered for this problem:

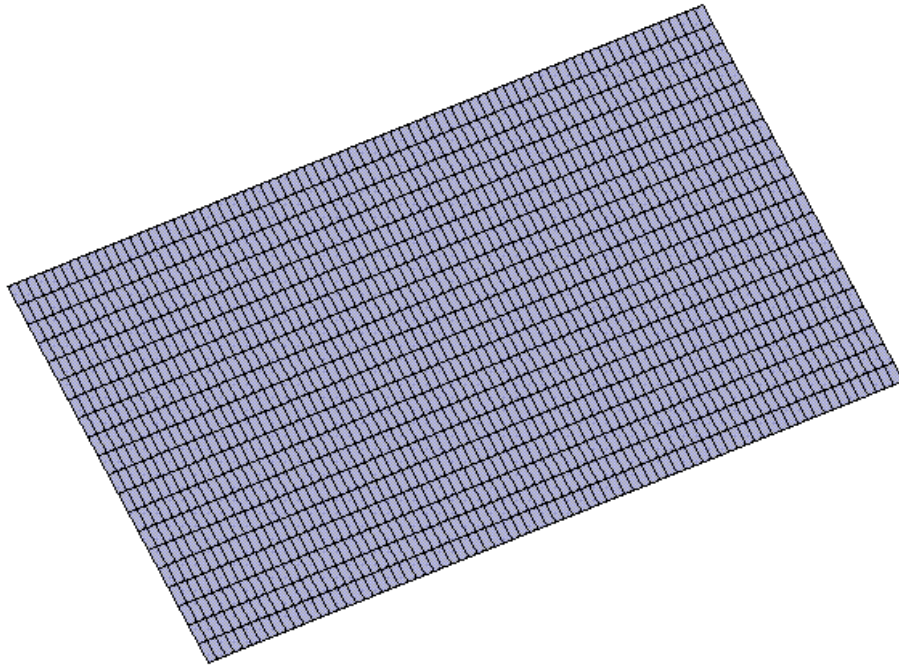
Full panel model using:

- Layered shell modeling approach
- Layered shell/solid modeling approach
- Sandwich element modeling approach

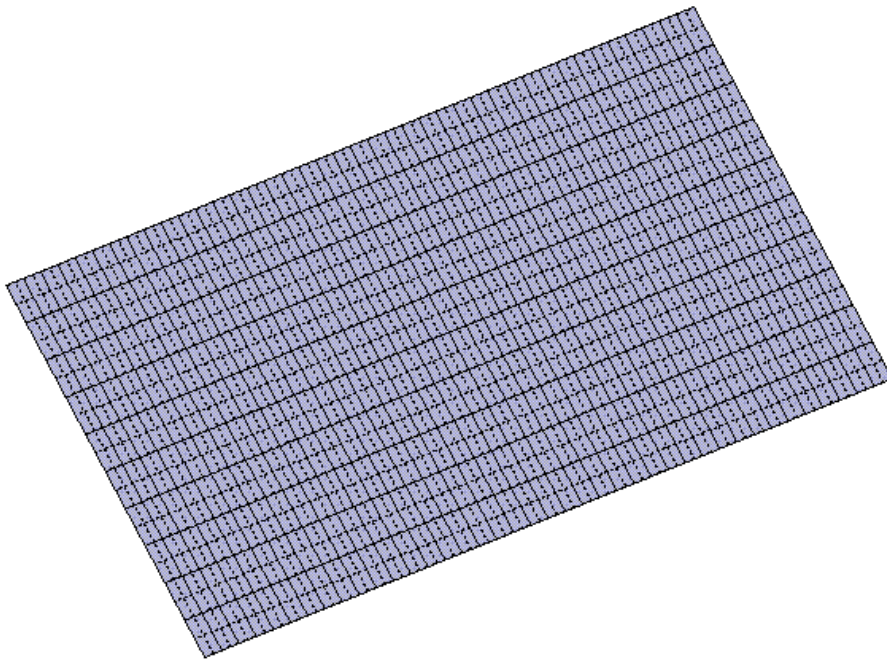
Local strip model using:

- Sandwich element modeling approach

The STAGS models for the layered shell and sandwich element modeling approaches (full panel and local strip) are generated using a single shell unit for the rectangular panel surface geometry (ISHHELL=1). Finite element models for the thick sandwich case are shown in Figure 51 for the layered shell approach, in Figure 52 for the sandwich element approach, in Figure 53 for the layered shell/solid approach, and in Figure 54 for the local strip model.



(a) 4-node E410 quadrilateral shell element.



(b) 9-node E480 quadrilateral shell element.

Figure 51. Finite element model for the layered shell approach.

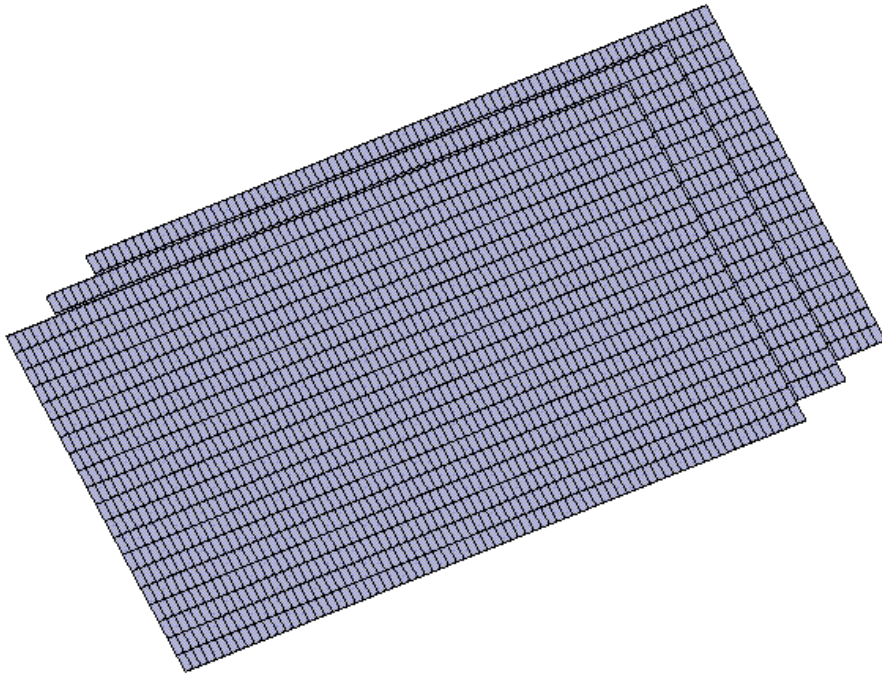


Figure 52. Finite element model for the sandwich element approach with two sandwich elements through the thickness – three nodal planes, one “phantom” face sheet on the interior of the panel.

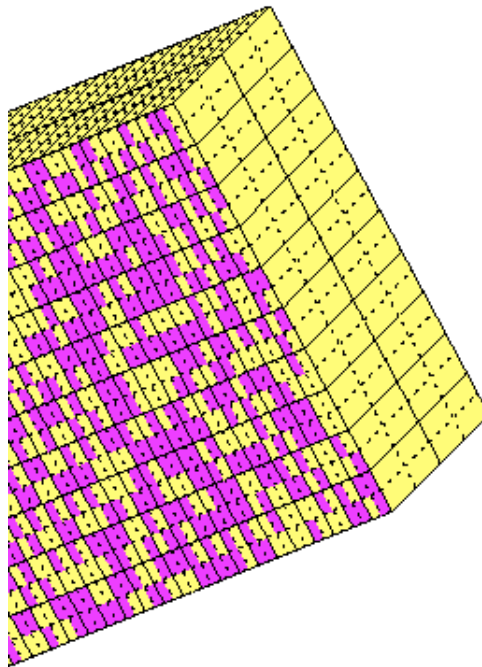


Figure 53. Portion of a finite element model for the layered shell/solid modeling approach with two E883 solid elements through the core thickness – five nodal planes plus E480 shell elements for each face sheet. Note: some of the solid element faces shown in this view are “showing through” the face-sheet shell elements in some locations.

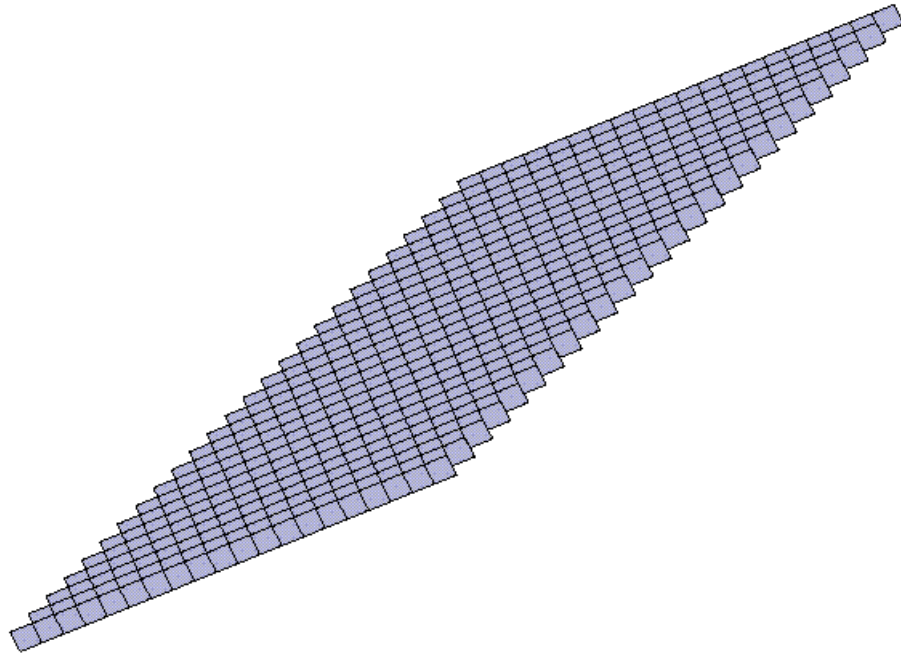


Figure 54. Finite element model for the local strip model using 25 layers of sandwich elements through the thickness, one element in width, 20 elements along the 2.5-in.-long strip length.

In these approaches, the reference surface is also the middle surface of the panel with no eccentricity specified. The STAGS model for the layered shell/solid modeling approach is generated using three shell units – one for each face sheet and one for the core. In the layered shell/solid approach, the reference surface can be defined as the middle surface of the panel provided the face sheet shell elements are located properly. The reference surface for the bottom face sheet (nodal plane) is located by translating the nodal plane to $z = -0.5h_c$ using the M-4d record and the middle surface of the shell element has an eccentricity of $e_z = -0.5t_f$ on the M-5 record. Similarly, the reference surface for the top face sheet is located by translating the nodal plane to $z = +0.5h_c$ using the M-4d record and the middle surface of the shell element has an eccentricity of $e_z = +0.5t_f$ on the M-5 record. The shell unit modeling the core using solid elements locates the reference surface at the middle of the accumulated thickness of the solid elements – the bounding nodal planes are located at $z = \pm 0.5h_c$.

Material properties and sandwich construction are defined using the GCP approach and also using the historical STAGS approach (I and K records). Material modeling using the current GCP approach requires data on the I-5a and I-6a records to define the material properties and records I-5a, I-21a, I-21b, I-21c, I-21d, and I-21e to define the shell fabrication. In addition, records I-5a, I-22a, and I-22b are used to define the solid fabrication. For the sandwich elements, the core material properties are defined using the solid fabrication records, while the face sheet properties are defined using the shell fabrication records. The core material is defined using a solid fabrication type where the thickness represents half the total core thickness (the finite element models used here have just two elements through the thickness). The face sheet material is defined using the shell fabrication type. Two solid fabrications are included to represent a thin core ($h_c = 0.20$ in.) and a thick core ($h_c = 5.50$ in.). Two shell fabrications are also included to represent a thin face sheet ($t_f = 0.02$ in.) and a thick face sheet ($t_f = 0.11$ in.).

Mesh discretization studies include different levels of mesh refinement and different element types. Mesh refinement is readily performed by changing the number of rows and columns of nodes in each planar direction on the F-1 record. Element type is selected using the N-1 record (KELT). Multiple solid elements through the thickness are specified using the NLAYS and NFABS parameters on the M-1 record in combination with NFABS M-5 records. All of the full panel finite element models use 81 grid points along the panel length and 21 grid points along the panel width.

Boundary conditions on the displacements are specified using the P-1 and P-2 records for the layered shell modeling approach. Boundary conditions for the layered shell/solid and sandwich modeling approaches are specified using the Q records – the P records will only constrain the degrees of freedom associated with the first nodal plane of a solid model. In the pre-stress condition, the sandwich panel is loaded by a uniform end shortening, u_0 , applied to the sandwich face sheets on the ends of the panel at $x=0$ and $x=a$ (see Figure 52). The boundary conditions applied to all grid points along each edge are: $u = u_0$ and $w = \theta_x = \theta_z = 0$ along Edge 1 ($x=0$); $w = \theta_y = 0$ along Edges 2 and 4 ($y=b$ and $y=0$, respectively); and $u = -u_0$ and $w = \theta_x = \theta_z = 0$ along Edge 3 ($x=a$). In addition, the v displacement component is fixed at the center of the panel on all nodal planes.

Numerical Results and Discussion

Full panel models are defined as finite element models of the entire sandwich panel. Spatial discretization of the full panel is related to the anticipated buckling mode. Thus, some knowledge of the panel buckling response is needed to develop these full panel analysis models. For a rectangular panel, the number of half-waves, m , along the panel length in a general-instability panel-buckling mode is a function of the

panel aspect ratio a/b , assuming a single half-wave across the width of the panel. Generally, five to six grid points per half-wave are required for accurate buckling predictions. To capture a face-sheet-wrinkling mode, the finite element mesh needs to be sufficiently refined to represent short-wavelength buckles.

Local strip models are defined as finite element models of a localized region with significant through-the-thickness modeling detail so that short wavelength wrinkling modes can readily be detected. A local strip model is used to verify short-wavelength face-sheet-wrinkling behavior predictions obtained with the full panel models. Local strip models represent a thin longitudinal slice of a panel away from edge effects. In the present study this strip model has a width equal to 0.1 inches (2.54 mm) and has 25 layers of sandwich elements through the core thickness. One integration point is used through the thickness of each core layer. The length of the local strip model depends on the wavelength of the buckling mode. Therefore, several local models, with different lengths, are typically analyzed to ensure that the lowest buckling load is determined. For the thick case, the buckling halfwave length from the full panel models is 2.5 inches (8 halfwaves along the panel length).

Analytical solution from Brush and Almroth (1975) is obtained from:

$$P_{cr} = k \frac{\pi^2 D}{b} \quad \text{where} \quad k = \frac{\left(\frac{mb}{a} + \frac{a}{mb}\right)^2}{1 + r \left[1 + \left(\frac{mb}{a}\right)^2\right]}$$

$$D = \frac{1}{2} E_f t_f (h_c + t_f)^2 \quad C_Q = G_c h_c \quad r = \frac{\pi^2 D}{b^2 C_Q}$$

PANDA2 solutions have also been computed. Face sheet wrinkling using Vinson's model and general panel instability buckling are predicted using PANDA2.

Results for two cases are presented. The first case has thin face sheets (each 0.02-inches thick) and a thin core (0.2-inches thick), and the buckling results are given in Table 13. The general instability buckling behavior predicted by the STAGS models has two halfwaves in the loading direction and one across the panel width – the analytical solution corresponds to three but is very close to the value corresponding to two halfwaves (within 0.4%). The buckling loads predicted using the layered shell modeling approach are quite unconservative (~30% higher buckling load) for both the E410 and E480 shell elements when the shear correction factors are set to 5/6 because the layered shell model ignores through the thickness effects. However, when the shear correction factors (SCFs) are computed internally by the STAGS generic constitutive processor (GCP) if the SCFs are defined as -1 for the GCP shell fabrication input, the results obtained using the E480 element in the layered shell model gives very good results. The computed shear correction factors are reported in the S1 output as 0.0186 and 0.0112 rather than 5/6. The layered shell/solid and sandwich element modeling approaches give results consistent with the result obtained using PANDA2. The local strip model predicted short wave length buckling modes with the buckling load dependent upon the length of the local strip. For a one-inch-long strip, the panel wrinkling instability load is 260.915 lb. with 20 halfwaves; for a 5.0-in.-long strip, it is 90.442 lb. with 8 halfwaves; and for a 10.0-in.-long strip, it is 91,376 lb. with 8 halfwaves. Buckling mode shapes for the global and local models are given in Figure 55. Users need to examine different local strip lengths in order to account for various wave length buckles. PANDA2 provides insight into this aspect of the modeling. Hence the global result is the critical buckling load.

The second case has thick face sheets (each 0.11-inches thick) and a thick core (5.5-inches thick), and the buckling results are given in Table 14. The general short wavelength instability buckling behavior

predicted by the STAGS sandwich element models has eight halfwaves in the loading direction and one across the panel width – the analytical solution corresponds to eight as well. Buckling loads predicted using the layered shell modeling approach are in significant error since these shell elements neglect the transverse normal stiffness of the core and the core thickness is quite large (half the panel width). Use of this modeling approach for this geometry (*i.e.*, $h_c \approx a$ or b) is not appropriate unless three-dimensional effects are accounted for in the model. The layered shell/solid and sandwich element modeling approaches give comparable results consistent with the result obtained using PANDA2. The local strip model (0.1 inches wide) also predicts the short wave length buckling mode shape. For a 1.25-inch-long strip, the panel wrinkling instability load is 182,652 lb. with 16 halfwaves; for a 2.50-in.-long strip, it is 90,208 lb. with 8 halfwaves; and for a 5.0-in.-long strip, it is 90,442 lb. with 8 halfwaves. Buckling mode shapes for the global and local models are given in Figure 56. Again the global result is the critical value, which is also confirmed by the local strip analysis.

Table 13. Sandwich panel buckling results for the thin face sheet, thin core case.

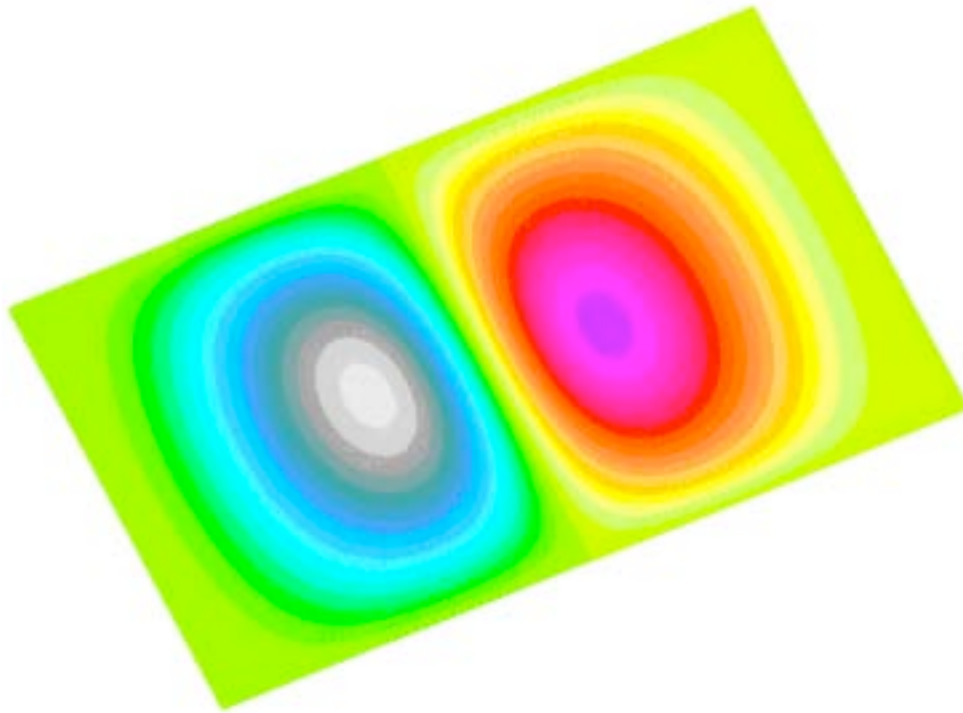
Analysis Type	Modeling	Buckling factor, λ	Critical Buckling Load, lb.
Brush & Almroth	Analytical	---	13,620
PANDA2	Face Sheet Wrinkling	---	33,400
PANDA2	Panel Buckling	---	12,100
STAGS	Layered Shell, E410	0.5276	21,107
STAGS	Layered Shell, E480 w/SCF=5/6	0.5221	20,886
STAGS	Layered Shell, E480 w/SCF computed	0.3565	14,261
STAGS	Layered Shell/Solid, E480/E883	0.3707	14,603
STAGS	Sandwich element, E840	0.3709	14,675
STAGS	Local strip, E840, 5-inch-long	0.2055	90,442*

*The buckling load for the local strip model is obtained by computing the critical running load for the local strip width (0.1 in.) and then multiplying by the panel width (10 in.).

Table 14. Sandwich panel buckling results for the thick face sheet, thick core case.

Analysis Type	Modeling	Buckling factor, λ	Critical Buckling Load, lb.
Brush & Almroth	Analytical	---	699,656
PANDA2	Face Sheet Wrinkling	---	88,400
PANDA2	Panel Buckling	---	557,000
STAGS	Layered Shell/Solid, E480/E883	0.4959	98,486
STAGS	Sandwich element, E840	0.4694	94,651
STAGS	Local strip, E840, 2.5-inch-long	0.1025	90,208*

*The buckling load for the local strip model is obtained by computing the critical running load for the local strip width (0.1 in.) and then multiplying by the panel width (10 in.).

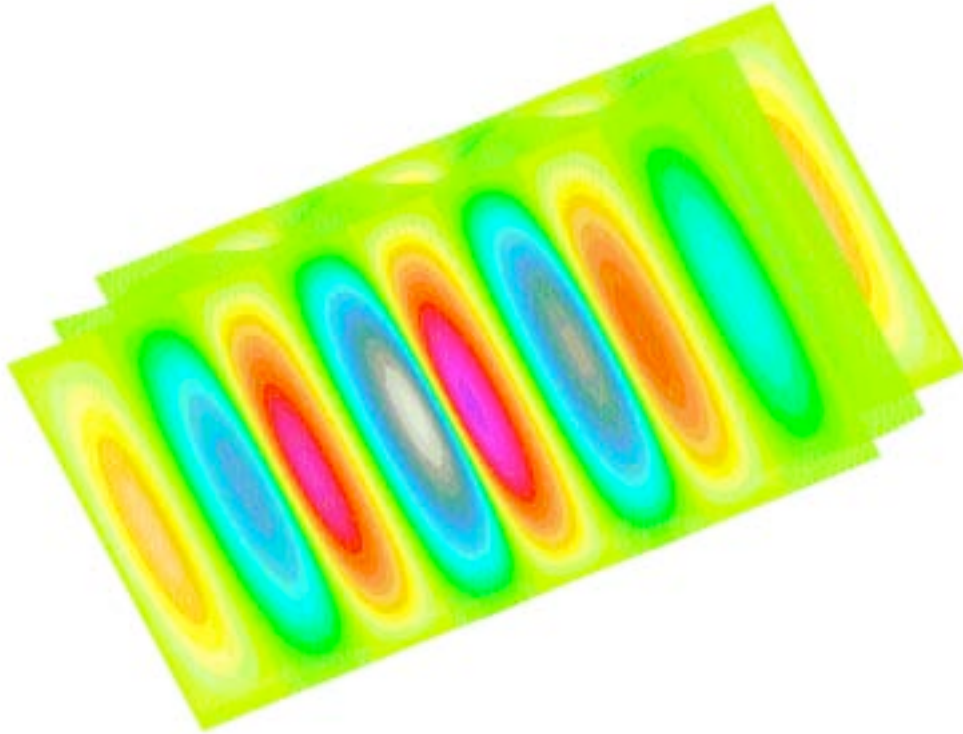


(a) Global model result.



(b) Local strip model result.

Figure 55. Buckling results using the sandwich element for the thin face sheets, thin core case.



(a) Global model result.



(b) Local strip model result.

Figure 56. Buckling results using the sandwich element for the thick face sheets, thick core case.

STAGS Input Files

The modeling strategy for sandwich panels depends on the nature of the structural response that is anticipated. However, a thorough examination of other possible response patterns needs to be performed. This strategy is needed due to the nature of the sandwich panel structural response. It may be governing by overall or general instability buckling mode shapes having a halfwave length on the order of the panel planar dimensions. These long wavelength mode shapes are easily represented using coarse finite element models over the plane of the sandwich panel. Face sheet wrinkling response, on the other hand, required a refined finite element model because halfwave length of the wrinkling mode (symmetric or asymmetric) is typically of the order of the sandwich panel thickness. Asymmetric face sheet wrinkling can be described as a short wave length general instability mode shape that does not cause compression or extension of the core material along the panel length. This behavior can be captured by full panel finite element models that are sufficiently refined (*i.e.*, element size on the order of the sandwich thickness). Symmetric face sheet wrinkling requires, in addition to a refined planar mesh discretization, through-the-thickness effects to be accounted for in the finite element model (*i.e.*, layered shell/solid models or sandwich element models). The STAGS input files included herein illustrate the various finite element modeling approaches. These input files are located under the following subdirectory:

```
$STAGSHOME/Advanced-Testcases/Type-A-sandwich
```

with specific modeling approaches given under the appropriate subdirectory as given by: layered-shell; layered-shell-solid; sandwich-element; and local-strip

Full Panel Layered Shell Model Input Files with E410

In this modeling approach, the sandwich panel is represented by shell elements only. Through-the-thickness modeling involves a three-layer laminate (bottom face sheet, core, and top face sheet) definition of the sandwich. The 4-node displacement-based E410 shell element is used. The E410 element neglects transverse shear flexibility but does have a cubic C^1 bending approximation.

sand410.inp (for S1 processor)

```
Sandwich panel buckling under compressive loading    $ A-1
C
C Layered shell modeling approach using the 410 shell element
C
C Ref. Brush & Almroth, "Buckling of Bars, Plates, and Shells,"
C      McGraw-Hill, 1975, pp. 108-112.
C
C a=20 in., b=10 in., simple-supported on all edges
C
0 0 0 0          $ B-1
1 0 0 0 0 0 0 0 0 $ B-2
0 0 0 0 0 1      $ B-3
81 21           $ F-1 Planar mesh definition over "a" by "b" panel
$-----GCP-----
ORTHOELAST_MATERIAL 1 1 1          $ core material
100.0 100.0 10.0e3,                $ E1, E2, E3
38.4 12.E3 7.2e3,                  $ G12, G13, G23
0.30 0.01 0.01,                   $ P12, P13, P23
0. 0. 0. 0. 0. 0. 0. 0. 0.        $ Filler spaces
ORTHOELAST_MATERIAL 2 1 1          $ isotropic face sheet material
10.0E6 10.0e6 10.0E6,              $ E1, E2, E3
3.846E6 3.846e6 3.846e6,           $ G12, G13, G23
0.30 0.30 0.30,                   $ P12, P13, P23
0. 0. 0. 0. 0. 0. 0. 0. 0.        $ Filler spaces
C
C Laminate definition of the sandwich structure
```

```

C
SHELL_FABRICATION 1 3 0 1 0 $i-21 Thin F/S and thin core
2 1 2 $i-21 Facesheet/Core/Facesheet
0.02 0.2 0.02 $i-21 h_fs=0.02 in.; h_core=0.2 in.
3*0.0
0.83333 0.83333 $i-21 shear correction factors, 5/6
SHELL_FABRICATION 2 3 0 1 0 $i-21 Thick F/S and thin core
2 1 2 $i-21 Facesheet/Core/Facesheet
0.11 0.2 0.11 $i-21 h_fs=0.11 in.; h_core=0.2 in.
3*0.0
0.83333 0.83333 $i-21 shear correction factors, 5/6
SHELL_FABRICATION 3 3 0 1 0 $i-21 Thin F/S and thick core
2 1 2 $i-21 Facesheet/Core/Facesheet
0.02 5.5 0.02 $i-21 h_fs=0.02 in.; h_core=5.5 in.
3*0.0
0.83333 0.83333 $i-21 shear correction factors, 5/6
SHELL_FABRICATION 4 3 0 1 0 $i-21 Thick F/S and thick core
2 1 2 $i-21 Facesheet/Core/Facesheet
0.11 5.5 0.11 $i-21 h_fs=0.11 in.; h_core=5.5 in.
3*0.0
0.83333 0.83333 $i-21 shear correction factors, 5/6
END
$-----GCP-----
$ Define the shell unit for the rectangular panel
2 0 0 0 0 0 $ M-1 Unit No. 1
0.0 20.0 0.00 10.00 $ M-2 Define Geometry of rectangular plate
-1 $ M-5 layered shell model
410 $ N-1 Select element type
0 0 0 0 $ P-1 Specify BC's on each edge
110 010 $ P-2, w=ru=rw=0 along x=0
110 101 $ P-2, w=rv=0 along y=b
110 010 $ P-2, w=ru=rw=0 along x=a
110 101 $ P-2, w=rv=0 along y=0
1 $ Q-1 Loading system
1 3 $ Q-2 Load system A only; 3 records
-0.1 -1 1 81 0 0 0 0 0 0 0 $ Q-3 Applied end shortening at x=a
+0.1 -1 1 1 0 0 0 0 0 0 0 $ Q-3 Applied end shortening at x=0
+0.0 -1 2 41 11 0 0 0 0 0 0 $ Q-3 Remove rigid body motion; v=0 at center
C+0.0 -1 6 0 0 0 0 0 0 0 0 $ Q-3 RW=0 everywhere for 480 element
1 4*0 1 $ R-1 Output displ. and internal forces

```

sand410.bin (for S2 processor)

```

Sandwich panel buckling under compressive loading $ A-1
C *** analysis type definition ***
C indic ipost  ilist  icor  impthe  ioptim  iflu  newent  $ b-1
1 1 1 0 0 0 0 -1 $ b-1
C *** load multiplier record ***
C stld(1) step(1) facm(1) stld(2) step(2) facm(2) itemp $ c-1
1.0 0.0 0.0 0.0 0.0 0.0 0 $ c-1
C
C *** eigenvalue control **** d-2
C nsec  delevev  iprint  *** d-2
100 .0001 1 $ d-2
C
C **** eigenvalue cluster definition **** d-3
C neig  shift  eiga  eigb  ***** d-3
4 0.00 $ d-3

```

sand410.pin (for STAPL processor)

```

Sandwich panel studies
4 0 0 0 $PL-2 NPLOT,IPREP,IPRS,KDEV
2 0 4 0 1 0 0 3 $SPL-3 KPLOT,VIEW,ITEM,STEP,MODE,IFRNG,COLOR,ICOMP

```

```

0.0  0  0.0  0.0  0.0  $PL-5  DSCALE,NROTS,LWSCALE,RNGMIN,RGMAX
2   0  4   0  2  0  0  3   $PL-3  KPLOT,VIEW,ITEM,STEP,MODE,IFRNG,COLOR,ICOMP
0.0  0  0.0  0.0  0.0  $PL-5  DSCALE,NROTS,LWSCALE,RNGMIN,RGMAX
2   0  4   0  3  0  0  3   $PL-3  KPLOT,VIEW,ITEM,STEP,MODE,IFRNG,COLOR,ICOMP
0.0  0  0.0  0.0  0.0  $PL-5  DSCALE,NROTS,LWSCALE,RNGMIN,RGMAX
2   0  4   0  4  0  0  3   $PL-3  KPLOT,VIEW,ITEM,STEP,MODE,IFRNG,COLOR,ICOMP
0.0  0  0.0  0.0  0.0  $PL-5  DSCALE,NROTS,LWSCALE,RNGMIN,RGMAX
2   0  4   0  1  0  0  3   $PL-3  KPLOT,VIEW,ITEM,STEP,MODE,IFRNG,COLOR,ICOMP
0.0  3  0.0  0.0  0.0  $PL-5  DSCALE,NROTS,LWSCALE,RNGMIN,RGMAX
1  0.0 / 2  0.0 / 3  0.0
2   0  4   0  1  0  0  3   $PL-3  KPLOT,VIEW,ITEM,STEP,MODE,IFRNG,COLOR,ICOMP
0.0  3  0.0  0.0  0.0  $PL-5  DSCALE,NROTS,LWSCALE,RNGMIN,RGMAX
1 -90.0 / 2  0.0 / 3  0.0
2   0  4   0  3  0  0  3   $PL-3  KPLOT,VIEW,ITEM,STEP,MODE,IFRNG,COLOR,ICOMP
0.0  3  0.0  0.0  0.0  $PL-5  DSCALE,NROTS,LWSCALE,RNGMIN,RGMAX
1  0.0 / 2  0.0 / 3  0.0
2   0  4   0  3  0  0  3   $PL-3  KPLOT,VIEW,ITEM,STEP,MODE,IFRNG,COLOR,ICOMP
0.0  3  0.0  0.0  0.0  $PL-5  DSCALE,NROTS,LWSCALE,RNGMIN,RGMAX
1 -90.0 / 2  0.0 / 3  0.0

```

Full Panel Layered Shell Model Input Files with E480

In this modeling approach, the sandwich panel is represented by shell elements only. Through-the-thickness modeling involves a three-layer laminate (bottom face sheet, core, and top face sheet) definition of the sandwich. The 9-node ANS-based E480 shell element is used since it includes transverse shear flexibility. As result, the number of rows and columns defined on the F-1 record must be odd numbers because the element has three nodes per edge (e.g., a model with three rows and three columns defines just a single 9-node element). Also, this element does not include drilling freedoms, and hence they must be suppressed (see the last Q-3 record).

sand480.inp (for S1 processor)

```

Sandwich panel buckling under compressive loading   $ A-1
C
C Layered shell modeling approach using the 480 shell element
C
C Ref.  Brush & Almroth, "Buckling of Bars, Plates, and Shells,"
C       McGraw-Hill, 1975, pp. 108-112.
C
C a=20 in., b=10 in., simple-supported on all edges
C
0  0  0  0          $ B-1
1  0  0  0  0  0  0  0  0  0  $ B-2
0  0  0  0  0  1    $ B-3
81 21              $ F-1  Planar mesh definition over "a" by "b" panel
$-----GCP-----
ORTHOELAST_MATERIAL 1 1 1          $ core material
100.0 100.0 10.0e3,                $ E1, E2, E3
38.4 12.E3 7.2e3,                  $ G12, G13, G23
0.30 0.01 0.01,                    $ P12, P13, P23
0. 0. 0. 0. 0. 0. 0. 0. 0. 0.    $ Filler spaces
ORTHOELAST_MATERIAL 2 1 1          $ isotropic face sheet material
10.0E6 10.0e6 10.0E6,              $ E1, E2, E3
3.846E6 3.846e6 3.846e6,          $ G12, G13, G23
0.30 0.30 0.30,                    $ P12, P13, P23
0. 0. 0. 0. 0. 0. 0. 0. 0. 0.    $ Filler spaces
C
C Laminate definition of the sandwich structure
C
SHELL_FABRICATION 1 3 0 1 0        $i-21 Thin F/S and thin core

```

```

2 1 2 $i-21 Facesheet/Core/Facesheet
0.02 0.2 0.02 $i-21 h_fs=0.02 in.; h_core=0.2 in.
3*0.0
0.83333 0.83333 $i-21 shear correction factors, 5/6
SHELL_FABRICATION 2 3 0 1 0 $i-21 Thick F/S and thin core
2 1 2 $i-21 Facesheet/Core/Facesheet
0.11 0.2 0.11 $i-21 h_fs=0.11 in.; h_core=0.2 in.
3*0.0
0.83333 0.83333 $i-21 shear correction factors, 5/6
SHELL_FABRICATION 3 3 0 1 0 $i-21 Thin F/S and thick core
2 1 2 $i-21 Facesheet/Core/Facesheet
0.02 5.5 0.02 $i-21 h_fs=0.02 in.; h_core=5.5 in.
3*0.0
0.83333 0.83333 $i-21 shear correction factors, 5/6
SHELL_FABRICATION 4 3 0 1 0 $i-21 Thick F/S and thick core
2 1 2 $i-21 Facesheet/Core/Facesheet
0.11 5.5 0.11 $i-21 h_fs=0.11 in.; h_core=5.5 in.
3*0.0
0.83333 0.83333 $i-21 shear correction factors, 5/6
END
$-----GCP-----
$ Define the shell unit for the rectangular panel
2 0 0 0 0 0 $ M-1 Unit No. 1
0.0 20.0 0.00 10.00 $ M-2 Define Geometry of rectangular plate
-1 $ M-5 layered shell model
480 $ N-1 Select element type
0 0 0 0 $ P-1 Specify BC's on each edge
110 010 $ P-2, w=ru=rw=0 along x=0
110 101 $ P-2, w=rv=0 along y=b
110 010 $ P-2, w=ru=rw=0 along x=a
110 101 $ P-2, w=rv=0 along y=0
1 $ Q-1 Loading system
1 4 $ Q-2 Load system A only; 3 records
-0.1 -1 1 81 0 0 0 0 0 0 0 $ Q-3 Applied end shortening at x=a
+0.1 -1 1 1 0 0 0 0 0 0 0 $ Q-3 Applied end shortening at x=0
+0.0 -1 2 41 11 0 0 0 0 0 0 $ Q-3 Remove rigid body motion; v=0 at center
+0.0 -1 6 0 0 0 0 0 0 0 0 $ Q-3 RW=0 everywhere for 480 element
1 4*0 1 $ R-1 Output displ. and internal forces

```

Full Panel Layered Shell/Solid Model Input Files

In this modeling approach, the sandwich panel is modeled using shell elements for each face sheet (with appropriate reference surface eccentricities) and one or more solid elements through the core thickness. This approach is the layered shell/solid (LSS) approach. Using this approach within STAGS, limits the finite element selection to only the E480 shell element with bi-quadratic displacement shape functions and the E883 solid element with bi-quadratic shape functions on each element face – displacement field compatibility over the connected face. The finite element model used herein has two solid elements through the core thickness (one of either side of the middle surface). Two input files are included since the input differs for the thin and thick sandwich panel models. Only a single set of the S2 and STAPL input files are included since they are identical in either case – except for file name, of course.

thinLSS.inp (for S1 processor; thin sandwich case)

```

Compression-loaded rectangular sandwich panel $A-1
C
C Sandwich panel modeled using the layered shell/solid approach
C with two E883 solid elements through the core thickness
C and the E480 shell elements for the face sheets
C (i.e., five planes of nodes through the sandwich thickness)
C Shell unit 1 = bottom face sheet using E480 9-node shell element
C Shell unit 2 = top face sheet using E480 9-node shell element

```

```

C Shell unit 3 = core using two E883 27-node bricks through thickness
C
C Ref. Brush & Almroth, "Buckling of Bars, Plates, and Shells,"
C McGraw-Hill, 1975, pp. 108-112.
C
C a=20 in., b=10 in., simple-supported on all edges
C
0 0 0 0 $ B-1
3 0 0 0 0 0 0 0 0 2 $ B-2
1 0 3 0 0 1 $ B-3
81 21 81 21 81 21 $ F-1 Three shell units (2 face sheets & core)
1 0 0 1 0 3 0 0 1 0/ 0 $G-2c/G-2d
2 0 0 1 0 3 0 0 5 0/ 0 $G-2c/G-2d
1 $ I-1 Face-sheet data
10.0E6 0.300 3.85E6 0.100 6.0E-7 10.00E6 1.9439E-5 $ I-2
$-----GCP-----
$ sandwich core,
ORTHOELAST_MATERIAL 1 1 1 $ core material
100.0 100.0 100.0e2, $ E1, E2, E3
38.4 12.0e3 7.2e3, $ G12, G13, G23
0.30 0.01 0.01, $ P12, P13, P23
0. 0. 0. 0. 0. 0. 0. 0. 0. 0. $ Filler spaces
ORTHOELAST_MATERIAL 2 1 1 $ isotropic face sheet material
10.0E6 10.0e6 10.0E6, $ E1, E2, E3
3.846E6 3.846e6 3.846e6, $ G12, G13, G23
0.30 0.30 0.30, $ P12, P13, P23
0. 0. 0. 0. 0. 0. 0. 0. 0. 0. $ Filler spaces
C Core definitions - 2 layers across core
SOLID_FABRICATION 1 1 0 0 $ fabid, matid, iang, nipz: thin core
0.10 $ thickness of core element
SOLID_FABRICATION 2 1 0 0 $ fabid, matid, iang, nipz: thick core
2.75 $ thickness of core element
C Face sheet definitions
SHELL_FABRICATION 1 1 0 0 0 $i-21 Thin F/S
2 $i-21 Facesheet material
0.02 $i-21 h_fs=0.02 in.
0.0
SHELL_FABRICATION 2 1 0 0 0 $i-21 Thick F/S
2 $i-21 Facesheet material
0.11 $i-21 h_fs=0.11 in.
0.0
END
$-----GCP-----
$----Shell Wall Data using historical STAGS approach -----
1 1 1 / 1 .020 0.0 $K-1/K-2 Thin face sheet
2 1 1 / 1 .110 0.0 $K-1/K-2 Thick face sheet
3 1 1 / 1 .000 0.0 $K-1/K-2 Phantom face sheet definition
C
C Shell unit to define Bottom Face Sheet
C
2 4 0 0 0 1 $ M-1 Unit No. 1
0.0 20.0 0.00 10.00 $ M-2
0.0 0.0 -0.10 / 3*0.0 $ M-4d/M-4e shift reference plane by -h_c/2
-1 0 0.0 -0.010 0 0 0 $ M-5 Lower Face Sheet with ecz=-t_fs/2
480 $ N-1 Element definition for face sheet
0 0 0 0 $ P-1 Specify BC's on each edge
110 010 $ P-2, w=ru=rw=0 along x=0
110 101 $ P-2, w=rv=0 along y=b
110 010 $ P-2, w=ru=rw=0 along x=a
110 101 $ P-2, w=rv=0 along y=0
1 $ Q-1
1 4 $ Q-2
-.1 -1 1 81 0 0 0 0 0 0 1 $ Q-3 u=-u0 at x=a on face sheet

```

```

+.1 -1 1 1 0 0 0 0 0 0 1 $ Q-3 u=+u0 at x=0 on face sheet
0.0 -1 2 41 11 0 0 0 0 0 1 $ Q-3 v=0 at center of face sheet
0.0 -1 6 0 0 0 0 0 0 0 1 $ Q-3 RW=0 everywhere (no drilling freedoms)
1 4*0 1 $ R-1
C
C Shell unit to define Upper Face Sheet
C
2 4 0 0 0 1 $ M-1 Unit No. 2
0.0 20.0 0.00 10.00 $ M-2
0.0 0.0 +0.10 / 3*0.0 $ M-4d/M-4e shift reference plane by +h_c/2
-1 0 0.0 +0.010 0 0 0 $ M-5 Lower Face Sheet with ecz=+t_fs/2
480 $ N-1
0 0 0 0 $ P-1 Specify BC's on each edge
110 010 $ P-2, w=ru=rw=0 along x=0
110 101 $ P-2, w=rv=0 along y=b
110 010 $ P-2, w=ru=rw=0 along x=a
110 101 $ P-2, w=rv=0 along y=0
1 $ Q-1
1 4 $ Q-2
-.1 -1 1 81 0 0 0 0 0 0 1 $ Q-3 u=-u0 at x=a on face sheet
+.1 -1 1 1 0 0 0 0 0 0 1 $ Q-3 u=+u0 at x=0 on face sheet
0.0 -1 2 41 11 0 0 0 0 0 1 $ Q-3 v=0 at center of face sheet
0.0 -1 6 0 0 0 0 0 0 0 1 $ Q-3 RW=0 everywhere (no drilling freedoms)
1 4*0 1 $ R-1
C
C Shell unit definition for the core using 2 layers of E883 elements
C
2 0 0 0 2 1 $ M-1 Unit No. 3
0.0 20.0 0.00 10.00 $ M-2
-1 0 0.0 0.0 0 0 0 $ M-5 Core using GCP solid fab.
883 $ N-1 Element definition for core
3 3 3 $ P-1 Specify BC's on each edge, solids have no rotations
1 $ Q-1 Loading system
1 21 $ Q-2 Load system A; 21 records for intermediate nodal planes
C impose uniform end shortening
-.1 -1 1 81 0 0 0 0 0 0 2 $ Q-3 u=-u0 at x=a on 2nd nodal plane
+.1 -1 1 1 0 0 0 0 0 0 2 $ Q-3 u=+u0 at x=0 on 2nd nodal plane
-.1 -1 1 81 0 0 0 0 0 0 3 $ Q-3 u=-u0 at x=a on 3rd nodal plane
+.1 -1 1 1 0 0 0 0 0 0 3 $ Q-3 u=+u0 at x=0 on 3rd nodal plane
-.1 -1 1 81 0 0 0 0 0 0 4 $ Q-3 u=-u0 at x=a on 4th nodal plane
+.1 -1 1 1 0 0 0 0 0 0 4 $ Q-3 u=+u0 at x=0 on 4th nodal plane
C impose w=0 along edges
0. -1 3 1 0 0 0 0 0 0 2 $ Q-3 w=0 at x = 0, layer 2
0. -1 3 1 0 0 0 0 0 0 3 $ Q-3 w=0 at x = 0, layer 3
0. -1 3 1 0 0 0 0 0 0 4 $ Q-3 w=0 at x = 0, layer 4
0. -1 3 81 0 0 0 0 0 0 2 $ Q-3 w=0 at x = a, layer 2
0. -1 3 81 0 0 0 0 0 0 3 $ Q-3 w=0 at x = a, layer 3
0. -1 3 81 0 0 0 0 0 0 4 $ Q-3 w=0 at x = a, layer 4
0. -1 3 0 1 0 0 0 0 0 2 $ Q-3 w=0 at y = 0, layer 2
0. -1 3 0 1 0 0 0 0 0 3 $ Q-3 w=0 at y = 0, layer 3
0. -1 3 0 1 0 0 0 0 0 4 $ Q-3 w=0 at y = 0, layer 4
0. -1 3 0 21 0 0 0 0 0 2 $ Q-3 w=0 at y = b, layer 2
0. -1 3 0 21 0 0 0 0 0 3 $ Q-3 w=0 at y = b, layer 3
0. -1 3 0 21 0 0 0 0 0 4 $ Q-3 w=0 at y = b, layer 4
0.0 -1 2 41 11 0 0 0 0 0 2 $ Q-3 v=0 at center of layer 2
0.0 -1 2 41 11 0 0 0 0 0 3 $ Q-3 v=0 at center of layer 3
0.0 -1 2 41 11 0 0 0 0 0 4 $ Q-3 v=0 at center of layer 4
1 4*0 1 $ R-1 Print displacements and internal forces

```

thickLSS.inp (for S1 processor; thick sandwich case)
Compression-loaded rectangular sandwich panel \$A-1


```

C
C Sandwich panel modeled using the layered shell/solid approach
C with two E883 solid elements through the core thickness
C and the E480 shell elements for the face sheets
C (i.e., five planes of nodes through the sandwich thickness)
C Shell unit 1 = bottom face sheet using E480 9-node shell element
C Shell unit 2 = top face sheet using E480 9-node shell element
C Shell unit 3 = core using two E883 27-node bricks through thickness
C
C Ref. Brush & Almroth, "Buckling of Bars, Plates, and Shells,"
C McGraw-Hill, 1975, pp. 108-112.
C
C a=20 in., b=10 in., simple-supported on all edges
C
0 0 0 0 $ B-1
3 0 0 0 0 0 0 0 0 2 $ B-2
1 0 3 0 0 1 $ B-3
81 21 81 21 81 21 $ F-1 Three shell units (2 face sheets & core)
1 0 0 1 0 3 0 0 1 0/ 0 $G-2c/G-2d
2 0 0 1 0 3 0 0 5 0/ 0 $G-2c/G-2d
1 $ I-1 Face-sheet data
10.0E6 0.300 3.85E6 0.100 6.0E-7 10.00E6 1.9439E-5 $ I-2
$-----GCP-----
$ sandwich core,
ORTHOELAST_MATERIAL 1 1 1 $ core material
100.0 100.0 100.0e2, $ E1, E2, E3
38.4 12.0e3 7.2e3, $ G12, G13, G23
0.30 0.01 0.01, $ P12, P13, P23
0. 0. 0. 0. 0. 0. 0. 0. 0. 0. $ Filler spaces
ORTHOELAST_MATERIAL 2 1 1 $ isotropic face sheet material
10.0E6 10.0e6 10.0E6, $ E1, E2, E3
3.846E6 3.846e6 3.846e6, $ G12, G13, G23
0.30 0.30 0.30, $ P12, P13, P23
0. 0. 0. 0. 0. 0. 0. 0. 0. 0. $ Filler spaces
C Core definitions - 2 layers across core
SOLID_FABRICATION 1 1 0 0 $ fabid, matid, iang, nipz: thin core
0.10 $ thickness of core element
SOLID_FABRICATION 2 1 0 0 $ fabid, matid, iang, nipz: thick core
2.75 $ thickness of core element
C Face sheet definitions
SHELL_FABRICATION 1 1 0 1 0 $i-21 Thin F/S
2 $i-21 Facesheet material
0.02 $i-21 h_fs=0.02 in.
0.0
0.83333 0.83333 $i-21 shear correction factors, 5/6
SHELL_FABRICATION 2 1 0 1 0 $i-21 Thick F/S
2 $i-21 Facesheet material
0.11 $i-21 h_fs=0.11 in.
0.0
0.83333 0.83333 $i-21 shear correction factors, 5/6
END
$-----GCP-----
$----Shell Wall Data using historical STAGS approach -----
1 1 1 / 1 .020 0.0 $K-1/K-2 Thin face sheet
2 1 1 / 1 .110 0.0 $K-1/K-2 Thick face sheet
3 1 1 / 1 .000 0.0 $K-1/K-2 Phantom face sheet definition
C
C Shell unit to define Bottom Face Sheet
C
2 4 0 0 0 1 $ M-1 Unit No. 1
0.0 20.0 0.00 10.00 $ M-2
0.0 0.0 -2.75 / 3*0.0 $ M-4d/M-4e shift reference plane by -h_c/2
-2 0 0.0 -0.055 0 0 0 $ M-5 Lower Face Sheet with ecz=-t_fs/2

```

```

480                                $ N-1 Element definition for face sheet
0 0 0 0 $ P-1 Specify BC's on each edge
110 010 $ P-2, w=ru=rw=0 along x=0
110 101 $ P-2, w=rv=0 along y=b
110 010 $ P-2, w=ru=rw=0 along x=a
110 101 $ P-2, w=rv=0 along y=0
1 $ Q-1
1 4 $ Q-2
-.1 -1 1 81 0 0 0 0 0 0 1 $ Q-3 u=-u0 at x=a on face sheet
+.1 -1 1 1 0 0 0 0 0 0 1 $ Q-3 u=+u0 at x=0 on face sheet
0.0 -1 2 41 11 0 0 0 0 0 1 $ Q-3 v=0 at center of face sheet
0.0 -1 6 0 0 0 0 0 0 0 1 $ Q-3 RW=0 everywhere (no drilling freedoms)
1 4*0 1 $ R-1
C
C Shell unit to define Upper Face Sheet
C
2 4 0 0 0 1 $ M-1 Unit No. 2
0.0 20.0 0.00 10.00 $ M-2
0.0 0.0 +2.75 / 3*0.0 $ M-4d/M-4e shift reference plane by +h_c/2
-2 0 0.0 +0.055 0 0 0 $ M-5 Lower Face Sheet with ecz=+t_fs/2
480 $ N-1
0 0 0 0 $ P-1 Specify BC's on each edge
110 010 $ P-2, w=ru=rw=0 along x=0
110 101 $ P-2, w=rv=0 along y=b
110 010 $ P-2, w=ru=rw=0 along x=a
110 101 $ P-2, w=rv=0 along y=0
1 $ Q-1
1 4 $ Q-2
-.1 -1 1 81 0 0 0 0 0 0 1 $ Q-3 u=-u0 at x=a on face sheet
+.1 -1 1 1 0 0 0 0 0 0 1 $ Q-3 u=+u0 at x=0 on face sheet
0.0 -1 2 41 11 0 0 0 0 0 1 $ Q-3 v=0 at center of face sheet
0.0 -1 6 0 0 0 0 0 0 0 1 $ Q-3 RW=0 everywhere (no drilling freedoms)
1 4*0 1 $ R-1
C
C Shell unit definition for the core using 2 layers of E883 elements
C
2 0 0 0 2 1 $ M-1 Unit No. 3
0.0 20.0 0.00 10.00 $ M-2
-2 0 0.0 0.0 0 0 0 $ M-5 Core using GCP solid fab.
883 $ N-1 Element definition for core
3 3 3 3 $ P-1 Specify BC's on each edge, solids have no rotations
1 $ Q-1 Loading system
1 21 $ Q-2 Load system A; 21 records for intermediate nodal planes
C impose uniform end shortening
-.1 -1 1 81 0 0 0 0 0 0 2 $ Q-3 u=-u0 at x=a on 2nd nodal plane
+.1 -1 1 1 0 0 0 0 0 0 2 $ Q-3 u=+u0 at x=0 on 2nd nodal plane
-.1 -1 1 81 0 0 0 0 0 0 3 $ Q-3 u=-u0 at x=a on 3rd nodal plane
+.1 -1 1 1 0 0 0 0 0 0 3 $ Q-3 u=+u0 at x=0 on 3rd nodal plane
-.1 -1 1 81 0 0 0 0 0 0 4 $ Q-3 u=-u0 at x=a on 4th nodal plane
+.1 -1 1 1 0 0 0 0 0 0 4 $ Q-3 u=+u0 at x=0 on 4th nodal plane
C impose w=0 along edges
0. -1 3 1 0 0 0 0 0 0 2 $ Q-3 w=0 at x = 0, layer 2
0. -1 3 1 0 0 0 0 0 0 3 $ Q-3 w=0 at x = 0, layer 3
0. -1 3 1 0 0 0 0 0 0 4 $ Q-3 w=0 at x = 0, layer 4
0. -1 3 81 0 0 0 0 0 0 2 $ Q-3 w=0 at x = a, layer 2
0. -1 3 81 0 0 0 0 0 0 3 $ Q-3 w=0 at x = a, layer 3
0. -1 3 81 0 0 0 0 0 0 4 $ Q-3 w=0 at x = a, layer 4
0. -1 3 0 1 0 0 0 0 0 2 $ Q-3 w=0 at y = 0, layer 2
0. -1 3 0 1 0 0 0 0 0 3 $ Q-3 w=0 at y = 0, layer 3
0. -1 3 0 1 0 0 0 0 0 4 $ Q-3 w=0 at y = 0, layer 4
0. -1 3 0 21 0 0 0 0 0 2 $ Q-3 w=0 at y = b, layer 2
0. -1 3 0 21 0 0 0 0 0 3 $ Q-3 w=0 at y = b, layer 3
0. -1 3 0 21 0 0 0 0 0 4 $ Q-3 w=0 at y = b, layer 4

```

```

0.0 -1 2 41 11 0 0 0 0 0 2 $ Q-3 v=0 at center of layer 2
0.0 -1 2 41 11 0 0 0 0 0 3 $ Q-3 v=0 at center of layer 3
0.0 -1 2 41 11 0 0 0 0 0 4 $ Q-3 v=0 at center of layer 4
1 4*0 1 $ R-1 Print displacements and internal forces

```

thickLSS.bin (for S2 processor; thick sandwich case)

```

Sandwich panel buckling under compressive loading $ A-1
C *** analysis type definition ***
C indic ipost ilist icor impthe ioptim iflu newent $ b-1
  1 1 0 0 0 0 0 -1 $ b-1
C *** load multiplier record ***
C stld(1) step(1) facm(1) stld(2) step(2) facm(2) itemp $ c-1
  1.0 0.0 0.0 0.0 0.0 0.0 0 $ c-1
C
C *** eigenvalue control **** d-2
C nsec deletv iprint *** d-2
2000 .0001 0 $ d-2
C
C **** eigenvalue cluster definition **** d-3
C neig shift eiga eigb ***** d-3
  4 0.0 $ d-3

```

thickLSS.pin (for STAPL processor; thick sandwich case)

```

Sandwich panel studies
  4 0 0 0 $PL-2 NPLOT,IPREP,IPRS,KDEV
  2 0 4 0 1 0 0 3 $PL-3 KPLOT,VIEW,ITEM,STEP,MODE,IFRNG,COLOR,ICOMP
  0.0 0 0.0 0.0 0.0 $PL-5 DSCALE,NROTS,LWSCALE,RNGMIN,RGMAX
  2 0 4 0 2 0 0 3 $PL-3 KPLOT,VIEW,ITEM,STEP,MODE,IFRNG,COLOR,ICOMP
  0.0 0 0.0 0.0 0.0 $PL-5 DSCALE,NROTS,LWSCALE,RNGMIN,RGMAX
  2 0 4 0 3 0 0 3 $PL-3 KPLOT,VIEW,ITEM,STEP,MODE,IFRNG,COLOR,ICOMP
  0.0 0 0.0 0.0 0.0 $PL-5 DSCALE,NROTS,LWSCALE,RNGMIN,RGMAX
  2 0 4 0 4 0 0 3 $PL-3 KPLOT,VIEW,ITEM,STEP,MODE,IFRNG,COLOR,ICOMP
  0.0 0 0.0 0.0 0.0 $PL-5 DSCALE,NROTS,LWSCALE,RNGMIN,RGMAX
  2 0 4 0 1 0 0 3 $PL-3 KPLOT,VIEW,ITEM,STEP,MODE,IFRNG,COLOR,ICOMP
  0.0 3 0.0 0.0 0.0 $PL-5 DSCALE,NROTS,LWSCALE,RNGMIN,RGMAX
  1 0.0 / 2 0.0 / 3 0.0
  2 0 4 0 1 0 0 3 $PL-3 KPLOT,VIEW,ITEM,STEP,MODE,IFRNG,COLOR,ICOMP
  0.0 3 0.0 0.0 0.0 $PL-5 DSCALE,NROTS,LWSCALE,RNGMIN,RGMAX
  1 -90.0 / 2 0.0 / 3 0.0
  2 0 4 0 3 0 0 3 $PL-3 KPLOT,VIEW,ITEM,STEP,MODE,IFRNG,COLOR,ICOMP
  0.0 3 0.0 0.0 0.0 $PL-5 DSCALE,NROTS,LWSCALE,RNGMIN,RGMAX
  1 0.0 / 2 0.0 / 3 0.0
  2 0 4 0 3 0 0 3 $PL-3 KPLOT,VIEW,ITEM,STEP,MODE,IFRNG,COLOR,ICOMP
  0.0 3 0.0 0.0 0.0 $PL-5 DSCALE,NROTS,LWSCALE,RNGMIN,RGMAX
  1 -90.0 / 2 0.0 / 3 0.0

```

Full Panel Sandwich Model Input Files

In this modeling approach, the sandwich panel is modeled using one or more sandwich elements through the thickness of the sandwich panel. If multiple sandwich elements are used through the thickness, the intermediate face sheets are “phantom face sheets” having zero thickness and are only used for modeling purposes through the core thickness. A piecewise linear approximation can thereby be represented. The STAGS sandwich element denoted by E840 exploits the E410 shell element for the face sheet response as well as for the core deformations. This finite element model has twice the number of elements over the surface of the panel compared to models using the 9-node E480 elements – the number of nodes on each plane is the same for the two element types.

The finite element model used herein has two sandwich elements through the core thickness (one of either side of the middle surface). This gives one "phantom face sheet" with zero thickness at the middle surface of the sandwich panel. Users also may select the number of the through-the-thickness integration points (one or two). Depending on the sandwich panel thickness and the structural response for the specified loading, spurious zero-energy mechanisms, stemming from the E840 dependence on the E410 shell element, may occur that can be suppressed by increasing the number of through-the-thickness integration points or increasing the through-the-thickness discretization (more sandwich elements). The reference surface is the middle of the sandwich panel.

sandwich2.inp (for S1 processor)

```

Compression-loaded rectangular sandwich panel $A-1
C
C Sandwich panel modeled using the E840 sandwich element
C with two elements through the core thickness (i.e., three
C planes of nodes)
C
C Ref. Brush & Almroth, "Buckling of Bars, Plates, and Shells,"
C McGraw-Hill, 1975, pp. 108-112.
C
C a=20 in., b=10 in., simple-supported on all edges
C
0 0 0 0 $ B-1
1 0 0 0 0 0 0 0 0 $ B-2
1 0 3 0 0 1 $ B-3
81 21 $ F-1 Planar mesh definition over "a" by "b" panel
1 $ I-1 Face-sheet data using historical STAGS approach
10.0E6 0.300 3.85E6 0.100 6.0E-7 10.00E6 1.9439E-5 $ I-2
$-----GCP-----
$ Homogeneous core
ORTHOELAST_MATERIAL 1 1 1 $ core material
100.0 100.0 100.0E2, $ E1, E2, E3
38.4 12.0E3 7.2E3, $ G12, G13, G23
0.30 0.01 0.01, $ P12, P13, P23
0. 0. 0. 0. 0. 0. 0. 0. 0. $ Filler spaces
ORTHOELAST_MATERIAL 2 1 1 $ isotropic face sheet material
10.0E6 10.0e6 10.0E6, $ E1, E2, E3
3.846E6 3.846e6 3.846e6, $ G12, G13, G23
0.30 0.30 0.30, $ P12, P13, P23
0. 0. 0. 0. 0. 0. 0. 0. 0. $ Filler spaces
C Core definitions - 2 layers across core
SOLID_FABRICATION 1 1 0 1 $ fabid, matid, iang, nipz: thin core
0.10 $ thickness of core element
SOLID_FABRICATION 2 1 0 1 $ fabid, matid, iang, nipz: thick core
2.75 $ thickness of core element
C Face sheet definitions
SHELL_FABRICATION 1 1 0 0 0 $i-21 Thin F/S
2 $i-21 Facesheet material
0.02 $i-21 h_fs=0.02 in.
0.0
SHELL_FABRICATION 2 1 0 0 0 $i-21 Thick F/S
2 $i-21 Facesheet material
0.11 $i-21 h_fs=0.11 in.
0.0
SHELL_FABRICATION 3 1 0 0 0 $i-21 Phantom F/S
2 $i-21 Facesheet material
0.0 $i-21 h_fs=0.0
0.0
END
$-----GCP-----
$----Shell Wall Data using historical STAGS approach-----
1 1 1 / 1 .020 0.0 $K-1/K-2 Thin face sheet

```

```

2 1 1 / 1 .110 0.0          $K-1/K-2 Thick face sheet
3 1 1 / 1 .000 0.0          $K-1/K-2 Phantom face sheet definition
$ Define the shell unit for the rectangular sandwich panel
2 0 0 0 2 5          $ M-1 Unit No. 1 - two layers of sandwich elements
0.0 20.0 0.00 10.00  $ M-2
-2 0 0.0 0.0 0 0 0  $ M-5 Bottom Face Sheet - GCP shell fab.
-2 0 0.0 0.0 0 0 0  $ M-5 First core element - GCP solid fab.
-2 0 0.0 0.0 0 0 0  $ M-5 Second core element - GCP solid fab.
-2 0 0.0 0.0 0 0 0  $ M-5 Top Face Sheet - GCP shell fab.
-3 0 0.0 0.0 0 0 0  $ M-5 Phantom Face Sheet - GCP shell fab.
840          $ N-1 Selement element type
3 3 3 3  $ P-1 Specify BC's on each edge using Q records
1          $ Q-1 Loading system
1 39          $ Q-2 Load system A; 39 records
+0.1 -1 1 1 0 0 0 0 0 0 1 $ Q-3 u=+u0 at x=0 in bottom face sheet
+0.1 -1 1 1 0 0 0 0 0 0 2 $ Q-3 u=+u0 at x=0 in phantom face sheet
+0.1 -1 1 1 0 0 0 0 0 0 3 $ Q-3 u=+u0 at x=0 in top face sheet
-0.1 -1 1 81 0 0 0 0 0 0 1 $ Q-3 u=-u0 at x=a in bottom face sheet
-0.1 -1 1 81 0 0 0 0 0 0 2 $ Q-3 u=-u0 at x=a in phantom face sheet
-0.1 -1 1 81 0 0 0 0 0 0 3 $ Q-3 u=-u0 at x=a in top face sheet
C w=rx=rz=0 on x=0 edge
0.0 -1 3 1 0 0 0 0 0 0 1 $ Q-3 w=0 at x=0 in bottom face sheet
0.0 -1 4 1 0 0 0 0 0 0 1 $ Q-3 rx=0 at x=0 in bottom face sheet
0.0 -1 6 1 0 0 0 0 0 0 1 $ Q-3 rz=0 at x=0 in bottom face sheet
0.0 -1 3 1 0 0 0 0 0 0 2 $ Q-3 w=0 at x=0 in phantom face sheet
0.0 -1 4 1 0 0 0 0 0 0 2 $ Q-3 rx=0 at x=0 in phantom face sheet
0.0 -1 6 1 0 0 0 0 0 0 2 $ Q-3 rz=0 at x=0 in phantom face sheet
0.0 -1 3 1 0 0 0 0 0 0 3 $ Q-3 w=0 at x=0 in top face sheet
0.0 -1 4 1 0 0 0 0 0 0 3 $ Q-3 rx=0 at x=0 in top face sheet
0.0 -1 6 1 0 0 0 0 0 0 3 $ Q-3 rz=0 at x=0 in top face sheet
C w=rx=rz=0 on x=a edge
0.0 -1 3 81 0 0 0 0 0 0 1 $ Q-3 w=0 at x=a in bottom face sheet
0.0 -1 4 81 0 0 0 0 0 0 1 $ Q-3 rx=0 at x=a in bottom face sheet
0.0 -1 6 81 0 0 0 0 0 0 1 $ Q-3 rz=0 at x=a in bottom face sheet
0.0 -1 3 81 0 0 0 0 0 0 2 $ Q-3 w=0 at x=a in phantom face sheet
0.0 -1 4 81 0 0 0 0 0 0 2 $ Q-3 rx=0 at x=a in phantom face sheet
0.0 -1 6 81 0 0 0 0 0 0 2 $ Q-3 rz=0 at x=a in phantom face sheet
0.0 -1 3 81 0 0 0 0 0 0 3 $ Q-3 w=0 at x=a in top face sheet
0.0 -1 4 81 0 0 0 0 0 0 3 $ Q-3 rx=0 at x=a in top face sheet
0.0 -1 6 81 0 0 0 0 0 0 3 $ Q-3 rz=0 at x=a in top face sheet
C w=ry=0 on y=0 edge
0.0 -1 3 0 1 0 0 0 0 0 0 1 $ Q-3 w=0 at y=0 in bottom face sheet
0.0 -1 5 0 1 0 0 0 0 0 0 1 $ Q-3 ry=0 at y=0 in bottom face sheet
0.0 -1 3 0 1 0 0 0 0 0 0 2 $ Q-3 w=0 at y=0 in phantom face sheet
0.0 -1 5 0 1 0 0 0 0 0 0 2 $ Q-3 ry=0 at y=0 in phantom face sheet
0.0 -1 3 0 1 0 0 0 0 0 0 3 $ Q-3 w=0 at y=0 in top face sheet
0.0 -1 5 0 1 0 0 0 0 0 0 3 $ Q-3 ry=0 at y=0 in top face sheet
C w=ry=0 on y=b edge
0.0 -1 3 0 21 0 0 0 0 0 0 1 $ Q-3 w=0 at y=b in bottom face sheet
0.0 -1 5 0 21 0 0 0 0 0 0 1 $ Q-3 ry=0 at y=b in bottom face sheet
0.0 -1 3 0 21 0 0 0 0 0 0 2 $ Q-3 w=0 at y=b in phantom face sheet
0.0 -1 5 0 21 0 0 0 0 0 0 2 $ Q-3 ry=0 at y=b in phantom face sheet
0.0 -1 3 0 21 0 0 0 0 0 0 3 $ Q-3 w=0 at y=b in top face sheet
0.0 -1 5 0 21 0 0 0 0 0 0 3 $ Q-3 ry=0 at y=b in top face sheet
C v=0 at center of nodal plane
0.0 -1 2 41 11 0 0 0 0 0 0 1 $ Q-3 v=0 at center in bottom face sheet
0.0 -1 2 41 11 0 0 0 0 0 0 2 $ Q-3 v=0 at center in phantom face sheet
0.0 -1 2 41 11 0 0 0 0 0 0 3 $ Q-3 v=0 at center in top face sheet
1 4*0 1  $ R-1 Print displacements and internal forces

```

sandwich2.bin (for S2 processor)

```
Sandwich panel buckling under compressive loading $ A-1
C *** analysis type definition ***
C indic ipost  ilist  icor  impthe  ioptim  iflu  newent $ b-1
  1      1      0      0      0      0      0      -1 $ b-1
C *** load multiplier record ***
C stld(1) step(1) facm(1) stld(2) step(2) facm(2) itemp $ c-1
  1.0    0.0    0.0    0.0    0.0    0.0    0      $ c-1
C
C *** eigenvalue control **** d-2
C nsec  delet  iprint  *** d-2
1000   .0001    0      $ d-2
C
C **** eigenvalue cluster definition **** d-3
C neig  shift  eiga  eigb  ***** d-3
  4     0.0                    $ d-3
```

sandwich2.pin (for STAPL processor)

```
Sandwich panel studies
  4  0  0  0  $PL-2  NPLOT,IPREP,IPRS,KDEV
  2  0  4  0  1  0  0  3  $PL-3  KPLOT,VIEW,ITEM,STEP,MODE,IFRNG,COLOR,ICOMP
  0.0  0  0.0  0.0  0.0  0.0  $PL-5  DSCALE,NROTS,LWSCALE,RNGMIN,RGMAX
  2  0  4  0  2  0  0  3  $PL-3  KPLOT,VIEW,ITEM,STEP,MODE,IFRNG,COLOR,ICOMP
  0.0  0  0.0  0.0  0.0  0.0  $PL-5  DSCALE,NROTS,LWSCALE,RNGMIN,RGMAX
  2  0  4  0  3  0  0  3  $PL-3  KPLOT,VIEW,ITEM,STEP,MODE,IFRNG,COLOR,ICOMP
  0.0  0  0.0  0.0  0.0  0.0  $PL-5  DSCALE,NROTS,LWSCALE,RNGMIN,RGMAX
  2  0  4  0  4  0  0  3  $PL-3  KPLOT,VIEW,ITEM,STEP,MODE,IFRNG,COLOR,ICOMP
  0.0  0  0.0  0.0  0.0  0.0  $PL-5  DSCALE,NROTS,LWSCALE,RNGMIN,RGMAX
```

Local Strip Sandwich Model Input Files

In this modeling approach, a local strip of the sandwich panel is modeled using many sandwich elements through the thickness of the sandwich panel. The intermediate face sheets are “phantom face sheets” having zero thickness and are only used for modeling purposes through the core thickness. A piecewise linear approximation results from layer to layer. The local strip is very narrow compared to the panel width, and its length is typically less than the panel length. Care must be taken in choosing the local strip length so that the lowest buckling load is captured. That is, the length of the local strip should be a multiple of the buckling mode shape halfwave length corresponding to the lowest buckling load. It may be necessary to examine more than one local strip length.

strip.inp (for S1 processor)

```
Local Strip Model of compression-loaded rectangular sandwich panel $A-1
C
C Local strip model with 25 layers through the thickness
C (strip length=2.5 in., strip width=0.1 in. based on
C full panel model which gave 8 halfwaves along length;
C so if more than 1 halfwave in local strip then local
C buckling may occur if buckling load below full panel
C buckling load).
C
C Ref. Brush & Almroth, "Buckling of Bars, Plates, and Shells,"
C McGraw-Hill, 1975, pp. 108-112.
C
C a=20 in., b=10 in., simple-supported on all edges
C
  0  0  0  0          $ B-1
  1 8*0 1          $ B-2
  1  0  3  0  0  1  $ B-3
```

```

21 2          $ F-1
1 1 1 1 2      1 0 1 1 2/ 26 5*0 3*0 1 0      $G-2c/G-2d
C
C face sheet material data using historical STAGS approach
C
1 $ I-1 Face-sheet data
10.0E6  0.300  3.85E6  0.100  6.0E-7  10.00E6  1.9439E-5  $ I-2
$-----GCP-----
$ Homogeneous core
ORTHOELAST_MATERIAL 1 1 1          $ core material
100.0  100.0  100.0E2,          $ E1, E2, E3
38.4  12.0E3  7.2E3,          $ G12, G13, G23
0.30  0.01  0.01,          $ P12, P13, P23
0. 0. 0. 0. 0. 0. 0. 0. 0. 0.  $ Filler spaces (unused)
SOLID_FABRICATION  1 1 0 1      $ fabid & matid for core material - thick case
.22000          $ element thickness (5.5 in./25 ele.=0.22 in.)
SOLID_FABRICATION  2 1 0 1      $ fabid & matid for core material - thin case
.00800          $ element thickness (0.2 in./25 ele.=0.008 in.)
END
$-----GCP-----
$----Shell Wall Data using historical STAGS approach -----
1 1 1 / 1  .110 0.0          $K-1/K-2 Face sheet thickness
2 1 1 / 1  .020 0.0          $K-1/K-2 Face sheet thickness
3 1 1 / 1  0.          $K-1/K-2 Phantom face sheet
C
C Local strip model (2.5 in. long by 0.1 inches wide)
C
2 0 0 0 25 28          $ M-1 Unit No. 1
0.0  1.25  0.00  .100  $ M-2
+1 0 0.0  0.0  0 0 0 0  $ M-5 Bottom Face Sheet
-1 0 0.0  0.0  0 0 0 0  $ M-5 Core element 1
-1 0 0.0  0.0  0 0 0 0  $ M-5 Core element 2
-1 0 0.0  0.0  0 0 0 0  $ M-5 Core element 3
-1 0 0.0  0.0  0 0 0 0  $ M-5 Core element 4
-1 0 0.0  0.0  0 0 0 0  $ M-5 Core element 5
-1 0 0.0  0.0  0 0 0 0  $ M-5 Core element 6
-1 0 0.0  0.0  0 0 0 0  $ M-5 Core element 7
-1 0 0.0  0.0  0 0 0 0  $ M-5 Core element 8
-1 0 0.0  0.0  0 0 0 0  $ M-5 Core element 9
-1 0 0.0  0.0  0 0 0 0  $ M-5 Core element 10
-1 0 0.0  0.0  0 0 0 0  $ M-5 Core element 11
-1 0 0.0  0.0  0 0 0 0  $ M-5 Core element 12
-1 0 0.0  0.0  0 0 0 0  $ M-5 Core element 13
-1 0 0.0  0.0  0 0 0 0  $ M-5 Core element 14
-1 0 0.0  0.0  0 0 0 0  $ M-5 Core element 15
-1 0 0.0  0.0  0 0 0 0  $ M-5 Core element 16
-1 0 0.0  0.0  0 0 0 0  $ M-5 Core element 17
-1 0 0.0  0.0  0 0 0 0  $ M-5 Core element 18
-1 0 0.0  0.0  0 0 0 0  $ M-5 Core element 19
-1 0 0.0  0.0  0 0 0 0  $ M-5 Core element 20
-1 0 0.0  0.0  0 0 0 0  $ M-5 Core element 21
-1 0 0.0  0.0  0 0 0 0  $ M-5 Core element 22
-1 0 0.0  0.0  0 0 0 0  $ M-5 Core element 23
-1 0 0.0  0.0  0 0 0 0  $ M-5 Core element 24
-1 0 0.0  0.0  0 0 0 0  $ M-5 Core element 25
+1 0 0.0  0.0  0 0 0 0  $ M-5 Top Face Sheet
+3 0 0.0  0.0  0 0 0 0  $ M-5 Phantom face sheets
840 4*0 0          $ N-1
0 4 4 0          $ P-1
111 100          $ P-2 Edge at x=0
111 010          $ P-2 Edge at y=0
1          $ Q-1 Loading system
1 27          $ Q-2 Load system A; 27 records

```

```

0.1 -1 1 1 0 0 0 0 0 0 1 $ Q-3 u=u0 along edge at x=0 on nodal plane 1
0.1 -1 1 1 0 0 0 0 0 0 2 $ Q-3 u=u0 along edge at x=0 on nodal plane 2
0.1 -1 1 1 0 0 0 0 0 0 3 $ Q-3 u=u0 along edge at x=0 on nodal plane 3
0.1 -1 1 1 0 0 0 0 0 0 4 $ Q-3 u=u0 along edge at x=0 on nodal plane 4
0.1 -1 1 1 0 0 0 0 0 0 5 $ Q-3 u=u0 along edge at x=0 on nodal plane 5
0.1 -1 1 1 0 0 0 0 0 0 6 $ Q-3 u=u0 along edge at x=0 on nodal plane 6
0.1 -1 1 1 0 0 0 0 0 0 7 $ Q-3 u=u0 along edge at x=0 on nodal plane 7
0.1 -1 1 1 0 0 0 0 0 0 8 $ Q-3 u=u0 along edge at x=0 on nodal plane 8
0.1 -1 1 1 0 0 0 0 0 0 9 $ Q-3 u=u0 along edge at x=0 on nodal plane 9
0.1 -1 1 1 0 0 0 0 0 0 10 $ Q-3 u=u0 along edge at x=0 on nodal plane 10
0.1 -1 1 1 0 0 0 0 0 0 11 $ Q-3 u=u0 along edge at x=0 on nodal plane 11
0.1 -1 1 1 0 0 0 0 0 0 12 $ Q-3 u=u0 along edge at x=0 on nodal plane 12
0.1 -1 1 1 0 0 0 0 0 0 13 $ Q-3 u=u0 along edge at x=0 on nodal plane 13
0.1 -1 1 1 0 0 0 0 0 0 14 $ Q-3 u=u0 along edge at x=0 on nodal plane 14
0.1 -1 1 1 0 0 0 0 0 0 15 $ Q-3 u=u0 along edge at x=0 on nodal plane 15
0.1 -1 1 1 0 0 0 0 0 0 16 $ Q-3 u=u0 along edge at x=0 on nodal plane 16
0.1 -1 1 1 0 0 0 0 0 0 17 $ Q-3 u=u0 along edge at x=0 on nodal plane 17
0.1 -1 1 1 0 0 0 0 0 0 18 $ Q-3 u=u0 along edge at x=0 on nodal plane 18
0.1 -1 1 1 0 0 0 0 0 0 19 $ Q-3 u=u0 along edge at x=0 on nodal plane 19
0.1 -1 1 1 0 0 0 0 0 0 20 $ Q-3 u=u0 along edge at x=0 on nodal plane 20
0.1 -1 1 1 0 0 0 0 0 0 21 $ Q-3 u=u0 along edge at x=0 on nodal plane 21
0.1 -1 1 1 0 0 0 0 0 0 22 $ Q-3 u=u0 along edge at x=0 on nodal plane 22
0.1 -1 1 1 0 0 0 0 0 0 23 $ Q-3 u=u0 along edge at x=0 on nodal plane 23
0.1 -1 1 1 0 0 0 0 0 0 24 $ Q-3 u=u0 along edge at x=0 on nodal plane 24
0.1 -1 1 1 0 0 0 0 0 0 25 $ Q-3 u=u0 along edge at x=0 on nodal plane 25
0.1 -1 1 1 0 0 0 0 0 0 26 $ Q-3 u=u0 along edge at x=0 on nodal plane 26
0.0 -1 3 1 1 0 0 0 0 0 1 $ Q-3 w=0 at point to remove rigid body motion
1 4*0 1 $ R-1

```

strip.bin (for S2 processor)

```

Sandwich panel buckling under compressive loading - local strip $ A-1
C *** analysis type definition ***
C indic ipost  ilist  icor  impthe  ioptim iflu newent $ b-1
  1      1      1      0      0      0      0      -1 $ b-1
C *** load multiplier record ***
C stld(1) step(1) facm(1) stld(2) step(2) facm(2) itemp $ c-1
  1.0    0.0    0.0    0.0    0.0    0.0    0 $ c-1
C
C *** eigenvalue control **** d-2
C nsec  delet  iprint  *** d-2
  100   .0001    1      $ d-2
C
C **** eigenvalue cluster definition **** d-3
C neig  shift  eiga  eigb  ***** d-3
  4     0.0      $ d-3

```

strip.pin (for STAPL processor)

```

Local Strip model of sandwich panel (25 layers) $A-1
  2  0  0  0  $PL-2  NPLOT,IPREP,IPRS,KDEV
  2  0  4  0  1  0  0  3  $PL-3  KPLOT,VIEW,ITEM,STEP,MODE,IFRNG,COLOR,ICOMP
0.0  3  0.0  0.0  0.0  0.0  $PL-5  DSCALE,NROTS,LWSCALE,RNGMIN,RGMAX
  1 -90.0 /2  0.0 / 3  0.0
  2  0  4  0  1  0  0  3  $PL-3  KPLOT,VIEW,ITEM,STEP,MODE,IFRNG,COLOR,ICOMP
0.0  3  0.0  0.0  0.0  0.0  $PL-5  DSCALE,NROTS,LWSCALE,RNGMIN,RGMAX
  1 -64.0 /2  -4.0 / 3  -135.0

```


Problem References

Brush, D. O. and Almroth, B. O., *Buckling of Bars, Plates, and Shells*, McGraw-Hill Book Company, New York, 1975.

Bushnell, D., "Optimum Design via PANDA2 of Composite Sandwich Panels with Honeycomb or Foam Cores," AIAA Paper No. 97-1142, April 1997.

Riks, E. and Rankin, C. C., "Sandwich Modeling with an Application to the Residual Strength Analysis of a Damaged Composite Compression Panel," AIAA Paper No. 2001-1323, April 2001.

Riks, E. and Rankin, C. C., "Sandwich Modeling with an Application to the Residual Strength Analysis of a Damaged Compression Panel," *International Journal of Non-Linear Mechanics*, Vol. 37, Nos. 4-5, June-July 2002, pp. 897-908.

Rose, C. A., Moore, D. F., Knight, N. F., Jr., and Rankin, C. C., "Finite Element Modeling of the Buckling Response of Sandwich Panels," AIAA Paper No. 2002-1517, April 2002.

Crack Growth Simulation for Middle-Crack Tension Panel

Background

An isotropic linear elastic panel with a center through-crack loaded in tension (M(T) panel) is a common analysis problem in fracture mechanics applications. The geometry is a standard configuration used in material testing and validation of computational methods (*e.g.*, Riks *et al.*, 1992; Dawicke *et al.*, 1994, Viz *et al.*, 1995; Dawicke, 1997; Seshadri and Newman, 1998; Seshadri *et al.*, 1998; Gullerud *et al.*, 1999; Rankin and Riks, 2000, 2001). The total panel length is $2L$, the total panel width is $2w$, and the initial total crack length is $2a$. The initial crack is located at $x=L$ and is centered about the line $y=0$. The geometry and material properties of the problem are defined in Figure 57 using U.S. customary units and SI units and represent a test configuration of Dawicke (1997).

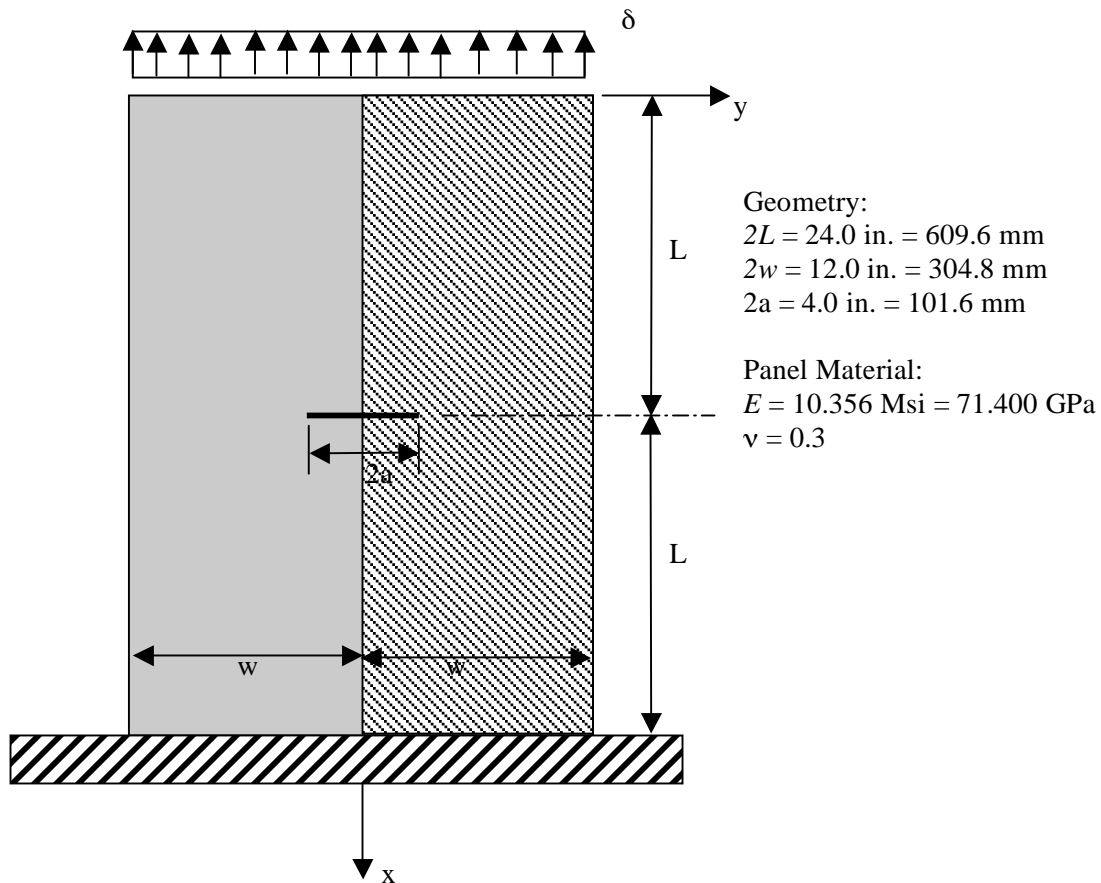


Figure 57. Center-crack panel problem: geometry and material properties.

Modeling and Analysis Process

The finite element model represents half the width and the full length of the panel even though quarter symmetry could have been used. While the rectangular panel can easily be modeled with a single shell unit, multiple shell units are used in order to refine the finite element mesh near the crack at panel midlength. The overall finite element model is shown in Figure 58 with inset figures showing the model near the crack (shell unit 5) for the shell-element and solid-element models. The inset figures represent the linear solution under a small load level so that the crack location can be viewed.

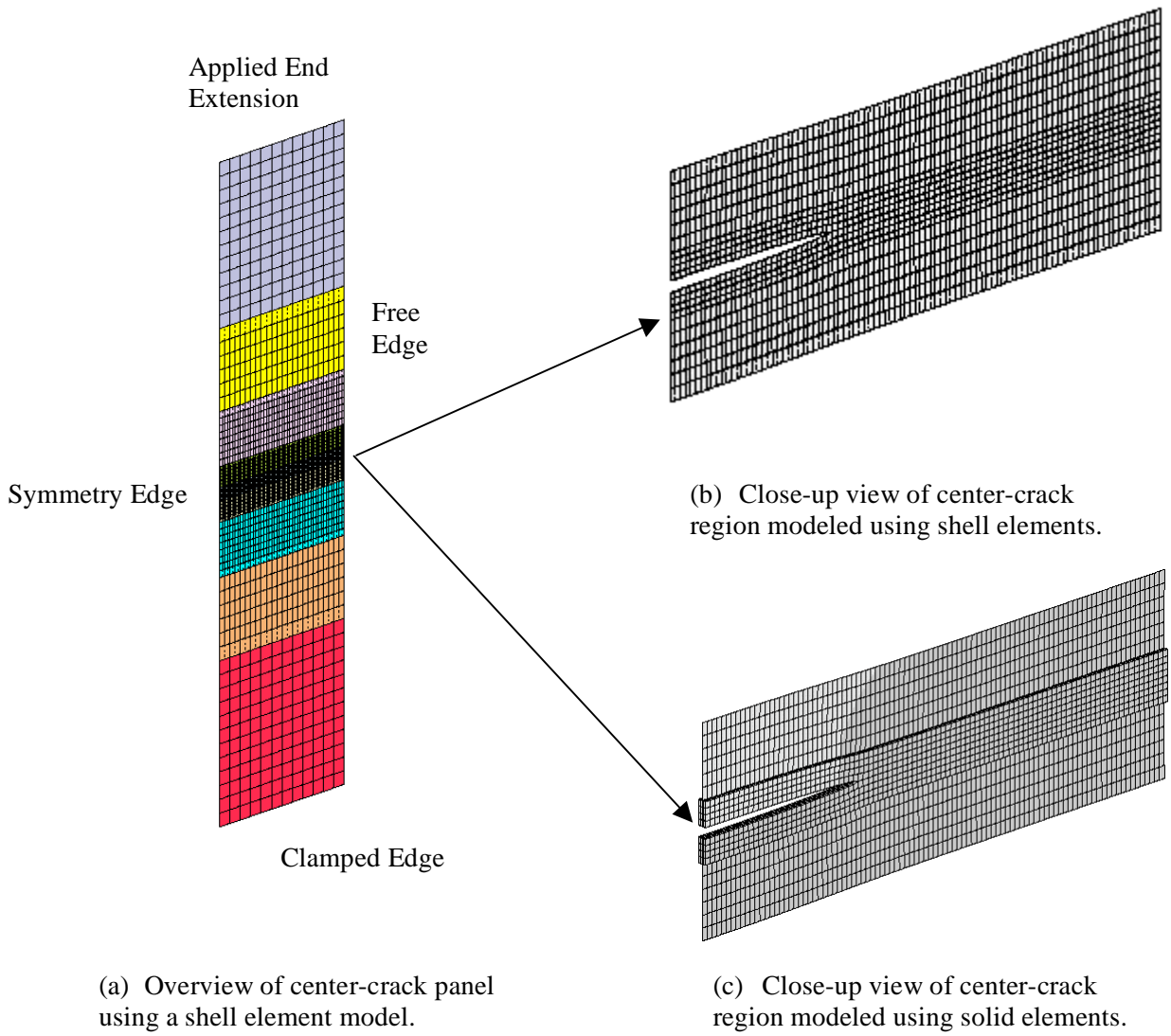


Figure 58. Overall finite element model and close-up views near the crack.

Table 15. Stress-strain data for 2024-T3 (LT) aluminum alloy.

Strain, ϵ (in./in.)	Stress, σ (MPa)	Stress, σ (psi)
0.0	0	0
0.00483	345	50,000
0.15	390	56,600
0.4	430	62,300
0.1	470	68,200
0.16	491	71,200

Material properties and shell wall construction are defined using the GCP approach.. Material modeling using the current GCP approach requires data on the I-5a and I-6a records to define the material properties and records I-5a, I-21a, I-21b, I-21c, I-21d, and I-21e to define the shell fabrication. The elastic-plastic stress-strain curve for 2024-T3 (LT) aluminum alloy (0.09-inches or 2.3-mm thick) is defined for the White-Besseling plasticity model in STAGS using the values given in Table 15. Note that STAGS does not require (or allow) the origin of the stress-strain curve to be defined – it is implicitly assumed.

From this data, the elastic modulus E of the material is 10.35197 Msi (71.400 GPa) and Poisson’s ratio ν is taken as 0.3. STAGS compares the computed value of the elastic modulus from the first nonzero pair of stress-strain values with the input modulus value on the I-2 record (or appropriate GCP record). The ratio of this difference and the elastic modulus read as input must be less than 10^{-6} or STAGS will stop. The yield stress is 50,000 psi or 345 MPa, and the ultimate stress is 71,200 psi or 491 MPa. The stress-strain curve is treated as a piecewise linear curve using table-lookup in STAGS with linear interpolation for values between data points. In the finite element model, shell units 4, 5, and 6 (*i.e.*, the center two inches of the model) use the elasto-plastic material definition while the other shell units use only the elastic properties.

Boundary condition on the displacements are specified using the P-1 and P-2 records. An applied end displacement is specified across edge 1 on shell unit 1. Because of the coordinate system used, extensional end displacements have a negative value. The opposite end of the panel is clamped, the right edge of the finite element model is free, and the left edge has symmetric conditions imposed. Even though the degrees of freedom associated with interior nodes are unrestrained, a nonlinear analysis will not automatically lead to out-of-plane deflections (local buckling) near the crack unless an initial geometric surface imperfection is used to “trigger” the nonlinear effects. The initial geometric imperfection can be generated by first performing a buckling calculation and then using the mode shape corresponding to the lowest eigenvalue scaled by a small number (*e.g.*, 1% of panel thickness) as the initial imperfection. Such a buckling-mode-based imperfection is defined using the B-6 record.

Mesh refinement using shell transition elements (E510 and E710) is performed automatically across shell unit boundaries. In the present case, there are four shell units on either side of a center shell unit since the entire panel length is modeled as shown in Figure 58. The element size in the width direction is cut in half in each shell unit as the center shell unit is approached. The element width is 0.5 inches in shell unit 1, 0.25 inches in shell unit 2, 0.125 inches in shell unit 3, and 0.0625 inches in shell unit 4. The element width in the center shell unit is held at 0.0625 inches. This level of mesh refinement gives 96 elements across the half width of the panel.

Transition from shell elements to solid elements is defined using several STAGS input records. In this discussion (and in the example case provided), the shell-to-solid transition occurs along shell unit boundaries. In the `crack1sm.inp` file, shell units 4 and 6 are modeled using E410 shell elements, while shell unit 5 is modeled using four layers of E881 solid elements through the thickness of the panel. The number of grid points along the shell-to-solid transition boundary is the same for the affected shell units (*i.e.*, the same number of rows in shell units 4, 5, and 6 in this case). The first step is to define a set of G-3/G-4 records along the shell/solid transition boundary for averaging the translational degrees of freedom between the shell element node and the solid element nodes. The second step is to define “softlinks” (element E121) between the shell element node and the through-the-thickness nodes of the solid elements at that planar nodal location. This step is performed by defining an element unit with nodes (S-1 records) and elements (T-1 records) defined along the shell-to-solid transition boundary. These nodes and elements are defined using the existing shell unit values and their generation exploits the in-line looping capability of the STAGS S1 input processor. No shell unit connection record (G-1 record) is defined for these boundaries. The connections are done explicitly with the constraints just described and the element unit definition for the E121 softlink elements. This shell-to-solid modeling approach is illustrated in the S1 input file named `crack1sm.inp` – for *manual* input of the shell-to-solid connections.

This overall shell-to-solid modeling process is rather cumbersome and error prone; hence, an automated procedure is available within STAGS to connect shell and solid elements along shell-unit boundary lines. The analyst simply defines the shell units as before using shell elements and solid elements in the appropriate shell units. Then define a shell unit connection record (G-1 record) for the shell-to-solid juncture using a negative value for MUNIT. STAGS then examines the two shell units and automatically generates the constraints and softlinks along the shell-to-solid element boundary line. . This shell-to-solid modeling approach is illustrated in the S1 input file named `crack1sa.inp` – for *automatic* input of the shell-to-solid connections.

Crack modeling is achieved using the G-5, G-6 and G-7 records that generate constraints along a predetermined path with coincident nodes generated along that path. A single crack definition is defined with “open” segments as well as “closed” segments. Crack tips occur at the intersection of open and closed segments. That is, a 2-inch-long crack would require 32 0.0625-inch-long elements with node 33 defining the crack tip (assuming nodes 1 through 32 are used with the 32 elements along the initial crack length). Additional nodes are then used to define a “closed” crack. Crack growth is then defined along a predetermined path built directly into the finite element model.

Modeling a single crack with a single tip using three-dimensional solid elements is slightly more complex than for shell element models. For a through-crack in a solid element model, the open and closed crack concept is applied for each plane of nodes through the thickness. For the bounding surface planes of the solid model, a single element crack record (G-7 record) is required. For interior planes, two records are needed to account for adjacent elements through the thickness.

Single cracks with multiple tips can be generated to simulate multi-site damage (MSD) cases. In such cases, multiple nodal-crack records (G-6 records) are needed to define several open and closed crack segments (single crack with multiple crack tips). These records are mesh dependent in their definition but are straightforward to generate.

Crack growth is simulated using the nodal release procedure in combination with the load relaxation procedure to re-establish equilibrium in the structure once a crack growth criterion is met and nodal release occurs. STAGS currently uses the crack-tip opening angle or CTOA criterion for crack growth. The analyst provides the critical value consistent for the material, the panel thickness, the kinematics assumption near the crack (plane stress or plane strain), and the finite element mesh size near the crack

tip. The critical CTOA value strongly affects the computed solution and typically involves repeated solution of standard test configurations for a particular material and a particular thickness before an *analysis* critical value for a given finite element model can be defined.

Numerical Results and Discussion

Dawicke (1997) reported M(T) fracture test results for 0.090-inch-thick 2024-T3 aluminum panels in the LT orientation. The test configuration for a 12-inch-wide M(T) panel with an initial 4.0-inch-long center through-crack is analyzed in this study. Fracture test results are report by Dawicke (1997) for specimens with and without guide plates to prevent local buckling near the crack. Test results are also reported for multiple-site damage cases.

The present modeling strategy for these panels assumes a symmetrical response in the width direction. The finite element discretization process uses the mesh transition feature with the E410 shell elements and doubles the number of the elements (or halves the element size) in the width direction as the panel midlength is approached. Initially the element size in the width direction of shell unit 1 is one inch. Then several shell units are used to change the mesh refinement. Mesh doubling occurs in the first four shell units so that the element size in the width direction of shell unit 5 is reduced to 0.0625 inches. This element size is somewhat larger than the 1-mm-rule (0.040-inch-rule) recommended for finite element models near the crack front – based on the constant-strain triangular element. Then mesh halving is used in the last four shell units. The critical value of CTOA is taken as 4.6 degrees. This value is strongly dependent on the material, geometry, and finite element discretization near the crack front. There is no initial geometric surface imperfection used with the finite element model and thus the simulation is for the M(T) panel with guide plates to present local buckling near the crack.

After each converged load step, a computation is made to evaluate the current value of the CTOA. If this computed value exceeds the critical value given on the G-5 input record, then the constraints on the coincident nodes at the crack tip are released (*i.e.*, nodal release). At this point, the model is no longer in equilibrium unless forces necessary to keep the “released” nodes together (*i.e.*, to “close” the crack) are applied to the released nodes. This force imbalance is treated as a right-hand-side vector with its own load factor P_X while holding the applied load factors (P_A and P_B) fixed. This new load factor P_X is then decremented from a value of one to zero and nonlinear solutions are obtained for each P_X value until the load imbalance is relaxed and the structure with the new crack extension is again in equilibrium. This procedure is called *load relaxation* and facilitates the crack growth simulation in an automated manner using the CTOA criterion.

The first analysis case is an M(T) panel 12-inches wide, 24-inches long, 0.09-inches thick, and with an initial 4-inch-long center through-crack. This panel was analyzed first using 4-node plane-stress shell E410 elements throughout the finite element model. Then the panel is analyzed again using three-dimensional 8-node solid E881 elements in shell unit 5 which treats a 0.25-inch region above and below the crack as a three-dimensional region.

Results from the two-dimensional plane stress model are summarized in Figures 59 through 61. Crack extension Δa as a function of the far-field stress is shown in Figure 59. Test data from Tables 10 (with buckling guide plates) and 13 (without buckling guide plates) of Dawicke (1997) are compared with the STAGS predictions. The far-field stress from the STAGS model is computed by dividing the equilibrium force summation across the loaded edge of the panel by the panel cross-sectional area (product of panel width and thickness). Crack extension is in terms of discrete incremental changes associated with the nodal-release approach and is based on the element size at the crack front. Test and simulation results are compared in Figure 59. The load relaxation steps are shown in this figure to illustrate the process; however, only the peak far-field stress values for a given value of crack extension are typically plotted.

Good correlation between test and analysis is indicated for the case when local buckling near the crack is prevented. Contour plots of the longitudinal displacement component and the longitudinal stress component are shown in Figures 60 and 61, respectively, for three solution steps. A compression-dominated region around the crack is evident from Figure 61 and indicates that a local instability may occur.

Results from the transition shell/solid model are summarized in Figures 62 through 64. Crack extension as a function of the far-field stress is shown in Figure 62 where test data from Table 10 of Dawicke (1997) are compared with the STAGS predictions (plane stress model and local solid model). The load relaxation process is again illustrated in this figure. Good correlation between test and analysis is indicated. Contour plots of the longitudinal displacement component and the longitudinal stress component are shown in Figures 63 and 64, respectively, for three solution steps. These plots illustrate that the response transitions smoothly across the shell/solid transition boundary. The results from the local solid model are below those obtained from the plane stress model due to using the same critical CTOA value.

A second analysis case is considered that includes multiple-site damage (MSD) in the form of two 0.30-inch-long cracks on either side of the center 4-inch-long crack with approximately 0.70-inch spacing between crack tips. The crack lengths and spacing between the crack tips in the test are not exactly symmetric across the panel centerline. In addition, the finite element mesh size used in the single crack case is also used for the MSD case and therefore certain limitations are imposed. In the STAGS model, the spacing between the crack tips (*i.e.*, “closed” crack regions) is 0.6875 inches and the length of the smaller cracks (*i.e.*, “open” crack regions) is 0.3125 inches – clearly some differences between test and simulation are anticipated. STAGS does have the capability to specialize the mesh layout (using the N-1 and N-9 records) to match the test configuration; however, since only a symmetric model was being considered this was not done. Within the STAGS modeling approach, this case is treated as a single crack with multiple tips rather than multiple cracks.

Results from the two-dimensional plane stress model are summarized in Figures 65 through 68. Crack extension as a function of the far-field stress is shown in Figure 65 where test data from Table 19 of Dawicke (1997) for the 5-crack MSD case (configuration E shown in Figure 3 of that report) are compared with the STAGS predictions. Good correlation between test and analysis is indicated. Contour plots of the longitudinal displacement component and the longitudinal stress component are shown in Figures 66 and 67, respectively, for three solution steps. These results illustrate the crack “linking” behavior where the center crack grows and links with the smaller cracks as load is applied. The size of the compression-dominated region appears to expand quickly as the link-up process occurs.

Contour plots of the plastic strain component in the longitudinal direction are shown in Figure 68 for the center two-inch region of the panel. As the load increases the crack extends and the local plastic strain field also expands around each of the cracks in the MSD panel. In these simulations, it was assumed that the elasto-plastic behavior was confined to this region. This modeling assumption appears to be true.

- 12-in. wide, $2a/W=1/3$, without guides, Dawicke, 1997 - NASA TM-112869, Table 13
- 12-in. wide, $2a/W=1/3$, with guides, Dawicke, 1997 - NASA TM-112869, Table 10
- △ STAGS shell element model

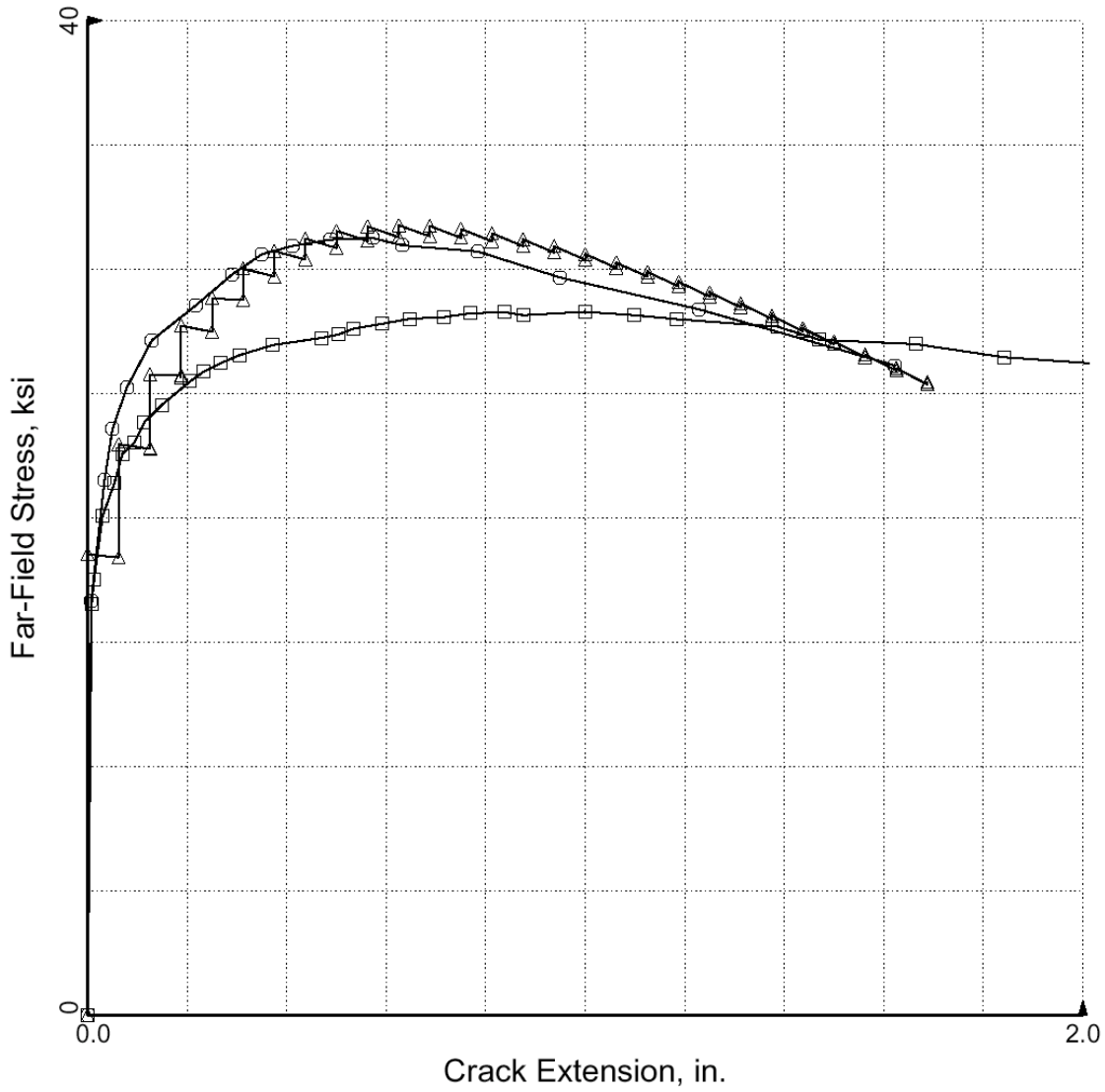
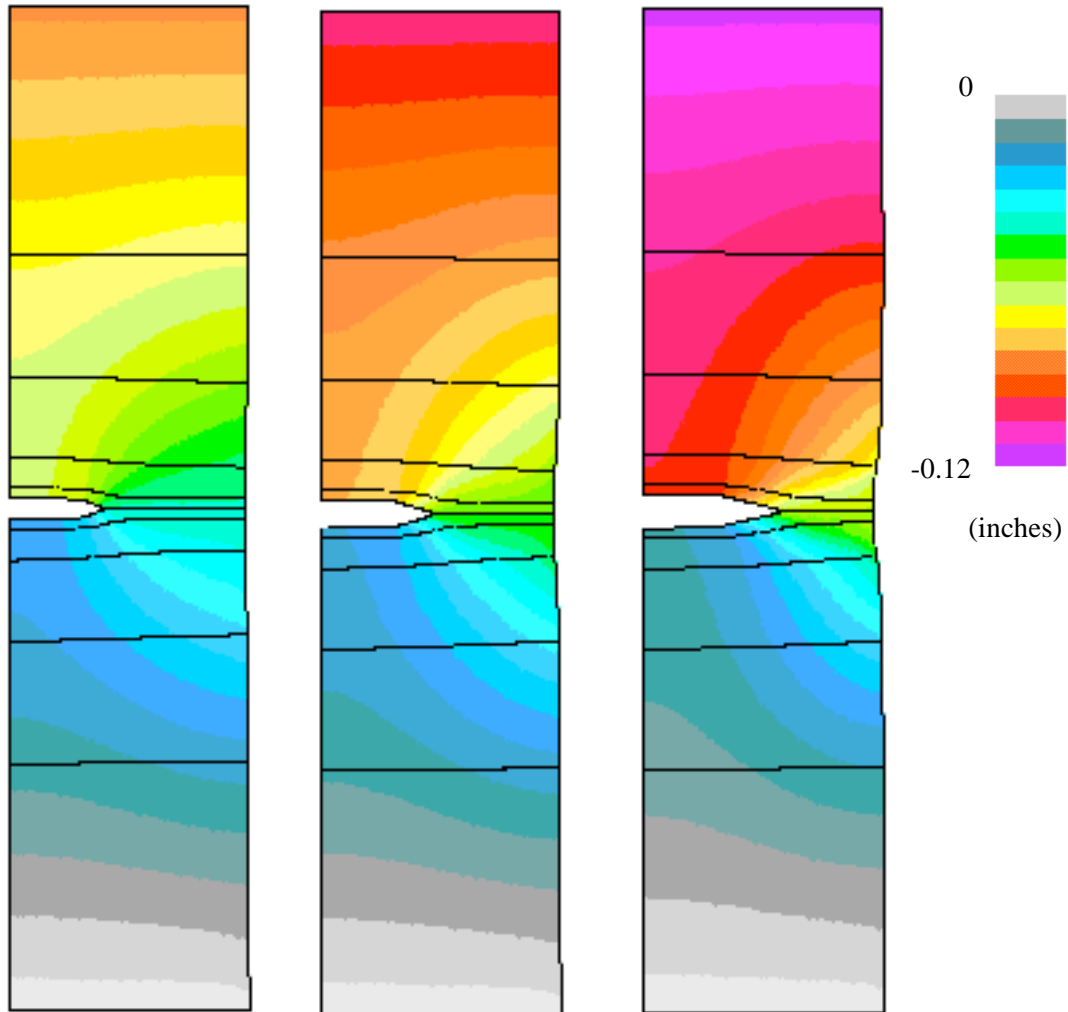
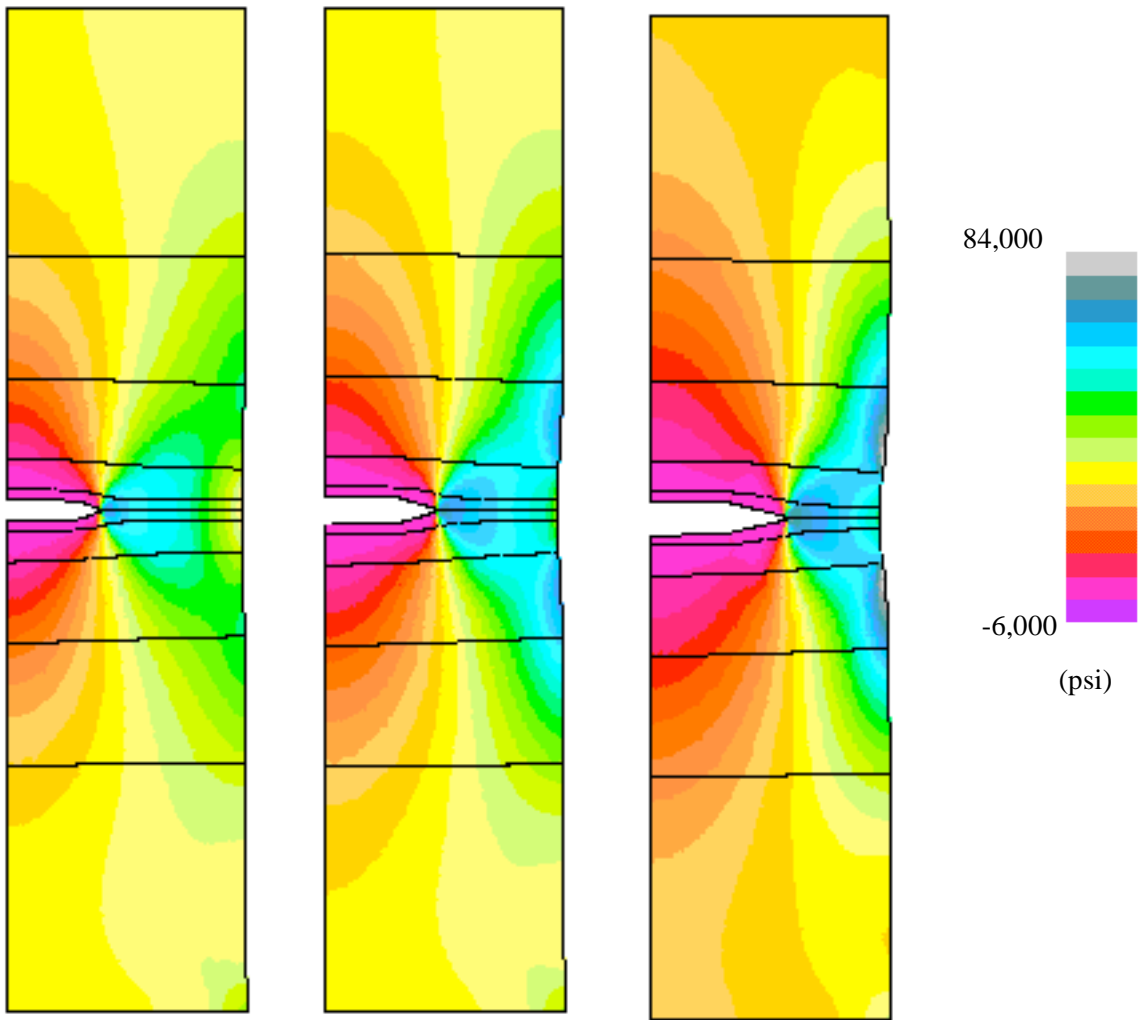


Figure 59. Crack extension as a function of far-field applied stress for NASA M(T) 0.09-inch-thick, 12-inch-wide panel with a 4-inch-long center through-crack using plane stress modeling



(a) Step 40, $\Delta a=0.5$ in. (b) Step 90, $\Delta a=1.0$ in. (c) Step 166, $\Delta a=1.6875$ in.

Figure 60. Contour plots of the longitudinal displacement component from the plane stress model for NASA M(T) 0.09-inch-thick, 12-inch-wide panel with a 4-inch-long center through-crack.



(a) Step 40, $\Delta a = 0.5$ in. (b) Step 90, $\Delta a = 1.0$ in. (c) Step 166, $\Delta a = 1.6875$ in.

Figure 61. Contour plots of the longitudinal stress component from the plane stress model for NASA M(T) 0.09-inch-thick, 12-inch-wide panel with a 4-inch-long center through-crack.

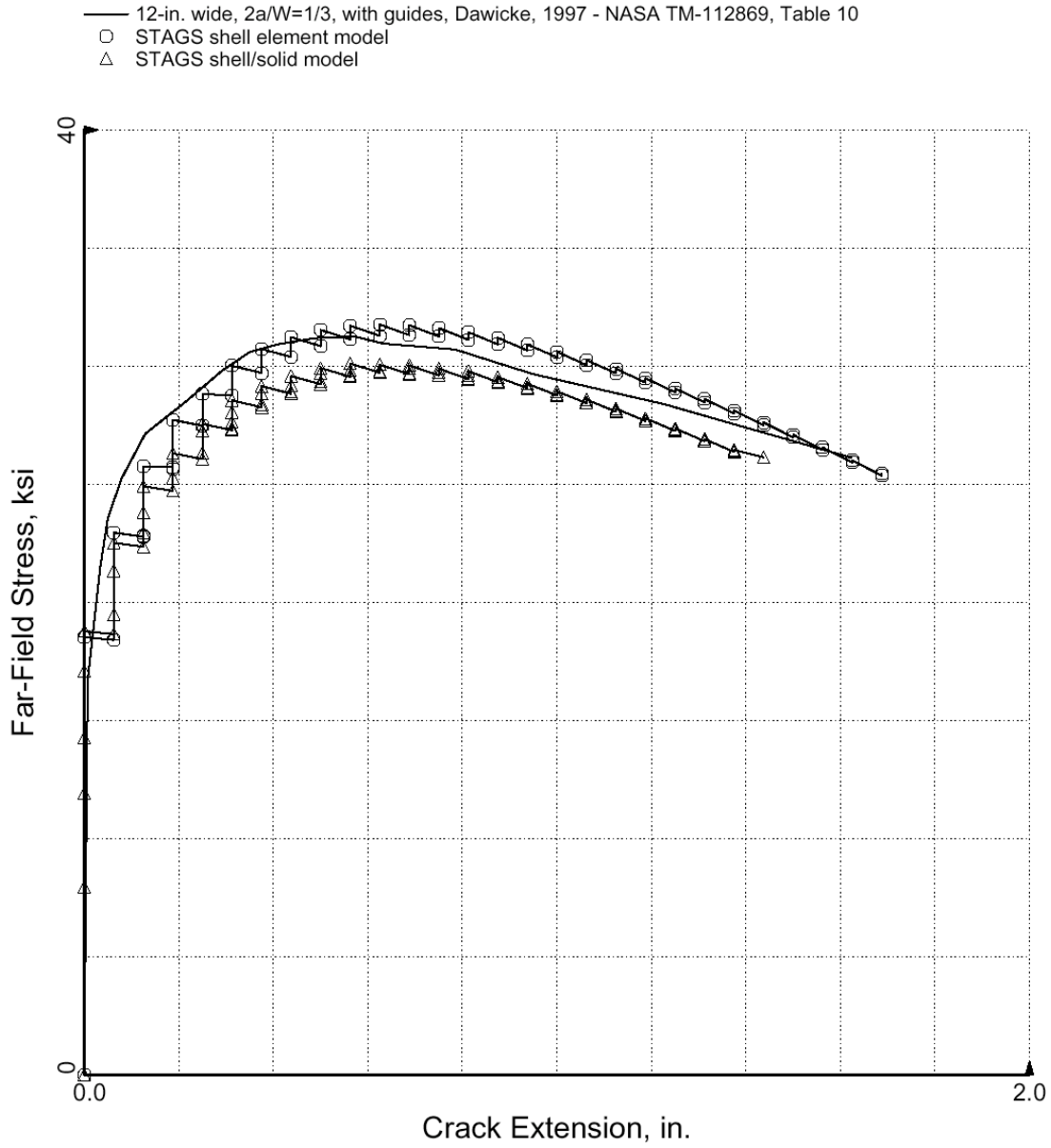
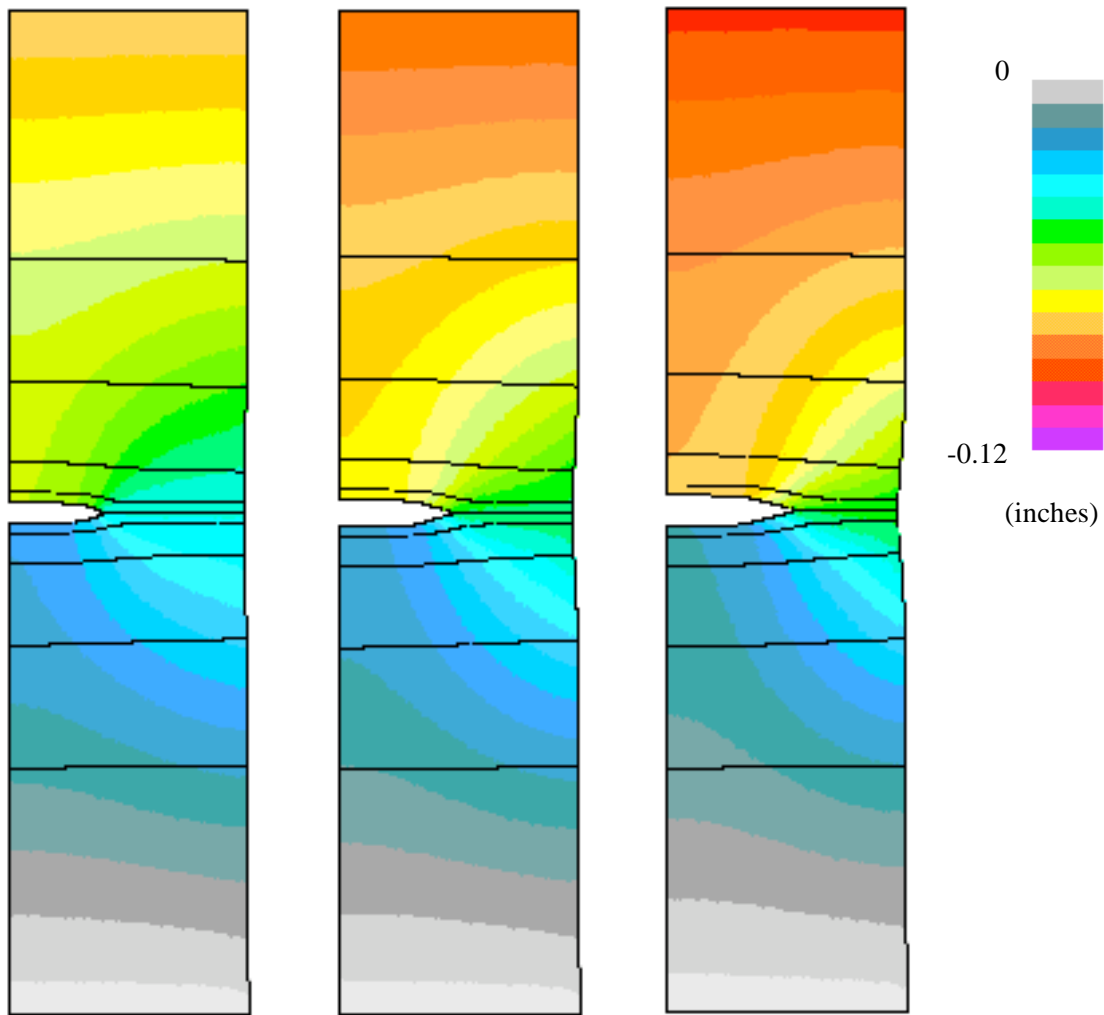
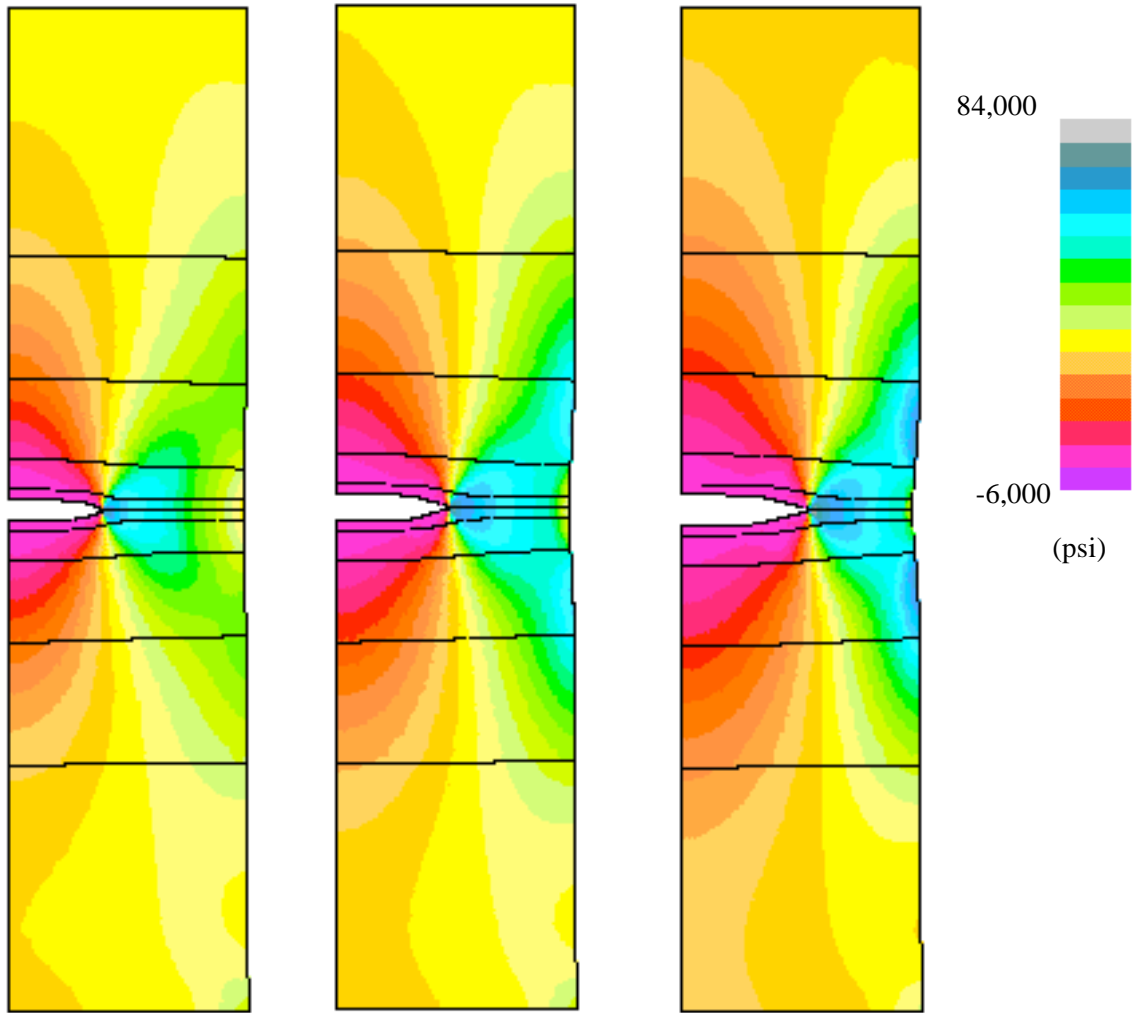


Figure 62. Crack extension as a function of far-field applied stress for NASA M(T) 0.09-inch-thick, 12-inch-wide panel with a 4-inch-long center through-crack using shell-solid transition modeling



(a) Step 52, $\Delta a=0.5$ in. (b) Step 111, $\Delta a=1.0$ in. (c) Step 151, $\Delta a=1.4375$ in.

Figure 63. Contour plots of the longitudinal displacement component from the shell-solid transition model for NASA M(T) 0.09-inch-thick, 12-inch-wide panel with a 4-inch-long center through-crack.



(a) Step 52, $\Delta a=0.5$ in. (b) Step 111, $\Delta a=1.0$ in. (c) Step 151, $\Delta a=1.4375$ in.

Figure 64. Contour plots of the longitudinal stress component from the shell-solid transition model for NASA M(T) 0.09-inch-thick, 12-inch-wide panel with a 4-inch-long center through-crack.

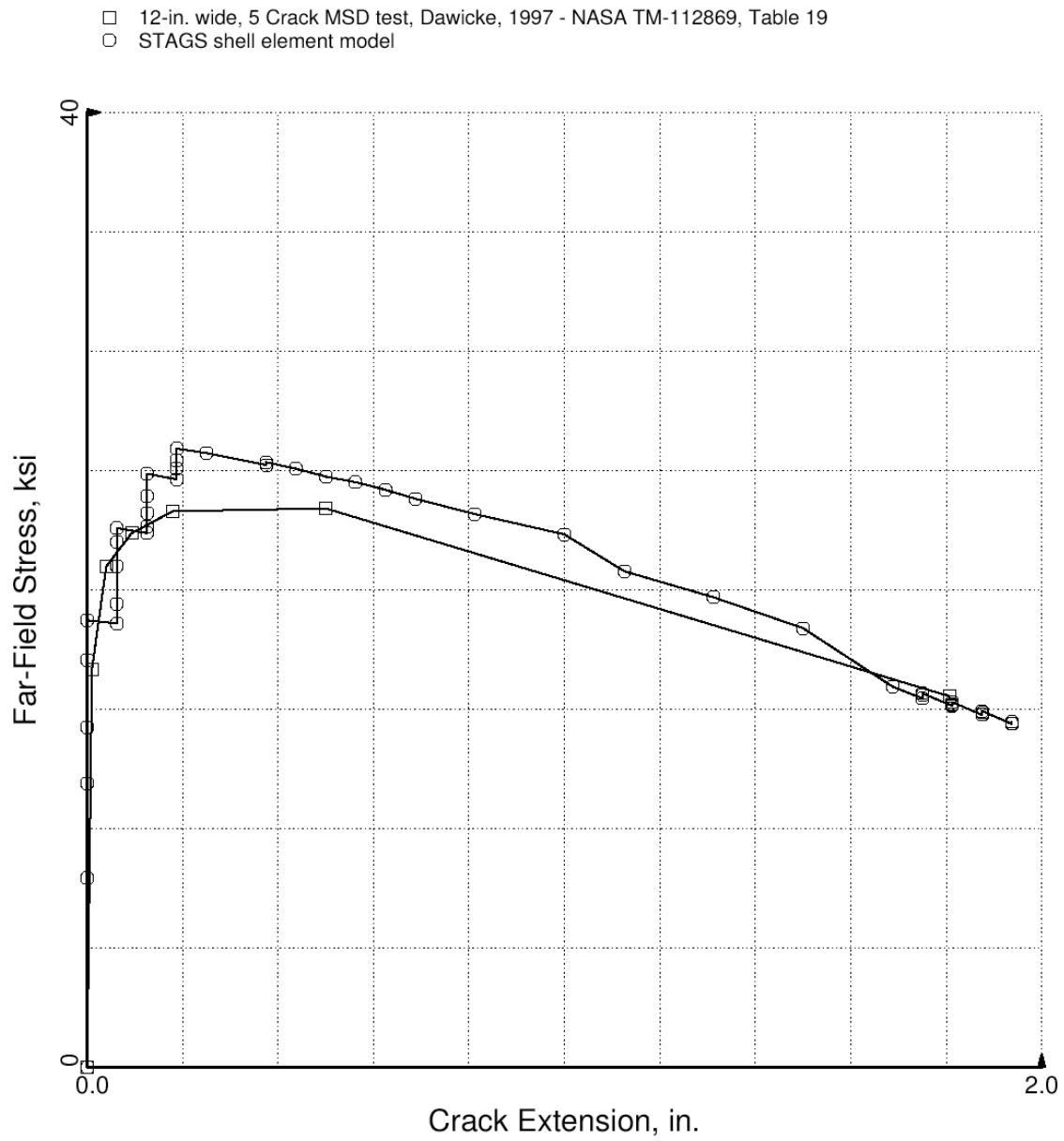
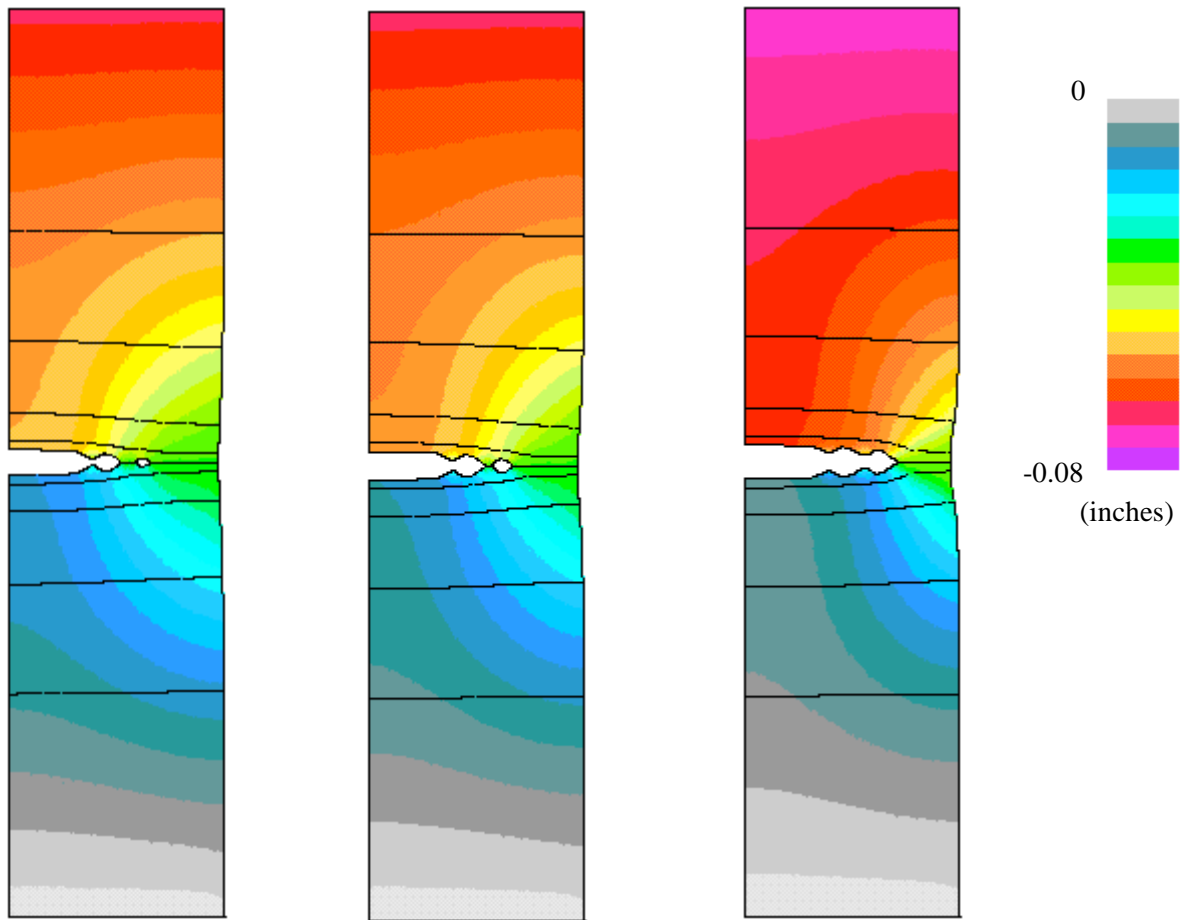
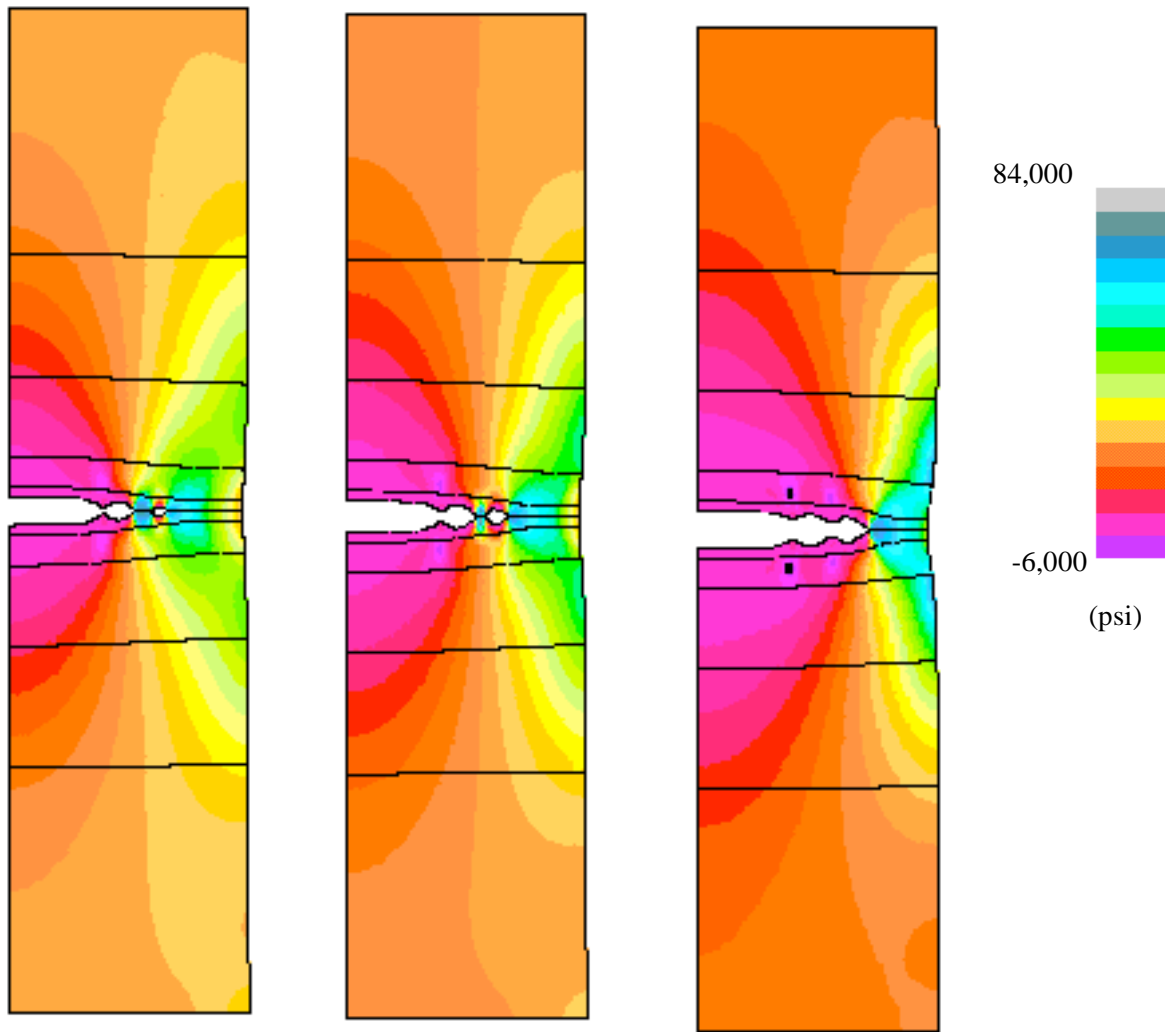


Figure 65. Crack extension as a function of far-field applied stress for NASA M(T) 0.09-inch-thick, 12-inch-wide panel with multiple site damage using plane stress modeling



(a) Step 61, $\Delta a=1.125$ in. (b) Step 71, $\Delta a=1.5$ in. (c) Step 100, $\Delta a=1.9375$ in.

Figure 66. Contour plots of the longitudinal displacement component from the plane stress model for NASA M(T) 0.09-inch-thick, 12-inch-wide panel with multiple site damage.



(a) Step 61, $\Delta a=1.125$ in. (b) Step 71, $\Delta a=1.5$ in. (c) Step 100, $\Delta a=1.9375$ in.

Figure 67. Contour plots of the longitudinal stress component from the plane stress model for NASA M(T) 0.09-inch-thick, 12-inch-wide panel with multiple site damage.

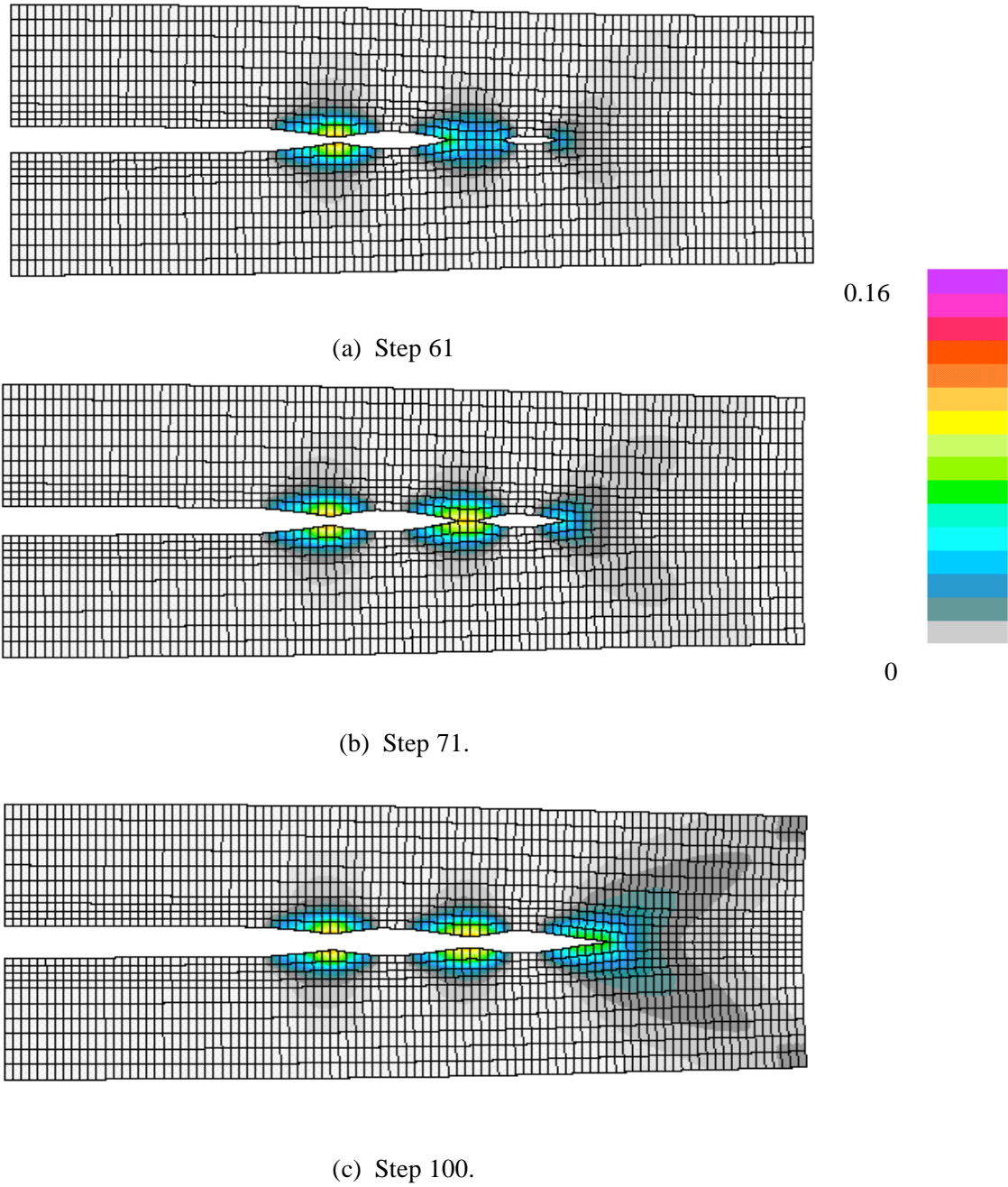


Figure 68. Contour plots of longitudinal plastic strain component from the plane stress model for NASA M(T) 0.09-inch-thick, 12-inch-wide panel with multiple site damage – close-up view of shell units 4, 5, and 6 (center two inches of the panel).

STAGS Input Files

These STAGS input files are located under the following subdirectory:

```
$STAGSHOME/Advanced-Testcases/Type-B-crack
```

where separate subdirectories are provided for three cases: center-crack shell-element model; center-crack shell/solid-element model; and multiple-site-damage shell-element model. These directories are:

```
shell
solid/manual
solid/auto
msd
```

Three different STAGS models are presented here. The first two models are for the middle-crack-tension (or M(T)) panel. Both models have the same planar finite element discretization and both use nine shell units over the full panel length and half the width (half symmetry model). However, one model uses shell elements (E410) only for all shell units, while the other model uses four solid elements (E881) through the shell thickness for the shell unit containing the crack (shell unit 5) and shell elements (E410) elsewhere.

The third STAGS model is a variation on the first model except that there are two additional smaller cracks along the panel midlength. It can be viewed as a single crack with multiple tips. This model exhibits multiple-site damage or MSD. This simulation is similar to the 5-crack MSD fracture test reported by Dawicke (1997). The finite element model approximates the actual test configuration because of the uniform element size along the panel width and the symmetry conditions. The MSD configuration features a center 4-inch-long crack followed by a 0.6875-inch-long space then a 0.3125-inch-long crack then another 0.6875-inch-long space and another 0.3125-inch-long crack. The remainder of the panel width (2-inches) has no additional initial cracks but forms the crack extension path. The finite element model of the MSD case assumes a symmetric distribution of the damage across the panel width even though the test configuration is not precisely symmetric.

Typical Center-Crack Panel Input Files – Shell Element Model

crack1.inp (for S1 processor)

```
Middle crack tension panel - M(T) $a-1
C
C 24 in. long, 12 in. wide, 0.09 in. thick
C with 4" long through center crack
C (2L=24; 2W=12; 2a=4; 2a/2W=1/3)
C
C Modeled region is 24 in. long, 6 in. wide
C with a 2 inch long crack (full length, half
C width).
C
0 0 0 0 0 0 0 $B-1 ANALYSIS TYPE
9 0 0 8 1 0 0 0 1 $B-2 MODEL SUMMARY
2 0 2 0 0 1 $B-3 DATA TABLE SUMMARY -> use gcp
C
C Use mesh refinement
C Unit 1 is 6" x 6"; use dx=0.5" and dy=0.5"
C Unit 2 is 3" x 6"; use dx=0.5" and dy=0.25"
C Unit 3 is 2" x 6"; use dx=0.25" and dy=0.125"
C Unit 4 is .75" x 6"; use dx=0.125" and dy=0.0625"
C Unit 5 is .50" x 6"; use dx=0.0625" and dy=0.0625"
```

```

C Unit 6 is .75" x 6"; use dx=0.125" and dy=0.0625"
C Unit 7 is 2" x 6"; use dx=0.25" and dy=0.125"
C Unit 8 is 3" x 6"; use dx=0.5" and dy=0.25"
C Unit 9 is 6" x 6"; use dx=dy=1.0"
C
13 13 7 25 9 49 ,
7 97 9 97 7 97 ,
9 49 7 25 13 13 $F-1 GRID SUMMARY
C
C Shell unit connection records
C - don't connect solids to shells with g-1 records
C
1 3 2 1 $G-1
2 3 3 1 $G-1
3 3 4 1 $G-1
4 3 5 1 $G-1
5 3 6 1 $G-1
6 3 7 1 $g-1
7 3 8 1 $g-1
8 3 9 1 $g-1
C
C Impose u=u at row 1 col. 1 across top of panel
C
1 1 1 1 1 1 0 1 $G-2 PARTIAL COMPATIBILITY U=CONSTANT AT EDGE
C
C Crack definition (element size is 0.0625")
C Note: nodes 1 to 32 open which gives an initial half crack length
C equal to 32 elements or 2" long; node 33 is at crack tip
C
1 2 1 1 4.6 0.0625 $G-5 Crack Inserted Node Set
1 5 5 1 5 32 $G-6 "open" crack (2" long)
0 5 5 33 5 97 $G-6 "closed" crack (4" long)
0 5 4 1 4 96 $G-7
C
C Input historical STAGS material tables
C
1 0 0 $I-1 Elastic only
10.351967E+6 0.3 0.0 0.1 $I-2 E, nu, skip, rho_weight
2 5 0 $i-1 Elasto-plastic
10.351967E+6 0.3 0.0 0.1 $I-2 E, nu, skip, rho_weight
0.00483 50000.0, $i-3 yield stress
0.015 56600.0, $i-3
0.04 62400.0, $I-3
0.1 68200.0, $I-3
0.16 71100.0 $I-3 ultimate stress
C -----GCP-----
C 2024-T3 (LT) Aluminum alloy - ISOTROPIC MATERIAL
C
ISOELASTIC_MATERIAL 1 1 1 $I-5A GCP COMMAND RECORD
10.351967E+6, $I-7A E
0.30 , $I-7A NU
2.59E-5 , $I-7A MASS DENSITY
0.0 , $I-7A CTE (alpha)
0.0 , $I-7A CHE (beta)
0.0 0.0 $I-7A REF. TEMP AND REF. MOISTURE CONTENT

PLASTIC_WB_MATERIAL 2 1 1 2 0 $ WHITE-BESSELING PLASTICITY MODEL
10.351967E+6 0.3 2.59E-5 0.0 5 $I-9a E, nu, rho, cte, npoints
0.00483 50000.0, $i-9b yield stress
0.015 56600.0, $i-9b
0.04 62400.0, $I-9b
0.1 68200.0, $I-9b
0.16 71100.0 $I-9b ultimate stress

```

```

C
SHELL_FABRICATION 1 1 0 0 0 $I-5A Elastic only
1                $I-21A Aluminum MATID
0.090           $I-21C LAYER THICKNESSES
0.0             $I-21D LAYER ORIENTATION
SHELL_FABRICATION 2 1 1 0 0 $I-5A Elasto-plastic
2                $I-21A Aluminum MATID
5                $I-21B Integration points through thickness
0.090           $I-21C LAYER THICKNESSES
0.0             $I-21D LAYER ORIENTATION
SOLID_FABRICATION 1 2 0 1 0 $I-5A Elasto-plastic
0.0225          $I-21C Solid Element THICKNESSES
END $I-5A END GCP INPUT
C -----
C
C define historical STAGS shell wall data
C
1 1 1 0 $K-1 elastic regions
1 0.09 0.0 0 $k-2 single layer
2 1 1 5 $K-1 elastic regions
2 0.09 0.0 0 $k-2 single layer
C
C Unit 1 - top part of panel
C
2 0 $M-1 SHELL SURFACE DEFINITION - RECTANGULAR PLATE
0.0 6.0 0.0 6.0 $M-2 24-IN BY 12-IN. PLATE (half width model)
+1 0 $M-5 SHELL WALL SELECTION -> USE GCP
410 0 0 $N-1 ELEMENT SELECTION, UNIFORM MESH
0 3 6 4 $P-1 BOUNDARY CONDITIONS GIVEN (0=FIXED; 1=FREE)
110 000 $P-2 X=0 EDGE
1 0 0 $Q-1 LOADING (base load with Area=1.08 sq. in. gives
1 1 0 $Q-2 LOAD SET far field stress of 10 ksi)
-0.02 -1 1 1 1 0 $Q-3 applied displ. at point plus constraints
C-10800.0 1 1 1 1 0 $Q-3 applied load at point plus constraints
0 0 0 0 0 0 1 0 $R-1 OUTPUT FLAGS
1 0 $ output displacements across top of panel
C
C Unit 2 - segment 2
C
2 0 $M-1 SHELL SURFACE DEFINITION - RECTANGULAR PLATE
6.0 9.0 0.0 6.0 $M-2 24-IN BY 12-IN. PLATE (half width model)
+1 0 $M-5 SHELL WALL SELECTION -> USE GCP
410 0 0 $N-1 ELEMENT SELECTION, UNIFORM MESH
6 3 6 4 $P-1 BOUNDARY CONDITIONS GIVEN (0=FIXED; 1=FREE)
0 0 0 $Q-1 NO LOADING
0 0 $R-1 OUTPUT FLAGS
C
C Unit 3 - segment 3
C
2 0 $M-1 SHELL SURFACE DEFINITION - RECTANGULAR PLATE
9.0 11.0 0.0 6.0 $M-2 24-IN BY 12-IN. PLATE (half width model)
+1 0 $M-5 SHELL WALL SELECTION -> USE GCP
410 0 0 $N-1 ELEMENT SELECTION, UNIFORM MESH
6 3 6 4 $P-1 BOUNDARY CONDITIONS GIVEN (0=FIXED; 1=FREE)
0 0 0 $Q-1 NO LOADING
0 0 $R-1 OUTPUT FLAGS
C
C Unit 4 - segment 4
C
2 0 0 0 0 0 $M-1 SHELL SURFACE DEFINITION - RECTANGULAR PLATE
11.0 11.75 0.0 6.0 $M-2 24-IN BY 12-IN. PLATE (half width model)
+2 0 0.0 0.0 0 1 $M-5 SHELL WALL SELECTION -> USE GCP
410 0 0 $N-1 ELEMENT SELECTION, UNIFORM MESH

```

```

6 3 6 4 $P-1 BOUNDARY CONDITIONS GIVEN (0=FIXED; 1=FREE)
0 0 0 $Q-1 NO LOADING
0 0 0 0 0 0 0 0 $R-1 OUTPUT FLAGS
C
C Unit 5 - center section with center crack - can be elasto-plastic
C
2 0 0 0 0 0 $M-1 SHELL SURFACE DEFINITION - RECTANGULAR PLATE
11.75 12.25 0.0 6.0 $M-2 24-IN BY 12-IN. PLATE (half width model)
+2 0 0.0 0.0 0 1 $M-5 Solid Fabrication SELECTION -> USE GCP
410 0 0 $N-1 ELEMENT SELECTION, UNIFORM MESH
6 3 6 4 $P-1 BOUNDARY CONDITIONS GIVEN (0=FIXED; 1=FREE)
0 0 0 $Q-1 NO LOADING
0 0 0 0 0 0 0 0 $R-1 OUTPUT FLAGS
C
C Unit 6 - section 6 - can be elasto-plastic
C
2 0 0 0 0 0 $M-1 SHELL SURFACE DEFINITION - RECTANGULAR PLATE
12.25 13.0 0.0 6.0 $M-2 24-IN BY 12-IN. PLATE (half width model)
+2 0 0.0 0.0 0 1 $M-5 SHELL WALL SELECTION -> USE GCP
410 0 0 $N-1 ELEMENT SELECTION, UNIFORM MESH
6 3 6 4 $P-1 BOUNDARY CONDITIONS GIVEN (0=FIXED; 1=FREE)
0 0 0 $Q-1 NO LOADING
0 0 0 0 0 0 0 0 $R-1 OUTPUT FLAGS
C
C Unit 7 - segment 7
C
2 0 $M-1 SHELL SURFACE DEFINITION - RECTANGULAR PLATE
13.0 15.0 0.0 6.0 $M-2 24-IN BY 12-IN. PLATE (half width model)
+1 0 $M-5 SHELL WALL SELECTION -> USE GCP
410 0 0 $N-1 ELEMENT SELECTION, UNIFORM MESH
6 3 6 4 $P-1 BOUNDARY CONDITIONS GIVEN (0=FIXED; 1=FREE)
0 0 0 $Q-1 NO LOADING
0 0 $R-1 OUTPUT FLAGS
C
C Unit 8
C
2 0 $M-1 SHELL SURFACE DEFINITION - RECTANGULAR PLATE
15.0 18.0 0.0 6.0 $M-2 24-IN BY 12-IN. PLATE (half width model)
+1 0 $M-5 SHELL WALL SELECTION -> USE GCP
410 0 0 $N-1 ELEMENT SELECTION, UNIFORM MESH
6 3 6 4 $P-1 BOUNDARY CONDITIONS GIVEN (0=FIXED; 1=FREE)
0 0 0 $Q-1 NO LOADING
0 0 $R-1 OUTPUT FLAGS
C
C Unit 9 Bottom section
C
2 0 $M-1 SHELL SURFACE DEFINITION - RECTANGULAR PLATE
18.0 24.0 0.0 6.0 $M-2 24-IN BY 12-IN. PLATE (half width model)
+1 0 $M-5 SHELL WALL SELECTION -> USE GCP
410 0 0 $N-1 ELEMENT SELECTION, UNIFORM MESH
6 3 2 4 $P-1 BOUNDARY CONDITIONS GIVEN (0=FIXED; 1=FREE)
0 0 0 $Q-1 NO LOADING
0 0 0 0 $R-1 OUTPUT FLAGS

```

crack1.bin (for S2 processor)

```

Middle crack tension panel X_ck $a-1
C
C nonlinear elasto-plastic crack growth analysis
C
3 1 0 0 0 0 0 -1 $b-1 analysis type and options

```

```

1.0 0.50 6.0          $c-1
0 6000 10 -20 0 1.0e-4 $d-1
0 0 0          $set-1
C
C linear elastic stress analysis
C
0 1 0 0 0 0 0 -1      $b-1 analysis type and options
1.0 1.00 1.0          $c-1 Apply just the base load

```

crack1.pin (for STAPL processor)

```

Panel with center crack
4 0 1 0 $PL-2 NPLOT,IPREP,IPRS,KDEV
C contour plot of u-displ component
2 0 1 20 0 0 1 1 $PL-3 KPLOT,VIEW,ITEM,STEP,MODE,IFRNG,COLOR,ICOMP
0.0 3 -1. -.12 0.0 $PL-5 DSCALE,NROTS,LWSCALE,RNGMIN,RGMAX
1 0.0 / 2 0.0 / 3 -90.0 $PL-6 rotations
2 0 1 40 0 0 1 1 $PL-3 KPLOT,VIEW,ITEM,STEP,MODE,IFRNG,COLOR,ICOMP
0.0 3 -1. -.12 0.0 $PL-5 DSCALE,NROTS,LWSCALE,RNGMIN,RGMAX
1 0.0 / 2 0.0 / 3 -90.0 $PL-6 rotations
2 0 1 90 0 0 1 1 $PL-3 KPLOT,VIEW,ITEM,STEP,MODE,IFRNG,COLOR,ICOMP
0.0 3 -1. -.12 0.0 $PL-5 DSCALE,NROTS,LWSCALE,RNGMIN,RGMAX
1 0.0 / 2 0.0 / 3 -90.0 $PL-6 rotations
2 0 1 166 0 0 1 1 $PL-3 KPLOT,VIEW,ITEM,STEP,MODE,IFRNG,COLOR,ICOMP
0.0 3 -1. -.12 0.0 $PL-5 DSCALE,NROTS,LWSCALE,RNGMIN,RGMAX
1 0.0 / 2 0.0 / 3 -90.0 $PL-6 rotations
C contour plot of longitudinal stress component
2 0 7 20 0 0 1 1 $PL-3 KPLOT,VIEW,ITEM,STEP,MODE,IFRNG,COLOR,ICOMP
0.0 3 -1. -6000. 84000. $PL-5 DSCALE,NROTS,LWSCALE,RNGMIN,RGMAX
1 0.0 / 2 0.0 / 3 -90.0 $PL-6 rotations
2 0 7 40 0 0 1 1 $PL-3 KPLOT,VIEW,ITEM,STEP,MODE,IFRNG,COLOR,ICOMP
0.0 3 -1. -6000. 84000. $PL-5 DSCALE,NROTS,LWSCALE,RNGMIN,RGMAX
1 0.0 / 2 0.0 / 3 -90.0 $PL-6 rotations
2 0 7 90 0 0 1 1 $PL-3 KPLOT,VIEW,ITEM,STEP,MODE,IFRNG,COLOR,ICOMP
0.0 3 -1. -6000. 84000. $PL-5 DSCALE,NROTS,LWSCALE,RNGMIN,RGMAX
1 0.0 / 2 0.0 / 3 -90.0 $PL-6 rotations
2 0 7 166 0 0 1 1 $PL-3 KPLOT,VIEW,ITEM,STEP,MODE,IFRNG,COLOR,ICOMP
0.0 3 -1. -6000. 84000. $PL-5 DSCALE,NROTS,LWSCALE,RNGMIN,RGMAX
1 0.0 / 2 0.0 / 3 -90.0 $PL-6 rotations
C plot model
0 0 0 0 0 0 0 0 $PL-3 KPLOT,VIEW,ITEM,STEP,MODE,IFRNG,COLOR,ICOMP
0.0 3 -1.0 0.0 0.0 $PL-5 DSCALE,NROTS,LWSCALE,RNGMIN,RGMAX
1 20.0 / 2 45.0 / 3 -90.0 $PL-6 rotations
C plot first solution close to crack so you can see it!
1 3 1 1 0 0 0 1 $PL-3 KPLOT,VIEW,ITEM,STEP,MODE,IFRNG,COLOR,ICOMP
4 5 6          $PL-4 plot unit = 5 only
0.0 3 0. -0.1 0.0 $PL-5 DSCALE,NROTS,LWSCALE,RNGMIN,RGMAX
1 20.0 / 2 45.0 / 3 -90.0 $PL-6 rotations

```

Typical Center-Crack Panel Input Files – Manual Shell/Solid Element Model

crack1sm.inp (for S1 processor)

```

Middle crack tension panel - M(T) $a-1
C
C 24 in. long, 12 in. wide, 0.09 in. thick
C with 4" long through center crack
C (2L=24; 2W=12; 2a=4; 2a/2W=1/3)
C
C Modeled region is 24 in. long, 6 in. wide
C with a 2 inch long crack (full length, half

```

```

C width). 3D model near crack (.25 inches on
C either side).
C
0 0 0 0 0 0 0          $B-1 ANALYSIS TYPE
9 1 0 6 1 -6 0 0 5     $B-2 MODEL SUMMARY
2 0 2 0 0 1           $B-3 DATA TABLE SUMMARY -> use gcp
C
C Use mesh refinement
C Unit 1 is 6" x 6"; use dx=0.5" and dy=0.5"
C Unit 2 is 3" x 6"; use dx=0.5" and dy=0.25"
C Unit 3 is 2" x 6"; use dx=0.25" and dy=0.125"
C Unit 4 is .75" x 6"; use dx=0.125" and dy=0.0625"
C Unit 5 is .50" x 6"; use dx=0.0625" and dy=0.0625"
C Unit 6 is .75" x 6"; use dx=0.125" and dy=0.0625"
C Unit 7 is 2" x 6"; use dx=0.25" and dy=0.125"
C Unit 8 is 3" x 6"; use dx=0.5" and dy=0.25"
C Unit 9 is 6" x 6"; use dx=dy=1.0"
C
13 13 7 25 9 49 ,
7 97 9 97 7 97 ,
9 49 7 25 13 13 $F-1 GRID SUMMARY
C
C Shell unit connection records
C - don't connect solids to shells with g-1 records
C
1 3 2 1 $G-1
2 3 3 1 $G-1
3 3 4 1 $G-1
6 3 7 1 $g-1
7 3 8 1 $g-1
8 3 9 1 $g-1
C
C Impose u=u at row 1 col. 1 across top of panel
C
1 1 1 1 1 1 0 1 $G-2 PARTIAL COMPATIBILITY U=CONSTANT AT EDGE
C
C Impose Lagrtanian constraints to average displacements at
C shell-solid interface
C
6 97 0 0 1 0          $G-3
4 7 1 1 -5.e4         $G-4
5 1 1 1 +1.e4 1       $G-4
5 1 1 1 +1.e4 2       $G-4
5 1 1 1 +1.e4 3       $G-4
5 1 1 1 +1.e4 4       $G-4
5 1 1 1 +1.e4 5       $G-4
C
6 97 0 0 1 0          $G-3
4 7 1 2 -5.e4         $G-4
5 1 1 2 +1.e4 1       $G-4
5 1 1 2 +1.e4 2       $G-4
5 1 1 2 +1.e4 3       $G-4
5 1 1 2 +1.e4 4       $G-4
5 1 1 2 +1.e4 5       $G-4
C
6 97 0 0 1 0          $G-3
4 7 1 3 -5.e4         $G-4
5 1 1 3 +1.e4 1       $G-4
5 1 1 3 +1.e4 2       $G-4
5 1 1 3 +1.e4 3       $G-4
5 1 1 3 +1.e4 4       $G-4
5 1 1 3 +1.e4 5       $G-4
C

```



```

6 97 0 0 1 0          $G-3
6 1 1 1 -5.e4         $G-4
5 9 1 1 +1.e4 1      $G-4
5 9 1 1 +1.e4 2      $G-4
5 9 1 1 +1.e4 3      $G-4
5 9 1 1 +1.e4 4      $G-4
5 9 1 1 +1.e4 5      $G-4
C
6 97 0 0 1 0          $G-3
6 1 1 2 -5.e4         $G-4
5 9 1 2 +1.e4 1      $G-4
5 9 1 2 +1.e4 2      $G-4
5 9 1 2 +1.e4 3      $G-4
5 9 1 2 +1.e4 4      $G-4
5 9 1 2 +1.e4 5      $G-4
C
6 97 0 0 1 0          $G-3
6 1 1 3 -5.e4         $G-4
5 9 1 3 +1.e4 1      $G-4
5 9 1 3 +1.e4 2      $G-4
5 9 1 3 +1.e4 3      $G-4
5 9 1 3 +1.e4 4      $G-4
5 9 1 3 +1.e4 5      $G-4
C
C Crack definition (element size is 0.0625")
C Note: nodes 1 to 32 open which gives an initial crack length
C       equal to 32 elements or 2" long; node 33 is at crack tip
C
1 2 1 1 4.6 0.0      $G-5 Crack Inserted Node Set
1 5 5 1 1 5 32 1 $G-6 "open" crack (2" long)
0 5 5 33 1 5 97 1 $G-6 "closed" crack (4" long)
0 5 4 1 1 4 96 1 $G-7
C
2 2 2 1 4.6 0.0      $G-5 Crack Inserted Node Set
1 5 5 1 2 5 32 2 $G-6 "open" crack (2" long)
0 5 5 33 2 5 97 2 $G-6 "closed" crack (4" long)
0 5 4 1 1 4 96 1 $G-7
0 5 4 1 2 4 96 2 $G-7
C
3 2 2 1 4.6 0.0      $G-5 Crack Inserted Node Set
1 5 5 1 3 5 32 3 $G-6 "open" crack (2" long)
0 5 5 33 3 5 97 3 $G-6 "closed" crack (4" long)
0 5 4 1 2 4 96 2 $G-7
0 5 4 1 3 4 96 3 $G-7
C
4 2 2 1 4.6 0.0      $G-5 Crack Inserted Node Set
1 5 5 1 4 5 32 4 $G-6 "open" crack (2" long)
0 5 5 33 4 5 97 4 $G-6 "closed" crack (4" long)
0 5 4 1 3 4 96 3 $G-7
0 5 4 1 4 4 96 4 $G-7
C
5 2 1 1 4.6 0.0      $G-5 Crack Inserted Node Set
1 5 5 1 5 5 32 5 $G-6 "open" crack (2" long)
0 5 5 33 5 5 97 5 $G-6 "closed" crack (4" long)
0 5 4 1 4 4 96 4 $G-7
C
C Define element unit data for softlink elements
C
1164 776 $H-1 spring "softlink" elements connecting shells and solids
C
C Input historical STAGS material tables
C
1 0 0          $I-1 Elastic only

```

```

10.351967E+6 0.3 0.0 0.1 $I-2 E, nu, skip, rho_weight
2 5 0 $i-1 Elasto-plastic
10.351967E+6 0.3 0.0 0.1 $I-2 E, nu, skip, rho_weight
0.00483 50000.0, $i-3 yield stress
0.015 56600.0, $i-3
0.04 62400.0, $I-3
0.1 68200.0, $I-3
0.16 71100.0 $I-3 ultimate stress
C -----GCP-----
C 2024-T3 (LT) Aluminum alloy - ISOTROPIC MATERIAL
C
ISOELASTIC_MATERIAL 1 1 1 $I-5A GCP COMMAND RECORD
10.351967E+6, $I-7A E
0.30 , $I-7A NU
2.59E-5 , $I-7A MASS DENSITY
0.0 , $I-7A CTE (alpha)
0.0 , $I-7A CHE (beta)
0.0 0.0 $I-7A REF. TEMP AND REF. MOISTURE CONTENT
PLASTIC_WB_MATERIAL 2 1 1 2 0 $ WHITE-BESSELING PLASTICITY MODEL
10.351967E+6 0.3 2.59E-5 0.0 5 $I-9a E, nu, rho, cte, npoints
0.00483 50000.0, $i-9b yield stress
0.015 56600.0, $i-9b
0.04 62400.0, $I-9b
0.1 68200.0, $I-9b
0.16 71100.0 $I-9b ultimate stress
C
SHELL_FABRICATION 1 1 0 0 0 $I-5A Elastic only
1 $I-21A Aluminum MATID
0.090 $I-21C LAYER THICKNESSES
0.0 $I-21D LAYER ORIENTATION
SHELL_FABRICATION 2 1 1 0 0 $I-5A Elasto-plastic
2 $I-21A Aluminum MATID
5 $I-21B Integration points through thickness
0.090 $I-21C LAYER THICKNESSES
0.0 $I-21D LAYER ORIENTATION
SOLID_FABRICATION 1 2 0 1 0 $I-5A Elasto-plastic
0.0225 $I-21C Solid Element THICKNESSES
END $I-5A END GCP INPUT
C -----
C
C define historical STAGS shell wall data
C
1 1 1 0 $K-1 elastic regions
1 0.09 0.0 0 $k-2 single layer
2 1 1 5 $K-1 elastic regions
2 0.09 0.0 0 $k-2 single layer
C
C Unit 1 - top part of panel
C
2 0 $M-1 SHELL SURFACE DEFINITION - RECTANGULAR PLATE
0.0 6.0 0.0 6.0 $M-2 24-IN BY 12-IN. PLATE (half width model)
+1 0 $M-5 SHELL WALL SELECTION -> USE GCP
410 0 0 $N-1 ELEMENT SELECTION, UNIFORM MESH
0 3 6 4 $P-1 BOUNDARY CONDITIONS GIVEN (0=FIXED; 1=FREE)
110 000 $P-2 X=0 EDGE
1 0 0 $Q-1 LOADING (base load with Area=1.08 sq. in. gives
1 1 0 $Q-2 LOAD SET far field stress of 10 ksi)
-0.02 -1 1 1 1 0 $Q-3 applied displ. at point plus constraints
C-10800.0 1 1 1 1 0 $Q-3 applied load at point plus constraints
0 0 0 0 0 0 1 0 $R-1 OUTPUT FLAGS
1 0 $ output displacements across top of panel
C
C Unit 2 - segment 2

```

```

C
2 0 $M-1 SHELL SURFACE DEFINITION - RECTANGULAR PLATE
6.0 9.0 0.0 6.0 $M-2 24-IN BY 12-IN. PLATE (half width model)
+1 0 $M-5 SHELL WALL SELECTION -> USE GCP
410 0 0 $N-1 ELEMENT SELECTION, UNIFORM MESH
6 3 6 4 $P-1 BOUNDARY CONDITIONS GIVEN (0=FIXED; 1=FREE)
0 0 0 $Q-1 NO LOADING
0 0 $R-1 OUTPUT FLAGS
C
C Unit 3 - segment 3
C
2 0 $M-1 SHELL SURFACE DEFINITION - RECTANGULAR PLATE
9.0 11.0 0.0 6.0 $M-2 24-IN BY 12-IN. PLATE (half width model)
+1 0 $M-5 SHELL WALL SELECTION -> USE GCP
410 0 0 $N-1 ELEMENT SELECTION, UNIFORM MESH
6 3 6 4 $P-1 BOUNDARY CONDITIONS GIVEN (0=FIXED; 1=FREE)
0 0 0 $Q-1 NO LOADING
0 0 $R-1 OUTPUT FLAGS
C
C Unit 4 - segment 4
C
2 0 0 0 0 0 $M-1 SHELL SURFACE DEFINITION - RECTANGULAR PLATE
11.0 11.75 0.0 6.0 $M-2 24-IN BY 12-IN. PLATE (half width model)
+2 0 0 0 0 0 1 $M-5 SHELL WALL SELECTION -> USE GCP
410 0 0 $N-1 ELEMENT SELECTION, UNIFORM MESH
6 3 6 4 $P-1 BOUNDARY CONDITIONS GIVEN (0=FIXED; 1=FREE)
0 0 0 $Q-1 NO LOADING
0 0 0 0 0 0 0 0 $R-1 OUTPUT FLAGS
C
C Unit 5 - center section with center crack - can be elasto-plastic
C
2 0 0 0 4 4 $M-1 SHELL SURFACE DEFINITION - RECTANGULAR PLATE
11.75 12.25 0.0 6.0 $M-2 24-IN BY 12-IN. PLATE (half width model)
-1 0 0.0 0.0 0 1 $M-5 Solid Fabrication SELECTION -> USE GCP
-1 0 0.0 0.0 0 1 $M-5 Solid Fabrication SELECTION -> USE GCP
-1 0 0.0 0.0 0 1 $M-5 Solid Fabrication SELECTION -> USE GCP
-1 0 0.0 0.0 0 1 $M-5 Solid Fabrication SELECTION -> USE GCP
881 0 0 $N-1 ELEMENT SELECTION, UNIFORM MESH
6 3 6 4 $P-1 BOUNDARY CONDITIONS GIVEN (0=FIXED; 1=FREE)
0 0 0 $Q-1 NO LOADING
0 0 0 0 0 0 0 0 $R-1 OUTPUT FLAGS
C
C Unit 6 - section 6 - can be elasto-plastic
C
2 0 0 0 0 0 $M-1 SHELL SURFACE DEFINITION - RECTANGULAR PLATE
12.25 13.0 0.0 6.0 $M-2 24-IN BY 12-IN. PLATE (half width model)
+2 0 0.0 0.0 0 1 $M-5 SHELL WALL SELECTION -> USE GCP
410 0 0 $N-1 ELEMENT SELECTION, UNIFORM MESH
6 3 6 4 $P-1 BOUNDARY CONDITIONS GIVEN (0=FIXED; 1=FREE)
0 0 0 $Q-1 NO LOADING
0 0 0 0 0 0 0 0 $R-1 OUTPUT FLAGS
C
C Unit 7 - segment 7
C
2 0 $M-1 SHELL SURFACE DEFINITION - RECTANGULAR PLATE
13.0 15.0 0.0 6.0 $M-2 24-IN BY 12-IN. PLATE (half width model)
+1 0 $M-5 SHELL WALL SELECTION -> USE GCP
410 0 0 $N-1 ELEMENT SELECTION, UNIFORM MESH
6 3 6 4 $P-1 BOUNDARY CONDITIONS GIVEN (0=FIXED; 1=FREE)
0 0 0 $Q-1 NO LOADING
0 0 $R-1 OUTPUT FLAGS
C
C Unit 8

```

```

C
2 0 $M-1 SHELL SURFACE DEFINITION - RECTANGULAR PLATE
15.0 18.0 0.0 6.0 $M-2 24-IN BY 12-IN. PLATE (half width model)
+1 0 $M-5 SHELL WALL SELECTION -> USE GCP
410 0 0 $N-1 ELEMENT SELECTION, UNIFORM MESH
6 3 6 4 $P-1 BOUNDARY CONDITIONS GIVEN (0=FIXED; 1=FREE)
0 0 0 $Q-1 NO LOADING
0 0 $R-1 OUTPUT FLAGS
C
C Unit 9 Bottom section
C
2 0 $M-1 SHELL SURFACE DEFINITION - RECTANGULAR PLATE
18.0 24.0 0.0 6.0 $M-2 24-IN BY 12-IN. PLATE (half width model)
+1 0 $M-5 SHELL WALL SELECTION -> USE GCP
410 0 0 $N-1 ELEMENT SELECTION, UNIFORM MESH
6 3 2 4 $P-1 BOUNDARY CONDITIONS GIVEN (0=FIXED; 1=FREE)
0 0 0 $Q-1 NO LOADING
0 0 0 0 $R-1 OUTPUT FLAGS
C
C Generate the "softlinks" to connect shells to solids
C
C Connect unit 4 shells to unit 5 solids
C
1 4 7 1 3*0. 3*0 97 / 1 0 0 1 $S1/S1-1A
98 5 1 1 3*0. 3*0 97 1 / 1 0 0 1 $S1/S1-1A
195 5 1 1 3*0. 3*0 97 2 / 1 0 0 1 $S1/S1-1A
292 5 1 1 3*0. 3*0 97 3 / 1 0 0 1 $S1/S1-1A
389 5 1 1 3*0. 3*0 97 4 / 1 0 0 1 $S1/S1-1A
486 5 1 1 3*0. 3*0 97 5 / 1 0 0 1 $S1/S1-1A
C
C Connect unit 6 shells to unit 5 solids
C
583 6 1 1 3*0. 3*0 97 / 1 0 0 1 $S1/S1-1A
680 5 9 1 3*0. 3*0 97 1 / 1 0 0 1 $S1/S1-1A
777 5 9 1 3*0. 3*0 97 2 / 1 0 0 1 $S1/S1-1A
874 5 9 1 3*0. 3*0 97 3 / 1 0 0 1 $S1/S1-1A
971 5 9 1 3*0. 3*0 97 4 / 1 0 0 1 $S1/S1-1A
1068 5 9 1 3*0. 3*0 97 5 / 1 0 0 1 $S1/S1-1A
C
C generate softlinks from unit 4 shells to unit 5 solids
C
1 98 195 121 97 1 1 1 / 1.e4 $T1/T1-B
1 98 292 121 97 1 1 1 / 1.e4 $T1/T1-B
1 98 389 121 97 1 1 1 / 1.e4 $T1/T1-B
1 98 486 121 97 1 1 1 / 1.e4 $T1/T1-B
C
C generate softlinks from unit 6 shells to unit 5 solids
C
583 680 777 121 97 1 1 1 / 1.e4 $T1/T1-B
583 680 874 121 97 1 1 1 / 1.e4 $T1/T1-B
583 680 971 121 97 1 1 1 / 1.e4 $T1/T1-B
583 680 1068 121 97 1 1 1 / 1.e4 $T1/T1-B
C
0 0 $U
0 $ 1 0 0 0 0 1 $V

```

crack1sm.bin (for S2 processor)

```

Middle crack tension panel $a-1
C
C nonlinear elasto-plastic crack growth analysis
C
3 1 0 0 0 0 0 -1 $b-1 analysis type and options

```

```

1.0 0.50 6.0          $c-1
0 30000 20 -20 0 1.0e-4 $d-1
0 0 0                $et-1
C
C linear elastic stress analysis
C
0 1 0 0 0 0 0 -1      $b-1 analysis type and options
1.0 1.00 1.0          $c-1 Apply just the base load

```

crack1sm.pin (for STAPL processor)

Panel with center crack

```

4 0 1 0 $PL-2 NPLOT,IPREP,IPRS,KDEV
C contour plot of longitudinal stress component
2 0 7 22 0 0 1 1 $PL-3 KPLOT,VIEW,ITEM,STEP,MODE,IFRNG,COLOR,ICOMP
0.0 3 -1. -6000. 84000. $PL-5 DSCALE,NROTS,LWSCALE,RNGMIN,RGMAX
1 0.0 / 2 0.0 / 3 -90.0 $PL-6 rotations
2 0 7 52 0 0 1 1 $PL-3 KPLOT,VIEW,ITEM,STEP,MODE,IFRNG,COLOR,ICOMP
0.0 3 -1. -6000. 84000. $PL-5 DSCALE,NROTS,LWSCALE,RNGMIN,RGMAX
1 0.0 / 2 0.0 / 3 -90.0 $PL-6 rotations
2 0 7 111 0 0 1 1 $PL-3 KPLOT,VIEW,ITEM,STEP,MODE,IFRNG,COLOR,ICOMP
0.0 3 -1. -6000. 84000. $PL-5 DSCALE,NROTS,LWSCALE,RNGMIN,RGMAX
1 0.0 / 2 0.0 / 3 -90.0 $PL-6 rotations
2 0 7 151 0 0 1 1 $PL-3 KPLOT,VIEW,ITEM,STEP,MODE,IFRNG,COLOR,ICOMP
0.0 3 -1. -6000. 84000. $PL-5 DSCALE,NROTS,LWSCALE,RNGMIN,RGMAX
1 0.0 / 2 0.0 / 3 -90.0 $PL-6 rotations
C contour plot of u-displ component
2 0 1 22 0 0 1 1 $PL-3 KPLOT,VIEW,ITEM,STEP,MODE,IFRNG,COLOR,ICOMP
0.0 3 -1. -.12 0.0 $PL-5 DSCALE,NROTS,LWSCALE,RNGMIN,RGMAX
1 0.0 / 2 0.0 / 3 -90.0 $PL-6 rotations
2 0 1 52 0 0 1 1 $PL-3 KPLOT,VIEW,ITEM,STEP,MODE,IFRNG,COLOR,ICOMP
0.0 3 -1. -.12 0.0 $PL-5 DSCALE,NROTS,LWSCALE,RNGMIN,RGMAX
1 0.0 / 2 0.0 / 3 -90.0 $PL-6 rotations
2 0 1 111 0 0 1 1 $PL-3 KPLOT,VIEW,ITEM,STEP,MODE,IFRNG,COLOR,ICOMP
0.0 3 -1. -.12 0.0 $PL-5 DSCALE,NROTS,LWSCALE,RNGMIN,RGMAX
1 0.0 / 2 0.0 / 3 -90.0 $PL-6 rotations
2 0 1 151 0 0 1 1 $PL-3 KPLOT,VIEW,ITEM,STEP,MODE,IFRNG,COLOR,ICOMP
0.0 3 -1. -.12 0.0 $PL-5 DSCALE,NROTS,LWSCALE,RNGMIN,RGMAX
1 0.0 / 2 0.0 / 3 -90.0 $PL-6 rotations
C plot model
0 0 0 0 0 0 0 0 $PL-3 KPLOT,VIEW,ITEM,STEP,MODE,IFRNG,COLOR,ICOMP
0.0 3 -1.0 0.0 0.0 $PL-5 DSCALE,NROTS,LWSCALE,RNGMIN,RGMAX
1 20.0 / 2 45.0 / 3 -90.0 $PL-6 rotations
C plot first solution close to crack so you can see it!
1 3 1 1 0 0 0 1 $PL-3 KPLOT,VIEW,ITEM,STEP,MODE,IFRNG,COLOR,ICOMP
4 5 6 $PL-4 plot unit = 5 only
0.0 3 0. -0.1 0.0 $PL-5 DSCALE,NROTS,LWSCALE,RNGMIN,RGMAX
1 20.0 / 2 45.0 / 3 -90.0 $PL-6 rotations

```

Typical Center-Crack Panel Input Files – *Automatic* Shell/Solid Element Model

crack1sa.inp (for S1 processor)

```

Middle crack tension panel - M(T) $a-1
C
C 24 in. long, 12 in. wide, 0.09 in. thick
C with 4" long through center crack
C
0 0 0 0 1 3 0          $B-1 ANALYSIS TYPE
5
3 -90.0 / 2 0.0 / 1 -20.0
9 0 0 8 1 0 0 0 5     $B-2 MODEL SUMMARY

```

```

2 0 2 0 0 1          $B-3 DATA TABLE SUMMARY -> use gcp
C
C Use mesh refinement
C Unit 1 is 6" x 6"; use dx=0.5" and dy=0.5"
C Unit 2 is 3" x 6"; use dx=0.5" and dy=0.25"
C Unit 3 is 2" x 6"; use dx=0.25" and dy=0.125"
C Unit 4 is .75" x 6"; use dx=0.125" and dy=0.0625"
C Unit 5 is .50" x 6"; use dx=0.0625" and dy=0.0625"
C Unit 6 is .75" x 6"; use dx=0.125" and dy=0.0625"
C Unit 7 is 2" x 6"; use dx=0.25" and dy=0.125"
C Unit 8 is 3" x 6"; use dx=0.5" and dy=0.25"
C Unit 9 is 6" x 6"; use dx=dy=1.0"
C
13 13 7 25 9 49 ,
7 97 9 97 7 97 ,
9 49 7 25 13 13 $F-1 GRID SUMMARY
C
C Shell unit connection records
C - don't connect solids to shells with g-1 records
C
1 3 2 1 $G-1
2 3 3 1 $G-1
3 3 4 1 $G-1
-4 3 5 1 $G-1
-5 3 6 1 $G-1
6 3 7 1 $g-1
7 3 8 1 $g-1
8 3 9 1 $g-1
C
C Impose u=u at row 1 col. 1 across top of panel
C
1 1 1 1 1 1 0 1 $G-2 PARTIAL COMPATIBILITY U=CONSTANT AT EDGE
C
C Crack definition (element size is 0.0625")
C Note: nodes 1 to 32 open which gives an initial crack length
C equal to 32 elements or 2" long; node 33 is at crack tip
C
1 2 1 1 4.6 0.0 $G-5 Crack Inserted Node Set
1 5 5 1 1 5 32 1 $G-6 "open" crack (2" long)
0 5 5 33 1 5 97 1 $G-6 "closed" crack (4" long)
0 5 4 1 1 4 96 1 $G-7
C
2 2 2 1 4.6 0.0 $G-5 Crack Inserted Node Set
1 5 5 1 2 5 32 2 $G-6 "open" crack (2" long)
0 5 5 33 2 5 97 2 $G-6 "closed" crack (4" long)
0 5 4 1 1 4 96 1 $G-7
0 5 4 1 2 4 96 2 $G-7
C
3 2 2 1 4.6 0.0 $G-5 Crack Inserted Node Set
1 5 5 1 3 5 32 3 $G-6 "open" crack (2" long)
0 5 5 33 3 5 97 3 $G-6 "closed" crack (4" long)
0 5 4 1 2 4 96 2 $G-7
0 5 4 1 3 4 96 3 $G-7
C
4 2 2 1 4.6 0.0 $G-5 Crack Inserted Node Set
1 5 5 1 4 5 32 4 $G-6 "open" crack (2" long)
0 5 5 33 4 5 97 4 $G-6 "closed" crack (4" long)
0 5 4 1 3 4 96 3 $G-7
0 5 4 1 4 4 96 4 $G-7
C
5 2 1 1 4.6 0.0 $G-5 Crack Inserted Node Set
1 5 5 1 5 5 32 5 $G-6 "open" crack (2" long)
0 5 5 33 5 5 97 5 $G-6 "closed" crack (4" long)

```

```

0 5 4 1 4 4 96 4 $G-7
C
C Input historical STAGS material tables
C
1 0 0 $I-1 Elastic only
10.359834E+6 0.3 0.0 0.1 $I-2 E, nu, skip, rho_weight
2 5 0 $i-1 Elasto-plastic
10.359834E+6 0.3 0.0 0.1 $I-2 E, nu, skip, rho_weight
0.00483 50000.0, $i-3 yield stress
0.015 56600.0, $i-3
0.04 62400.0, $I-3
0.1 68200.0, $I-3
0.16 71100.0 $I-3 ultimate stress
C -----GCP-----
C 2024-T3 (LT) Aluminum alloy - ISOTROPIC MATERIAL
C
ISOELASTIC_MATERIAL 1 1 1 $I-5A GCP COMMAND RECORD
10.359834E+6, $I-7A E
0.30 , $I-7A NU
2.59E-5 , $I-7A MASS DENSITY
0.0 , $I-7A CTE (alpha)
0.0 , $I-7A CHE (beta)
0.0 0.0 $I-7A REF. TEMP AND REF. MOISTURE CONTENT
PLASTIC_WB_MATERIAL 2 1 1 2 0 $ WHITE-BESSELING PLASTICITY MODEL
10.359834E+6 0.3 2.59E-5 0.0 5 $I-9a E, nu, rho, cte, npoints
0.00483 50000.0, $i-9b yield stress
0.015 56600.0, $i-9b
0.04 62400.0, $I-9b
0.1 68200.0, $I-9b
0.16 71100.0 $I-9b ultimate stress
C
SHELL_FABRICATION 1 1 0 0 0 $I-5A Elastic only
1 $I-21A Aluminum MATID
0.090 $I-21C LAYER THICKNESSES
0.0 $I-21D LAYER ORIENTATION
SHELL_FABRICATION 2 1 1 0 0 $I-5A Elasto-plastic
2 $I-21A Aluminum MATID
5 $I-21B Integration points through thickness
0.090 $I-21C LAYER THICKNESSES
0.0 $I-21D LAYER ORIENTATION
SOLID_FABRICATION 1 2 0 1 0 $I-5A Elasto-plastic
0.0225 $I-21C Solid Element THICKNESSES
END $I-5A END GCP INPUT
C -----
C
C define historical STAGS shell wall data
C
1 1 1 0 $K-1 elastic regions
1 0.09 0.0 0 $k-2 single layer
2 1 1 5 $K-1 elastic regions
2 0.09 0.0 0 $k-2 single layer
C
C Unit 1 - top part of panel
C
2 0 $M-1 SHELL SURFACE DEFINITION - RECTANGULAR PLATE
0.0 6.0 0.0 6.0 $M-2 24-IN BY 12-IN. PLATE (half width model)
-1 0 $M-5 SHELL WALL SELECTION -> USE GCP
410 0 0 $N-1 ELEMENT SELECTION, UNIFORM MESH
0 3 6 4 $P-1 BOUNDARY CONDITIONS GIVEN (0=FIXED; 1=FREE)
110 000 $P-2 X=0 EDGE
1 0 0 $Q-1 LOADING (base load with Area=1.08 sq. in. gives
1 1 0 $Q-2 LOAD SET far field stress of 10 ksi)
-10800.0 1 1 1 1 0 $Q-3 applied load at point plus constraints

```

```

0 0 0 0 0 0 1 0 $R-1 OUTPUT FLAGS
1 0 $ output displacements across top of panel
C
C Unit 2 - segment 2
C
2 0 $M-1 SHELL SURFACE DEFINITION - RECTANGULAR PLATE
6.0 9.0 0.0 6.0 $M-2 24-IN BY 12-IN. PLATE (half width model)
-1 0 $M-5 SHELL WALL SELECTION -> USE GCP
410 0 0 $N-1 ELEMENT SELECTION, UNIFORM MESH
6 3 6 4 $P-1 BOUNDARY CONDITIONS GIVEN (0=FIXED; 1=FREE)
0 0 0 $Q-1 NO LOADING
0 0 $R-1 OUTPUT FLAGS
C
C Unit 3 - segment 3
C
2 0 $M-1 SHELL SURFACE DEFINITION - RECTANGULAR PLATE
9.0 11.0 0.0 6.0 $M-2 24-IN BY 12-IN. PLATE (half width model)
-1 0 $M-5 SHELL WALL SELECTION -> USE GCP
410 0 0 $N-1 ELEMENT SELECTION, UNIFORM MESH
6 3 6 4 $P-1 BOUNDARY CONDITIONS GIVEN (0=FIXED; 1=FREE)
0 0 0 $Q-1 NO LOADING
0 0 $R-1 OUTPUT FLAGS
C
C Unit 4 - segment 4
C
2 0 0 0 0 0 $M-1 SHELL SURFACE DEFINITION - RECTANGULAR PLATE
11.0 11.75 0.0 6.0 $M-2 24-IN BY 12-IN. PLATE (half width model)
-2 0 0.0 0.0 0 1 $M-5 SHELL WALL SELECTION -> USE GCP
410 0 0 $N-1 ELEMENT SELECTION, UNIFORM MESH
6 3 6 4 $P-1 BOUNDARY CONDITIONS GIVEN (0=FIXED; 1=FREE)
0 0 0 $Q-1 NO LOADING
0 0 0 0 0 0 0 0 $R-1 OUTPUT FLAGS
C
C Unit 5 - center section with center crack - can be elasto-plastic
C
2 0 0 0 4 4 $M-1 SHELL SURFACE DEFINITION - RECTANGULAR PLATE
11.75 12.25 0.0 6.0 $M-2 24-IN BY 12-IN. PLATE (half width model)
-1 0 0.0 0.0 0 1 $M-5 Solid Fabrication SELECTION -> USE GCP
-1 0 0.0 0.0 0 1 $M-5 Solid Fabrication SELECTION -> USE GCP
-1 0 0.0 0.0 0 1 $M-5 Solid Fabrication SELECTION -> USE GCP
-1 0 0.0 0.0 0 1 $M-5 Solid Fabrication SELECTION -> USE GCP
881 0 0 $N-1 ELEMENT SELECTION, UNIFORM MESH
6 3 6 4 $P-1 BOUNDARY CONDITIONS GIVEN (0=FIXED; 1=FREE)
0 0 0 $Q-1 NO LOADING
0 0 0 0 0 0 0 0 $R-1 OUTPUT FLAGS
C
C Unit 6 - section 6 - can be elasto-plastic
C
2 0 0 0 0 0 $M-1 SHELL SURFACE DEFINITION - RECTANGULAR PLATE
12.25 13.0 0.0 6.0 $M-2 24-IN BY 12-IN. PLATE (half width model)
-2 0 0.0 0.0 0 1 $M-5 SHELL WALL SELECTION -> USE GCP
410 0 0 $N-1 ELEMENT SELECTION, UNIFORM MESH
6 3 6 4 $P-1 BOUNDARY CONDITIONS GIVEN (0=FIXED; 1=FREE)
0 0 0 $Q-1 NO LOADING
0 0 0 0 0 0 0 0 $R-1 OUTPUT FLAGS
C
C Unit 7 - segment 7
C
2 0 $M-1 SHELL SURFACE DEFINITION - RECTANGULAR PLATE
13.0 15.0 0.0 6.0 $M-2 24-IN BY 12-IN. PLATE (half width model)
-1 0 $M-5 SHELL WALL SELECTION -> USE GCP
410 0 0 $N-1 ELEMENT SELECTION, UNIFORM MESH
6 3 6 4 $P-1 BOUNDARY CONDITIONS GIVEN (0=FIXED; 1=FREE)

```



```

0 0 0 $Q-1 NO LOADING
0 0 $R-1 OUTPUT FLAGS
C
C Unit 8
C
2 0 $M-1 SHELL SURFACE DEFINITION - RECTANGULAR PLATE
15.0 18.0 0.0 6.0 $M-2 24-IN BY 12-IN. PLATE (half width model)
-1 0 $M-5 SHELL WALL SELECTION -> USE GCP
410 0 0 $N-1 ELEMENT SELECTION, UNIFORM MESH
6 3 6 4 $P-1 BOUNDARY CONDITIONS GIVEN (0=FIXED; 1=FREE)
0 0 0 $Q-1 NO LOADING
0 0 $R-1 OUTPUT FLAGS
C
C Unit 9 Bottom section
C
2 0 $M-1 SHELL SURFACE DEFINITION - RECTANGULAR PLATE
18.0 24.0 0.0 6.0 $M-2 24-IN BY 12-IN. PLATE (half width model)
-1 0 $M-5 SHELL WALL SELECTION -> USE GCP
410 0 0 $N-1 ELEMENT SELECTION, UNIFORM MESH
6 3 2 4 $P-1 BOUNDARY CONDITIONS GIVEN (0=FIXED; 1=FREE)
0 0 0 $Q-1 NO LOADING
0 0 0 0 $R-1 OUTPUT FLAGS

```

Typical MSD Panel Input Files – Shell Element Model

crack5.inp (for S1 processor)

```

Middle crack tension panel - M(T) 5-crack MSD simulation $a-1
C
C 24 in. long, 12 in. wide, 0.09 in. thick
C with 4" long through center crack + MSD
C (2L=24; 2W=12; 2a=4; 2a/2W=1/3)
C
C Modeled region is 24 in. long, 6 in. wide
C with a 2 inch long crack (full length, half
C width). MSD Configuration E with 5 total
C cracks - 2 additional 0.3125" long cracks
C on either side of center crack. The spacing
C between the center crack and the next crack is
C 0.75" and between the next 2 cracks is 0.6875"
C
0 0 0 0 0 0 0 $B-1 ANALYSIS TYPE
9 0 0 8 1 0 0 0 1 $B-2 MODEL SUMMARY
2 0 2 0 0 1 $B-3 DATA TABLE SUMMARY -> use gcp
C
C Use mesh refinement
C Unit 1 is 6" x 6"; use dx=0.5" and dy=0.5"
C Unit 2 is 3" x 6"; use dx=0.5" and dy=0.25"
C Unit 3 is 2" x 6"; use dx=0.25" and dy=0.125"
C Unit 4 is .75" x 6"; use dx=0.125" and dy=0.0625"
C Unit 5 is .50" x 6"; use dx=0.0625" and dy=0.0625"
C Unit 6 is .75" x 6"; use dx=0.125" and dy=0.0625"
C Unit 7 is 2" x 6"; use dx=0.25" and dy=0.125"
C Unit 8 is 3" x 6"; use dx=0.5" and dy=0.25"
C Unit 9 is 6" x 6"; use dx=dy=1.0"
C
13 13 7 25 9 49 ,
7 97 9 97 7 97 ,
9 49 7 25 13 13 $F-1 GRID SUMMARY
C
C Shell unit connection records

```

```

C - don't connect solids to shells with g-1 records
C
1 3 2 1 $G-1
2 3 3 1 $G-1
3 3 4 1 $G-1
4 3 5 1 $G-1
5 3 6 1 $G-1
6 3 7 1 $g-1
7 3 8 1 $g-1
8 3 9 1 $g-1
C
C Impose u=u at row 1 col. 1 across top of panel
C
1 1 1 1 1 1 0 1 $G-2 PARTIAL COMPATIBILITY U=CONSTANT AT EDGE
C
C Crack definition (element size is 0.0625")
C Note: nodes 1 to 32 open which gives an initial half crack length
C equal to 32 elements or 2" long; node 33 is at crack tip
C plus 2 MSD 0.3125"-long cracks with a spacing of 0.75"
C and 0.6875" (tip-to-tip)
C
1 6 1 1 4.6 0.0625 $G-5 Crack Inserted Node Set
1 5 5 1 5 32 $G-6 "open" crack (2" long)
0 5 5 33 5 45 $G-6 "closed" crack (0.75" long)
1 5 5 46 5 49 $G-6 "open" crack (.3125" long)
0 5 5 50 5 61 $G-6 "closed" crack (0.6875" long)
1 5 5 62 5 65 $G-6 "open" crack (.3125" long)
0 5 5 66 5 97 $G-6 "closed" crack (1.9375" long)
0 5 4 1 4 96 $G-7
C
C Input historical STAGS material tables
C
1 0 0 $I-1 Elastic only
10.351967E+6 0.3 0.0 0.1 $I-2 E, nu, skip, rho_weight
2 5 0 $i-1 Elasto-plastic
10.351967E+6 0.3 0.0 0.1 $I-2 E, nu, skip, rho_weight
0.00483 50000.0, $i-3 yield stress
0.015 56600.0, $i-3
0.04 62400.0, $I-3
0.1 68200.0, $I-3
0.16 71100.0 $I-3 ultimate stress
C -----GCP-----
C 2024-T3 (LT) Aluminum alloy - ISOTROPIC MATERIAL
C
ISOELASTIC_MATERIAL 1 1 1 $I-5A GCP COMMAND RECORD
10.351967E+6, $I-7A E
0.30 , $I-7A NU
2.59E-5 , $I-7A MASS DENSITY
0.0 , $I-7A CTE (alpha)
0.0 , $I-7A CHE (beta)
0.0 0.0 $I-7A REF. TEMP AND REF. MOISTURE CONTENT
PLASTIC_WB_MATERIAL 2 1 1 2 0 $ WHITE-BESSELING PLASTICITY MODEL
10.351967E+6 0.3 2.59E-5 0.0 5 $I-9a E, nu, rho, cte, npoints
0.00483 50000.0, $i-9b yield stress
0.015 56600.0, $i-9b
0.04 62400.0, $I-9b
0.1 68200.0, $I-9b
0.16 71100.0 $I-9b ultimate stress
C
SHELL_FABRICATION 1 1 0 0 0 $I-5A Elastic only
1 $I-21A Aluminum MATID
0.090 $I-21C LAYER THICKNESSES
0.0 $I-21D LAYER ORIENTATION

```

```

SHELL_FABRICATION 2 1 1 0 0 $I-5A Elasto-plastic
2 $I-21A Aluminum MATID
5 $I-21B Integration points through thickness
0.090 $I-21C LAYER THICKNESSES
0.0 $I-21D LAYER ORIENTATION
SOLID_FABRICATION 1 2 0 1 0 $I-5A Elasto-plastic
0.0225 $I-21C Solid Element THICKNESSES
END $I-5A END GCP INPUT
C -----
C
C define historical STAGS shell wall data
C
1 1 1 0 $K-1 elastic regions
1 0.09 0.0 0 $k-2 single layer
2 1 1 5 $K-1 elastic regions
2 0.09 0.0 0 $k-2 single layer
C
C Unit 1 - top part of panel
C
2 0 $M-1 SHELL SURFACE DEFINITION - RECTANGULAR PLATE
0.0 6.0 0.0 6.0 $M-2 24-IN BY 12-IN. PLATE (half width model)
+1 0 $M-5 SHELL WALL SELECTION -> USE GCP
410 0 0 $N-1 ELEMENT SELECTION, UNIFORM MESH
0 3 6 4 $P-1 BOUNDARY CONDITIONS GIVEN (0=FIXED; 1=FREE)
110 000 $P-2 X=0 EDGE
1 0 0 $Q-1 LOADING (base load with Area=1.08 sq. in. gives
1 1 0 $Q-2 LOAD SET far field stress of 10 ksi)
-0.02 -1 1 1 1 0 $Q-3 applied displ. at point plus constraints
C-10800.0 1 1 1 1 0 $Q-3 applied load at point plus constraints
0 0 0 0 0 0 1 0 $R-1 OUTPUT FLAGS
1 0 $ output displacements across top of panel
C
C Unit 2 - segment 2
C
2 0 $M-1 SHELL SURFACE DEFINITION - RECTANGULAR PLATE
6.0 9.0 0.0 6.0 $M-2 24-IN BY 12-IN. PLATE (half width model)
+1 0 $M-5 SHELL WALL SELECTION -> USE GCP
410 0 0 $N-1 ELEMENT SELECTION, UNIFORM MESH
6 3 6 4 $P-1 BOUNDARY CONDITIONS GIVEN (0=FIXED; 1=FREE)
0 0 0 $Q-1 NO LOADING
0 0 $R-1 OUTPUT FLAGS
C
C Unit 3 - segment 3
C
2 0 $M-1 SHELL SURFACE DEFINITION - RECTANGULAR PLATE
9.0 11.0 0.0 6.0 $M-2 24-IN BY 12-IN. PLATE (half width model)
+1 0 $M-5 SHELL WALL SELECTION -> USE GCP
410 0 0 $N-1 ELEMENT SELECTION, UNIFORM MESH
6 3 6 4 $P-1 BOUNDARY CONDITIONS GIVEN (0=FIXED; 1=FREE)
0 0 0 $Q-1 NO LOADING
0 0 $R-1 OUTPUT FLAGS
C
C Unit 4 - segment 4
C
2 0 0 0 0 0 $M-1 SHELL SURFACE DEFINITION - RECTANGULAR PLATE
11.0 11.75 0.0 6.0 $M-2 24-IN BY 12-IN. PLATE (half width model)
+2 0 0.0 0.0 0 1 $M-5 SHELL WALL SELECTION -> USE GCP
410 0 0 $N-1 ELEMENT SELECTION, UNIFORM MESH
6 3 6 4 $P-1 BOUNDARY CONDITIONS GIVEN (0=FIXED; 1=FREE)
0 0 0 $Q-1 NO LOADING
0 0 0 0 0 0 0 0 $R-1 OUTPUT FLAGS
C
C Unit 5 - center section with center crack - can be elasto-plastic

```

```

C
2 0 0 0 0 0 $M-1 SHELL SURFACE DEFINITION - RECTANGULAR PLATE
11.75 12.25 0.0 6.0 $M-2 24-IN BY 12-IN. PLATE (half width model)
+2 0 0.0 0.0 0 1 $M-5 Solid Fabrication SELECTION -> USE GCP
410 0 0 $N-1 ELEMENT SELECTION, UNIFORM MESH
6 3 6 4 $P-1 BOUNDARY CONDITIONS GIVEN (0=FIXED; 1=FREE)
0 0 0 $Q-1 NO LOADING
0 0 0 0 0 0 0 0 $R-1 OUTPUT FLAGS

```

```

C
C Unit 6 - section 6 - can be elasto-plastic
C

```

```

2 0 0 0 0 0 $M-1 SHELL SURFACE DEFINITION - RECTANGULAR PLATE
12.25 13.0 0.0 6.0 $M-2 24-IN BY 12-IN. PLATE (half width model)
+2 0 0.0 0.0 0 1 $M-5 SHELL WALL SELECTION -> USE GCP
410 0 0 $N-1 ELEMENT SELECTION, UNIFORM MESH
6 3 6 4 $P-1 BOUNDARY CONDITIONS GIVEN (0=FIXED; 1=FREE)
0 0 0 $Q-1 NO LOADING
0 0 0 0 0 0 0 0 $R-1 OUTPUT FLAGS

```

```

C
C Unit 7 - segment 7
C

```

```

2 0 $M-1 SHELL SURFACE DEFINITION - RECTANGULAR PLATE
13.0 15.0 0.0 6.0 $M-2 24-IN BY 12-IN. PLATE (half width model)
+1 0 $M-5 SHELL WALL SELECTION -> USE GCP
410 0 0 $N-1 ELEMENT SELECTION, UNIFORM MESH
6 3 6 4 $P-1 BOUNDARY CONDITIONS GIVEN (0=FIXED; 1=FREE)
0 0 0 $Q-1 NO LOADING
0 0 $R-1 OUTPUT FLAGS

```

```

C
C Unit 8
C

```

```

2 0 $M-1 SHELL SURFACE DEFINITION - RECTANGULAR PLATE
15.0 18.0 0.0 6.0 $M-2 24-IN BY 12-IN. PLATE (half width model)
+1 0 $M-5 SHELL WALL SELECTION -> USE GCP
410 0 0 $N-1 ELEMENT SELECTION, UNIFORM MESH
6 3 6 4 $P-1 BOUNDARY CONDITIONS GIVEN (0=FIXED; 1=FREE)
0 0 0 $Q-1 NO LOADING
0 0 $R-1 OUTPUT FLAGS

```

```

C
C Unit 9 Bottom section
C

```

```

2 0 $M-1 SHELL SURFACE DEFINITION - RECTANGULAR PLATE
18.0 24.0 0.0 6.0 $M-2 24-IN BY 12-IN. PLATE (half width model)
+1 0 $M-5 SHELL WALL SELECTION -> USE GCP
410 0 0 $N-1 ELEMENT SELECTION, UNIFORM MESH
6 3 2 4 $P-1 BOUNDARY CONDITIONS GIVEN (0=FIXED; 1=FREE)
0 0 0 $Q-1 NO LOADING
0 0 0 0 $R-1 OUTPUT FLAGS

```

crack5.bin (for S2 processor)

```

Middle crack tension panel $a-1
3 1 0 0 0 0 0 -1 $b-1 analysis type and options
1.0 0.50 6.0 $c-1
0 6000 10 -20 0 1.0e-4 $d-1
0 0 0 $et-1

```

crack5.pin (for STAPL processor)

```

Panel with center crack and MSD (5 cracks total)
6 0 0 0 $PL-2 NPLOT,IPREP,IPRS,KDEV
C contour plot of longitudinal stress component
2 0 7 20 0 0 1 1 $PL-3 KPLOT,VIEW,ITEM,STEP,MODE,IFRNG,COLOR,ICOMP
0.0 3 -1. -6000. 84000. $PL-5 DSCALE,NROTS,LWSCALE,RNGMIN,RGMAX

```

```

1 0.0 / 2 0.0 / 3 -90.0 $PL-6 rotations
2 0 7 38 0 0 1 1 $PL-3 KPLOT,VIEW,ITEM,STEP,MODE,IFRNG,COLOR,ICOMP
0.0 3 -1. -6000. 84000. $PL-5 DSCALE,NROTS,LWSCALE,RNGMIN,RGMAX
1 0.0 / 2 0.0 / 3 -90.0 $PL-6 rotations
2 0 7 61 0 0 1 1 $PL-3 KPLOT,VIEW,ITEM,STEP,MODE,IFRNG,COLOR,ICOMP
0.0 3 -1. -6000. 84000. $PL-5 DSCALE,NROTS,LWSCALE,RNGMIN,RGMAX
1 0.0 / 2 0.0 / 3 -90.0 $PL-6 rotations
2 0 7 71 0 0 1 1 $PL-3 KPLOT,VIEW,ITEM,STEP,MODE,IFRNG,COLOR,ICOMP
0.0 3 -1. -6000. 84000. $PL-5 DSCALE,NROTS,LWSCALE,RNGMIN,RGMAX
1 0.0 / 2 0.0 / 3 -90.0 $PL-6 rotations
2 0 7 80 0 0 1 1 $PL-3 KPLOT,VIEW,ITEM,STEP,MODE,IFRNG,COLOR,ICOMP
0.0 3 -1. -6000. 84000. $PL-5 DSCALE,NROTS,LWSCALE,RNGMIN,RGMAX
1 0.0 / 2 0.0 / 3 -90.0 $PL-6 rotations
2 0 7 100 0 0 1 1 $PL-3 KPLOT,VIEW,ITEM,STEP,MODE,IFRNG,COLOR,ICOMP
0.0 3 -1. -6000. 84000. $PL-5 DSCALE,NROTS,LWSCALE,RNGMIN,RGMAX
1 0.0 / 2 0.0 / 3 -90.0 $PL-6 rotations
C contour plot of plastic strain Ep_xx in shell units 4,5,6
2 3 8 20 0 0 0 1 $PL-3 KPLOT,VIEW,ITEM,STEP,MODE,IFRNG,COLOR,ICOMP
4 5 6 $PL-4 plot units = 4,5,6
0.0 3 0.0 0.0 0.16 $PL-5 DSCALE,NROTS,LWSCALE,RNGMIN,RGMAX
1 0.0 / 2 0.0 / 3 -90.0 $PL-6 rotations
2 3 8 38 0 0 0 1 $PL-3 KPLOT,VIEW,ITEM,STEP,MODE,IFRNG,COLOR,ICOMP
4 5 6 $PL-4 plot units = 4,5,6
0.0 3 0.0 0.0 0.16 $PL-5 DSCALE,NROTS,LWSCALE,RNGMIN,RGMAX
1 0.0 / 2 0.0 / 3 -90.0 $PL-6 rotations
2 3 8 61 0 0 0 1 $PL-3 KPLOT,VIEW,ITEM,STEP,MODE,IFRNG,COLOR,ICOMP
4 5 6 $PL-4 plot units = 4,5,6
0.0 3 0.0 0.0 0.16 $PL-5 DSCALE,NROTS,LWSCALE,RNGMIN,RGMAX
1 0.0 / 2 0.0 / 3 -90.0 $PL-6 rotations
2 3 8 71 0 0 0 1 $PL-3 KPLOT,VIEW,ITEM,STEP,MODE,IFRNG,COLOR,ICOMP
4 5 6 $PL-4 plot units = 4,5,6
0.0 3 0.0 0.0 0.16 $PL-5 DSCALE,NROTS,LWSCALE,RNGMIN,RGMAX
1 0.0 / 2 0.0 / 3 -90.0 $PL-6 rotations
2 3 8 80 0 0 0 1 $PL-3 KPLOT,VIEW,ITEM,STEP,MODE,IFRNG,COLOR,ICOMP
4 5 6 $PL-4 plot units = 4,5,6
0.0 3 0.0 0.0 0.16 $PL-5 DSCALE,NROTS,LWSCALE,RNGMIN,RGMAX
1 0.0 / 2 0.0 / 3 -90.0 $PL-6 rotations
2 3 8 100 0 0 0 1 $PL-3 KPLOT,VIEW,ITEM,STEP,MODE,IFRNG,COLOR,ICOMP
4 5 6 $PL-4 plot units = 4,5,6
0.0 3 0.0 0.0 0.16 $PL-5 DSCALE,NROTS,LWSCALE,RNGMIN,RGMAX
1 0.0 / 2 0.0 / 3 -90.0 $PL-6 rotations
C contour plot of u-displ component
2 0 1 20 0 0 1 1 $PL-3 KPLOT,VIEW,ITEM,STEP,MODE,IFRNG,COLOR,ICOMP
0.0 3 -1. -0.08 1.0e-6 $PL-5 DSCALE,NROTS,LWSCALE,RNGMIN,RGMAX
1 0.0 / 2 0.0 / 3 -90.0 $PL-6 rotations
2 0 1 38 0 0 1 1 $PL-3 KPLOT,VIEW,ITEM,STEP,MODE,IFRNG,COLOR,ICOMP
0.0 3 -1. -0.08 1.0e-6 $PL-5 DSCALE,NROTS,LWSCALE,RNGMIN,RGMAX
1 0.0 / 2 0.0 / 3 -90.0 $PL-6 rotations
2 0 1 61 0 0 1 1 $PL-3 KPLOT,VIEW,ITEM,STEP,MODE,IFRNG,COLOR,ICOMP
0.0 3 -1. -0.08 1.0e-6 $PL-5 DSCALE,NROTS,LWSCALE,RNGMIN,RGMAX
1 0.0 / 2 0.0 / 3 -90.0 $PL-6 rotations
2 0 1 71 0 0 1 1 $PL-3 KPLOT,VIEW,ITEM,STEP,MODE,IFRNG,COLOR,ICOMP
0.0 3 -1. -0.08 1.0e-6 $PL-5 DSCALE,NROTS,LWSCALE,RNGMIN,RGMAX
1 0.0 / 2 0.0 / 3 -90.0 $PL-6 rotations
2 0 1 80 0 0 1 1 $PL-3 KPLOT,VIEW,ITEM,STEP,MODE,IFRNG,COLOR,ICOMP
0.0 3 -1. -0.08 1.0e-6 $PL-5 DSCALE,NROTS,LWSCALE,RNGMIN,RGMAX
1 0.0 / 2 0.0 / 3 -90.0 $PL-6 rotations
2 0 1 100 0 0 1 1 $PL-3 KPLOT,VIEW,ITEM,STEP,MODE,IFRNG,COLOR,ICOMP
0.0 3 -1. -0.08 1.0e-6 $PL-5 DSCALE,NROTS,LWSCALE,RNGMIN,RGMAX
1 0.0 / 2 0.0 / 3 -90.0 $PL-6 rotations

```

Problem References

Rankin, C. C., Loden, W. A., and Swenson, L. W., *STAGS Element Manual – Version 5.0 Preliminary*, Lockheed Martin Advanced Technology Center, Palo Alto, CA, September 2001.

Rankin, C. C., Brogan, F. A., Loden, W., and Cabiness, H., *Structural Analysis of General Shells – STAGS User Manual, Version 4.0*, Lockheed Martin Advanced Technology Center, Palo Alto, CA, June 2000.

Riks, E., Rankin, C. C., and Brogan, F. A., “The Buckling Behavior of a Central Crack in a Plate under Tension,” *Engineering Fracture Mechanics*, Vol. 143, No. 4, 1992, pp. 529-548.

Rankin, C. C., Brogan, F. A., and Riks, E., “Some Computational Tools for the Analysis of Through Cracks in Stiffened Fuselage Shells,” *Computational Mechanics*, Vol. 13, 1993, pp. 143-156.

Dawicke, D. S., Newman, J. C., Jr., Sutton, M. A., and Amstutz, B. E., *Stable Tearing Behavior of a Thin-Sheet Material with Multiple Cracks*, NASA TM-109131, July 1994.

Viz, M. J., Potyondy, D. O., Zehnder, A. T., Rankin, C. C., and Riks, E., “Computation of Membrane and Bending Stress Intensity Factors for Thin, Cracked Plates,” *International Journal of Fracture*, Vol. 72, No. 1, 1995, pp. 21-38.

Dawicke, D. S., *Fracture Tests on 0.09 Inch Thick 2024-T3 Aluminum Alloy*, NASA TM-112869, 1997. Unofficial draft document.

Seshadri, B. R. and Newman, J. C., Jr., *Analyses of Buckling and Stable Tearing in Thin-Sheet Materials*, NASA TM-1998-208428, May 1998.

Seshadri, B. R., Newman, J. C., Jr., Dawicke, D. S., and Young, R. D., *Fracture Analysis of the FAA/NASA Wide Stiffened Panels*, NASA TM-1998-208976, December 1998.

Gullerud, A. S., Dodds, R. H., Jr., Hampton, R. W., and Dawicke, D. S., “Three-Dimensional Modeling of Ductile Crack Growth in Thin Sheet Metals: Computational Aspects and Validation,” *Engineering Fracture Mechanics*, Vol. 63, No. 4, July 1999, pp. 347-374.

Rankin, C. C. and Riks, E., “On the Simulation of Crack-Propagation in Pressurized Fuselages,” AIAA Paper No. 2000-1594, April 2000.

Rankin, C. C. and Riks, E., “Tools for the Evaluation of the Residual Strength of Cracked Pressurized Fuselage Shells,” AIAA Paper No. 2001-1325, April 2001.

Rankin, C. C., “Riks Path Parameter Solution Control During Crack Node Release,” unpublished notes, June 9, 1998.

Hybrid Quasi-Static/Transient Solution Procedures Application

Background

Thin-walled plates and shells often can carry loads well in excess of its buckling load determined from a linear bifurcation buckling analysis. The structural response for load levels below the buckling load is referred to as the primary solution or pre-buckling solution. It may be linear or nonlinear. Beyond the buckling load, the response is referred to as postbuckling behavior when the response is stable and collapse when the response is unstable. For these structures, the analyst needs to examine the role initial geometry imperfections and “generalized” imperfections if possible. Generalized imperfections refer to surface imperfections, thickness variations, variations in lamination, fabrication inconsistencies, eccentricities in loading, and other aspects that cause the structure, its boundary conditions, and its loading to be less than ideal (*e.g.*, see Hilburger and Starnes, 2002).

Complex nonlinear response often involves changes in structural behavior that may develop gradually or may suddenly occur. Transition from a pre-buckled state to a post-buckled state for plates can be a gradual process depending on the imperfections. Shell structures, on the other hand, often exhibit collapse behavior. In some cases, the structural response involves changes in the buckle pattern in the post-buckled state. Stein (1961) explored this behavior and also presented test results illustrating the phenomenon of buckle pattern changes. Supple (1967, 1968, 1970) has studied this phenomena as well and provides insight into the structural response for simple configurations. Tiwari and Hyer (1996, 2000) also explored secondary buckling response predictions. However, Riks *et al.* (1993, 1996, 1997) provided the first computational procedure for nonlinear finite element analysis codes. Their approach involves the use of a nonlinear static solution procedure for a period and then switching to a nonlinear transient dynamics solution procedure. After the dynamic behavior has “settled” then the nonlinear static solution procedure is resumed after equilibrium is re-established. The term “load relaxation” is used for the procedure to re-establish equilibrium at a fixed load level. The procedure has been implemented in QSTAGS (early 1990’s version) and improved on each version since then (currently at STAGS Version 4.0, Rankin, *et al.*, 2001).

For structures exhibiting changes in their deformation pattern as part of the nonlinear response, the analysis effort can exhibit convergence difficulties and even non-convergence may result. In some cases, there is a mode change (or a mode jump), and equilibrium paths that are not statically connected may be involved. These difficulties may be signaled by the nonlinear analysis in several forms depending on the solution control procedure (load control, displacement control, or arc-length control) being used. One signal indicating convergence problems regardless of the solution control procedure is a large number of iterations and repeated step size reductions. Another signal is when the determinant of the stiffness matrix tends to zero indicating a limit point in the nonlinear response. Another signal is the occurrence of more than one negative roots in the tangent stiffness matrix due to the nonlinear response (*i.e.*, not including negative roots due to Lagrangian constraints). In the past such problems have been called “drop dead” problems because the solution procedure essentially “died” and further predictions were not possible. However, Riks, Rankin and Brogan (1993, 1996) proposed a hybrid static-transient solution procedure including load relaxation as a method to overcome these non-convergence issues.

The basic steps of the computational procedure are described as followed:

1. After defining the finite element model (geometry, discretization, material definitions, boundary conditions, and loading), perform a basic linear elastic stress analysis to check out the overall response of the model.
2. Perform a linear buckling analysis for the loading system considered. This step helps the analyst define the initial load level and starting load step size for the nonlinear analysis. The buckling mode

shapes may be used individually or in a linear combination to form an initial geometric surface imperfection.

3. Perform a linear free vibration analysis of the structure to determine the lowest natural frequency of vibration. This value is used in the transient dynamic analysis to define the coefficients associated with structural damping.
4. Perform a nonlinear static analysis. Examine the results to determine whether non-convergence occurred, whether convergence difficulties were encountered, or whether multiple negative roots from decomposition of the “tangent” stiffness matrix.
5. If no difficulties encountered, then perform a restart of the nonlinear solution process and continue the nonlinear static analysis until difficulties are encountered or until the desired load level is reached.
6. If difficulties or multiple negative roots are encountered, then perform a nonlinear transient dynamic analysis with either a slight increase in load or with a slight initial velocity. The analyst needs to have some insight into the nonlinear response in choosing this amplitude – too little and the solution will return to a neighboring static equilibrium solution instead of “passing through” or “jumping to” a new deformation mode.
7. Perform the nonlinear transient dynamic analysis using direct time integration methods for a given time period. The length of this time period is somewhat arbitrary – in essence, until the inertial forces become negligible. However, the definition of negligible is analyst dependent. The initial time step using the implicit Park’s method of STAGS can be chosen using the vibration frequencies from the linear vibration analysis. An initial time step size can be defined using $\Delta t = \frac{2}{\omega}$ where ω is the frequency associated with the highest anticipated vibration mode (*i.e.*, perhaps the third or fourth value assuming the lowest four are global mode shapes).
8. Perform a load relaxation step for each of one or more steps from the transient dynamic solution process. The load relaxation process computes a new right-hand-side “load” vector using the transient solution for that step. This “load” vector represents the inertial forces due to accelerations and velocities. In this case, these forces are the d’Alembert required to put the system in static equilibrium given the displacements from the transient solution at the specified load step; these forces are applied so long as the load factor PX on this new “load” vector is nonzero. Holding the applied external loads fixed, the load factor PX is decremented from a value of unity, and nonlinear solutions for each decrement are obtained until PX is zero. When PX is zero, static equilibrium is now re-established in a consistent, rigorous basis.
9. Once equilibrium is re-established, a restart of the nonlinear solution process is performed again until another problem is encountered.

The postbuckling response of a curved cylindrical composite panel with a central cutout shown in Figure 69 and loaded by in-plane compression is studied. This configuration corresponds to Panel CP8 in Knight and Starnes (1985). The curved panel is 14-inch-square projected-planform with a 15-inch radius. The curved panel is clamped along the curved edges and the straight edges are restrained using knife-edge supports that simulate a near simple support condition. The cutout is a 2-inch-diameter circular cutout in the panel center. Constraints are imposed along the top curved edge to enforce a uniform end-shortening condition similar to the test conditions. The material is T300/5208 graphite-epoxy, and nominal material data and geometry are defined on Figure 69 using U.S. customary units.

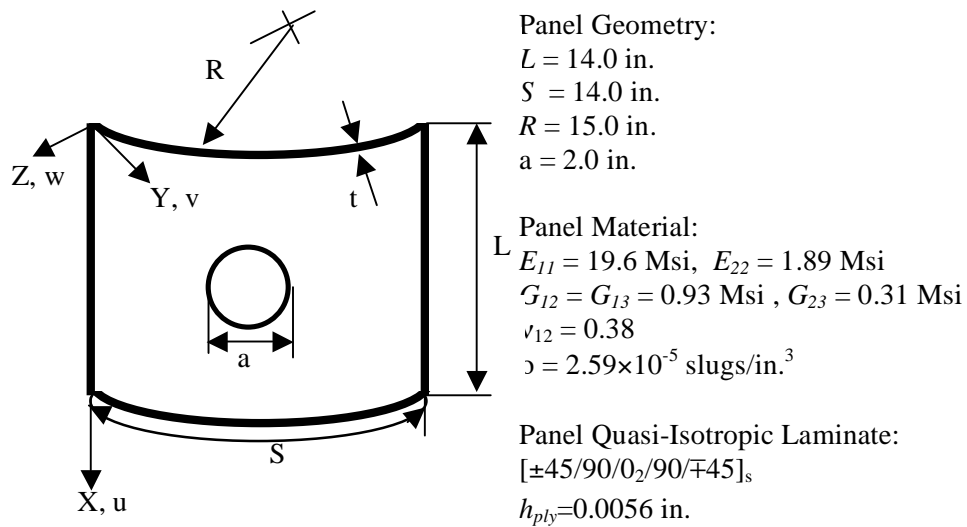


Figure 69. Compression-loaded curved panel: geometry and material properties.

Modeling and Analysis Process

The finite element model represents the entire panel with twelve shell units as shown in Figure 70. Eight shell units are used to model a six-inch-square region surrounding the central circular cutout using the LAME user-written subroutine – this region will be referred to as the cutout region (see Knight, October 1999). Two shell units are used to model the full width of the panel across the top and bottom. Two additional shell units are then used to complete the left and right sides of the panel adjacent to the cutout region. The finite element mesh in the cutout region is more refined than the other regions using the E510 transition elements (automatic).

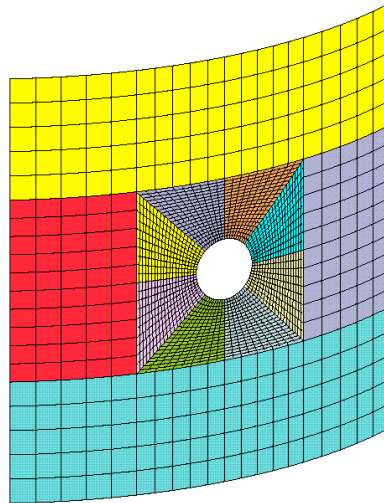


Figure 70. Finite element model of the curved panel with central circular cutout.

Material properties and shell wall construction are defined using the GCP approach. Material modeling using the current GCP approach requires data on the I-5a and I-6a records to define the material properties and records I-5a, I-21a, I-21b, I-21c, I-21d, and I-21e to define the shell fabrication. The 16-ply quasi-isotropic laminate has a $[\pm 45/90/0_2/90/ -45]_s$ stacking sequence and an average ply thickness of 0.0056 inches (based on measurements of the panel thickness). The value of the elastic modulus in the fiber direction E_{11} is modified for the nonlinear postbuckling analysis in order to better correlate the initial slope of the load-shortening curve (EA) with the value obtained from the test (EA=8,620,000 pounds). As a result, a value of 18.4 Msi is used instead of 19.0 Msi.

Boundary condition on the displacements are specified using the P-1 and P-2 records. An applied end displacement is specified across top curved edge (edge 3 on shell unit 12). The opposite curved end of the panel (edge 1 of shell unit 10) is clamped. The right and left straight edges of the finite element model (*i.e.*, edge 2 of shell unit 9 and edge 4 of shell unit 11, respectively) have knife-edge boundary conditions imposed (*i.e.*, $w = \theta_y = 0$).

Numerical Results and Discussion

The panel was observed during the test to buckle into a local mode shape around the cutout. This local mode shape was observed to be embedded within a more global deformation pattern at buckling. After buckling two regions of local deformation were noted. Panel failure occurred at a load nearly six times the buckling load in the test.

Linear buckling analysis is performed with four eigenvalues requested. The lowest buckling load is used to establish the initial load level and initial solution step size for the nonlinear analysis. In addition, these four mode shapes are then used to form an initial geometric surface imperfection for the nonlinear analysis. Contour plots of the out-of-plane displacement component of the first four buckling mode shapes are shown in Figure 71. The buckling modes are scaled (5%, 1%, 0.5% and 0.5% times the panel thickness) and then combined as a linear combination to form the initial geometric surface imperfection as shown in Figure 72. Note that STAGS normalizes the buckling modes by the largest component in the eigenvector (*i.e.*, the largest components will correspond to ± 1 ; typically an out-of-plane displacement degree of freedom has the maximum value in many applications).

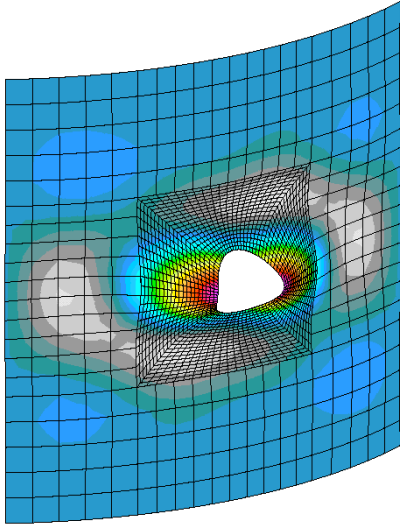
Nonlinear elastic analysis results and test results are shown on Figure 73. The end-shortening displacement as a function of the applied compressive load is shown in Figure 73. The test results are indicated by the open square symbols, and the elastic postbuckling analysis results obtained using arc-length control are shown by the open circles. Good correlation is shown for the assumed initial imperfection shape and nominal elastic properties up to buckling. The static solution predicted using the arc-length control procedure proceeded through the unstable regions of the response with no more than one negative root.

Nonlinear elastic results were also predicted using displacement control wherein the amplitude of the end-shortening displacement is controlled. In this case, the unstable branches of the nonlinear response are not predicted. Instead, one or more negative roots are detected once the collapse load had been reached. Hence, following an initial nonlinear static analysis, the results are reviewed and the analyst may choose to start the transient response from any of the archived nonlinear static solutions. Examination of the archived solutions indicate that the sixth solution step had no negative roots and the seventh step had just one negative root; however, there was a significant increase in load level between these solution steps. Therefore, the analyst needs to either restart the nonlinear solution and perform a few more static steps to more closely approach the collapse point, initiate the transient at step 6 with a high enough amplitude to cause the collapse to occur, or to initiate the transient at step 7 with a small increase in amplitude to

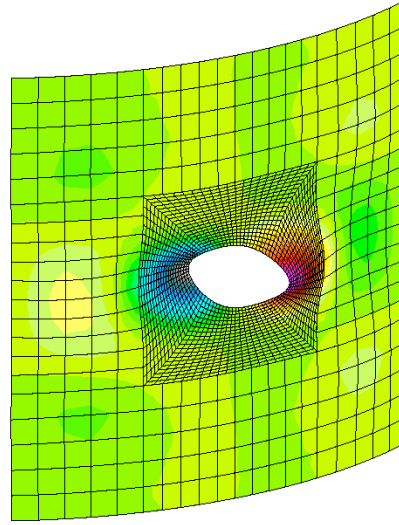
trigger the collapse. The results shown in Figure 73 are obtained using step 7 to initiate the transient with $\Delta t=0.0001$ sec. The values used for the damping parameters are based on the first fundamental frequency from a linear free vibration analysis. The fundamental frequency ϖ is 1434 hertz. The damping parameters, assuming 0.1% critical damping, are:

$$\alpha = 2\pi\varpi\zeta = 901.3 \quad \text{and} \quad \beta = \frac{\zeta}{2\pi\varpi} = 1.11 \times 10^{-5}$$

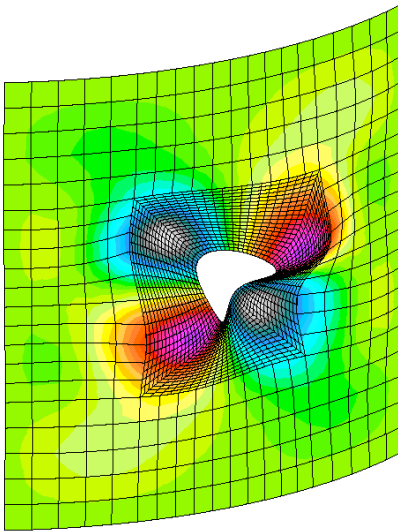
Following the transient, a load relaxation step is performed automatically on a nonlinear restart to re-establish equilibrium and subsequent increase in loading to advance the nonlinear solution.



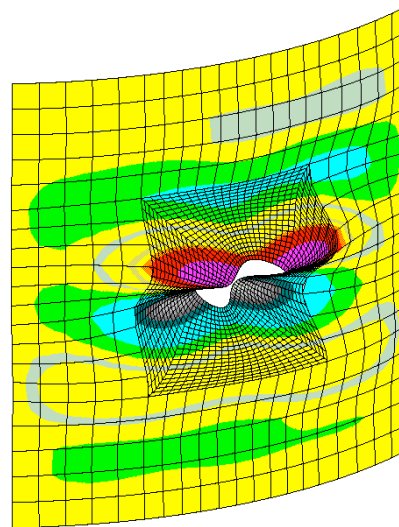
(a) Mode 1.



(b) Mode 2.



(c) Mode 3.



(d) Mode 4.

Figure 71. Contour plots of the out-of-plane displacement component of the buckling mode shapes.

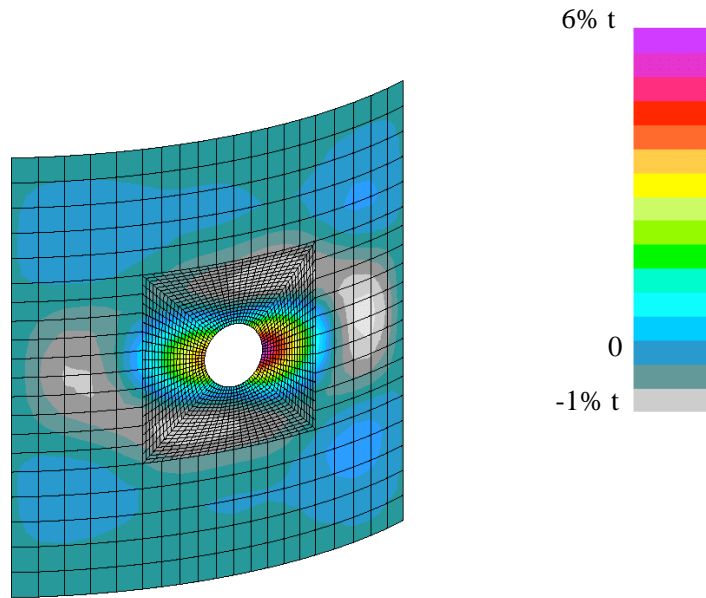


Figure 72. Contour plot of out-of-plane component of the initial geometric surface imperfection based on a linear combination of the lowest four buckling mode shapes.

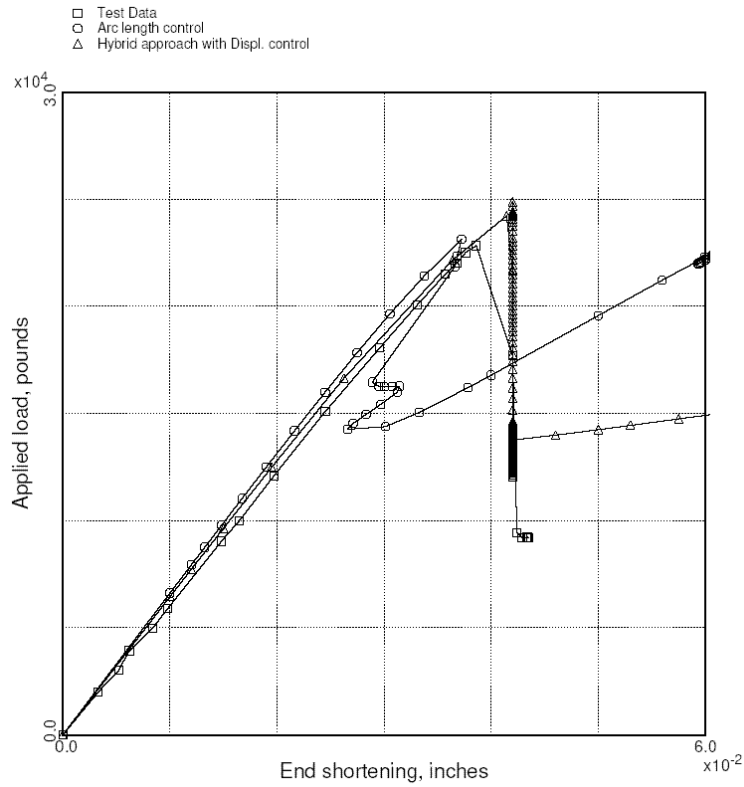


Figure 73. Load versus end-shortening results.

STAGS Input Files

These STAGS input files are located under the following subdirectory:

`$STAGSHOME/Advanced-Testcases/Type-D-Hybrid`

The 2-D shell analysis model is defined using entirely shell units in combination with the LAME user-written subroutine to model the circular cutout as a sequence of eight shell units (45-degrees each) around the hole.

Typical Shell Element Model

cp8.inp (for S1 processor)

```
Curved panel with a central cutout - using LAME.F
$ R=15" R_hole=1", Total length=14", 16-ply laminate
$ local 3" region around cutout
$ 2-to-1 transition for other shell units
$ top and bottom units span 3 middle shell units
$ first 8 shell units model local region around cutout
$
$ Panel is 53.5-degrees in arc, R=15 in. and L=14 in.
$ with the origin of the coord sys at the cylinder
$ mid-length on its axis
$
$ 8 segments around hole (+/- 45 degrees) plus
$ additional segments on top and bottom and
$ on left and right (uniform spacing of mesh)
$
0 0 1 0 0 3 $B-1
1 20.0 / 2 30.0 / 3 90.0 $b-1b model rotations
12 0 0 8 12 0 4 $B-2 MODEL SUMMARY
0 0 0 0 0 1 $B-3 DATA TABLE SUMMARY - use GCP
C
C Define imperfections using buckling mode shapes
C
0.0044800 0 1 0 $b-5 5%*t for Mode 1
0.0008960 0 2 0 $b-5 1%*t for Mode 2
0.0000896 0 3 0 $b-5 0.1%*t for Mode 3
0.0000896 0 4 0 $b-5 0.1%*t for Mode 4
C
C define shell unit discretization (rows and columns)
C
21 11 11 21 11 21 21 11,
21 11 11 21 11 21 21 11,
11 6,
6 21,
11 6,
6 21
$ G-1--Please see documentation in LAME routine
1 2 2 3
2 1 3 3
3 1 4 4
4 2 5 4
5 2 6 3
6 1 7 3
7 1 8 4
1 4 8 2
```

```

$g-2 combine segments with hole to other cylinder units
$ do the left side
2 0 21 0 9 0 1 0 1 11 2 6 11 1 $g-2
3 0 21 0 9 0 1 0 1 11 2 1 6 1 $g-2
$ do the bottom
4 21 0 0 10 6 0 0 1 11 2 16 11 -1 $g-2
5 21 0 0 10 6 0 0 1 11 2 11 6 -1 $g-2
$ do the right side
6 0 21 0 11 0 6 0 1 11 2 6 1 -1 $g-2
7 0 21 0 11 0 6 0 1 11 2 11 6 -1 $g-2
$ do the top
8 21 0 0 12 1 0 0 1 11 2 6 11 1 $g-2
1 21 0 0 12 1 0 0 1 11 2 11 16 1 $g-2
$
$ now connect outer shell units together
$ left side
9 1 0 0 10 6 0 0 1 6 1 16 21 1 $g-2
9 11 0 0 12 1 0 0 1 6 1 16 21 1 $g-2
$ right side
10 6 0 0 11 1 0 0 1 6 1 1 6 1 $g-2
11 11 0 0 12 1 0 0 1 6 1 1 6 1 $g-2
$
C -----
C
C 16-PLY QUASI-ISOTROPIC LAMINATE [pm45/90/0/0/90/mp45]_s
C
ORTHOELAST_MATERIAL 1 1 1 $I-5A GCP COMMAND RECORD
18.4E+6 1.89E+6 1.89e+6, $I-7A E1, E2, E3=E2
0.93E6 0.93E6 0.93E6, $I-7A G12,G13=G12, G23=G12
0.38 0.38 0.38, $I-7A NU12, NU13=NU12, NU23=NU12
2.59E-5, $I-7A MASS DENSITY
0.0 0.0 0.0 , $I-7A CTE'S
0.0 0.0 0.0 , $I-7A CME'S
0.0 0.0 $I-7A REF. TEMP AND REF. MOISTURE CONTENT
C
C 16-PLY QUASI-ISOTROPIC LAMINATE
C
ORT_EL_BR 2 1 1 $I-5A GCP COMMAND RECORD
18.4E+6 1.89E+6 1.89e+6, $I-7A E1, E2, E3=E2
0.93E6 0.93E6 0.93E6, $I-7A G12,G13=G12, G23=G12
0.38 0.38 0.38, $I-7A NU12, NU13=NU12, NU23=NU12
2.59E-5, $I-7A MASS DENSITY
0.0 0.0 0.0 , $I-7A CTE'S
0.0 0.0 0.0 , $I-7A CME'S
0.0 0.0 , $I-7A REF. TEMP AND REF. MOISTURE CONTENT
0.0 0.0 0.0 0.0 0.0 0.0 0.0 0.0 0.0, $i-7a allowable strains
165.e+3 200.e+3 27.41e+3 11.74e+3 27.41e+3 11.74e+3, $i-7a allowable
9.0e+3 9.0e+3 10.0e+3, $i-7a allowable shears
0.8e-14 0.0 -1.0e-3 1 1, $i-7a alpha, F12, beta, ifail idgrd
3*0.0 $i-7a visf0, visf1, visff
C
SHELL_FABRICATION 1 16 0 1 0 $I-5A 24-PLY LAMINATE
16*1 $I-21A T300/5208 MATID
16*0.0056 $I-21C LAYER THICKNESSES
+45.0 -45.0 90.0 0.0 0.0 90.0 -45.0 +45.0 , $i-21d
+45.0 -45.0 90.0 0.0 0.0 90.0 -45.0 +45.0 $i-21d
1.0 1.0 $I-21E SHEAR CORRECTION FACTORS
C
SHELL_FABRICATION 2 16 1 1 0 $I-5A 16-PLY LAMINATE
16*2 $I-21A T300/5208 MATID
16*1 $I-21B SHELL INTEGRATION POINTS PER LAYER
16*0.0056 $I-21C LAYER THICKNESSES
+45.0 -45.0 90.0 0.0 0.0 90.0 -45.0 +45.0 , $i-21d

```

```

+45.0 -45.0 90.0 0.0 0.0 90.0 -45.0 +45.0    $i-21d
1.0 1.0 $I-21E SHEAR CORRECTION FACTORS
END $I-5A END GCP INPUT
C -----
C
C generate 45-degree wedges around the hole in a
C counter-clockwise manner starting at "Noon"
C
C -----
$ UNIT 1
C -----
1 0/1. 3.0 +11.46 1.0 15.0
-1
410 0 0 0 1 0 0 0 0 1 0
3 6 6 6
0 $q-1 no loads - interior unit
0 0 0 0 $r-1
C -----
$ UNIT 2
C -----
1 0/-1. 3.0 +11.46 1.0 15.0
-1
410 0 0 0 1 0 0 0 1 0 0
6 6 6 3
0 $q-1 no loads - interior unit
0 0 0 0 $r-1
C -----
$ UNIT 3
C -----
1 0/-1. -3.0 +11.46 1.0 15.0
-1
410 0 0 0 1 0 0 0 1 0 0
6 6 6 3
0 $q-1 no loads - interior unit
0 0 0 0 $R-1
C -----
$ UNIT 4
C -----
1 0/1. -3.0 -11.46 1.0 15.0
-1
410 0 0 0 1 0 0 0 0 1 0
3 6 6 6
0 $q-1 no loads - interior unit
0 0 0 0 $r-1
C -----
$ UNIT 5
C -----
1 0/1. -3.0 +11.46 1.0 15.0
-1
410 0 0 0 1 0 0 0 0 1 0
3 6 6 6
0 $q-1 no loads - interior unit
0 0 0 0 $r-1
C -----
$ UNIT 6
C -----
1 0/-1. 3.0 -11.46 1.0 15.0
-1
410 0 0 0 1 0 0 0 1 0 0
6 6 6 3
0 $q-1 no loads - interior unit
0 0 0 0 $r-1
C -----

```



```

$ UNIT 7
C -----
1 0/-1. -3.0 -11.46 1.0 15.0
-1
410 0 0 0 1 0 0 0 1 0 0
6 6 6 3
0 $q-1 no loads - interior unit
0 0 0 0 $r-1
C -----
$ UNIT 8
C -----
1 0/1. 3.0 -11.46 1.0 15.0
-1
410 0 0 0 1 0 0 0 0 1 0
3 6 6 6
0 $q-1 no loads - interior unit
0 0 0 0 $r-1
C -----
$ unit 9 left side of shell
C -----
5 0 $M-1
-3.0 3.0 11.46 26.74 15.0 $m-2
-1 $m-5 shell wall fabrication
410 0 0 $n-1
6 0 6 6 $p-1
110 101 $p-2 knife edge BC at theta=+60 deg
0 $q-1 no load
0 0 $r-1
C -----
$ unit 10 bottom of shell
C -----
5 0 $M-1
-7.0 -3.0 -26.74 26.74 15.0 $m-2
-1 $m-5 shell wall fabrication
410 0 3 $n-1
15.28 22.92 15.28 $n-5 y-segment lengths
5 10 5 $n-6 y-segment spacing
2 0 6 0 $p-1 clamped at x=-6
110 101 $p-2 knife edge BC at theta=+60 deg
110 101 $p-2 knife edge BC at theta=-60 deg
0 $q-1 no load
0 0 $r-1
C -----
$ unit 11 right side of shell
C -----
5 0 $M-1
-3.0 3.0 -26.74 -11.46 15.0 $m-2
-1 $m-5 shell wall fabrication
410 0 0 $n-1
6 6 6 0 $p-1
110 101 $p-2 knife edge BC at theta=-60 deg
0 $q-1 no load
0 0 $r-1
C -----
$ unit 12 top of shell
C -----
5 0 $M-1
3.0 7.0 -26.74 26.74 15.0 $m-2
-1 $m-5 shell wall fabrication
410 0 3 $n-1
15.28 22.92 15.28 $n-5 y-segment lengths
5 10 5 $n-6 y-segment spacing
6 0 0 0 $p-1

```

```

110 101 $p-2 knife edge BC at theta=+60 deg
100 000 $p-2 clamped except for applied u_0 at x=+6
110 101 $p-2 knife edge BC at theta=+60 deg
1 $q-1 applied end shortening
1 1 $q-2
-0.01 -1 1 6 0 $ q-3 applied u_0 across top at x=+6
0 0 0 0 0 0 1 $r-1
6 0 $r-2 selective displacements across the top

```

cp8.bin (for S2 processor)

This file contains the S2 input records for all the analyses performed on the panel (buckling, vibration, nonlinear static, transient dynamics, and nonlinear restart with load relaxation). Only the first set of commands is executed even though all records are read and echoed on input. In this manner, a record of all the analyses performed can be maintained in a single file.

```

Curved panel with central cutout - applied end shortening $a-1
C
C Nonlinear static restart after transient
C with load relaxation as a first step
C
3      1      5*0      -1      $B-1 ANALYSIS CONTROL
4.2 0.1 8.0          $C-1 LOAD MULTIPLIERS
422 4000 5 -20 1 1.0e-4 1.0 $d-1 strategy parameters
5 0 1 $et-1 do load relaxation and use previous solution as estimate
C
C Nonlinear transient dynamic solution control from static solution
C
6 1 0 0 0 0 0 -1 $b-1
4.14375 0.0 4.14375 $c-1
7 4000 10 -20 0 1.0e-4 $d-1
0.0 20.0 1.0e-4 100.0 901.335 1.11e-5 $e-1
0 4 1 0 0 1 0 $e-2
4.20 0.0 0.0 1000.0 1000.0 0.0 $e-3
C
C Nonlinear analysis - displ control
C
3 1 0 0 0 0 0 -1
1.0 0.2 8.0 $c-1
0 8000 10 -20 1 1.0e-4 $d-1
0 0 3 $et-1
C
C Nonlinear analysis - arc length control
C
3 1 0 0 0 0 0 -1
1.0 0.2 8.0 $c-1
0 8000 10 -20 0 1.0e-4 $d-1
0 0 3 $et-1
C
C Linear buckling analysis
C
1 1 1 0 0 0 0 -1 $b-1
1. 0. 1. $c-1
1000 1.0e-4 $d-2
4 $d-3
C
C Nonlinear static restart after transient
C with load relaxation as a first step
C
3      1      5*0      -1      $B-1 ANALYSIS CONTROL
4.50 0.1 8.0          $C-1 LOAD MULTIPLIERS
420 1000 5 20 1 1.0e-4 1.0 $d-1 strategy parameters
5 0 1 $et-1 do load relaxation and use previous solution as estimate

```

```

C
C Restart nonlinear analysis
C
3 1 0 0 0 0 0 -1
4.0 1.0 8.0 $c-1
28 8000 10 -20 0 1.0e-4 $d-1
0 0 3 $et-1
C
C Free vibration analysis
C
2 1 0 0 0 0 0 -1
1. 0. 1.
1000 1.0e-4 $d-2
4 $d-3

```

cp8.pin (for STAPL processor)

Curved panel with central cutout \$A-1

```
10 0 1 0 $PL-2 NPLOT,IPREP,IPRS,KDEV
```

```

C
C displacement plots for linear solution
C

```

```

2 0 1 0 0 0 0 1 $PL-3 KPLOT,NUNIT,ITEM,STEP,MODE,IFRNG,COLOR,ICOMP
0.0 3 0.0 $PL-5 DSCALE,NROTS,LWSCALE
1 20.0
2 30.0
3 90.0
2 0 1 0 0 0 0 2 $PL-3 KPLOT,NUNIT,ITEM,STEP,MODE,IFRNG,COLOR,ICOMP
0.0 3 0.0 $PL-5 DSCALE,NROTS,LWSCALE
1 20.0
2 30.0
3 90.0
2 0 1 0 0 0 0 3 $PL-3 KPLOT,NUNIT,ITEM,STEP,MODE,IFRNG,COLOR,ICOMP
0.0 3 0.0 $PL-5 DSCALE,NROTS,LWSCALE
1 20.0
2 30.0
3 90.0

```

```

C
C stress resultant plots for linear solution
C

```

```

2 0 5 0 0 0 0 1 $PL-3 KPLOT,NUNIT,ITEM,STEP,MODE,IFRNG,COLOR,ICOMP
-1.0 3 0.0 $PL-5 DSCALE,NROTS,LWSCALE
1 20.0
2 30.0
3 90.0
2 0 5 0 0 0 0 2 $PL-3 KPLOT,NUNIT,ITEM,STEP,MODE,IFRNG,COLOR,ICOMP
-1.0 3 0.0 $PL-5 DSCALE,NROTS,LWSCALE
1 20.0
2 30.0
3 90.0
2 0 5 0 0 0 0 3 $PL-3 KPLOT,NUNIT,ITEM,STEP,MODE,IFRNG,COLOR,ICOMP
-1.0 3 0.0 $PL-5 DSCALE,NROTS,LWSCALE
1 20.0
2 30.0
3 90.0

```

```

C
C buckling modes
C

```

```

2 0 4 0 1 0 0 3 $PL-3 KPLOT,NUNIT,ITEM,STEP,MODE,IFRNG,COLOR,ICOMP
0.0 3 0.0 $PL-5 DSCALE,NROTS,LWSCALE
1 20.0
2 30.0
3 90.0
2 0 4 0 2 0 0 3 $PL-3 KPLOT,NUNIT,ITEM,STEP,MODE,IFRNG,COLOR,ICOMP

```

```

0.0 3 0.0 $PL-5 DSCALE,NROTS,LWSCALE
1 20.0
2 30.0
3 90.0
2 0 4 0 3 0 0 3 $PL-3 KPLOT,NUNIT,ITEM,STEP,MODE,IFRNG,COLOR,ICOMP
0.0 3 0.0 $PL-5 DSCALE,NROTS,LWSCALE
1 20.0
2 30.0
3 90.0
2 0 4 0 4 0 0 3 $PL-3 KPLOT,NUNIT,ITEM,STEP,MODE,IFRNG,COLOR,ICOMP
0.0 3 0.0 $PL-5 DSCALE,NROTS,LWSCALE
1 20.0
2 30.0
3 90.0
C
C Nonlinear solution displacement plots
C
2 0 1 6 0 0 0 3 $PL-3 KPLOT,NUNIT,ITEM,STEP,MODE,IFRNG,COLOR,ICOMP
-1.0 3 0.0 $PL-5 DSCALE,NROTS,LWSCALE
1 20.0 / 2 30.0 / 3 90.0
2 0 1 9 0 0 0 3 $PL-3 KPLOT,NUNIT,ITEM,STEP,MODE,IFRNG,COLOR,ICOMP
-1.0 3 0.0 $PL-5 DSCALE,NROTS,LWSCALE
1 20.0 / 2 30.0 / 3 90.0
2 0 1 50 0 0 0 3 $PL-3 KPLOT,NUNIT,ITEM,STEP,MODE,IFRNG,COLOR,ICOMP
-1.0 3 0.0 $PL-5 DSCALE,NROTS,LWSCALE
1 20.0 / 2 30.0 / 3 90.0
2 0 1 100 0 0 0 3 $PL-3 KPLOT,NUNIT,ITEM,STEP,MODE,IFRNG,COLOR,ICOMP
-1.0 3 0.0 $PL-5 DSCALE,NROTS,LWSCALE
1 20.0 / 2 30.0 / 3 90.0
2 0 1 200 0 0 0 3 $PL-3 KPLOT,NUNIT,ITEM,STEP,MODE,IFRNG,COLOR,ICOMP
-1.0 3 0.0 $PL-5 DSCALE,NROTS,LWSCALE
1 20.0 / 2 30.0 / 3 90.0
2 0 1 300 0 0 0 3 $PL-3 KPLOT,NUNIT,ITEM,STEP,MODE,IFRNG,COLOR,ICOMP
-1.0 3 0.0 $PL-5 DSCALE,NROTS,LWSCALE
1 20.0 / 2 30.0 / 3 90.0
2 0 1 400 0 0 0 3 $PL-3 KPLOT,NUNIT,ITEM,STEP,MODE,IFRNG,COLOR,ICOMP
-1.0 3 0.0 $PL-5 DSCALE,NROTS,LWSCALE
1 20.0 / 2 30.0 / 3 90.0
2 0 1 424 0 0 0 3 $PL-3 KPLOT,NUNIT,ITEM,STEP,MODE,IFRNG,COLOR,ICOMP
-1.0 3 0.0 $PL-5 DSCALE,NROTS,LWSCALE
1 20.0 / 2 30.0 / 3 90.0
2 0 1 428 0 0 0 3 $PL-3 KPLOT,NUNIT,ITEM,STEP,MODE,IFRNG,COLOR,ICOMP
-1.0 3 0.0 $PL-5 DSCALE,NROTS,LWSCALE
1 20.0 / 2 30.0 / 3 90.0

```

Problem References

Hilburger, M. W. and Starnes, J. H., Jr., "Effects of Imperfections on the Buckling Response of Compression-Loaded Composite Shells," *International Journal of Non-Linear Mechanics*, Vol. 37, Nos. 4-5, June-July 2002, pp. 623-643.

Stein, M., *The Phenomenon of Change in Buckle Pattern in Elastic Structures*, NASA Technical Report R-39, 1959.

Supple, W. J., "Couple Branching Configurations in the Elastic Buckling of Symmetric Structural Systems," *International Journal of Mechanical Sciences*, Vol. 9, No. 2, 1967, pp. 97-112.

Supple, W. J., "On the Change in Buckle Pattern of Elastic Structures," *International Journal of Mechanical Sciences*, Vol. 10, 1968, pp. 737-745.

Supple, W. J., "Changes of Wave-Form of Plates in the Post-Buckling Range," *International Journal of Solid and Structures*, Vol. 6, No. 9, 1970, pp. 1243-1258.

Riks, E, Rankin, C. C., and Brogan, F. A., *The Numerical Simulation of the Collapse Process of Axially Compressed Cylindrical Shells with Measured Imperfections*, Delft University of Technology, Faculty of Aerospace Engineering, Report No. LR-705, 1993.

Riks, E, Rankin, C. C., and Brogan, F. A., "On the Solution of Mode Jumping Phenomena in Thin-Walled Shell Structures," *Computer Methods in Applied Mechanics and Engineering*, Vol. 136, Nos. 1-2, September 1996, pp. 59-92.

Riks, E. and Rankin, C. C., "Computer Simulation of the Buckling Behavior of Thin Shells Under Quasi-Static Loads," *Archives of Computational Methods in Engineering*, Vol. 4, No. 4, 1997, pp. 325-351.

Tiwari, N. and Hyer, M. W., "Secondary Buckling of Compression-Loaded Composite Plates," AIAA Paper No. 96-1626-CP, April 1996.

Tiwari, N. and Hyer, M. W., "Secondary Buckling of Laminated Composite Plates," AIAA Paper No. 2000-1457, April 2000.

Fujii, F., Noguchi, H., and Ramm, E., "Static Path Jumping to Attain Postbuckling Equilibria of a Compressed Circular Cylinder," *Computational Mechanics*, Vol. 26, No. 3, September 2000, pp. 259-266.

Everall, P. R. and Hunt, G. W., "Mode Jumping in the Buckling of Struts and Plates: A Comparative Study," *International Journal of Non-Linear Mechanics*, Vol. 35, No. 6, November 2000, pp. 1067-1079.

Godoy, Luis A., *Theory of Elastic Stability – Analysis and Sensitivity*, Taylor and Francis, Philadelphia, PA, 2000, Chapter 14.

Knight, N. F., Jr. and Starnes, J. H., Jr., "Postbuckling Behavior of Axially Compressed Graphite-Epoxy Panels with Circular Holes," *ASME Journal of Pressure Vessel Technology*, Vol. 107, No. 4, November 1985, pp. 394-402.

Hilburger, M. W., *Numerical and Experimental Study of the Compression Response of Composite Cylindrical Shells with Cutouts*, Ph.D. Dissertation, Department of Aerospace Engineering, University of Michigan, Ann Arbor, MI, 1998.

Hilburger, M. W., Britt, V. O., and Nemeth, M. P., "Buckling Behavior of Compression-Loaded Quasi-Isotropic Curved Panels with a Circular Cutout," *International Journal of Solids and Structures*, Vol. 38, 2001, pp. 1495-1522.

Ambur, D. R., Jaunky, N., Davila, C. G., and Hilburger, M. W., "Progressive Failure Studies of Composite Panels with and without Cutouts," AIAA Paper No. 2001-1182, April 2001.

Knight, Norman F., Jr., *Enhancement of STAGS Progressive Failure Capability*, Contract No. GS-35F-4503G, Final Report for MRJ Task 1410, October 1999.

Progressive Failure Analysis of Postbuckled Shear Panel

Background

Thin-walled plates and shells often can carry loads well in excess of its buckling load determined from a linear bifurcation buckling analysis. The structural response for load levels below the buckling load is referred to as the primary solution or pre-buckling solution. It may be linear or nonlinear. Above the buckling load, the response is referred to as postbuckling behavior when the response is stable and collapse when the response is unstable. For these structures, the analyst needs to examine the role initial geometry imperfections and “generalized” imperfections if possible. Generalized imperfections include to surface imperfections, thickness variations, variations in lamination, fabrication inconsistencies, eccentricities in loading, and other aspects that cause the structure, its boundary conditions, and its loading to be less than ideal (e.g., see Hilburger and Starnes, 2002).

In addition local material failures may initiate and then propagate – progressive failure. Nonlinear finite element analyses accounting for such behavior are quite computationally intense due to the large number of material points that need to be examined for one or more failure modes. Recent works on postbuckled panels exhibiting a progressive failure response include Knight, Rankin, and Brogan (2000, 2001, 2002), Ambur, Jaunky, Davila, and Hilburger (2001), Ambur, Jaunky, and Hilburger (2002), Engelstad, Reddy and Knight (1992), Sleight, Knight and Wang (1997), and Baranski and Biggers (1999).

The postbuckling response of a flat composite panel loaded by in-plane shear shown in Figure 74 is studied. This configuration corresponds to Panel B2 tested by Rouse (1985a,b). The panel is 12-inches square and is clamped along all edges in a picture-frame test fixture. The corners are pinned so that a uniform diagonal-tension field develops prior to buckling. Constraints are imposed on the edges to keep the edges straight and yet allow the edges to rotate about a normal to the plane. The material is AS4/3502 graphite-epoxy, and the nominal material data and geometry are defined on Figure 74 using U.S. customary units and SI units.

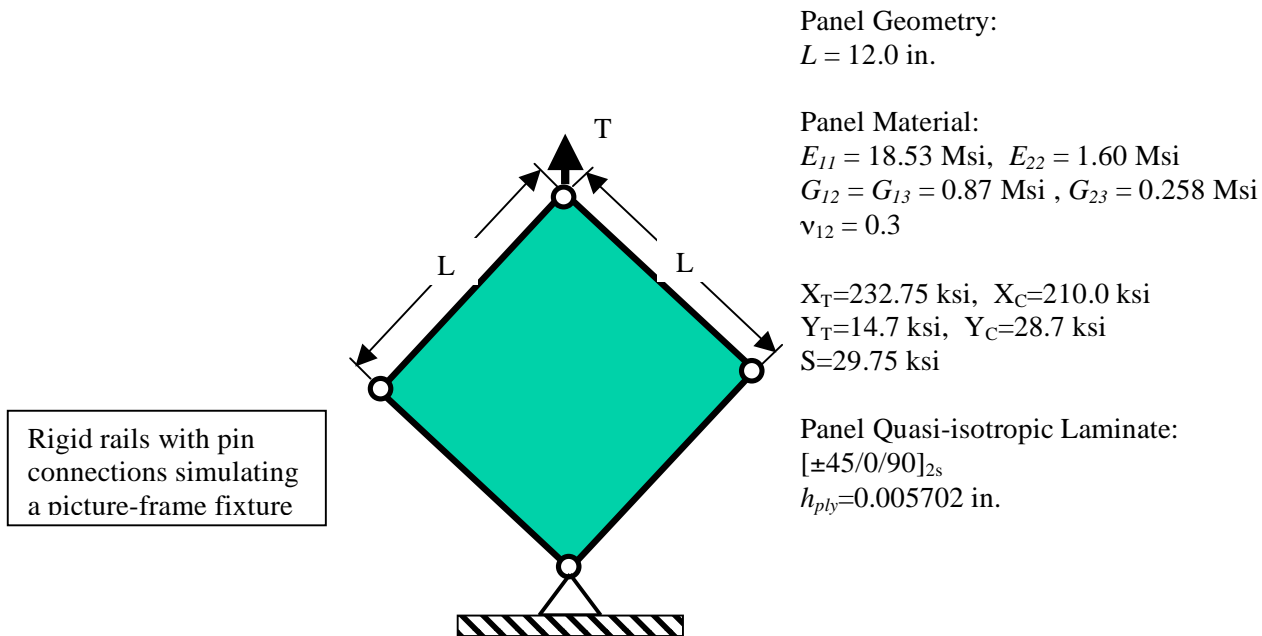


Figure 74. In-plane-shear-loaded flat panel: geometry and material properties.

Modeling and Analysis Process

The finite element model represents the entire panel with fifty 4-node E410 shell elements along each coordinate direction resulting in a total of 2500 4-node shell elements to model the entire panel. This finite element model is shown in Figure 75. The test fixture is not explicitly modeled; however, a series of constraints enforce a picture-frame-type in-plane loading. The behavior predicted by the finite element model is consistent with the test results.

Material properties and shell wall construction are defined using the GCP approach. Material modeling using the current GCP approach requires data on the I-5a and I-6a records to define the material properties and records I-5a, I-21a, I-21b, I-21c, I-21d, and I-21e to define the shell fabrication. The 16-ply quasi-isotropic laminate has a $[\pm 45/0/90]_{2s}$ stacking sequence and an average ply thickness of 0.005702 inches (based on measurements of the panel thickness). The progressive failure analysis will consider each layer to be represented individually with only a single integration point per layer. The E410 element has four surface-integration point and hence the number of material points to be examined for damage is given by the product of the number of elements which may experience damage (*i.e.*, those elements with an ORT_EL_BR GCP material type), the number of surface-integration points per element (*i.e.*, INTEG parameter on the N-1 record), the number of layers in the laminate (*i.e.*, NLAYERS on the I-21a record), and the number of through-the-thickness integration points per layer (*i.e.*, INTSHL on the I-21b record). For this finite element model of the square flat shear panel, the resulting multiplication corresponds to $2500 \times 4 \times 1 \times 16$ for a total of 160,000 material points.

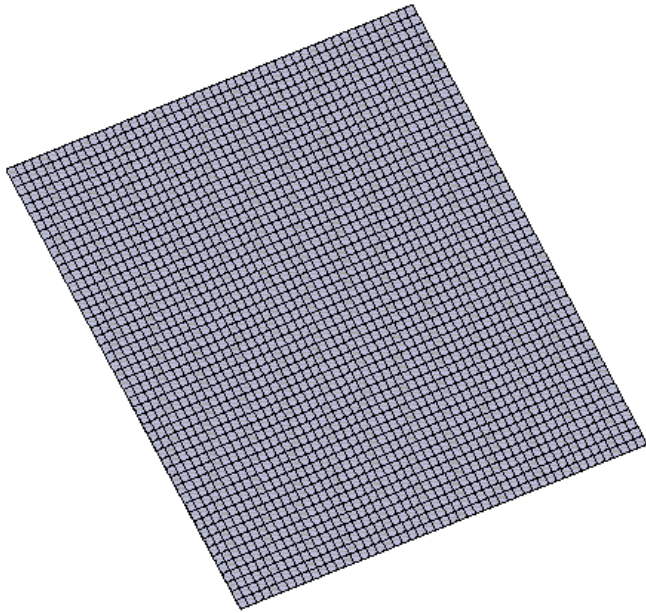


Figure 75. Finite element model of a shear panel using a 50×50 mesh of 4-node shell elements.

Boundary condition on the displacements are specified using the P-1 and P-2 records. An applied end displacement is specified across edge 1 on shell unit 1. The opposite end of the panel is clamped, the right edge of the finite element model is free, and the left edge has symmetric conditions imposed.

The edges of the panel are constrained to remain straight. Lagrangian constraints are written across the edge 1 ($x=0$) such that a linear variation in both in-plane displacement components results. Along row 1, the displacements vary linearly from zero at column 1 up to their values at column 51 (*i.e.*, assuming a model with 51 rows and 51 columns of nodes). Similar constraints are written along row 51 or edge 3. Partial compatibility constraints are defined along edge 2 that define uniform u and v displacements across that edge.

Numerical Results and Discussion

The panel was observed during the test to buckle into three halfwaves transverse to the diagonal-loading direction and one halfwave in the diagonal-loading direction. The diagonal-tension load at buckling T_{cr} and the diagonal load at failure are reported by Rouse (1985) to be 9,642 lbs. and 54,808 lbs. ($5.68 T_{cr}$), respectively. Rouse (1985) reported failure initiation along the fixture edges and then along the main diagonal of the panel where a severe displacement gradient developed. Panel failure occurred at a load nearly six times the buckling load in the test.

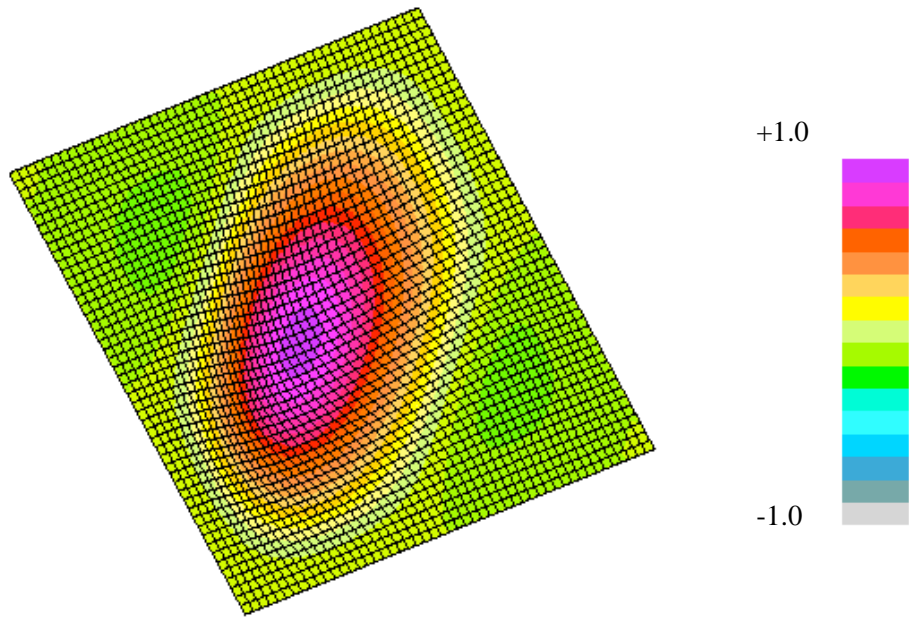
The analytical buckling load for this STAGS finite element model corresponds to a diagonal-tension load of 8,319 lbs. using nominal mechanical properties and NLIP equal to three (a value of 8,284 lbs is obtained for NLIP=1). Contour plots of the out-of-plane displacement component of the buckling mode shapes corresponding to the lowest two eigenvalues in shown in Figure 76. To initial the nonlinear postbuckling response for the flat panel, an initial geometric surface imperfection was generated using the

first buckling mode shape with a maximum amplitude equal to five percent of the panel thickness as shown in Figure 77. Note that STAGS normalizes the buckling modes by the largest component in the eigenvector (*i.e.*, the largest components will correspond to ± 1 ; typically an out-of-plane displacement degree of freedom has the maximum value in many applications).

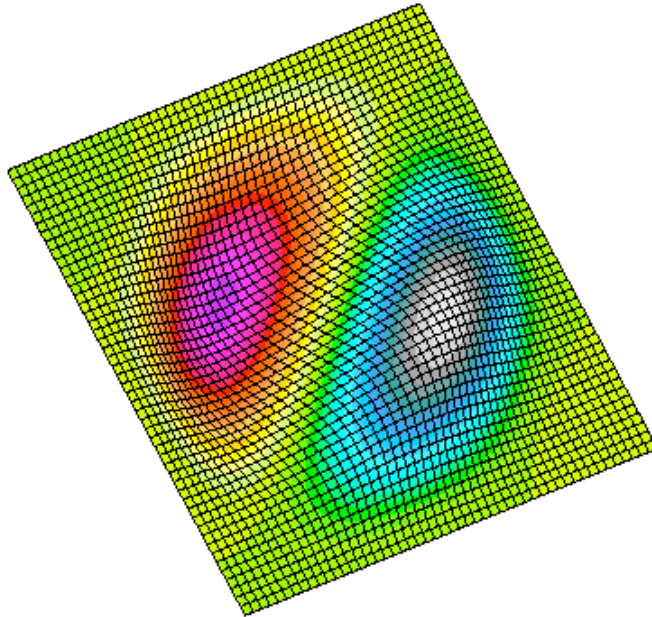
Nonlinear elastic analysis results and test results are shown on Figure 78. The out-of-plane displacement near the panel center normalized by the panel thickness as a function of the diagonal tension load is shown in Figure 78. The solid curve represents the test results and the elastic postbuckling analysis results are shown as a dashed curve. Good correlation is shown for the assumed initial imperfection shape and nominal elastic properties.

Nonlinear PFA analysis results were obtained using the maximum strain criteria and a small amount of artificial viscous damping. The out-of-plane displacement near the panel center normalized by the panel thickness as a function of the diagonal tension load is shown in Figure 78. Buckling occurs very early, and as the diagonal-tension load continues to increase, the buckles deep and the panel stiffens. Damage initiation (matrix tension failures) occurs at a diagonal-tension load of 44,324 lbs. (Step 21) in the corners. Damage progresses in the loaded diagonal corners first as shown in Figure 79. The plateau in load shown in Figure 78 is due to a rapid growth in damage along the edges near the corners. After some load redistribution, the load reaches a plateau at a value of 53,976 lbs. (Step 35). Along this plateau, damage propagates along the center buckle crest (Step 44). As the solution process continues, the extent of damage increases (*i.e.*, more damage through the thickness) and grows toward the opposite corners. This process is a slow process numerically as the material nonlinearity develops due to local discrete changes in material stiffness. Increasing the amount of artificial viscous damping may accelerate the process without changing the overall panel response.

A sequence of deformed geometry plots showing the percent ply damage by element is given in Figure 79. As mentioned previously, damage initiates in the loaded corners of the panel and first progresses along the edges before damage initiates along the crest of the center buckle. Damage grows along the center buckle crest and then transverse to the buckle crest until the computations are stopped.



(a) Mode 1 at 8,319 lbs.



(b) Mode 2 at 9,529 lbs.

Figure 76. Contour plots of the out-of-plane displacement component of the buckling mode shapes.

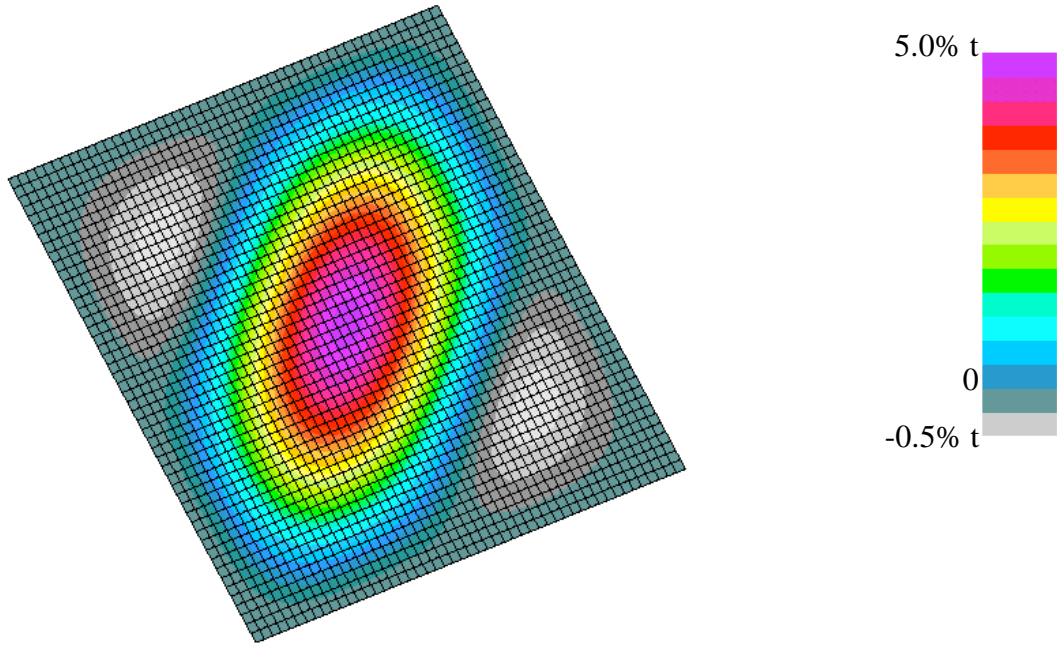


Figure 77. Contour plot of the initial surface imperfection formed from the first buckling mode shape with a maximum amplitude of 5% of the panel thickness.

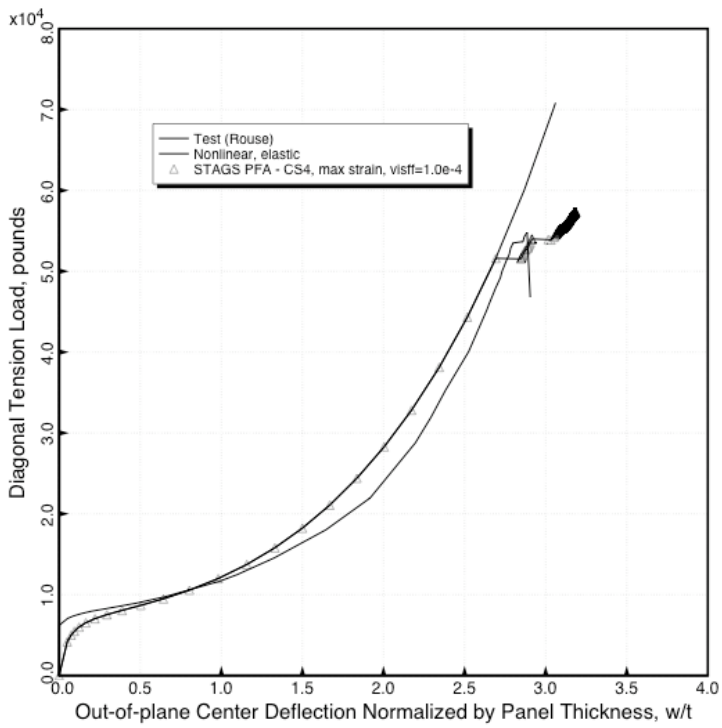
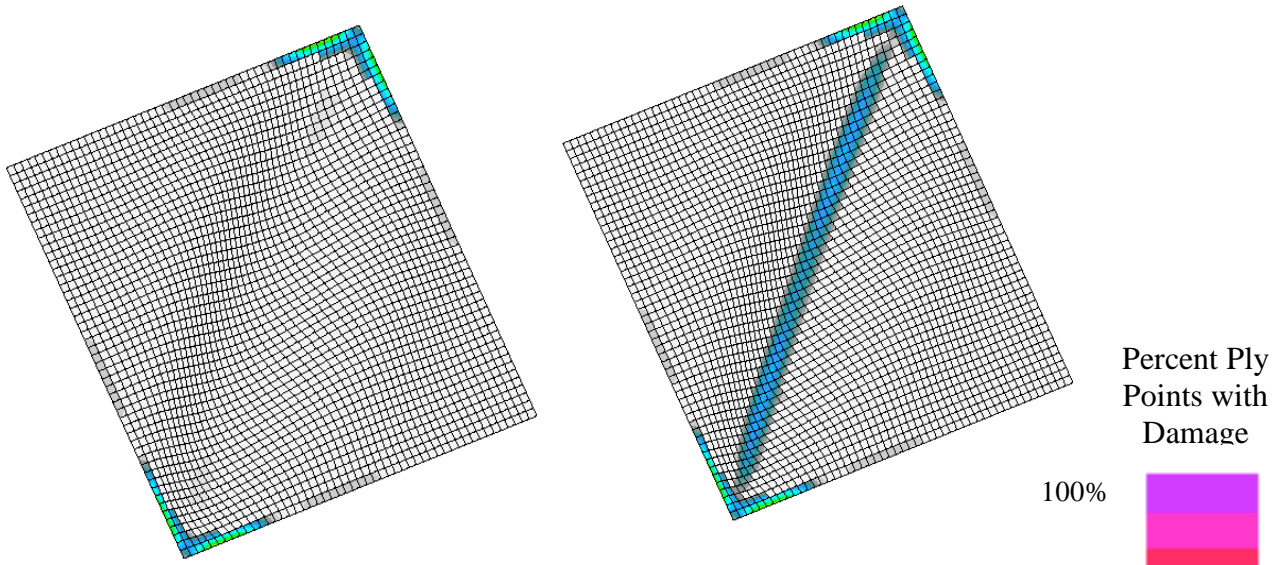
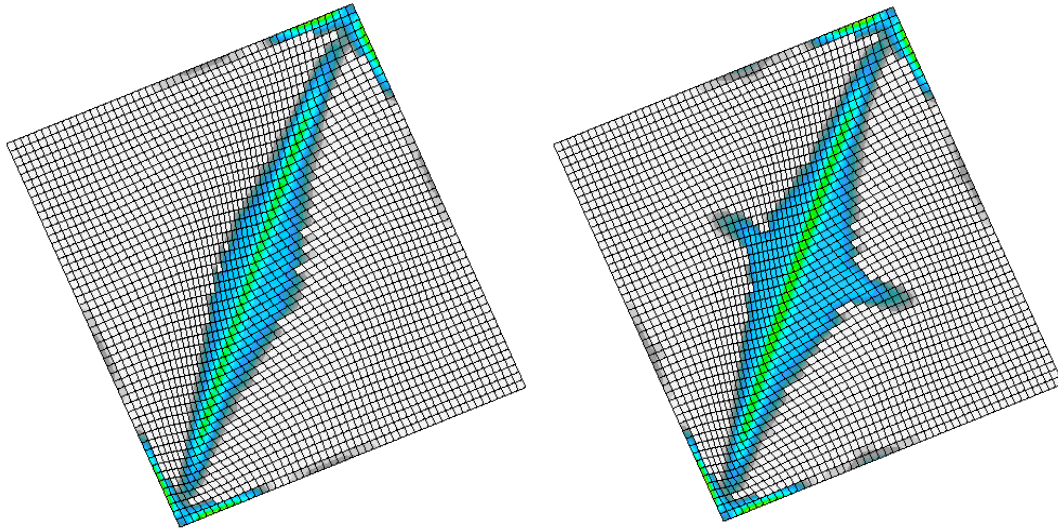


Figure 78. Diagonal-tension load versus out-of-plane deflection near panel center.



(a) Step 35 (52,976 lbs.) has 110 elements with damage (1,158 ply points)

(b) Step 44 (53,916 lbs.) has 324 elements with damage (2,945 ply points)



(c) Step 112 (55,358 lbs.) has 444 elements with damage (5,329 ply points)

(d) Step 395 (57,387 lbs.) has 687 elements with damage (9,060 ply points)

Figure 79. Percent ply points with damage for selected solution steps obtained using the maximum strain criteria. Total number of material points is 160,000.

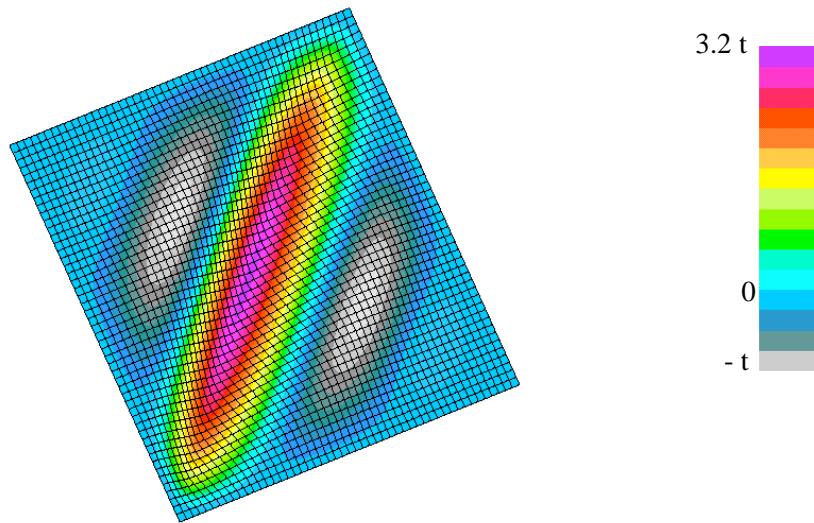


Figure 80. Contour plot of the out-of-plane deflection pattern for a solution step at the end of the simulation.

The deformation pattern of the postbuckled panel due to the in-plane shear loading is shown in Figure 80. The pattern has three halfwaves transverse to the diagonal tension loading and one halfwave along the diagonal tension loading direction.

STAGS Input Files

These STAGS input files are located under the following subdirectory:

\$STAGSHOME/Advanced-Testcases/Type-D-PFA

Typical Shell Element Model

b2.inp (for S1 processor)

```
Rouse B2 Panel with picture frame fixture and in-plane shear  $a-1
C
C Rouse, M., "Postbuckling of flat unstiffened graphite-epoxy
C plates in shear,", AIAA Paper No. 85-0771-CP, 1985.
C
0 0 1 0 0 0 0 $B-1 ANALYSIS TYPE
CC 3 45.0 $b-lb
1 1 0 0 5 -98 1 $B-2 MODEL SUMMARY
1 0 0 0 0 1 $B-3 DATA TABLE SUMMARY -> use gcp
0.45616E-2 0 1 0 $B-5 buckling mode imperfection 5% * thick * Mode 1
$ h=0.09123=16*0.005702
51 51 $F-1 GRID SUMMARY
1 1 51 1 1 0 51 1 $G-2 Keep Top edge straight--all U's the same
1 1 51 2 1 0 51 2 $G-2 Keep Top edge straight -- all V's the same
1 1 51 1 2 2 0 1 $G-2 At pin, force local node translations to be
$ equal, use rigid link to simulate beam
1 1 51 2 2 2 0 2 $G-2 --V
1 1 51 3 2 2 0 3 $ -- W
$ Keep left edge straight (x = 0, boundary line 1), but allow line
$ to rotate -- U and V handled simultaneously
2 2 0 0 0 1
```

```

1 1 51 1 .02e5 0
1 1 2 1 -1.e5 0
2 2 0 0 0 1
1 1 51 1 .04e5 0
1 1 3 1 -1.e5 0
2 2 0 0 0 1
1 1 51 1 .06e5 0
1 1 4 1 -1.e5 0
2 2 0 0 0 1
1 1 51 1 .08e5 0
1 1 5 1 -1.e5 0
2 2 0 0 0 1
1 1 51 1 .1e5 0
1 1 6 1 -1.e5 0
2 2 0 0 0 1
1 1 51 1 .12e5 0
1 1 7 1 -1.e5 0
2 2 0 0 0 1
1 1 51 1 .14e5 0
1 1 8 1 -1.e5 0
2 2 0 0 0 1
1 1 51 1 .16e5 0
1 1 9 1 -1.e5 0
2 2 0 0 0 1
1 1 51 1 .18e5 0
1 1 10 1 -1.e5 0
2 2 0 0 0 1
1 1 51 1 .2e5 0
1 1 11 1 -1.e5 0
2 2 0 0 0 1
1 1 51 1 .22e5 0
1 1 12 1 -1.e5 0
2 2 0 0 0 1
1 1 51 1 .24e5 0
1 1 13 1 -1.e5 0
2 2 0 0 0 1
1 1 51 1 .26e5 0
1 1 14 1 -1.e5 0
2 2 0 0 0 1
1 1 51 1 .28e5 0
1 1 15 1 -1.e5 0
2 2 0 0 0 1
1 1 51 1 .3e5 0
1 1 16 1 -1.e5 0
2 2 0 0 0 1
1 1 51 1 .32e5 0
1 1 17 1 -1.e5 0
2 2 0 0 0 1
1 1 51 1 .34e5 0
1 1 18 1 -1.e5 0
2 2 0 0 0 1
1 1 51 1 .36e5 0
1 1 19 1 -1.e5 0
2 2 0 0 0 1
1 1 51 1 .38e5 0
1 1 20 1 -1.e5 0
2 2 0 0 0 1
1 1 51 1 .4e5 0
1 1 21 1 -1.e5 0
2 2 0 0 0 1
1 1 51 1 .42e5 0
1 1 22 1 -1.e5 0
2 2 0 0 0 1

```

```
1 1 51 1 .44e5 0
1 1 23 1 -1.e5 0
2 2 0 0 0 1
1 1 51 1 .46e5 0
1 1 24 1 -1.e5 0
2 2 0 0 0 1
1 1 51 1 .48e5 0
1 1 25 1 -1.e5 0
2 2 0 0 0 1
1 1 51 1 .5e5 0
1 1 26 1 -1.e5 0
2 2 0 0 0 1
1 1 51 1 .52e5 0
1 1 27 1 -1.e5 0
2 2 0 0 0 1
1 1 51 1 .54e5 0
1 1 28 1 -1.e5 0
2 2 0 0 0 1
1 1 51 1 .56e5 0
1 1 29 1 -1.e5 0
2 2 0 0 0 1
1 1 51 1 .58e5 0
1 1 30 1 -1.e5 0
2 2 0 0 0 1
1 1 51 1 .6e5 0
1 1 31 1 -1.e5 0
2 2 0 0 0 1
1 1 51 1 .62e5 0
1 1 32 1 -1.e5 0
2 2 0 0 0 1
1 1 51 1 .64e5 0
1 1 33 1 -1.e5 0
2 2 0 0 0 1
1 1 51 1 .66e5 0
1 1 34 1 -1.e5 0
2 2 0 0 0 1
1 1 51 1 .68e5 0
1 1 35 1 -1.e5 0
2 2 0 0 0 1
1 1 51 1 .7e5 0
1 1 36 1 -1.e5 0
2 2 0 0 0 1
1 1 51 1 .72e5 0
1 1 37 1 -1.e5 0
2 2 0 0 0 1
1 1 51 1 .74e5 0
1 1 38 1 -1.e5 0
2 2 0 0 0 1
1 1 51 1 .76e5 0
1 1 39 1 -1.e5 0
2 2 0 0 0 1
1 1 51 1 .78e5 0
1 1 40 1 -1.e5 0
2 2 0 0 0 1
1 1 51 1 .8e5 0
1 1 41 1 -1.e5 0
2 2 0 0 0 1
1 1 51 1 .82e5 0
1 1 42 1 -1.e5 0
2 2 0 0 0 1
1 1 51 1 .84e5 0
1 1 43 1 -1.e5 0
2 2 0 0 0 1
```

```

1 1 51 1 .86e5 0
1 1 44 1 -1.e5 0
2 2 0 0 0 1
1 1 51 1 .88e5 0
1 1 45 1 -1.e5 0
2 2 0 0 0 1
1 1 51 1 .9e5 0
1 1 46 1 -1.e5 0
2 2 0 0 0 1
1 1 51 1 .92e5 0
1 1 47 1 -1.e5 0
2 2 0 0 0 1
1 1 51 1 .94e5 0
1 1 48 1 -1.e5 0
2 2 0 0 0 1
1 1 51 1 .96e5 0
1 1 49 1 -1.e5 0
2 2 0 0 0 1
1 1 51 1 .98e5 0
1 1 50 1 -1.e5 0
$ Keep right edge straight, same as above except for face #3
2 2 0 0 0 1
1 51 51 1 .02e5 0
1 51 2 1 -1.e5 0
2 2 0 0 0 1
1 51 51 1 .04e5 0
1 51 3 1 -1.e5 0
2 2 0 0 0 1
1 51 51 1 .06e5 0
1 51 4 1 -1.e5 0
2 2 0 0 0 1
1 51 51 1 .08e5 0
1 51 5 1 -1.e5 0
2 2 0 0 0 1
1 51 51 1 .1e5 0
1 51 6 1 -1.e5 0
2 2 0 0 0 1
1 51 51 1 .12e5 0
1 51 7 1 -1.e5 0
2 2 0 0 0 1
1 51 51 1 .14e5 0
1 51 8 1 -1.e5 0
2 2 0 0 0 1
1 51 51 1 .16e5 0
1 51 9 1 -1.e5 0
2 2 0 0 0 1
1 51 51 1 .18e5 0
1 51 10 1 -1.e5 0
2 2 0 0 0 1
1 51 51 1 .2e5 0
1 51 11 1 -1.e5 0
2 2 0 0 0 1
1 51 51 1 .22e5 0
1 51 12 1 -1.e5 0
2 2 0 0 0 1
1 51 51 1 .24e5 0
1 51 13 1 -1.e5 0
2 2 0 0 0 1
1 51 51 1 .26e5 0
1 51 14 1 -1.e5 0
2 2 0 0 0 1
1 51 51 1 .28e5 0
1 51 15 1 -1.e5 0

```


2	2	0	0	0	1
1	51	51	1	.3e5	0
1	51	16	1	-1.e5	0
2	2	0	0	0	1
1	51	51	1	.32e5	0
1	51	17	1	-1.e5	0
2	2	0	0	0	1
1	51	51	1	.34e5	0
1	51	18	1	-1.e5	0
2	2	0	0	0	1
1	51	51	1	.36e5	0
1	51	19	1	-1.e5	0
2	2	0	0	0	1
1	51	51	1	.38e5	0
1	51	20	1	-1.e5	0
2	2	0	0	0	1
1	51	51	1	.4e5	0
1	51	21	1	-1.e5	0
2	2	0	0	0	1
1	51	51	1	.42e5	0
1	51	22	1	-1.e5	0
2	2	0	0	0	1
1	51	51	1	.44e5	0
1	51	23	1	-1.e5	0
2	2	0	0	0	1
1	51	51	1	.46e5	0
1	51	24	1	-1.e5	0
2	2	0	0	0	1
1	51	51	1	.48e5	0
1	51	25	1	-1.e5	0
2	2	0	0	0	1
1	51	51	1	.5e5	0
1	51	26	1	-1.e5	0
2	2	0	0	0	1
1	51	51	1	.52e5	0
1	51	27	1	-1.e5	0
2	2	0	0	0	1
1	51	51	1	.54e5	0
1	51	28	1	-1.e5	0
2	2	0	0	0	1
1	51	51	1	.56e5	0
1	51	29	1	-1.e5	0
2	2	0	0	0	1
1	51	51	1	.58e5	0
1	51	30	1	-1.e5	0
2	2	0	0	0	1
1	51	51	1	.6e5	0
1	51	31	1	-1.e5	0
2	2	0	0	0	1
1	51	51	1	.62e5	0
1	51	32	1	-1.e5	0
2	2	0	0	0	1
1	51	51	1	.64e5	0
1	51	33	1	-1.e5	0
2	2	0	0	0	1
1	51	51	1	.66e5	0
1	51	34	1	-1.e5	0
2	2	0	0	0	1
1	51	51	1	.68e5	0
1	51	35	1	-1.e5	0
2	2	0	0	0	1
1	51	51	1	.7e5	0
1	51	36	1	-1.e5	0

```

2 2 0 0 0 1
1 51 51 1 .72e5 0
1 51 37 1 -1.e5 0
2 2 0 0 0 1
1 51 51 1 .74e5 0
1 51 38 1 -1.e5 0
2 2 0 0 0 1
1 51 51 1 .76e5 0
1 51 39 1 -1.e5 0
2 2 0 0 0 1
1 51 51 1 .78e5 0
1 51 40 1 -1.e5 0
2 2 0 0 0 1
1 51 51 1 .8e5 0
1 51 41 1 -1.e5 0
2 2 0 0 0 1
1 51 51 1 .82e5 0
1 51 42 1 -1.e5 0
2 2 0 0 0 1
1 51 51 1 .84e5 0
1 51 43 1 -1.e5 0
2 2 0 0 0 1
1 51 51 1 .86e5 0
1 51 44 1 -1.e5 0
2 2 0 0 0 1
1 51 51 1 .88e5 0
1 51 45 1 -1.e5 0
2 2 0 0 0 1
1 51 51 1 .9e5 0
1 51 46 1 -1.e5 0
2 2 0 0 0 1
1 51 51 1 .92e5 0
1 51 47 1 -1.e5 0
2 2 0 0 0 1
1 51 51 1 .94e5 0
1 51 48 1 -1.e5 0
2 2 0 0 0 1
1 51 51 1 .96e5 0
1 51 49 1 -1.e5 0
2 2 0 0 0 1
1 51 51 1 .98e5 0
1 51 50 1 -1.e5 0

```

```

$
$ H - 1 Element unit for single rigid link
$

```

```

2 1
1 0 0 $i-1
1.0E+7 0.3 $i-2

```

```

C -----

```

```

C Material Data for AS4/3502 Graphite Epoxy

```

```

C
C Elastic data only
C

```

```

ORTHOELAST_MATERIAL 1 1 1          $ I-5A GCP COMMAND RECORD
1.853E7 1.6E6 1.67E6,             $ I-10A E1, E2, E3
8.7E5 8.7E5 2.58E5,             $ I-10A G12, G13, G23
0.30 0.30 0.30,                 $ I-10A NU12, NU13, NU23
1.54e-4,                         $ I-10A MASS DENSITY
0.0 0.0 0.0 ,                   $ I-10A CTE'S
0.0 0.0 0.0 ,                   $ I-10A CHE'S
0.0 0.0                          $I-7A REF. TEMP AND REF. MOISTURE CONTENT
C

```

```

C Elastic data and PFA data for traditional failure criteria

```

```

C
ORT_EL_BR 2 1 1 $ I-5A GCP COMMAND RECORD
1.853E7 1.6E6 1.67E6, $ I-10A E1, E2, E3
8.7E5 8.7E5 2.58E5, $ I-10A G12, G13, G23
0.30 0.30 0.30, $ I-10A NU12, NU13, NU23
1.54e-4, $ I-10A MASS DENSITY
0. 0. 0. 0. 0. 0. 0. 0., $ I-10A CTEs, CHes, RT, RM
0.0 0.0 0.0 0.0 0.0, $ I-10A E1C, E1T, E2C, E2T, GAMMAF
0.0 0.0 0.0 0.0, $ I-10A E3C, E3T, GAM23F, GAM13F
210000. 232750., $ I-10A Xc, Xt
28700. 14700, $ I-10A Yc, Yt
29750., $ I-10A Sxy
28700. 14700., $ I-10A Zc, Zt
29750. 29750., $ I-10A Syz, Sxz
0.0 0.0 -1.E-6 1 1, $ I-10A alpha, F12, beta, IFAIL, IDGRD
1.0 1.0e-9 1.0e-4 $ I-10a visf0, visf1, visff

```

```

C
C 8-PLY [(pm45)_2]_s LAMINATE (Panel A2)
C

```

```

SHELL_FABRICATION 1 8 0 1 0 $ I-5A 8-PLY SYMMETRIC LAMINATE
8*1 $ I-21A MATID
8*0.005123 $ I-21C Layer thickness
+45.0 -45.0 +45.0 -45.0 , $ I-21D FAB. ORIENTATION ANGLES
-45.0 +45.0 -45.0 +45.0 $ I-21D FAB. ORIENTATION ANGLES
1.0 1.0 $I-21E SHEAR CORRECTION FACTORS

```

```

C
C 16-PLY [(pm45/0/90)_2]_s LAMINATE (Panel B2)
C

```

```

SHELL_FABRICATION 2 16 1 1 0 $I-5A 16-PLY SYMMETRIC LAMINATE
16*2 $I-21A MATID
16*1 $I-21A Number of layer integration points
16*0.005702 $I-21C LAYER THICKNESSES
+45.0 -45.0 0.0 90.0 , $I-21D
+45.0 -45.0 0.0 90.0 , $I-21D
90.0 0.0 -45.0 +45.0, $i-21d
90.0 0.0 -45.0 +45.0 $i-21d
1.0 1.0 $I-21E SHEAR CORRECTION FACTORS

```

```

SHELL_FABRICATION 3 16 0 1 0 $I-5A 16-PLY SYMMETRIC LAMINATE
16*1 $I-21A MATID
16*0.005702 $I-21C LAYER THICKNESSES
+45.0 -45.0 0.0 90.0 , $I-21D
+45.0 -45.0 0.0 90.0 , $I-21D
90.0 0.0 -45.0 +45.0, $i-21d
90.0 0.0 -45.0 +45.0 $i-21d
1.0 1.0 $I-21E SHEAR CORRECTION FACTORS

```

```

C
C 24-PLY [(pm45/0/90)_3]_s LAMINATE (Panel C4)
C

```

```

SHELL_FABRICATION 4 24 0 1 0 $I-5A 24-PLY SYMMETRIC LAMINATE
24*1 $I-21A MATID
24*0.005376 $I-21C LAYER THICKNESSES
+45.0 -45.0 0.0 90.0 , $I-21D
+45.0 -45.0 0.0 90.0 , $I-21D
+45.0 -45.0 0.0 90.0 , $I-21D
90.0 0.0 -45.0 +45.0, $i-21d
90.0 0.0 -45.0 +45.0, $i-21d
90.0 0.0 -45.0 +45.0 $i-21d
1.0 1.0 $I-21E SHEAR CORRECTION FACTORS

```

```

C
END $I-5A END GCP INPUT

```

```

C -----
2 0 $M-1 SHELL SURFACE DEFINITION - RECTANGULAR PLATE
0.0 12.0 0.0 12.0 $M-2 12-IN BY 12-IN. PLATE

```

```

-2 0          $M-5 SHELL WALL SELECTION -> USE GCP
410 0 0       $N-1 ELEMENT SELECTION, UNIFORM MESH
0 0 0 0       $P-1 BOUNDARY CONDITIONS GIVEN (0=FIXED; 1=FREE)
110 000       $P-2 X=0 EDGE
110 000       $P-2 Y=12 EDGE
110 000       $P-2 X=12 EDGE
000 000       $P-2 Y=0 EDGE
1 0 0         $Q-1 LOADING
1 1 0         $Q-2 LOAD SET
+5882.5094 1 1 1 51 0 $Q-3 Force component along +X axis
CC +0.0226239 -1 1 1 51 0 $Q-3 Displ component along +X axis
0 0 0 0 0 0 1 $R-1 OUTPUT FLAGS
0 51          $R-2 SELECTED OUTPUT ACROSS COLUMN 51
C
C One Rigid Link:
1 3*0 3*0. 000 001 $S-1
2 3*0 0. 12. 0. 110 001 $S-1
1 2 1 120 0
1.e3
0
0 0 0 0 0 0

```

b2.bin (for S2 processor)

```

Rouse shear panels with picture frame - Panel B2 $A-1
C nonlinear analysis options
3 1 0 4*0 -1 $b-1
0.50 .1 8.0 $c-1
0 8000 10 -20 0 1.e-4 $d-1
0 0 3 $et-1
c buckling analysis options
1 1 0 4*0 -1 $b-1
1.0 1.0 1.0 $c-1
1000 1.0e-4 1 $d-2
4 $d-3

```

b2.pin (for STAPL processor)

Rouse shear panels - Panel B2

5 0 0 \$PL-2 NPLOT,IPREP,IPRS,KDEV

C deformed shape

2 0 1 181 0 0 0 3 \$PL-3 KPLOT,VIEW,ITEM,STEP,MODE,IFRNG,COLOR,ICOMP

0 0.0 0.0 0.0 \$PL-5 DSCALE,NROTS,LWSCALE,RNGMIN,RGMAX

C percent ply damage for different load steps

2 0 8 34 0 0 0 0 \$PL-3 KPLOT,VIEW,ITEM,STEP,MODE,IFRNG,COLOR,ICOMP

0.0 0 0.0 0.0 0.0 \$PL-5 DSCALE,NROTS,LWSCALE,RNGMIN,RGMAX

2 0 8 40 0 0 0 0 \$PL-3 KPLOT,VIEW,ITEM,STEP,MODE,IFRNG,COLOR,ICOMP

0.0 0 0.0 0.0 0.0 \$PL-5 DSCALE,NROTS,LWSCALE,RNGMIN,RGMAX

2 0 8 112 0 0 0 0 \$PL-3 KPLOT,VIEW,ITEM,STEP,MODE,IFRNG,COLOR,ICOMP

0.0 0 0.0 0.0 0.0 \$PL-5 DSCALE,NROTS,LWSCALE,RNGMIN,RGMAX

2 0 8 181 0 0 0 0 \$PL-3 KPLOT,VIEW,ITEM,STEP,MODE,IFRNG,COLOR,ICOMP

0.0 0 0.0 0.0 0.0 \$PL-5 DSCALE,NROTS,LWSCALE,RNGMIN,RGMAX

C buckling modes

2 0 4 0 1 0 0 3 \$PL-3 KPLOT,VIEW,ITEM,STEP,MODE,IFRNG,COLOR,ICOMP

0.0 0 0.0 -1.0 +1.0 \$PL-5 DSCALE,NROTS,LWSCALE,RNGMIN,RGMAX

2 0 4 0 2 0 0 3 \$PL-3 KPLOT,VIEW,ITEM,STEP,MODE,IFRNG,COLOR,ICOMP

0.0 0 0.0 -1.0 +1.0 \$PL-5 DSCALE,NROTS,LWSCALE,RNGMIN,RGMAX

2 0 4 0 3 0 0 3 \$PL-3 KPLOT,VIEW,ITEM,STEP,MODE,IFRNG,COLOR,ICOMP

0.0 0 0.0 -1.0 +1.0 \$PL-5 DSCALE,NROTS,LWSCALE,RNGMIN,RGMAX

2 0 4 0 4 0 0 3 \$PL-3 KPLOT,VIEW,ITEM,STEP,MODE,IFRNG,COLOR,ICOMP

0.0 0 0.0 -1.0 +1.0 \$PL-5 DSCALE,NROTS,LWSCALE,RNGMIN,RGMAX

C Nxy distributions

2 0 5 30 0 0 0 3 \$PL-3 KPLOT,VIEW,ITEM,STEP,MODE,IFRNG,COLOR,ICOMP

0.0 0 0.0 0.0 4.5e3 \$PL-5 DSCALE,NROTS,LWSCALE,RNGMIN,RGMAX

2 0 5 40 0 0 0 3 \$PL-3 KPLOT,VIEW,ITEM,STEP,MODE,IFRNG,COLOR,ICOMP

0.0 0 0.0 0.0 4.5e3 \$PL-5 DSCALE,NROTS,LWSCALE,RNGMIN,RGMAX

Problem References

Hilburger, M. W. and Starnes, J. H., Jr., "Effects of Imperfections on the Buckling Response of Compression-Loaded Composite Shells," *International Journal of Non-Linear Mechanics*, Vol. 37, Nos. 4-5, June-July 2002, pp. 623-643.

Rouse, M., "Postbuckling of Flat Unstiffened Graphite-Epoxy Plates in Shear," AIAA Paper No. 85-0771-CP, 1985.

Rouse, M., *Postbuckling of Flat Unstiffened Graphite-Epoxy Plates in Shear*, Master's Thesis, School of Engineering and Applied Science, The George Washington University, Joint Institute for the Advancement of Flight Sciences, Hampton, VA, October 29, 1985.

Knight, Norman F., Jr., Rankin, Charles C., and Brogan, Frank A., "Controlling a Nonlinear Solution Procedure During a Progressive Failure Analysis," AIAA Paper No. 2000-1460, April 2000.

Knight, Norman F., Jr., Rankin, Charles C., and Brogan, Frank A., "Controlling a Progressive Failure Analysis using Artificial Viscous Damping," AIAA Paper No. 2001-1180, April 2001.

Knight, Norman F., Jr., Rankin, Charles C., and Brogan, Frank A., "STAGS Computational Procedure for Progressive Failure Analysis of Laminated Composite Structures," *International Journal of Non-Linear Mechanics*, Vol. 37, Nos. 4-5, June-July 2002, pp. 833-849.

Ambur, D. R., Jaunky, N., Davila, C. G., and Hilburger, M. W., "Progressive Failure Studies of Composite Panels with and without Cutouts," AIAA Paper No. 2001-1182, April 2001.

Ambur, D. R., Jaunky, N., and Hilburger, M. W., "Progressive Failure Studies of Stiffened Panels Subjected to Shear Loading," AIAA Paper No. 2002-1404, April 2002

Baranski, A. T. and Biggers, S. B., "Postbuckling Analysis of Tailored Composite Plates with Progressive Failure," *Composite Structures*, Vol. 46, 1999, pp. 245-255.

Sleight, D. W., Knight, N. F., Jr., and Wang, J. T., "Evaluation of a Progressive Failure Analysis Methodology for Laminated Composite Structures," AIAA Paper No. 97-1187, April 1997.

Engelstad, S. P., Reddy, J. N., and Knight, N. F., Jr., "Postbuckling Response and Failure Prediction of Graphite Epoxy Plates Loaded in Compression," *AIAA Journal*, Vol. 30, No. 8, August 1992, pp. 2106-2113.

Membrane Wrinkling Problems

Background

Research on ultra-thin membrane structures for space applications such as solar sails and sun shields is motivated by the need for advanced space propulsion concepts (see Leifer *et al.* (1997), Frisbee and Leifer (1998), and Garner *et al.* (2000, 2001)). One of the leading concepts is the solar sail concept using ultra-thin membrane films. The square solar sail architecture with separate triangular quadrants (Greschik and Mikulas (2001)) is being developed and ground tests at NASA Langley are planned (Garner *et al.* (2001)). State-of-the-art literature reviews for membrane structures have been published (Jenkins and Leonard (1991) and Jenkins (1996)) as well as a review of deployment simulations for inflatable structures (Jenkins (2001) and Fang (1999)). In addition, a recent monograph by Jenkins (2001) on gossamer structures has been published by AIAA covering mission, materials, structural mechanics, deployment and inflation, structural dynamics, and controls. Examples of NASA efforts in inflatable structures and ultra-thin membranes include antenna structures such as the IAE, NMP solar sail propulsion concepts, and NGST sunshields (*e.g.*, Salma *et al.* (2000), Freeland (2001), Smalley *et al.* (2001a, 2001b), Johnston (2002), Johnston and Lienard (2001), and Slade *et al.* (2001)). These efforts highlight the need for more advanced structural analysis tools for this class of structures.

Research topics in solar sail structures include efforts to predict and understand the influence of wrinkles on the performance of these structures (*e.g.*, Murphey *et al.* (1999, 2002), Talley *et al.* (2002)). While the formation of wrinkles in thin membrane structures is well known, only recently have researchers measured wrinkle amplitudes and wavelengths (*e.g.*, Jenkins *et al.* (1998), Blandino *et al.* (2001, 2002), Dharamsi *et al.* (2002)). Specialized experimental measurement procedures using non-contacting instrumentation such as photogrammetry are needed (Pappa *et al.* (2002)). Additional ground tests are either planned or underway and new data are anticipated (Garner *et al.* (2001)).

Analysis methods have generally fallen into one of two categories. The first category analyzes the structure as a membrane using a modified constitutive matrix so that no compression stresses are supported. Methods in this category generally predict the regions where wrinkling is anticipated to develop and average strains and displacements but give no information regarding the wrinkle amplitude or wavelength. The second category analyzes the structure as a very thin shell structure that exhibits general and local instability characteristics. Methods in this category typically apply finite element analysis methods to these thin structures and may need to adjust the nonlinear solution procedure in order to obtain converged solutions for wrinkled membranes.

Very early work on wrinkled membrane structures is tied to tension field theory. Stein and Hedgepeth (1961) presented an analytical approach for partly wrinkled membranes and demonstrated its capability on three basic configurations. The basic approach is to examine the principal stresses and determine whether or not a local region of the membrane is taut or slack. Mikulas (1964) extended this approach for pre-tensioned circular membranes with a central hub being twisted. Both examined global response functions and overall structural behavior for the partly wrinkled membranes rather than detailed examination of the wrinkles.

Moriya and Uemura (1971) extended the Stein-Hedgepeth approach (1961) using the finite element method to determine the boundary between wrinkled and unwrinkled regions. They applied the method to square panels in a picture-frame shear test fixture rather than ultra-thin membranes.

Haug and Powell (1971) developed a nonlinear finite element formulation for membrane structures with applications to fabric roof structures. They developed a complete finite element formulation for large

deformations. With regards to wrinkling, the principal stresses are examined. In addition, prestress elements are defined that exhibit an isotropic state of stress and are of constant thickness and thin. As a result these elements have geometric stiffness but no elastic stiffness. Limited applications were presented.

Miller *et al.* (1982, 1985) formulated an algorithm for partly wrinkled membrane from a finite element analysis perspective using Stein and Hedgepeth's approach. This model is often referred to as the Miller-Hedgepeth model; however, this approach is herein referred to as the Stein-Hedgepeth-Miller (or SHM) model to reflect contributions by each main contributor.

Tabarrok and Qin (1992) applied this wrinkling model to tension structures that were essentially tent structures for civil engineering applications. The emphasis of their work is on form finding, loads analysis and cutting patterns. Typically the civil engineering tension structure is not ultra-thin and hence the nonlinear analysis issue associated with non-convergence and singularities observed for solar sail applications were not detected.

Adler *et al.* (2000a, 2000b, 2001) incorporated the SHM model within the Iterative Membrane Properties (IMP) method and MSC/NASTRAN. Difficulties in controlling the nonlinear solution procedure and being limited to examining only an element centroid for wrinkling led to a subsequent implementation of the SHM model as a user-defined material or UMAT for HKS/ABAQUS. This UMAT implementation is commonly used by other investigators working on gossamer structures. However, this approach still only provides general information regarding the wrinkled region.

Roddean *et al.* (1987a, 1987b, 1991) formulated a large deformation finite element for planar membrane wrinkling analysis. This formulation is based on the use of a modified deformation tensor. The principal stresses determine whether a region is wrinkled, slack, or taut. A new membrane finite element was developed and tested on a membrane in shear.

Chiu *et al.* (1994) extended this formulation to account for thermal effects being motivated by the thermal printing process. Muttin (1996) further extended the Roddean model to curved membranes. The applications were then focused on sailboat sails, tension fabric structures, and airbags.

Contri and Schrefler (1988) used a total Lagrangian formulation for a geometrically nonlinear finite element analysis with a no-compression material model. The process involves a two-step procedure. The first step involves determining the equilibrium state of the membrane with both tensile and compressive stresses active. Once determined, the principal stresses are evaluated and compressive stresses eliminated. New tensile stresses are defined that maintain the same absolute value and direction of the principal tensile stress. These new trial stresses are then used in the nonlinear equilibrium iteration process. The method was demonstrated for an airbag inflation problem.

Kang and Im (1997) also start with the basic nonlinear finite element formulation for a membrane and incorporate the wrinkling criterion based on a combination of principal stresses and principal strains. Additionally a reconstruction of the stress update procedure during the nonlinear iteration process is presented which has an impact on the internal force vector and tangent stiffness matrix. Results are presented for a flat membrane and an airbag application. Wrinkled regions are identified; however, wrinkle amplitudes and wrinkle pattern wavelengths are not determined.

Yang and his colleagues (2001, 2002) have proposed an approach using a two-field variational statement for wrinkling predictions using first a bar-network approach and then for a two-dimensional membrane approach. He refers to it as a parameter variation principle or PVP. The total potential energy

formulation is augmented with a term having two parameters related to the wrinkle state. Results are shown to be in good correlation with test data for wrinkle pattern and wrinkle distribution.

Lee and Lee (2002) applied solid shell formulations to gossamer structures. Their approach dealt with near singularities stemming from these ultra-thin membranes. Two techniques were considered. The first technique scaled the material moduli by a factor related to the ratio of overall planar membrane size to membrane thickness (*i.e.*, L/t). The second technique involved performing the computations in “quadruple” precision. Both techniques essentially have the same effect in that the accuracy of their elements was extended to extremely thin structures. The implication may be that a judicious choice of units for the membrane geometry and material properties may alleviate some of the numerical issues.

Haseganu and Steigmann (1994) applied a dynamic relaxation solution procedure to partly wrinkled membranes and thereby avoided some of the quasi-static solution procedure problems associated with non-convergence and near singularities. Their formulation is based on the relaxed strain energy concept (Pipkin (1988, 1994)). Epstein and Forcinito (2001) have completed the formulation for anisotropic membrane wrinkling.

Liu, Jenkins, and Schur (2000) describe two levels of analysis for wrinkled membranes. The coarse-scale analysis uses a penalty parameter to degrade material stiffness if local wrinkling is detected. The wrinkling criterion associated with the SHM model is used for this step in combination with a UMAT and HKS/ABAQUS. Only general wrinkling behavior (regions and distributions) is obtained. The second level is the fine-scale analysis that provides details about the wrinkles. The fine-scale analysis extracts information from the coarse-scale analysis and assumes a uniform wrinkled zone (based on coarse-scale analysis). Within this zone wrinkle parameters are calculated in a global/local approach.

Wong (2000) and Wong and Pellegrino (2002a, 2002b) employed HKS/ABAQUS shell elements to simulate the membrane wrinkling response of the ultra-thin structures. Their approach differs from others using HKS/ABAQUS in that no UMAT is involved. Since the simulation is based on the use of shell elements rather than membrane elements, wrinkling details may be predicted including wrinkle amplitude and wavelength. A membrane with in-plane shear loading was analyzed by first performing the pre-stress calculation followed by a nonlinear equilibrium check, then a linear buckling analysis that provides the basis for initial geometric surface imperfections, and finally a nonlinear analysis of an imperfect (“wrinkled”) membrane. Convergence difficulties encountered in the nonlinear solution process were addressed using the automatic stabilization function available in HKS/ABAQUS. In addition, Wong and Pellegrino (2002a, 2002b) observed and predicted the changes in mode shape (mode jumping) as the in-plane shear loading increased. Loading and unloading of the membrane was also examined. Excellent correlation between test (Jenkins *et al.* (1998)) and analysis is shown for wrinkle details (number of wrinkles, amplitude, wavelength and angle).

Stanuszek (2002) membrane wrinkling is treated using a cable analogy – which is not clearly described. The finite element formulation is based on the natural approach of Argyris using a total Lagrangian formulation. Nonlinear continuum mechanics approach is used within membrane theory. Stanuszek (2002) comments that stochastic considerations are necessary for determining the number and distribution of folds and wrinkles.

The key developments related to finite element prediction for wrinkled membrane structures are represented by the works of Adler *et al.* (2000a, 2000b, 2001), Kang and Im (1997), Wong (2000), and Wong and Pellegrino (2002a, 2002b). The approach implemented in STAGS under this effort is to first study the Stein-Hedgepeth-Miller (SHM) membrane model since it is now widely used in the finite element analysis of gossamer structures. This model is applied to membrane structures to determine

overall behavior and regions susceptible to wrinkling rather than details of the wrinkles (*e.g.*, wrinkle wavelength, wrinkle height).

Modeling and Analysis Process

The basic concept behind the Stein-Hedgepeth-Miller model is to examine points within the thin membrane structure and determine the current stress state. Since the structure is ultra-thin, bending is often neglected and the stress state is assumed constant through the thickness at a given planar coordinate. Denoting the planar deformation field as the xy -plane and given the state of strain ($\epsilon_{xx}, \epsilon_{yy}, \gamma_{xy}$) at a material point in that plane, the principal strains (ϵ_1, ϵ_2) are determined from:

$$\epsilon_1, \epsilon_2 = \frac{\epsilon_{xx} + \epsilon_{yy}}{2} \pm \sqrt{\left(\frac{\epsilon_{xx} - \epsilon_{yy}}{2}\right)^2 + \left(\frac{\gamma_{xy}}{2}\right)^2}$$

where the subscript 1 denotes major principal value and subscript 2 denotes the minor principal value. The orientation of the principal axes relative to x -axis is obtained from:

$$\tan 2\alpha = \frac{\gamma_{xy}}{\epsilon_{xx} - \epsilon_{yy}}$$

The stress state at that material point can be determined using the strain state and the generalized Hooke's law for an isotropic linear elastic material:

$$\begin{Bmatrix} \sigma_{xx} \\ \sigma_{yy} \\ \sigma_{xy} \end{Bmatrix} = \begin{bmatrix} Q_{11} & Q_{12} & Q_{16} \\ Q_{12} & Q_{22} & Q_{26} \\ Q_{16} & Q_{26} & Q_{66} \end{bmatrix} \begin{Bmatrix} \epsilon_{xx} \\ \epsilon_{yy} \\ \gamma_{xy} \end{Bmatrix}$$

where

$$Q_{11} = Q_{22} = \frac{E}{1 - \nu^2}$$

$$Q_{12} = \frac{\nu E}{1 - \nu^2}$$

$$Q_{66} = G = \frac{E}{2(1 + \nu)}$$

$$Q_{16} = Q_{26} = 0$$

and E is the elastic or Young's modulus and ν is Poisson's ratio. Given this plane stress state, the principal stresses can be calculated according to:

$$\sigma_1, \sigma_2 = \frac{\sigma_{xx} + \sigma_{yy}}{2} \pm \sqrt{\left(\frac{\sigma_{xx} - \sigma_{yy}}{2}\right)^2 + (\sigma_{xy})^2}$$

where the subscript 1 denotes major principal value and subscript 2 denotes the minor principal value. The orientation of the principal axes relative to x -axis is obtained from:

$$\tan 2\beta = \frac{2\sigma_{xy}}{\sigma_{xx} - \sigma_{yy}}$$

The Stein-Hedgepeth-Miller model then examines these principal stress values and modifies the local constitutive relations for the membrane. Kang and Im (1997), Wong (2000), and Adler (2000) consider three criteria to define the membrane state: stress criteria; strain criteria; and a combined or mixed stress-strain criteria. While similar in concept, the actual criteria are slightly different and six different ones are implemented. The first three follow Wong (2000) and the next three follow Adler (2000). These criteria are:

- Wong (2000) stress criteria based on principal stresses (IWRINK=1)
 - Taut state: $\sigma_2 > 0$
 - Slack state: $\sigma_1 \leq 0$ and $\sigma_2 \leq 0$
 - Wrinkled state: $\sigma_1 > 0$ and $\sigma_2 \leq 0$
- Wong (2000) strain criteria based on principal strains (IWRINK=2)
 - Taut state: $\varepsilon_2 > 0$
 - Slack state: $\varepsilon_1 \leq 0$ and $\varepsilon_2 \leq 0$
 - Wrinkled state: $\varepsilon_1 > 0$ and $\varepsilon_2 \leq 0$
- Wong (2000) mixed stress-strain criteria based on both principal stresses and principal strains (IWRINK=3)
 - Taut state: $\sigma_2 > 0$
 - Slack state: $\varepsilon_1 \leq 0$ and $\sigma_1 \leq 0$
 - Wrinkled state: $\varepsilon_1 > 0$ and $\sigma_2 \leq 0$
- Adler (2000) stress criteria based on principal stresses (IWRINK=4)
 - Taut state: $\sigma_2 > 0$
 - Slack state: $\sigma_1 \leq 0$
 - Wrinkled state: $\sigma_1 > 0$ and $\sigma_2 \leq 0$
- Adler (2000) strain criteria based on principal strains (IWRINK=5)
 - Taut state: $\varepsilon_1 > 0$ and $\varepsilon_2 > -\nu\varepsilon_1$
 - Slack state: $\varepsilon_1 \leq 0$
 - Wrinkled state: $\varepsilon_1 > 0$ and $\varepsilon_2 \leq -\nu\varepsilon_1$
- Adler (2000) mixed stress-strain criteria based on both principal stresses and principal strains (IWRINK=6)
 - Taut state: $\sigma_2 > 0$
 - Slack state: $\varepsilon_1 \leq 0$
 - Wrinkled state: $\varepsilon_1 > 0$ and $\sigma_2 \leq 0$

Of these criteria, the mixed stress-strain criteria appear to be the more commonly accepted criteria. Once the membrane state is determined at a material point, the constitutive model for the material point is set accordingly:

$$Q_{ij} = \begin{cases} Q_{ij}^{slack} & \dots \text{slack state} \\ Q_{ij}^{wrinkle} & \dots \text{wrinkled state} \\ Q_{ij}^{taut} & \dots \text{taut state} \end{cases}$$

For the slack behavior, the constitutive coefficients are set to a penalty factor κ (input parameter PENLTY) that is typically a very small number approaching zero and are given by:

$$[Q^{slack}] = \kappa \begin{bmatrix} 1 & 1 & 1 \\ 1 & 1 & 1 \\ 1 & 1 & 1 \end{bmatrix}$$

For the taut behavior, the constitutive coefficients are the original plane stress values for a linear elastic, isotropic material given by:

$$[Q^{taut}] = \frac{E}{1 - \nu^2} \begin{bmatrix} 1 & \nu & 0 \\ \nu & 1 & 0 \\ 0 & 0 & \frac{1 - \nu}{2} \end{bmatrix}$$

For the wrinkled behavior, the constitutive coefficients are changed and are given by:

$$[Q^{wrinkle}] = \frac{E}{4} \begin{bmatrix} 2(1 + P) & 0 & Q \\ 0 & 2(1 - P) & Q \\ Q & Q & 1 \end{bmatrix}$$

$$\text{where } P = \cos 2\alpha = \frac{\epsilon_{xx} - \epsilon_{yy}}{\epsilon_1 - \epsilon_2} \text{ and } Q = \sin 2\alpha = \frac{\gamma_{xy}}{\epsilon_1 - \epsilon_2}$$

The wrinkling process is considered to be an elastic process where wrinkles may form and then disappear if the local stress state at a material point would permit it.

This material model can be used with membrane elements (constraint all bending degrees of freedom to zero using the Q-records) and also with plate/shell elements. Within STAGS, membrane behavior is modeled by constraining all out-of-plane deformation degrees of freedom (transverse displacement and two bending rotations) using the loading records (Q-records). The E410 shell element uses the “drilling degree of freedom” to increase the order of the in-plane displacement field approximations; the E480 and E330 shell elements do not have this freedom and so it must also be constrained. Using this material model with plate/shell elements means that the local material stiffness terms are modified in the same way based on the wrinkling criteria and in addition, the bending stiffness terms are computed and used in the stiffness matrix evaluation.

The basic computation process for each iteration of a nonlinear solution step starts with a given estimate of the displacement solution for the current iteration. Then within the loop over the number of elements in the finite element model, the local element strain resultants are computed at each element surface integration point. Then point strains through the thickness are computed – even though the membrane is

very thin. The membrane strains are examined and principal values computed. Stresses are computed either using the original plane stress values that assumes the membrane is taut or using the values extracted from the historical material database. The principal values are used to determine the state of the membrane (taut, slack, or wrinkled). The default criteria will be the stress-strain or mixed criteria. However, the stress criteria and the strain criteria will also be implemented as options to be used for comparisons.

Once the membrane state is determined, then the constitutive coefficients are evaluated and new trial stresses are computed. The constitutive coefficients (Q_{11} , Q_{12} , Q_{16} , Q_{22} , Q_{26} , Q_{66}), principal strains (ϵ_1 , ϵ_2), principal angle for strains (α), principal stresses (σ_1 , σ_2), principal angle for stresses (β), and the membrane state variable (M_{state}) are archived, upon convergence for this solution step, to the historical material database for this material point – thirteen words per material point. This record is written for every material that has changed from an initially taut state to any other state – even when it possibly returns to a taut state. As long as the membrane state remains in its initially taut state, no data are written to historical material database for that material point. Once all elements are evaluated, the iteration process is continued until no compressive regions are found and convergence is achieved.

Numerical Results and Discussion

Pellegino Rectangular Membrane:

The first problem is the rectangular membrane loaded by in-plane shearing displacement studied by Wong (2000) and Wong and Pellegrino (2002a, 2002b). Finite element results are available for comparison. The basic geometry and initial finite element model are shown in Figure 81. The finite element mesh is uniform having 3960 (99×40) 4-node elements. The STAGS input files are also listed.

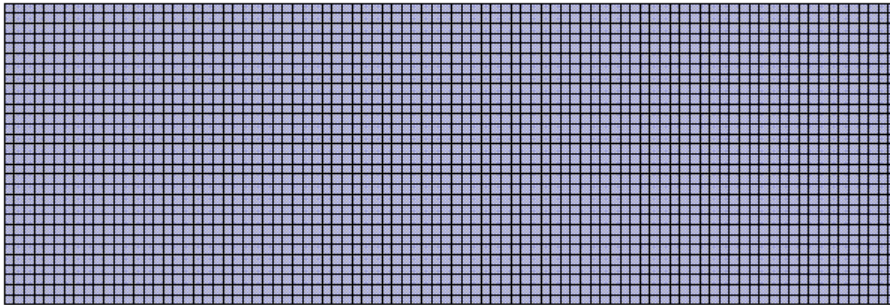


Figure 81. Initial finite element of rectangular membrane loaded by in-plane shear.

The rectangular membrane has dimensioned of 128 mm by 380 mm and an assumed uniform thickness of 0.025 mm. The material is a Kapton foil with an elastic modulus of 3530 N/mm², a Poisson’s ratio of 0.3, and a mass density of 1.5×10⁻⁶ kg/mm³. The bottom edge is completely restrained, the side edges are free, and the top edge is loaded. The loading has two stages. First, a pre-tensioned stretching of the membrane is done by imposing an edge displacement (normal to the top edge) of 0.5 mm. Then from this pre-tensioned state, a shearing displacement (parallel to the top edge) is imposed and increased to a maximum value of 3.0 mm.

The simulation is performed in two stages. First, a pre-tensioning vertical displacement is imposed in two solution steps (Load Set B). Then a shearing horizontal displacement is imposed over several solution steps (Load Set A). Contour plots of the wrinkle indicator are shown in Figures 82 and 83. Results for the pre-tensioning state are given in Figure 82 and indicate only minor edge wrinkling. Then the shearing

displacement is superimposed with the pre-tensioning displacement and the results are shown in Figure 83. The wrinkle region extends from the free vertical edges very quickly until the entire membrane is wrinkled – quantitatively consistent with the available results.

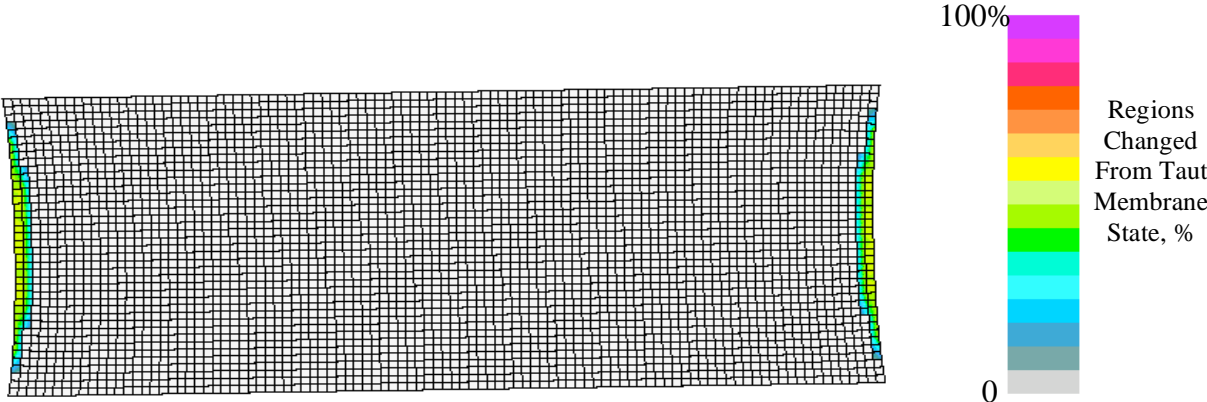
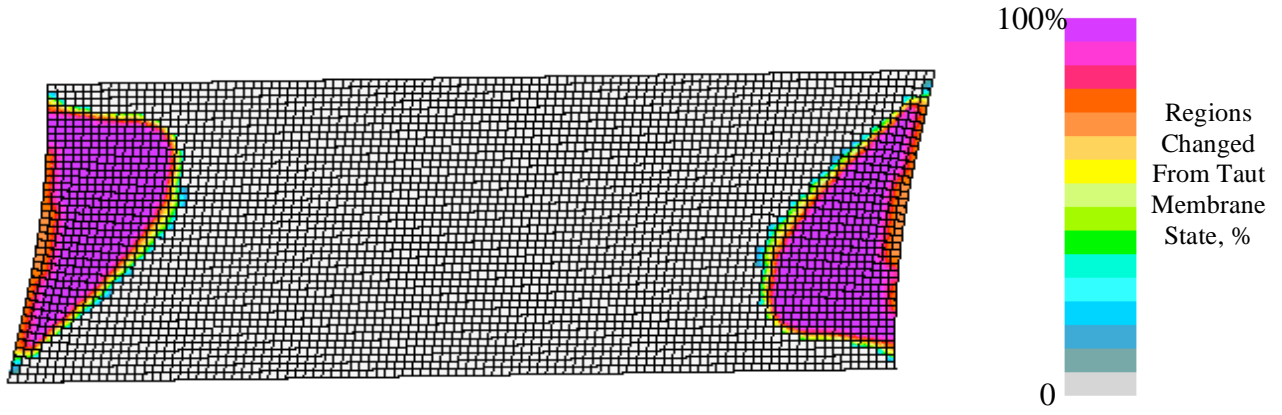
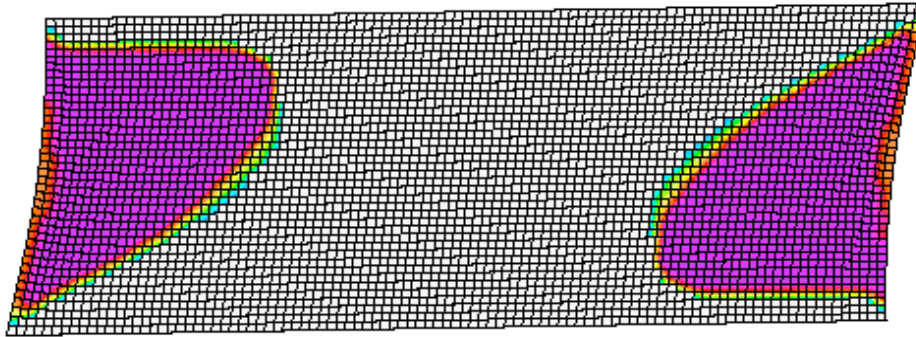


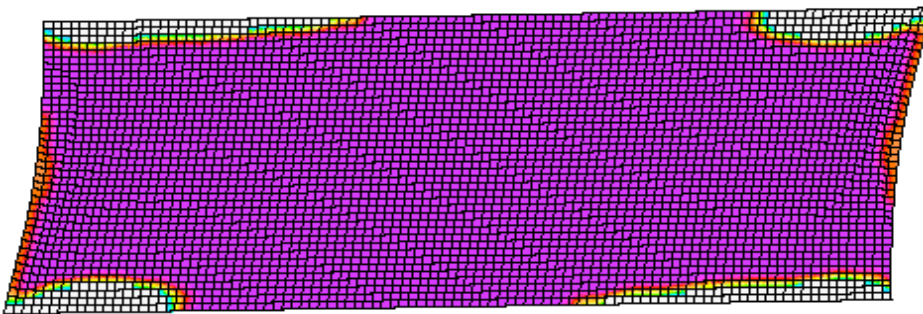
Figure 82. Contour plot of wrinkling indicator for the pre-tensioning step (Step 2, PA=0.0, PB=1.0, 112 affected elements).



(a) Step 3, PA=0.20, PB=1.0, 826 affected elements.

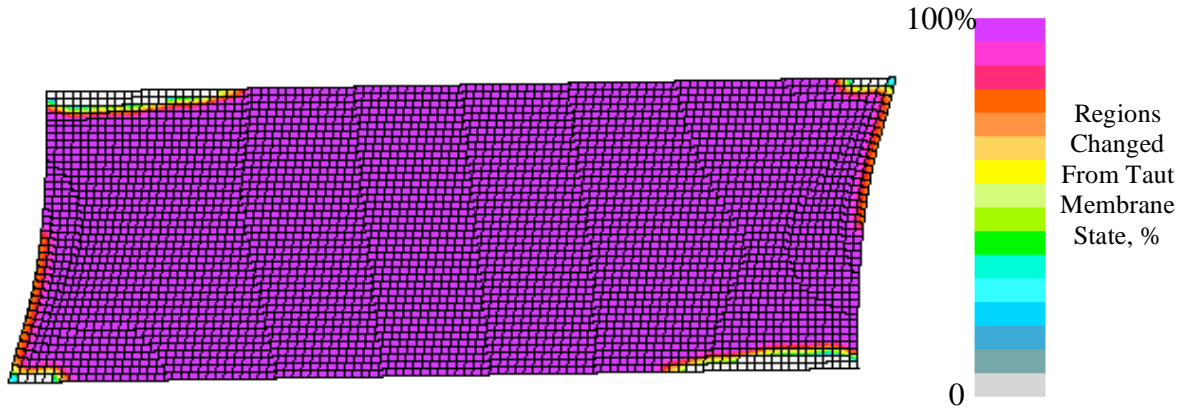


(b) Step 4, PA=0.24, PB=1.0, 1465 affected elements.

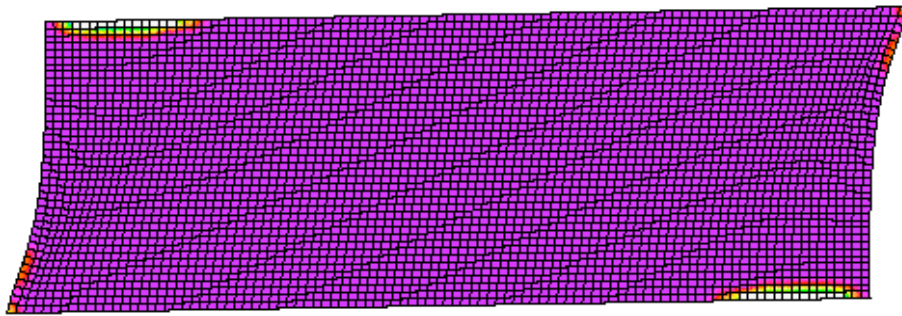


(c) Step 5, PA=0.28, PB=1.0, 3730 affected elements.

Figure 83. Contour plot of wrinkling indicator for the pre-tensioning step



(d) Step 8, PA=0.40, PB=1.0, 3886 affected elements.



(e) Step 10, PA=1.0, PB=1.0, 3900 affected elements.

Figure 83. Concluded.

Square Solar Sail

The second problem is related to the NASA effort in solar sail propulsion concepts. One of the square sail architectures defined by Greschik and Mikulas (2001) has four separate triangular quadrants. Ground testing at NASA Langley is underway for a 10-m solar sail testbed (Slade *et al.* (2002)) (a two quadrant model including a center boom). The basic geometry and initial finite element model of a scaled 200-mm model are shown in Figure 84.

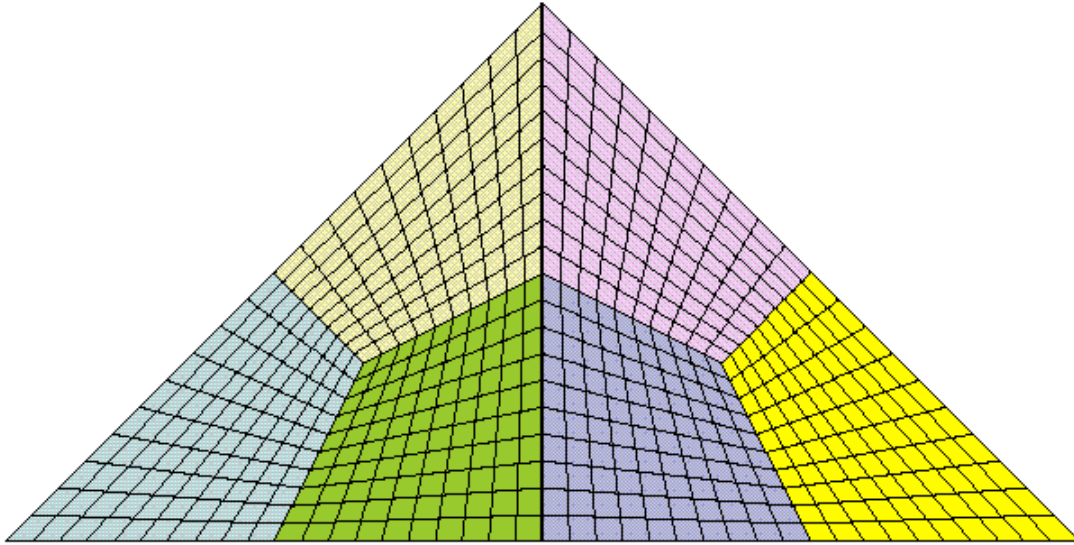
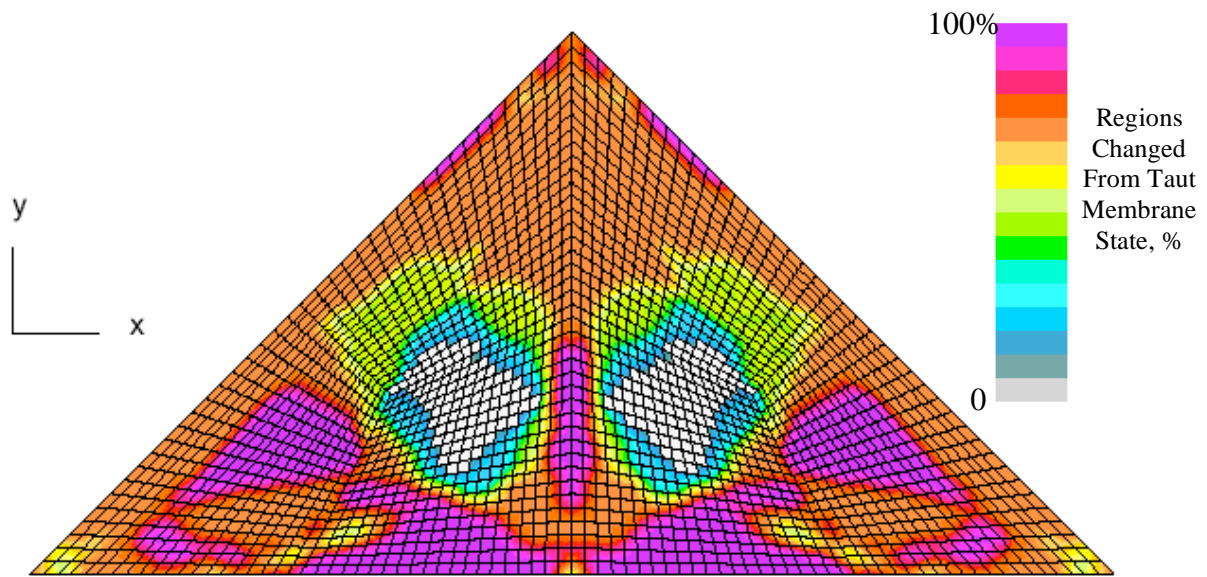


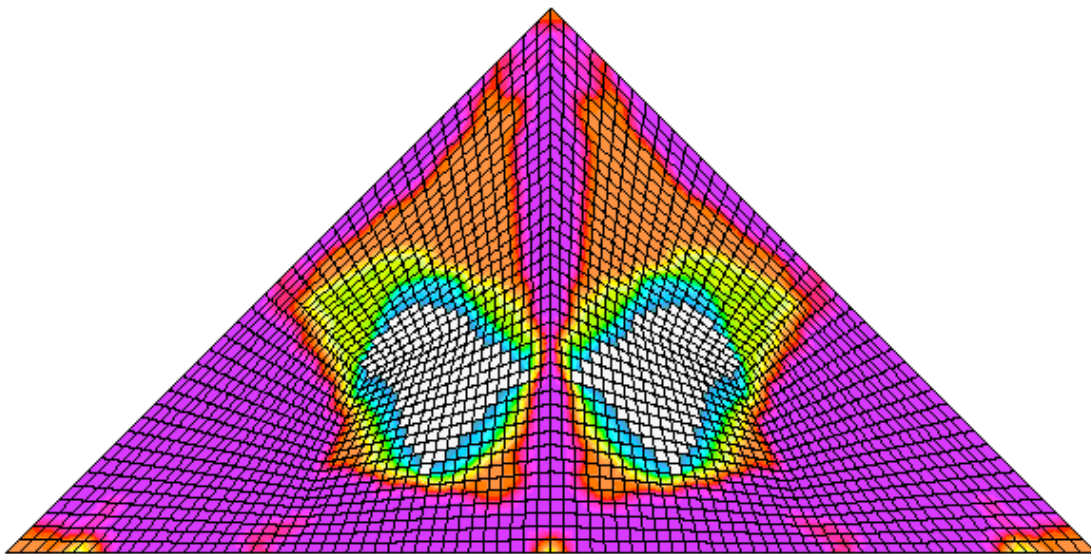
Figure 84. Initial finite element model of two quadrants of the 200-mm solar sail.

The hypotenuse of each triangular segment of the membrane is 200 mm and an assumed uniform thickness of 0.0254 mm. The material is a Kapton foil with an elastic modulus of 2964.8 N/mm^2 , a Poisson's ratio of 0.34, and a mass density of $1.4172 \times 10^{-6} \text{ kg/mm}^3$. Along the lower horizontal edge, three points are fully restrained (the end points and the center point). Between the two triangular regions is a single beam element to model a center boom structure. The membrane structure is only attached to the center boom at the end points and not along its length. At the upper vertex, the center boom is loaded by an applied vertical force with a base magnitude of 1 N.

Nonlinear static solutions are obtained using the SHM membrane wrinkling model with a relaxed tolerance on the convergence criterion. Contour plots of the wrinkling indicator for several solution steps are shown in Figure 85. These results indicate that wrinkling develops from the membrane edges and does evolve as the loading increases. The center region of each quadrant apparently stays taut.

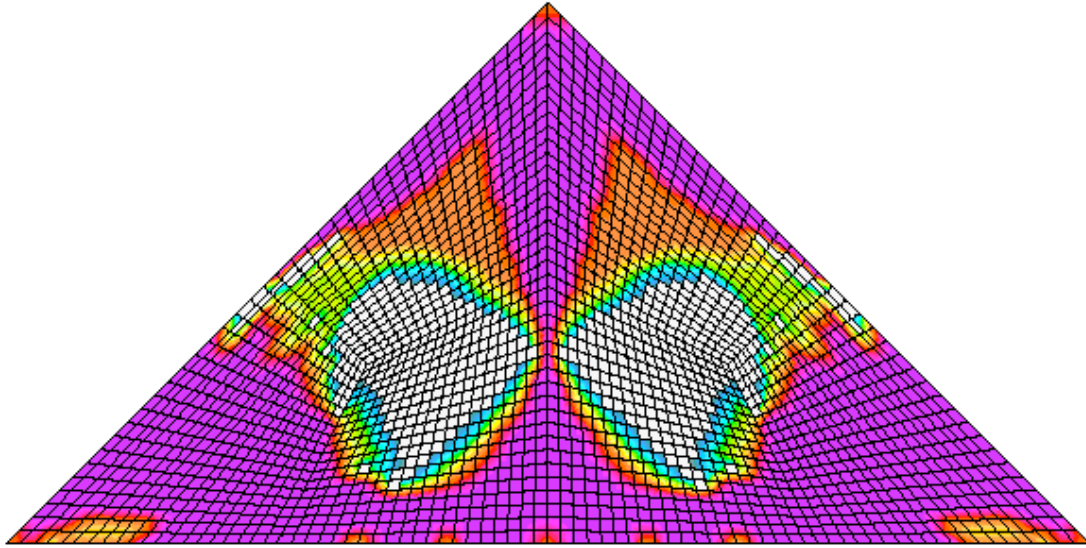


(a) Step 1, $PA=0.020$, 2110 affected elements.

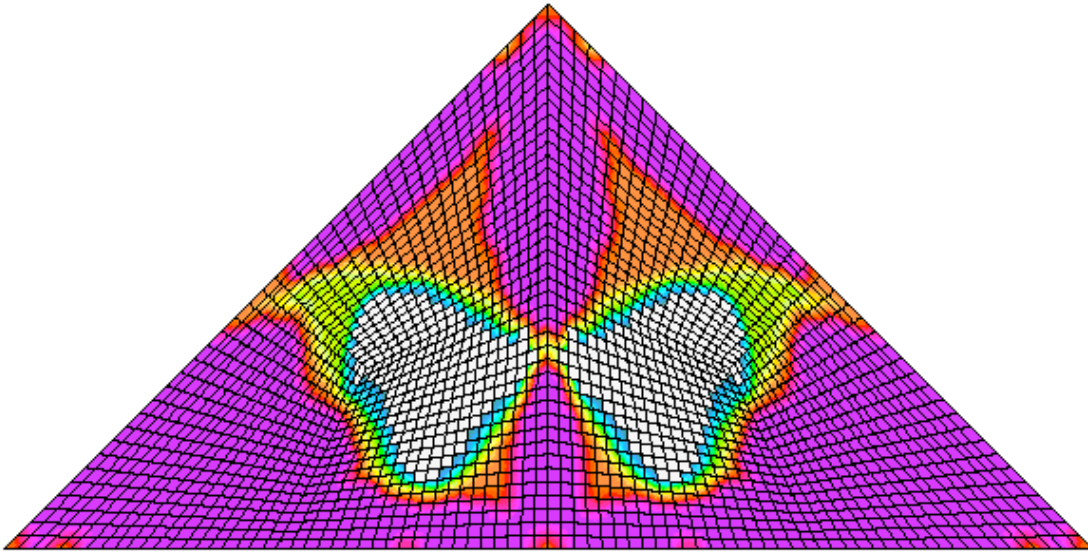


(b) Step 2, $PA=0.040$, 2200 affected elements.

Figure 85. Contour plots of the wrinkling indicator for several solution steps.

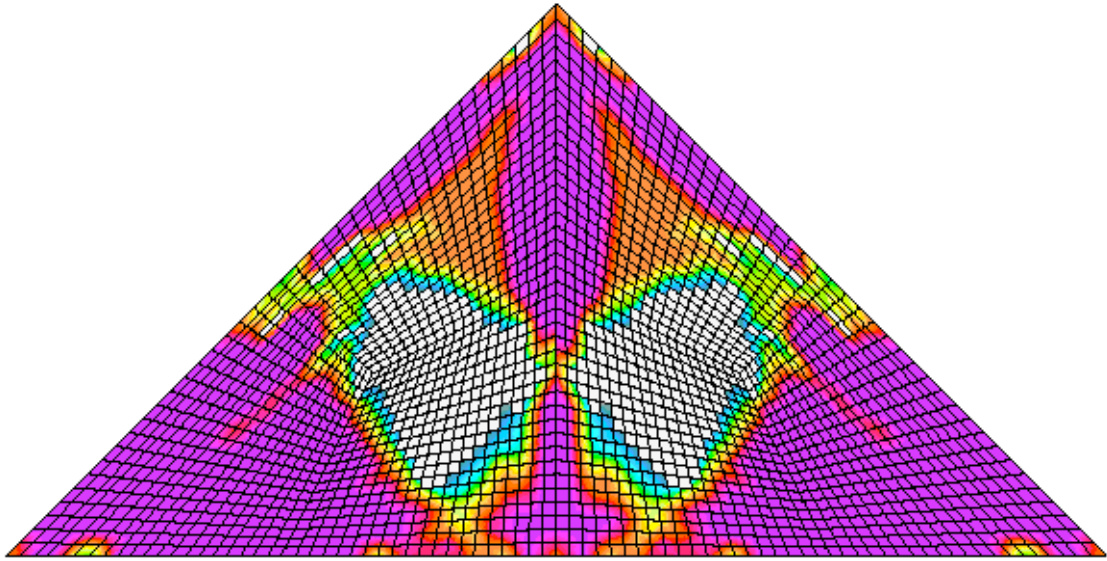


(c) Step 3, $PA=0.0597$, 2074 affected elements.

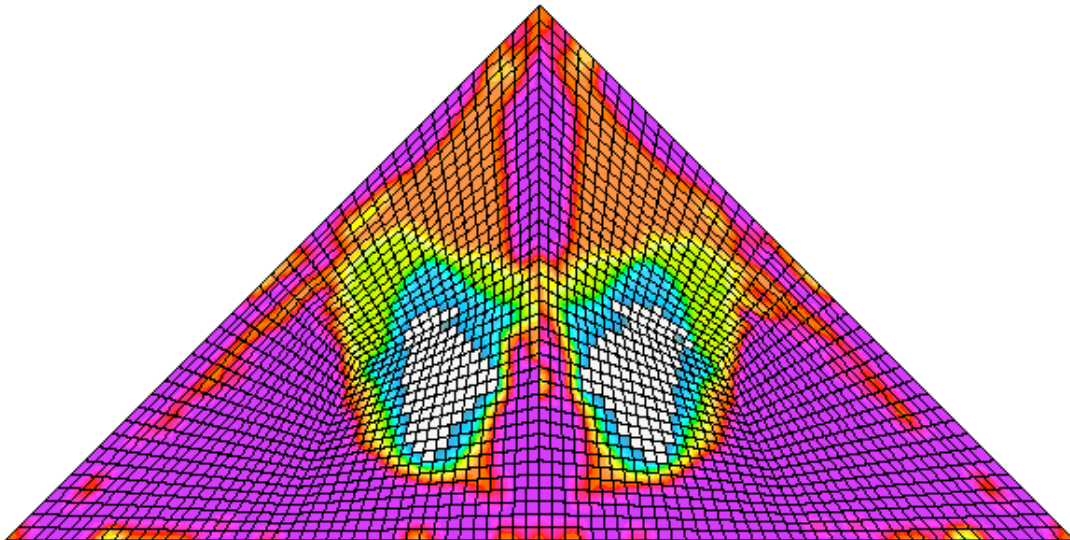


(d) Step 5, $PA=0.1479$, 2040 affected elements.

Figure 85. Continued.

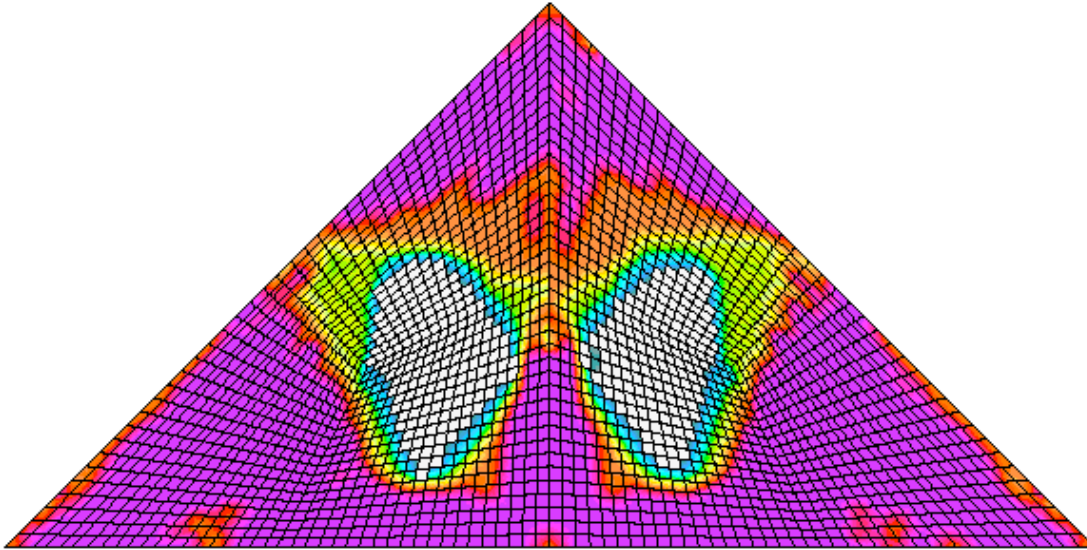


(e) Step 6, PA=0.2132, 1978 affected elements.



(f) Step 8, PA=0.5115, 2281 affected elements.

Figure 85. Continued.



(g) Step 10, PA=1.0, 2073 affected elements.

Figure 85. Concluded.

STAGS Input Files

These input files are located under the following subdirectory:

```
$STAGSHOME/Advanced-Testcases/Type-E-wrinkling
```

with the first case under the subdirectory pellegrino and the second case under the subdirectory sail2m.

pellegrino.inp

```
Rectangular Kapton membrane with in-plane shear loading $a-1
C
C Membrane wrinkling test case studied by Wong & Pellegrino
C
C Ref.: Wong & Pellegrino, "Computation of Wrinkle
C Amplitudes in Thin Membranes," AIAA Paper
C No. 2002-1369, April 2002, SDM in Denver.
C
C MODEL INPUT CONTROLS
1 0 1 0 0 3 0 $B-1
1 0.0 / 2 0.0 / 3 0.0 $B-1b model rotations
1 0 0 0 0 0 0 1 $B-2 include inertial loads
1 0 1 0 0 1 $B-3 INCLUDE GCP INPUT
9814.56 $b-4 acceleration due to gravity mm/s/s (=386.4 in/s/s)
1 1 0 0 0 $B-6 gravity load in y-direction
0.0 0.0 0.0 $b-6a neg y-global to center of earth
C 0.0 9814.56 0.0 $b-6a neg y-global to center of earth
100 41 $f-1 row and columns in each unit (3960 4-node elements)
C
C HISTORICAL STAGS MATERIAL DEFINITION
C
```

```

C Kapton Type H film
C E=430 ksi = 2964.8 N/mm^2; nu=0.34
C rho(mass) = 0.0512 lbm/in^3 = 1.4172E-6 kg/mm^3 = 0.013909 N/mm^3
C
1      $I-1 MATERIAL NO. 1 (HISTORICAL STAGS APPROACH)
3530.0 0.30 0.0 1.4722E-2 $I-2 ISOTROPIC ELASTIC MATERIAL
C =====
C BEGIN GCP INPUT FOR MATERIAL AND FABRICATION
C
ISOELASTIC_MATERIAL 1 1 1 0 0 $I-5A MATERIAL NO. 1 (GCP APPROACH)
3530.0,      $I-6A YOUNG'S MODULUS, N/mm^2
0.30,      $I-6A POISSON'S RATIO
1.5000E-6,  $I-6A MASS DENSITY, kg/mm^3
4*0.0      $I-6A UNUSED MATERIAL PARAMETERS
C Membrane wrinkling model
SHM_MEMB 2 1 1 0 0 $I-5A MATERIAL NO. 2 (GCP APPROACH)
3530.0,      $I-6A YOUNG'S MODULUS, N/mm^2
0.30,      $I-6A POISSON'S RATIO
1.5000E-6,  $I-6A MASS DENSITY, kg/mm^3
4*0.0,      $I-6A UNUSED MATERIAL PARAMETERS
1.0e-3,     $I-6a Penalty factor for slack state
3,          $I-6a Wrinkling criteria
1          $I-6a Initial membrane state for each iteration
SHELL_FABRICATION 1 1 1 0 0 $I-5A GCP SHELL FABRICATION RECORD
2          $I-21A GCP LAYER MATERIAL ID
1          $I-21A GCP LAYER INTEGRATION POINTS
25.0e-3    $I-21C GCP LAYER THICKNESS, mm (= 25 micro-meters)
0.0        $I-21D GCP LAYER ORIENTATION, DEGREES
END        $I-5A END GCP INPUT
C END GCP INPUT FOR MATERIAL AND FABRICATION
C =====
C
C HISTORICAL STAGS SHELL FABRICATION DEFINITION
C
1          1          1          0          $K-1 SHELL WALL RECORD
1          25.0e-3 0.0          0          $K-2 LAYERED WALL, mm (= 25 micro-meters)
C
C SHELL UNIT 1 MODEL DEFINITION (right side)
C
2 0 0 0 0 0 0          $M-1 RECTANGULAR PLATE GEOMETRY
0.0 380.0 0.0 128.0    $M-2 rectangle dimensions, mm
-1 0 0.0 0.0 0 0 0    $M-5 SHELL WALL RECORD, USE GCP FAB. # 1
410 0 0          $N-1 ELEMENT SELECTION
C
C Boundary conditions
C (horizontal edges in rigid blocks at fixed distance apart
C and the vertical edges are free)
C
0 0 0 2 $P-1 EDGE 4 IS CLAMPED
110 000
110 000
110 000
C
C Load definition
C
2 0 0 0 $Q-1 LOADING SUMMARY
C load system A - horizontal edge displacement - shears membrane
1 1 0 $Q-2 LOAD SET A SUMMARY
3.0 -1 1 0 41 0 0 0 0 0 $Q-3 uniform horizontal displ.
C load system B - vertical edge displacement - tensions membrane
2 4 0 $Q-2 LOAD SET B SUMMARY
0.5 -1 2 0 41 0 0 0 0 0 $Q-3 uniform vertical displ.
0.0 -1 3 0 0 0 0 0 0 0 $Q-3 w=0
0.0 -1 4 0 0 0 0 0 0 0 $Q-3 ru=0
0.0 -1 5 0 0 0 0 0 0 0 $Q-3 rv=0

```

```

C
C Output Control
C
0 0 0 0 0 0 0 0 0 $r-1

pellegrino.bin

Wong & Pellegrino rectangular membrane under shear loading $a-1
C
C Nonlinear restart adding in shearing with tensioning
C ( Increment Load Set A with constant Load Set B)
C
3 1 5*0 -1 $B-1 ANALYSIS Type
0.1 0.1 1.0 1.0 0.0 1.0 $C-1 LOAD MULTIPLIERS
2 2000 5 -20 0 1.0e-4 $d-1 Solution controls
0 0 1 $et-1
C
C Nonlinear solution for tensioning first (Load Set B)
C
3 1 5*0 -1 $B-1 ANALYSIS Type
0.0 0.0 0.0 0.5 0.5 1.0 $C-1 LOAD MULTIPLIERS
0 2000 5 -20 0 1.0e-4 $d-1 Solution controls
0 0 1 $et-1
C
C Linear solution
C
0 1 5*0 -1 $B-1 ANALYSIS CONTROL
0.0 0.0 0.0 1.0 1.0 1.0 $C-1 Pre-tensioning
C
C linear buckling analysis
C
1 1 0 4*0 -1 $b-1
1.0 0.0 1.0 1.0 0.0 1.0 $c-1 load factor
6000 1.0e-4 0 $d-2
10 0.0215 $d-3
C
C Nonlinear solution
C
3 1 5*0 -1 $B-1 ANALYSIS CONTROL
0.0 0.1 0.2 1.0 1.0 1.0 $C-1 LOAD MULTIPLIERS
0 2000 5 -20 0 1.0e-4 $d-1
0 0 1 $et-1
C
C Nonlinear solution
C
3 1 5*0 -1 $B-1 ANALYSIS CONTROL
1.0 1.0 5.0 $C-1 LOAD MULTIPLIERS
0 200 5 -20 0 1.0e-4 $d-1
0 0 0 $et-1
C
C linear vibration with gravity prestress
C
5 1 5*0 -1 $b-1
1.0 $c-1 load factor
1 4 $c-3 number of modes
1.0 $c-4
0 200 5 -20 1 1.0e-4 $d-1
0 0 0 $et-1
C
C free vibration analysis
C
2 1 5*0 -1 $b-1
1.0 $c-1 load factor
200 1.0e-4 0 $d-2
4 $d-3

```

pellegrino.pin

Wong & Pellegrino rectangular Kapton membrane in shear \$a-1

10 0 0 0 \$PL-2 NPLOT,IPREP,IPRS,KDEV

C plot membrane state - state variable

```
2 0 14 1 0 0 1 13 1 $PL-3 KPLOT,VIEW,ITEM,STEP,MODE,IFRNG,COLOR,ICOMP
-1.0 3 0.0 -1.0 1.0 $PL-5 DSCALE,NROTS,LWSCALE,RNGMIN,RGMAX
1 1.0 / 2 1.0 / 3 1.0
2 0 14 2 0 0 1 13 1 $PL-3 KPLOT,VIEW,ITEM,STEP,MODE,IFRNG,COLOR,ICOMP
-1.0 3 0.0 -1.0 1.0 $PL-5 DSCALE,NROTS,LWSCALE,RNGMIN,RGMAX
1 1.0 / 2 1.0 / 3 1.0
2 0 14 3 0 0 1 13 1 $PL-3 KPLOT,VIEW,ITEM,STEP,MODE,IFRNG,COLOR,ICOMP
-1.0 3 0.0 -1.0 1.0 $PL-5 DSCALE,NROTS,LWSCALE,RNGMIN,RGMAX
1 1.0 / 2 1.0 / 3 1.0
2 0 14 4 0 0 1 13 1 $PL-3 KPLOT,VIEW,ITEM,STEP,MODE,IFRNG,COLOR,ICOMP
-1.0 3 0.0 -1.0 1.0 $PL-5 DSCALE,NROTS,LWSCALE,RNGMIN,RGMAX
1 1.0 / 2 1.0 / 3 1.0
2 0 14 5 0 0 1 13 1 $PL-3 KPLOT,VIEW,ITEM,STEP,MODE,IFRNG,COLOR,ICOMP
-1.0 3 0.0 -1.0 1.0 $PL-5 DSCALE,NROTS,LWSCALE,RNGMIN,RGMAX
1 1.0 / 2 1.0 / 3 1.0
2 0 14 6 0 0 1 13 1 $PL-3 KPLOT,VIEW,ITEM,STEP,MODE,IFRNG,COLOR,ICOMP
-1.0 3 0.0 -1.0 1.0 $PL-5 DSCALE,NROTS,LWSCALE,RNGMIN,RGMAX
1 1.0 / 2 1.0 / 3 1.0
2 0 14 8 0 0 1 13 1 $PL-3 KPLOT,VIEW,ITEM,STEP,MODE,IFRNG,COLOR,ICOMP
-1.0 3 0.0 -1.0 1.0 $PL-5 DSCALE,NROTS,LWSCALE,RNGMIN,RGMAX
1 1.0 / 2 1.0 / 3 1.0
2 0 14 10 0 0 1 13 1 $PL-3 KPLOT,VIEW,ITEM,STEP,MODE,IFRNG,COLOR,ICOMP
-1.0 3 0.0 -1.0 1.0 $PL-5 DSCALE,NROTS,LWSCALE,RNGMIN,RGMAX
1 1.0 / 2 1.0 / 3 1.0
```

C plot wrinkling flag

```
2 0 8 2 0 0 0 0 $PL-3 KPLOT,VIEW,ITEM,STEP,MODE,IFRNG,COLOR,ICOMP
0.0 3 0.0 0.0 0.0 $PL-5 DSCALE,NROTS,LWSCALE,RNGMIN,RGMAX
1 1.0 / 2 1.0 / 3 1.0
2 0 8 3 0 0 0 0 $PL-3 KPLOT,VIEW,ITEM,STEP,MODE,IFRNG,COLOR,ICOMP
0.0 3 0.0 0.0 0.0 $PL-5 DSCALE,NROTS,LWSCALE,RNGMIN,RGMAX
1 1.0 / 2 1.0 / 3 1.0
2 0 8 4 0 0 0 0 $PL-3 KPLOT,VIEW,ITEM,STEP,MODE,IFRNG,COLOR,ICOMP
0.0 3 0.0 0.0 0.0 $PL-5 DSCALE,NROTS,LWSCALE,RNGMIN,RGMAX
1 1.0 / 2 1.0 / 3 1.0
2 0 8 5 0 0 0 0 $PL-3 KPLOT,VIEW,ITEM,STEP,MODE,IFRNG,COLOR,ICOMP
0.0 3 0.0 0.0 0.0 $PL-5 DSCALE,NROTS,LWSCALE,RNGMIN,RGMAX
1 1.0 / 2 1.0 / 3 1.0
2 0 8 6 0 0 0 0 $PL-3 KPLOT,VIEW,ITEM,STEP,MODE,IFRNG,COLOR,ICOMP
0.0 3 0.0 0.0 0.0 $PL-5 DSCALE,NROTS,LWSCALE,RNGMIN,RGMAX
1 1.0 / 2 1.0 / 3 1.0
2 0 8 7 0 0 0 0 $PL-3 KPLOT,VIEW,ITEM,STEP,MODE,IFRNG,COLOR,ICOMP
0.0 3 0.0 0.0 0.0 $PL-5 DSCALE,NROTS,LWSCALE,RNGMIN,RGMAX
1 1.0 / 2 1.0 / 3 1.0
2 0 8 8 0 0 0 0 $PL-3 KPLOT,VIEW,ITEM,STEP,MODE,IFRNG,COLOR,ICOMP
0.0 3 0.0 0.0 0.0 $PL-5 DSCALE,NROTS,LWSCALE,RNGMIN,RGMAX
1 1.0 / 2 1.0 / 3 1.0
2 0 8 10 0 0 0 0 $PL-3 KPLOT,VIEW,ITEM,STEP,MODE,IFRNG,COLOR,ICOMP
0.0 3 0.0 0.0 0.0 $PL-5 DSCALE,NROTS,LWSCALE,RNGMIN,RGMAX
1 1.0 / 2 1.0 / 3 1.0
2 0 8 12 0 0 0 0 $PL-3 KPLOT,VIEW,ITEM,STEP,MODE,IFRNG,COLOR,ICOMP
0.0 3 0.0 0.0 0.0 $PL-5 DSCALE,NROTS,LWSCALE,RNGMIN,RGMAX
1 1.0 / 2 1.0 / 3 1.0
2 0 8 14 0 0 0 0 $PL-3 KPLOT,VIEW,ITEM,STEP,MODE,IFRNG,COLOR,ICOMP
0.0 3 0.0 0.0 0.0 $PL-5 DSCALE,NROTS,LWSCALE,RNGMIN,RGMAX
1 1.0 / 2 1.0 / 3 1.0
2 0 8 16 0 0 0 0 $PL-3 KPLOT,VIEW,ITEM,STEP,MODE,IFRNG,COLOR,ICOMP
0.0 3 0.0 0.0 0.0 $PL-5 DSCALE,NROTS,LWSCALE,RNGMIN,RGMAX
1 1.0 / 2 1.0 / 3 1.0
```



```

2 0 8 18 0 0 0 0 $PL-3 KPLOT,VIEW,ITEM,STEP,MODE,IFRNG,COLOR,ICOMP
0.0 3 0.0 0.0 0.0 $PL-5 DSCALE,NROTS,LWSCALE,RNGMIN,RGMAX
1 1.0 / 2 1.0 / 3 1.0
C plot state variable term
2 0 14 18 0 0 1 7 $PL-3 KPLOT,VIEW,ITEM,STEP,MODE,IFRNG,COLOR,ICOMP
0.0 3 0.0 .0 .0 $PL-5 DSCALE,NROTS,LWSCALE,RNGMIN,RGMAX
1 1.0 / 2 1.0 / 3 1.0
2 0 14 18 0 0 1 10 $PL-3 KPLOT,VIEW,ITEM,STEP,MODE,IFRNG,COLOR,ICOMP
0.0 3 0.0 .0 .0 $PL-5 DSCALE,NROTS,LWSCALE,RNGMIN,RGMAX
1 1.0 / 2 1.0 / 3 1.0
2 0 14 12 0 0 1 13 $PL-3 KPLOT,VIEW,ITEM,STEP,MODE,IFRNG,COLOR,ICOMP
0.0 3 0.0 -1.0 1.0 $PL-5 DSCALE,NROTS,LWSCALE,RNGMIN,RGMAX
1 1.0 / 2 1.0 / 3 1.0
2 0 14 18 0 0 1 13 $PL-3 KPLOT,VIEW,ITEM,STEP,MODE,IFRNG,COLOR,ICOMP
0.0 3 0.0 -1.0 1.0 $PL-5 DSCALE,NROTS,LWSCALE,RNGMIN,RGMAX
1 1.0 / 2 1.0 / 3 1.0
C plot displacements
2 0 1 2 0 0 0 1 $PL-3 KPLOT,VIEW,ITEM,STEP,MODE,IFRNG,COLOR,ICOMP
0.0 3 0.0 0.0 0.0 $PL-5 DSCALE,NROTS,LWSCALE,RNGMIN,RGMAX
1 1.0 / 2 1.0 / 3 1.0
2 0 1 3 0 0 0 2 $PL-3 KPLOT,VIEW,ITEM,STEP,MODE,IFRNG,COLOR,ICOMP
0.0 3 0.0 0.0 0.0 $PL-5 DSCALE,NROTS,LWSCALE,RNGMIN,RGMAX
1 1.0 / 2 1.0 / 3 1.0
C plot mode shapes
2 0 4 0 1 0 0 3 $PL-3 KPLOT,VIEW,ITEM,STEP,MODE,IFRNG,COLOR,ICOMP
0.0 3 0.0 -1.0 1.0 $PL-5 DSCALE,NROTS,LWSCALE,RNGMIN,RGMAX
1 -5.0 / 2 -5.0 / 3 1.0
2 0 4 0 2 0 0 3 $PL-3 KPLOT,VIEW,ITEM,STEP,MODE,IFRNG,COLOR,ICOMP
0.0 3 0.0 -1.0 1.0 $PL-5 DSCALE,NROTS,LWSCALE,RNGMIN,RGMAX
1 -5.0 / 2 -5.0 / 3 1.0
2 0 4 0 3 0 0 3 $PL-3 KPLOT,VIEW,ITEM,STEP,MODE,IFRNG,COLOR,ICOMP
0.0 3 0.0 -1.0 1.0 $PL-5 DSCALE,NROTS,LWSCALE,RNGMIN,RGMAX
1 -5.0 / 2 -5.0 / 3 1.0
2 0 4 0 4 0 0 3 $PL-3 KPLOT,VIEW,ITEM,STEP,MODE,IFRNG,COLOR,ICOMP
0.0 3 0.0 -1.0 1.0 $PL-5 DSCALE,NROTS,LWSCALE,RNGMIN,RGMAX
1 -5.0 / 2 -5.0 / 3 1.0
C plot principal stresses
2 0 7 2 0 0 0 7 $PL-3 KPLOT,VIEW,ITEM,STEP,MODE,IFRNG,COLOR,ICOMP
0.0 3 0.0 0.0 0.0 $PL-5 DSCALE,NROTS,LWSCALE,RNGMIN,RGMAX
1 1.0 / 2 1.0 / 3 1.0
2 0 7 2 0 0 0 8 $PL-3 KPLOT,VIEW,ITEM,STEP,MODE,IFRNG,COLOR,ICOMP
0.0 3 0.0 0.0 0.0 $PL-5 DSCALE,NROTS,LWSCALE,RNGMIN,RGMAX
1 1.0 / 2 1.0 / 3 1.0
2 0 8 2 0 0 0 0 $PL-3 KPLOT,VIEW,ITEM,STEP,MODE,IFRNG,COLOR,ICOMP
0.0 3 0.0 0.0 0.0 $PL-5 DSCALE,NROTS,LWSCALE,RNGMIN,RGMAX
1 1.0 / 2 1.0 / 3 1.0
C
2 0 1 6 0 0 0 1 $PL-3 KPLOT,VIEW,ITEM,STEP,MODE,IFRNG,COLOR,ICOMP
0.0 3 0.0 0.0 0.0 $PL-5 DSCALE,NROTS,LWSCALE,RNGMIN,RGMAX
1 1.0 / 2 1.0 / 3 1.0
2 0 1 6 0 0 0 2 $PL-3 KPLOT,VIEW,ITEM,STEP,MODE,IFRNG,COLOR,ICOMP
0.0 3 0.0 0.0 0.0 $PL-5 DSCALE,NROTS,LWSCALE,RNGMIN,RGMAX
1 1.0 / 2 1.0 / 3 1.0
C plot stress resultants
2 0 5 0 0 0 0 1 $PL-3 KPLOT,VIEW,ITEM,STEP,MODE,IFRNG,COLOR,ICOMP
0.0 3 0.0 0.0 0.0 $PL-5 DSCALE,NROTS,LWSCALE,RNGMIN,RGMAX
1 0.0 / 2 -45.0 / 3 15.0
2 0 5 0 0 0 0 2 $PL-3 KPLOT,VIEW,ITEM,STEP,MODE,IFRNG,COLOR,ICOMP
0.0 3 0.0 0.0 0.0 $PL-5 DSCALE,NROTS,LWSCALE,RNGMIN,RGMAX
1 0.0 / 2 -45.0 / 3 15.0
2 0 5 0 0 0 0 3 $PL-3 KPLOT,VIEW,ITEM,STEP,MODE,IFRNG,COLOR,ICOMP
0.0 3 0.0 0.0 0.0 $PL-5 DSCALE,NROTS,LWSCALE,RNGMIN,RGMAX
1 0.0 / 2 -45.0 / 3 15.0
C plot strains
2 0 6 0 0 0 0 1 $PL-3 KPLOT,VIEW,ITEM,STEP,MODE,IFRNG,COLOR,ICOMP

```

```

0.0 3 0.0 0.0 0.0 $PL-5 DSCALE,NROTS,LWSCALE,RNGMIN,RGMAX
1 0.0 / 2 -45.0 / 3 15.0
2 0 6 0 0 0 0 2 $PL-3 KPLOT,VIEW,ITEM,STEP,MODE,IFRNG,COLOR,ICOMP
0.0 3 0.0 0.0 0.0 $PL-5 DSCALE,NROTS,LWSCALE,RNGMIN,RGMAX
1 0.0 / 2 -45.0 / 3 15.0
C plot principal stresses
2 0 7 0 0 0 0 7 $PL-3 KPLOT,VIEW,ITEM,STEP,MODE,IFRNG,COLOR,ICOMP
0.0 3 0.0 0.0 0.0 $PL-5 DSCALE,NROTS,LWSCALE,RNGMIN,RGMAX
1 0.0 / 2 -45.0 / 3 15.0
2 0 7 0 0 0 0 8 $PL-3 KPLOT,VIEW,ITEM,STEP,MODE,IFRNG,COLOR,ICOMP
0.0 3 0.0 0.0 0.0 $PL-5 DSCALE,NROTS,LWSCALE,RNGMIN,RGMAX
1 0.0 / 2 -45.0 / 3 15.0
C plot displacements
2 0 1 0 0 0 0 0 $PL-3 KPLOT,VIEW,ITEM,STEP,MODE,IFRNG,COLOR,ICOMP
0.0 3 0.0 0.0 0.0 $PL-5 DSCALE,NROTS,LWSCALE,RNGMIN,RGMAX
1 0.0 / 2 0.0 / 3 0.0
2 0 1 1 0 0 0 0 $PL-3 KPLOT,VIEW,ITEM,STEP,MODE,IFRNG,COLOR,ICOMP
0.0 3 0.0 0.0 0.0 $PL-5 DSCALE,NROTS,LWSCALE,RNGMIN,RGMAX
1 0.0 / 2 0.0 / 3 0.0

```

sail2m.inp

```

Two quadrants of square solar sail including center boom $A-1
C
C Tension load applied at tip of center boom then
C shearing displacement
C
C MODEL INPUT CONTROLS
1 0 1 0 3 0 $B-1
1 0.0 / 2 0.0 / 3 0.0 $B-1b model rotations
6 1 0 6 2 0 0 0 $B-2 include inertial loads
1 1 1 0 0 1 $B-3 INCLUDE GCP INPUT
9814.56 $b-4 acceleration due to gravity mm/s/s (=386.4 in/s/s)
C1 1 0 0 0 $B-6 gravity load in y-direction
C0.0 9814.56 0.0 $b-6a neg y-global to center of earth
21 21 21 21 21 21, $f-1 row and columns in each unit on right
21 21 21 21 21 21 $f-1 row and columns in each unit on left
C
C Shell unit connections
C
1 3 2 1
1 2 3 4
2 2 3 3
4 1 5 3
4 2 6 4
5 2 6 -1
C
C Partial compatibility at two end points along center
C
4 21 1 0 1 1 1 0
6 21 21 0 3 1 21 0
C
C Element unit specifics
C
3 0 1 0 0 $h-1 element unit (3 nodes and 1 beam element)
C
C HISTORICAL STAGS MATERIAL DEFINITION
C
C Kapton Type H film
C E=430 ksi = 2964.8 N/mm^2; nu=0.34
C rho(mass) = 0.0512 lbm/in^3 = 1.4172E-6 kg/mm^3 = 0.013909 N/mm^3
C
1 $I-1 MATERIAL NO. 1 (HISTORICAL STAGS APPROACH)

```

```

2964.8 0.34 0.0 1.3909E-2 $I-2 ISOTROPIC ELASTIC MATERIAL
C =====
C BEGIN GCP INPUT FOR MATERIAL AND FABRICATION
C
ISOELASTIC_MATERIAL 1 1 1 0 0 $I-5A MATERIAL NO. 1 (GCP APPROACH)
2964.8, $I-6A YOUNG'S MODULUS, N/mm^2
0.34, $I-6A POISSON'S RATIO
1.4172E-6, $I-6A MASS DENSITY, kg/mm^3
4*0.0 $I-6A UNUSED MATERIAL PARAMETERS
C Membrane Wrinkling Model
SHM_MEMB 2 1 1 0 0 $I-5A MATERIAL NO. 2 (GCP APPROACH)
2964.8, $I-6A YOUNG'S MODULUS, N/mm^2
0.34, $I-6A POISSON'S RATIO
1.4172E-6, $I-6A MASS DENSITY, kg/mm^3
4*0.0, $I-6A UNUSED MATERIAL PARAMETERS
1.0e-6, $I-6a Penalty factor for slack state
3 0 $I-6a Wrinkling criteria
SHELL_FABRICATION 1 1 1 0 0 $I-5A GCP SHELL FABRICATION RECORD
2 $I-21A GCP LAYER MATERIAL ID
1 $I-21B GCP Layer integration points
25.4e-3 $I-21C GCP LAYER THICKNESS, mm (= 1 mil)
0.0 $I-21D GCP LAYER ORIENTATION, DEGREES
END $I-5A END GCP INPUT
C END GCP INPUT FOR MATERIAL AND FABRICATION
C =====
C
C define center boom stiffnesses
C
1 1 1 0 0.0 $j-1
10.0 1000. 1000. 0.0 $j-2a A, Iyy, Izz, Iyz
C
C HISTORICAL STAGS SHELL FABRICATION DEFINITION
C
1 1 1 0 $K-1 SHELL WALL RECORD
1 25.4e-3 0.0 0 $K-2 LAYERED WALL, mm (= 1 mil)
C
C SHELL UNIT 1 MODEL DEFINITION (right side)
C
3 0 0 0 0 0 $M-1 QUADRILATERAL PLATE GEOMETRY
0.0000 0.0000 , $M-2 coordinates
0.0000 70.7107 , $M-2 coordinates
47.1405 47.1405 , $M-2 coordinates
70.7107 0.0000 $M-2 coordinates
-1 0 0.0 0.0 0 0 0 $M-5 SHELL WALL RECORD, USE GCP FAB. # 1
410 0 0 $N-1 ELEMENT SELECTION
C
C Boundary conditions
C
6 6 6 3 $P-1
C
C Load definition
C
1 0 0 0 $Q-1 LOADING SUMMARY
1 4 0 $Q-2 LOAD SET SUMMARY
0.0 -1 3 0 0 0 0 0 0 0 $Q-3 w=0
0.0 -1 4 0 0 0 0 0 0 0 $Q-3 ru=0
0.0 -1 5 0 0 0 0 0 0 0 $Q-3 rv=0
0.0 -1 1 1 1 0 6 1 0 0 $Q-3 Fix one point
C
C Output Control
C
0 $r-1
C

```

```

C SHELL UNIT 2 MODEL DEFINITION (right side)
C
3 0 0 0 0 0          $M-1 QUADRILATERAL PLATE GEOMETRY
    70.7107      0.0000 , $M-2 coordinates
    47.1405      47.1405 , $M-2 coordinates
    70.7107      70.7107 , $M-2 coordinates
    141.4214     0.0000  $M-2 coordinates
-1 0 0.0 0.0 0 0 0    $M-5 SHELL WALL RECORD, USE GCP FAB. # 1
410 0 0              $N-1 ELEMENT SELECTION
C
C Boundary conditions
C
6 6 3 3 $P-1
C
C Load definition
C
1 0 0 0 $Q-1 LOADING SUMMARY
1 4 0   $Q-2 LOAD SET SUMMARY
0.0 -1 3 0 0 0 0 0 0 0 $Q-3 w=0
0.0 -1 4 0 0 0 0 0 0 0 $Q-3 ru=0
0.0 -1 5 0 0 0 0 0 0 0 $Q-3 rv=0
0.0 -1 1 21 1 0 6 1 0 0 $Q-3 Fix one point
C
C Output Control
C
0 $r-1
C
C SHELL UNIT 3 MODEL DEFINITION (right side)
C
3 0 0 0 0 0          $M-1 QUADRILATERAL PLATE GEOMETRY
    0.0000      70.7107 , $M-2 coordinates
    0.0000     141.4214 , $M-2 coordinates
    70.7107     70.7107 , $M-2 coordinates
    47.1405     47.1405  $M-2 coordinates
-1 0 0.0 0.0 0 0 0    $M-5 SHELL WALL RECORD, USE GCP FAB. # 1
410 0 0              $N-1 ELEMENT SELECTION
C
C Boundary conditions
C
6 3 6 6 $P-1
C
C Load definition
C
1 0 0 0 $Q-1 LOADING SUMMARY
1 4 0   $Q-2 LOAD SET SUMMARY
0.0 -1 3 0 0 0 0 0 0 0 $Q-3 w=0
0.0 -1 4 0 0 0 0 0 0 0 $Q-3 ru=0
0.0 -1 5 0 0 0 0 0 0 0 $Q-3 rv=0
0.0 -1 3 1 21 0 4 1 0 0 $Q-3 Fix one point
C
C Output Control
C
0 $r-1
C
C SHELL UNIT 4 MODEL DEFINITION (left side)
C
3 0 0 0 0 0          $M-1 QUADRILATERAL PLATE GEOMETRY
   -70.7107     0.0000 , $M-2 coordinates
   -47.1405     47.1405 , $M-2 coordinates
    0.0000      70.7107 , $M-2 coordinates
    0.0000      0.0000  $M-2 coordinates
-1 0 0.0 0.0 0 0 0    $M-5 SHELL WALL RECORD, USE GCP FAB. # 1
410 0 0              $N-1 ELEMENT SELECTION

```

```

C
C Boundary conditions
C
6 6 6 3 $P-1
C
C Load definition
C
1 0 0 0 $Q-1 LOADING SUMMARY
1 3
0.0 -1 3 0 0 0 0 0 0 0 $Q-3 w=0
0.0 -1 4 0 0 0 0 0 0 0 $Q-3 ru=0
0.0 -1 5 0 0 0 0 0 0 0 $Q-3 rv=0
C
C Output Control
C
0 $r-1
C
C SHELL UNIT 5 MODEL DEFINITION (left side)
C
3 0 0 0 0 0 $M-1 QUADRILATERAL PLATE GEOMETRY
-141.4214 0.0000 , $M-2 coordinates
-70.7107 70.7107 , $M-2 coordinates
-47.1405 47.1405 , $M-2 coordinates
-70.7107 0.0000 $M-2 coordinates
-1 0 0.0 0.0 0 0 0 $M-5 SHELL WALL RECORD, USE GCP FAB. # 1
410 0 0 $N-1 ELEMENT SELECTION
C
C Boundary conditions
C
3 6 6 3 $P-1
C
C Load definition
C
1 0 0 0 $Q-1 LOADING SUMMARY
1 4 0 $Q-2 LOAD SET SUMMARY
0.0 -1 3 0 0 0 0 0 0 0 $Q-3 w=0
0.0 -1 4 0 0 0 0 0 0 0 $Q-3 ru=0
0.0 -1 5 0 0 0 0 0 0 0 $Q-3 rv=0
0.0 -1 1 1 1 0 6 1 0 0 $Q-3 Fix one point
C
C Output Control
C
0 $r-1
C
C SHELL UNIT 6 MODEL DEFINITION (left side)
C
3 0 0 0 0 0 $M-1 QUADRILATERAL PLATE GEOMETRY
-47.1405 47.1405 , $M-2 coordinates
-70.7107 70.7107 , $M-2 coordinates
0.0000 141.4214 , $M-2 coordinates
0.0000 70.7107 $M-2 coordinates
-1 0 0.0 0.0 0 0 0 $M-5 SHELL WALL RECORD, USE GCP FAB. # 1
410 0 0 $N-1 ELEMENT SELECTION
C
C Boundary conditions
C
6 3 6 6 $P-1
C
C Load definition
C
1 0 0 0 $Q-1 LOADING SUMMARY
1 3
0.0 -1 3 0 0 0 0 0 0 0 $Q-3 w=0

```

```

0.0  -1  4  0  0  0  0  0  0  0  0  $Q-3 ru=0
0.0  -1  5  0  0  0  0  0  0  0  0  $Q-3 rv=0
C
C Output Control
C
0    $r-1
C
C Define 3 nodes for the center vertical boom between the
C two triangular quadrants
C
1  1  1  1  3*0.0  110 000  0  $$s-1 base point
2  3  1  21  3*0.0  110 000  0  $$s-1 end of strut where load is applied
3  2  21  1  3*0.0  000 000  0  $$s-1 reference point defining xy plane
C
C define the beam element - only one required
C
1  2  3  210  1  0.0  0.0  0.0  0  0  $T-2 beam element
C
C tip load on center boom
C
1  0  0  0  $u-1
1  1  $u-2
1.0  1  2  2  0  1  $u-3 tip load in y-direction at node 2 Fy=100 N
1  0  0  0  0  1  $v-1

```

sail2m.bin

Two quadrants of the square solar sail with gravity loading \$a-1

```

C
C Nonlinear solution
C
3      1      5*0      -1      $B-1 ANALYSIS Type
0.02  0.02  1.0      $C-1 LOAD MULTIPLIERS
0  2000  8  -20  0  1.0e-1  $d-1 Solution Controls
0  0  0      $et-1
C
C Linear solution
C
0      1      5*0      -1      $B-1 ANALYSIS CONTROL
1.0  1.0  1.0      $C-1 LOAD MULTIPLIERS
C
C linear vibration with gravity prestress
C
5  1  5*0  -1  $b-1
1.0      $c-1 load factor
1  4      $c-3 number of modes
1.0      $c-4
0  200  5  -20  1  1.0e-4  $d-1
0  0  0  $et-1
C
C free vibration analysis
C
2  1  5*0  -1  $b-1
1.0      $c-1 load factor
200  1.0e-4  0  $d-2
4  $d-3
C
C linear vibration with gravity prestress
C
5  1  5*0  -1  $b-1
1.0      $c-1 load factor
1  4      $c-3 number of modes
1.0      $c-4

```

```
0 200 5 -20 1 1.0e-4 $d-1
0 0 0 $set-1
```

sail2m.pin

Two quadrants of square solar sail

```
10 0 0 0 $PL-2 NPLOT,IPREP,IPRS,KDEV
C plot wrinkling indicator
  2 0 8 1 0 0 0 0 $PL-3 KPLOT,VIEW,ITEM,STEP,MODE,IFRNG,COLOR,ICOMP
-1.0 3 0.0 0.0 0.0 $PL-5 DSCALE,NROTS,LWSCALE,RNGMIN,RGMAX
1 0.0 / 2 0.0 / 3 0.0
  2 0 8 2 0 0 0 0 $PL-3 KPLOT,VIEW,ITEM,STEP,MODE,IFRNG,COLOR,ICOMP
-1.0 3 0.0 0.0 0.0 $PL-5 DSCALE,NROTS,LWSCALE,RNGMIN,RGMAX
1 0.0 / 2 0.0 / 3 0.0
  2 0 8 3 0 0 0 0 $PL-3 KPLOT,VIEW,ITEM,STEP,MODE,IFRNG,COLOR,ICOMP
-1.0 3 0.0 0.0 0.0 $PL-5 DSCALE,NROTS,LWSCALE,RNGMIN,RGMAX
1 0.0 / 2 0.0 / 3 0.0
  2 0 8 4 0 0 0 0 $PL-3 KPLOT,VIEW,ITEM,STEP,MODE,IFRNG,COLOR,ICOMP
-1.0 3 0.0 0.0 0.0 $PL-5 DSCALE,NROTS,LWSCALE,RNGMIN,RGMAX
1 0.0 / 2 0.0 / 3 0.0
  2 0 8 5 0 0 0 0 $PL-3 KPLOT,VIEW,ITEM,STEP,MODE,IFRNG,COLOR,ICOMP
-1.0 3 0.0 0.0 0.0 $PL-5 DSCALE,NROTS,LWSCALE,RNGMIN,RGMAX
1 0.0 / 2 0.0 / 3 0.0
  2 0 8 6 0 0 0 0 $PL-3 KPLOT,VIEW,ITEM,STEP,MODE,IFRNG,COLOR,ICOMP
-1.0 3 0.0 0.0 0.0 $PL-5 DSCALE,NROTS,LWSCALE,RNGMIN,RGMAX
1 0.0 / 2 0.0 / 3 0.0
  2 0 8 8 0 0 0 0 $PL-3 KPLOT,VIEW,ITEM,STEP,MODE,IFRNG,COLOR,ICOMP
-1.0 3 0.0 0.0 0.0 $PL-5 DSCALE,NROTS,LWSCALE,RNGMIN,RGMAX
1 0.0 / 2 0.0 / 3 0.0
  2 0 8 10 0 0 0 0 $PL-3 KPLOT,VIEW,ITEM,STEP,MODE,IFRNG,COLOR,ICOMP
-1.0 3 0.0 0.0 0.0 $PL-5 DSCALE,NROTS,LWSCALE,RNGMIN,RGMAX
1 0.0 / 2 0.0 / 3 0.0
C plot membrane state - state variable
  2 0 14 1 0 0 1 13 1 $PL-3 KPLOT,VIEW,ITEM,STEP,MODE,IFRNG,COLOR,ICOMP
-1.0 3 0.0 -1.0 1.0 $PL-5 DSCALE,NROTS,LWSCALE,RNGMIN,RGMAX
1 0.0 / 2 -45.0 / 3 15.0
  2 0 14 2 0 0 1 13 1 $PL-3 KPLOT,VIEW,ITEM,STEP,MODE,IFRNG,COLOR,ICOMP
-1.0 3 0.0 -1.0 1.0 $PL-5 DSCALE,NROTS,LWSCALE,RNGMIN,RGMAX
1 0.0 / 2 -45.0 / 3 15.0
  2 0 14 3 0 0 1 13 1 $PL-3 KPLOT,VIEW,ITEM,STEP,MODE,IFRNG,COLOR,ICOMP
-1.0 3 0.0 -1.0 1.0 $PL-5 DSCALE,NROTS,LWSCALE,RNGMIN,RGMAX
1 0.0 / 2 -45.0 / 3 15.0
  2 0 14 4 0 0 1 13 1 $PL-3 KPLOT,VIEW,ITEM,STEP,MODE,IFRNG,COLOR,ICOMP
-1.0 3 0.0 -1.0 1.0 $PL-5 DSCALE,NROTS,LWSCALE,RNGMIN,RGMAX
1 0.0 / 2 -45.0 / 3 15.0
  2 0 14 5 0 0 1 13 1 $PL-3 KPLOT,VIEW,ITEM,STEP,MODE,IFRNG,COLOR,ICOMP
-1.0 3 0.0 -1.0 1.0 $PL-5 DSCALE,NROTS,LWSCALE,RNGMIN,RGMAX
1 0.0 / 2 -45.0 / 3 15.0
  2 0 14 6 0 0 1 13 1 $PL-3 KPLOT,VIEW,ITEM,STEP,MODE,IFRNG,COLOR,ICOMP
-1.0 3 0.0 -1.0 1.0 $PL-5 DSCALE,NROTS,LWSCALE,RNGMIN,RGMAX
1 0.0 / 2 -45.0 / 3 15.0
  2 0 14 8 0 0 1 13 1 $PL-3 KPLOT,VIEW,ITEM,STEP,MODE,IFRNG,COLOR,ICOMP
-1.0 3 0.0 -1.0 1.0 $PL-5 DSCALE,NROTS,LWSCALE,RNGMIN,RGMAX
1 0.0 / 2 -45.0 / 3 15.0
  2 0 14 10 0 0 1 13 1 $PL-3 KPLOT,VIEW,ITEM,STEP,MODE,IFRNG,COLOR,ICOMP
-1.0 3 0.0 -1.0 1.0 $PL-5 DSCALE,NROTS,LWSCALE,RNGMIN,RGMAX
1 0.0 / 2 -45.0 / 3 15.0
C plot displacements
  2 0 1 2 0 0 0 1 $PL-3 KPLOT,VIEW,ITEM,STEP,MODE,IFRNG,COLOR,ICOMP
0.0 3 0.0 0.0 0.0 $PL-5 DSCALE,NROTS,LWSCALE,RNGMIN,RGMAX
1 0.0 / 2 -45.0 / 3 15.0
  2 0 1 2 0 0 0 2 $PL-3 KPLOT,VIEW,ITEM,STEP,MODE,IFRNG,COLOR,ICOMP
0.0 3 0.0 0.0 0.0 $PL-5 DSCALE,NROTS,LWSCALE,RNGMIN,RGMAX
```

```

1 0.0 / 2 -45.0 / 3 15.0
C plot strains
  2 0 7 2 0 0 0 11 $PL-3 KPLOT,VIEW,ITEM,STEP,MODE,IFRNG,COLOR,ICOMP
0.0 3 0.0 0.0 0.0 $PL-5 DSCALE,NROTS,LWSCALE,RNGMIN,RGMAX
1 0.0 / 2 -45.0 / 3 15.0
  2 0 7 2 0 0 0 12 $PL-3 KPLOT,VIEW,ITEM,STEP,MODE,IFRNG,COLOR,ICOMP
0.0 3 0.0 0.0 0.0 $PL-5 DSCALE,NROTS,LWSCALE,RNGMIN,RGMAX
1 0.0 / 2 -45.0 / 3 15.0
C plot principal stresses
  2 0 7 2 0 0 0 7 $PL-3 KPLOT,VIEW,ITEM,STEP,MODE,IFRNG,COLOR,ICOMP
0.0 3 0.0 0.0 0.0 $PL-5 DSCALE,NROTS,LWSCALE,RNGMIN,RGMAX
1 0.0 / 2 -45.0 / 3 15.0
  2 0 7 2 0 0 0 8 $PL-3 KPLOT,VIEW,ITEM,STEP,MODE,IFRNG,COLOR,ICOMP
0.0 3 0.0 0.0 0.0 $PL-5 DSCALE,NROTS,LWSCALE,RNGMIN,RGMAX
1 0.0 / 2 -45.0 / 3 15.0
C plot stress resultants
  2 0 5 0 0 0 0 1 $PL-3 KPLOT,VIEW,ITEM,STEP,MODE,IFRNG,COLOR,ICOMP
0.0 3 0.0 0.0 0.0 $PL-5 DSCALE,NROTS,LWSCALE,RNGMIN,RGMAX
1 0.0 / 2 -45.0 / 3 15.0
  2 2 5 0 0 0 0 1 $PL-3 KPLOT,VIEW,ITEM,STEP,MODE,IFRNG,COLOR,ICOMP
4 5
0.0 3 0.0 0.0 0.0 $PL-5 DSCALE,NROTS,LWSCALE,RNGMIN,RGMAX
1 0.0 / 2 -45.0 / 3 15.0
  2 3 5 0 0 0 0 1 $PL-3 KPLOT,VIEW,ITEM,STEP,MODE,IFRNG,COLOR,ICOMP
4 5 6
0.0 3 0.0 0.0 0.0 $PL-5 DSCALE,NROTS,LWSCALE,RNGMIN,RGMAX
1 0.0 / 2 -45.0 / 3 15.0
  2 1 5 0 0 0 0 1 $PL-3 KPLOT,VIEW,ITEM,STEP,MODE,IFRNG,COLOR,ICOMP
6
0.0 3 0.0 0.0 0.0 $PL-5 DSCALE,NROTS,LWSCALE,RNGMIN,RGMAX
1 0.0 / 2 -45.0 / 3 15.0
  2 0 5 0 0 0 0 2 $PL-3 KPLOT,VIEW,ITEM,STEP,MODE,IFRNG,COLOR,ICOMP
0.0 3 0.0 0.0 0.0 $PL-5 DSCALE,NROTS,LWSCALE,RNGMIN,RGMAX
1 0.0 / 2 -45.0 / 3 15.0
  2 0 5 0 0 0 0 3 $PL-3 KPLOT,VIEW,ITEM,STEP,MODE,IFRNG,COLOR,ICOMP
0.0 3 0.0 0.0 0.0 $PL-5 DSCALE,NROTS,LWSCALE,RNGMIN,RGMAX
1 0.0 / 2 -45.0 / 3 15.0
C plot vibration mode shapes
  2 0 4 1 1 0 0 3 $PL-3 KPLOT,VIEW,ITEM,STEP,MODE,IFRNG,COLOR,ICOMP
0.0 3 0.0 0.0 0.0 $PL-5 DSCALE,NROTS,LWSCALE,RNGMIN,RGMAX
1 0.0 / 2 -45.0 / 3 15.0
  2 0 4 1 2 0 0 3 $PL-3 KPLOT,VIEW,ITEM,STEP,MODE,IFRNG,COLOR,ICOMP
0.0 3 0.0 0.0 0.0 $PL-5 DSCALE,NROTS,LWSCALE,RNGMIN,RGMAX
1 0.0 / 2 1.0 / 3 0.0
  2 0 4 0 3 0 0 0 $PL-3 KPLOT,VIEW,ITEM,STEP,MODE,IFRNG,COLOR,ICOMP
0.0 3 0.0 0.0 0.0 $PL-5 DSCALE,NROTS,LWSCALE,RNGMIN,RGMAX
1 0.0 / 2 0.0 / 3 0.0
  2 0 4 0 4 0 0 0 $PL-3 KPLOT,VIEW,ITEM,STEP,MODE,IFRNG,COLOR,ICOMP
0.0 3 0.0 0.0 0.0 $PL-5 DSCALE,NROTS,LWSCALE,RNGMIN,RGMAX
1 0.0 / 2 0.0 / 3 0.0

```


Problem References

- Leifer, S. D., Frisbee, R. H., and Brophy, J. R., "The NASA Advanced Propulsion Concepts Program at the Jet Propulsion Laboratory," AIAA Paper No. 97-2792, 1997.
- Frisbee, R. H. and Leifer, S. D., "Evaluation of Propulsion Options for Interstellar Missions," AIAA Paper No. 98-3403, 1998.
- Garner, C. and Leipold, M., "Developments and Activities in Solar Sail Propulsion," AIAA Paper No. 2000-3858, July 2000.
- Garner, C., Price, H., Edwards, D., and Baggett, R., "Developments and Activities in Solar Sail Propulsion," AIAA Paper No. 2001-3234, July 2001.
- Greschik, G. and Mikulas, M. M., "Design Study of a Square Solar Sail Architecture," AIAA Paper No. 2001-1259, April 2001.
- Jenkins, C. H. and Leonard, J. W., "Nonlinear Dynamic Response of Membranes: State of the Art," *Applied Mechanics Reviews*, Vol. 44, No. 7, July 1991, pp. 319-328.
- Jenkins, C. H., "Nonlinear Dynamic Response of Membranes: State of the Art – Update," *Applied Mechanics Reviews*, Vol. 49, No. 10, Part 2, October 1996, pp. S41-S48.
- Jenkins, C. H. M. (editor), *Gossamer Spacecraft: Membrane and Inflatable Structures Technology for Space Applications*, AIAA Progress in Astronautics and Aeronautics Series, Vol. 191, Paul Zarchan (editor-in-chief), Reston, Virginia, 2001.
- Fang, H. and Lou, M., "Analytical Characterization of Space Inflatable Structures – An Overview," AIAA Paper No. 99-1272, April 1999.
- Salama, M., Lou, M., and Fang, H., "Deployment of Inflatable Space Structures: A Review of Recent Developments," AIAA Paper No. 2000-1730, April 2000.
- Freeland, R. F., "History of Relevant Inflatable High-Precision Space Structures Technology Development," *Gossamer Spacecraft: Membrane and Inflatable Structures Technology for Space Applications*, C. H. M. Jenkins (editor), AIAA Progress in Astronautics and Aeronautics Series, Vol. 191, 2001, pp. 35-47.
- Smalley, K. B., Tinker, M. L., and Fischer, R. T., "Investigation of Nonlinear Pressurization and Modal Restart in MSC/NASTRAN for Modeling Thin Film Inflatable Structures," AIAA Paper No. 2001-1409, April 2001.
- Smalley, K. B., Tinker, M. L., and Taylor, W. S., "Structural Modeling of a Five-Meter Thin Film Inflatable Antenna/Concentrator with Rigidized Support Struts," AIAA Paper No. 2001-1412, April 2001.
- Johnston, John D., "Finite Element Analysis of Wrinkled Membrane Structures for Sunshield Applications," AIAA Paper No. 2002-1456, April 2002.
- Johnston, J. and Lienard, S., "Modeling and Analysis of Structural Dynamics for a One-Tenth Scale Model NGST Sunshield," AIAA Paper No. 2001-1407, April 2001.

- Slade, K. N., Tinker, M. L., Lassiter, J. O., and Engberg, R., "Dynamics of an Inflatable Structure in Vacuum and Ambient Conditions," *AIAA Journal*, Vol. 39, No. 6, June 2001, pp. 1-8.
- Murphey, T. W. and Mikulas, M. M., "Nonlinear Effects of Material Wrinkles on the Stiffness of Thin Polymer Films," AIAA Paper No. 99-1341, April 1999.
- Murphey, T. W., Murphy D. M., Mikulas, M. M., Jr., and Adler, A. L., "A Method to Quantify the Thrust Degradation Effects of Structural Wrinkles in Solar Sails," AIAA Paper No. 2002-1560, April 2002.
- Talley, C., Clayton, W., Gierow, P., McGee, J., and Moore, J., "Advanced Membrane Materials for Improved Solar Sail Capabilities," AIAA Paper No. 2002-1561, April 2002.
- Jenkins, C. H., Haugen, F., and Spicher, W. H., "Experimental Measurement of Wrinkling in Membranes Undergoing Planar Deformation," *Experimental Mechanics*, Vol. 38, No. 2, June 1998, pp. 147-152.
- Blandino, J. R., Johnston, J. D., Miles, J. J., and Soplop, J. S., "Thin Film Membrane Wrinkling due to Mechanical and Thermal Loads," AIAA Paper No. 2001-1345, April 2001.
- Blandino, J. R., Johnston, J. D., Miles, J. J., and Dharamsi, U. K., "The Effect of Asymmetric Mechanical and Thermal Loading on Membrane Wrinkling," AIAA Paper No. 2002-1371, April 2002.
- Dharamsi, U. K., Evanchik, D. M., and Blandino, J. R., "Comparing Photogrammetry with a Conventional Displacement Measurement Technique on a 0.5m Square Kapton Membrane," AIAA Paper No. 2002-1258, April 2002.
- Pappa, R. S., Jones, T. W., Black, J. T., Walford, A., Robson, S., and Shortis, M. R., "Photogrammetry Methodology Development for Gossamer Spacecraft Structures," AIAA Paper No. 2002-1375, April 2002.
- Stein, Manuel and Hedgepeth, John M., *Analysis of Partly Wrinkled Membranes*, NASA TN D-813, July 1961.
- Mikulas, Martin M., Jr., *Behavior of a Flat Stretched Membrane Wrinkled by the Rotation of an Attached Hub*, NASA TN D-2456, September 1964.
- Moriya, K. and Uemura, M., "An Analysis of the Tension Field after Wrinkling in Flat Membrane Structures," *IASS Pacific Symposium – Part II on Tension Structures and Space Frames*, October 17-23, 1971, Tokyo and Kyoto, International Association for Shell and Spatial Structures, pp. 2-5-1 to 2-5-12.
- Haug, E. and Powell, G. H., "Finite Element Analysis of Nonlinear Membrane Structures," *IASS Pacific Symposium – Part II on Tension Structures and Space Frames*, October 17-23, 1971, Tokyo and Kyoto, International Association for Shell and Spatial Structures, pp. 2-3-1 to 2-3-13.
- Miller, Richard K. and Hedgepeth, John M., "An Algorithm for Finite Element Analysis of Partly Wrinkled Membranes," *AIAA Journal*, Vol. 20, No. 12, December 1982, pp. 1761-1763.
- Miller, Richard K., Hedgepeth, John M., Weingarten, Victor I., Das, Prasanta, and Kahyai, Shahrzad, "Finite Element Analysis of Partly Wrinkled Membranes," *Computers and Structures*, Vol. 20, Nos. 1-3, 1985, pp. 631-639.

Tabarrok, B. and Qin, Z., "Nonlinear Analysis of Tension Structures," *Computers and Structures*, Vol. 45, Nos. 5-6, 1992, pp. 973-984.

Adler, A. L., Mikulas, M. M., and Hedgepeth, J. M., "Static and Dynamic Analysis of Partially Wrinkled Membrane Structures," AIAA Paper No. 2000-1810, April 2000.

Adler, A. L., *Finite Element Approaches for Static and Dynamic Analysis of Partially Wrinkled Membrane Structures*, PhD Dissertation, Department of Aerospace Engineering, University of Colorado, Boulder, CO, December 2000.

Adler, A. L. and Mikulas, M. M., "Application of a Wrinkled Membrane Finite Element Approach to Advanced Membrane Structures," AIAA Paper No. 2001-4646, August 2001.

Roddeman, D. G., Drukker, J., Oomens, C. W. J., and Janssen, J. D., "The Wrinkling of Thin Membranes: Part 1 – Theory," *ASME Journal of Applied Mechanics*, Vol. 54, No. 4, December 1987, pp. 884-887.

Roddeman, D. G., Drukker, J., Oomens, C. W. J., and Janssen, J. D., "The Wrinkling of Thin Membranes: Part 2 – Numerical Analysis," *ASME Journal of Applied Mechanics*, Vol. 54, No. 4, December 1987, pp. 888-892.

Roddeman, D. G., "Finite Element Analysis of Wrinkling Membranes," *Communications in Applied Numerical Methods*, Vol. 7, 1991, pp. 299-307.

Chiu, H. C., Benson, R. C., Fiscella, M. D., and Burns, S. J., "Mechanical and Thermal Wrinkling of Polymer Membranes," *ASME Journal of Applied Mechanics*, Vol. 61, No. 1, March 1994, pp. 67-70.

Muttin, F., "A Finite Element for Wrinkled Curved Elastic Membranes, and Its Applications to Sails," *Communications in Numerical Methods in Engineering*, Vol. 12, No. 11, November 1996, pp. 775-785.

Contri, P. and Schrefler, B. A., "A Geometrically Nonlinear Finite Element Analysis of Wrinkled Membrane Surfaces by a No-Compression Material Model," *Communications in Applied Numerical Methods*, Vol. 4, No. 1, January-February 1988, pp. 5-15.

Kang, S. and Im, S., "Finite Element Analysis of Wrinkling Membranes," *ASME Journal of Applied Mechanics*, Vol. 64, No. 2, June 1997, pp. 263-269.

Yang, B., Ding, H., Lou, M., and Fang, H., "A New Approach to Wrinkling Prediction for Space Membrane Structures," AIAA Paper No. 2001-1348, April 2001.

Ding, H., Yang, B., and Lou, M., "A Two-Viable Parameter Membrane Model for Wrinkling Analysis of Membrane Structures," AIAA Paper No. 2002-1460, April 2002.

Lee, Keejoo and Lee, S. W., "Analysis of Gossamer Space Structures using Assumed Strain Formulation Solid Shell Elements," AIAA Paper No. 2002-1559, April 2002.

Haseganu, E. M. and Steigmann, D. J., "Analysis of Partly Wrinkled Membranes by the Method of Dynamic Relaxation," *Computational Mechanics*, Vol. 14, No. 6, September 1994, pp. 596-614.

Pipkin, A. C., "Relaxed Energy Densities for Isotropic Membranes," *Journal of Applied Mathematics*, Vol. 36, 1988, pp. 85-99.

Pipkin, A. C., "Relaxed Energy Densities for Large Deformations of Membranes," *Journal of Applied Mathematics*, Vol. 52, 1994, pp. 297-308.

Epstein, Marcelo and Forcinito, Mario A., "Anisotropic Membrane Wrinkling: Theory and Analysis," *International Journal of Solids and Structures*, Vol. 38, No. 30-31, June 2001, pp. 5253-5272.

Liu, X., Jenkins, C. H., and Schur, W. W., "Fine Scale Analysis of Wrinkled Membranes," *International Journal of Computational Engineering Science*, Vol. 1, No. 2, 2000, pp. 281-298.

Wong, Yew Wei, *Analysis of Wrinkle Patterns in Prestressed Membrane Structures*, Master of Philosophy Dissertation, Department of Engineering, University of Cambridge, U.K., August 2000.

Wong, Y. W. and Pellegrino, S., "Computation of Wrinkle Amplitudes in Thin Membranes," AIAA Paper No. 2002-1369, April 2002.

Wong, Y. W. and Pellegrino, S., "Amplitude of Wrinkles in Thin Membranes," in *New Approaches to Structural Mechanics, Shells and Biological Structures*, H. Drew and S. Pellegrino (editors), Kluwer Academic Publishers, 2002

Stanuszek, M., "FE Analysis of Large Deformations of Membranes with Wrinkling," *Finite Elements in Analysis and Design*, in press, 2002.

Slade, K. N., Belvin, W. K., and Behun, V., "Solar Sail Loads, Dynamics, and Membrane Studies," AIAA Paper No. 2002-1265, April 2002.

Actuator Problems

Background

A very simple actuator element can be based on enforcing the relative distance between the two endpoints to be a function of the applied load factor. Output from this element would in this case be the force required in the actuator mechanism to maintain the specified distance. Conversely, a specified force directed along the line between the two endpoints can be applied, resulting in a modified distance between the two points. The geometry of the actuator element is shown in Figure 86.

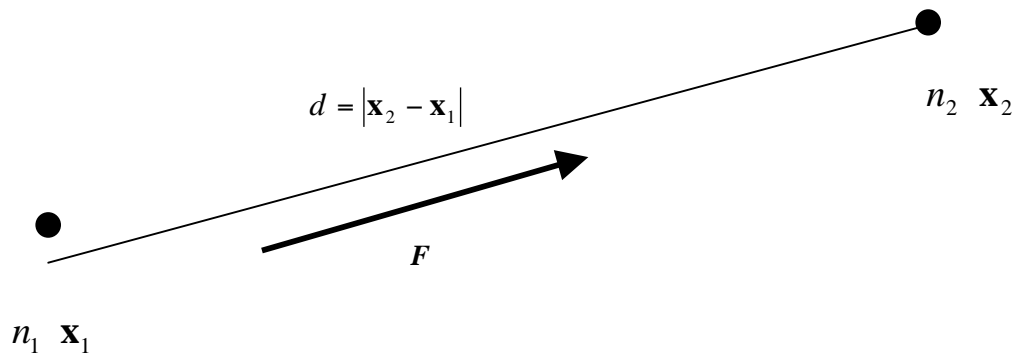


Figure 86. Illustration of a simple actuator

Modeling and Analysis Process

This sample case involves two flat strips separated initially by a distance of 0.1 inches. Each strip is clamped at one end and has an actuator element at the corners of the other end. The actuator elements then drive the two ends apart through specified stroke (ub910.inp) and through specified force (ubl910.inp). Note that while STAPL plotting of user-written elements is still pending, STAPL plots can be generated for those parts of the finite element that use intrinsic STAGS features.

Numerical Results and Discussion

The deformed geometry plots for the two-strip test case with tip actuator elements is shown in Figure 87. These results indicate that the present actuator element functions properly for large-displacements and large-rotation applications.

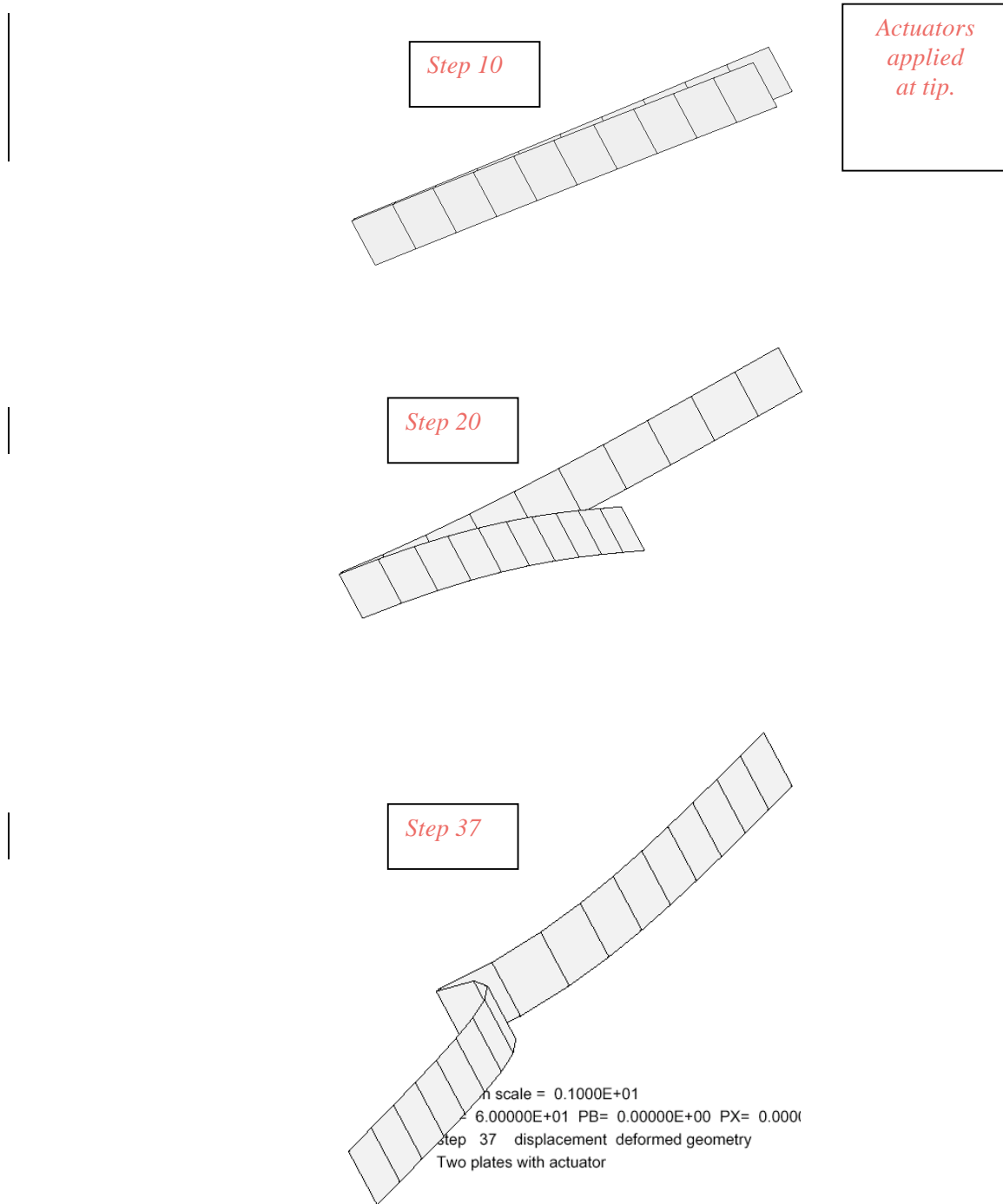


Figure 87. Selected deformed geometry plots for the Charles Rankin two actuator test case.

Sample output from the actuator elements is shown next. The displacements and rotations of each node on any actuator are printed using the frequency specified for the STAGS Element Unit input. In addition, actuator specific results (force and stroke) are available as shown:

```
Force in actuator Uel Type: 910
Element      Force
1           -6.29449E-03
2           -6.29449E-03
Length change in actuator Uel Type: 910
Element      Delta Length
1            8.25516E+00
2            8.25516E+00
```

XYTRANS is fully capable of producing a history plot of actuator stroke or resultant (reaction or loading) force. No “remaking” of software is necessary since the actuator is a permanent STAGS element. To obtain the stroke, the user should *choose option 14* “total strain and reference surface” and *choose option 1* (labeled “xx”), when the request “Enter component for total strain & reference surface:” comes up. The element number to be input is the actual STAGS *global element number* (not the actuator number). The user can input 0 for the element number, and then answer the next request with unit and local element number, as is done for all other elements. The next prompt requests the user to enter “C” for centroid and “I” for integration point data: *enter C*.

For the resultant (reaction or loading force) *choose option 13* “integrated stresses.” Follow that with *component 1* (Nx), and the *global element number* (as described above). Then *choose the C* option (as above). Other questions in the interview are exactly the same as for other elements.

The results of these operations go into a {casename}.plt file exactly as in other XYTRANS executions. This file can be processed with PLOTPS or imported into an EXCEL spreadsheet for display.

An example of an XYTRANS execution followed by PLOTPS processing yields the plot in Figure 88 for the test case described above:

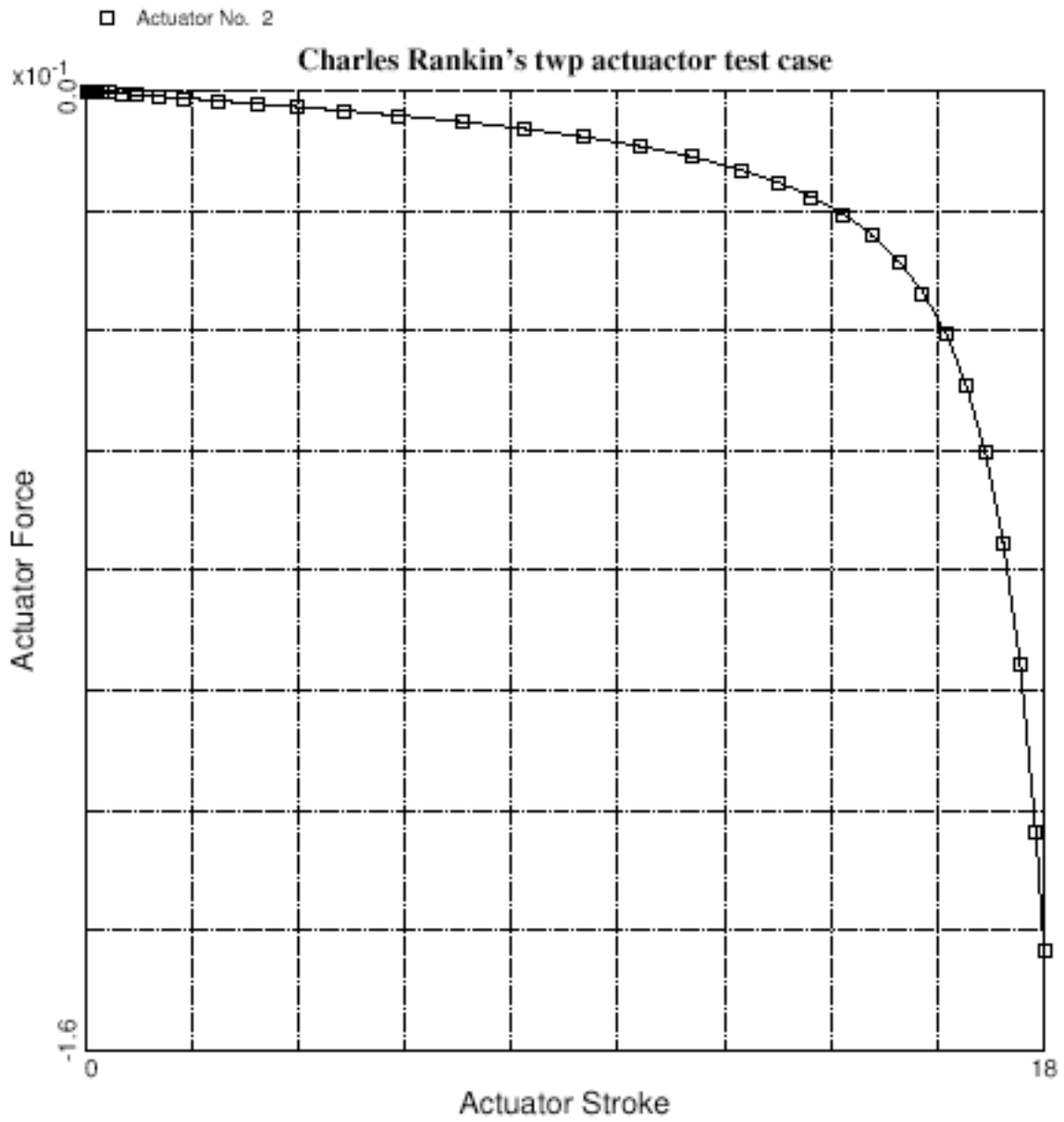


Figure 88. Representative actuator stroke versus force plot.

STAGS Input Files

These input files are located under the following subdirectory:

```
$STAGSHOME/Advanced-Testcases/Type-F-actuator
```

STAGS S1 Input:

```
Two strips clamped at one end and actuators at another
0 0 0 0 0 0 0 $ b1
2 1 0 0 0 0 0 0 0 $ b2
1 0 1 0 0 0 $ b3
11 2 11 2 $ f1
-1 -1 0 0 0 0 $ h1
$ Material for plates
1 /1.e7 .03 $I1/I2
$ Wall for plates
1 1 1 $K1
1 .01 $K2
$ Unit 1
2 0 $M1
0. 10. 0. 1. $M2
1 $M5
410 $N1
2 3 3 3 $P1
0 $Q1
1 0 0 0 0 1 $R1
$ Unit 2
2 4
0. 10. 0. 1.
0. 0. .1
0. 0. 0.
1
410
2 3 3 3
1/1 1
0. 5 3 0 0
1 0 0 0 0 1

$=====
$--User Element Definitions-----
$=====
$
*userElement name="Actuator Element" type=910 nodes=3

*dofOrdering

$ Node DOF...
$ -----
1 1 2 3
2 1 2 3
3 1

*nodeSequence

$ Nodes...
$ -----
1 2 3

*floatVariables
```

```

$ Name          Size
$ -----
FactA           1
FactB           1
Length          1
*integervariables

$ Name          Size
$ -----
spec_disp       1

*end userElement

*userProperty name="Standard Data -- Actuator Element" id=910

*integerProps

$ Required Standard Data
$ -----
ActiveNodes     2
SamplingCount    1
StrainCount      1
StressCount      1

*end userProperty
$
$=====
$--Element Unit-----
$=====
0 1 11 1 0.0 0.0 0.0 111 111 0 2 0      $ s3
1 0 0 1 .0 0.0 0.0                          $ s3a
0 2 11 1 0.0 0.0 0.0 111 111 0 2 0      $ s3
1 0 0 1 .0 0.0 0.0                          $ s3a
0 3*0 5.0 1.0 0.0 000 000 0 1 0          $ s3
END                                         $ s3
$
$ -----
E9XX_elements 1                          $ t100
910 1 0 0 0 0 2 1 1                      $ ----
1 3 5                                     $ nodes
1 1 0 1                                  $ {nodes} & elt x-incs
.3 0. 0.                                  $ FactA, FactB, length
1                                          $ Spec_disp
END                                         $ t100
$=====
$--Specified displacements & forces-----
$=====
0
$-----
1 1 1 0 0 1 0 0 0 0 0                    $ v1

```

STAGS S2 Input:

```

Two plates with actuator (specified stroke)
3 1 1 0 0 0 0 -1
.1 .1 60.
0 0 5 -20 -1 1.e-7
0

```

STAGS STAPL Input:

Two plates with actuators

```
4 0 1 0 $PL-2 NPLOT,IPREP,IPRS,KDEV
C Plot deformed shapes
1 0 1 10 0 $PL-3 KPLOT,VIEW,ITEM,STEP,MODE
-1.0 0 0.0 0.0 0.0 $PL-5 DSCALE,NROTS,LWSCALE,RNGMIN,RGMAX
1 0 1 20 0 $PL-3 KPLOT,VIEW,ITEM,STEP,MODE
-1.0 0 0.0 0.0 0.0 $PL-5 DSCALE,NROTS,LWSCALE,RNGMIN,RGMAX
1 0 1 30 0 $PL-3 KPLOT,VIEW,ITEM,STEP,MODE
-1.0 0 0.0 0.0 0.0 $PL-5 DSCALE,NROTS,LWSCALE,RNGMIN,RGMAX
1 0 1 37 0 $PL-3 KPLOT,VIEW,ITEM,STEP,MODE
-1.0 0 0.0 0.0 0.0 $PL-5 DSCALE,NROTS,LWSCALE,RNGMIN,RGMAX
```

Problem References

None.

Summary

This document summarizes the STAGS development effort, STAGS performance for selected demonstration problems, and STAGS application problems illustrating selected advanced features available in the STAGS Version 5.0. Each problem is discussed including selected background information and reference solutions when available. The modeling and solution approach for each problem is described and illustrated. Numerical results are presented and compared with reference solutions, test data, and/or results obtained from mesh refinement studies. These solutions provide an indication of the overall capabilities of the STAGS nonlinear finite element analysis tool and provide users with representative cases, including input files, to explore these capabilities that may then be tailored to other applications.

References

1. Almroth, B. O., Brogan, F. A., and Pittner, E. V., *Buckling Analysis of Segmented Orthotropic Cylinders Under Nonuniform Stress Distribution*, Lockheed Missiles & Space Company, Report No. M-77-65-4, July 1965.
2. Bushnell, D., Amroth, B. O., and Sobel, L. H., *Buckling of Shells of Revolution with Various Wall Constructions - Volume 2: Basic Equations and Method of Solution*, NASA CR-1050, May 1968.
3. Bushnell David, *Numerical Methods for the Analysis of Shells*, Lockheed Missiles & Space Company, Report No. 6-77-67-36, October 1968.
4. Brogan, F. A. and Stern, P., *Analysis of Stiffened Shells with Cutouts*, Lockheed Missiles & Space Company, Report No. N-3M-69-1, 1969.
5. Almroth, B. O. and Holmes, A. M. C., "Buckling of Shells with Cutouts: Experiment and Analysis," *International Journal of Solids and Structures*, Vol. 8, 1972, pp. 1057-1071.
6. Besseling, J. F., *A Theory of Elastic, Plastic, and Creep Deformations of an Initially Isotropic Material*, Stanford University, Department of Aeronautical Engineering, SUDAER Report No. 78, 1958.
7. Marlowe , M. B. and Flugge, W., *Some New Developments in the Foundations of Shell Theory*, Lockheed Missiles & Space Company, Report No. LMSC-6-78-68-13, May 1968
8. Almroth, B. O., Brogan, F. A., and Marlowe, M. B., *Computer Analysis of Shells of General Shape - Volume I: Analysis*, AFFDL-TR-71-8, August 1972.
9. Almroth, B. O., Brogan, F. A., Meller, E., Zele, F., and Petersen, H. T., *Collapse Analysis for Shells of General Shape - Volume II: User's Manual for the STAGS-A Computer Code*, AFFDL TR-71-8, March 1973.
10. Anon., *Collected Papers on Instability of Shell Structures -1962*, NASA TN-D-1510, December 1962.
11. Hartung, R. F. (editor), *Computer Oriented Analysis of Shell Structures*, proceedings of a conference held in Palo Alto, CA, August 10-14, 1970, AFFDL Report No. TR-71-79, 1971.
12. Hartung, R. F. and Ball, R. E., *A Comparison of Several Computer Solutions to Three Structural Shell Problems*, AFFDL, Report No. TR-73-15, 1973.

13. Almroth, B. O., Meller, E., and Brogan, F. A., "Computer Solutions for Static and Dynamic Buckling of Shells," in *Buckling of Structures*, B. Budiansky (editor). Proceedings of the IUTAM Symposium, June 17-21, 1974, Springer-Verlag, Berlin, 1976, pp. 52-66.
14. Almroth, B. O., Brogan, F. A., Meller, E., and Petersen, H. T., *User's Manual for the STAGS: Volume 3 - User's Instructions*, LMSC Report LMSC-D351897, January 1974. (STAGSB users manual)
15. Almroth, B. O., Brogan, F. A., and Stanley, G. M., *User's Manual for STAGS - Volume I: Theory*, NASA CR-165670, March 1978. (mainly for STAGSC)
16. Almroth, B. O. and Brogan, F. A., *The STAGS Computer Code*, NASA CR-2950, February 1978. (STAGSC overview)
17. Melosh, R. J., "Basis of Derivation of Matrices for the Direct Stiffness Method," *AIAA Journal*, Vol. 1, No. 7, 1963, pp. 1631-1637.
18. Willam, K. J., *Finite Element Analysis of Cellular Structures*, PhD Thesis, University of California at Berkeley, Department of Civil Engineering, 1969.
19. Rankin, Charles and Brogan, Frank, *The Computational Structural Mechanics Testbed Structural Element Processor ES5: STAGS Shell Element*, NASA CR-4358, May 1991.
20. Ahmad, S., Irons, B. M., and Zienkiewicz, O. C., "Analysis of Thick and Thin Shell Structures by Curved Elements," *International Journal for Numerical Methods in Engineering*, Vol. 2, 1970, pp. 419-451.
21. Giles, Gary L., *Digital Computer Programs for Generating Oblique Orthographic Projections and Contour Plots*, NASA TN D-7797, January 1975.
22. Almroth, B. O., Brogan, F. A., and Stanley, G. M., *Structural Analysis of General Shells - Volume II: User Instructions for STAGSC-1*, Lockheed Missiles & Space Company, Report No. LMSC-D633873, December 1982.
23. Almroth, B. O. and Brogan, F. A., "Computational Efficiency of Shell Elements," in *Nonlinear Finite Element Analysis of Plates and Shells*, T. J. R. Hughes, A. Pifko, and A. Jay (editors), ASME AMD-Vol. 48, 1981, pp. 147-165.
24. Thomas, K. and Sobel, L. H., *Evaluation of the STAGSC-1 Shell Analysis Computer Program*, Westinghouse Electric Corporation, Advanced Reactor Division, Report No. WARD-10881, August 1981.
25. Woytowicz, Peter J., *Sample Problems for STAGSC-1*, Air Force Wright Aeronautical Laboratories, Report No. AFWAL-TR-84-3088, February 1985.
26. L. H. Sobel and K. Thomas (editors), *Collapse Analysis of Structures*, ASME PVP- Vol. 84, June 1984.
27. Riks, E., *On the Numerical Solution of Snapping Problems in the Theory of Elastic Stability*, Stanford University, Report SUDAAR No. 401, 1970. Also available as AFOSR 70-2258TR.
28. Riks, E., Brogan, F. A., and Rankin, C. C., "Numerical Aspects of Shell Stability Analysis," *Computational Mechanics of Nonlinear Response of Shells*, W. B. Kratzig and E. Onate (editors), Springer-Verlag, Berlin, 1990, pp. 125-151.

29. Riks, E., "On Formulations of Path-Following Techniques for Structural Stability Analysis," *New Advances in Computational Structural Mechanics*, P. Ladeveze and O. C. Zienkiewicz (editors), Elsevier Science Publishers, 1992, pp. 65-79.
30. Knight, N. F., Jr. and Starnes, J. H., Jr., "Postbuckling Behavior of Axially Compressed Graphite-Epoxy Panels with Circular Holes," *ASME Journal of Pressure Vessel Technology*, Vol. 107, No. 4, November 1985, pp. 394-402.
31. Rankin, C. C., Stehlin, P., and Brogan, F. A., *Enhancements to the STAGS Computer Code*, NASA CR-4000, November 1986.
32. Rankin, C. C. and Brogan, F. A., "An Element-Independent Corotational Procedure for the Treatment of Large Rotations," *ASME Journal of Pressure Vessel Technology*, Vol. 108, 1986, pp. 165-174. Also available in *Collapse Analysis of Structures*, L. H. Sobel and K. Thomas (editors), ASME PVP- Vol. 84, June 1984, pp. 85-100.
33. Rankin, C. C., *Consistent Linearization of the Element-Independent Corotational Formulation for the Structural Analysis of General Shells*, Lockheed Missiles & Space Company, Report No. LMSC-F202439, March 1987.
34. Rankin, C. C. and Nour-Omid, B., "The Use of Projectors to Improve Finite Element Performance," *Computers and Structures*, Vol. 30, Nos. 1-2, 1988, pp. 257-267.
35. Nour-Omid, B and Rankin, C. C., "Finite Rotation Analysis and Consistent Linearization Using Projectors," *Computer Methods in Applied Mechanics and Engineering*, Vol. 93, 1991, pp. 353-384.
36. Thurston, G. A., Brogan, F. A., and Stehlin, P., "Postbuckling Analysis Using a General-Purpose Code," *AIAA Journal*, Vol. 24, No. 6, June 1986, pp. 1013-1020.
37. Rankin, C. C. and Brogan, F. A., "Application of the Thurston Bifurcation Solution Strategy to Problems with Modal Interaction," AIAA Paper No. 88-2286, April 1988.
38. Davila, Carlos, "Pad Elements for Gaps, Contact Problems and Crack Closure in Fracture Mechanics," unpublished NRC Progress Report, August 18, 1992.
39. Rankin, C. C., Chien, L. S., Loden, W. A., and Swenson, L. W., Jr., "Line-to-Line Contact Behavior of Shell Structures," AIAA Paper No. AIAA-99-1237, April 1999.
40. Almroth, B. O., Stern, P., and Brogan, F. A., "Automatic Choice of Global Shape Functions in Structural Analysis," *AIAA Journal*, Vol. 16, No. 5, May 1978, pp. 525-528.
41. Almroth, B. O., Stehlin, P., and Brogan, F. A., "Use of Global Functions for Improvement in Efficiency of Nonlinear Analysis," AIAA Paper No. 81-0575, April 1981.
42. Almroth, B. O., Stehlin, P., and Brogan, F. A., *Global Function Approach in Structural Analysis: Basic Approach, Numerical Results*, NASA CR-165669, April 1981.
43. Stehlin, P., Brogan, F. A., and Almroth, B. O., *RRSYS Integrated Modular Program System for the Static and Dynamic Analysis of Elastic Structures by Means of the Rayleigh-Ritz Method - User's Manual*, Lockheed Missiles & Space Company, December 1981.
44. Stehlin, P., Brogan, F. A., and Almroth, B. O., *RRSYS - System Reference Manual (second revision)*, NASA CR-178096, July 1986.

45. Knight, N. F., Jr. and Stroud, W. J., *Computational Structural Mechanics: A New Activity at the NASA Langley Research Center*, NASA TM-87612, 1985.
46. Rankin, C., Stanley, G., and DeRuntz, J., *Formulation of Improved Plasticity Calculations in the STAGSC-1 and NICE-SPAR Computer Codes*, Lockheed Missiles & Space Company, Report No. LMSC-F183026, 1987.
47. Rankin, C. and Brogan, F., *STAGS/Testbed Interface*, Lockheed Missiles & Space Company, Report No. LMSC-255539, April 1988.
48. Rankin, C. and Brogan, F., *Improved Plasticity and Imperfections in the STAGSC-1 Computer Code - Phase 2: Implementation*, Lockheed Missiles & Space Company, Report No. LMSC-F386402, July 1990.
49. Young, Richard D., "STAGS Sample Problems," presentation notes dated May 17, 1993.
50. Young, Richard D. "Introduction to STAGS," presentation charts from STAGS short course at NASA Langley, June 30 - July 1, 1993. (based on QSTAGS)
51. Brogan, F. A., Rankin, C. C., and Cabiness, H. D., *STAGS User Manual - Version 2.0*, Lockheed Missiles & Space Company, Report No. LMSC-P032594, June 1994.
52. Brogan, F. A., Rankin, C. C., and Cabiness, H. D., *STAR Reference Manual - Version 2.0*, Lockheed Martin Missiles & Space Company, Inc., Report No. LMMS-P032595, July 1996.
53. Rankin, C. C., Brogan, F. A., Loden, W., and Cabiness, H. D., *Structural Analysis of General Shells (STAGS) User Manual - Version 2.4*, Lockheed Martin Missiles & Space Company, Report No. LMMS-P032594, June 1997.
54. Hurlbut, B. J. and Stehlin, B. P., *Computational Mechanics Testbed (COMET) Generic Constitutive Processor*, Lockheed Missiles & Space Company, Report No. LMSC-F318484, May 1991.
55. Stanley, Gary M., *The Computational Structural Mechanics Testbed Structural Element Processor ES1: Basic SRI and ANS Shell Elements*, NASA CR-4357, May 1991.
56. Rankin, C. C., Brogan, F. A., and Riks, E., "Some Computational Tools for the Analysis of Through Cracks in Stiffened Fuselage Shells," *Computational Mechanics*, Vol. 13, 1993, pp. 143-156.
57. Riks, E., Rankin, C. C., and Brogan, F. A., "On the Solution of Mode Jumping Phenomena in Thin-Walled Shell Structures," *Computer Methods in Applied Mechanics and Engineering*, Vol. 136, Nos. 1-2, September 1996, pp. 59-92.
58. Riks, E. and Rankin, C. C., "Computer Simulation of the Buckling Behavior of Thin Shells Under Quasi-Static Loads," *Archives of Computational Methods in Engineering*, Vol. 4, No. 4, 1997, pp. 325-351.
59. Rankin, C. C., Brogan, F. A., Loden, W., and Cabiness, H. D., *Structural Analysis of General Shells (STAGS) User Manual - Version 3.0*, Lockheed Martin Missiles & Space Company, Report No. LMMS-P032594, June 1998.
60. Rankin, C. C., Brogan, F. A., Loden, W. A., and Cabiness, H. D., *STAGS Users Manual - Version 4.0*, Lockheed Martin Missiles & Space Co., Inc., Report No. LMSC P032594, June 2000.

61. Knight, N. F., Jr., Rankin, C. C., and Brogan, F. A., "STAGS Computational Procedure for Progressive Failure Analysis of Laminated Composite Structures," *International Journal of Non-Linear Mechanics*, Vol. 37, Nos. 4-5, June-July 2002, pp. 833-849.
62. Riks, E. and Rankin, C. C., "Sandwich Modeling with an Application to the Residual Strength Analysis of a Damaged Composite Compression Panel," AIAA Paper No. 2001-1323, April 2001.
63. Riks, E. and Rankin, C. C., "Sandwich Modeling with an Application to the Residual Strength Analysis of a Damaged Compression Panel," *International Journal of Non-Linear Mechanics*, Vol. 37, Nos. 4-5, 2002, pp. 897-908.
64. Rose, C. A., Moore, D. F., Knight, N. F., Jr., and Rankin, C. C., "Finite Element Modeling of the Buckling Response of Sandwich Panels," AIAA Paper No. 2002-1517, April 2002.
65. Rankin, C. C., Brogan, F. A., Loden, W. A., Cabiness, H. D., "STAGS User Manual – Version 5.0," Rhombus Consultants Group, Inc., Palo Alto, CA, revised January 2005 (on-line). *Previously Report No. LMSC P032594, Lockheed Martin Missiles and Space Company, Palo Alto, CA.*
66. Hurlbut, B. J. and Stehlin, B. P., "Computational Mechanics Testbed (COMET) Generic Constitutive Processor Manual," Lockheed Palo Alto Research Laboratory, Palo Alto, CA, Contract Report No. F318484, May 1991.
67. Rankin, C. C., Loden, W. A., and Swenson, L. W., "STAGS Elements Manual – Version 5.0, Preliminary," Rhombus Consultants Group, Inc., Palo Alto, CA, revised January 2005.
68. Brogan, F. A., Rankin, C. C., and Cabiness, H. D., STAR Reference Manual – Version 2.0," Lockheed Martin Missiles and Space Company, Palo Alto, CA, July 1996.
69. Loden, W. A., Rankin, C. C., and Young, R. W., "STAGS Test Cases Manual – Preliminary," Lockheed Martin Missiles and Space Company, Palo Alto, CA, February 2001.
70. Rankin, C., "STAGS UEL Post-processing and GCP Interface: UEL Developer Requirements and Interface Enhancements," January 2005.
71. Rankin, C., "Characterization of STAGS Thermal Capabilities," January 2005.
72. Rankin, C., "STAGS UEL Post-processing and GCP Interface: UEL Developer Requirements and Interface Enhancements," January 2005.
73. Jacoby, M., "STAGS Viewer and Mesher," December 2004.
74. Rankin, C. "An Actuator Element for STAGS V5," revised January, 2005.

REPORT DOCUMENTATION PAGE			Form Approved OMB No. 0704-0188		
<p>The public reporting burden for this collection of information is estimated to average 1 hour per response, including the time for reviewing instructions, searching existing data sources, gathering and maintaining the data needed, and completing and reviewing the collection of information. Send comments regarding this burden estimate or any other aspect of this collection of information, including suggestions for reducing this burden, to Department of Defense, Washington Headquarters Services, Directorate for Information Operations and Reports (0704-0188), 1215 Jefferson Davis Highway, Suite 1204, Arlington, VA 22202-4302. Respondents should be aware that notwithstanding any other provision of law, no person shall be subject to any penalty for failing to comply with a collection of information if it does not display a currently valid OMB control number. PLEASE DO NOT RETURN YOUR FORM TO THE ABOVE ADDRESS.</p>					
1. REPORT DATE (DD-MM-YYYY) 01- 03 - 2006		2. REPORT TYPE Contractor Report		3. DATES COVERED (From - To)	
4. TITLE AND SUBTITLE STAGS Example Problems Manual			5a. CONTRACT NUMBER		
			5b. GRANT NUMBER		
			5c. PROGRAM ELEMENT NUMBER		
6. AUTHOR(S) Knight, Norman F., Jr.; and Rankin, Charles			5d. PROJECT NUMBER NNL05AC09T		
			5e. TASK NUMBER Task 8		
			5f. WORK UNIT NUMBER 732759.07.11		
7. PERFORMING ORGANIZATION NAME(S) AND ADDRESS(ES) NASA Langley Research Center Hampton, VA 23681-2199			8. PERFORMING ORGANIZATION REPORT NUMBER		
General Dynamics Advanced Information Systems, Inc. 14700 Lee Road Chantilly, VA 20151					
9. SPONSORING/MONITORING AGENCY NAME(S) AND ADDRESS(ES) National Aeronautics and Space Administration Washington, DC 20546-0001			10. SPONSOR/MONITOR'S ACRONYM(S) NASA		
			11. SPONSOR/MONITOR'S REPORT NUMBER(S) NASA/CR-2006-214281		
12. DISTRIBUTION/AVAILABILITY STATEMENT Unclassified - Unlimited Subject Category 39 Availability: NASA CASI (301) 621-0390					
13. SUPPLEMENTARY NOTES Prepared for Langley Research Center under GSA Task Order GS-00F-0067M, NASA Order No. NNL05AC09T. Langley Technical Monitor: Richard D. Young An electronic version can be found at http://ntrs.nasa.gov					
14. ABSTRACT This document summarizes the STructural Analysis of General Shells (STAGS) development effort, STAGS performance for selected demonstration problems, and STAGS application problems illustrating selected advanced features available in the STAGS Version 5.0. Each problem is discussed including selected background information and reference solutions when available. The modeling and solution approach for each problem is described and illustrated. Numerical results are presented and compared with reference solutions, test data, and/or results obtained from mesh refinement studies. These solutions provide an indication of the overall capabilities of the STAGS nonlinear finite element analysis tool and provide users with representative cases, including input files, to explore these capabilities that may then be tailored to other applications.					
15. SUBJECT TERMS Finite elements; STAGS; Plates; Shells					
16. SECURITY CLASSIFICATION OF:			17. LIMITATION OF ABSTRACT	18. NUMBER OF PAGES	19a. NAME OF RESPONSIBLE PERSON
a. REPORT	b. ABSTRACT	c. THIS PAGE			STI Help Desk (email: help@sti.nasa.gov)
U	U	U	UU	289	19b. TELEPHONE NUMBER (Include area code) (301) 621-0390